Aus dem Cécile und Oskar Vogt-Institut für Hirnforschung
Direktorin: Prof. Dr. Katrin Amunts

Neuroanatomische Grundlagen für intelligentes Verhalten bei Vögeln – Eine Vergleichsstudie

Habilitationsschrift
zur Erlangung der Venia Legendi
für das Fach Neurowissenschaften
an der Hohen Medizinischen Fakultät
der Heinrich-Heine-Universität Düsseldorf

Vorgelegt von
Dr. rer. nat. Christina Herold
Düsseldorf 2019

Eidesstattliche Erklärung:

Ich versichere an Eides statt, dass ich die vorliegende Habilitationsschrift ohne unerlaubte Hilfe angefertigt habe, und dass das benutzte Schrifttum vollständig erwähnt wurde. Ethische Grundsätze sowie die Empfehlungen zur Sicherung der guten wissenschaftlichen Praxis wurden eingehalten. Diese Habilitationsschrift wurde bislang keiner anderen Fakultät vorgelegt.

Dr. rer. nat. Christina Herold
Düsseldorf, Juli 2019

Für meine Mama.

Inhaltsverzeichnis

1. Zusammenfassung

Die ersten Landwirbeltiere haben sich vor mehr als 365 Millionen Jahren in unterschiedliche Gruppen diversifiziert und sich unter der Bildung einer Vielzahl von neuen konkurrierenden Arten parallel zueinander bis heute weiterentwickelt. Neben den verschiedenen angeborenen Verhaltensweisen haben sie sich dabei Fähigkeiten angeeignet, die es ihnen erlauben, den Bereich ihrer ökologischen Nische möglichst optimal zu nutzen. Einige Arten zeigen dabei herausragende Fähigkeiten im Rahmen von intelligentem Verhalten, welches mit der Weiterentwicklung des Gehirns und insbesondere des Vorderhirns in Zusammenhang gesehen wird. Es ist daher hochinteressant, dass das Vorderhirn der Vögel, welches mit den Säugern den gleichen pallialen/subpallialen Ursprung teilt, keine laminierten Cortexareale aufweist, sondern nuklear aufgebaute Hirnstrukturen, und dass sich trotz der strukturellen Diversifizierung der Gehirne viele Funktionen parallel entwickelt haben. Diese ermöglichen es einigen Vögeln, wie z.B. aus der Familie der Rabenvögel (*Corvidae*) oder aus der Ordnung der Papageienvögel (*Psittaciformes*), die gleichen kognitiven Fähigkeiten wie Primaten zu erreichen, oder diese sogar noch zu übertreffen. Trotz dieser Erkenntnis ist es bisher nicht gelungen, die zugrundeliegenden Mechanismen von intelligentem Verhalten in Bezug auf die neuroanatomischen Korrelate hinreichend zu klären.

In dieser Habilitation wurde daher unter anderem die Neuroanatomie verschiedener Hirnareale, die an Lern- und Gedächtnisprozessen beteiligt sind, in unterschiedlichen Spezies untersucht. Hierbei lag der Schwerpunkt der Arbeit auf dem Gehirn der Taube (*Columba livia f.d.*). Durch detaillierte Untersuchungen der zellulären Architektur, der Neurotransmitter-Rezeptordichten und der Verbindungen der Areale wurden z.B. für die Hippocampus-formation, das Nidopallium caudolaterale (funktionell vergleichbar zum präfrontalen Cortex) und den Arcopallium/Amygdala-Kernkomplex (teilweise funktionell vergleichbar zum motorischen und somatosensorischen Cortex) neue Hirnatlaskarten für die Taube erstellt. Diese bereiteten die Grundlagen für den vergleichenden Ansatz. Es konnte so ein Vergleich zur Rezeptorarchitektur funktionell vergleichbarer Hirnstrukturen bei der Maus (*Mus musculus*), der Ratte (*Rattus norvegicus*), dem Makaken-Affen (*Macaca fascicularis*), dem Marmoset-Affen (*Callithrix jacchus*) und dem Menschen (*Homo sapiens*) erfolgen. Darüber hinaus wurde mit Verhaltenstests und *Real-time* PCR-Analysen gezeigt, dass die Konzentrationen von Dopamin-Rezeptoren sich im Nidopallium caudolaterale testabhängig plastisch anpassen können. Dies ist eine Form der Plastizität, die sich ebenfalls im präfrontalen Cortex von Säugern beobachten lässt. Zusätzlich wurde herausgefunden, dass die Hippocampusformation, ein entwicklungsgeschichtlich betrachtet sehr alter Teil des Palliums, in der Organisation der Konnektivität und dem Vorkommen adulter Neurogenese eine ähnliche topografische Gliederung wie die der Säuger aufweist.

Die Untersuchungen in dieser Arbeit zeigten, dass zwischen den Vertretern verschiedener Wirbeltierklassen, neben spezies-spezifischen Befunden, Parallelen in der neurochemischen Basis, in der neuronalen Plastizität und in der Konnektivität der funktionell an Lern- und Gedächtnisprozessen beteiligten Areale existieren. Somit wurde ein Grundlagenverständnis geschaffen, das einen Teilbeitrag für ein besseres Verständnis der Evolution von Kognition und

Verhalten leistet. In der Zukunft sind diese Ergebnisse nicht nur für neue Modellansätze im Rahmen der neuropathologischen Kognitionsforschung hilfreich, sondern auch für computerbasierte Ansätze bei der Entwicklung von Lernalgorithmen oder Transkriptom-Analysen.

2. Einleitung

2.1 Lernen und Gedächtnis

Seit den ersten dokumentierten pathologischen Befunden über Verhaltensänderungen und Gedächtnisstörungen beim Menschen, die mit einer Verletzung des Gehirns in Verbindung gebracht werden konnten, und der damit verbundenen Erkenntnis, dass das Gehirn als zentrales Organ im Verlauf der Evolution für viele Lern- und Gedächtnisprozesse eine tragende Rolle übernommen hat, ist das Wissen in Bezug auf diese Prozesse stetig erweitert und entwickelt worden. Ein Meilenstein in dieser Forschungsrichtung entstand in den 1970er Jahren durch Eric Kandel, der die molekularen Vorgänge des Lernens an den Neuronen des Seehasen (*Aplysia californica*) untersuchte und damit nicht nur ein Grundlagenverständnis für die Vorgänge an der Synapse beim Konditionierungslernen schaffte, sondern auch zeigte, dass sogar wirbellose Tiere die Fähigkeit besitzen zu lernen (Kandel, 2013[1981]). Aus dieser Erkenntnis wird deutlich, dass sich die grundlegenden Mechanismen, um Erinnerungen zu bilden, schon vor mehr als 600 Millionen Jahren entwickelt haben müssen, denn wirbellose Lebewesen sind schon für diese Zeit datiert (Wood et al., 2019). Mit der Evolution weiterer Spezies und der Weiterentwicklung des Gehirns wurden die molekularen Vorgänge des Lernens zunehmend komplexer. Es ließ sich jedoch speziesübergreifend zeigen, dass Prozesse wie Langzeitpotenzierung (englisch: *long-term potentiation, LTP*) und Langzeitdepression (englisch: *long-term depression, LTD*) als zelluläre Korrelate für Eingangsspezifität, Kooperativität und Assoziation von Signalen/Informationen im Sinne von assoziativem bzw. Extinktionslernen gelten (Bliss & Lomo, 1973; Levy & Steward, 1983; Brandon et al., 1995; Margrie et al., 1998; Huang et al., 2005; Bliss et al., 2018). Beiden Prozessen liegt die andauernde Verstärkung oder andauernde Abschwächung eines synaptischen Signals durch Aktionspotentiale an der Synapse/den Synapsen zwischen zwei Nervenzellen zu Grunde. Hierbei sind die beteiligten Neurotransmitterrezeptoren von großer Bedeutung, die bei der Signalvermittlung steuernd mitwirken. Mit zunehmender Komplexität des Nervensystems, der Weiterentwicklung der Sinne wie Geruch, Geschmack, Sehen, Hören, Fühlen und der Erschließung neuer ökologischer Nischen und Räume wurden für das Lernen zusätzliche Aspekte relevanter, die z.B. Motorik, Emotion, Motivation/Belohnung und Informationsinhalt/Kontext einschließen, aber auch der Zeitraum an sich, wie lange und in welcher Reihenfolge etwas abgespeichert werden muss. Hier ergab sich ein weiterer Ausgangspunkt bei der Erforschung der Lernprozesse aus dem Fall Henry Molaison (*1926; Patient H.M.), der nach der Resektion beider Hippocampi eine anterograde und zeitlich abgestufte retrograde Amnesie erlitt (Scoville & Milner, 1957; Squire, 2009). Im Gegensatz dazu blieben die Langzeiterinnerungen und weitere Lern- und Gedächtnisprozesse bei H.M. auch nach der Operation erhalten. Untersuchungen an Mäusen und anderen Säugern bestätigten die Bedeutung des Hippocampus für die Bildung von Langzeiterinnerungen sowie für das episodische und das räumliche Gedächtnis (Bird & Burgess, 2008). Es stellte sich zudem heraus, dass die Langzeitpotenzierung besonders stark im Hippocampus ausgeprägt ist, wohingegen im Kleinhirn der Prozess der Langzeitdepression als dominierend nachgewiesen wurde, welches eine wichtige Rolle in Zusammenhang mit dem prozeduralen Gedächtnis, z.B.

beim Erlernen von koordinierten Bewegungsabläufen, einnimmt (Ito et al., 1982; Aiba et al., 1994). Bei anderen Aspekten von Motorik im Rahmen von Lernprozessen sind die Basalganglien und insbesondere das dorsale Striatum von Bedeutung (Alexander et al., 1986; Liljeholm & O'Doherty, 2012). Läsionsstudien an Tiermodellen und Studien im Rahmen neuropathologischer Erkrankungen des menschlichen Gehirns führten zu der Erkenntnis, dass die emotionale Einfärbung der Gedächtnisinhalte stark von der Amygdala abhängt (Phelps, 2004). In diesem Zusammenhang nimmt die Amygdala mit ihren unterschiedlichen Anteilen und Verbindungen zum Hippocampus, dem ventralen Striatum und dem präfrontalen Cortex (PFC) sowie dem Hypothalamus eine zentrale Rolle als Schaltstelle für bewusstes Erleben und autonome Reaktion ein (Kim et al., 2011; Janak & Tye, 2015). Für die Gesamtkoordination der Abspeicherung von Gedächtnisinhalten lokalisierte man hingegen den PFC. Dieser wird deswegen auch als zentrale Exekutive oder übergeordnetes Zentrum bezeichnet (Baddeley, 1992). Die Erforschung des PFC und seine Bedeutung für das so genannte Arbeitsgedächtnis im Rahmen „höherer" kognitiver Funktionen wurde unter anderem durch den Fall Phineas Gage (*1823; P.G.) und die Aufzeichnungen durch seinen Arzt Harlow initiiert (Damasio et al., 1994). Durch einen Arbeitsunfall erlitt P.G. im linken frontalen Cortex und im PFC große Läsionen, die zu einer starken Persönlichkeitsveränderung führten. Diese war unter anderem durch fehlende Inhibition unangemessenen Verhaltens, Vergesslichkeit, Wutausbrüche und die Unfähigkeit zum Planen gekennzeichnet. Weitere Studien in Zusammenhang mit dem PFC und dem Arbeitsgedächtnis definierten dieses als Gedächtniskomponente, die gleichzeitig über einen kurzen Zeitraum eine bestimmte Anzahl an Informationseinheiten (nach George Miller maximal sieben) zwischenspeichert und manipulieren kann und so intelligentes Verhalten ermöglicht (Fuster & Alexander, 1971; Funahashi et al., 1989; Miller et al., 1996; Miller et al., 2018).

Auf dem heutigen Stand der Forschung ist man davon abgewichen, die einzelnen Lern- und Gedächtnisprozesse funktionell in nur einer Hirnregion zu lokalisieren, zumal durch Weiterentwicklung der Methoden und Rekonstruktionen auch die Fälle von H.M. und P.G. neu bewertet werden konnten (Thiebaut de Schotten et al., 2015). Vielmehr geht man davon aus, dass die Modulation der Verbindungen und die Netzwerke, die sich aufgrund der Verbindungen innerhalb sowie auch mit unterschiedlichen Hirnregionen bilden, speziellen Funktionen unterliegen und so „höhere" kognitive Funktionen ermöglichen, welche sich dann in intelligentem Verhalten widerspiegeln.

2.2 Neuronale Plastizität im adulten Gehirn

Im adulten Gehirn gibt es verschiedene Formen der neuronalen Plastizität, die einen wichtigen Beitrag im Rahmen von Lernen und Gedächtnis sowie weiteren kognitiven Funktionen leisten. Eine Form ist die synaptische Plastizität, welche Prozesse einschließt, die z.B. zur Bildung oder zum Abbau von Synapsen führen können, um so das gezielte Abspeichern von Informationen in neuronalen Netzen zu ermöglichen. In Bezug auf die Lernprozesse sind in Zusammenhang mit der synaptischen Plastizität LTP und LTD zu erwähnen. Durch LTP und LTD ist unter anderem das Knüpfen/Lösen von neuen/alten Verbindungen von Neuronen möglich, so dass

letztendlich Informationen gespeichert werden oder zerfallen. Ebenso fallen Veränderungen der Zusammensetzung von Rezeptoren an einer Synapse, welche einen weitreichenden Einfluss auf die Modulation von Information haben können, unter den Begriff der synaptischen Plastizität. Eine weitere Form der neuronalen Plastizität ist die adulte Neurogenese, also die Entstehung neuer Neurone im adulten Gehirn. Das Vorkommen adulter Neurogenese ist in verschiedenen Hirnarealen speziesabhängig nachgewiesen worden und wird jedoch nach wie vor stark diskutiert (Alvarez-Buylla & Nottebohm, 1988; Eriksson et al., 1998; Ming & Song, 2011; Ernst et al., 2014; Kempermann et al., 2018; Sorrells et al., 2018). Am besten untersucht ist die adulte Neurogenese im Gyrus dentatus bei Nagern (*Rodentia*; Abb. 1).

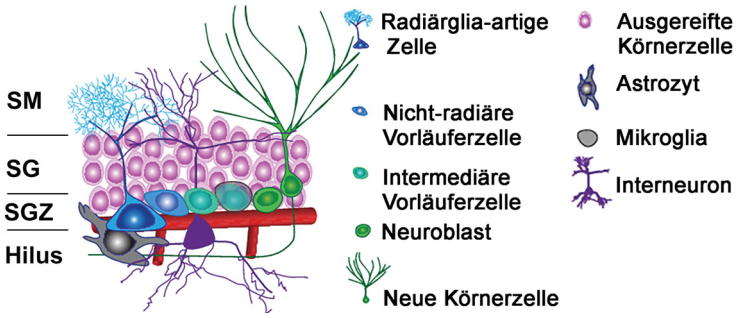

Abbildung 1: Schematische Darstellung der adulten Neurogenese im Gyrus dentatus der Hippocampusformation. Neue Neurone entstehen über Zwischenstufen (nicht-radiäre Vorläuferzelle ▶intermediäre Vorläuferzelle ▶Neuroblast) aus teilungsfähigen Stammzellen (Radiärglia-artige Zellen, blau) in der subgranulären Zone (SGZ) unterhalb des Stratum granulosum (SG; Körnerzellen, pink). Die Fortsätze der Radiärglia-artigen Zellen reichen bis in das Stratum moleculare (SM) des Gyrus dentatus hinein. Die Vorläuferzellen stehen dabei in engem Kontakt zu Blutgefäßen (rot). Die Neuroblasten differenzieren sich weiter zu neuen Körnerzellen (grün mit langen Fortsätzen) und wandern in das Stratum granulosum hinein. Neben den bereits genannten Zelltypen tragen außerdem noch die Astrozyten, Mikroglia und Interneurone zur zellulären Architektur der Stammzellnische bei (Abbildung modifiziert nach Ming & Song (2011) mit freundlicher Genehmigung von Elsevier).

Mit Hilfe von Nagermodellen konnte gezeigt werden, dass verschiedene neurologische Erkrankungen, wie z.B. Epilepsie und Morbus Alzheimer, aber auch eine stimulierende/angereicherte Umgebung und Bewegung, zu einer veränderten adulten Neurogenese im Hippocampus führen (Mu & Gage, 2011; Jessberger & Parent, 2015). Die Funktion der adulten Neurogenese im Hippocampus, aber auch in anderen Arealen, ist bei weitem noch nicht aufgeklärt. Im Rahmen von Lern- und Gedächtnisprozessen scheint sie wichtig für das Separieren von benachbarten/konkurrierenden Informationen zu sein (*pattern separation*), um in einem ähnlichen räumlichen Kontext neue Informationen gezielt abzubilden oder zu speichern (Clelland et al., 2009). Des Weiteren wurde eine Beteiligung in Zusammenhang mit kognitiver Flexibilität nachgewiesen (Anacker & Hen, 2017). Die unterschiedliche Bedeutung der adulten Neurogenese für die vorgenannten Funktionen könnte dabei von der Konnektivität und der topografischen Anordnung der Afferenzen und Efferenzen des Hippocampus abhängen. Bei Vögeln wurde die adulte Neurogenese bisher vor allem im Rahmen des „*Song*"-Systems oder in Abhängigkeit von verschiedenen Umweltfaktoren untersucht (Sherry & Hoshooley, 2010; Barnea & Pravosudov, 2011; Brenowitz & Larson, 2015; Melleu et al., 2016; Pozner et al., 2018).

2.3 Das Vogelgehirn im Vergleich zum Säuger

Bereits vor mehr als 365 Millionen Jahren trennte sich die Gruppe der Amnioten, eine Großgruppe der Landwirbeltiere, die bereits zu diesem Zeitpunkt dauerhaft an Land lebte und sich an Land fortpflanzte, in zwei unterschiedliche Hauptlinien auf: Sauropsida und Mammalia (Abb.2).

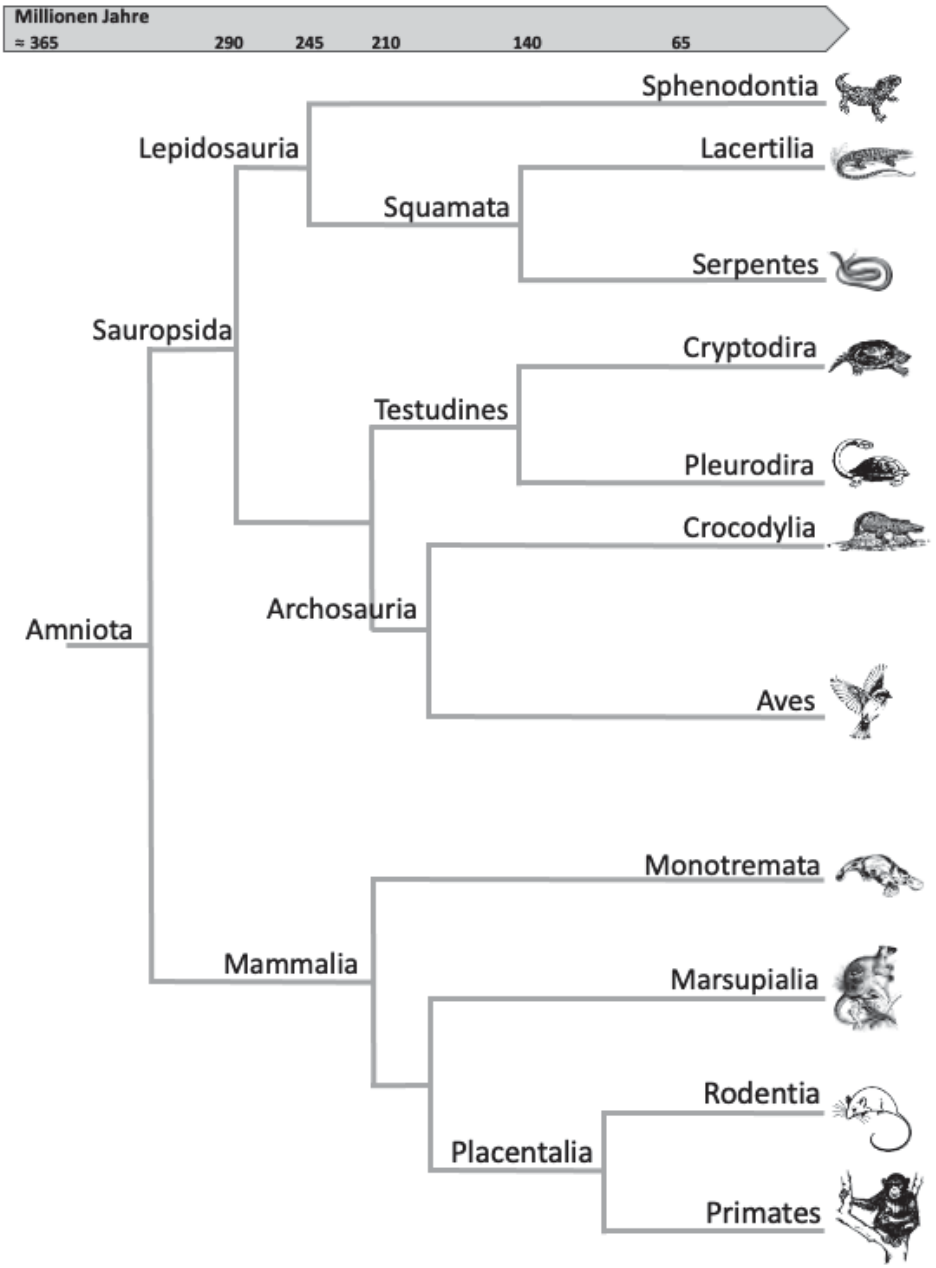

Abbildung 2: Vereinfachter phylogenetischer Baum der Amnioten. Demnach haben sich Vögel (*Aves*) aus einem Zweig der Archosauria entwickelt. Die Archosauria bilden ebenfalls einen Ursprung, aus dem die Krokodile (*Crocodylia)* hervorgingen. Die Krokodile bilden ihre eigene Ordnung und stehen den Vögeln abstammungsgeschichtlich näher als die Schildkröten (*Testudines*; Abbildung modifiziert nach Herold et al., 2019 mit freundlicher Genehmigung von Elsevier).

Im Laufe der letzten Jahrzehnte hat sich die Sichtweise auf das Vogelhirn im Vergleich zum Säugerhirn stark geändert (Reiner et al., 2004; Jarvis et al., 2005; Brusatte et al., 2015; Güntürkün & Bugnyar, 2016). Während man zunächst aufgrund des nuklearen Hirnaufbaus

davon ausging, dass große Teile des Vorderhirns der Vögel ein hypertrophiertes Striatum darstellen (Abb. 3A), haben genetische und entwicklungsbiologische Studien gezeigt, dass der Großteil des Vorderhirns vergleichbar zum Säugerhirn einen pallialen Ursprung hat (Abb. 3B-D). Dennoch ist es bisher im Hinblick auf mögliche Homologien und Homoplasien (Analogien) im Vergleich zum Säugergehirn mit keiner Methode gelungen, für alle Hirnareale eine einheitliche Evolutionstheorie zu etablieren (Abb. 3B-D).

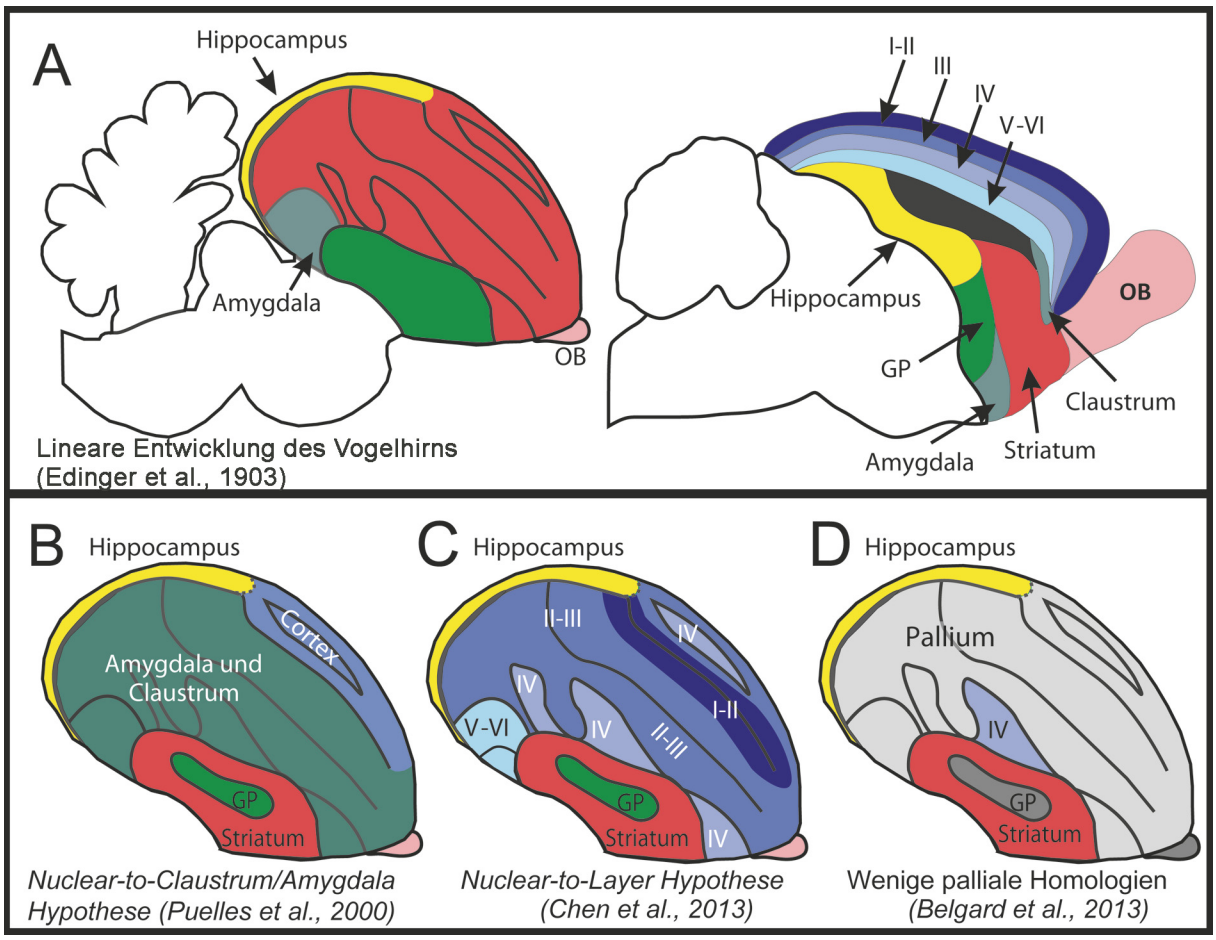

Abbildung 3: Unterschiedliche Hypothesen zu den Homologien zwischen dem Telencephalon von Vögeln und Säugern. Während in A die veraltete Sicht auf das Vogelgehirn im Vergleich zum Säugergehirn dargestellt ist, zeigen B-D die aktuellen Hypothesen, welche aufgrund von entwicklungsbiologischen und genetischen Analysen aufgestellt wurden. Die Farbkodierung spiegelt hier die möglichen Homologien wider. Dunkelgraue Bereiche wurden nicht analysiert. Demnach entwickelte sich der Großteil des Telencephalons in B homolog zur Amygdala und zum Claustrum (*Nuclear-to-Claustrum/Amygdala*-Hypothese). Hier entspräche nur ein kleiner Teil dem Cortex. In C werden die Kernstrukturen als homolog zu den verschiedenen Schichten des Cortex angesehen (*Nuclear-to-Layer*-Hypothese). In D existieren nur wenige Homologien zu Säugerstrukturen oder Schichten des Cortex (Abbildung modifiziert und im Original freundlicher Weise von Onur Güntürkün zur Verfügung gestellt). GP, Globus pallidus; OB, Bulbus olfactorius; I-VI, Schichten des Cortex.

Trotz der unterschiedlichen evolutionsbiologischen Hypothesen besteht Übereinkunft darin, dass Vögel hochintelligente Lebewesen sind, deren kognitive und kommunikative Fähigkeiten zum Teil sogar die von Menschenaffen überschreiten können (Jarvis, 2004; Emery, 2006; Güntürkün & Bugnyar, 2016; Mouritsen et al., 2016; Olkowicz et al., 2016; Letzner et al., 2017; Nieder, 2017; Pika et al., 2018; Pepperberg, 2019). Bei allen Parallelen und Unterschieden zwischen Vogel- und Säugerhirnen stellt sich daher immer wieder die Frage: Was gehört zur neuronalen Basis für intelligentes Verhalten und welche strukturellen oder molekularen

Komponenten sind variabel? Die Klärung dieser Frage ist komplex und aufgrund des aktuellen Forschungsstandes scheinbar nicht mit einer einzigen Methode zu beantworten (Striedter, 2005; Striedter et al., 2014). Daher wurden in dieser Arbeit unterschiedliche Methoden gewählt, um sich dieser Fragestellung zu nähern. Im Fokus stand dabei die Analyse von Hirnstrukturen bei Tauben, die als analog/homolog zu den Hirnstrukturen gesehen werden, welche bei Säugern an unterschiedlichen Lern- und Gedächtnisprozessen beteiligt sind.

2.3.1 Nidopallium caudolaterale

Das Nidopallium caudolaterale (NCL) ist eine halbmondförmige, assoziative Region im hinteren Teil des Vorderhirns, die funktionell analog zum PFC der Säuger ist (Waldmann & Güntürkün, 1993; Güntürkün, 2005; Herold et al., 2011). Das NCL hat sich eigenständig entwickelt und stellt damit ein herausragendes Beispiel konvergenter Entwicklung dar (Güntürkün & Bugnyar, 2016). Genau wie der PFC ist das NCL in viele exekutive Funktionen eingebunden und funktioniert als multimodales Integrationszentrum für eine Vielzahl von Informationen. Es ist, wie auch der PFC, mit aufsteigenden sensorischen wie auch absteigenden motorischen Systemen verbunden und wird stark durch den Neurotransmitter Dopamin innerviert (Waldmann & Güntürkün, 1993; Durstewitz et al., 1999; Kröner & Güntürkün, 1999). Insbesondere spielt es eine Rolle bei Arbeitsgedächtnisaufgaben, Entscheidungsprozessen, Aufmerksamkeits-gesteuertem und regelbasiertem Verhalten, und bei der Assoziation bzw. Beurteilung einer Belohnung für zielgerichtetes Verhalten (Kalt et al., 1999; Diekamp et al., 2002; Lissek & Güntürkün, 2003; Kalenscher et al., 2005; Karakuyu et al., 2007; Herold et al., 2008; Starosta et al., 2013).

2.3.2 Die Hippocampusformation

Im Gegensatz zum NCL entwickelt sich die Hippocampusformation (HF) verglichen mit Säugern zu großen Anteilen aus identischen pallialen Anlagen. Die HF der Vögel besitzt jedoch einen anderen strukturellen Aufbau (Atoji & Wild, 2006; Herold et al., 2014; Striedter, 2016; Medina et al., 2017; Tosches et al., 2018). Zudem weicht die räumliche Lage der HF im Vorderhirn, caudal-medial, dorsal des Vorderhirnventrikels und oberflächlich, im Vergleich zum Säuger ab. Solche Lageabweichungen gibt es für die HF auch innerhalb der Säugetiere, wie z.B. bei Nagern (*Rodentia*) und bei Affen (*Primates*), welche beide zu der Überordnung der Euarchontoglires und damit zur Unterklasse der höheren Säugetiere (*Eutheria*) gezählt werden sowie auch im Vergleich zu den Ursäugern (*Protheria*), welche eine weitere Unterklasse der Säugetiere bilden. Dies deutet daraufhin, dass sich die HF bei den Säugetieren im Verlauf der Evolution ebenfalls weiterentwickelt hat (Andersen et al., 2007). Die HF bei Vögeln zeigt ein zu Säugern vergleichbares Konnektivitätsmuster und wird neben den klassischen Transmittern wie Glutamat und γ-Aminobuttersäure (GABA) ebenfalls stark von Noradrenalin innerviert (Krebs et al., 1991; Moons et al., 1995; Balthazart & Absil, 1997; Mello et al., 1998; Atoji & Wild, 2006; Herold et al., 2019). Wie beim Säuger stellt die HF eine wichtige Struktur im Rahmen von Lernprozessen dar, und ist speziell in räumliches und assoziatives Lernen eingebunden (Colombo & Broadbent, 2000; Rattenborg & Martinez-Gonzalez, 2011; Sherry, 2011; Mayer et

al., 2013; Coppola et al., 2014; Lengersdorf et al., 2014; Scarf et al., 2014; Herold et al., 2015; Striedter, 2016; Bingman & Muzio, 2017).

2.3.3 Der Arcopallium/Amygdala-Komplex

Der Arcopallium/Amygdala-Komplex umschreibt eine Kerngruppe im caudo-ventralen Bereich des Vorderhirns. Die Kerngruppe beginnt auf der anterior-posterior Achse in etwa auf der Höhe der Hälfte des Vorderhirns lateral vom Striatum. Mit zunehmender Komplexität zieht die Kerngruppe sich dann weiter nach medial und endet dann ventro-lateral im Bereich des caudalen Nidopalliums (Herold et al., 2018b; Mello et al., 2019). Auf die Hirnentwicklung bezogen geht diese Kerngruppe nach heutigem Erkenntnisstand bei Vögeln sowohl auf subpalliale als auch auf palliale Bereiche zurück und entwickelt sich teilweise aus Anteilen, aus denen sich bei Säugern im Verlauf der Hirnentwicklung die Amygdala entwickelt (Puelles et al., 2000; Moreno & Gonzalez, 2007). Auch bei Säugern besteht die Amygdala aus einem Kernkomplex mit subpallialen wie auch pallialen Anteilen (Amunts et al., 2005; Janak & Tye, 2015; Kedo et al., 2018). Bei Vögeln sind Teile des Arcopallium/Amygdala-Komplexes aufgrund ihres Konnektivitätsmusters funktionell eher vergleichbar zum prämotorischen Cortex der Säuger und somit an zielgerichtetem Verhalten beteiligt. Gleichzeitig nimmt der Kernkomplex Informationen verschiedener Sinnesmodalitäten auf, die bereits prozessiert sind und ist dementsprechend assoziativ (Shanahan et al., 2013). Andere Anteile des Komplexes wiederum erfüllen funktionell die gleichen Aufgaben wie die Amygdala bei Säugern und sind mit emotionalen Aspekten von Lern- und Gedächtnisprozessen assoziiert (McGaugh, 2000; Saint-Dizier et al., 2009). Die genauen Anteile von anatomischen/funktionellen Homologien/Analogien sind in dem Komplex bisher immer noch weitestgehend ungeklärt, da es scheinbar bei Vögeln im Verlauf der Evolution viele spezies-spezifische Anpassungen gab (Herold et al., 2018b; Mello et al., 2019).

2.4 Neurotransmitterrezeptoren im Telencephalon

Neurotransmitterrezeptoren sind Transmembranproteine, die spezifisch Transmitter wie Glutamat, γ- Aminobuttersäure (GABA), Acetylcholin (ACh), Noradrenalin, Dopamin, Serotonin (5-HT) und teilweise weitere Co-Faktoren binden. Die Bindung des Transmitters an den Rezeptor und die damit verbundene Rezeptorvermittlung eines exzitatorischen oder inhibitorischen Signals ist zum einen abhängig davon, für welche Ionen der Ionenkanal des Rezeptors durchlässig ist (ionotrope Rezeptoren) und zum anderen davon, welches G-Protein an den Rezeptor gekoppelt ist (metabotrope Rezeptoren). G-Proteine können unterschiedliche Signalkaskaden initiieren, wie z.B. den Phospholipase C-Weg oder den Adenylatcyclase-Weg und darüber dann die Aktivität der Zelle modulieren. Das Vorkommen der Neurotransmitterrezeptoren im Gehirn steht oft in Zusammenhang mit der Funktion und/oder der Modalität der jeweiligen Hirnareale (Rehkämper & Zilles, 1991; Zilles et al., 2004; Zilles & Amunts, 2009; Zilles & Palomero-Gallagher, 2016). Im humanen Cortex weisen Neurotransmitterrezeptoren zudem in den meisten Cortex-Arealen ein spezifisches Laminierungsmuster auf (Zilles & Palomero-Gallagher, 2017). Im Folgenden bezieht sich die

molekulare Beschreibung und die Verteilung einzelner Rezeptoren, wenn nicht anders vermerkt, auf Ergebnisse, die aus Studien mit Säugern bekannt sind. Die Verteilung der Rezeptoren im Vogelgehirn ist ein wesentlicher Bestandteil dieser Arbeit und wird daher in der Darstellung der eigenen Arbeiten ausführlicher beschrieben. Aus molekularer Sicht ist aufgrund genetischer Analysen davon auszugehen, dass die Neurotransmitterrezeptoren der Vertebraten und der Invertebraten größtenteils homolog sind und daher die gleichen Signale vermitteln. Dies spiegelt sich ebenfalls in der Beteiligung der Rezeptoren an bestimmten Funktionen wider. Dennoch ist nicht auszuschließen, dass auch hier spezies-spezifische Anpassungen erfolgt sind, die bisher gar nicht oder kaum untersucht wurden.

2.4.1 Glutamaterge Rezeptoren

Zu den glutamatergen Rezeptoren zählen sowohl ionotrope als auch metabotrope Transmembranproteine, die den Neurotransmitter Glutamat binden. Die ionotropen Glutamat-Rezeptoren sind die *α-Amino-3-hydroxy-5-methyl-4-isoazolpropionic acid* (AMPA)-, N-Methyl-D-Aspartat (NMDA)- und Kainat-Rezeptoren, die sich aufgrund der der Zusammensetzung der Untereinheiten ihres Ionenkanals und der damit verbundenen Ionenleitfähigkeit in ihrer Funktion unterscheiden. Sie wirken exzitatorisch. Im Vergleich zu AMPA- und NMDA-Rezeptoren ist das Vorkommen von Kainat-Rezeptoren im Telencephalon geringer und regional spezifischer. So weisen sie z.B. im Gyrus dentatus (DG) oder Cornu ammonis Feld 3 (CA3) in der Hippocampusformation (HF) eine deutlich höhere Dichte im Vergleich zu weiteren Arealen der HF auf (Zilles et al., 2000; Palomero-Gallagher et al., 2003; Zeineh et al., 2017). AMPA- und NMDA-Rezeptoren sind hingegen in der CA1 Region erhöht, was mit ihrer Funktion im Rahmen von Lern- und Gedächtnisprozessen in Einklang steht. Sie besitzen eine große Bedeutsamkeit für die synaptische Plastizität in Bezug auf LTP und LTD (Bliss & Collingridge, 1993; Malenka & Nicoll, 1999; Andersen et al., 2007). Die Funktion der Kainat-Rezeptoren ist weniger einfach einzugrenzen. Kainat-Rezeptoren wurden bisher vor allem in Zusammenhang mit der Entstehung von epileptischen Anfällen untersucht und steuern an der Präsynapse die Transmitterausschüttung (Carta et al., 2014). Die metabotropen Glutamat-Rezeptoren werden aufgrund der Bindung verschiedener G-Proteine in drei Gruppen eingeteilt. Sie spielen bei vielen Hirnfunktionen eine Rolle, was sich in ihrer relativ homogenen Verteilung im Gehirn spiegelt. Eine besondere Eigenschaft verschiedener glutamaterger Rezeptoren ist, dass sie, je nach Lage an der Synapse, auch die Wirkung anderer Neurotransmitter wie Dopamin und Noradrenalin beeinflussen können (Wang et al., 2008; Maletic et al., 2017; Herold et al., 2018a). Bei Vögeln konnte eine Beteiligung der Glutamat-Rezeptoren beim Erlernen von spezifischen Liedmustern im Rahmen des *„Song“*-Systems (Wada et al., 2004), für das Abspeichern räumlicher Informationen (Shiflett et al., 2004), beim Umlernen (Herold, 2010), beim Extinktionslernen (Lissek & Güntürkün, 2003; Gao et al., 2018) und beim Problemlösen (Audet et al., 2018) gezeigt werden.

2.4.2 GABAerge Rezeptoren

Vergleichbar zu den Glutamat-Rezeptoren sind die GABAergen Rezeptoren ubiquitär im Gehirn verteilt, zeigen Subtyp-spezifische heterogene Rezeptordichten und existieren als

ionotrope und metabotrope Rezeptoren. Zu den ionotropen zählen die $GABA_A$-Rezeptoren, die eine inhibitorische Reizweiterleitung vermitteln, welche je nach Zusammensetzung der Untereinheiten moduliert werden kann. Unter anderem sind $GABA_A$-Rezeptoren im Rahmen der Bildung und Integration neuer Neurone in der HF sowohl in der Embryonalentwicklung als auch im adulten Zustand von Bedeutung. Dies spiegelt sich in den verschiedenen Stadien in einer erhöhten Rezeptordichte im DG wider (Kraemer et al., 1995; Ge et al., 2007; Maguire et al., 2009; Licheri et al., 2015). $GABA_B$-Rezeptoren sind metabotrop und regulieren vielseitig die Transmitterausschüttung an der Präsynapse. Im Allgemeinen können GABAerge Rezeptoren über lange Strecken die Signalmodulation bis in die Projektionsgebiete der Neuronen beeinflussen. So können sie z.B. über die Projektionen der HF zum PFC zur optimalen Funktion des Arbeitsgedächtnisses besteuern sowie Aufmerksamkeitsprozesse modulieren (Bast et al., 2017). Darüber hinaus beeinflusst die Aktivierung GABAerger Rezeptoren in der HF direkt wie auch indirekt, welche Informationen zeitlich abgestuft ins Langzeitgedächtnis überführt werden (Paulsen & Moser, 1998; Lamsa & Lau, 2019). Wie Glutamat-Rezeptoren können auch GABA-Rezeptoren durch Wechselwirkungen mit anderen Neurotransmittersystemen die Weiterleitung der Informationen an den Synapsen zusätzlich modulieren. Im Zusammenhang mit Lern- und Gedächtnisprozessen wurde das GABAerge System bei Vögeln bisher wenig untersucht. Einige wenige Studien beschreiben eine Beteiligung im Rahmen des Vermeidungslernens (Daisley & Rose, 2002), des Kurzzeitgedächtnisses (Gibbs & Johnston, 2005), der Konsolidierung (Gibbs & Bowser, 2009) und von Lernprozessen innerhalb des „*Song*"-Systems (Yanagihara & Yazaki-Sugiyama, 2016).

2.4.3 Acetylcholinerge Rezeptoren

Diese Rezeptortypen teilen sich in zwei Gruppen, die nikotinischen (ionotrop) und die muskarinischen (M; metabotrop) Rezeptoren. Letztere Gruppe schließt fünf Isoformen ein. Für die Untersuchungen dieser Arbeit sind vor allem die nikotinischen- ($n\alpha_4\beta_2$), die M_1- und die M_2- Rezeptoren relevant. M_1-, M_2-, und $n\alpha_4\beta_2$- Rezeptoren kommen sowohl prä- als auch postsynaptisch vor, wobei der M_1- Rezeptor im Cortex bisher in der Regel an der Postsynapse lokalisiert wurde. Die Verteilung der cholinergen Rezeptoren im Gehirn ist heterogen. Der $n\alpha_4\beta_2$-Subtyp zeigt hohe Dichten in den Basalganglien, wohingegen die M_1-Rezeptoren sowohl in den Basalganglien als auch im Hippocampus eine hohe Rezeptordichte aufweisen. Ein erhöhtes Vorkommen von M_2-Rezeptoren wurde in primär visuellen, auditorischen und somatosensorischen Cortex-Arealen nachgewiesen (Zilles, 2005; Zilles & Palomero-Gallagher, 2017). Acetylcholin (ACh) wird verstärkt im Nucleus basalis Meynert, im Striatum und in den Septumkernen gebildet. Von diesen Gebieten aus reichen Projektionen in fast alle Bereiche des Telencephalons (Zaborszky, 2002; Picciotto et al., 2012). Die Stimulation der ACh-Rezeptoren im PFC, der HF und in der Amygdala bzw. ihrer Afferenzen und Efferenzen wird im Rahmen von Lernen und Gedächtnis vielfach mit Aufmerksamkeitsprozessen, der Enkodierung von Informationen, Angst-assoziiertem Lernen und Extinktionslernen assoziiert (Levey, 1996; Hasselmo, 2006; Picciotto et al., 2012; Pepeu & Grazia Giovannini, 2017; Wilson & Fadel, 2017). Des Weiteren ist bekannt, dass systemische Injektionen verschiedener

cholinerger Rezeptorantagonisten auch bei Vögeln zu Gedächtnisdefiziten führen (Santi et al., 1988; Patterson et al., 1990).

2.4.4 Monoaminerge Rezeptoren

Zu den monoaminergen Rezeptoren zählen unter anderem Rezeptortypen, die die Signalvermittlung durch die Neurotransmitter Adrenalin, Noradrenalin, Dopamin und Serotonin (5-HT) beeinflussen. Mit Ausnahme des 5-HT-Rezeptor-Subtyps 3 sind die Rezeptortypen der genannten Neurotransmitter alle metabotrop und an unterschiedliche G-Proteine gekoppelt.

Adrenerge Rezeptoren werden in 2 Gruppen eingeteilt, α und β. Hier werden nur die α_1- und α_2-Rezeptoren vorgestellt. Sie kommen sowohl präsynaptisch als auch postsynaptisch vor, und man findet unter anderem hohe Konzentrationen im Hippocampus, im Striatum, in der Amygdala und in einigen primären Cortex-Arealen, wobei zu beachten ist, dass die Dichten der α-Rezeptoren speziesabhängig schwanken (Zilles et al., 1993). In Bezug auf Lern- und Gedächtnisprozesse sind adrenerge Rezeptoren besonders in Aspekte von Motivation, emotionalem Gedächtnis und Aufmerksamkeit eingebunden. In der HF und in der Amygdala, welche beide mit Noradrenalin aus dem Locus coeruleus versorgt werden, modulieren α-Rezeptoren im Rahmen von Lernprozessen LTP und LTD. Dies wirkt aufgrund der Verbindungen der HF und der Amygdala auf weitere Hirnareale, wie z.B. auf den PFC oder den Nucleus accumbens im ventralen Striatum (Liang et al., 1986; Izumi & Zorumski, 1999; Kandel, 2001; Tully & Bolshakov, 2010; Atucha et al., 2017; Datta et al., 2019). Bei Vögeln scheinen α-Rezeptoren eine Rolle bei Konsolidierungsprozessen zu spielen (Gibbs & Summers, 2001; 2003). Bei Säugern besitzen α-Rezeptoren zusätzlich eine wichtige Funktion im Rahmen der Steuerung des Energiehaushaltes durch Gliazellen (Bekar et al., 2008). Dies wurde auch bei Vögeln beobachtet und hat möglicherweise Auswirkungen auf zeitlich abgestufte Gedächtnisprozesse (Gibbs & Bowser, 2010; Hutchinson et al., 2011).

Dopamin-Rezeptoren werden ebenfalls in zwei Gruppen eingeteilt, D_1 und D_2. In der jeweiligen Gruppe der Dopamin-Rezeptoren existiert eine speziesabhängige Anzahl von Isoformen, die sich genetisch alle auf einen Ursprung der jeweiligen Gruppe zurückführen lassen (Callier et al., 2003; Yamamoto et al., 2013). So existiert bei Vögeln neben den Isoformen D_1 (D_{1A}) und D_5 (D_{1B}) noch eine dritte Isoform (D_{1D}), deren Sequenz Homologien mit dem D_5-Rezeptor aufweist, womit diese Isoform zu der D_1-Gruppe gezählt wird (Herold et al., 2012; Kubikova et al., 2010). Rezeptoren der D_2-Rezeptorgruppe kommen auch präsynaptisch vor, während Rezeptoren der D_1-Rezeptorgruppe bisher nur postsynaptisch beobachtet wurden. Dopamin-Rezeptoren besitzen die höchsten Dichten im PFC und in den Basalganglien. Sie interagieren mit Glutamat-, GABA- und ACh-Rezeptoren und modulieren sowohl bei Säugern als auch bei Vögeln vor allem Funktionen des Arbeitsgedächtnisses, belohnungs-assoziierte Prozesse, kognitive Flexibilität und das Ausführen von zielgerichteten Verhaltens (Sawaguchi & Goldman-Rakic, 1994; Williams & Goldman-Rakic, 1995; Robbins & Everitt, 1996; Diekamp et al., 2000; Ding & Perkel, 2002; Herold et al., 2008; Herold, 2010; Floresco, 2013; Rose et al., 2013; Jenni et al., 2017).

Serotonin-Rezeptoren sind sehr vielfältig und werden daher in fünf Gruppen eingeteilt. Im Rahmen der vorliegenden Arbeit sind besonders die 5-HT_{1A}-Rezeptoren relevant. Sie wurden prä- und postsynaptisch nachgewiesen (Polter & Li, 2010) und man findet sie in hoher Dichte in der HF und der Amygdala (Pazos et al., 1987; Hannon & Hoyer, 2008). 5-HT_{1A}-Rezeptoren sind sowohl bei Säugern als auch bei Vögeln an einer Reihe von grundlegenden Prozessen wie z.B. dem Schlaf-Wach-Rhythmus, Angst-assoziiertem Verhalten oder der Nahrungsaufnahme beteiligt (Bendotti & Samanin, 1987; Groenink et al., 2000; Boutrel et al., 2002; Dos Santos et al., 2009; Li et al., 2010; Hoeller et al., 2013). Sie interagieren zudem mit Glutamat-Rezeptoren und modulieren so unterschiedliche glutamaterge Signale, wie auch LTP und LTD (Yuen et al., 2005). Im Rahmen von Lernen und Gedächtnis sind 5-HT_{1A}-Rezeptoren an Prozessen wie dem Inhibitionslernen, der Bildung von räumlichem Gedächtnis und Hippocampus-abhängigen Aufgaben beteiligt (Carli et al., 1992; Ogren et al., 2008; Elvander-Tottie et al., 2009). Im Hippocampus stimulieren sie außerdem die adulte Neurogenese (Gould, 1999; Klempin et al., 2010). Bei Vögeln ist kaum etwas über die Funktion der 5-HT_{1A}-Rezeptoren im Rahmen von Lern- und Gedächtnisprozessen bekannt.

2.5 Analysemethoden

Für weitreichende neuroanatomische Untersuchungen der Grundlagen der Evolution von Kognition und Verhalten ist es unabdingbar, einen multimodalen Ansatz zu wählen. Zum einen lässt sich eine so komplexe Fragestellung nicht durch eine einzelne Methode beantworten, und zum anderen sind durch die Weiterentwicklung bestehender und die Entwicklung neuer Analysemethoden immer detailliertere Untersuchungen möglich. Dies eröffnet die Möglichkeit, vorhandene Daten zu ergänzen, neues Wissen zu generieren und neue Forschungsrichtungen anzustoßen. Neben den klassischen Färbemethoden zur Analyse der Zyto- und Myeloarchitektur von Hirnstrukturen wurden in dieser Arbeit daher die Rezeptorautoradiografie, Expressionsanalysen, immunhistochemische Methoden und die dreidimensionale Polarisationsmikroskopie (3D-PLI) gewählt, deren spezifische Vorteile und Limitierungen in Bezug auf die Fragestellung beschrieben werden. Eine detaillierte Methodenbeschreibung befindet sich in den jeweiligen Originalpublikationen.

2.5.1 Rezeptorautoradiografie

Anhand einer großen Anzahl von Publikationen, in denen verschiedene Spezies untersucht wurden, konnte nachgewiesen werden, dass die Rezeptorautoradiografie nicht nur eine Methode zur genauen Kartierung und Abgrenzung von Gehirnarealen ist, sondern auch in funktionellem Zusammenhang mit den Hirnarealen steht (Zilles et al., 2002; Zilles & Palomero-Gallagher, 2017). Mit dieser Methode ist es möglich, mit Hilfe von radioaktiv markierten Liganden, die spezifisch an ihre Rezeptoren binden und einer anschließenden quantitativen Auswertung, die Verteilung verschiedener Rezeptoren in den zu analysierenden Hirnregionen (ROIs; englisch: *regions of interest*) darzustellen. Diese lassen sich dann in farbkodierten Bildern mit Bezug zur Rezeptordichte (fmol/mg protein) optimiert darstellen, so dass die heterogene oder homogene Verteilung der Rezeptoren sichtbar wird. Mit Hilfe der

Darstellung in einem Netzdiagramm ist es zudem möglich, einen sogenannten Fingerabdruck (*fingerprint*) aus den gesammelten Daten z.B. pro Region zu erstellen, um so ähnliche Verteilungsmuster zwischen Regionen zu zeigen, die man anschließend z.B. in einer Clusteranalyse oder multidimensionalen Analyse statistisch untersuchen kann. Darüber hinaus ist eine Darstellung und Auswertung der Laminierungsmuster, sofern in den ROIs vorhanden, möglich. Der Nachteil der Methode besteht darin, dass einige Liganden mehrere Rezeptorsubtypen binden, und dass in solchen Fällen keine Ergebnisse über spezifische Subtypen oder die Zusammensetzung der Rezeptoruntereinheiten gewonnen werden können. Diese Informationen über die Zusammensetzung der Rezeptoruntereinheiten können relevant sein, wenn man etwas über die genaue funktionelle Beteiligung der Rezeptoren wissen möchte, da je nach Untereinheitenzusammensetzung, der Rezeptor andere funktionelle Eigenschaften besitzen kann. Zudem kann man mit dieser Methode nichts über die Lage der Rezeptoren, prä- oder postsynaptisch, aussagen und keine einzelnen Zelltypen darstellen. Auf der Größenskala befindet man sich hier in der mesoskopischen Ebene.

2.5.2 *Real-time* PCR

Im Gegensatz zur Rezeptorautoradiografie ist es mit Hilfe der *Real-time* PCR möglich, die mRNA Expressionslevel unterschiedlicher Rezeptoren und gegebenenfalls ihrer Untereinheiten in einer Gewebeprobe der ROIs, zu bestimmen (Pfaffl, 2004). Dabei kann man eine absolute oder relative Quantifizierung der mRNA Level durchführen. Letztere hat den Vorteil, da man in Relation zu einem nicht regulierten Haushaltsgen misst, dass ein direkter Vergleich der Expressionslevel der untersuchten mRNAs zwischen verschiedenen Proben möglich ist und methodische Fehler in den unterschiedlichen Arbeitsschritten sehr klein gehalten werden. Je nachdem, wie viele Gene man untersucht, sind neben den klassischen statistischen Analysen wie ANOVAs ebenfalls Clusteranalysen oder Korrelationsanalysen möglich. Die Expressionslevel spiegeln normalerweise in guter Näherung die relativen Proteinlevel wider. Allerdings gibt es auch hier Ausnahmen, so dass die Ergebnisse entsprechend validiert werden müssen, oder mögliche andere Ursachen im Rahmen des Prozessierens der mRNA und des Einbaus der Rezeptoren in die Membran in Betracht gezogen werden müssen. Zudem ist es nicht für jede ROI möglich, unter dem binokularen Mikroskop Hirnproben mit hoher Genauigkeit zu entnehmen. Dazu müsste man mit einem Laser an den Hirnblöckchen/Hirnschnitten arbeiten, welches wiederum andere methodische Einschränkungen in Bezug auf die Probe mit sich bringt. Auf der Größenskala bewegt sich die Methode in der vorliegenden Arbeit in der mesoskopischen Ebene.

2.5.3 Immunhistochemie

Mit Hilfe immunhistochemischer Untersuchungen kann man nahezu jedes beliebige Protein in Hirnschnitten oder Gewebeproben untersuchen. Dabei nutzt man das Prinzip der Antikörper-Antigen-Bindung. Dies bringt den Vorteil, dass die räumliche Auflösung erhalten bleibt und einzelne ROIs zu identifizieren sind, so dass mit verschiedenen Methoden eine quantitative Auswertung erfolgen kann. Hinzu kommt, dass eine immunhistochemische Färbung die Anwendung verschiedener Mikroskope, wie z.B. des Durchlicht-, Fluoreszenz-,

oder Konfokalmikroskops ermöglicht, so dass weitere Untersuchungen bezüglich des Zelltyps oder zellulärer Strukturen angestellt werden können. Außerdem können durch die Kopplung der Antikörper an unterschiedliche Fluoreszenzfarbstoffe Kolokalisationen von Proteinen betrachtet werden. Bei der Analyse von Gewebeproben wurde die *Western*-Blot-Methode verwendet. Diese Methode kann man unter anderem zur Validierung des Antikörpers nutzen, um Splice-Varianten des untersuchten Proteins darzustellen, oder um die Proteinkonzentration in einer Probe zu bestimmen. Vorausgesetzt, dass der Antikörper das zu untersuchende Protein spezifisch bindet, liegt der Hauptnachteil immunhistochemischer Methoden darin, dass sie stark von der Art und Weise der Einbettung (z.B. Paraffin), der Fixierung (z.B. Formalin) und vom Probenzustand abhängig sind. Der Auflösungsbereich hängt vom Mikroskop, der Probenart und der Methode ab. In den histologischen Schnitten der vorliegenden Arbeit befindet man sich im mikroskopischen Bereich.

2.5.4 3D-Polarisationsmikroskopie (3D-PLI)

Die Polarisationsmikroskopie ist ein bildgebendes Verfahren, mit dem man auf der Mikroskala Verbindungen zwischen Hirnarealen (lange oder kurze Distanz, englisch: *long- oder short-range*) oder innerhalb von Hirnarealen (lokal) mit Hilfe eines Polarisationsmikroskops untersuchen kann (Axer et al., 2011a; Axer et al., 2011b; Zilles, 2016; Zeineh et al., 2017). Dazu nutzt man die doppelbrechenden Eigenschaften von (myelinisierten) Axonen in fixierten Hirnschnitten aus, ohne den Hirnschnitt mit weiteren Färbemethoden behandeln zu müssen. Mit Hilfe verschiedener Winkeleinstellungen der Polarisationsfilter sowie eines in der z-Ebene verstellbaren Tisches ist eine 3D-Betrachtung der Faserbahnarchitektur des Gehirns/des Hirnschnittes möglich. Dabei werden die Richtungen und Richtungsänderungen der Fasern sowie Faserbahndichten über eine Farbkodierung bzw. Farbintensitäten dargestellt (Abb. 4). Anschließend lassen sich die Daten der Hirnschnitte in einem 3D-Hirnmodell rekonstruieren, so dass die gesamte Faserbahnarchitektur analysiert werden kann. Darüber hinaus lässt sich die Methode zur Kartierung der Hirnareale oder zur Darstellung von Gefäßstrukturen einsetzen. Ein Vorteil gegenüber anderen bildgebenden Verfahren wie z.B. der Diffusion-Tensor-Bildgebung ist die hohe Auflösung und die geringere Anfälligkeit für Fehlsignale. Der größte Nachteil liegt darin, dass man nicht bestimmen kann, ob es sich bei den Verbindungen um Afferenzen oder Efferenzen handelt, so dass man entweder vorhandene Daten aus *Tracing*-Studien zur Hilfe nehmen muss, oder dies nach der Neubeschreibung von Verbindungen mit zusätzlichen Methoden eingehender untersucht.

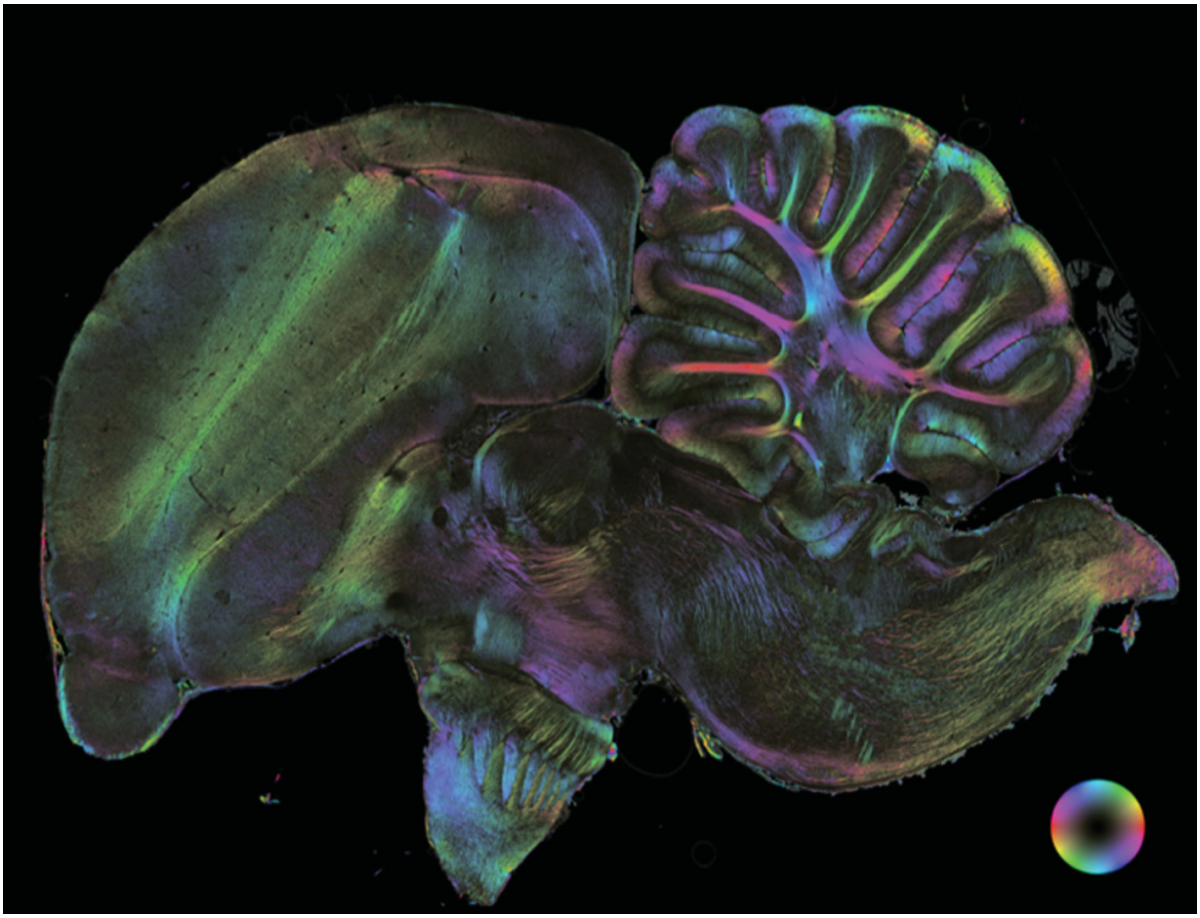

Abbildung 4: Sagittaler Schnitt des Taubengehirns in der 3D-PLI Darstellung. Die Farbkodierung unten rechts im Bild gibt die Richtungen der Faserbahnen an. Die Farbwechsel innerhalb einer Faserbahn zeigen Richtungswechsel der Fasern an. Dunklere Bereiche entsprechen entweder dem Verlauf der Fasern durch die Ebene oder vielen Faserbahnkreuzungen.

3. Eigene Arbeiten

In diesem Abschnitt sind die Ergebnisse und Erkenntnisse aus den eigenen vergleichenden Studien an Vögeln und Säugern in Bezug auf strukturelle und funktionelle Gemeinsamkeiten und Unterschiede zusammengefasst. Hierbei liegt der Fokus auf den Strukturen, die funktionell für Lern- und Gedächtnisprozesse relevant sind, da diese die Basis für intelligentes Verhalten darstellen. Darüber hinaus wurden in den eigenen Arbeiten teilweise zusätzliche Strukturen und funktionelle Fragestellungen bearbeitet, auf die hier nur am Rande eingegangen wird. Die eigenen Arbeiten sind jeweils unter den einzelnen Untertiteln nochmals gesondert aufgeführt und benannt.

3.1 Die Rezeptorarchitektur des Nidopallium caudolaterale (NCL) der Taube und umliegender Strukturen im Vergleich zu funktionell verwandten Säugerarealen

(Herold et al., 2011; Herold et al., 2012a; Vogt et al., 2013)

Vorausgehende Arbeiten haben gezeigt, dass das NCL stark durch Dopamin innerviert wird, und dass es aufgrund dopaminerger Korbzellen und der Dichte an Dopamin-Rezeptoren als halbmondförmige Struktur im Vorderhirn der Vögel zum restlichen Nidopallium abgrenzbar

ist (Waldmann & Güntürkün, 1993; Durstewitz et al., 1999). Neben den neurochemischen Gemeinsamkeiten zeigten funktionelle Studien, dass das NCL im Rahmen höherer kognitiver Funktionen vergleichbar mit dem präfrontalen Cortex (PFC) bei Säugern ist, ähnlich verschaltet ist und sich konvergent entwickelt hat (Güntürkün, 2005). Da die ersten anatomischen Studien schon mehr als 20 Jahre zurücklagen, und in der Zwischenzeit neue Erkenntnisse bezüglich weiterer beteiligter Neurotransmittersysteme und Rezeptoren an den Funktionen des NCL gewonnen werden konnten, wurde in einer der ersten Studien dieser Arbeit auf der Basis von elf verschiedenen ^{3}[H]-Liganden die Neurotransmitter-Rezeptorarchitektur des NCL mit Hilfe der Autoradiografie detaillierter untersucht (Abb. 5; Herold et al., 2011).

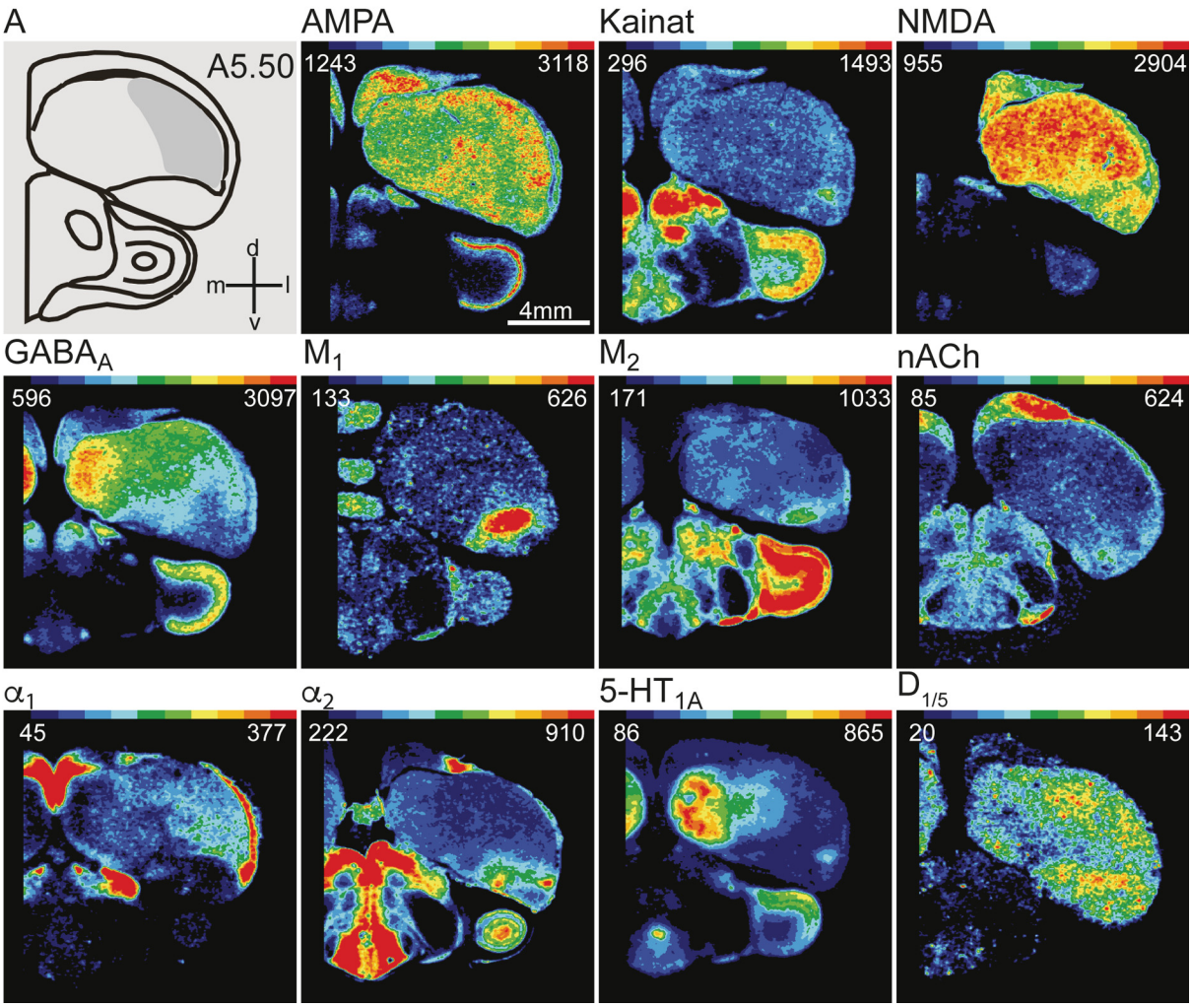

Abbildung 5: Rezeptorverteilung im Nidopallium der Taube. Die farb-kodierten Autoradiogramme zeigen die Rezeptordichten für glutamaterge AMPA-, Kainat- und NMDA-Rezeptoren, GABAerge $GABA_A$-Rezeptoren, muskarinerge M_1- und M_2-Acetylcholinrezeptoren, nikotinische Acetylcholinrezeptoren (nACh; Subtyp: $n\alpha_4\beta_2$), noradrenerge α_1- und α_2-Rezeptoren, serotonerge 5-HT_{1A}-Rezeptoren und dopaminerge $D_{1/5}$ ($D_{1\text{-like}}$) -Rezeptoren in Frontalschnitten auf der Höhe des Atlaslevels A 5.50 (Karten & Hodos, 1967). Die dunkelgrau schattierte Struktur in der Atlasabbildung stellt das Nidopallium caudolaterale (NCL) dar. Die Farbkodierung in den Autoradiogrammen zeigt die Konzentration der Rezeptoren in fmol/mg Protein an. Sie ist auf die Gesamtansicht des Frontalschnitts optimiert und spiegelt nicht die Maxima der Rezeptordichten wider. d, dorsal; m, medial; l, lateral; v, ventral; modifiziert nach Herold et al., 2011 mit freundlicher Genehmigung des Springer-Verlags).

Um die Ergebnisse mit umliegenden Strukturen quantitativ zu vergleichen, wurden zusätzlich die Rezeptordichten im Nidopallium caudocentrale (NCC) und in der Area corticoidea dorsolateralis (CDL) bestimmt. Die CDL wird funktionell von einzelnen Forschern mit dem cingulären Cortex (Cg) von Säugern verglichen (Atoji & Wild, 2005; Csillag & Montagnese, 2005; Yamamoto & Reiner, 2005). Für den weiteren Vergleich zu Säugern wurden daher die gleichen Rezeptordichten in der (prä-)frontalen Cortex-Region 2 (Fr2) und der medialen frontalen Cortex-Region Cg1 bei der Ratte (*Rattus norvegicus*; Zilles, 1985; Uylings et al., 2003) und im Brodmann-Areal 10 des humanen (*Homo sapiens*) präfrontalen Cortex (BA10) bestimmt. BA10 zählt bei Primaten zum anterioren PFC, und unterliegt während der Reifung des menschlichen Gehirns (postnatal) großen Volumenänderungen (Semendeferi et al., 2001; Sowell et al., 2004; Burgess et al., 2007). Es wird daher darüber diskutiert, ob dieses Areal entwicklungsgeschichtlich ein relativ junges Areal im Vergleich zu anderen neocortikalen Arealen darstellt. Aufgrund zytoarchitektonischer Unterschiede wurde BA10 in der vorliegenden Arbeit zusätzlich in eine mediale und eine laterale Region unterteilt (Bludau et al., 2014). Da die verschiedenen Evolutionshypothesen (Abb. 3) weitere Unterteilungen des Nidopalliums nahelegten, wurde das NCL auf Basis der Rezeptordichten ebenfalls auf weitere Subregionen untersucht. Gleichzeitig ließ sich so im Rahmen der *Nuclear-to-Layer*-Hypothese (Abb. 3) testen, inwiefern Subregionen im NCL möglicherweise den supra- oder infragranulären Schichten im PFC der Säuger gleichen. Die quantitative Auswertung der Rezeptorarchitektur des NCL zeigte, dass sich das NCL von beiden benachbarten Strukturen, NCC und CDL, abgrenzen ließ (Abb. 6A). Lediglich die Glutamat-Rezeptoren sind homogen in allen Arealen verteilt, während alle anderen Rezeptoren signifikante Unterschiede zeigen, was sich in den *fingerprints* für die Areale visuell widerspiegelt (Abb. 6A). Die größte Verschiebung der Rezeptordichten (fmol/mg Protein) zwischen den Arealen bei der Taube zeigte sich für die $GABA_A$-, M_2-, α_1-, α_2-, 5-HT_{1A}- und $D_{1/5}$-Rezeptoren. Im Vergleich zu den Säugerarealen Fr2, Cg1 und BA10 fällt besonders auf, dass das Verhältnis von Glutamat-Rezeptoren und $GABA_A$-Rezeptoren bei Vögeln und Säugern umgekehrt ist (Abb. 6B-C). Die Glutamat-Rezeptoren haben im Nidopallium verglichen mit den Säugerarealen eine deutlich höhere Dichte. Es lässt sich jedoch feststellen, dass die Dichten der Kainat-Rezeptoren sich für den NCL und BA10 nicht unterscheiden, aber in Fr2 und Cg1 eine deutlich geringere Dichte sowohl im Vergleich zum NCL als auch zu BA10 aufweisen. Für die $GABA_A$-Rezeptoren ist im Vergleich zwischen NCL, BA10, Fr2 und Cg1 kein Konzentrationsunterschied zu finden.

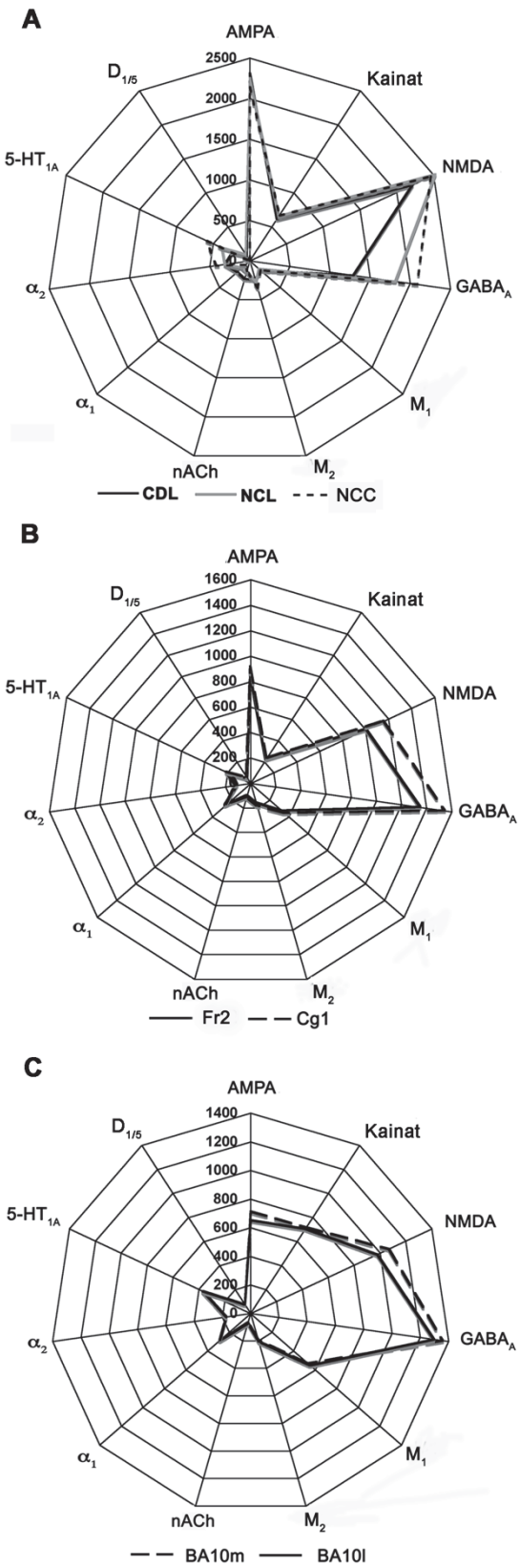

Abbildung 6: Darstellung der Rezeptordichten in Form von „Fingerabdrücken“ in der CDL, im NCL und NCC der Taube (A), im Fr2 und Cg1 der Ratte (B) und im BA10m und BA10l des Menschen (C). Die Mittelwerte der Rezeptordichten für glutamaterge AMPA-, Kainat- und NMDA-Rezeptoren, GABAerge $GABA_A$-Rezeptoren, muskarinerge Acetylcholinrezeptoren M_1 und M_2, nikotinische Acetylcholinrezeptoren (nACh; Subtyp: $n\alpha_4\beta_2$), noradrenerge α_1- und α_2-Rezeptoren, serotonerge 5-HT_{1A}-Rezeptoren und dopaminerge $D_{1/5}$-Rezeptoren in fmol/mg Protein sind im Netzdiagramm auf der Hauptachse des jeweiligen Rezeptors dargestellt. Die Verbindungslinien zwischen den Rezeptordichten pro Areal definieren das Aussehen des „Fingerabdrucks“ eines Areals für alle gemessenen Rezeptoren. BA10l, Brodmann-Area 10, Pars lateralis; BA10m, Brodmann-Area 10, Pars medialis; CDL, Area corticoidea dorsolateralis; Cg1, Cingulärer Cortex, Area 1; Fr2, (Prä-)Frontaler Cortex, Area2; NCC, Nidopallium caudocentrale; NCL, Nidopallium caudolaterale (modifiziert nach Herold et al., 2011 mit freundlicher Genehmigung des Springer-Verlags).

Ebenso wie für das NCL konnte gezeigt werden, dass die $GABA_A$-Rezeptordichte auch für die CDL und die Subareale des cingulären Cortex bei der Maus (*Mus musculus*), der Ratte (*Rattus norvegicus*), dem Makaken-Affen (*Macaca fascicularis*) und dem Menschen (*Homo sapiens*) vergleichbar ist, welches aus einer weiteren Studie dieser Arbeit hervorging, in der die cingulären Cortex-Areale in den vorgenannten Säugern in Bezug auf die Glutamat- und GABA-Rezeptorverteilung detaillierter untersucht wurden (Abb. 7; Vogt et al., 2013). Im Gegensatz zur $GABA_A$-Rezeptordichte scheint die Konzentration der Kainat-Rezeptoren in den cingulären Cortex-Arealen generell spezies-spezifisch zu variieren, da sich hier sowohl Unterschiede zwischen den verschiedenen Ordnungen (*Primates* und *Rodentia*) als auch innerhalb einer Ordnung bei den Säugetieren zeigen (Abb. 7).

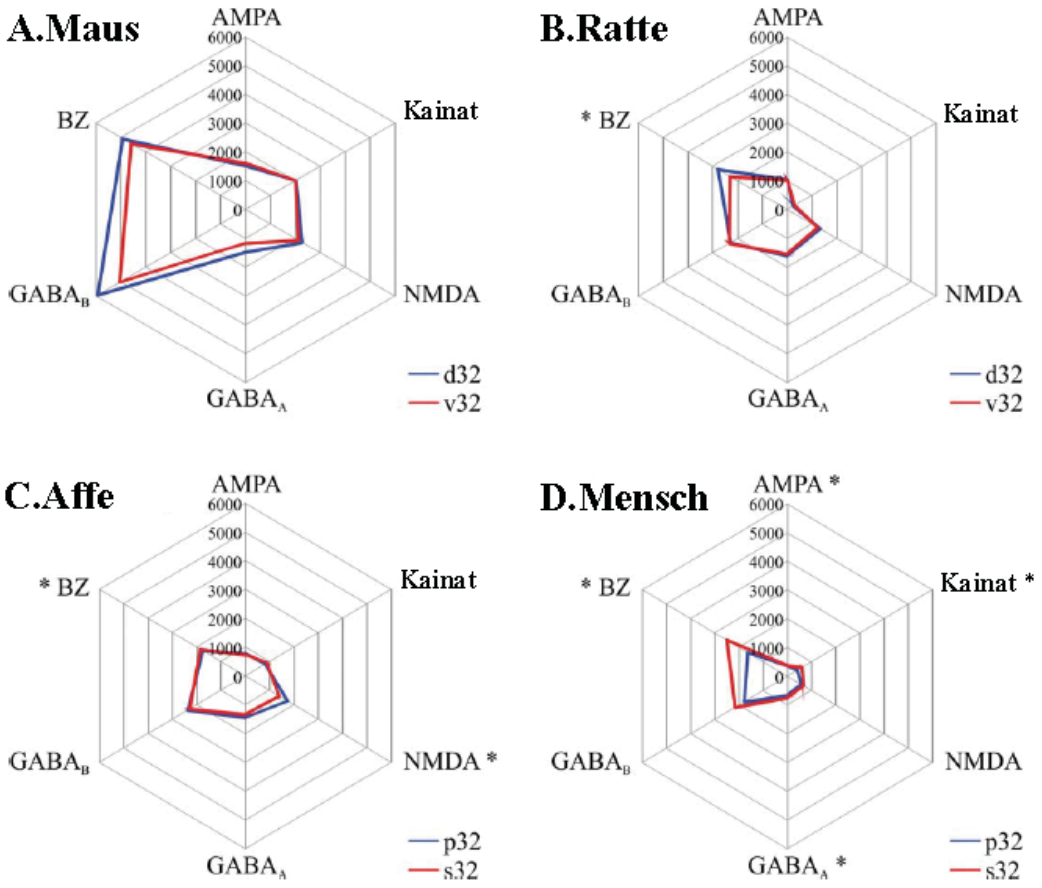

Abbildung 7: Rezeptor-„Fingerabdrücke“ der räumlich unterteilten Area 32 des cingulären Cortex. Die Achsen kodieren die Rezeptordichten in fmol/mg Protein für glutamaterge AMPA-, Kainat- und NMDA-Rezeptoren und GABAerge $GABA_A$- und $GABA_B$-Rezeptoren, sowie die Benzodiazepinbindestellen für GABAerge $GABA_A$-Rezeptoren (BZ). *signifikante Unterschiede ($p<0.01$) zwischen den Rezeptordichten in d32 (dorsal) und v32 (ventral) bzw. p32 (prägenual) und s32 (subgenual; modifiziert nach Vogt et al., 2013 mit freundlicher Genehmigung von Wiley Periodicals, Inc.).

Betrachtet man die metabotropen Rezeptortypen, so lässt sich feststellen, dass die pallialen Strukturen bei der Taube im Vergleich zu den Säugerarealen zusätzlich ein invertiertes Verhältnis für die M_1-/M_2- und die α_1-/α_2-Rezeptoren aufweisen (Abb. 6). Das umgekehrte Verhältnis dieser Rezeptoren bei Vögeln erhöht die Möglichkeit einer lokalen inhibitorischen Kontrolle und stellt wahrscheinlich einen kompensatorischen Mechanismus für die erhöhte Konzentration der Glutamatrezeptoren und der damit verbundenen exzitatorischen Reizweiterleitung dar. Die $5\text{-}HT_{1A}$-Rezeptoren zeigten vergleichbare Rezeptordichten zwischen NCL und BA10, während sie in Fr2 und Cg1 niedrigere Konzentrationen aufwiesen. D_1-Rezeptoren haben in allen hier studierten Arealen die niedrigste Rezeptordichte. Es wird vermutet, dass die D_1-Rezeptordichten sich im NCL und im PFC nicht unterscheiden, weil der Mechanismus der Volumentransmission von Dopamin in diesen Arealen konserviert ist, also zwischen den verschiedenen Wirbeltierklassen gleichermaßen vorhanden ist. Dies spiegelt sich auch in der Beteiligung der Dopamin-Rezeptoren in Zusammenhang mit exekutiven Funktionen und belohnungs-assoziierten Aufgaben in den präfrontalen Arealen aller untersuchten Klassen wider (Herold et al., 2012a; Puig et al., 2014). Insgesamt lässt sich daher festhalten, dass das GABAerge und das dopaminerge System scheinbar eine besondere

Stellung im Rahmen der Modulation höherer kognitiver Prozesse einnehmen, um adäquates Verhalten zu produzieren (Herold et al., 2011).
Die beobachteten Unterteilungen des NCL ähneln einer Unterteilung, wie sie auch in BA10 vorzufinden ist (Abb. 6C und 8) und sind am ehesten mit der neuronalen Verschaltung dieser Strukturen sowie der damit verbundenen Modulation durch verschiedene Neurotransmittersysteme zu erklären.

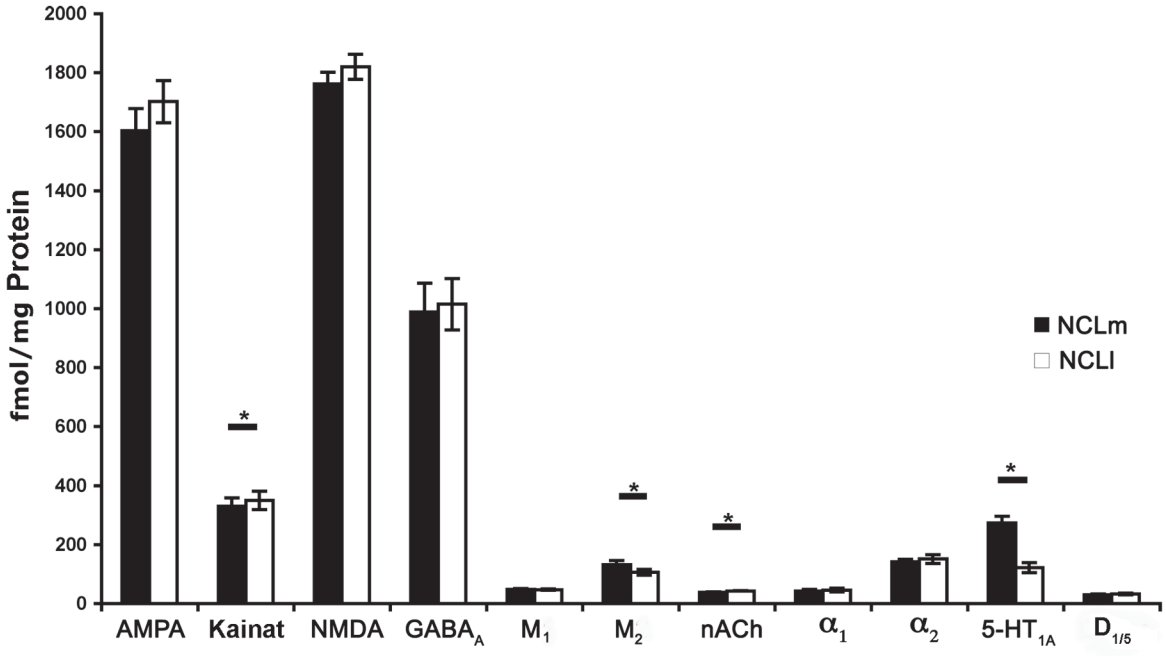

Abbildung 8: Histogramm der Mittelwerte der Rezeptordichten im medialen und lateralen Nidopallium caudolaterale (NCLm und NCLl). Die Werte für glutamaterge AMPA-, Kainat-und NMDA-Rezeptoren, GABAerge $GABA_A$-Rezeptoren, muskarinerge Acetylcholinrezeptoren M_1 und M_2, nikotinische Acetylcholinrezeptoren (nACh; Subtyp: $n\alpha_4\beta_2$), noradrenerge α_1- und α_2-Rezeptoren, serotonerge 5-HT_{1A}-Rezeptoren und dopaminerge $D_{1/5}$-Rezeptoren sind in fmol/mg Protein angegeben. Die Fehlerbalken zeigen die Standardabweichung an. *signifikanter Unterschied ($p<0.05$) in der Rezeptordichte (modifiziert nach Herold et al., 2011 mit freundlicher Genehmigung des Springer-Verlages).

Eine Aussage zu möglichen Homologien zwischen der Einteilung in einen medialen und lateralen NCL und einzelnen Cortexschichten im Säugergehirn war aus diesen Ergebnissen nicht sicher abzuleiten. Im Gegensatz dazu konnte die Analyse der Rezeptorarchitektur der supra- und infragranulären Schichten im cingulären Cortex von Maus, Ratte, Affe und Mensch sehr gut dazu benutzt werden, um Homologien zwischen den Säugern zu zeigen und dennoch die Unterschiede in den Ordnungen der Nager und der Primaten, inklusive des Vergleichs zwischen Arten der gleichen Familie (Langschwanzmäuse (*Muridae*)) und verschiedener Familien (Meerkatzenverwandte (*Cercopithecidae*) und große Menschenaffen (*Hominidae*)), darzustellen (Abb. 9; Vogt et al., 2013). So konnte z.B. gezeigt werden, dass der cinguläre Cortex bei Menschen, der wie die Makaken zur Unterordnung der Altweltaffen (*Catarrhini*) zählt, viel differenzierter ist und nicht alle cingulären Areale ein Pendant im Gehirn von Affen (hier speziell in der Überfamilie der geschwänzten Altweltaffen (*Cercopithecoidea*)) oder Nagern (hier speziell in der Überfamilie der *Muroidea*) haben. Dies legt den Schluss nahe, dass

der cinguläre Cortex sich beim Menschen, der zur Überfamilie der Menschenaffen (*Hominoidea*) gezählt wird, weiter/höher entwickelt hat.

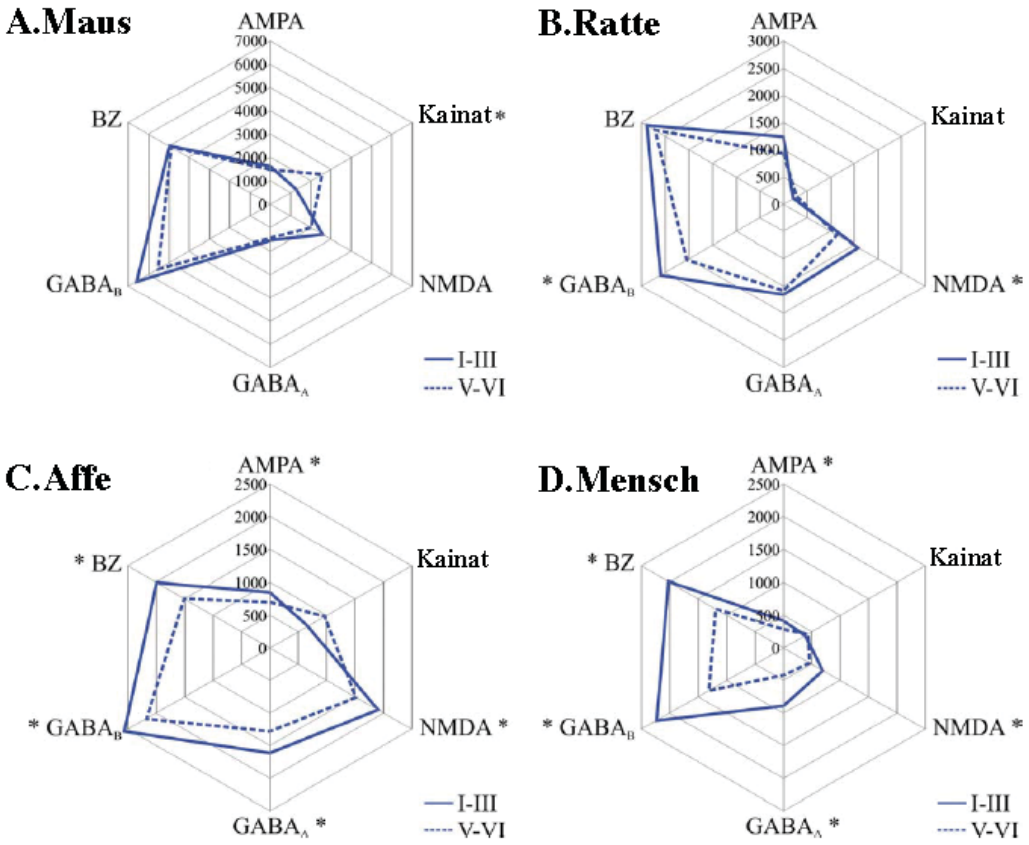

Abbildung 9: Rezeptor-„Fingerabdrücke“ der supra- (I-III) und infragranulären (V-VI) Schichten der Area d32 (dorsal) des cingulären Cortex von Maus und Ratte (A-B) und p32 (prägenual) von Affe und Mensch (C-D). Die Achsen kodieren die Rezeptordichten für glutamaterge AMPA-, Kainat- und NMDA-Rezeptoren und GABAerge $GABA_A$- und $GABA_B$-Rezeptoren sowie die Benzodiazepinbindestellen für GABAerge $GABA_A$-Rezeptoren (BZ) in fmol/mg Protein, angepasst an die jeweilige Spezies (Maus: *Mus musculus*; Ratte: *Rattus norvegicus*; Affe: *Macaca fascicularis*; Mensch: *Homo sapiens*). *signifikante Unterschiede ($p<0.01$) zwischen den Rezeptordichten in den supra- und infragranulären Schichten (modifiziert nach Vogt et al., 2013 mit freundlicher Genehmigung von Wiley Periodicals, Inc.).

Mit Hilfe der detaillierten Analyse der Rezeptordichten im NCL (Abb. 5; Abb. 6A) konnten, zusätzlich zu der Einteilung in einen medialen NCL und einen lateralen NCL (Abb. 8), die rostralen und caudalen Grenzen des NCL genauer bestimmt werden, so dass ein neuer Atlas erstellt wurde (Abb. 10; Herold et al., 2011).

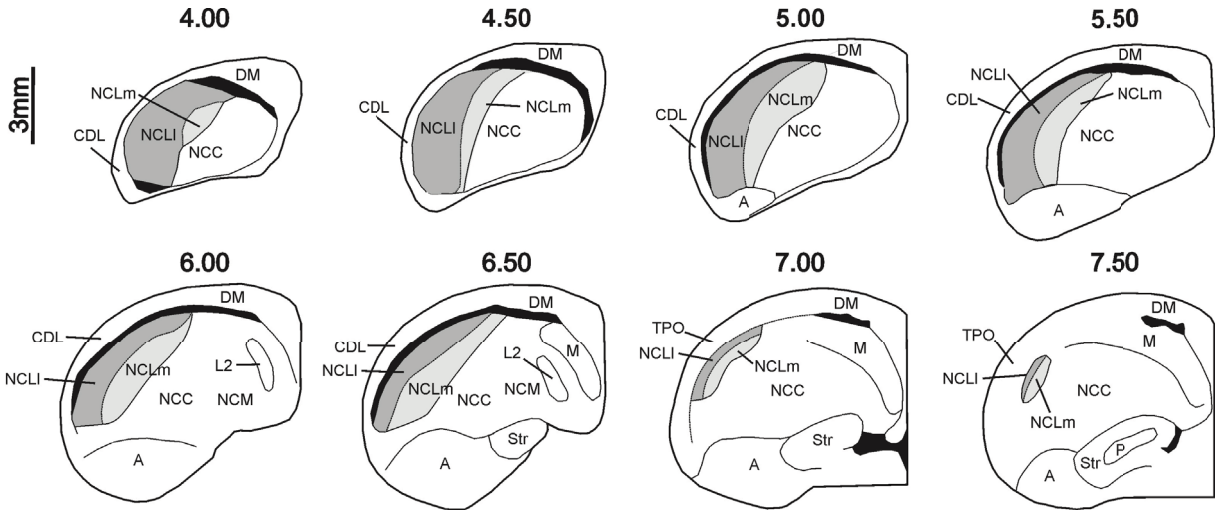

Abbildung 10: Atlas des NCL in einer Serie von Frontalschnitten basierend auf signifikanten Unterschieden in den Rezeptordichten. A, Arcopallium; CDL, Area corticoidea dorsolateralis; DM, dorsomediale Region der Hippocampusformation; L2, Feld L2; M, Mesopallium; NCC, Nidopallium caudocentrale; NCLm, Nidopallium caudolaterale, Pars medialis; NCLl, Nidopallium caudolaterale, Pars lateralis; NCM, Nidopallium caudomediale; P, Pallidum; Str, Striatum; TPO, Area temporo-parieto-occipitalis (modifiziert nach Herold et al., 2011 mit freundlicher Genehmigung des Springer-Verlages).

Dies bietet zukünftig zum einen die Möglichkeit die Funktionen des NCL noch spezifischer zu untersuchen, und zum anderen, im Vergleich mit weiteren Vogelspezies, die Evolution des NCL genauer in den Fokus zu nehmen und dies mit den kognitiven Fähigkeiten der jeweiligen Vogelspezies in Korrelation zu setzen.

Die in der Autoradiografie-Studie beobachtete konservierte Funktion des dopaminergen Systems zeigte sich auch in Untersuchungen zur Plastizität der Dopamin-Rezeptoren (Herold et al., 2012a). Grundlage für diese Studie war, dass die Stimulation oder Blockade der $D_{1/5}$-Rezeptoren während Arbeitsgedächtnisaufgaben sowohl bei Säugern als auch bei Vögeln abhängig von der Stärke der Stimulation ein invertiertes U in der Dosis-Wirkungskurve aufwiesen (Castner & Williams, 2007; Puig et al., 2014). Diese Dosis-Wirkungskurve ließ sich auch bei hochtrainierten Tieren in Abhängigkeit davon beobachten, ob die Tiere zuvor eine sehr gute oder nicht so gute Arbeitsgedächtnisleistung hatten (Herold et al., 2008). Um die genaueren Zusammenhänge zwischen den verschiedenen Leistungsniveaus, Lern- und Gedächtnisprozessen sowie möglichen Unterschieden in der Rezeptorstimulation an der Synapse zu verstehen, wurden zunächst vier unterschiedliche Gruppen gebildet, in denen die Tauben verschiedene Subkomponenten einer typischen Arbeitsgedächtnisaufgabe (*Delayed-Matching-To-Sample, DMTS*) erlernten (Abb. 11; Herold et al., 2012a).

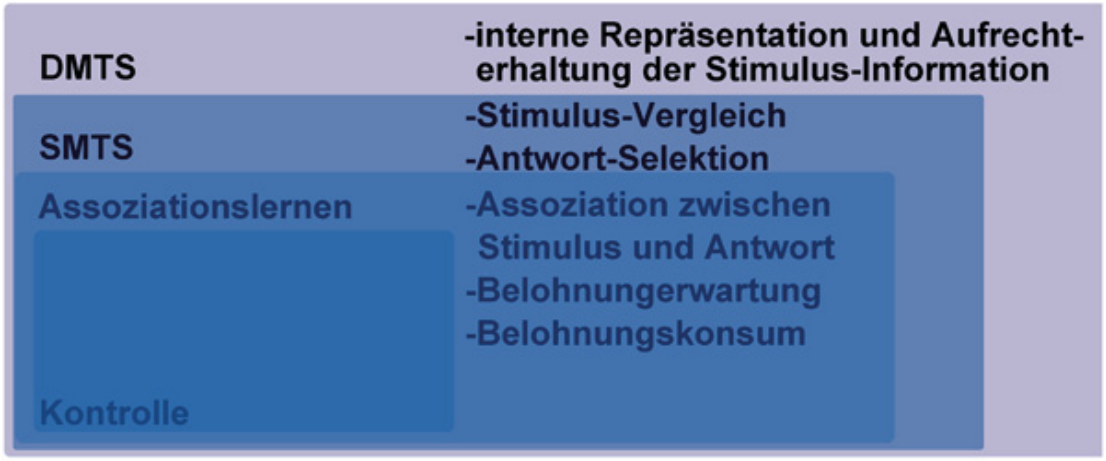

Abbildung 11: Schematische Darstellung der Prozesse des kognitiven Trainings. Die Expressionslevel der Dopamin-Rezeptoren wurden jeweils nachdem die Tiere das Lernkriterium für eine Aufgabenstufe erreicht hatten, gemessen. Das Design ähnelt dem einer Matrjoschka-Puppe. Jede Trainings-Aufgabe enthält die kognitiven Komponenten der vorangegangenen Gruppe, während immer neue Komponenten (jeweils rechts in der Box) dazukommen. DMTS, *Delayed-Matching-To-Sample*; SMTS, *Simultaneous-Matching-To-Sample* (modifiziert nach Herold et al., 2012a).

Die Kontrollgruppe sowie die DMTS-Gruppe wurden bereits in der Promotion untersucht. Im Rahmen der Habilitation wurden zwei zusätzliche Gruppen untersucht: die operante Konditionierungsgruppe (Assoziationslernen zwischen Stimulus und Antwort, englisch: *Stimulus-Response,* SR) und die *Simultaneous-Matching-To-Sample* (SMTS)-Gruppe, um die verschiedenen Belohnungs-, Lern-, und Gedächtniskomponenten der DMTS-Aufgabe zu extrahieren. Anschließend wurde die Expression der D_1-Rezeptorsubtypen und der D_2-Rezeptoren mit Hilfe der *Real-time* PCR in einer relativen Quantifizierung im NCL untersucht. Im Ergebnis zeigte sich, dass die D_1-Rezeptoren im NCL abhängig von der trainierten Aufgabe exprimiert werden, während das Level der D_2-Rezeptoren im NCL konstant bleibt (Abb. 12). Dabei zeigte der Subtyp D_{1B} (homolog zu D_5 bei Säugern) erst nach dem Training in der DMTS-Aufgabe eine veränderte und erhöhte Expression, wohingegen die D_{1A} (homolog zu D_1 bei Säugern) und die D_{1D} (geringe Homologie zu D_5 bei Säugern) Level nach dem SR-Lernen sanken und durch das DMTS-Training wieder auf Kontroll-Niveau anstiegen. Die SMTS-Aufgabe, in der es nicht notwendig ist, eine Repräsentation des Stimulus im Arbeitsgedächtnis aufrechtzuerhalten, sondern nur den Stimulus zu vergleichen und auszuwählen, beeinflusste die Expression der D_1-Rezeptoren hingegen nicht, so dass die Tiere auf dem SR-Niveau blieben. Der Stimulus-Vergleich und die Antwort-Auswahl scheinen somit nicht mit der Stimulation der Plastizität der gemessenen Dopamin-Rezeptoren in Verbindung zu stehen.

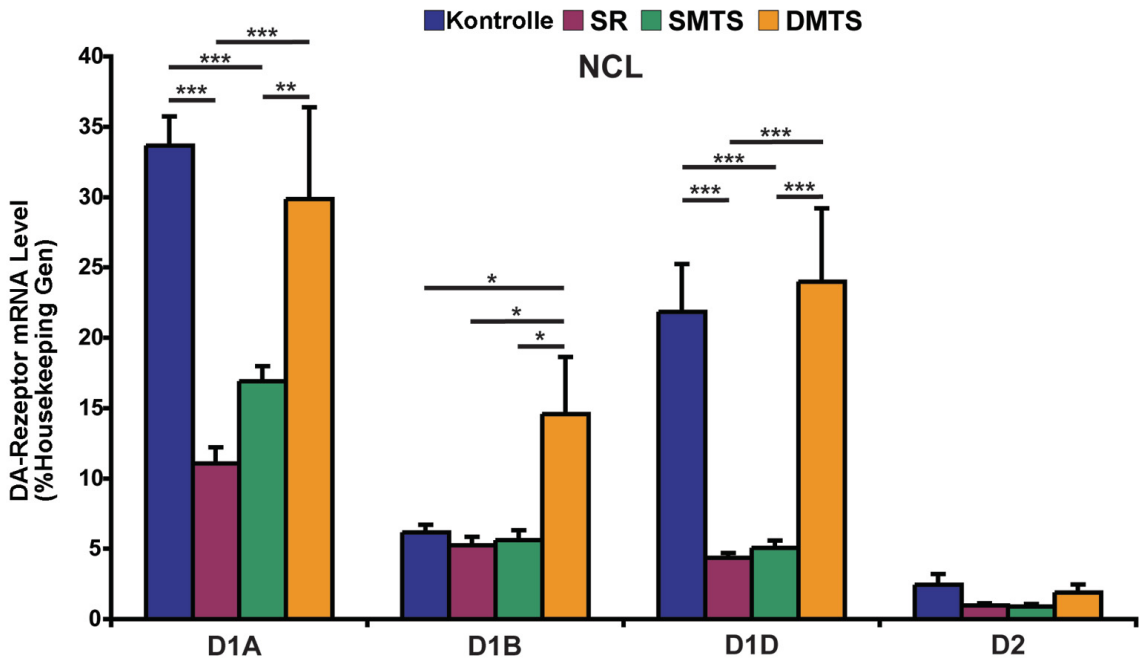

Abbildung 12: Quantifizierung der Dopamin-Rezeptor-mRNA-Level im Nidopallium caudolaterale (NCL) der verschiedenen Trainings-Gruppen. Die Expression der Dopamin-Rezeptoren ist relativ zum *housekeeping*-Gen Histon H3.3B dargestellt (Mittelwert ± Standardfehler; n=10 für jede Gruppe). Signifikante Unterschiede sind mit Sternchen markiert (*p<0.05; **p<0.01; ***p<0.001). DMTS, *Delayed-Matching-To-Sample*; SMTS, *Simultaneous-Matching-To-Sample*; SR, *Stimulus-Response* (modifiziert nach Herold et al., 2012a).

Durch diese Studie wurde deutlich, dass die Modulation durch die D_1-Subtypen im NCL bei Vögeln an spezifische kognitive Prozesse und Lernparadigmen gekoppelt ist. In Kombination mit den Ergebnissen aus elektrophysiologischen, pharmakologischen und molekularbiologischen Studien (Bergson et al., 1995; Diekamp et al., 2002; Seamans & Yang, 2004; Castner & Williams, 2007; Vijayraghavan et al., 2007; Bordelon-Glausier et al., 2008; Glausier et al., 2009) ließ sich aus den Ergebnissen außerdem ableiten, dass die D_1-Subtypen im NCL, analog zum PFC, vermutlich unterschiedlich auf die zelluläre Aktivität von Neuronen wirken, die in kognitive Prozesse eingebunden sind. Somit ergaben sich in dieser Studie sowohl Befunde, die eine molekulare Erklärung für die invertierte U-Kurve lieferten, als auch Hinweise darauf, warum sich möglicherweise die Aktivitätsmuster und Rezeptordichten im PFC nach kognitivem Training beim Menschen ändern könnten (McNab et al., 2009; Klingberg, 2010). Darüber hinaus lieferte die Studie einen weiteren Beleg dafür, dass die Funktionen und die molekulare Basis des dopaminergen Systems zwischen den Vögeln und Säugern gleich sind (Herold et al., 2012a). Die Modulation der neuronalen Aktivität durch Dopamin hat demnach scheinbar eine sehr konservierte Stellung im Rahmen von Belohnungsmechanismen und Arbeitsgedächtnisprozessen. Insgesamt lässt sich aus den Ergebnissen schließen, dass der neuroanatomische Aufbau einer definierten Struktur scheinbar nicht allein entscheidend für das Maß an möglichen Fähigkeiten zur Kognition ist. Vielmehr haben besonders die verschiedenen funktionellen Systeme und hier insbesondere Neurotransmittersysteme einen hohen Beitrag daran, welche kognitiven Leistungen erzielt werden können. Dabei scheint es im Verlauf der Evolution so zu sein, dass einige Systeme hochkonserviert sind und so die Grundlagen für intelligentes Verhalten ermöglichen.

3.2 Eine multimodale Analyse der Hippocampusformation (HF) der Taube im Vergleich zum Säuger

(Herold et al., 2012b; Herold et al., 2014; dos Santos et al., 2015; Herold et al., 2019)

Neben den herausragenden kognitiven Leistungen, die Vögel zeigen, wie z.B. „*Song*“ („Sprach“)- Erwerb, Werkzeuggebrauch, „*Theory of mind*“, Problemlösen und *Multitasking*, die eher assoziativen Arealen und deren Netzwerken zuzuordnen sind, zeichnen sich viele Vogelarten, auch Tauben, besonders durch ihre räumlichen Gedächtnisfähigkeiten und durch räumliche Orientierung aus (Herold et al., 2015; Mouritsen et al., 2016; Letzner et al., 2017; Nieder, 2017; Boeckle & Clayton, 2018; Pika et al., 2018; Pepperberg, 2019). Es zeigte sich, dass für diese Funktionen, die HF, in Abgrenzung zum NCL, die entscheidende Rolle spielt (Abb.13; Bingman et al., 2005; Kahn & Bingman, 2009; Herold et al., 2015; Bingman & MacDougall-Shackleton, 2017).

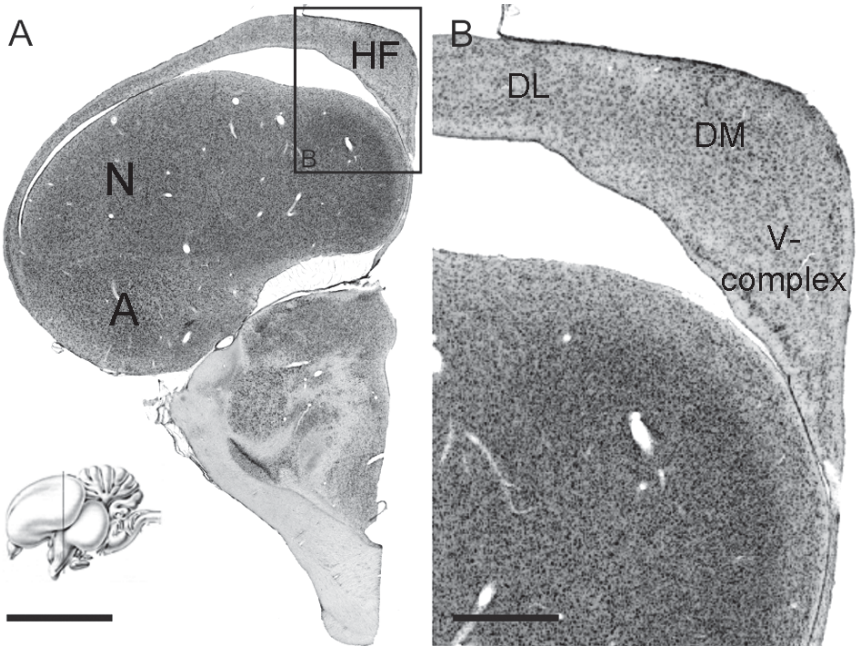

Abbildung 13: Nissl-gefärbter Frontalschnitt durch das Vorderhirn der Taube. (A) Gesamter Schnitt einer Hirnhälfte auf der Höhe des Atlas-Levels A 6.75 (Karten & Hodos, 1967). Der gerahmte Bereich zeigt die Hippocampusformation (HF) in (B). Am Rand unten links ist eine laterale Ansicht des Taubengehirns zu sehen (nicht skaliert), in der die Schnitthöhe markiert ist. Der Skalierungsbalken in (A) entspricht 2,5 mm, in (B) 500 µm. A, Arcopallium; DL, dorsolaterale Region der HF; DM, dorsomediale Region der HF; HF, Hippocampusformation; N, Nidopallium (modifiziert nach Herold et al., 2014 mit freundlicher Genehmigung von Wiley Periodicals, Inc.; Miniatur des Taubengehirns modifiziert und im Original freundlicherweise zur Verfügung gestellt von Prof. Dr. Onur Güntürkün, Co-Autor in der Publikation Herold et al., 2014).

Dennoch ist die HF über ihre zahlreichen Verschaltungen direkt wie indirekt auch in viele höhere kognitive Funktionen eingebunden (Atoji & Wild, 2004; 2006; Herold et al., 2019). Somit erfüllt die HF bei Vögeln ähnliche Funktionen wie bei Säugern, auch wenn nicht alle Verschaltungen identisch sind (Atoji & Wild, 2006; Andersen et al., 2007). Obwohl sich die HF bei Vögeln und Säugern vom gleichen Teil des Palliums ausgehend entwickelt und daher als homolog anzusehen ist (Jarvis et al., 2013; Tosches et al., 2018), gibt uns die HF der Vögel seit mehr als 30 Jahren Rätsel auf, da sie sich in ihrem strukturellen Aufbau stark von der HF beim

Säuger unterscheidet (Herold et al., 2014; Herold et al., 2015; Atoji et al., 2016). Insbesondere gilt dies für die Definition unterschiedlicher Subareale in Bezug auf die klar organisierten und trilaminären Strukturen des Säuger-Hippocampus, Gyrus dentatus (DG) und Cornu ammonis (CA1-4). Betrachtet man die Anordnung der Zellen in den Subarealen der HF bei Vögeln, gleichen sie, wie viele andere palliale Strukturen im Vogelhirn, eher Kerngebieten. Es gibt außer im Bereich der caudalen HF und des V-Komplexes keine unmittelbar sichtbare Laminierung und auch die lokalen Verbindungen sind eher wie ein Netzwerk organisiert und nicht so getrennt, wie z.B. der trisynaptische Verschaltungsweg zwischen DG, CA3 und CA1 beim Säuger (Herold et al., 2015). Aktuellere Studien bei Vögeln zeigen zudem deutliche Abweichungen zu der ursprünglich in nur zwei Subareale unterteilten HF des Taubengehirns im Atlas von Karten und Hodos (Karten & Hodos, 1967; Atoji et al., 2002; Atoji & Wild, 2006). Zudem sind eine genaue funktionelle Betrachtung und der Vergleich schwierig, wenn keine einheitliche Einteilung einer Struktur vorliegt. Daher wurde in der vorliegenden Arbeit die HF der Taube auf der Basis der Zyto- und der Rezeptorarchitektur sowie einer speziellen Zink-Färbung (Timm-Färbung) neu analysiert und ein Atlas, der an die Arbeiten von Atoji und Wild (Atoji & Wild, 2004; 2006) angelehnt ist, auf Basis der quantitativ ermittelten Rezeptordichteunterschiede in den Subarealen erstellt (Abb. 14 und 15; Herold et al., 2014).

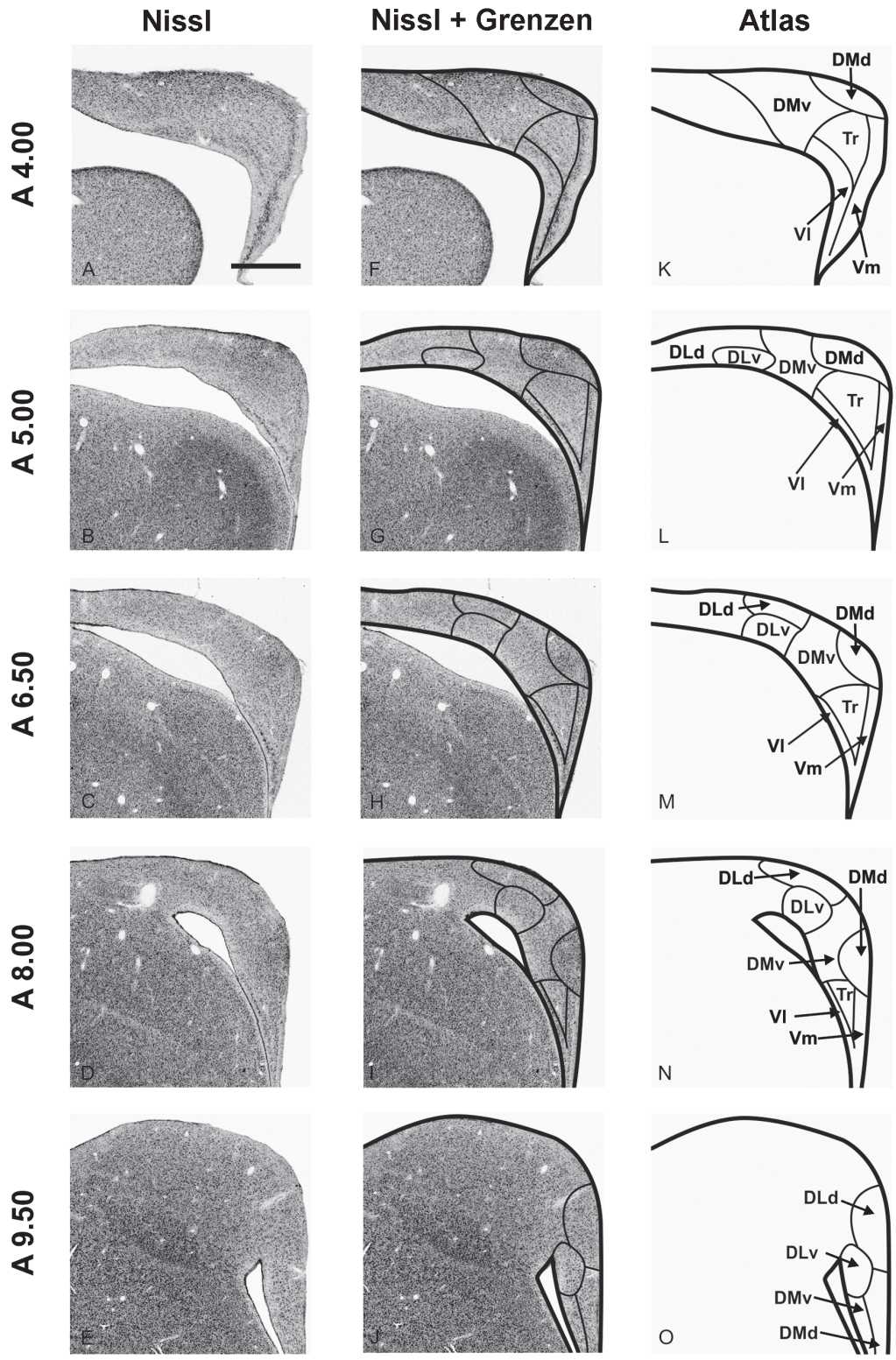

Abbildung 14: Nissl-gefärbte Frontalschnitte und Schemata der Subareale der Hippocampusformation bei der Taube für die Atlas-Level A 4.00- A 9.50 (Karten & Hodos, 1967). A-J Nisslgefärbte Frontalschnitte ohne und mit Grenzen für die Subareale definiert von Atoji und Wild (2004;2006). K-0 Schematische Darstellung der Subareale, um die Rezeptordichten und die Zink-Färbung zu analysieren. Die HF der Taube setzt sich aus sieben Subarealen zusammen: der V-Region, bestehend aus dem ventrolateralen Zellband (Vl), dem ventromedialen Zellband (Vm) und der triangulären Zwischenregion (Tr), der dorsomedialen Region (DM), die sich in einen ventralen (DMv) und einen dorsalen (DMd) Teil unterscheiden lässt, und der dorsolateralen Region (DL), ebenfalls unterteilt in einen ventralen (DLv) und in einen dorsalen Teil (DLd). Der Skalierungsbalken entspricht 500µm (modifiziert nach Herold et al., 2014 mit freundlicher Genehmigung von Wiley Periodicals, Inc.).

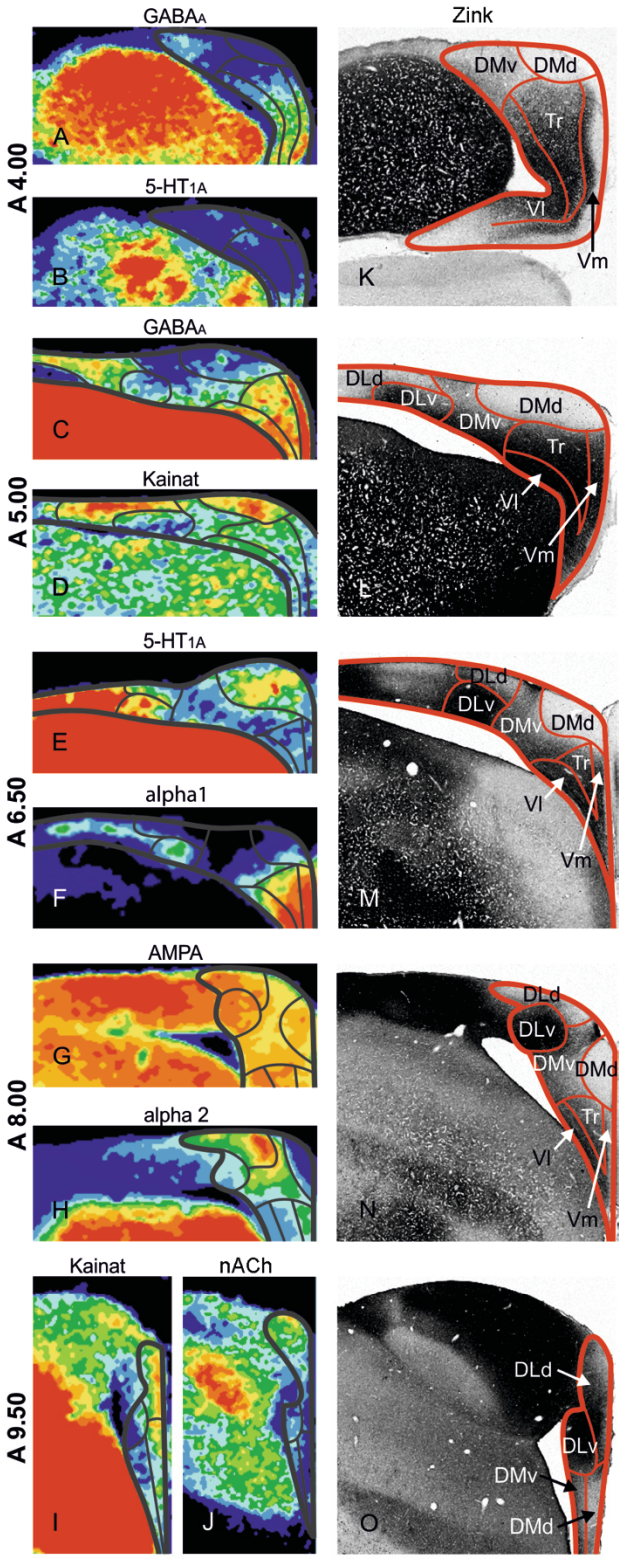

Abbildung 15: Farbkodierte Autoradiogramme und Zink-Färbungen in der HF der Taube. A-J zeigen ausgewählte Beispiele für die Dichte und die Verteilung verschiedener Rezeptortypen in unterschiedlichen Atlasebenen in der rostro-caudalen Achse. Rot zeigt eine hohe Dichte, blau eine niedrige Dichte des Rezeptors an. K-O zeigen die unterschiedliche Markierung mit Zink in den Subarealen der HF in etwa auf den gleichen Atlasebenen. Schwarz zeigt eine hohe Konzentration von Zink an, grau eine niedrige. alpha 1 und 2, noradrenerge Rezeptor-Subtypen 1 und 2; AMPA, glutamaterger AMPA-Rezeptor; DMd, dorsale dorsomediale Region; DMv, ventrale dorsomediale Region; DLd, dorsale dorsolaterale Region; DLv, ventrale dorsolaterale Region; $GABA_A$, GABAerger Rezeptor-Subtyp A; $5\text{-}HT_{1A}$, serotonerger Rezeptor-Subtyp 1A; Kainat, glutamaterger Kainat-Rezeptor; nACh, nikotinischer cholinerger Rezeptor-Subtyp $\alpha_4\beta_2$; Tr, Trianguläre Zwischenregion; Vm, ventromediales Zellband; Vl, ventrolaterales Zellband (modifiziert nach Herold et al., 2014 mit freundlicher Genehmigung von Wiley Periodicals, Inc.).

Um die unterschiedlichen Subareale nun genauer mit der Einteilung der HF beim Säuger zu vergleichen, wurden die ermittelten Rezeptordichten semi-quantitativ verglichen, und relative Werte herangezogen, um absolute Konzentrationsabweichungen in den Rezeptordichten zwischen Vögeln und Säugern zu nivellieren (Tab. 1). Die Zinkfärbung wurde benutzt, um glutamaterge Synapsen, die man in den CA-Feldern beim Säuger klassisch damit anfärben kann, darzustellen.

Tabelle 1. Vergleich der Neurotransmitterrezeptordichten zwischen den Subarealen der Hippocampusformation (HF) der Taube (*Columba livia f.d.*), der Ratte (*Rattus norvegicus*), der Maus (*Mus musculus*) und dem Marmoset-Affen (*Callithrix jacchus*). Die Zahlen geben den relativen Wert der Rezeptordichte für jedes Areal, bezogen auf die Gesamtkonzentration des Rezeptors in der HF der jeweiligen Spezies, in Prozent an. Die Schlussfolgerungen daraus sind in Abbildung 16 dargestellt.

	Relative Rezeptordichten in der HF der Taube							**Relative Rezeptordichten in der HF der Säuger (%)**					
Rezeptor	**Vl**	**Tr**	**Vm**	**DMv**	**DMd**	**DLd**	**DLv**	**CA1**	**CA2**	**CA3**	**DG**	**EC**	**Spezies**
AMPA	107	109	99	99	71	104	111	109[1],114[2],117[5],102[6]	90[1],87[2],94[5]	86[1],78[2],94[5]	97[1],104[2],95[5],98[6]	68[6]	Ratte
								110[4],115[7]		95[4],90[7]	96[4],94[7]		Maus
Kainat	101	96	81	79	109	132	102	52[1],67[2,6],59[5]	74[1],58[2],69[5]	140[1],127[2],174[5]	124[1],113[2],132[6],97[5]	134[6]	Ratte
								71[4],63[7]		116[4],113[7]	113[4],125[7]		Maus
NMDA	110	116	91	102	81	96	103	120[1],124[2],130[5],105[6]	84[1],83[2],99[5]	74[1],71[2],83[5]	90[1],101[2],89[5],95[6]	77[6]	Ratte
								126[4],135[7]		81[4],69[7]	93[4],97[7]		Maus
								110[3]	88[3]	82[3]	94[3]		Marmoset
$GABA_A$	147	110	100	76	40	107	120	80[2],87[6]	70[2]	47[2]	119[2],111[6]	118[6]	Ratte
								122[4],106[7]		62[4],58[7]	114[4],137[7]		Maus
								111[3]	72[3]	60[3]	112[3]		Marmoset
M_1	74	65	52	109	61	132	206	118[2],128[12]	74[2],67[12]	65[2],94[12]	109[2],139[12]	111[12]	Ratte
								119[7],113[8]		71[7],70[8]	110[7],117[8]		Maus
								101[3]	104[3]	97[3]	99[3]		Marmoset
M_2	99	89	69	79	46	127	190	115[2],141[12]	101[2],86[12]	105[2],104[12]	86[2],89[12]	146[12]	Ratte
								91[7],124[8]		142[7],79[8]	74[7],97[8]		Maus
								103[3]	110[3]	111[3]	88[3]		Marmoset
nACh	83	126	80	131	91	109	80	56[12]	56[12]	56[12]	260[12]	185[12]	Ratte
								103[7]		45[7]	152[7]		Maus
α_1	156	206	161	33	15	61	67	95[2]	102[2]	101[2]	103[2]	104[13]	Ratte
								108[7]		104[7]	88[7]		Maus
								88[3]	101[3]	95[3]	110[3]		Marmoset
α_2	92	68	75	150	52	142	120	103[2]	90[2]	86[2]	105[2]	132[13]	Ratte
$5\text{-}HT_{1A}$	130	100	93	87	101	97	93	93[2],79[9]	44[2]	73[2]	130[2],119[9]	27[13]	Ratte
								205[7]		29[7]	66[7]		Maus
$D_{1/5}$	96	89	87	98	72	110	148	39[2],76[10]	58[2]	54[2]	177[2],147[10]	170[11]	Ratte

[1] Palomero-Gallagher et al. (2003); [2] Topic et al., 2007; [3] Kraemer et al., 1995; [4] Zilles et al., 2000; [5] Martens et al., 1998; [6] Cremer et al., 2009; [7] Cremer et al., 2011; [8] Wolff et al., 2008; [9] Zavitsanou et al., 2010; [10] Savasta et al., 1986; [11] Cremer et al., 2010; [12] Sihver et al., 1997; [13] eigene Daten. AMPA, Glutamaterger AMPA-Rezeptor; Kainat, Glutamaterger Kainat-Rezeptor; NMDA, Glutamaterger NMDA-Rezeptor; $GABA_A$, GABAerger Rezeptor-Subtyp A; M_1 und M_2, Muscarinische acetylcholinerge Rezeptor- Subtypen 1 und 2; nACh, Nikotinischer cholinerger Rezeptor-Subtyp $\alpha_4\beta_2$; α_1 und α_2, Noradrenerge α-Rezeptor-Subtypen 1 und 2; $5\text{-}HT_{1A}$, Serotonerger Rezeptor-Subtyp 1A; $D_{1/5}$, Dopaminerge $D_{1/5}$-Rezeptoren (Tabelle modifiziert nach Herold et al., 2014 mit freundlicher Genehmigung von Wiley Periodicals, Inc.).

Das Ergebnis dieser umfangreichen Analysen zwischen Taube, Maus, Ratte und Marmoset-Affen (*Callithrix jacchus*) ist in Abbildung 16 dargestellt.

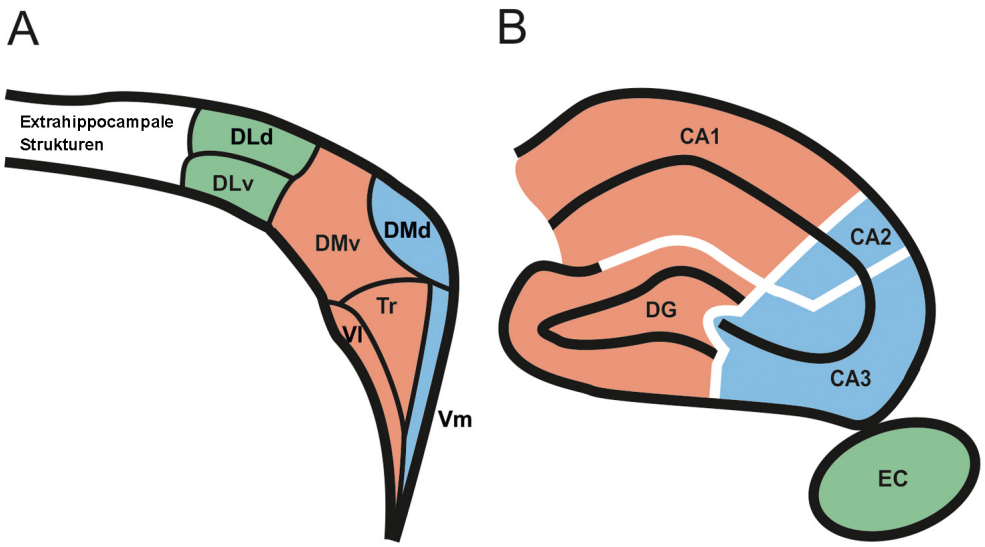

Abbildung 16: Beobachtete Übereinstimmungen in der Rezeptorverteilung zwischen den Subarealen der Hippocampusformation (HF) der Taube (A) und der Säuger (B). Gleiche Farben zeigen Überlappungen basierend auf einer semi-quantitativen Analyse zwischen den verschiedenen Arealen der HF bei der Taube und bei der Ratte an. Das ventrolaterale Zellband des V-Komplexes (Vl), die trianguläre Zwischenregion (Tr) und die ventrale dorsomediale Region (DMv) sind mit dem Gyrus dentatus (DG) und dem Cornu ammonis 1 (CA1) vergleichbar (orange). Das ventromediale Zellband des V-Komplexes (Vm) und die dorsale dorsomediale Region (DMd) sind mit dem Cornu ammonis 2 (CA2) und dem Cornu ammonis 3 (CA3) vergleichbar (blau), und die dorsale dorsolaterale Region (DLd) und die ventrale dorsolaterale Region (DLv) sind zum entorhinalen Cortex (EC) vergleichbar (grün; modifiziert nach Herold et al., 2014 mit freundlicher Genehmigung von Wiley Periodicals, Inc.).

Im Vergleich zeigten sich folgende Gemeinsamkeiten bezüglich der Rezeptordichten in der HF: Vögel und Säuger besitzen generell hohe Dichten an glutamatergen Rezeptoren in der gesamten HF. Sowohl die Vl-, die Tr- und die DMd-Region bei der Taube als auch der DG und das CA3 bei Nagern sowie die DLd-Region und der entorhinale Cortex (EC) zeigten gleich hohe relative Dichten an glutamatergen Kainat-Rezeptoren, wohingegen diese in der Vm- und DMv-Region im Vergleich zu CA1 und CA3 ähnlich niedrig verteilt sind (Tab. 1). Die glutamatergen NMDA- und AMPA-Rezeptoren zeigten Gemeinsamkeiten zwischen der Vl-, der Tr- und der DMv-Region und dem DG und CA1 (Tab. 1). Hohe Dichten lassen sich ebenfalls für die $GABA_A$-Rezeptoren bei Vögeln und Säugern finden. Bei der Maus, der Ratte und beim Marmoset-Affen nimmt die Dichte in der Reihenfolge EC, DG, CA1, CA2 und CA3 ab. Die größten Gemeinsamkeiten für die $GABA_A$-Rezeptoren konnten für die Regionen des V-Komplexes und den DG und das CA1 sowie für die DL-Region und den EC festgestellt werden. Die relativen Dichten waren ebenfalls in der DMv-Region und CA2 gleich. DMd und CA3 hingegen zeichneten sich beide durch eine sehr niedrige Konzentration an $GABA_A$-Rezeptoren aus (Tab. 1). Muskarinische acetylcholinerge Rezeptoren sind in der HF der untersuchten Säuger höher exprimiert als bei Tauben, während nikotinische acetylcholinerge Rezeptoren wiederum in der HF der Taube höhere Werte aufweisen. In Bezug auf die cholinergen Rezeptoren ließen sich keine Gemeinsamkeiten in der HF zwischen den beiden Wirbeltierklassen Vögel und Säuger feststellen (Tab. 1). Von den monoaminergen Rezeptoren zeigten noradrenerge α_2-

Rezeptoren in der Vl- und der DMv-Region Übereinstimmungen mit dem DG und dem CA1-Areal, wohingegen niedrige Konzentrationen in der Tr-, der Vm- und der DMd-Region gefunden wurden, welche ebenfalls im CA2 und CA3 beobachtet werden konnten. Serotonerge 5-HT_{1A}-Rezeptoren wiesen in der VL-Region und im DG sowie in der Vm-Region und im CA1 der Ratte gleiche Dichten auf, nicht aber im Vergleich zur Maus. Dopaminerge $D_{1/5}$-Rezeptoren sind im DG und der Vl- und der DMv-Region gleichverteilt. Eine hohe $D_{1/5}$-Rezeptor Konzentration, wie sie in der DL-Region detektiert wurde, fand sich ebenfalls im EC. Zusammenfassend ließen sich daher die größten Gemeinsamkeiten zwischen Vl/Tr/DMv und DG/CA1 sowie Vm/DMd und CA2/CA3 finden, wohingegen die Rezeptorarchitektur der DL-Region eher der des EC glich (Abb. 16). Die Schlussfolgerungen aus der Betrachtung der Rezeptorverteilung stehen ebenfalls in Einklang mit den Ergebnissen aus der Zink-Färbung, die besonders in den Subarealen ein starkes Signal hervorbrachte, die eine hohe Dichte an glutamatergen Rezeptoren aufwies (Abb. 15; Tab. 1). Allerdings deutete die eher diffus verteilte Zink-Konzentration daraufhin, dass insbesondere der V-Komplex sich ähnlich wie die CA-Areale bei Primaten anfärbt (Amaral et al., 2017). Eine spezifische Färbung der Moosfasern, wie sie typisch für den DG bei Ratten ist (Danscher et al., 1973; Danscher & Haug, 1978; Zimmer & Haug, 1978), konnte bei der Taube nicht beobachtet werden.

Neben morphologischen, physiologischen und neurochemischen Gemeinsamkeiten liefert der Vergleich der Rezeptordichten eine gute Erklärung für die übereinstimmenden Funktionen, an denen die HF sowohl bei Vögeln als auch bei Säugern beteiligt ist. Gleichzeitig zeigt die Analyse der Zyto- und Myeloarchitektur, dass die HF der Vögel sich andersartig entwickelt hat als die der Säuger. Trotzdem zum Zeitpunkt der Studie die Erkenntnis existierte, dass sich die HF bei Vögeln und Säugern aus dem dorso-medialen Pallium entwickelt, diskutierten einige Forscher noch darüber, ob die Zelltypen der HF aufgrund ihres Expressionsprofils mehr den Zelltypen des Cortex oder der Amygdala gleichen (Reiner et al., 2004; Dugas-Ford et al., 2012; Chen et al., 2013; Jarvis et al., 2013) oder spekulierten darüber, ob der DG eine Neuentwicklung der Säuger ist (Kempermann, 2012). Außerdem zeigten Untersuchungen der Konnektivität der Vogel-HF neben den Unterschieden in den *Long-Range*-Verbindungen insbesondere Unterschiede in der lokalen Konnektivität, die als nicht-laminar und netzwerkartige Verschaltung beschrieben wurde (Atoji et al., 2002; Hough et al., 2002; Kahn et al., 2003). In Kombination mit den Befunden aus der hier durchgeführten Studie lässt sich daher schließen, dass möglicherweise im Gegensatz zu Säugern ein nicht so hoher Selektionsdruck für anatomisch diskrete Subareale bestand, so dass sich die HF bei Vögeln innerhalb von 300 Jahren getrennter Evolution anatomisch diversifizierte. Offen blieb auch, ob es tatsächlich bei Vögeln ein homologes Areal zum DG der Säuger gibt oder sich möglicherweise konvergent ein funktionelles Äquivalent entwickelte, wie es für den NCL und den PFC der Fall ist. Dies wäre eine mögliche Erklärung für das Mosaik an Gemeinsamkeiten und aus Unterschieden zwischen der HF der Vögel und der HF der Säuger, zeigt aber auch deutlich, dass weitere Untersuchungen notwendig sind, um die Evolution der HF und ihre Funktionen besser zu verstehen. Im Folgenden wurden dafür zwei unterschiedlich funktionell-anatomisch kombinierte Ansätze gewählt: Erstens wurden die serotonergen 5-HT_{1A}-Rezeptoren im Hirnstamm und im Hypothalamus und ihre Aufgabe in 5-HT-induziertem Schlaf und

induzierter Nahrungsaufnahme in Kombination mit einer Analyse der 5-HT-Level in der HF und im Arcopallium/Amygdala-Komplex der Taube studiert (dos Santos et al., 2015). Zweitens wurden die adulte Neurogenese sowie die *Long-Range*-Verbindungen der HF in Bezug auf Topografie und Unterschiede in der rostro-caudalen Achse in den Blick genommen (Herold et al., 2019).

Der erstgenannten Arbeit war eine umfangreiche Analyse der Verteilung der 5-HT_{1A}-Rezeptoren im Taubengehirn vorausgegangen (Herold et al., 2012b), die zeigte, dass die HF und der Arcopallium/Amygdala-Komplex im Vergleich zu anderen pallialen Strukturen nur eine moderate 5-HT_{1A}-Rezeptordichte aufwiesen, während diese in diencephalen, mesencephalen und rhombencephalen Kernen häufig sehr hoch war, wobei nicht alle Kerngebiete analysiert wurden (Abb. 17). Dies erfolgte dann in einer zweiten Studie, in der unter anderem auch der Hypothalamus und der Hirnstamm genauer analysiert wurde (Abb. 18; dos Santos et al., 2015), so dass hier gezieltere Schlussfolgerungen zum Wirkmechanismus des serotonergen Systems auf Schlaf und Nahrungsaufnahme gestellt werden konnten. Schlaf stellt bei Vögeln wie auch bei Säugern eine wichtige Komponente für das Aufbauen des räumlichen Gedächtnisses dar und ist eng mit einer optimalen Funktion der HF verknüpft, welches sich z.B. durch die Konnektivität der HF mit dem Hypothalamus erklären lässt (Stickgold, 2005; Rattenborg & Martinez-Gonzalez, 2011; Vorster & Born, 2015).

Für die funktionell-anatomische Studie wurde neben der Analyse der 5-HT_{1A}-Rezeptoren eine bilaterale intracerebroventrikuläre Applikation von 5,7-DHT in die lateralen Ventrikel des Taubengehirns vorgenommen (dos Santos et al., 2015). 5,7-DHT ist ein Neurotoxin, welches die 5-HT-Level im Gehirn senkt und in Bezug auf die Funktionen der prä- und postsynaptischen 5-HT_{1A}-Rezeptoren selektiv wirkt (Alesci & Bagnoli, 1988; Choi et al., 2004). In unserer Studie senkte es die 5-HT-Level im Hirnstamm, im Hypothalamus und in der HF, aber nicht im Arcopallium/Amygdala-Komplex. Es induzierte darüber hinaus längere Schlafphasen. Die Schlafphasen erhöhten sich noch weiter, wenn den Tieren nach der Behandlung mit 5,7-DHT zusätzlich 5-HT injiziert wurde. Es wurde jedoch kein Effekt im Unterschied zur Kontrolle beobachtet, wenn der 5-HT_{1A}-Rezeptor Agonist DPAT zusätzlich injiziert wurde. Beides, 5-HT und DPAT Applikation in die Ventrikel, hatten zuvor veränderte EEG-Aktivität in der HF der Taube bewirkt (Hoeller et al., 2013), die in Zusammenhang mit Schlaf und räumlichem Gedächtnis steht (Lesku & Rattenborg, 2014). Weitere Untersuchungen in unserer Studie ergaben zwei Vermutungen bezüglich des Wirkmechanismus von 5-HT via 5-HT_{1A}-Rezeptoren: Erstens, eine chronische Reduktion von 5-HT beeinflusst solche Neuronenkreise nachhaltig, die eine Verbindung zur HF haben und den Schlaf steuern. Zweitens, diese Neuronenkreise werden höchstwahrscheinlich unter anderem über Hetero- und Auto-5-HT_{1A}-Rezeptoren (terminal oder somatodendritisch) an präoptisch-hypothalamischen Neuronen mit Kontakt zur Cerebrospinalflüssigkeit, die wiederum nicht serotonerg sind, moduliert. Somit zeigten sich hier mögliche mechanistische Unterschiede zwischen Säugern und Vögeln unter Erhaltung der gleichen Funktion (dos Santos et al., 2015).

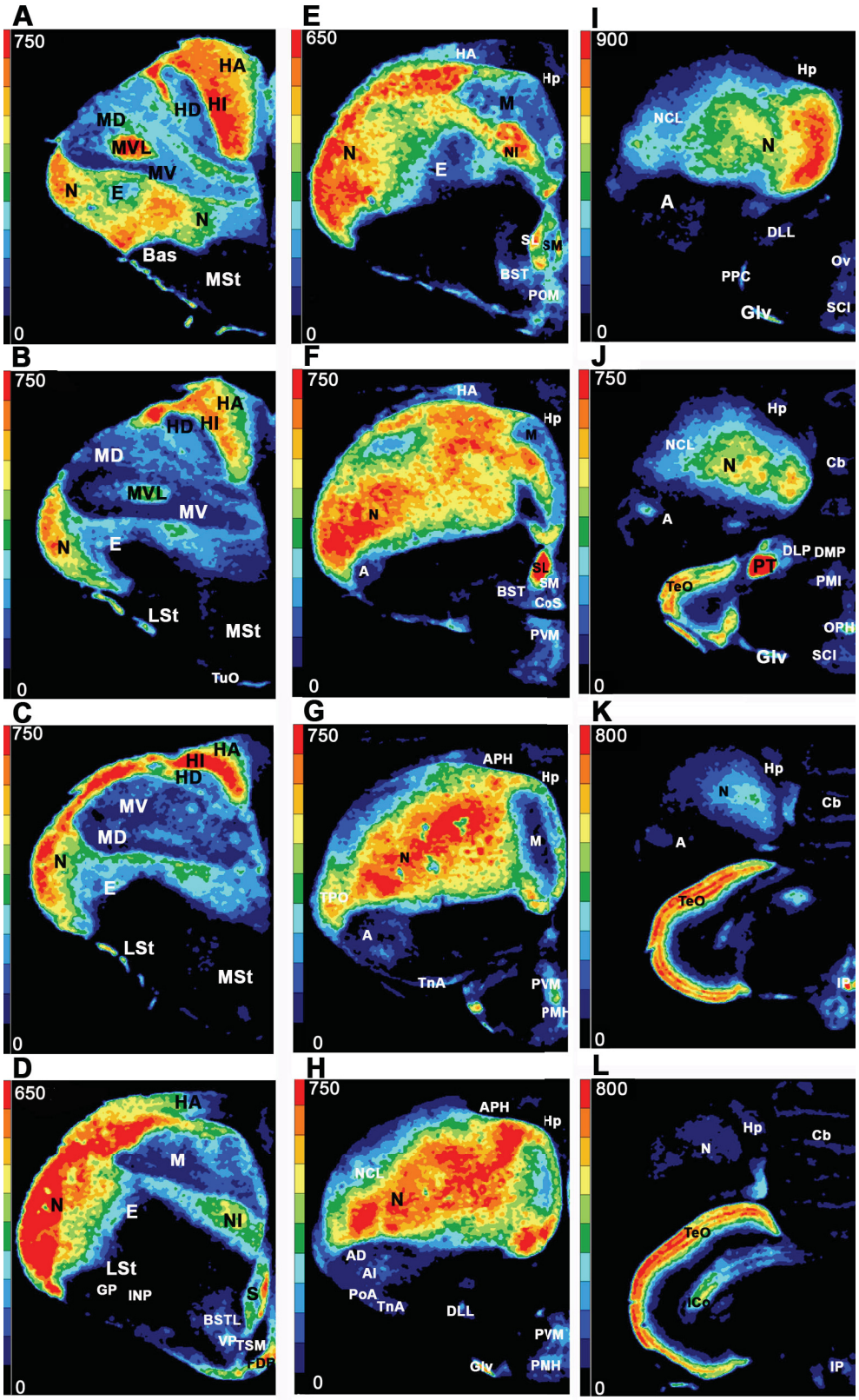

Abbildung 17: Farbkodierte Autoradiogramme der 5-HT_{1A}-Rezeptorverteilung im Gehirn der Taube von rostral nach caudal (A-L). Die Farbkodierung zeigt die Dichte der Rezeptoren in fmol/mg Protein an. Die Bilder wurden im Verhältnis zur höchsten Intensität und den vorliegenden Strukturen optimiert und spiegeln daher nicht das Maximum der Rezeptordichten wider. Die Hippocampusformation (Hp und Area parahippocampalis (APH)) zeigt eine niedrigere Dichte im Vergleich zum Nidopallium (N). A, Arcopallium; AD, Arcopallium dorsale; AI, Arcopallium intermedium; APH, Area parahippocampalis; Bas, Nucleus basorostralis pallii; BST, Nucleus interstitialis striae terminalis; BSTL, Nucleus interstitialis striae terminalis, Pars lateralis; Cb, Cerebellum; CoS, Nucleus commissuralis septi; DLL, Nucleus dorsolateralis anterior thalami, Pars lateralis; DLP, Nucleus dorsolateralis posterior thalami; DMP, Nucleus dorsomedialis posterior thalami; E, Entopallium; FDB, Fasciculus diagonalis Broca; Glv, Nucleus geniculatus lateralis, Pars ventralis; GP, Globus pallidus; HA, Hyperpallium apicale; HD, Hyperpallium

densocellulare; HI, Hyperpallium intercalatum; Hp, Hippocampus; ICo, Nucleus intercollicularis; INP, Nucleus intrapeduncularis; IP, Nucleus interpeduncularis; LSt, Striatum laterale; M, Mesopallium; MD, Mesopallium dorsale; MSt, Striatum mediale; MV, Mesopallium ventrale; MVL, Mesopallium ventrolaterale; N, Nidopallium; NCL, Nidopallium caudolaterale; NI, Nidopallium intermedium; OPH, Organum paraventriculare; Ov, Nucleus ovoidalis; PMH, Nucleus medialis hypothalami posterioris; PMI, Nucleus paramedianus internus thalami; PoA, Nucleus posterioris amygdalopallii; POM, Nucleus preopticus medialis; PPC, Nucleus principalis precommissuralis; PT, Nucleus pretectalis; PVM, Nucleus periventricularis magnocellularis; S, Septumregion; SCI, Stratum cellulare internum; SL, Nucleus septalis lateralis; SM, Nucleus septalis medialis; TeO, Tectum opticum; TnA, Nucleus taeniae amygdalae; TSM, Tractus septopallio-mesencephalicus; TuO, Tuberculum olfactorium; VP, Pallidum ventrale (modifiziert nach Herold et al., 2012b mit freundlicher Genehmigung von Elsevier).

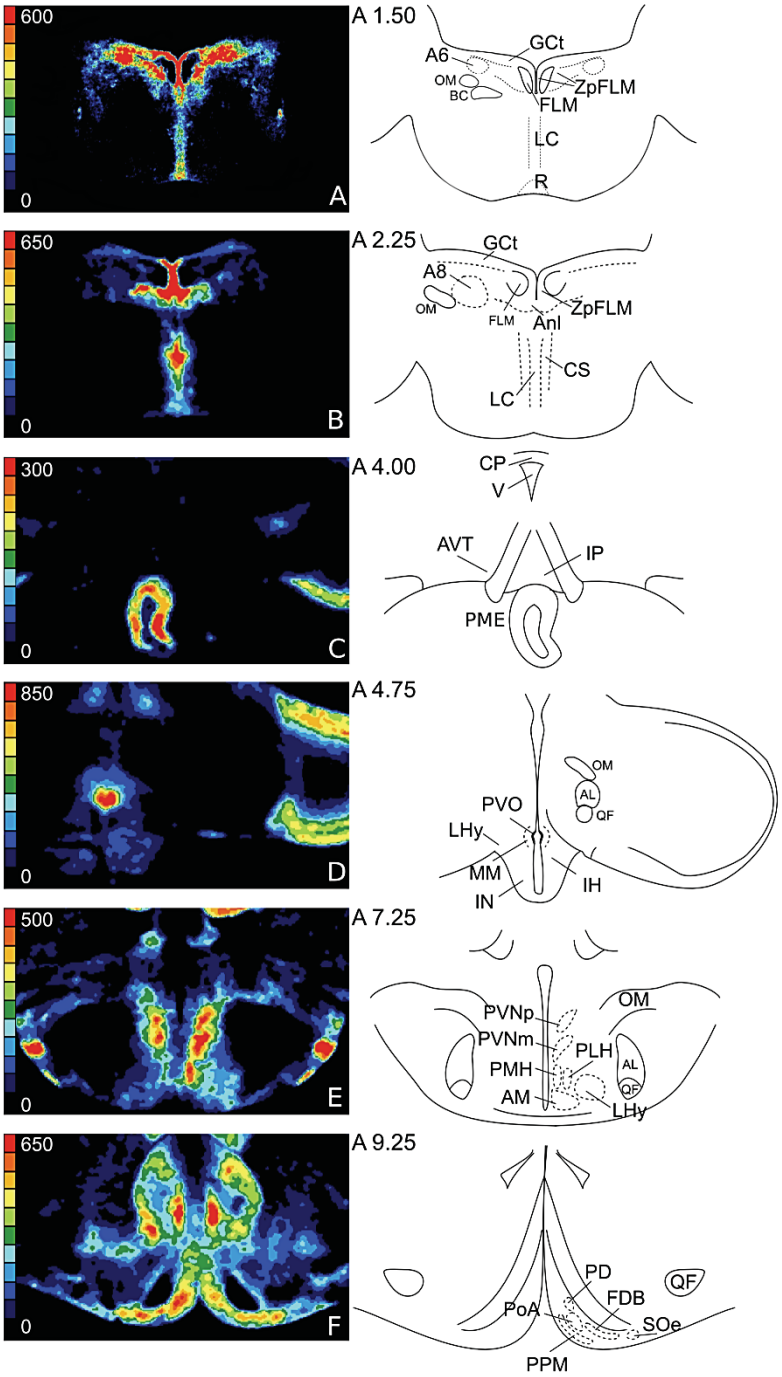

Abbildung 18: Farbkodierte Autoradiogramme der 5-HT_{1A}-Rezeptorverteilung im Hirnstamm und im Hypothalamus der Taube von rostral nach caudal (A-F). Die Farbkodierung zeigt die Dichte der Rezeptoren in fmol/mg Protein an. Die Bilder wurden im Verhältnis zur höchsten Intensität und den vorliegenden Strukturen optimiert und spiegeln daher nicht das Maximum der Rezeptordichten wider. In der rechten Spalte sind die analysierten Strukturen in Form von schematischen Zeichnungen anhand der Atlas-Level A1.50 bis 9.25 nach Karten & Hodos (1967) dargestellt. Die höchsten 5-HT_{1A}-Rezeptordichten im

Hirnstamm wurden im Nucleus annularis (Anl) und der anliegenden Zone des Fasciculus longitudinalis medialis (ZpFLM) detektiert. In der Hypothalamus-Region war die 5-HT_{1A}-Rezeptordichte am höchsten im paraventrikulären Organ (PVO) und im Nucleus preopticus anterior (PoA). A6, Locus coeruleus, Pars caudalis; A8, Locus coeruleus, Pars rostralis; AL, Ansa lenticularis; AM, Arcopallium mediale; Anl, Nucleus annularis; AVT, Area tegmentalis ventralis; BC, Brachium conjunctivum; CP, Commissura posterior; CS, Nucleus centralis superior; FDB, Fasciculus diagonalis Broca; FLM, Fasciculus longitudinalis medialis; GCt, Griseum centrale; IN, Nucleus infundibuli hypothalami; IP, Nucleus interpeduncularis; LC, Nucleus linearis caudalis; LHy, Lateraler Hypothalamus; MM, Nucleus mamillaris medialis; OM, Tractus occipitomesencephalicus; PD, Nucleus preopticus, Pars dorsalis; PLH, Nucleus lateralis hypothalami posterioris; PME, Eminentia mediana posterior; PMH, Nucleus medialis hypothalami posterioris; PoA, Nucleus preopticus anterior; PPM, Nucleus preopticus magnocellularis; PVNm, Nucleus paraventricularis, Pars magnocellularis; PVNp, Nucleus paraventricularis, Pars parvocellularis; PVO, Organum paraventriculare; QF, Tractus quintofrontalis; R, Nucleus raphe pontis; SOe, Nucleus supraopticus externus; V, Ventriculus; ZpFLM, Zona perifasciculus longitudinalis medialis (modifiziert nach dos Santos et al., 2015 mit freundlicher Genehmigung von Elsevier).

Die Idee für die zweite anatomisch-funktionelle Studie entstand zum einen aufgrund der Befunde der Autoradiografie-Studie über die HF in dieser Arbeit (Herold et al., 2014) und zum anderen aufgrund der Befunde bei Säugern. Basierend auf genetischen und Konnektivitäts-Studien ist bekannt, dass die HF innerhalb der rostro-caudalen (bei Primaten) und der dorso-ventralen (bei Nagern) Achse in viele weitere Regionen unterteilbar ist, die an unterschiedlichen Funktionen beteiligt sind (Thompson et al., 2008; Dong et al., 2009; Witter et al., 2017). Diese funktionellen Unterschiede betreffen bei Säugern auch das Vorkommen und die Funktion der adulten Neurogenese (Colombo et al., 1998; Fanselow & Dong, 2010; Strange et al., 2014; Anacker & Hen, 2017). Erste Studien bei Vögeln in Kombination mit Stress-assoziiertem Verhalten führten zu ähnlichen Erkenntnissen (Robertson et al., 2017; Smulders, 2017). Die Befunde bei Säugern weisen darauf hin, dass der dorsale Hippocampus (septaler Pol oder caudal in Primaten) stärker in räumliches Gedächtnis und Navigation eingebunden ist, während der ventrale Hippocampus (temporaler Pol oder rostral in Primaten) eher in emotionales Verhalten, Angst, Stress und kognitive Flexibilität involviert ist (Strange et al., 2014; Anacker & Hen, 2017; Witter et al., 2017). Um diese Zusammenhänge in der HF der Tauben zu untersuchen, wurden zunächst die *Longe-Range*-Verbindungen der HF und der einzelnen Subareale mit Hilfe der 3D-PLI-Mikroskopie in Bezug auf eine topografische Gliederung hin detailliert analysiert. Dies ist das erste Mal gewesen, dass die mögliche Anwendung der 3D-PLI beim Vogelgehirn erfolgreich gezeigt wurde. Außerdem wurden die adulte Neurogenese in der HF sowie Unterschiede in der rostro-caudalen Achse mit Hilfe immunhistochemischer Methoden untersucht. Dazu wurden fünf Atlasebenen $\pm$ 500 µm, wie in Abbildung 19 dargestellt, gewählt (Herold et al., 2019).

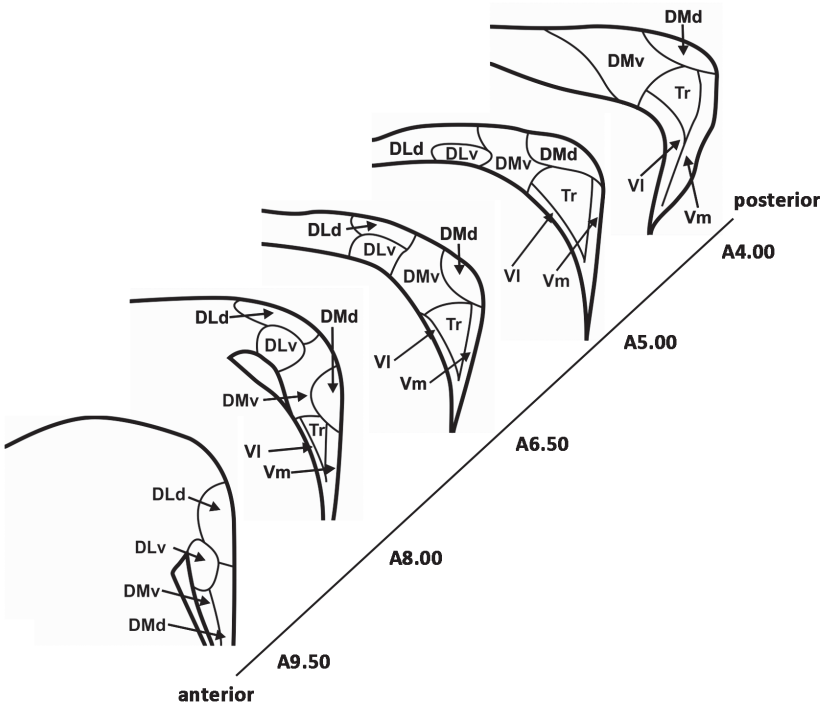

Abbildung 19: Die Hippocampusformation der Taube im Verlauf von rostral nach caudal (nach Herold et al., 2014). Die Atlas-Level beziehen sich auf den Taubenhirnatlas von Karten & Hodos (1967). Die Ebenen wurden bei der Analyse der adulten Neurogenese berücksichtigt. Die Hauptregionen umfassen die V-Region, welche sich aus dem lateralen Zellband (Vl), der triangulären Zwischenregion (Tr) und dem medialen Zellband (Vm) zusammensetzt, die dorsomediale Region (DM) mit den ventralen (DMv) und dorsalen (DMd) Subarealen, und die dorsolaterale Region (DL) mit den ventralen (DLv) und dorsalen (DLd) Subarealen (modifiziert nach Herold et al., 2019 mit freundlicher Genehmigung von Elsevier).

Die Untersuchungen der Konnektivität in sagittalen wie frontalen Schnitten des Taubengehirns zeigten eine topografische Gliederung für die meisten Verbindungen der verschiedenen Subareale der HF entlang der rostro-caudalen Achse, die zuvor noch nicht beschrieben wurde (Abb. 20 und 21).

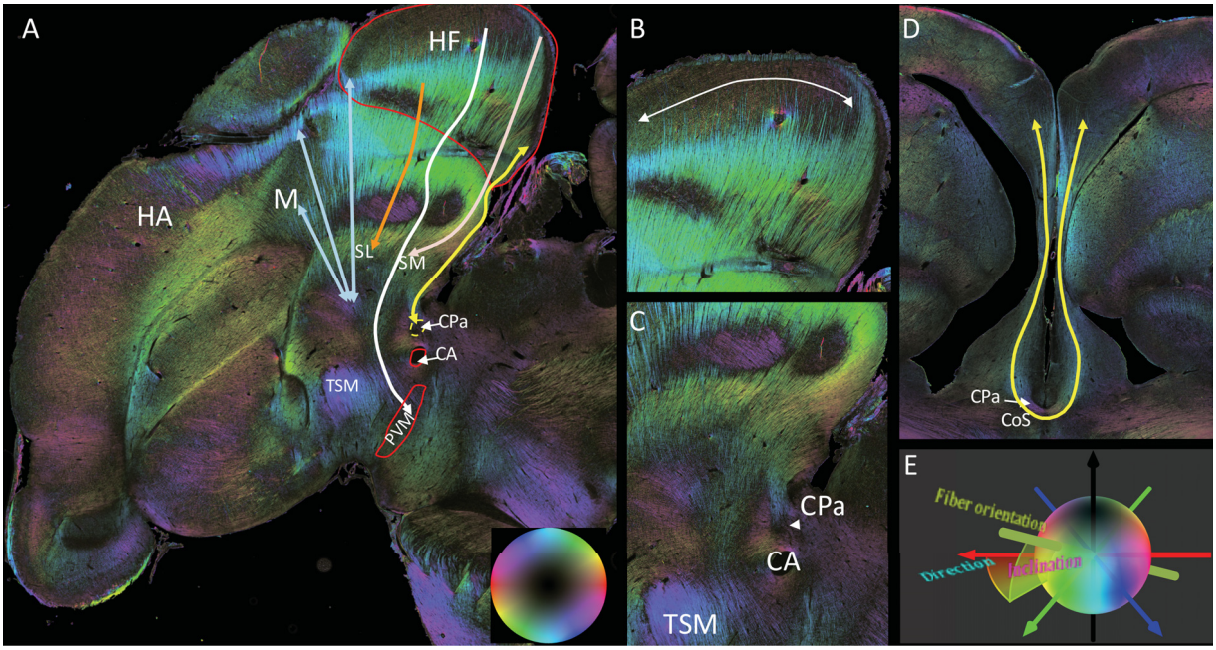

Abbildung 20: Verlauf der *Long-Range*-Verbindungen der Hippocampusformation bei der Taube entlang der rostro-caudalen Achse. A: 3D-PLI Aufnahme eines Sagittalschnitts um das laterale Level Lat 0.00 nahe der interhemisphärischen Fissur/medialen Wand. Der Farbton des Farbkreises zeigt die Richtung der Faserbahnen innerhalb der Schnittebene an. Die Helligkeit/Dunkelheit (peripher/zentral im Farbkreis) spiegelt den Verlauf der Fasern innerhalb/durch die Ebene wider. Rote Linien markieren die Hippocampusformation. Die weiße Linie zeigt eine direkte Verbindung zwischen dem Hypothalamus, dem Nucleus periventricularis magnocellularis (PVM), und der caudalen dorsomedialen Region der Hippocampusformation. Die orange Linie zeigt die hippocampalen-septalen Verbindungen mit dem lateralen Septum (SL) und die rosafarbene Linie mit dem medialen Septum (SM). Der Weg der kommissuralen Fasern, die durch die Commissura pallii (CPa) verlaufen, ist mit einer gelben Linie markiert. Fasern, die aus der äußersten medialen Position des Tractus septopallio-mesencephalicus (TSM) auftauchen und Verbindungen mit der rostralen Hippocampusformation, dem Hyperpallium apicale (HA) und dem Mesopallium (M) zeigen, sind mit hellblauen Linien markiert. Weitere dorsale Verbindungen der Septum-Region gehören zu den Tractus cortico-habenularis et cortico-septalis (CHCS). B: Die V-Region und die ventrale dorsomediale (DMv) Region zeigen eine hohe Dichte dicker Fasern oder Faserbündel, die topografisch organisiert sind und entlang der rostro-caudalen Achse verlaufen, wohingegen in den dorsalen Regionen viele dünne Fasern verlaufen, die die rostralen und caudalen Bereiche verbinden (weiße Linie). C: Vergrößerte Ansicht der Verbindung zwischen PVM und DM und der Organisation der Fasern der CPa und der Septum-Region. D: Visualisierung der CPa in einem Frontalschnitt auf der Atlashöhe A 7.50 (Karten & Hodos, 1967). Wie die Farbumkehrung (weißer Pfeil) zeigt, kreuzen die Fasern der V-Region und der DM-Region zwischen den Hemisphären und ziehen dann auf der anderen Seite wieder nach oben (gelbe Linie). Der Vergleich zwischen den frontalen und sagittalen Schnitten und die Berücksichtigung der Inklinationsbilder zeigt, dass die Fasern topografisch verlaufen. E: Zusätzliche Legende, die die Sinus-Abhängigkeit der 3D-PLI Bilder erklärt. Hemisphärische Faserorientierungen werden durch Farbton, Sättigung und Helligkeit kodiert. Eine Farbveränderung zeigt eine Änderung der Richtung der Fasern an. Bei einer hohen Inklination der Fasern erscheinen sie schwarz. CA, Commissura anterior, CoS, Nucleus commissuralis septi (modifiziert nach Herold et al., 2019 mit freundlicher Genehmigung von Elsevier).

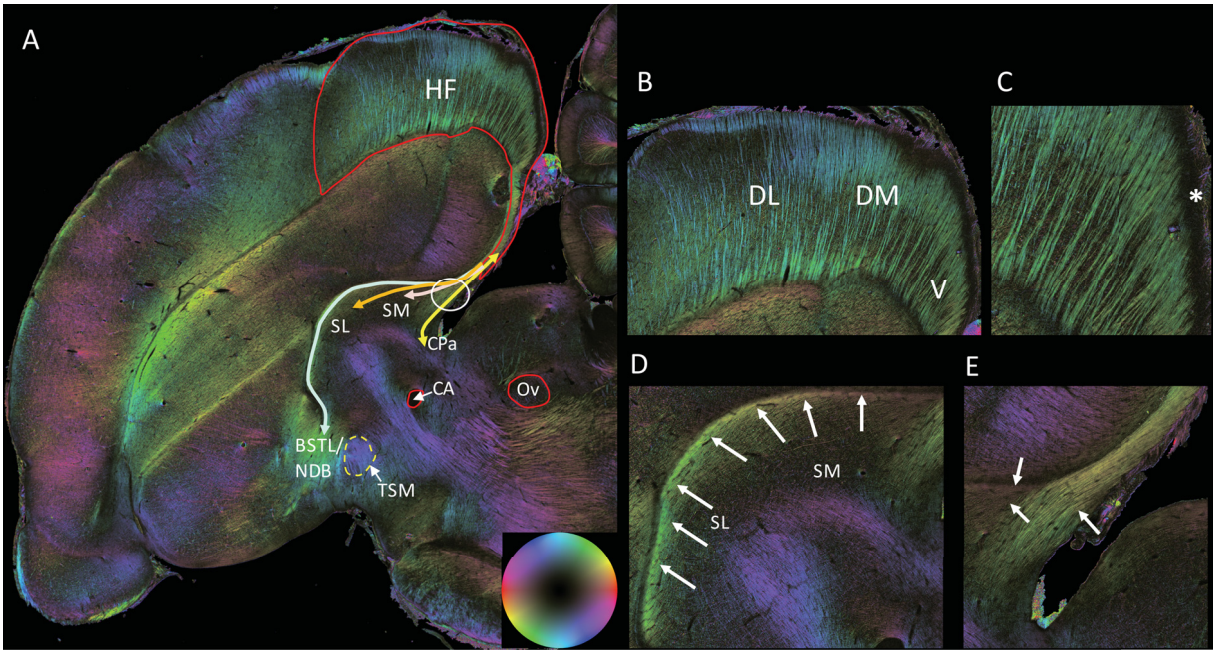

Abbildung 21: 3D-PLI Darstellung der Verbindungen der Hippocampusformation (HF) im Sagittalschnitt in der rostro-caudalen Achse um das Level Lat 0.50. A: In dieser Ebene wurden vier große Bahnen mit Efferenzen und Afferenzen identifiziert, die durch die mediale Wand verlaufen (weißer Kreis). Die hellblaue Linie markiert Fasern zwischen der HF und BSTL und der HF und NDB, die durch den gleichen Pfad laufen. B: Vergrößerte Ansicht der HF, in der die Organisation der Fasern zu erkennen ist, die von der medialen Wand über die V-Region (V), die dorsomediale Region (DM) und die dorsolaterale Region (DL) verlaufen. Die Faserarchitektur folgt der Einteilung der Zyto-/Rezeptorarchitektur der HF. C: Die Vergrößerung der V-Region zeigt, dass es eine superfizielle Bahn am caudalen Pol der HF gibt, die sich entlang des ventromedialen Zellbandes (Vm) zieht (weißes Sternchen). D: Vergrößerte Ansicht der Septum-Region, die den Pfad der Fasern um diese Region herum anzeigt. Die weißen Pfeile zeigen den Pfad der Verbindungen der HF zu BSTL und NDB an. E: Vergrößerte Ansicht in die Region, in der sich die Fasern der Septum-Region und Fasern der CPa vermischen (weiße Pfeile). CA, Commissura anterior; CPa, Commissura pallii; BSTL, Nucleus interstitialis striae terminalis, Pars lateralis; NDB, Nucleus diagonalis Brocae; Ov, Nucleus ovoidalis; SM, Mediales Septum; SL, Laterales Septum; TSM, Tractus septopallio-mesencephalicus (modifiziert nach Herold et al., 2019 mit freundlicher Genehmigung von Elsevier).

Die Resultate dieser Studie zeigten, dass der rostrale Teil der HF mit weiteren Hirnstrukturen verbunden ist, die in visuell-räumliche Verarbeitungsprozesse eingebunden sind. Diese Spezialisierung ist im Vergleich weniger stringent als in der HF der Säuger, ließe sich aber mit der Idee in Einklang bringen, dass man den anterioren Pol bei Vögeln mit dem temporalen Pol bei Säugern vergleichen kann. Ebenso sprechen die Befunde aus den Untersuchungen der Konnektivität dafür, dass man den caudalen Pol mit dem septalen Pol bei Säugern vergleichen kann. Darüber hinaus konnte eine direkte Verbindung der DM-Region der HF zum Nucleus periventricularis magnocellularis (PVM) beschrieben werden. Dieser Kern ist homolog zu Anteilen des Nucleus paraventricularis des Hypothalamus bei Säugern und in die Ausschüttung von Hormonen in der Hypophyse eingebunden. Zusätzlich besitzt der PVM Projektionsneurone die in das limbische System ziehen, ist in die hormonelle Kontrolle von Stress eingebunden, und moduliert den Schlaf-Wach-Rhythmus (dos Santos et al., 2015). Eine weitere Auffälligkeit zeigte sich im Vorkommen vieler longitudinaler Fasern in DM. Im Vergleich zum Säuger ist es somit möglich, dass DM sowohl typische Faserverläufe des Subiculums als auch der CA1/CA3 Region aufweist. In der Folge deutet dies auf eine weitere Unterteilung von DM neben der Unterteilung in DMd und DMv hin, die in der Zukunft genauer untersucht werden muss.

Die quantitative Analyse verschiedener Marker für die adulte Neurogenese (Abb. 22) ergab große Unterschiede in den Subarealen der HF.

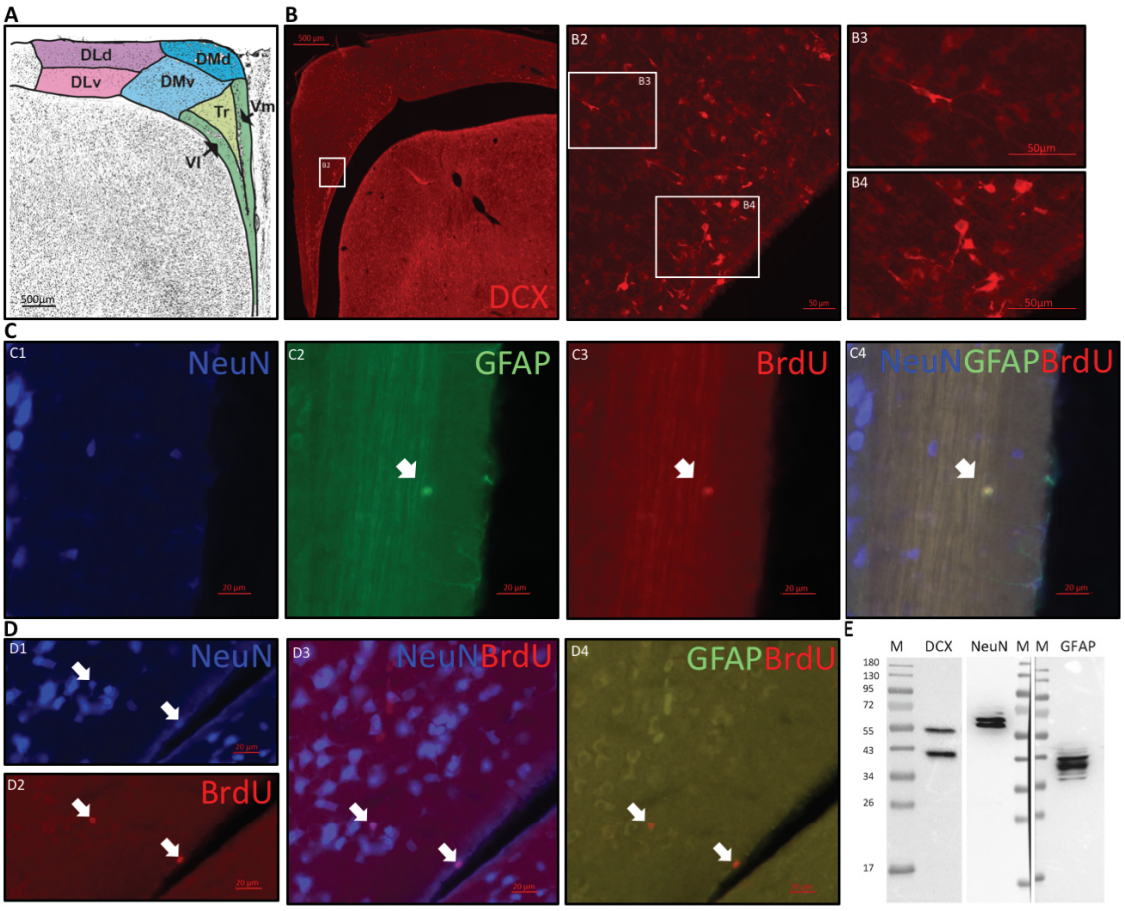

Abbildung 22: Expression verschiedener Markerproteine für adulte Neurogenese in der Hippocampusformation (HF) der Taube. A: Untersuchte Subareale der HF. B: Doublecortin (DCX)-Expression in der HF. In B2 ist ein vergrößerter Ausschnitt zu sehen (weißer Kasten in B). B3 zeigt DCX-positive Zellen, die eine ovoide Form haben (weißer Kasten oben in B2) und B4 zeigt DCX-positive Zellen, die eine trianguläre Form aufweisen. Beide Ausschnitte stammen aus der V-Region. C: Neuron-Nuclei-Marker-Protein (NeuN; C1), saures Gliafaser-Protein (GFAP; C2) und Bromdesoxyuridin (BrdU; C3) Dreifachfärbung in Vm, bei der man in C4 eine doppelgefärbte BrdU/GFAP-Zelle sieht (weißer Pfeil). D: NeuN (D1), GFAP, BrdU (D2) Dreifachfärbung in Vl. In D3 sind doppelgefärbte BrdU/NeuN Zellen zu sehen (weiße Pfeile) und D4 zeigt die Spezifität dieser Markierung, da keine Markierung von GFAP nachzuweisen ist (weiße Pfeile). E: Western-Blots von Hirnproben der Taube um die benutzten Antikörper zu validieren (M, Marker). Sie zeigen die erwarteten Banden zwischen 55-40 kDa (DCX), 72-55 kDa (NeuN) und 43-34 kDa (GFAP). DMv, ventrale dorsomediale Region der HF; DMd, dorsale dorsomediale Region der HF; DLv, ventrale dorsolaterale Region der HF; DLd, dorsale dorsolaterale Region der HF; Tr, Trianguläre Zwischenregion der HF; Vl, ventrolaterales Zellband der HF; Vm, ventromediales Zellband der HF (modifiziert Herold et al., 2019 mit freundlicher Genehmigung von Elsevier).

Die höchsten Werte adulter Neurogenesemarker wurden in der Vl-Region gemessen und stehen in Einklang damit, dass diese zusammen mit anderen Subarealen der V-Region in Teilen vergleichbar zum DG bei Säugern ist, da dort ebenfalls die höchste neuronale Plastizität zu beobachten ist (Kempermann, 2012). In Bezug auf Unterschiede in der rostro-caudalen Achse wurde im Bereich des caudalen Pols ein geringeres Level an unreifen Neuronen in der HF gemessen (Abb. 23; Herold et al., 2019), welches ebenfalls die Hypothese stützen würde, dass der caudale Pol der HF bei der Taube vergleichbar zum ventralen Pol der HF bei Säugern ist.

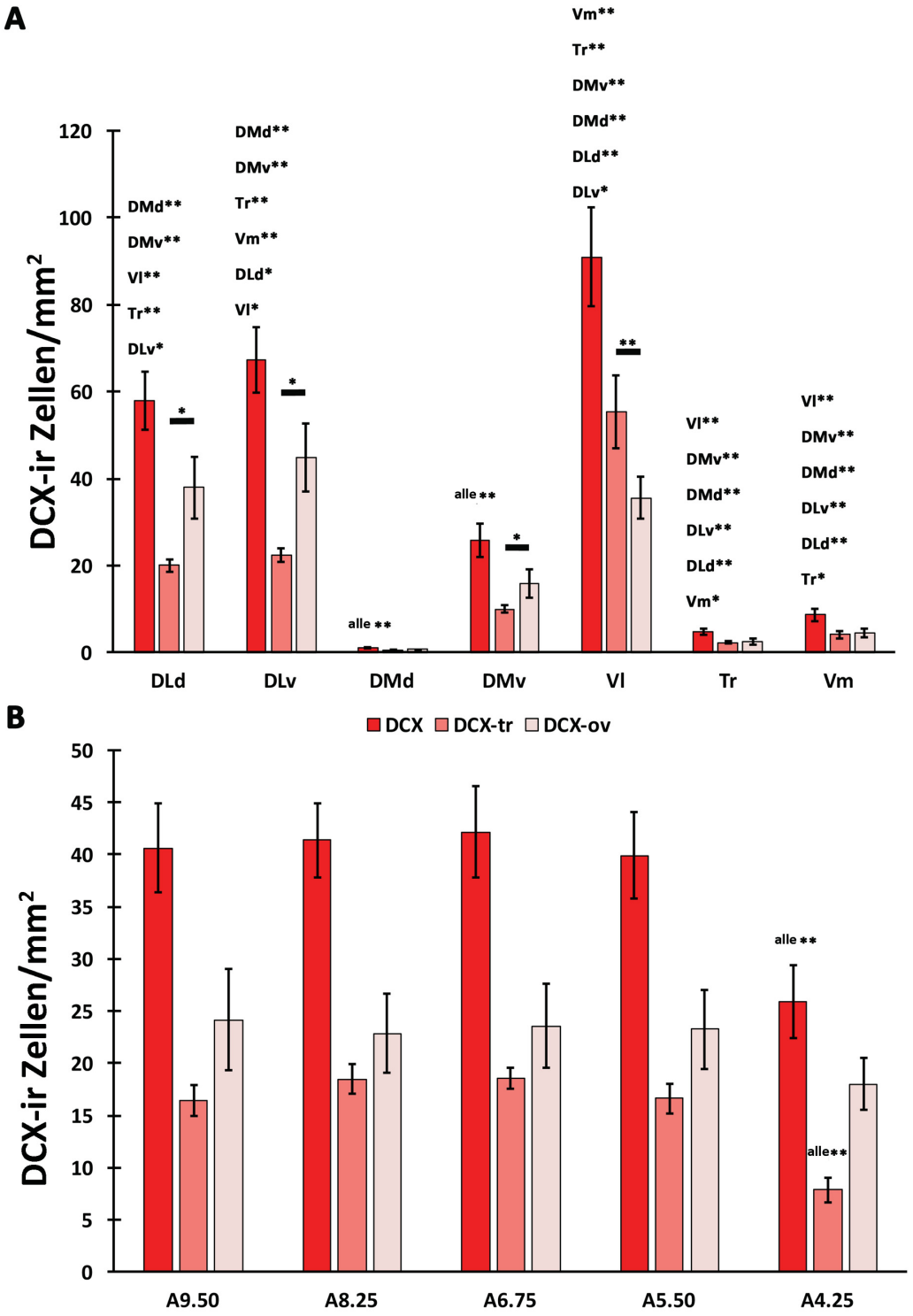

Abbildung 23: Neuronale Plastizität in der adulten Hippocampusformation (HF) der Taube. A: Verteilung der Doublecortin (DCX)- positiven Zellen in verschiedenen Regionen der HF (n=9). B: DCX-positive Zellen in der HF entlang der rostro-caudalen Achse unter Berücksichtigung der verschiedenen Neuronentypen, die ein DCX-positives Signal zeigen: DCX-triangulär (DCX-tr) und DCX-ovoid (DCX-ov). Die Balken entsprechen dem Standardfehler. Sternchen markieren signifikante Unterschiede (*p<0.05; **p<0.01). DLd, dorsale dorsolaterale Region der HF; DLv, ventrale dorsolaterale Region der HF; DMd, dorsale dorsomediale Region der HF; DMv, ventrale dorsomediale Region der HF; Tr, Trianguläre Zwischenregion der HF; Vl, ventrolaterales Zellband der HF; Vm, ventromediales Zellband der HF (modifiziert nach Herold et al., 2019 mit freundlicher Genehmigung von Elsevier).

Darüber hinaus wurde gezeigt, dass im Verlauf der rostro-caudalen Achse die Anzahl neu entstandener Gliazellen in Vl abnimmt (Abb. 24).

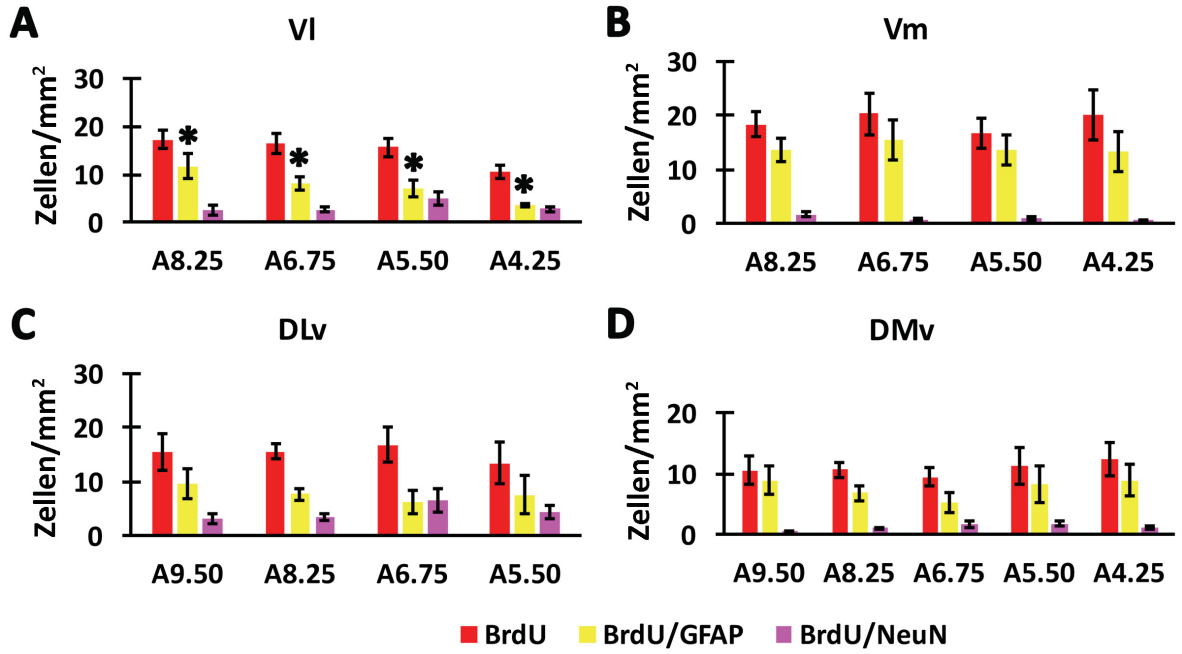

Abbildung 24: Verteilung der Bromdesoxyuridin (BrdU)-markierten Zellen in den Subarealen der Hippocampusformation (HF), die eine moderate bis hohe Plastizität entlang der rostro-caudalen Achse zeigten. Nur BrdU/saures Gliafaserprotein (GFAP)-positive Zellen in Vl zeigten eine immer geringer werdende Anzahl in Richtung des caudalen Pols. Die Balken entsprechen dem Standardfehler. Sternchen markieren signifikante Unterschiede (*p<0.05). DLv, ventrale dorsolaterale Region der HF; DMv, ventrale dorsomediale Region der HF; Vl, ventrolaterales Zellband der HF; Vm, ventromediales Zellband der HF (modifiziert nach Herold et al., 2019 mit freundlicher Genehmigung von Elsevier).

Dieser Aspekt ist vollkommen neu und wurde bisher bei Vögeln noch nicht untersucht. Beide Befunde zur Neuro- und zur Gliogenese deuten darauf hin, dass es bei Vögeln tatsächlich eine regionale und funktionelle Spezialisierung der Subregionen entlang der rostro-medialen zur caudo-lateralen HF gibt. Im Unterschied zu der HF beim Säuger, in der die adulte Neurogenese hauptsächlich auf den DG beschränkt ist, zeigte die HF bei Vögeln allerdings in allen Subarealen eine hohe neuronale Plastizität. Dies wurde bereits auch für Knochenfische (*Osteichthyes*), Reptilien (als Ausschlusstaxon definiert) und Amphibien (*Lissamphibia*) gezeigt und gilt auch für weitere Strukturen außerhalb der HF der Vögel (Melleu et al., 2013; Ernst & Frisen, 2015). Die Unterschiede in den verschiedenen Wirbeltierklassen deuten darauf hin, dass das Vogelgehirn plastischer ist, sich möglicherweise im adulten Stadium stärker weiterentwickelt und dadurch schneller auf Veränderungen in der Umwelt reagieren kann.
In Bezug auf die Evolution der HF unterstreichen die Ergebnisse der vorliegenden Arbeit, dass sich die HF sowohl bei Vögeln als auch bei Säugern deutlich von der basalen Form einer HF in anderen Landwirbeltierklassen, wie Amphibien oder Reptilien, sowie auch innerhalb der Überklasse der Kiefermäuler (*Gnasthostomata*), zu der auch die Knochenfische zählen, diversifiziert hat (Striedter, 2016; Bingman & Muzio, 2017). Von den Landwirbeltieren (Tetrapoda) spalteten sich phylogenetisch gesehen dabei nach heutigem Erkenntnisstand zuerst die Amphibien ab, noch bevor es innerhalb der Amnioten zur Aufspaltung in zwei Hauptlinien kam: Synapsida (rezent Mammalia) und Sauropsida (rezent Lepidosauromorpha

und Archosauromorpha; Abb. 2). Innerhalb des Taxons der Archosauria entwickelten sich zwei weitere Gruppen, die Crurotarsi, zu der die Krokodile gehören, und die Ornithodira, die als Klade definiert ist, die den letzten gemeinsamen Vorfahren von Flugsauriern und Dinosauriern umfasst. Die Vögel sind dabei ein Entwicklungszweig der Dinosaurier und somit die einzige rezente Wirbeltierklasse dieser Klade. Im Vergleich zu der basalen Form der HF, die vermutlich auch bei den Ur-Amnioten zu finden war, ist die HF bei Vögeln und Säugern jedoch viel voluminöser, weist eine andere Zytoarchitektur auf und ist in komplexe Verschaltungsmuster eingebunden (Striedter, 2016; Bingman & Muzio, 2017). Zudem nimmt die HF in den verschiedenen Wirbeltierklassen im Zuge der Entwicklung des Cortex eine andere Position im Gehirn ein. Im Vergleich zu Reptilien, bei denen man eine dreischichtige hippocampale Struktur vorfindet, hat die HF bei Vögeln sich stark vergrößert und eine zelluläre (kernähnliche) Struktur gebildet, die möglicherweise eine Reduktion der Schichtung zur Folge hatte (Hevner, 2016; Striedter, 2016; Bingman & Muzio, 2017). Bei Säugern ist die Laminierung der HF abhängig von den Cajal-Retzius Zellen, welche während der Hirnentwicklung der Vögel vor allem im medialen Pallium zu finden sind (Nomura et al., 2009). Im Gegensatz zu den Säugern, aber auch zu den Eidechsen (*Lacertidae*), die zur Klasse der Reptilien zählen, wandern die Cajal-Retzius Zellen und auch andere Progenitorzellen bei Vögeln jedoch scheinbar nicht in eine dorsale Position (Cabrera-Socorro et al., 2007; Garcia-Moreno et al., 2018), so dass dieser Einfluss auf die Entwicklung einer Laminierung hier entfällt. Dies und die Expansion der HF könnten eine mögliche Ursache dafür sein, warum sich die Morphologie der V-Region im Verlauf der rostro-caudalen Achse so unterscheidet, da sich bei Vögeln große Anteile der HF aus einer weiter dorsalen Position entwickeln. Am caudalen Ende der HF bei Vögeln existiert nämlich noch eine trilaminäre Struktur, deren Zellband sich im weiteren Verlauf nach rostral und dorsal aufteilt und so die Tr-Region einschließt und die V-Region bildet (Abb. 25; Herold et al., 2019).

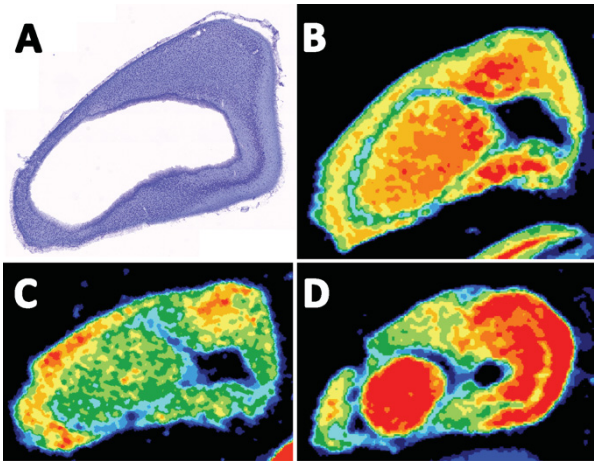

Abbildung 25: Die V-Region in der caudalen Hippocampusformation der Taube. A: Nissl-Färbung, die die dreischichtige Struktur der V-Region in einem Frontalschnitt am caudalen Ende der HF auf Höhe der Atlas-Level A 3.50-3.25 zeigt. B-D: glutamaterge AMPA- (B), Kainat- (C) und NMDA- (D) Rezeptor-Verteilung in der caudalen V-Region (nicht gezeigte zusätzliche Ebenen aus der Studie Herold et al., 2014). Die farbkodierten Autoradiogramme spiegeln die Rezeptordichten in fmol/mg Protein wider. Die Skalen sind verschieden. Rot bedeutet hohe und blau bedeutet niedrige Rezeptordichten (modifiziert nach Herold et al., 2019 mit freundlicher Genehmigung von Elsevier).

Aktuelle genetische Einzelzell-Analysen im sich entwickelnden Reptiliengehirn legen nahe, dass es höchstwahrscheinlich schon bereits vor 350 Millionen Jahren eine Anlage für den DG und die CA-Felder gab (Tosches et al., 2018). Die Untersuchungen der HF bei Vögeln deuten daher darauf hin, dass die Morphologie dieser Strukturen sich im Verlauf der getrennten

Evolution stark verändert und selektiv angepasst hat, während die funktionellen Verbindungen größtenteils konserviert wurden. Vögel haben es so in einer hoch kompetitiven Umgebung geschafft, außerordentliche kognitive Fähigkeiten zu entwickeln, ohne dabei laminierte Hirnstrukturen, wie sie für das Pallium der Säuger typisch sind, auszubilden. Die vorgefundene erhöhte Plastizität könnte unter Umständen zusätzlich ein Selektionsvorteil im Rahmen dieser (Um-?) Strukturierung sein, der auch weitere Hirnbereiche im Telencephalon der Vögel betrifft.

3.3 Die Abgrenzung einzelner Nuclei im Arcopallium/Amygdala-Komplex der Taube (Herold et al., 2018b)

Der Arcopallium/Amygdala-Komplex besteht aus einer Kerngruppe im ventralen Pallium der Vögel, dessen Herkunft und Funktion aufgrund der Heterogenität dieses Kerngebietes noch nicht vollständig geklärt ist (Abb. 26; Herold et al., 2018b).

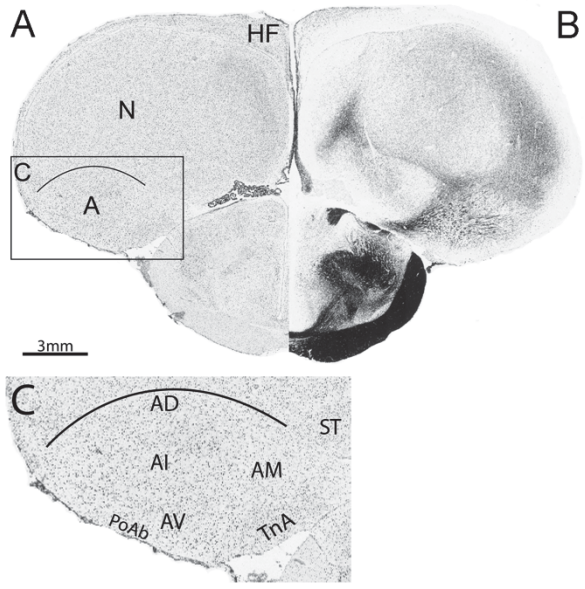

Abbildung 26: Nissl- und Myelin-gefärbte Frontalschnitte des Taubengehirns. A: Nissl- und B: Myelin-gefärbter Schnitt auf der Höhe des Atlas-Levels 6.75 (Karten & Hodos, 1967). Der Kasten markiert den Arcopallium/Amygdala-Komplex. Maßstab: 3mm. C: Vergrößerte Ansicht des Arcopallium/Amygdala-Komplexes, der in A markiert ist. A, Arcopallium; AD, Arcopallium dorsale; AI, Arcopallium intermedium; AM, Arcopallium mediale; AV, Arcopallium ventrale; HF, Hippocampusformation; N, Nidopallium; PoAb, Nucleus posterioris amygdalopallii, Pars basalis; ST, Striatum; TnA, Nucleus taeniae amygdalae (modifiziert nach Herold et al., 2018b mit freundlicher Genehmigung von Wiley Periodicals, Inc.).

Auf der Basis genetischer, funktioneller, entwicklungsbiologischer und neurochemischer Studien ist es höchstwahrscheinlich, dass dieser Komplex zum Großteil aus Kerngebieten besteht die in ihrer Funktion dem prämotorischen Cortex gleichen, während nur ein kleiner Anteil vergleichbar zur Amygdala ist. Teile des Komplexes sind in Lern- und Gedächtnisprozesse involviert, und dabei in unterschiedliche Netzwerke eingebunden (Shanahan et al., 2013). Um dies in der Zukunft spezifischer untersuchen zu können, wurde in dieser Arbeit die Zyto-, Myelo- und Rezeptorarchitektur detailliert analysiert, und ein neuer Atlas dieser Region für die Taube erstellt (Abb. 27; Herold et al., 2018b). Neuste Studien zeigen darüber hinaus spezies-spezifische Abweichungen bei anderen Vogelarten wie z.B. dem Zebrafinken (*Taeniopygia guttata*), der zur Ordnung der Sperlingsvögel (*Passeriformes*) zählt (Mello et al., 2019).

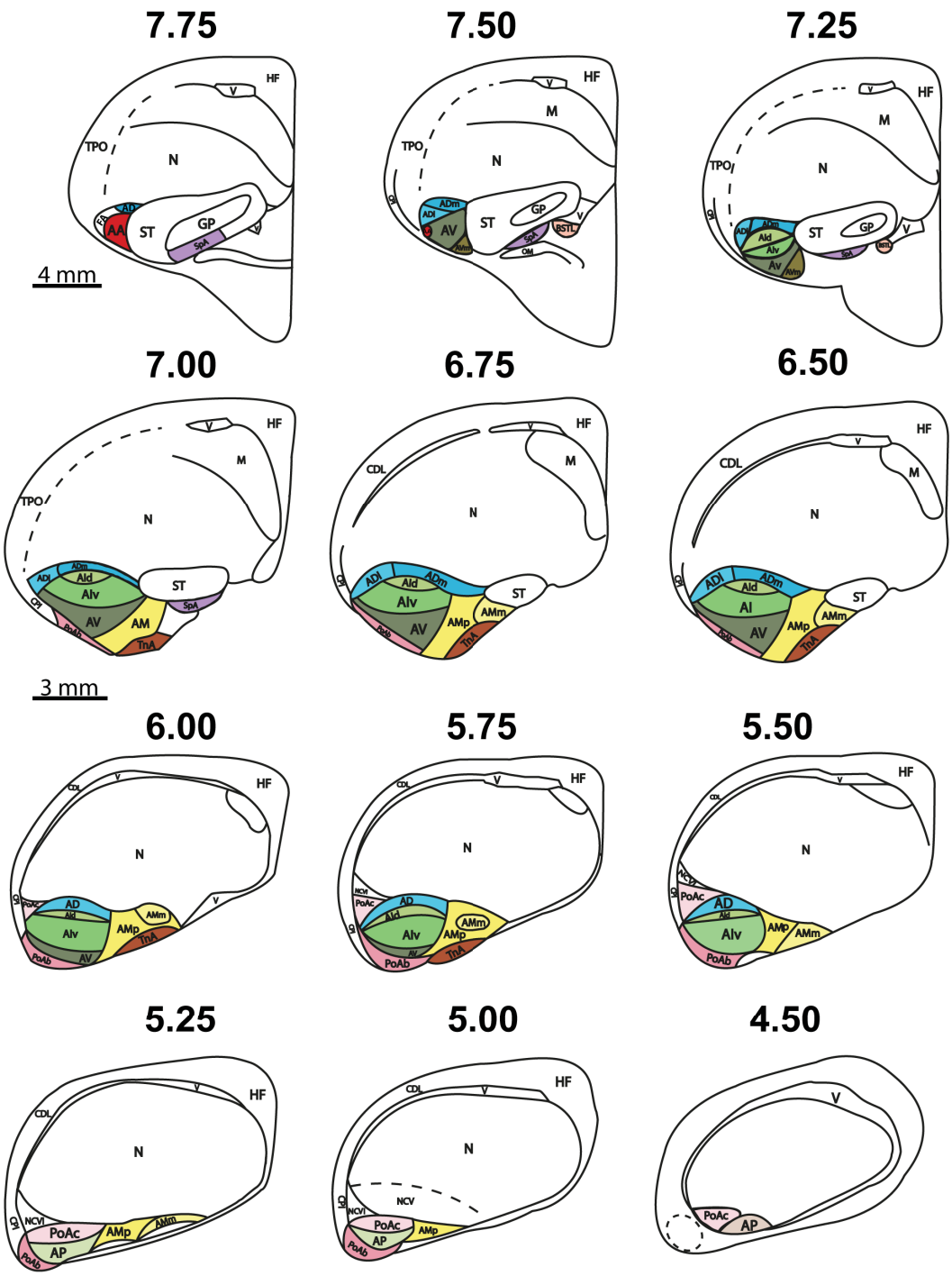

Abbildung 27: Schematischer Atlas des Arcopallium/Amygdala-Komplexes der Taube in einer Serie von Frontalschnitten. Der Atlas basiert auf den beobachteten und gemessenen Unterschieden in der Zyto-, Myelo- und Rezeptorarchitektur. Die Atlas-Level korrespondieren zu den rostro-caudalen Leveln A 7.75 bis A 4.50 (Karten & Hodos, 1967). AA, Arcopallium anterius; AD, Arcopallium dorsale; ADl, Arcopallium dorsale, Pars lateralis; ADm, Arcopallium dorsale, Pars medialis; AI, Arcopallium intermedium; Ald, Arcopallium intermedium, Pars dorsalis; Alv, Arcopallium intermedium, Pars ventralis; Alvm, Arcopallium intermedium, Pars ventromedialis; AM, Arcopallium mediale; AMm, Arcopallium mediale, Pars magnocellularis; AMp, Arcopallium mediale, Pars parvocellularis; AP, Arcopallium posterior; AV, Arcopallium ventrale; AVm, Arcopallium ventrale, Pars medialis; BSTL, Nucleus interstitialis striae terminalis, Pars lateralis; CDL, Area corticoidea dorsolateralis; CPi, Cortex piriformis; FA, Tractus fronto-arcopallialis; GP, Globus pallidus; HF, Hippocampusformation; LSt, Striatum laterale; M, Mesopallium; N, Nidopallium; NCV, Nidopallium caudoventrale; NCVl, Nidopallium caudoventrale, Pars lateralis; OM, Tractus occipitomesencephalicus; PoAb, Nucleus posterioris amygdalopallii, Pars basalis; PoAc, Nucleus posterioris amygdalopallii, Pars compacta; SpA, Area subpallialis amygdalae; ST, Striatum; TnA, Nucleus taeniae amygdalae; TPO, Area temporo-parieto-occipitalis; V, Ventriculus (modifiziert nach Herold et al., 2018b mit freundlicher Genehmigung von Wiley Periodicals, Inc.).

Die Clusteranalyse der Rezeptordichten der einzelnen Kerngebiete des Arcopallium/Amygdala-Komplexes und umliegender Strukturen ergab zwei Hauptcluster (Abb. 28).

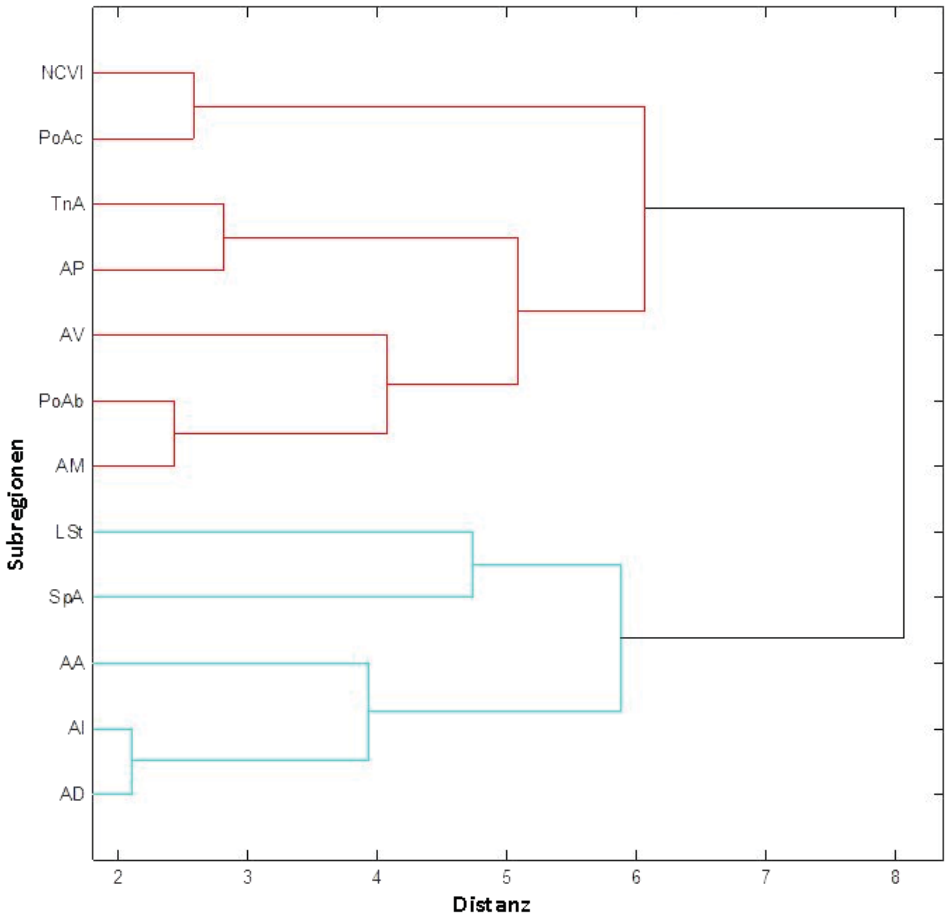

Abbildung 28: Clusteranalyse zwischen den gemessenen Rezeptordichten in den unterschiedlichen und benachbarten Regionen des Arcopallium/Amygdala-Komplexes. X-Achse: Euklidische Distanz. Y-Achse: Subregionen. Das Kladogramm zeigt zwei Hauptcluster (rot und blau) mit weiteren Untergruppen mit verschiedenen Abzweigungen (kophenetischer Korrelationskoeffizient c= 0.60). AA, Arcopallium anterius; AD, Arcopallium dorsale; AI, Arcopallium intermedium; AM, Arcopallium mediale; AP, Arcopallium posterior; AV, Arcopallium ventrale; LSt, Striatum laterale; NCVl, Nidopallium caudoventrale, Pars lateralis; PoAb, Nucleus posterioris amygdalopallii, Pars basalis; PoAc, Nucleus posterioris amygdalopallii, Pars compacta; SpA, Area subpallialis amygdalae; TnA, Nucleus taeniae amygdalae (modifiziert nach Herold et al., 2018b mit freundlicher Genehmigung von Wiley Periodicals, Inc.).

Innerhalb dieser Cluster wurden weitere Untergruppen entdeckt. Im „(prä-)motorischen Cluster“ werden AA, AI und AD zusammengefasst, wobei AA separiert ist, sowie die Untergruppe aus LSt und SpA. LST und SpA sind mit motorischen und affektiven Funktionen verknüpft, und beide Strukturen sind subpallialer Herkunft. Im „limbischen Cluster“ bilden die analysierten Kerngebiete drei Untergruppen. Hier können PoAb, AM und AV zusammengefasst werden, wobei AV separiert ist, TnA und AP bilden eine weitere Untergruppe, die eine nähere Beziehung zur ersten Gruppe hat, und damit nochmals getrennt von PoAc und NCVl dargestellt wird, welche die dritte Untergruppe im „limbischen“ Cluster bilden (Abb. 28). Aufgrund der neuen Kartierung ist der funktionelle Vergleich mit vorausgegangen Studien erschwert. AA, AI und AD befinden sich im Rahmen der funktionellen

Netzwerkanalyse von Shanahan und Kollegen (2013) im assoziativen prämotorischen Modul, in dem AI und AD eine zentrale Stellung einnehmen. Dies steht in Einklang damit, dass AA auf Basis der Rezeptorarchitektur innerhalb der Untergruppe separiert werden kann und AI und AD eine weitere Subgruppe bilden (Herold et al., 2018b). Alle Strukturen im „limbischen Cluster“, sind nach aktuellem Forschungsstand mit Funktionen des limbischen Systems verknüpft. Die Separierung von AV innerhalb der Untergruppe mit AM und PoAb findet sich auch in der Netzwerkanalyse wieder (Shanahan et al., 2013). AV zählt dort jedoch zum präfrontalen assoziativen Modul, wohingegen PoA und AM im viscero-limbischen Modul eingeordnet sind. Eine Unterteilung in PoAb und PoAc erfolgte dort nicht. AP wurde ebenfalls nicht analysiert und wurde in unserer Studie zum ersten Mal definiert (Herold et al., 2018b). Die Rezeptoranalyse zeigt eine stärkere Beziehung von TnA und AP zu der ersten Untergruppe, verglichen mit der dritten Untergruppe NCVl und PoAc (Abb. 28). NCVl und PoA befinden sich in der Netzwerkanalyse im viscero-limbischen Modul, TnA im cortico-hippocampalen Modul (Shanahan et al., 2013). Alleine diese Unterschiede machen deutlich, wie wichtig es ist anatomisch gut definierte Hirnkarten vorzulegen. Dies erlaubt es funktionelle Zusammenhänge innerhalb einer Spezies sowie zwischen verschiedenen Spezies zu prüfen, und so ein besseres Verständnis für die Funktionen und mögliche Funktionsausfälle zu erhalten.

In der vergleichenden Analyse zum Rattengehirn ließen sich auf Basis der Rezeptoranalyse sowohl Ähnlichkeiten mit der Amygdala der Ratte als auch zwischen den arcopallialen Kernen und dem (prä-)motorischen Cortex und dem Inselcortex der Ratte finden (Abb. 29; Herold et al., 2018b). In Abbildung 29 sind die Rezeptoren gezeigt, die regionsspezifische Unterschiede bei der Ratte in der Amygdala und im Cortex aufweisen, und deren Expression im relativen Verhältnis eine hohe Vergleichbarkeit zwischen der Taube und der Ratte zeigte. Da die Expression von Rezeptoren in der Amygdala bei Säugern neben den vergleichbaren Mustern ebenfalls spezies-spezifische Unterschiede zeigt, und die Amygdala auch bei Säugern eine sehr heterogene Struktur mit pallialen und subpallialen Anteilen ist, wird anhand des Vergleiches deutlich, dass in Kombination mit der Rezeptoranalyse weitere Daten, z.B. über die Konnektivität, erfasst werden müssen, um genauere Aussagen treffen zu können. Diese Daten müssten im besten Fall kombiniert mit elektrophysiologischen Studien und auf Einzelzellebene analysiert werden sowie dazu weitere Transkriptomanalysen erfolgen sollten. Bei Säugern hat man z.B. innerhalb der Amygdala Netzwerke analysiert und festgestellt, dass sich in einem einzigen Kerngebiet parallel lokale Netzwerke ausbilden können, die unterschiedliche Funktionen wie z.B. die Modulation von Belohnung und Angst steuern (Janak & Tye, 2015). In der vorliegenden Arbeit ließen sich die meisten Gemeinsamkeiten zwischen PoAc und TnA im Vergleich zur lateralen bzw. medialen, lateralen und basolateralen Amygdala der Säuger finden (Herold et al., 2018b).

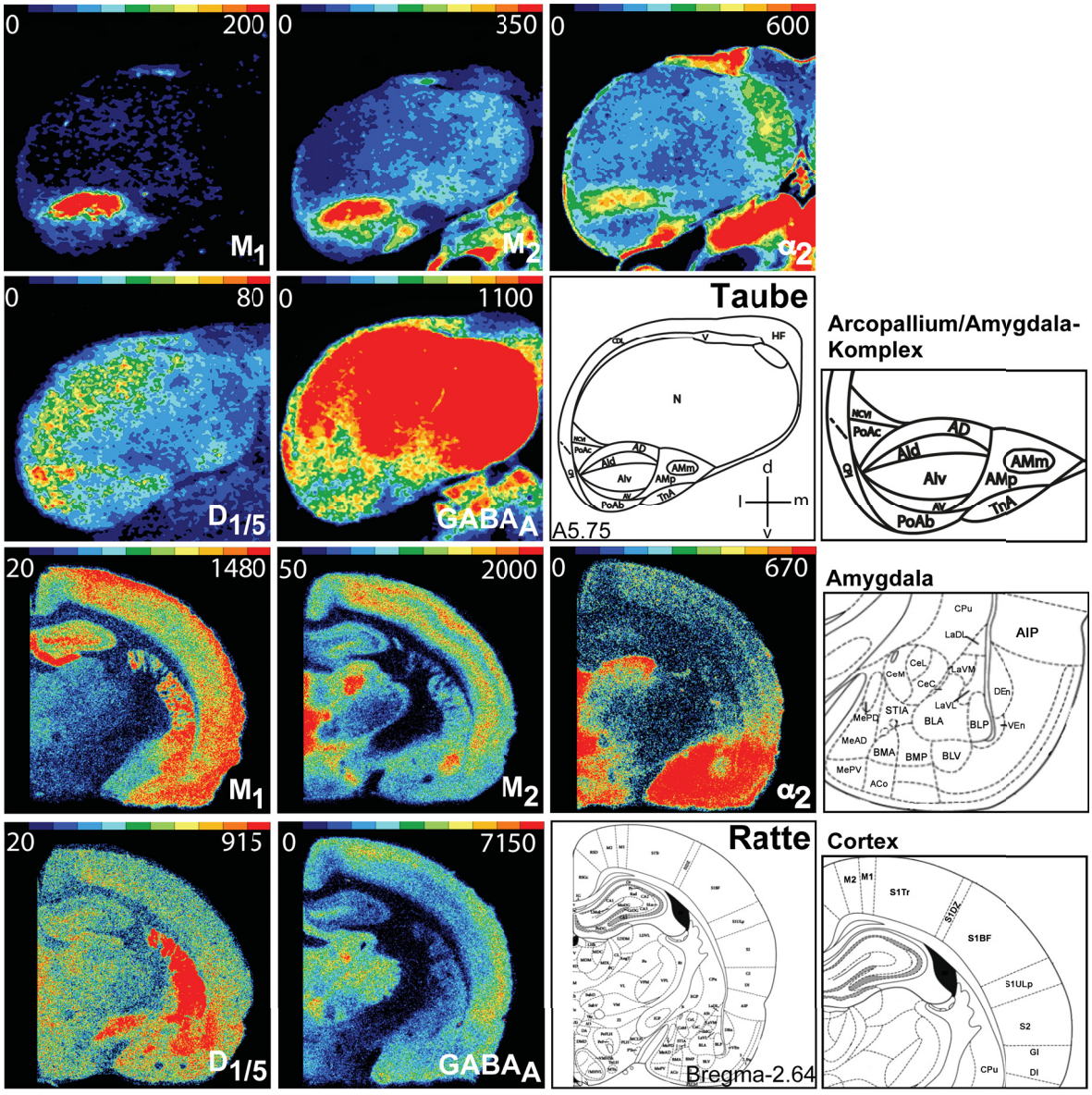

Abbildung 29: Vergleich der Verteilung verschiedener Rezeptoren zwischen dem Arcopallium/Amygdala-Komplex der Taube auf Höhe des Atlas-Levels 5.75 (Karten & Hodos, 1967) und der Amygdala sowie verschiedenen Cortex-Arealen bei der Ratte auf Höhe des Atlas-Levels Bregma -2.64 (Paxinos & Watson, 2005). Die Farbkodierung zeigt die Dichte der GABAergen $GABA_A$-Rezeptoren, muskarinergen M_1- und M_2-Acetylcholinrezeptoren, noradrenergen α_1- und α_2-Rezeptoren und dopaminergen $D_{1/5}$-Rezeptoren in fmol/mg Protein an. Die Bilder wurden im Verhältnis zur höchsten Intensität und den vorliegenden Strukturen optimiert und spiegeln daher nicht das Maximum der Rezeptordichten wider. Taube: AD, Arcopallium dorsale; AId, Arcopallium intermedium, Pars dorsalis; AIv, Arcopallium intermedium, Pars ventralis; AIvm, Arcopallium intermedium, Pars ventromedialis; AMm, Arcopallium mediale, Pars magnocellularis; AMp, Arcopallium mediale, Pars parvocellularis; AV, Arcopallium ventrale; CDL, Area corticoidea dorsolateralis; CPi, Cortex piriformis; d, dorsal; HF, Hippocampusformation; l, lateral; m, medial; N, Nidopallium; NCVl, Nidopallium caudoventrale, Pars lateralis; PoAb, Nucleus posterioris amygdalopallii, Pars basalis; PoAc, Nucleus posterioris amygdalopallii, Pars compacta; TnA, Nucleus taeniae amygdalae; v, ventral; V, Ventrikel; Ratte: ACo, Amygdala, Nucleus corticalis anterior; AIP, Area insularis agranularis posterior; BLA, Amygdala, Nucleus basolateralis, Pars anterior; BLP, Amygdala, Nucleus basolateralis, Pars posterior; BLV, Amygdala, Nucleus basolateralis, Pars ventralis; BMA, Amygdala, Nucleus basomedialis, Pars anterior; BMP, Amygdala, Nucleus basomedialis, Pars posterior; CPu, Nucleus caudatus/Putamen; CeC, Amygdala, Nucleus centralis, Pars capsularis; CeM, Amygdala, Nucleus centralis, Pars medialis; CeL, Amygdala, Nucleus centralis, Pars lateralis; DEn, Nucleus endopiriformis dorsalis; VEn, Nucleus endopiriformis ventralis; DI, Cortex insularis dysgranularis; GI, Cortex insularis granularis; LaDL, Amygdala, Nucleus lateralis, Pars dorsolateralis; LaVL, Amygdala, Nucleus lateralis, Pars ventrolateralis; LaVM, Amygdala, Nucleus lateralis, Pars ventromedialis; M1, Motorcortex, primär; M2, Motorcortex, sekundär; MeAD, Amygdala, Nucleus medialis, Pars anterodorsalis; MePD, Amygdala, Nucleus medialis, Pars posterodorsalis; MePV, Amygdala, Nucleus medialis, Pars posteroventralis; S1, Somatosensorischer Cortex, primär; S2, Somatosensorischer Cortex, sekundär; STIA, Nucleus intersitialis

striae terminalis, Pars intra-amygdaloideum (modifiziert nach Herold et al., 2018b mit freundlicher Genehmigung von Wiley Periodicals, Inc.).

Durch die Rezeptoranalyse der arcopallialen Strukturen im Vergleich zu verschiedenen Cortex-Arealen der Ratte fanden sich bei Betrachtung der M_1-, M_2-, $D_{1/5}$-, α_2- und $GABA_A$-Rezeptorverteilungen Übereinstimmungen von AA, AD, AI, AV und AP mit den (prä-) motorischen Arealen FR1 (M1), FR2 (M2) und den Inselcortex-Arealen AIP, GI, DI bei der Ratte. Demnach scheinen hier Parallelen zwischen den pallialen Strukturen zu existieren, die in einem funktionellen Zusammenhang stehen könnten. Jedoch konnten keine genaueren Aussagen getroffen werden, welche arcopallialen Areale genau als korrespondierend zu den Cortex-Arealen betrachtet werden könnten, da gleichzeitig auch viele Unterschiede existierten. Die hier untersuchten pallialen Strukturen bei der Taube und bei der Ratte scheinen sich demnach eher konvergent entwickelt zu haben und sind möglicherweise ein Resultat der getrennten, parallelen Evolution sowie Adaptionen.
Insgesamt lässt sich daher festhalten, dass die Heterogenität des Arcopallium/Amygdala-Komplexes eine große Herausforderung für Vergleichsstudien darstellt, obwohl funktionell viele Gemeinsamkeiten existieren. Der hier erstellte Atlas nimmt daher in zukünftigen vergleichenden Studien einen hohen Stellenwert ein, der sowohl innerhalb der verschiedenen Vogelordnungen, z.B. im Vergleich zu den Sperlingsvögeln (*Passeriformes*), bei denen der Komplex unter anderem in das *„Song"- (*„Sprach"-) System eingebunden ist als auch zwischen Säugern oder weiteren Wirbeltierklassen funktionell berücksichtigt werden muss.

4. Resümee und Ausblick

Die hier beschriebenen Arbeiten zeigen auf, dass es neurochemische und strukturelle Gemeinsamkeiten zwischen Vogel- und Säugerhirnen gibt, obwohl der zytoarchitektonische Aufbau der Gehirne verschieden ist. Diese Gemeinsamkeiten lassen sich insbesondere in den Arealen finden, die funktionell an Lern- und Gedächtnisprozessen beteiligt sind und liefern grundlegende Erkenntnisse, um die Basis für intelligentes Verhalten besser zu verstehen und diese noch intensiver zu erforschen. Auf der anderen Seite existieren auch Unterschiede, welche nicht nur die Laminierung der pallialen Hirnregionen, sondern auch die molekulare Zusammensetzung innerhalb der Strukturen betreffen, und die im Zuge einer mehr als 300 Millionen Jahre getrennt ablaufenden Evolution verdeutlichen, dass die Gehirne der verschiedenen Wirbeltierklassen sich weiterentwickeln und Evolution im Rahmen von Selektionsprozessen nach wie vor stattfindet. Gleichzeitig stellt sich dadurch die hochinteressante Frage, wieviel Spielraum im Rahmen des Hirnaufbaus möglich ist und welche anderen Optionen ein Organismus hat, um hohe kognitive Leistungen zu erzielen. In der Gänze könnte dieses Wissen gerade in Bezug auf die Entwicklung von theoretischen Lern- und Gedächtnismodellen im Rahmen von Lernalgorithmen für die Entwicklung künstlicher Intelligenz große Vorteile erbringen, um die Möglichkeit verschiedene Lösungsansätze für die Lernalgorithmen zu testen. Dazu könnte man z.B. in Kombination mit genetischen Verfahren,

die die Rezeptorfunktion beeinflussen und Verhaltenstests am Tiermodell unterschiedliche Lernbedingungen und Strategien untersuchen. Neben der weiteren Untersuchung des grundsätzlichen Aufbaus von Hirnstrukturen und funktionellen Netzwerken wäre es zudem in der Zukunft z.B. interessant, ob weitere Neurotransmitterrezeptoren abseits der Dopamin-Rezeptoren plastische Veränderungen nach kognitivem Training aufweisen und inwieweit dies auf andere beteiligte Hirnstrukturen außerhalb des Nidopallium caudolaterale, wie z.B. die Hippocampusformation, Auswirkungen zeigt. Da das Vogelgehirn im Vergleich zum Säugerhirn insgesamt plastischer zu sein scheint, wäre es außerdem spannend zu untersuchen, welche Bedeutung die adulte Neurogenese und die Gliogenese in diesem Zusammenhang spielen. Darüber hinaus lässt sich untersuchen, ob sich Vögel möglicherweise als Modell für bestimmte neurologische Erkrankungen, wie z.B. die Epilepsie oder Morbus Parkinson, bei denen Veränderungen kritischer Faktoren wie Neuro- und Gliogenese bestimmt wurden, besser nutzen lassen als die in der Regel etablierten Maus- oder Rattenmodelle. Aber auch für Nager-Modelle, wäre es interessant genauer zu untersuchen, welche Zusammenhänge es zwischen der neuronalen und der neurochemischen Plastizität gibt. Ergänzend dazu wäre es sehr wichtig, die zu Grunde liegenden neuronalen Schaltkreise speziesübergreifend noch detaillierter zu erforschen, wofür sich z.B. die neu entwickelte 3D-Polarisationsmikroskopie bestens eignet. Durch die Entwicklung neuer optischer Techniken in Kombination mit elektrophysiologischen Messungen ist es außerdem zusätzlich möglich, einzelne Strukturen und Zellen viel genauer zu untersuchen und kausale Zusammenhänge zu erfassen und auszuwerten. Auch im Rahmen der vergleichenden Forschung werden immer häufiger bildgebende Verfahren eingesetzt, die funktionelle Zusammenhänge in Form von Aktivitätsmustern und Netzwerkanalysen im Gehirn darstellen können. Die vorliegenden Arbeiten zeigen jedoch deutlich, dass es dafür unabdingbar ist, die Neuroanatomie der beteiligten Strukturen im Detail zu erfassen und hierbei zelluläre Strukturen, Verbindungen, den neurochemischen Aufbau, entwicklungsbiologische und genetische Analysen einzubeziehen und folglich multimodale Ansätze zu verfolgen. Darüber hinaus wurde ebenfalls anschaulich dargelegt, dass es wichtig ist, sich dabei nicht nur auf einzelne Spezies zu beziehen, sondern den Blick möglichst weit zu fassen, da es speziesübergreifend verschiedene Anpassungen gibt und selbst zwischen nahverwandten Gattungen, wie z.B. Ratten und Mäusen, Unterschiede existieren. Bei Vögeln wird dies besonders erkennbar, wenn man sich z.B. die Unterschiede im Hirnaufbau zwischen verschiedenen Ordnungen wie den Taubenvögeln (*Columbiformes*), den Hühnervögeln (*Galliformes*), den Sperlingsvögeln (*Passeriformes*) und den Papageien (*Psittaciformes*) ansieht. Auch innerhalb der Unterordnung der Singvögel (*Passeri*), die zu den Sperlingsvögeln gehört, gibt es deutliche Unterschiede im Hirnaufbau zwischen den verschiedenen dazugehörigen Familien, wie z.B. den Prachtfinken (*Estrildidae*), zu denen die Gattung der Zebrafinken (*Taeniopygia*) zählt, und den Rabenvögeln (*Corvidae*), zu denen die Gattung der Krähen und Raben (*Corvus*) zählt (Jarvis et al., 2013; Pfenning et al., 2014; Chakraborty et al., 2015; Olkowicz et al., 2016). Diese Unterschiede betreffen unter anderem auch das *Song*-System, welches vergleichend zum Sprachnetzwerk des Menschen angesehen wird, und liefern z.B. eine Erklärung dafür, warum sich die *Song-/*Sprachfähigkeiten der Singvögel nochmals unterschieden. Die zu Grunde

liegenden Netzwerke und die beteiligten Strukturen sind sowohl in der Aufnahme und im Erlernen von *Song*-/Sprachinformationen, dem Enkodieren, z.B. von Silben, wie auch in der Ausführung des *Songs*/der Sprache, zwischen Vögeln und Menschen fast identisch (Jarvis, 2007; Woolley, 2013; Chakraborty & Jarvis, 2015). Die Bedeutung der Sprache nimmt im Rahmen von intelligentem Verhalten im Vergleich zu Säugern nochmal einen besonderen Stellenwert ein, da die Entwicklung/Evolution der Sprache beim Menschen mit der Entwicklung vieler kognitiven Fähigkeiten in Zusammenhang zu stehen scheint. So könnte es hier ebenfalls zu bedeutsamen Erkenntnissen kommen, wenn man diese Netzwerke zwischen den verschiedenen Vogelordnungen noch spezifischer untersucht. Nicht zuletzt sind die Papageienvögel (*Psittaciformes*) sogar in der Lage, die menschliche Sprache bis zu einem gewissen Grad zu erlernen, zu imitieren und zu „verstehen“. Inwieweit dabei auch weitere Hirnstrukturen, welche die Lern- und Gedächtnisprozesse unterstützen, beteiligt sind, ist insbesondere in der Gattung der Krähen und Raben und in der Ordnung der Papageien erst sehr wenig erforscht, so dass es in der Zukunft an dieser Stelle sicher noch viele interessante Forschungsfragen zu beantworten gibt.

5. Literatur

Aiba A, Kano M, Chen C, Stanton ME, Fox GD, Herrup K, Zwingman TA, Tonegawa S. 1994. Deficient cerebellar long-term depression and impaired motor learning in mGluR1 mutant mice. Cell 79(2):377-388.

Alesci R, Bagnoli P. 1988. Endogenous levels of serotonin and 5-hydroxyindoleacetic acid in specific areas of the pigeon CNS: effects of serotonin neurotoxins. Brain Res 450(1-2):259-271.

Alexander GE, DeLong MR, Strick PL. 1986. Parallel organization of functionally segregated circuits linking basal ganglia and cortex. Annu Rev Neurosci 9:357-381.

Alvarez-Buylla A, Nottebohm F. 1988. Migration of young neurons in adult avian brain. Nature 335(6188):353-354.

Amaral DG, Scharfman HE, Lavenex P. 2007. The dentate gyrus: fundamental neuroanatomical organization (dentate gyrus for dummies). Prog Brain Res 163:3-22.

Amunts K, Kedo O, Kindler M, Pieperhoff P, Mohlberg H, Shah NJ, Habel U, Schneider F, Zilles K. 2005. Cytoarchitectonic mapping of the human amygdala, hippocampal region and entorhinal cortex: intersubject variability and probability maps. Anat Embryol (Berl) 210(5-6):343-352.

Anacker C, Hen R. 2017. Adult hippocampal neurogenesis and cognitive flexibility - linking memory and mood. Nature reviews Neuroscience 18(6):335-346.

Andersen P, Morris R, Amaral D, O'Keefe J, Bliss B. 2007. The hippocampus book. Oxford; New York: Oxford University Press.

Atoji Y, Sarkar S, Wild JM. 2016. Proposed homology of the dorsomedial subdivision and V-shaped layer of the avian hippocampus to Ammon's horn and dentate gyrus, respectively. Hippocampus 26(12):1608-1617.

Atoji Y, Wild JM. 2004. Fiber connections of the hippocampal formation and septum and subdivisions of the hippocampal formation in the pigeon as revealed by tract tracing and kainic acid lesions. J Comp Neurol 475(3):426-461.

Atoji Y, Wild JM. 2005. Afferent and efferent connections of the dorsolateral corticoid area and a comparison with connections of the temporo-parieto-occipital area in the pigeon (Columba livia). J Comp Neurol 485(2):165-182.

Atoji Y, Wild JM. 2006. Anatomy of the avian hippocampal formation. Rev Neurosci 17(1-2):3-15.

Atoji Y, Wild JM, Yamamoto Y, Suzuki Y. 2002. Intratelencephalic connections of the hippocampus in pigeons (Columba livia). J Comp Neurol 447(2):177-199.

Atucha E, Vukojevic V, Fornari RV, Ronzoni G, Demougin P, Peter F, Atsak P, Coolen MW, Papassotiropoulos A, McGaugh JL, de Quervain DJ, Roozendaal B. 2017. Noradrenergic activation of the basolateral amygdala maintains hippocampus-dependent accuracy of remote memory. Proc Natl Acad Sci U S A 114(34):9176-9181.

Audet JN, Kayello L, Ducatez S, Perillo S, Cauchard L, Howard JT, O'Connell LA, Jarvis ED, Lefebvre L. 2018. Divergence in problem-solving skills is associated with differential expression of glutamate receptors in wild finches. Sci Adv 4(3):eaao6369.

Axer M, Amunts K, Grassel D, Palm C, Dammers J, Axer H, Pietrzyk U, Zilles K. 2011a. A novel approach to the human connectome: ultra-high resolution mapping of fiber tracts in the brain. Neuroimage 54(2):1091-1101.

Axer M, Grassel D, Kleiner M, Dammers J, Dickscheid T, Reckfort J, Hutz T, Eiben B, Pietrzyk U, Zilles K, Amunts K. 2011b. High-resolution fiber tract reconstruction in the human brain by means of three-dimensional polarized light imaging. Front Neuroinform 5:34.

Baddeley A. 1992. Working memory. Science 255(5044):556-559.

Balthazart J, Absil P. 1997. Identification of catecholaminergic inputs to and outputs from aromatase-containing brain areas of the Japanese quail by tract tracing combined with tyrosine hydroxylase immunocytochemistry. J Comp Neurol 382(3):401-428.

Barnea A, Pravosudov V. 2011. Birds as a model to study adult neurogenesis: bridging evolutionary, comparative and neuroethological approaches. Eur J Neurosci 34(6):884-907.

Bast T, Pezze M, McGarrity S. 2017. Cognitive deficits caused by prefrontal cortical and hippocampal neural disinhibition. Br J Pharmacol 174(19):3211-3225.

Bekar LK, He W, Nedergaard M. 2008. Locus coeruleus alpha-adrenergic-mediated activation of cortical astrocytes in vivo. Cerebral cortex 18(12):2789-2795.

Belgard TG, Montiel JF, Wang WZ, Garcia-Moreno F, Margulies EH, Ponting CP, Molnar Z. 2013. Adult pallium transcriptomes surprise in not reflecting predicted homologies across diverse chicken and mouse pallial sectors. Proc Natl Acad Sci U S A 110(32):13150-13155.

Bendotti C, Samanin R. 1987. The role of putative 5-HT1A and 5-HT1B receptors in the control of feeding in rats. Life Sci 41(5):635-642.

Bergson C, Mrzljak L, Smiley JF, Pappy M, Levenson R, Goldman-Rakic PS. 1995. Regional, cellular, and subcellular variations in the distribution of D1 and D5 dopamine receptors in primate brain. J Neurosci 15(12):7821-7836.

Bingman VP, Gagliardo A, Hough GE, 2nd, Ioale P, Kahn MC, Siegel JJ. 2005. The avian hippocampus, homing in pigeons and the memory representation of large-scale space. Integr Comp Biol 45(3):555-564.

Bingman VP, MacDougall-Shackleton SA. 2017. The avian hippocampus and the hypothetical maps used by navigating migratory birds (with some reflection on compasses and migratory restlessness). J Comp Physiol A Neuroethol Sens Neural Behav Physiol 203(6-7):465-474.

Bingman VP, Muzio RN. 2017. Reflections on the Structural-Functional Evolution of the Hippocampus: What Is the Big Deal about a Dentate Gyrus? Brain Behav Evol 90(1):53-61.

Bird CM, Burgess N. 2008. The hippocampus and memory: insights from spatial processing. Nature reviews Neuroscience 9(3):182-194.

Bliss TV, Collingridge GL. 1993. A synaptic model of memory: long-term potentiation in the hippocampus. Nature 361(6407):31-39.

Bliss TV, Lomo T. 1973. Long-lasting potentiation of synaptic transmission in the dentate area of the anaesthetized rabbit following stimulation of the perforant path. The Journal of physiology 232(2):331-356.

Bliss TV, Collingridge GL, Morris RGM, Reymann KG. 2018. Long-term potentiation in the hippocampus: discovery, mechanisms and function. Neuroforum 24(3):A103-A120.

Bludau S, Eickhoff SB, Mohlberg H, Caspers S, Laird AR, Fox PT, Schleicher A, Zilles K, Amunts K. 2014. Cytoarchitecture, probability maps and functions of the human frontal pole. Neuroimage 93(2):260-275.

Boeckle M, Clayton NS. 2018. Theory of Mind. Encyclopedia of Animal Cognition and Behavior, Springer, Vonk J, Shackelford T (eds).

Bordelon-Glausier JR, Khan ZU, Muly EC. 2008. Quantification of D1 and D5 dopamine receptor localization in layers I, III, and V of Macaca mulatta prefrontal cortical area 9: coexpression in dendritic spines and axon terminals. J Comp Neurol 508(6):893-905.

Boutrel B, Monaca C, Hen R, Hamon M, Adrien J. 2002. Involvement of 5-HT1A receptors in homeostatic and stress-induced adaptive regulations of paradoxical sleep: studies in 5-HT1A knock-out mice. J Neurosci 22(11):4686-4692.

Brandon EP, Zhuo M, Huang YY, Qi M, Gerhold KA, Burton KA, Kandel ER, McKnight GS, Idzerda RL. 1995. Hippocampal long-term depression and depotentiation are defective in mice carrying a targeted disruption of the gene encoding the RI beta subunit of cAMP-dependent protein kinase. Proc Natl Acad Sci U S A 92(19):8851-8855.

Brenowitz EA, Larson TA. 2015. Neurogenesis in the adult avian song-control system. Cold Spring Harb Perspect Biol 7(6).

Brusatte SL, O'Connor JK, Jarvis ED. 2015. The Origin and Diversification of Birds. Curr Biol 25(19):R888-898.

Burgess PW, Gilbert SJ, Dumontheil I. 2007. Function and localization within rostral prefrontal cortex (area 10). Philos Trans R Soc Lond B Biol Sci 362(1481):887-899.

Cabrera-Socorro A, Hernandez-Acosta NC, Gonzalez-Gomez M, Meyer G. 2007. Comparative aspects of p73 and Reelin expression in Cajal-Retzius cells and the cortical hem in lizard, mouse and human. Brain Res 1132(1):59-70.

Callier S, Snapyan M, Le Crom S, Prou D, Vincent JD, Vernier P. 2003. Evolution and cell biology of dopamine receptors in vertebrates. Biology of the cell / under the auspices of the European Cell Biology Organization 95(7):489-502.

Carli M, Lazarova M, Tatarczynska E, Samanin R. 1992. Stimulation of 5-HT1A receptors in the dorsal hippocampus impairs acquisition and performance of a spatial task in a water maze. Brain Res 595(1):50-56.

Carta M, Fievre S, Gorlewicz A, Mulle C. 2014. Kainate receptors in the hippocampus. Eur J Neurosci 39(11):1835-1844.

Castner SA, Williams GV. 2007. Tuning the engine of cognition: a focus on NMDA/D1 receptor interactions in prefrontal cortex. Brain and cognition 63(2):94-122.

Chakraborty M, Jarvis ED. 2015. Brain evolution by brain pathway duplication. Philos Trans R Soc Lond B Biol Sci 370(1684).

Chakraborty M, Walloe S, Nedergaard S, Fridel EE, Dabelsteen T, Pakkenberg B, Bertelsen MF, Dorrestein GM, Brauth SE, Durand SE, Jarvis ED. 2015. Core and Shell Song Systems Unique to the Parrot Brain. PLoS One 10(6):e0118496.

Chen CC, Winkler CM, Pfenning AR, Jarvis ED. 2013. Molecular profiling of the developing avian telencephalon: Regional timing and brain subdivision continuities. J Comp Neurol 521(16):3666-3701.

Choi S, Jonak E, Fernstrom JD. 2004. Serotonin reuptake inhibitors do not prevent 5,7-dihydroxytryptamine-induced depletion of serotonin in rat brain. Brain Res 1007(1-2):19-28.
Clelland CD, Choi M, Romberg C, Clemenson GD, Jr., Fragniere A, Tyers P, Jessberger S, Saksida LM, Barker RA, Gage FH, Bussey TJ. 2009. A functional role for adult hippocampal neurogenesis in spatial pattern separation. Science 325(5937):210-213.
Colombo M, Broadbent N. 2000. Is the avian hippocampus a functional homologue of the mammalian hippocampus? Neurosci Biobehav Rev 24(4):465-484.
Colombo M, Fernandez T, Nakamura K, Gross CG. 1998. Functional differentiation along the anterior-posterior axis of the hippocampus in monkeys. Journal of neurophysiology 80(2):1002-1005.
Coppola VJ, Hough G, Bingman VP. 2014. Age-related spatial working memory deficits in homing pigeons (Columba livia). Behav Neurosci 128(6):666-675.
Cremer CM, Bidmon HJ, Görg B, Palomero-Gallagher N, Escobar JL, Speckmann EJ, Zilles K. 2010. Inhibition of glutamate/glutamine cycle in vivo results in decreased benzodiazepine binding and differentially regulated GABAergic subunit expression in the rat brain. Epilepsia 51(8):1446-1455.
Cremer CM, Lübke JH, Palomero-Gallagher N, Zilles K. 2011. Laminar distribution of neurotransmitter receptors in different reeler mouse brain regions. Brain Struct Funct 216(3):201-218.
Cremer CM, Palomero-Gallagher N, Bidmon HJ, Schleicher A, Speckmann EJ, Zilles K. 2009. Pentylenetetrazole-induced seizures affect binding site densities for GABA, glutamate and adenosine receptors in the rat brain. Neuroscience 163(1):490-499.
Csillag A, Montagnese CM. 2005. Thalamotelencephalic organization in birds. Brain Res Bull 66(4-6):303-310.
Daisley JN, Rose SP. 2002. Amino acid release from the intermediate medial hyperstriatum ventrale (IMHV) of day-old chicks following a one-trial passive avoidance task. Neurobiol Learn Mem 77(2):185-201.
Damasio H, Grabowski T, Frank R, Galaburda AM, Damasio AR. 1994. The return of Phineas Gage: clues about the brain from the skull of a famous patient. Science 264(5162):1102-1105.
Danscher G, Haug FM, Fredens K. 1973. Effect of diethyldithiocarbamate (DEDTC) on sulphide silver stained boutons. Reversible blocking of Timm's sulphide silver stain for "heavy" metals in DEDTC treated rats (light microscopy). Exp Brain Res 16(5):521-532.
Danscher G, Zimmer J. 1978. An improved Timm sulphide silver method for light and electron microscopic localization of heavy metals in biological tissues. Histochemistry 55(1):27-40.
Datta D, Yang ST, Galvin VC, Solder J, Luo F, Morozov YM, Arellano J, Duque A, Rakic P, Arnsten AFT, Wang M. 2019. Noradrenergic alpha1-Adrenoceptor Actions in the Primate Dorsolateral Prefrontal Cortex. J Neurosci 39(14):2722-2734.
Diekamp B, Kalt T, Güntürkün O. 2002. Working memory neurons in pigeons. J Neurosci 22(4):RC210.
Diekamp B, Kalt T, Ruhm A, Koch M, Güntürkün O. 2000. Impairment in a discrimination reversal task after D1 receptor blockade in the pigeon "prefrontal cortex". Behav Neurosci 114(6):1145-1155.
Ding L, Perkel DJ. 2002. Dopamine modulates excitability of spiny neurons in the avian basal ganglia. J Neurosci 22(12):5210-5218.
Dong HW, Swanson LW, Chen L, Fanselow MS, Toga AW. 2009. Genomic-anatomic evidence for distinct functional domains in hippocampal field CA1. Proc Natl Acad Sci U S A 106(28):11794-11799.
Dos Santos MM, Hoeller AA, dos Santos TS, Felisbino MB, Herdt MA, da Silva ES, Paschoalini MA, Marino-Neto J. 2009. Behavioural and electroencephalographic effects of systemic injections of 8-OH-DPAT in the pigeon (Columba livia). Behav Brain Res 201(2):244-256.
dos Santos TS, Krüger J, Melleu FF, Herold C, Zilles K, Poli A, Güntürkün O, Marino-Neto J. 2015. Distribution of serotonin 5-HT1A-binding sites in the brainstem and the hypothalamus, and their roles in 5-HT-induced sleep and ingestive behaviors in rock pigeons (Columba livia). Behav Brain Res 295:45-63.
Dugas-Ford J, Rowell JJ, Ragsdale CW. 2012. Cell-type homologies and the origins of the neocortex. Proc Natl Acad Sci U S A 109(42):16974-16979.
Durstewitz D, Kröner S, Güntürkün O. 1999. The dopaminergic innervation of the avian telencephalon. Progress in neurobiology 59(2):161-195.
Elvander-Tottie E, Eriksson TM, Sandin J, Ogren SO. 2009. 5-HT(1A) and NMDA receptors interact in the rat medial septum and modulate hippocampal-dependent spatial learning. Hippocampus 19(12):1187-1198.
Emery NJ. 2006. Cognitive ornithology: the evolution of avian intelligence. Philos Trans R Soc Lond B Biol Sci 361(1465):23-43.
Eriksson PS, Perfilieva E, Bjork-Eriksson T, Alborn AM, Nordborg C, Peterson DA, Gage FH. 1998. Neurogenesis in the adult human hippocampus. Nat Med 4(11):1313-1317.
Ernst A, Alkass K, Bernard S, Salehpour M, Perl S, Tisdale J, Possnert G, Druid H, Frisen J. 2014. Neurogenesis in the striatum of the adult human brain. Cell 156(5):1072-1083.

Ernst A, Frisen J. 2015. Adult neurogenesis in humans- common and unique traits in mammals. PLoS Biol 13(1):e1002045.
Fanselow MS, Dong HW. 2010. Are the dorsal and ventral hippocampus functionally distinct structures? Neuron 65(1):7-19.
Floresco SB. 2013. Prefrontal dopamine and behavioral flexibility: shifting from an "inverted-U" toward a family of functions. Front Neurosci 7:62.
Funahashi S, Bruce CJ, Goldman-Rakic PS. 1989. Mnemonic coding of visual space in the monkey's dorsolateral prefrontal cortex. Journal of neurophysiology 61(2):331-349.
Fuster JM, Alexander GE. 1971. Neuron activity related to short-term memory. Science 173(3997):652-654.
Gao M, Lengersdorf D, Stüttgen MC, Güntürkün O. 2018. NMDA receptors in the avian amygdala and the premotor arcopallium mediate distinct aspects of appetitive extinction learning. Behav Brain Res 343:71-82.
Garcia-Moreno F, Anderton E, Jankowska M, Begbie J, Encinas JM, Irimia M, Molnar Z. 2018. Absence of Tangentially Migrating Glutamatergic Neurons in the Developing Avian Brain. Cell Rep 22(1):96-109.
Ge S, Yang CH, Hsu KS, Ming GL, Song H. 2007. A critical period for enhanced synaptic plasticity in newly generated neurons of the adult brain. Neuron 54(4):559-566.
Gibbs ME, Bowser DN. 2009. Astrocytes and interneurons in memory processing in the chick hippocampus: roles for G-coupled protein receptors, GABA(B) and mGluR1. Neurochem Res 34(10):1712-1720.
Gibbs ME, Bowser DN. 2010. Astrocytic adrenoceptors and learning: alpha1-adrenoceptors. Neurochem Int 57(4):404-410.
Gibbs ME, Johnston GA. 2005. Opposing roles for GABAA and GABAC receptors in short-term memory formation in young chicks. Neuroscience 131(3):567-576.
Gibbs ME, Summers RJ. 2001. Stimulation of alpha1-adrenoceptors inhibits memory consolidation in the chick. Eur J Neurosci 14(8):1369-1376.
Gibbs ME, Summers RJ. 2003. Alpha 2-adrenoceptors in the basal ganglia have a role in memory consolidation and reinforcement. Neuropharmacology 45(3):355-367.
Glausier JR, Khan ZU, Muly EC. 2009. Dopamine D1 and D5 receptors are localized to discrete populations of interneurons in primate prefrontal cortex. Cerebral cortex 19(8):1820-1834.
Gould E. 1999. Serotonin and hippocampal neurogenesis. Neuropsychopharmacology 21(2 Suppl):46S-51S.
Groenink L, Joordens RJ, Hijzen TH, Dirks A, Olivier B. 2000. Infusion of flesinoxan into the amygdala blocks the fear-potentiated startle. Neuroreport 11(10):2285-2288.
Güntürkün O. 2005. The avian 'prefrontal cortex' and cognition. Curr Opin Neurobiol 15(6):686-693.
Güntürkün O, Bugnyar T. 2016. Cognition without Cortex. Trends Cogn Sci 20(4):291-303.
Hannon J, Hoyer D. 2008. Molecular biology of 5-HT receptors. Behav Brain Res 195(1):198-213.
Hasselmo ME. 2006. The role of acetylcholine in learning and memory. Curr Opin Neurobiol 16(6):710-715.
Herold C. 2010. NMDA and D2-like receptors modulate cognitive flexibility in a color discrimination reversal task in pigeons. Behav Neurosci 124(3):381-390.
Herold C, Bidmon HJ, Pannek HW, Hans V, Gorji A, Speckmann EJ, Zilles K. 2018a. ATPase N-ethylmaleimide-sensitive Fusion Protein: A Novel Key Player for Causing Spontaneous Network Excitation in Human Temporal Lobe Epilepsy. Neuroscience 371:371-383.
Herold C, Bingman VP, Ströckens F, Letzner S, Sauvage M, Palomero-Gallagher N, Zilles K, Güntürkün O. 2014. Distribution of neurotransmitter receptors and zinc in the pigeon (Columba livia) hippocampal formation: A basis for further comparison with the mammalian hippocampus. J Comp Neurol 522(11):2553-2575.
Herold C, Coppola VJ, Bingman VP. 2015. The maturation of research into the avian hippocampal formation: Recent discoveries from one of the nature's foremost navigators. Hippocampus 25(11):1193-1211.
Herold C, Diekamp B, Güntürkün O. 2008. Stimulation of dopamine D1 receptors in the avian fronto-striatal system adjusts daily cognitive fluctuations. Behav Brain Res 194(2):223-229.
Herold C, Joshi I, Chehadi O, Hollmann M, Güntürkün O. 2012a. Plasticity in D1-like receptor expression is associated with different components of cognitive processes. PLoS One 7(5):e36484.
Herold C, Palomero-Gallagher N, Günturkün O, Zilles K. 2012b. Serotonin 5-HT(1A) receptor binding sites in the brain of the pigeon (Columba livia). Neuroscience 200:1-12.
Herold C, Palomero-Gallagher N, Hellmann B, Kröner S, Theiss C, Güntürkün O, Zilles K. 2011. The receptor architecture of the pigeons' nidopallium caudolaterale: an avian analogue to the mammalian prefrontal cortex. Brain Struct Funct 216(3):239-254.
Herold C, Paulitschek C, Palomero-Gallagher N, Güntürkün O, Zilles K. 2018b. Transmitter receptors reveal segregation of the arcopallium/amygdala complex in pigeons (Columba livia). J Comp Neurol 526(3):439-466.

Herold C, Schlömer P, Mafoppa-Fomat I, Mehlhorn J, Amunts K, Axer M. 2019. The hippocampus of birds in a view of evolutionary connectomics. Cortex 118:165-187.
Hevner RF. 2016. Evolution of the mammalian dentate gyrus. J Comp Neurol 524(3):578-594.
Hoeller AA, dos Santos TS, Bruxel RR, Dallazen AR, do Amaral Silva HT, Andre ES, Marino-Neto J. 2013. Serotonergic control of ingestive and post-ingestive behaviors in pigeons (Columba livia): the role of 5-HT1A receptor-mediated central mechanisms. Behav Brain Res 236(1):118-130.
Hough GE, 2nd, Pang KC, Bingman VP. 2002. Intrahippocampal connections in the pigeon (Columba livia) as revealed by stimulation evoked field potentials. J Comp Neurol 452(3):297-309.
Huang YY, Zakharenko SS, Schoch S, Kaeser PS, Janz R, Sudhof TC, Siegelbaum SA, Kandel ER. 2005. Genetic evidence for a protein-kinase-A-mediated presynaptic component in NMDA-receptor-dependent forms of long-term synaptic potentiation. Proc Natl Acad Sci U S A 102(26):9365-9370.
Hutchinson DS, Catus SL, Merlin J, Summers RJ, Gibbs ME. 2011. alpha(2)-Adrenoceptors activate noradrenaline-mediated glycogen turnover in chick astrocytes. J Neurochem 117(5):915-926.
Ito M, Sakurai M, Tongroach P. 1982. Climbing fibre induced depression of both mossy fibre responsiveness and glutamate sensitivity of cerebellar Purkinje cells. The Journal of physiology 324:113-134.
Izumi Y, Zorumski CF. 1999. Norepinephrine promotes long-term potentiation in the adult rat hippocampus in vitro. Synapse 31(3):196-202.
Janak PH, Tye KM. 2015. From circuits to behaviour in the amygdala. Nature 517(7534):284-292.
Jarvis ED. 2004. Learned birdsong and the neurobiology of human language. Annals of the New York Academy of Sciences 1016:749-777.
Jarvis ED. 2007. Neural systems for vocal learning in birds and humans: a synopsis. J Ornithol 148(1):35-44.
Jarvis ED, Güntürkün O, Bruce L, Csillag A, Karten H, Kuenzel W, Medina L, Paxinos G, Perkel DJ, Shimizu T, Striedter G, Wild JM, Ball GF, Dugas-Ford J, Durand SE, Hough GE, Husband S, Kubikova L, Lee DW, Mello CV, Powers A, Siang C, Smulders TV, Wada K, White SA, Yamamoto K, Yu J, Reiner A, Butler AB, Avian Brain Nomenclature C. 2005. Avian brains and a new understanding of vertebrate brain evolution. Nature reviews Neuroscience 6(2):151-159.
Jarvis ED, Yu J, Rivas MV, Horita H, Feenders G, Whitney O, Jarvis SC, Jarvis ER, Kubikova L, Puck AE, Siang-Bakshi C, Martin S, McElroy M, Hara E, Howard J, Pfenning A, Mouritsen H, Chen CC, Wada K. 2013. Global view of the functional molecular organization of the avian cerebrum: mirror images and functional columns. J Comp Neurol 521(16):Spc1.
Jenni NL, Larkin JD, Floresco SB. 2017. Prefrontal Dopamine D1 and D2 Receptors Regulate Dissociable Aspects of Decision Making via Distinct Ventral Striatal and Amygdalar Circuits. J Neurosci 37(26):6200-6213.
Jessberger S, Parent JM. 2015. Epilepsy and Adult Neurogenesis. Cold Spring Harb Perspect Biol 7(12).
Kahn MC, Bingman VP. 2009. Avian hippocampal role in space and content memory. Eur J Neurosci 30(10):1900-1908.
Kahn MC, Hough GE, 2nd, Ten Eyck GR, Bingman VP. 2003. Internal connectivity of the homing pigeon (Columba livia) hippocampal formation: an anterograde and retrograde tracer study. J Comp Neurol 459(2):127-141.
Kalenscher T, Windmann S, Diekamp B, Rose J, Güntürkün O, Colombo M. 2005. Single units in the pigeon brain integrate reward amount and time-to-reward in an impulsive choice task. Curr Biol 15(7):594-602.
Kalt T, Diekamp B, Güntürkün O. 1999. Single unit activity during a Go/NoGo task in the "prefrontal cortex" of pigeons. Brain Res 839(2):263-278.
Kandel ER. 2001. The molecular biology of memory storage: a dialogue between genes and synapses. Science 294(5544):1030-1038.
Kandel ER. 2013. Principles of neural science. New York: McGraw-Hill Medical. l, 1709 p. p.
Karakuyu D, Herold C, Güntürkün O, Diekamp B. 2007. Differential increase of extracellular dopamine and serotonin in the 'prefrontal cortex' and striatum of pigeons during working memory. Eur J Neurosci 26(8):2293-2302.
Karten H, Hodos W. 1967. A stereotaxic atlas of the brain of the pigeon (Columba livia). The Johns Hopkins University Press, Baltimore.
Kedo O, Zilles K, Palomero-Gallagher N, Schleicher A, Mohlberg H, Bludau S, Amunts K. 2018. Receptor-driven, multimodal mapping of the human amygdala. Brain Struct Funct 223(4):1637-1666.
Kempermann G. 2012. New neurons for 'survival of the fittest'. Nature reviews Neuroscience 13(10):727-736.
Kempermann G, Gage FH, Aigner L, Song H, Curtis MA, Thuret S, Kuhn HG, Jessberger S, Frankland PW, Cameron HA, Gould E, Hen R, Abrous DN, Toni N, Schinder AF, Zhao X, Lucassen PJ, Frisen J. 2018. Human Adult Neurogenesis: Evidence and Remaining Questions. Cell Stem Cell 23(1):25-30.

Kim MJ, Loucks RA, Palmer AL, Brown AC, Solomon KM, Marchante AN, Whalen PJ. 2011. The structural and functional connectivity of the amygdala: from normal emotion to pathological anxiety. Behav Brain Res 223(2):403-410.

Klempin F, Babu H, De Pietri Tonelli D, Alarcon E, Fabel K, Kempermann G. 2010. Oppositional effects of serotonin receptors 5-HT1a, 2, and 2c in the regulation of adult hippocampal neurogenesis. Front Mol Neurosci 3:14.

Klingberg T. 2010. Training and plasticity of working memory. Trends Cogn Sci 14(7):317-324.

Kraemer M, Zilles K, Schleicher A, Gebhard R, Robbins TW, Everitt BJ, Divac I. 1995. Quantitative receptor autoradiography of eight different transmitter-binding sites in the hippocampus of the common marmoset, Callithrix jacchus. Anat Embryol (Berl) 191(3):213-225.

Krebs JR, Erichsen JT, Bingman VP. 1991. The distribution of neurotransmitters and neurotransmitter-related enzymes in the dorsomedial telencephalon of the pigeon (Columba livia). J Comp Neurol 314(3):467-477.

Kröner S, Güntürkün O. 1999. Afferent and efferent connections of the caudolateral neostriatum in the pigeon (Columba livia): a retro- and anterograde pathway tracing study. J Comp Neurol 407(2):228-260.

Kubikova L, Wada K, Jarvis ED. 2010. Dopamine receptors in a songbird brain. J Comp Neurol 518(6): 741-769.

Lamsa K, Lau P. 2019. Long-term plasticity of hippocampal interneurons during in vivo memory processes. Curr Opin Neurobiol 54:20-27.

Lengersdorf D, Stüttgen MC, Uengoer M, Güntürkün O. 2014. Transient inactivation of the pigeon hippocampus or the nidopallium caudolaterale during extinction learning impairs extinction retrieval in an appetitive conditioning paradigm. Behav Brain Res 265:93-100.

Lesku JA, Rattenborg NC. 2014. Avian sleep. Curr Biol 24(1):R12-R14.

Letzner S, Güntürkün O, Beste C. 2017. How birds outperform humans in multi-component behavior. Curr Biol 27(18):R996-R998.

Levey AI. 1996. Muscarinic acetylcholine receptor expression in memory circuits: implications for treatment of Alzheimer disease. Proc Natl Acad Sci U S A 93(24):13541-13546.

Levy WB, Steward O. 1983. Temporal contiguity requirements for long-term associative potentiation/depression in the hippocampus. Neuroscience 8(4):791-797.

Li JX, Koek W, Rice KC, France CP. 2010. Differential effects of serotonin 5-HT1A receptor agonists on the discriminative stimulus effects of the 5-HT2A receptor agonist 1-(2,5-dimethoxy-4-methylphenyl)-2-aminopropane in rats and rhesus monkeys. J Pharmacol Exp Ther 333(1):244-252.

Liang KC, Juler RG, McGaugh JL. 1986. Modulating effects of posttraining epinephrine on memory: involvement of the amygdala noradrenergic system. Brain Res 368(1):125-133.

Licheri V, Talani G, Gorule AA, Mostallino MC, Biggio G, Sanna E. 2015. Plasticity of GABAA Receptors during Pregnancy and Postpartum Period: From Gene to Function. Neural Plast 2015:170435.

Liljeholm M, O'Doherty JP. 2012. Contributions of the striatum to learning, motivation, and performance: an associative account. Trends Cogn Sci 16(9):467-475.

Lissek S, Güntürkün O. 2003. Dissociation of extinction and behavioral disinhibition: the role of NMDA receptors in the pigeon associative forebrain during extinction. J Neurosci 23(22):8119-8124.

Maguire J, Ferando I, Simonsen C, Mody I. 2009. Excitability changes related to GABAA receptor plasticity during pregnancy. J Neurosci 29(30):9592-9601.

Malenka RC, Nicoll RA. 1999. Long-term potentiation--a decade of progress? Science 285(5435):1870-1874.

Maletic V, Eramo A, Gwin K, Offord SJ, Duffy RA. 2017. The Role of Norepinephrine and Its alpha-Adrenergic Receptors in the Pathophysiology and Treatment of Major Depressive Disorder and Schizophrenia: A Systematic Review. Front Psychiatry 8:42.

Margrie TW, Rostas JA, Sah P. 1998. Long-term potentiation of synaptic transmission in the avian hippocampus. J Neurosci 18(4):1207-1216.

Martens U, Capito B, Wree A. 1998. Septotemporal distribution of [^{3}H]MK-801, [^{3}H]AMPA and [^{3}H]Kainate binding sites in the rat hippocampus. Anat Embryol 198:195-204.

Mayer U, Watanabe S, Bischof HJ. 2013. Spatial memory and the avian hippocampus: research in zebra finches. J Physiol Paris 107(1-2):2-12.

McGaugh JL. 2000. Memory--a century of consolidation. Science 287(5451):248-251.

McNab F, Varrone A, Farde L, Jucaite A, Bystritsky P, Forssberg H, Klingberg T. 2009. Changes in cortical dopamine D1 receptor binding associated with cognitive training. Science 323(5915):800-802.

Medina L, Abellan A, Desfilis E. 2017. Contribution of Genoarchitecture to Understanding Hippocampal Evolution and Development. Brain Behav Evol 90(1):25-40.

Melleu FF, Pinheiro MV, Lino-de-Oliveira C, Marino-Neto J. 2016. Defensive behaviors and prosencephalic neurogenesis in pigeons (Columba livia) are affected by environmental enrichment in adulthood. Brain Struct Funct 221(4):2287-2301.
Melleu FF, Santos TS, Lino-de-Oliveira C, Marino-Neto J. 2013. Distribution and characterization of doublecortin-expressing cells and fibers in the brain of the adult pigeon (Columba livia). J Chem Neuroanat 47:57-70.
Mello CV, Kaser T, Buckner AA, Wirthlin M, Lovell PV. 2019. Molecular architecture of the zebra finch arcopallium. J Comp Neurol 527(15):2512-2556.
Mello CV, Pinaud R, Ribeiro S. 1998. Noradrenergic system of the zebra finch brain: immunocytochemical study of dopamine-beta-hydroxylase. J Comp Neurol 400(2):207-228.
Miller EK, Erickson CA, Desimone R. 1996. Neural mechanisms of visual working memory in prefrontal cortex of the macaque. J Neurosci 16(16):5154-5167.
Miller EK, Lundqvist M, Bastos AM. 2018. Working Memory 2.0. Neuron 100(2):463-475.
Ming GL, Song H. 2011. Adult neurogenesis in the mammalian brain: significant answers and significant questions. Neuron 70(4):687-702.
Moons L, D'Hondt E, Pijcke K, Vandesande F. 1995. Noradrenergic system in the chicken brain: immunocytochemical study with antibodies to noradrenaline and dopamine-beta-hydroxylase. J Comp Neurol 360(2):331-348.
Moreno N, Gonzalez A. 2007. Evolution of the amygdaloid complex in vertebrates, with special reference to the anamnio-amniotic transition. J Anat 211(2):151-163.
Mouritsen H, Heyers D, Güntürkün O. 2016. The Neural Basis of Long-Distance Navigation in Birds. Annu Rev Physiol 78:133-154.
Mu Y, Gage FH. 2011. Adult hippocampal neurogenesis and its role in Alzheimer's disease. Mol Neurodegener 6:85.
Nieder A. 2017. Evolution of cognitive and neural solutions enabling numerosity judgements: lessons from primates and corvids. Philos Trans R Soc Lond B Biol Sci 373(1740).
Nomura T, Hattori M, Osumi N. 2009. Reelin, radial fibers and cortical evolution: insights from comparative analysis of the mammalian and avian telencephalon. Dev Growth Differ 51(3):287-297.
Ogren SO, Eriksson TM, Elvander-Tottie E, D'Addario C, Ekstrom JC, Svenningsson P, Meister B, Kehr J, Stiedl O. 2008. The role of 5-HT(1A) receptors in learning and memory. Behav Brain Res 195(1):54-77.
Olkowicz S, Kocourek M, Lucan RK, Portes M, Fitch WT, Herculano-Houzel S, Nemec P. 2016. Birds have primate-like numbers of neurons in the forebrain. Proc Natl Acad Sci U S A 113(26):7255-7260.
Palomero-Gallagher N, Bidmon HJ, Zilles K. 2003. AMPA, kainate, and NMDA receptor densities in the hippocampus of untreated male rats and females in estrus and diestrus. J Comp Neurol 459(4):468-474.
Patterson TA, Lipton JR, Bennett EL, Rosenzweig MR. 1990. Cholinergic receptor antagonists impair formation of intermediate-term memory in the chick. Behav Neural Biol 54(1):63-74.
Paulsen O, Moser EI. 1998. A model of hippocampal memory encoding and retrieval: GABAergic control of synaptic plasticity. Trends Neurosci 21(7):273-278.
Paxinos G, Watson C. 2005. The rat brain in stereotaxic coordinates. Compact 6th edition, Academic Press, New York, 400.
Pazos A, Probst A, Palacios JM. 1987. Serotonin receptors in the human brain--III. Autoradiographic mapping of serotonin-1 receptors. Neuroscience 21(1):97-122.
Pepeu G, Grazia Giovannini M. 2017. The fate of the brain cholinergic neurons in neurodegenerative diseases. Brain Res 1670:173-184.
Pepperberg IM. 2019. Tool use in Goffin's cockatoos: Shape/frame matching. Learn Behav 47(1):1-2.
Pfaffl M. 2004. Relative Quantification. Real-time PCR, International University Line (Editor: TDorak) Chap.3:63-82.
Pfenning AR, Hara E, Whitney O, Rivas MV, Wang R, Roulhac PL, Howard JT, Wirthlin M, Lovell PV, Ganapathy G, Mountcastle J, Moseley MA, Thompson JW, Soderblom EJ, Iriki A, Kato M, Gilbert MTP, Zhang G, Bakken T, Bongaarts A, Bernard A, Lein E, Mello CV, Hartemink AJ, Jarvis ED. 2014. Convergent transcriptional specializations in the brains of humans and song-learning birds. Science 346(6215): 1256846.
Phelps EA. 2004. Human emotion and memory: interactions of the amygdala and hippocampal complex. Curr Opin Neurobiol 14(2):198-202.
Picciotto MR, Higley MJ, Mineur YS. 2012. Acetylcholine as a neuromodulator: cholinergic signaling shapes nervous system function and behavior. Neuron 76(1):116-129.
Pika S, Wilkinson R, Kendrick KH, Vernes SC. 2018. Taking turns: bridging the gap between human and animal communication. Proc Biol Sci 285: 20180598.
Polter AM, Li X. 2010. 5-HT1A receptor-regulated signal transduction pathways in brain. Cell Signal 22(10):1406-1412.

Pozner T, Vistoropsky Y, Moaraf S, Heiblum R, Barnea A. 2018. Questioning Seasonality of Neuronal Plasticity in the Adult Avian Brain. Sci Rep 8(1):11289.

Puelles L, Kuwana E, Puelles E, Bulfone A, Shimamura K, Keleher J, Smiga S, Rubenstein JL. 2000. Pallial and subpallial derivatives in the embryonic chick and mouse telencephalon, traced by the expression of the genes Dlx-2, Emx-1, Nkx-2.1, Pax-6, and Tbr-1. J Comp Neurol 424(3):409-438.

Puig MV, Rose J, Schmidt R, Freund N. 2014. Dopamine modulation of learning and memory in the prefrontal cortex: insights from studies in primates, rodents, and birds. Front Neural Circuits 8:93.

Rattenborg NC, Martinez-Gonzalez D. 2011. A bird-brain view of episodic memory. Behav Brain Res 222(1):236-245.

Rehkämper G, Zilles K. 1991. Parallel evolution in mammalian and avian brains: comparative cytoarchitectonic and cytochemical analysis. Cell Tissue Res 263(1):3-28.

Reiner A, Perkel DJ, Bruce LL, Butler AB, Csillag A, Kuenzel W, Medina L, Paxinos G, Shimizu T, Striedter G, Wild M, Ball GF, Durand S, Güntürkün O, Lee DW, Mello CV, Powers A, White SA, Hough G, Kubikova L, Smulders TV, Wada K, Dugas-Ford J, Husband S, Yamamoto K, Yu J, Siang C, Jarvis ED, Avian Brain Nomenclature F. 2004. Revised nomenclature for avian telencephalon and some related brainstem nuclei. J Comp Neurol 473(3):377-414.

Robbins TW, Everitt BJ. 1996. Neurobehavioural mechanisms of reward and motivation. Curr Opin Neurobiol 6(2):228-236.

Robertson BA, Rathbone L, Cirillo G, D'Eath RB, Bateson M, Boswell T, Wilson PW, Dunn IC, Smulders TV. 2017. Food restriction reduces neurogenesis in the avian hippocampal formation. PLoS One 12(12):e0189158.

Rose J, Schiffer AM, Güntürkün O. 2013. Striatal dopamine D1 receptors are involved in the dissociation of learning based on reward-magnitude. Neuroscience 230:132-138.

Saint-Dizier H, Constantin P, Davies DC, Leterrier C, Levy F, Richard S. 2009. Subdivisions of the arcopallium/posterior pallial amygdala complex are differentially involved in the control of fear behaviour in the Japanese quail. Brain Res Bull 79(5):288-295.

Santi A, Bogles J, Petelka S. 1988. The effect of scopolamine and physostigmine on working and reference memory in pigeons. Behav Neural Biol 49(1):61-73.

Savasta M, Dubois A, Scatton B. 1986. Autoradiographic localization of D1 dopamine receptors in the rat brain with [^{3}H]SCH 23390. Brain Res 375(2):291-301.

Sawaguchi T, Goldman-Rakic PS. 1994. The role of D1-dopamine receptor in working memory: local injections of dopamine antagonists into the prefrontal cortex of rhesus monkeys performing an oculomotor delayed-response task. Journal of neurophysiology 71(2):515-528.

Scarf D, Millar J, Pow N, Colombo M. 2014. Inhibition, the final frontier: the impact of hippocampal lesions on behavioral inhibition and spatial processing in pigeons. Behav Neurosci 128(1):42-47.

Scoville WB, Milner B. 1957. Loss of recent memory after bilateral hippocampal lesions. J Neurol Neurosurg Psychiatry 20(1):11-21.

Seamans JK, Yang CR. 2004. The principal features and mechanisms of dopamine modulation in the prefrontal cortex. Progress in neurobiology 74(1):1-58.

Semendeferi K, Armstrong E, Schleicher A, Zilles K, Van Hoesen GW. 2001. Prefrontal cortex in humans and apes: a comparative study of area 10. Am J Phys Anthropol 114(3):224-241.

Shanahan M, Bingman VP, Shimizu T, Wild M, Güntürkün O. 2013. Large-scale network organization in the avian forebrain: a connectivity matrix and theoretical analysis. Frontiers in computational neuroscience 7:89.

Sherry DF. 2011. The hippocampus of food-storing birds. Brain Behav Evol 78(2):133-135.

Sherry DF, Hoshooley JS. 2010. Seasonal hippocampal plasticity in food-storing birds. Philos Trans R Soc Lond B Biol Sci 365(1542):933-943.

Shiflett MW, Tomaszycki ML, Rankin AZ, DeVoogd TJ. 2004. Long-term memory for spatial locations in a food-storing bird (Poecile atricapilla) requires activation of NMDA receptors in the hippocampal formation during learning. Behav Neurosci 118(1):121-130.

Sihver W, Günther P, Schliebs R, Bigl V. 1997. Repeated administration of tacrine to normal rats: effects on cholinergic, glutamatergic and GABAergic receptor subtypes in rat brain using receptor autoradiography. Neurochem Int 31 (5):693-703.

Smulders TV. 2017. The Avian Hippocampal Formation and the Stress Response. Brain Behav Evol 90(1):81-91.

Sorrells SF, Paredes MF, Cebrian-Silla A, Sandoval K, Qi D, Kelley KW, James D, Mayer S, Chang J, Auguste KI, Chang EF, Gutierrez AJ, Kriegstein AR, Mathern GW, Oldham MC, Huang EJ, Garcia-Verdugo JM, Yang Z, Alvarez-Buylla A. 2018. Human hippocampal neurogenesis drops sharply in children to undetectable levels in adults. Nature 555(7696):377-381.

Sowell ER, Thompson PM, Leonard CM, Welcome SE, Kan E, Toga AW. 2004. Longitudinal mapping of cortical thickness and brain growth in normal children. J Neurosci 24(38):8223-8231.

Squire LR. 2009. The legacy of patient H.M. for neuroscience. Neuron 61(1):6-9.
Starosta S, Güntürkün O, Stüttgen MC. 2013. Stimulus-response-outcome coding in the pigeon nidopallium caudolaterale. PLoS One 8(2):e57407.
Stickgold R. 2005. Sleep-dependent memory consolidation. Nature 437(7063):1272-1278.
Strange BA, Witter MP, Lein ES, Moser EI. 2014. Functional organization of the hippocampal longitudinal axis. Nature reviews Neuroscience 15(10):655-669.
Striedter G. 2005. Prinicples of Brain Evolution. Sinauer Associates, Inc.
Striedter GF. 2016. Evolution of the hippocampus in reptiles and birds. J Comp Neurol 524(3):496-517.
Striedter GF, Belgard TG, Chen CC, Davis FP, Finlay BL, Güntürkün O, Hale ME, Harris JA, Hecht EE, Hof PR, Hofmann HA, Holland LZ, Iwaniuk AN, Jarvis ED, Karten HJ, Katz PS, Kristan WB, Macagno ER, Mitra PP, Moroz LL, Preuss TM, Ragsdale CW, Sherwood CC, Stevens CF, Stüttgen MC, Tsumoto T, Wilczynski W. 2014. NSF workshop report: discovering general principles of nervous system organization by comparing brain maps across species. Brain Behav Evol 83(1):1-8.
Thiebaut de Schotten M, Dell'Acqua F, Ratiu P, Leslie A, Howells H, Cabanis E, Iba-Zizen MT, Plaisant O, Simmons A, Dronkers NF, Corkin S, Catani M. 2015. From Phineas Gage and Monsieur Leborgne to H.M.: Revisiting Disconnection Syndromes. Cerebral cortex 25(12):4812-4827.
Thompson CL, Pathak SD, Jeromin A, Ng LL, MacPherson CR, Mortrud MT, Cusick A, Riley ZL, Sunkin SM, Bernard A, Puchalski RB, Gage FH, Jones AR, Bajic VB, Hawrylycz MJ, Lein ES. 2008. Genomic anatomy of the hippocampus. Neuron 60(6):1010-1021.
Topic B, Willuhn I, Palomero-Gallagher N, Zilles K, Huston JP, Hasenöhrl RU. 2007. Impaired maze performance in aged rats is accompanied by increased density of NMDA, 5-HT1A, and alpha-adrenoceptor binding in hippocampus. Hippocampus 17(1):68-77.
Tosches MA, Yamawaki TM, Naumann RK, Jacobi AA, Tushev G, Laurent G. 2018. Evolution of pallium, hippocampus, and cortical cell types revealed by single-cell transcriptomics in reptiles. Science 360(6391):881-888.
Tully K, Bolshakov VY. 2010. Emotional enhancement of memory: how norepinephrine enables synaptic plasticity. Mol Brain 3:15.
Uylings HB, Groenewegen HJ, Kolb B. 2003. Do rats have a prefrontal cortex? Behav Brain Res 146(1-2):3-17.
Vijayraghavan S, Wang M, Birnbaum SG, Williams GV, Arnsten AF. 2007. Inverted-U dopamine D1 receptor actions on prefrontal neurons engaged in working memory. Nature neuroscience 10(3):376-384.
Vogt BA, Hof PR, Zilles K, Vogt LJ, Herold C, Palomero-Gallagher N. 2013. Cingulate area 32 homologies in mouse, rat, macaque and human: cytoarchitecture and receptor architecture. J Comp Neurol 521(18):4189-4204.
Vorster AP, Born J. 2015. Sleep and memory in mammals, birds and invertebrates. Neurosci Biobehav Rev 50:103-119.
Wada K, Sakaguchi H, Jarvis ED, Hagiwara M. 2004. Differential expression of glutamate receptors in avian neural pathways for learned vocalization. J Comp Neurol 476(1):44-64.
Waldmann C, Güntürkün O. 1993. The dopaminergic innervation of the pigeon caudolateral forebrain: immunocytochemical evidence for a 'prefrontal cortex' in birds? Brain Res 600(2):225-234.
Wang M, Lee FJ, Liu F. 2008. Dopamine receptor interacting proteins (DRIPs) of dopamine D1-like receptors in the central nervous system. Molecules and cells 25(2):149-157.
Williams GV, Goldman-Rakic PS. 1995. Modulation of memory fields by dopamine D1 receptors in prefrontal cortex. Nature 376(6541):572-575.
Wilson MA, Fadel JR. 2017. Cholinergic regulation of fear learning and extinction. J Neurosci Res 95(3):836-852.
Witter MP, Kleven H, Kobro Flatmoen A. 2017. Comparative Contemplations on the Hippocampus. Brain Behav Evol 90(1):15-24.
Wolff SC, Hruska Z, Nguyen L, Dohanich GP. 2008. Asymmetrical distributions of muscarinic receptor binding in the hippocampus of female rats. Eur J Pharmacol 588(2-3):248-250.
Wood R, Liu AG, Bowyer F, Wilby PR, Dunn FS, Kenchington CG, Cuthill JFH, Mitchell EG, Penny A. 2019. Integrated records of environmental change and evolution challenge the Cambrian Explosion. Nat Ecol Evol 3(4):528-538.
Woolley S. 2013. The Songbird Auditory System. Animal Models of Speech and Language Disorders, Springer(Chap.4):61-88.
Yamamoto K, Mirabeau O, Bureau C, Blin M, Michon-Coudouel S, Demarque M, Vernier P. 2013. Evolution of dopamine receptor genes of the D1 class in vertebrates. Mol Biol Evol 30(4):833-843.
Yamamoto K, Reiner A. 2005. Distribution of the limbic system-associated membrane protein (LAMP) in pigeon forebrain and midbrain. J Comp Neurol 486(3):221-242.

Yanagihara S, Yazaki-Sugiyama Y. 2016. Auditory experience-dependent cortical circuit shaping for memory formation in bird song learning. Nat Commun 7:11946.

Yuen EY, Jiang Q, Chen P, Gu Z, Feng J, Yan Z. 2005. Serotonin 5-HT1A receptors regulate NMDA receptor channels through a microtubule-dependent mechanism. J Neurosci 25(23):5488-5501.

Zaborszky L. 2002. The modular organization of brain systems. Basal forebrain: the last frontier. Prog Brain Res 136:359-372.

Zavitsanou K, Wang H, Dalton VS, Nguyen V. 2010. Cannabinoid administration increases 5HT1A receptor binding and mRNA expression in the hippocampus of adult but not adolescent rats. Neuroscience 169(1):315-24.

Zeineh MM, Palomero-Gallagher N, Axer M, Grassel D, Goubran M, Wree A, Woods R, Amunts K, Zilles K. 2017. Direct Visualization and Mapping of the Spatial Course of Fiber Tracts at Microscopic Resolution in the Human Hippocampus. Cerebral cortex 27(3):1779-1794.

Zilles K. 1985. The Cortex of the Rat- A stereotaxic atlas. Springer-Verlag.

Zilles K. 2005. Evolution of the human brain and comparative cyto- and receptor architecture. In: From Monkey Brain to Human Brain (S Dehaene, J-R Duhamel, M Hauser, G Rizzolatti, eds), pp. 41-56. MIT Press, Cambridge.

Zilles K, Amunts K. 2009. Receptor mapping: architecture of the human cerebral cortex. Curr Opin Neurol 22(4):331-339.

Zilles K, Palomero-Gallagher N, Gräßel D, Schlömer P, Cremer M, Woods R, Amunts K, Axer M. 2016. High-Resolution Fiber and Fiber Tract Imaging Using Polarized Light Microscopy in the Human, Monkey, Rat, and Mouse Brain. In Axons and Brain Architecture (Rockland KS, ed), Elsevier, Chap.18:369-389.

Zilles K, Palomero-Gallagher N. 2016. Comparative analysis of receptor subtypes that identify primary cortical sensory areas. In (Kaas, J, Striedter, G, Krubitzer, L, Herculano-Houzel, S, Preuss, T, eds) Evolution of the Nervous System. Elsevier, Oxford: pp 225-245.

Zilles K, Palomero-Gallagher N. 2017. Multiple Transmitter Receptors in Regions and Layers of the Human Cerebral Cortex. Frontiers in neuroanatomy 11:78.

Zilles K, Palomero-Gallagher N, Schleicher A. 2004. Transmitter receptors and functional anatomy of the cerebral cortex. J Anat 205(6):417-432.

Zilles K, Qu M, Schleicher A. 1993. Regional distribution and heterogeneity of alpha-adrenoceptors in the rat and human central nervous system. J Hirnforsch 34(2):123-132.

Zilles K, Schleicher A, Palomero-Gallagher N, Amunts K. 2002. Quantitative analysis of cyto- and receptor architecture of the human brain. In: Mazziotta JC, Toga A (eds) Brain mapping: the methods Elsevier, Amsterdam: pp 573–602.

Zilles K, Wu J, Crusio WE, Schwegler H. 2000. Water maze and radial maze learning and the density of binding sites of glutamate, GABA, and serotonin receptors in the hippocampus of inbred mouse strains. Hippocampus 10(3):213-225.

Zimmer J, Haug FM. 1978. Laminar differentiation of the hippocampus, fascia dentata and subiculum in developing rats, observed with the Timm sulphide silver method. J Comp Neurol 179(3):581-617.

6. Abkürzungsverzeichnis

5-HT, Serotonin
A, Arcopallium
A6, Locus coeruleus, Pars caudalis
A8, Locus coeruleus, Pars rostralis (nach Karten & Hodos, 1967; dopaminerge Zellgruppe A8 nach Reiner et al., 2004 ohne lateinische Bezeichnung)
AA, Arcopallium anterius
ACh, Acetylcholin
ACo, Amygdala, Nucleus corticalis anterior
AD, Arcopallium dorsale
ADl, Arcopallium dorsale, Pars lateralis
ADm, Arcopallium dorsale, Pars medialis
AI, Arcopallium intermedium
AId, Arcopallium intermedium, Pars dorsalis
AIP, Area insularis agranularis posterior
AIv, Arcopallium intermedium, Pars ventralis
AIvm, Arcopallium intermedium, Pars ventromedialis
AL, Ansa lenticularis
AM, Arcopallium mediale
AMm, Arcopallium mediale, Pars magnocellularis
AMp, Arcopallium mediale, Pars parvocellularis
AMPA, (englisch: α-Amino-3-hydroxy-5-methyl-4-isoazolpropionic acid)
AMPA, Glutamaterger AMPA-Rezeptor (Abb.5,6,7,8,9,15)
Anl, Nucleus annularis
AP, Arcopallium posterior
APH, Area parahippocampalis
AV, Arcopallium ventrale
AVm, Arcopallium ventral, Pars medialis
AVT, Area tegmentalis ventralis
BA10l, Brodmann-Area 10, Pars lateralis
BA10m, Brodmann-Area 10, Pars medialis
Bas, Nucleus basorostralis pallii
BC, Brachium conjunctivum
BLA, Amygdala, Nucleus basolateralis, Pars anterior
BLP, Amygdala, Nucleus basolateralis, Pars posterior
BLV, Amygdala, Nucleus basolateralis, Pars ventralis
BMA, Amygdala, Nucleus basomedialis, Pars anterior
BMP, Amygdala, Nucleus basomedialis, Pars posterior
BrdU, Bromdesoxyuridin
BST, Nucleus interstitialis striae terminalis
BSTL, Nucleus interstitialis striae terminalis, Pars lateralis

CA, Commissura anterior (Vögel)
CA1-4, Cornu ammonis 1-4 (Säuger)
Cb, Cerebellum
CDL, Area corticoidea dorsolateralis
CeC, Amygdala, Nucleus centralis, Pars capsularis
CeL, Amygdala, Nucleus centralis, Pars lateralis
CeM, Amygdala, Nucleus centralis, Pars medialis
Cg, Cingulärer Cortex
CO, Chiasma opticum
CoS, Nucleus commissuralis septi
CP, Commissura posterior
CPa, Commissura pallii
CPi, Cortex piriformis
CPu, Nucleus caudatus/Putamen
CS, Nucleus centralis superior
d, dorsal
d32, Brodmann-Area 32, Pars dorsalis
DCX, Doublecortin
DEn, Nucleus endopiriformis dorsalis
DG, Gyrus dentatus
DI, Cortex insularis dysgranularis
DL, dorsolaterale Region der Hippocampusformation
DLd, dorsolaterale Region der Hippocampusformation, Pars dorsalis
DLL, Nucleus dorsolateralis anterior thalami, Pars lateralis
DLP, Nucleus dorsolateralis posterior thalami
DLv, dorsolaterale Region der Hippocampusformation, Pars ventralis
DM, dorsomediale Region der Hippocampusformation
DMd, dorsomediale Region der Hippocampusformation, Pars dorsalis
DMN, Nucleus dorsomedialis hypothalami
DMP, Nucleus dorsomedialis posterior thalami
DMTS, (englisch: Delayed-Matching-To-Sample)
DMv, dorsomediale Region der Hippocampusformation, Pars ventralis
DSD, Decussatio supraoptica, Pars dorsalis
DSV, Decussatio supraoptica, Pars ventralis
E, Entopallium
EC, Entorhinaler Cortex
FA, Tractus fronto-arcopallialis
FDB, Fasciculus diagonalis Broca
FLM, Fasciculus longitudinalis medialis
FR1 (M1), (Prä-)Frontaler Cortex, Area 1 (Primärer Motorcortex)
FR2 (M2), (Prä-)Frontaler Cortex, Area 2 (Sekundärer Motorcortex)
GABA, γ-Aminobuttersäure

$GABA_A$, GABAerger Rezeptor-Subtyp A (Abb. 5-9, 15, 29)
GCt, Griseum centrale
GFAP, Saures Gliafaserprotein (englisch: glial fibrillary acidic protein)
GI, Cortex insularis granularis
Glv, Nucleus geniculatus lateralis, Pars ventralis
GP, Globus pallidus
HA, Hyperpallium apicale
HD, Hyperpallium densocellulare
HF, Hippocampusformation
HI, Hyperpallium intercalatum
Hp, Hippocampus
I-VI, Schichten des Cortex
ICo, Nucleus intercollicularis
IF, Tractus infundibuli
IN, Nucleus infundibuli hypothalami
INP, Nucleus intrapeduncularis
IP, Nucleus interpeduncularis
Kainat, Glutamaterger Kainat-Rezeptor (Abb. 5-9, 15)
l, lateral
L2, Feld L2
LaDL, Amygdala, Nucleus lateralis, Pars dorsolateralis
LaVL, Amygdala, Nucleus lateralis, Pars ventrolateralis
LaVM, Amygdala, Nucleus lateralis, Pars ventromedialis
LC, Nucleus linearis caudalis
LHy, Lateraler Hypothalamus
LSt, Laterales Striatum
LTD, Langzeitdepression (englisch: long term depression)
LTP, Langzeitpotenzierung (englisch: long term potentiation)
m, medial
M, Mesopallium
MD, Mesopallium dorsale
MeAD, Amygdala, Nucleus medialis, Pars anterodorsalis
MePD, Amygdala, Nucleus medialis, Pars posterodorsalis
MePV, Amygdala, Nucleus medialis, Pars posteroventralis
ML, Nucleus mamillaris lateralis
MM, Nucleus mamillaris medialis
MSt, Striatum mediale
MV, Mesopallium ventrale
MVL, Mesopallium ventrolaterale
N, Nidopallium
nACh, Nikotinischer cholinerger Rezeptor-Subtyp $\alpha_4\beta_2$ (Abb. 5, 6, 8, 15)
NCL, Nidopallium caudolaterale

NCLl, Nidopallium caudolaterale, Pars lateralis
NCLm, Nidopallium caudolaterale, Pars medialis
NCM, Nidopallium caudomediale
NCV, Nidopallium caudoventrale
NCVl, Nidopallium caudoventrale, Pars lateralis
NDB, Nucleus diagonalis Brocae
NeuN, Neuron-Nuclei-Marker-Protein
NI, Nidopallium intermedium
NMDA, N-Methyl-D-Aspartat
NMDA, glutamaterger NMDA-Rezeptor (Abb. 5-9, 15)
OB, Bulbus olfactorius
OM, Tractus occipitomesencephalicus
OPH, Organum paraventriculare
Ov, Nucleus ovoidalis
P, Pallidum
p32, Brodmann-Area 32, Pars praegenual
PD, Nucleus preopticus, Pars dorsalis
PFC, Präfrontaler Cortex
PLH, Nucleus lateralis hypothalami posterioris
PME, Eminentia mediana posterior
PMH, Nucleus medialis hypothalami posterioris
PMI, Nucleus paramedianus internus thalami
PMM, Nucleus pre-mamillaris
PoA, Nucleus posterioris amygdalopallii
PoA, Nucleus preopticus anterior (Abb. 18)
PoAb, Nucleus posterioris amygdalopallii, Pars basalis
PoAc, Nucleus posterioris amygdalopallii, Pars compacta
POM, Nucleus preopticus medialis
PPC, Nucleus principalis precommissuralis
PPM, Nucleus preopticus magnocellularis
PT, Nucleus pretectalis
PVM, Nucleus periventricularis magnocellularis
PVNm, Nucleus paraventricularis, Pars magnocellularis
PVNp, Nucleus paraventricularis, Pars parvocellularis
PVO, Organum paraventriculare
QF, Tractus quintofrontalis
R, Nucleus raphe pontis
S, Septumregion
S1, Somatosensorischer Cortex, primär
S2, Somatosensorischer Cortex, sekundär
s32, Brodmann-Area 32, Pars subgenual
SCE, Stratum cellulare externum

SCI, Stratum cellulare internum
SG, Stratum granulosum
SGZ, subgranuläre Zone
SL, Laterales Septum (Abb. 20, 21)
SL, Nucleus septalis lateralis
SM, Mediales Septum (Abb. 20, 21)
SM, Nucleus septalis medialis
SM, Stratum moleculare (Abb. 1)
SMTS, englisch: Simultaneous-Matching-To-Sample
SOe, Nucleus supraopticus externus
SpA, Area subpallialis amygdalae
SR, englisch: Stimulus-Response
ST, Striatum
STIA, Nucleus interstitialis striae terminalis, Pars intra-amygdaloideum
TeO, Tectum opticum
TnA, Nucleus taeniae amygdalae
TPO, Area temporo-parieto-occipitalis
Tr, Trianguläre Zwischenregion der Hippocampusformation
TSM, Tractus septopallio-mesencephalicus
TuO, Tuberculum olfactorium
v, ventral
V, Ventrikel
v32, Brodmann-Area 32, Pars ventralis
VEn, Nucleus endopiriformis ventralis
Vl, Ventrolaterales Zellband der Hippocampusformation
Vm, Ventromediales Zellband der Hippocampusformation
VMN, Nucleus ventromedialis hypothalami
VP, Pallidum ventrale
ZpFLM, Zona perifasciculus longitudinalis medialis

7. Danksagung

Ich möchte mich bei Frau Prof. Dr. Katrin Amunts für Ihre großzügige Unterstützung meiner wissenschaftlichen Arbeit bedanken, insbesondere weil sie mir nach dem Direktionswechsel im C. & O. Vogt-Institut an der HHU die Möglichkeit gegeben hat im Rahmen meines eigenen Forschungsfeldes weiterhin selbständig zu arbeiten. Zudem danke ich dir herzlich für das entgegengebrachte Vertrauen in mich und meine wissenschaftlichen Arbeiten, deine Offenheit, und die Möglichkeit, sich in einem interdisziplinären Team weiterzuentwickeln und jederzeit über den Tellerrand zu schauen.

Prof. Dr. Dr. h.c. Karl Zilles danke ich dafür, dass er mich seinerzeit im C. & O. Vogt-Institut an der HHU eingestellt hat, mich zu jedem Zeitpunkt wohlwollend in meinen Ideen unterstützt hat und mir damit den Weg zu dieser Arbeit erst ermöglicht hat. Ich danke ihm darüber hinaus insbesondere für den andauernden wissenschaftlichen und fachlichen Austausch, der auch nach seiner „Pensionierung“ noch erfolgte (der abseits vom Balkon der 6.Etage des ehemaligen Vogt-Institutes auch im einzigen „Raucherbüro“ im FZ Jülich sehr angenehm war) und die Unterstützung bei gemeinsamen Publikationen. Ich danke Ihnen von Herzen für Ihr grundlegendes Interesse an der vergleichenden Neuroanatomie, die Aufrechterhaltung/ Erweiterung der Hirnsammlung und der Vielfältigkeit der möglichen Arbeiten, die dies auch für zukünftige Arbeiten mit sich bringen kann.

Prof. Dr. Dr. h.c. Onur Güntürkün möchte ich dafür danken, dass er mich auch nach Abschluss meiner Promotion und dem Weggang aus Bochum zunächst weiterhin fachlich begleitet hat, wir viele offene Diskussionen geführt haben und starke Kooperationspartner geworden sind. Auch möchte ich mich dafür bedanken, dass er immer wieder neue Kooperationspartner miteinschließt und so die Qualität der Arbeiten auf einem exzellenten Niveau hält. Onur, vielen Dank, ich schätze dich und dein Engagement für die Wissenschaft sehr und bin gerne zwischendurch immer mal wieder „zu Hause“ in Bochum.

Dr. Hans-Jürgen Bidmon danke ich für die vielen aufmunternden Flurgespräche, den wissenschaftlichen Austausch in jeder Hinsicht und Thematik und seine Hilfsbereitschaft im Labor. Hans, du bist einzigartig. Danke dafür!

Dr. Nicola Palomero-Gallagher danke ich für die kompetente Einarbeitung in die Methode der Rezeptorautoradiografie und ihr gutes Auge auf die korrekte Anwendung. Ich danke dir außerdem für deine andauernde Kooperationsbereitschaft liebe Nicola.

Dr. Markus Axer möchte ich danken, weil er mir die Möglichkeit gegeben hat, auch am Forschungszentrum Jülich eine Basis zu finden und mir im Rahmen seiner Arbeitsgruppe die Einführung und Nutzung in das 3D-PLI zur Verfügung gestellt hat. Ich danke dir Markus ebenfalls für den offenen Austausch und die Bereitschaft, dich fachlich in völlig unbekannte Gefilde zu begeben und somit gemeinsam mit mir wissenschaftlich neue Wege zu gehen.

Bei Herrn Dipl. Phys. David Gräßel möchte ich mich besonders herzlich dafür bedanken, dass er mich bei der Erlernung der Durchführung und der Auswertung des 3D-PLI zu jeder Tages- und Nachtzeit unterstützt hat und bereit war sich selbstlos kontinuierlich einzubringen. Danke, du gute Seele des 3D-PLI Labs!

Frau Nicole Delhaes möchte ich insbesondere für ihre Zuverlässigkeit im Labor und ihre Offenheit, sich methodisch immer weiterzuentwickeln, danken. Ich danke dir dafür, dass du mitdenkst und für das Vertrauen, dass sich in den Jahren daraus aufgebaut hat. Ich wünsche dir für Ohio nur das Allerbeste! Komm irgendwann wieder ;)
Frau Angelika Hallenberger, ich danke dir dafür, dass du mich damals in Düsseldorf so herzlich begrüßt hast und dich mit Eifer für meine Projekte ins Feuer gelegt hast.
Meinen vielen anderen Kollegen und Kolleginnen sowie Studierenden, sowohl an der HHU, an der RUB, im FZ Jülich als auch an der UCSD, die mir innerhalb meiner wissenschaftlichen Laufbahn und Lehre begegnet sind und so für weitläufigen und abwechslungsreichen Austausch gesorgt haben, möchte ich ebenfalls danken.
Ich danke den Tieren, den Körperspendern und den Patienten, die durch ihre Teilnahme meine Studien überhaupt erst ermöglicht haben.
Ich danke in höchstem Maß meiner Familie, meinen Freunden und meinen Wegbegleitern, die mich alle, ganz gleich auf welche Art, dabei unterstützt haben, diese Arbeit zu leisten.
Ich danke jedoch am allermeisten meinen Kindern, Lisa, Anna und Julius, die mich tagtäglich an mein eigenes inneres Kind erinnern, das immer bereit ist sich mit Freude auf die Reise zu begeben, Neues zu entdecken und neues Wissen zu erlangen.

8. Originalarbeiten

1. **Christina Herold,** Nicola Palomero-Gallagher, Burkhard Hellmann, Carsten Theiss, Sven Kröner, Onur Güntürkün and Karl Zilles (2011) *The Receptorarchitecture of the Pigeon's Nidopallium caudolaterale: An Avian Analogue to the Mammalian Prefrontal Cortex.* Brain Structure and Function 216: 239-254. doi: 10.1007/s00429-011-0301-5.
2. **Christina Herold,** Illah Joshi, Omar Chehadi, Michael Hollmann and Onur Güntürkün (2012a) *Plasticity in D1-Like Receptor Expression Is Associated with Different Components of Cognitive Processes.* PLOS ONE 7 (5) e36484. doi: 10.1371/journal.pone.0036484.
3. **Christina Herold,** Nicola Palomero-Gallagher, Onur Güntürkün and Karl Zilles (2012b) *Serotonin 5-HT1A Receptor Binding Sites in the Brain of the Pigeon (Columba livia).* Neuroscience 200: 1-12. doi: 10.1016/j.neuroscience.2011.10.050.
4. Brent Vogt, Patrick Hof, Karl Zilles, Leslie Vogt, **Christina Herold** and Nicola Palomero-Gallagher (2013) *Cingulate Area 32 Homologies in Mouse, Rat, Macaque and Human.* The Journal of Comparative Neurology 521(18): 4189-204. doi: 10.1002/cne.23409.
5. **Christina Herold**, Vern P. Bingman, Felix Ströckens, Sarah Letzner, Magdalena Sauvage, Nicola Palomero-Gallagher, Karl Zilles and Onur Güntürkün (2014) *Distribution of Neurotransmitter Receptors and Zinc in the Pigeon (Columba livia) Hippocampal Formation: A Basis for further Comparison with the Mammalian Hippocampus.* The Journal of Comparative Neurology 522(11): 2553-75. doi: 10.1002/cne.23549.
6. Tiago S. dos Santos, Jéssica Krüger, Fernando F. Melleu, **Christina Herold**, Karl Zilles, Anicleto Poli, Onur Güntürkün and José Marino-Neto (2015) *Distribution of Serotonin 5-HT_{1A}-binding Sites in the Brainstem and the Hypothalamus, and their Roles in 5-HT-induced Sleep and Ingestive Behaviors in Rock Pigeons (Columba livia).* Behavioral Brain Research 295:45-63. doi: 10.1016/j.bbr.2015.03.059.
7. **Christina Herold**, Christina Paulitschek, Nicola Palomero-Gallagher, Onur Güntürkün, Karl Zilles (2018b) *Transmitter receptors reveal segregation of the arcopallium/amygdala complex in pigeons (Columba livia)*. Journal of Comparative Neurology 526(3):439-466. doi: 10.1002/cne.24344.
8. **Christina Herold**, Philipp Schlömer, Isabelle Mafoppa-Fomat, Julia Mehlhorn, Katrin Amunts, Markus Axer (2019) *The Hippocampus of birds in a view of evolutionary connectomics.* Cortex 118: 165-187. doi: 10.1016/j.cortex.2018.09.025.

Brain Struct Funct
DOI 10.1007/s00429-011-0301-5

ORIGINAL ARTICLE

The receptor architecture of the pigeons' nidopallium caudolaterale: an avian analogue to the mammalian prefrontal cortex

Christina Herold · Nicola Palomero-Gallagher · Burkhard Hellmann · Sven Kröner · Carsten Theiss · Onur Güntürkün · Karl Zilles

Received: 26 October 2010 / Accepted: 12 January 2011
© Springer-Verlag 2011

Abstract The avian nidopallium caudolaterale is a multimodal area in the caudal telencephalon that is apparently not homologous to the mammalian prefrontal cortex but serves comparable functions. Here we analyzed binding-site densities of glutamatergic AMPA, NMDA and kainate receptors, GABAergic $GABA_A$, muscarinic M_1, M_2 and nicotinic (nACh) receptors, noradrenergic α_1 and α_2, serotonergic 5-HT_{1A} and dopaminergic D_1-like receptors using quantitative in vitro receptor autoradiography. We compared the receptor architecture of the pigeons' nidopallial structures, in particular the NCL, with cortical areas Fr2 and Cg1 in rats and prefrontal area BA10 in humans. Our results confirmed that the relative ratios of multiple receptor densities across different nidopallial structures (their "receptor fingerprints") were very similar in shape; however, the absolute binding densities (the "size" of the fingerprints) differed significantly. This finding enables a delineation of the avian NCL from surrounding structures and a further parcellation into a medial and a lateral part as revealed by differences in densities of nACh, M_2, kainate, and 5-HT_{1A} receptors. Comparisons of the NCL with the rat and human frontal structures showed differences in the receptor distribution, particularly of the glutamate receptors, but also revealed highly conserved features like the identical densities of $GABA_A$, M_2, nACh and D_1-like receptors. Assuming a convergent evolution of avian and mammalian prefrontal areas, our results support the hypothesis that specific neurochemical traits provide the molecular background for higher order processes such as executive functions. The differences in glutamate receptor distributions may reflect species-specific adaptations.

Keywords Receptor autoradiography · Prefrontal cortex · Nidopallium caudolaterale · Rat · Human · Fr2 · Cg1 · BA10 · Dopamine · Glutamate · GABA

Abbreviations

ACh	Acetylcholine
AMPA	α-Amino-3-hydroxy-5-methyl-4-isoxalone propionic acid
Cg1	Cingulate cortex 1
CDL	Dorsolateral corticoid area
EPSCs	Excitatory postsynaptic currents
FR2	Frontal area 2
GABA	γ-Aminobutyric acid
GLI	Gray level index
gluR1	Glutamate receptor subunit 1
HA	Hyperpallium apicale
HVC	Higher vocal center
IMM	Intermediate and medial mesopallium ventrale

C. Herold (✉) · K. Zilles
C. and O. Vogt-Institute of Brain Research,
University of Düsseldorf, 40225 Düsseldorf, Germany
e-mail: christina.herold@uni-duesseldorf.de

N. Palomero-Gallagher · K. Zilles
Institute of Neuroscience and Medicine INM-2,
Research Center Jülich, 52425 Jülich, Germany

B. Hellmann · O. Güntürkün
Department of Biopsychology,
Institute of Cognitive Neuroscience,
Faculty of Psychology, Ruhr-University Bochum,
44780 Bochum, Germany

C. Theiss
Institute of Anatomy and Molecular Embryology,
Faculty of Medicine, Ruhr-University Bochum,
44780 Bochum, Germany

S. Kröner
School of Behavioral and Brain Sciences, The University
of Texas at Dallas, Richardson, TX 75080, USA

Published online: 04 February 2011

MNH	Mediorostral nidopallium/hyperpallium
nACh	Nicotinic acetylcholine
NCC	Nidopallium caudocentrale
NCL	Nidopallium caudolaterale
NCLl	Nidopallium caudolaterale pars lateralis
NCLm	Nidopallium caudolaterale pars medialis
NCM	Nidopallium caudomediale
NFT	Nidopallium fronto-trigeminale
NIM	Nidopallium intermedium medialis
NMDA	*N*-methyl-D-aspartate
PFC	Prefrontal cortex

Introduction

The increasingly refined parcellation of the mammalian cerebral cortex with anatomical methods enables various analyses of its functional segregation (Uylings et al. 2000; Amunts et al. 2004; Eickhoff et al. 2006, Amunts et al. 2007; Naito et al. 2008; Palomero-Gallagher et al. 2009; Zilles and Amunts 2010). Similarly, in the last decades the avian forebrain has been subdivided by various means. These efforts have fostered a new understanding of the avian telencephalic organization and the assumed homologies between avian and mammalian brain components (Reiner et al. 2004). This new view, which is rooted in a series of seminal studies over the last 40 years (Karten 1969), assumes that mammalian and avian pallia are homologous in terms of shared pallial identity that derive from common ancestry (Jarvis et al. 2005). This assumption, however, does not imply that cortical or subcortical pallial areas have to be one-to-one homologous to pallial components in birds. Thus, pallial structures of birds and mammals might be similar in terms of anatomical, physiological and cognitive characteristics, but may still represent the result of convergent evolution.

The avian nidopallium caudolaterale (NCL) is such a case. Numerous studies show that the mammalian prefrontal cortex (PFC) and the avian NCL share several anatomical (Kröner and Güntürkün 1999), neurochemical (Bast et al. 2002; Karakuyu et al. 2007), electrophysiological (Diekamp et al. 2002a; Kalenscher et al. 2005; Rose and Colombo 2005), and functional (Güntürkün 1997; Diekamp et al. 2002b; Kalenscher et al. 2003; Lissek and Güntürkün 2005) characteristics; however, several genetic (Puelles et al. 2000) and topological arguments (Medina and Reiner 2000) make a homology between the PFC and the NCL unlikely. Therefore, the similarities of these two structures likely do not result from common ancestry but represent the outcome of an evolutionary convergence. Thus, a common selection pressure for an 'executive' behavioral repertoire possibly facilitates emergence of non-homologous forebrain areas of mammals and birds that share typical 'prefrontal' characteristics (Güntürkün 2005a; Kirsch et al. 2008).

The NCL displays a homogeneous cytoarchitecture and does not differ considerably from neighboring portions of the nidopallium either. The NCL was first defined by its dopaminergic innervation and high tyrosine hydroxylase density (Divac et al. 1985; Waldmann and Güntürkün 1993). To date, the outer borders and the internal structure of the NCL have been analyzed with immunocytochemical (Wynne and Güntürkün 1995; Bock et al. 1997; Schnabel et al. 1997; Durstewitz et al. 1998; Riters et al. 1999) and ultrastructural methods (Metzger et al. 2002) as well as in several tracing studies (Leutgeb et al. 1996; Metzger et al. 1998; Kröner and Güntürkün 1999). Receptor autoradiography is an additional powerful tool to define areal borders and to derive region-specific receptor-density combinations that define areas like 'fingerprints' (Zilles et al. 2002b). Therefore, the first aim of this study was to map the chemoarchitecture of the NCL. This approach is important to define the areal borders between the nidopallium caudocentrale (NCC) and the NCL, since different studies using tracing techniques or immunocytochemistry showed discrepant delineations (Wynne and Güntürkün 1995; Waldmann and Güntürkün 1993; Kröner and Güntürkün 1999; Atoji and Wild 2009). Although, the border to the laterally and supraventricular located dorsolateral corticoid area (CDL) and the NCL is easier to define, it was additionally included in the analysis here.

The second aim of this study was to investigate possible subdivisions within the NCL because numerous studies in mammals have implicated subdivisions of the PFC in the processing of different stimulus domains (Levy and Goldman-Rakic 1999). Similarly, there is also evidence for a parcellation of the NCL based on functional, neurochemical and hodological data (Leutgeb et al. 1996; Braun et al. 1999; Kröner and Güntürkün 1999; Riters et al. 1999; Diekamp et al. 2002b). Riters et al. (1999) proposed a dorsoventral distinction of the NCL based on the distribution of tyrosine hydroxylase, choline acetyltransferase and substance P labeled fibers and terminals. Accordingly, lesions of the dorsal NCL result in delay-specific working memory deficits (Diekamp et al. 2002b). The high density of tyrosine hydroxylase positive fibers in the dorsal NCL might be related to the important role of dopamine in working memory functions as shown in primates (Goldman-Rakic 1999) and birds (Karakuyu et al. 2007). Based on connectivity data, however, Kröner and Güntürkün (1999) assumed a frontocaudal distinction with the caudal portion being tightly embedded within the limbic system.

The third aim was to compare the receptor fingerprints of mammalian frontal and prefrontal areas with those of the avian NCL in order to examine whether a common

functional repertoire is reflected by a similar pattern of receptor architecture. For this purpose we studied the receptor fingerprints of the medial and the lateral portions of Brodmann's human prefrontal cortex area BA10 (BA10m and BA10l, respectively) and the rat frontal area 2 (Fr2) as well as the rat prefrontal cingulate area 1 (Cg1) (Brodmann 1909; Uylings et al. 2003). Owing to their connectivity patterns with other neocortical areas, the thalamus, the basal ganglia, and the amygdala, both Fr2 and Cg1 were structurally and functionally compared with the dorsolateral prefrontal cortex in primates (Uylings et al. 2003; Van de Werd et al. 2010). However, it has to be noted they there are still discrepancies in the delineations of rat prefrontal and motor cortical structures; furthermore, Fr2 is classified as the rodent's motor cortex (Van Eden et al. 1992; Zilles 1985).

Taken together, our receptor autoradiographic study was aimed to constitute an independent approach to these open questions.

Materials and methods

We examined a total of six pigeons (*Columba livia*) of unknown sex and eight male rats (*Long-Evans*). Animals were decapitated and the brains removed from the skull, frozen immediately in isopentane at −40°C and stored at −70°C. Serial coronal 10 µm sections were cut with a cryostat microtome (2800 Frigocut E, Reichert-Jung). Sections were thaw-mounted on gelatinized slides and freeze-dried.

Post-mortem human brain tissue was studied from 2 control subjects (age 72 male and age 77 female, post-mortem time 8 and 18 h) without a record of neurological or psychiatric disorders and was obtained from the body donor program of the Department of Anatomy, University of Düsseldorf, Germany. Causes of death were a heart attack and carcinoma. Serial coronal cryosections (20 µm) comprising the whole cross-section of unfixed brain blocks were prepared at −20°C using a large-scale cryostat microtome. Sections were thaw-mounted on gelatinized slides, freeze-dried and stained with a modified cell body staining for cytoarchitectonic analysis (Merker 1983; Palomero-Gallagher et al. 2008) or processed for receptor autoradiography.

Receptor autoradiography

Details of the autoradiographic labeling procedure have been published elsewhere (Zilles et al. 2002b; Palomero-Gallagher et al. 2009). Binding protocols are summarized in Table 1. Three steps were performed in the following sequence: (1) A preincubation step removed endogenous ligand from the tissue. (2) During the main incubation step, binding sites were labeled with triated ligand (total binding). Coincubation of the triated ligand and a 1,000 to 10,000-fold excess of an appropriate non-labeled ligand (displacer) determined non-specific and thus non-displaceable binding. Specific binding is the difference between total and non-specific binding. (3) A final rinsing step eliminated unbound radioactive ligand from the sections.

The following binding sites were labeled according to standardized protocols: α-amino-3-hydroxy-5-methyl-4-isoxalone propionic acid (AMPA) with [^{3}H] AMPA, kainate with [^{3}H]kainate, *N*-methyl-D-aspartate (NMDA) with [^{3}H]MK-801, γ-aminobutyric acid A ($GABA_A$) receptor with [^{3}H]muscimol, muscarinic cholinergic M_1 receptor with [^{3}H]pirenzepine, muscarinic cholinergic M_2 receptor with [^{3}H]oxotremorine-M, nicotinic cholinergic (nACh) receptor with [^{3}H]cytosine (pigeon) or [^{3}H]epibatidine (rat and human), noradrenergic α_1 adrenoreceptor with [^{3}H]prazosin, noradrenergic α_2 adrenoreceptor with [^{3}H] RX-821002, serotonergic 5-HT_{1A} receptor with [^{3}H]8-OH-DPAT, and dopaminergic D_1-like receptors with [^{3}H]SCH 23390. Sections were air-dried overnight and subsequently coexposed for 4–5 weeks against a tritium-sensitive film (Hyperfilm, Amersham, Braunschweig, Germany) with plastic [^{3}H]-standards (Microscales, Amersham) of known concentrations of radioactivity.

Image analysis

The resulting autoradiographs were subsequently processed using densitometry with a video-based image analyzing technique (Zilles et al. 2002b; Schleicher et al. 2005). Autoradiographs were digitized by means of a KS-400 image analyzing system (Kontron, Germany) connected to a CCD camera (Sony, Tokyo) equipped with a S-Ortho-planar 60-mm macro lens (Zeiss, Germany). The images were stored as binary files with a resolution of 512 × 512 pixels and 8-bit gray value. The gray value images of the coexposed microscales were used to compute a calibration curve by non-linear, least-squares fitting, which defined the relationship between gray values in the autoradiographs and concentrations of radioactivity. This enabled the pixel-wise conversion of the gray values of an autoradiograph into the corresponding concentrations of radioactivity. These concentrations of binding sites occupied by the ligand under incubation conditions are transformed into fmol binding site/mg protein at saturation conditions by means of the equation: $(K_D + L)/A_S \times L$, where K_D is the equilibrium dissociation constant of ligand-binding kinetics, L is the incubation concentration of ligand, and A_S the specific activity of the ligand. The mean of the gray values contained in a specific region over a series of 4–5 sections

Table 1 Incubation conditions for receptor autoradiography

Receptor	[^{3}H] ligand (incubation concentration)	Displacer (incubation concentration)	Incubation buffer	Preincubation step	Main incubation step	Rinsing step
AMPA	[^{3}H]AMPA (10 nM)	Quisqualate (10 μM)	50 mM Tris–acetate (pH 7.2)	3 × 10 min at 4°C in incubation buffer	45 min at 4°C in incubation buffer + 100 mM KSCN	4 × 4 s at 4°C in incubation buffer + 2 × 2 s at 4°C in acetone/glutaraldehyde
Kainate	[^{3}H]kainate (8 nM)	Kainate (100 μM)	50 mM Tris–citrate (pH 7.1)	3 × 10 min at 4°C in incubation buffer	45 min at 4°C in incubation buffer + 10 mM Ca-acetate	4 × 4 s at 4°C in incubation buffer + 2 × 2 s at 4°C in acetone/glutaraldehyde
NMDA	[^{3}H]MK-801 (5 nM)	MK-801 (100 μM)	50 mM Tris–HCl (pH 7.2)	15 min at 25°C in incubation buffer	60 min at 25°C in incubation buffer + 30 μM glycine + 50 μM spermidine	2 × 5 min at 4°C in incubation buffer
Muscarinergic cholinergic M_1	[^{3}H]pirenzipine (1nM)	Pirenzipine (10 μM)	Modified Krebs–Ringer buffer (pH 7.4)	20 min at 25°C in incubation buffer	60 min at 25°C in incubation buffer	2 × 5 min at 4°C in incubation buffer
Muscarinergic cholinergic M_2	[^{3}H]oxotremonine-M (0.8 nM)	Carbachol (1 μM)	20 mM Hepes–Tris (pH 7.5) + 10 mM $MgCl_2$	20 min at 25°C in incubation buffer	60 min at 25°C in incubation buffer	2 × 2 min at 4°C in incubation buffer
Nicotinic cholinergic	[^{3}H]cytisine [1 nM]	Nicotine (10 μM)	50 mM Tris–HCl (pH7.4) + 120 mM NaCl + 5 mM KCl + 1 mM $MgCl_2$ + 2.5 mM $CaCl_2$	15 min at 22°C in incubation buffer	90 min at 4°C in incubation buffer	2 × 2 min at 4°C in incubation buffer
	[^{3}H]epibatidine [0.5 nM]	Nicotine (10 μM)	15 mM Hepes–Tris (pH 7.5) + 10 mM NaCl + 5.4 mM KCl + 0.8 mM $MgCl_2$ + 1.8 mM $CaCl_2$	20 min at 22°C in incubation buffer	90 min at 4°C in incubation buffer	1 × 5 min at 4°C in incubation buffer 2 × up & down in distilled H_2O
α_1 Adrenoreceptor	[^{3}H]prazosin (0.2 nM)	Phentolamine (10 μM)	50 mM Tris–HCl (pH 7.4)	30 min at 37°C in incubation buffer	45 min at 30°C in incubation buffer	2 × 5 min at 4°C in incubation buffer
α_2 Adrenoreceptor	[^{3}H]UK-14304 (1.4 nM)	Noradrenalin (100 μM)	50 mM Tris–HCl (pH 7.7) + 100 μM $MnCl_2$	15 min at 22°C in incubation buffer	90 min at 22°C in incubation buffer	5 min at 4°C in incubation buffer
$GABA_A$	[^{3}H]muscimol (6 nM:pigeon and 3 nM:human)	GABA (10 μM)	50 mM Tris–citrate (pH 7.0)	3 × 5 min at 4°C in incubation buffer	40 min at 4°C in incubation buffer	3 × 3 s at 4°C in incubation buffer
Serotoninergic 5-HT_{1A}	[^{3}H]8-OH-DPAT (1 nM)	Serotonin (10 μM)	170 mM Tris–HCl (pH 7.6) + 4 mM $CaCl_2$ + 0.01% ascorbic acid	30 min at 22°C in incubation buffer	60 min at 22°C in incubation buffer	1 × 5 min at 4°C in incubation buffer
Dopaminergic D_1-like	[^{3}H]SCH-23390 (0.5 nM)	SKF 83566 (1 μM)	50 mM Tris–HCl (pH 7.4) + 120 mM NaCl + 5 mM KCl + 2 mM $CaCl_2$ + 1 mM $MgCl_2$ + 1 μM mianserin	20 min at 22° C in incubation buffer	90 min at 22° C in incubation buffer	2 × 10 min at 4° C in incubation buffer

from one animal is thus transformed into a receptor concentration (fmol/mg protein).

Anatomical identification

The borders of the NCL were identified based on previous neurochemical (Waldmann and Güntürkün 1993) and tract-tracing studies (Kröner and Güntürkün 1998). The borders of the NCL and surrounding structures as defined in the atlas of Karten and Hodos (1967) were traced on prints of the digitized autoradiographs. The borders of rat Fr2 and Cg1 were anatomically identified based on a rat cortex atlas (Zilles 1985). We decided to analyze these two regions because they are assumed to be a part of the rat frontal and prefrontal cortex (Uylings et al. 2003). The borders of human BA10 were identified based on criteria defined by Brodmann (Brodmann 1909). BA10m and BA10l were additionally defined and traced onto digitized autoradiographs ($n = 3$ hemispheres). The mean of the gray values contained in a specific region over a series of 4–5 sections from one hemisphere is thus transformed into a receptor concentration per unit protein (fmol/mg protein).

Statistical analysis

To investigate the chemoarchitectural differences between the NCL and the surrounding structures, the binding site concentrations of the NCL were compared with those of the nidopallium caudomediale (NCM, located medial to NCL) and the dorsolateral corticoid area (CDL, located dorsolaterally to NCL, above the ventricle). First, a Friedman ANOVA was conducted. If significant, pair wise comparisons were run with the Wilcoxon rank test. Binding site concentrations of the NCM were measured medial to Field L. Differences between nidopallium caudolaterale pars medialis (NCLm) and nidopallium caudolaterale pars lateralis (NCLl) were further analyzed with Wilcoxon rank tests.

Results

Receptor-binding site densities in avian pallial structures

The most caudal portion of the avian nidopallium displays a rather homogeneous cytoarchitecture. The only subventricular cytoarchitectural feature that is clearly different from the otherwise homogeneous pattern is Field L in the most medial part. Within Field L, especially, the granular layer L2 is readily visible. Ventrolaterally, the lamina arcopallialis dorsalis defines the borderline between the nidopallium and the arcopallial and the amygdalar substructures. Dorsally, the caudal cap of the lateral ventricle separates the nidopallium from the CDL and the hippocampal and parahippocampal structures. The distribution of different ligand-binding sites shows that the cytoarchitectonically seemingly homogeneous caudal nidopallium is in fact comprised of several substructures. Further, the examined receptor types not only enabled a clear delineation of the NCL from the adjoining areas, but also revealed the existence of two hitherto unknown subentities. Stereotaxic coordinates, A 5.50 and A 6.75, were chosen as exemplary levels for which all receptor types were shown in Fig. 1a and b. Different binding-site densities within the borders of the NCL could be followed up to the most caudal aspect of the subventricular forebrain where it constituted the most caudal tip of the nidopallium. Frontally, the NCL was visible up to A 7.50 (anterior–posterior coordinates according to the pigeon brain atlas of Karten and Hodos 1967). Further, binding-site densities of the different receptor ligands are presented relative to each other in a 2-dimensional coordinate plot to construct a receptor fingerprint for a given brain area (Fig. 2). This allows us to compare the shape and the absolute size of this receptor fingerprint across brain areas and between species.

As illustrated in the autoradiographs and in the fingerprints, glutamatergic AMPA and NMDA receptors show the highest densities of all measured receptors, and were followed by $GABA_A$ receptor densities. Conversely, lowest values were found for nACh, α_1 and D_1-like receptor densities (Figs. 1a/b, 2a).

The mean density of AMPA receptors for the whole NCL was 2,252 ± 269 fmol/mg protein. A comparison of binding densities between NCL, NCC and CDL using a Friedman ANOVA showed no significant overall effects [Chi Square ($N = 6$, df = 2) = 1, n.s.].

Overall densities for kainate receptor-binding sites were 660 ± 81 fmol/mg (Fig. 1a/b). Because kainate receptor-binding sites were approximately fivefold lower than those of AMPA receptors, and sixfold lower than those of NMDA receptors, this resulted in a considerable indentation in the fingerprint (Fig. 2a). Binding of [^{3}H]kainate was highest in the most lateral portion of the NCL (Figs. 1a/b, 3). We labeled this area nidopallium caudolaterale pars lateralis (NCLl) to differentiate it from the medial portion of the NCL (NCLm). The Friedman ANOVA showed a significant overall effect [Chi Square ($N = 6$, df = 2) = 10.33, $p < 0.01$]. Binding was higher both in NCL and NCC than in CDL (all $N = 6$, $T = 0$, $p < 0.05$). Additionally, a significant higher concentration of kainate receptors in the lateral than in the medial aspect of the NCL was detected ($N = 6$, $T = 1$, $p < 0.05$; Fig. 3).

Binding of [^{3}H]MK-801 was very high throughout the entire caudal nidopallium (Fig. 1a/b), indicating a high

density of NMDA receptors. Binding density reached 2,525 ± 143 fmol/mg protein (Figs. 1a, 2a) in NCL. Like for the AMPA receptors this results in a prominent peak in the fingerprints (c.f Fig. 2a). The Friedman ANOVA comparing NCL, NCC and CDL showed a significant overall effect [Chi Square ($N = 6$, df $= 2$) $= 8.33$, $p < 0.05$]. A subsequent Wilcoxon test revealed significantly higher values for NCL and NCM over CDL (all $N = 6$, $T \leq 1$, $p < 0.05$).

$GABA_A$ receptor-binding sites were labeled with [^{3}H]muscimol (mean density 1,810 ± 188 fmol/mg protein). Since binding increased medial to NCC, the border of the NCL could be easily visualized (Fig. 1a/b). The Friedman ANOVA showed a significant main effect [Chi Square ($N = 6$, df $= 2$) $= 12$, $p < 0.005$]. Subsequent Wilcoxon tests revealed a significantly stepwise decrease of binding from NCC over NCL to CDL (all $N = 6$, $T = 0$, $p < 0.05$) that is particularly illustrated in the fingerprints (Fig. 2a).

The study of binding sites for the neurotransmitter acetylcholine revealed low densities for all analyzed cholinergic receptors. Binding of [^{3}H]pirenzepine to muscarinergic cholinergic receptors of the M_1-type was very low in the caudolateral nidopallium (NCL: 151 ± 24 fmol/mg protein; Figs. 1a/b, 2a). A further differentiation within NCL was not visible. The Friedman ANOVA using the data from NCL, NCC and CDL showed a significant overall effect [Chi Square ($N = 6$, df $= 2$] $= 6.52$, $p < 0.05$). Subsequent Wilcoxon tests revealed that the concentration was significantly lower in NCL compared to both NCC and CDL ($N = 6$, $T \leq 1$, $p < 0.05$; Fig. 2).

M_2-receptors presented the highest densities of all determined cholinergic receptors in the nidopallial structures (269 ± 39 fmol/mg protein; Fig. 2a). The Friedman ANOVA comparing NCL, NCC and CDL showed a significant overall effect [Chi Square ($N = 6$, df $= 2$) $=$ 10.33, $p < 0.01$). Subsequent Wilcoxon tests revealed a

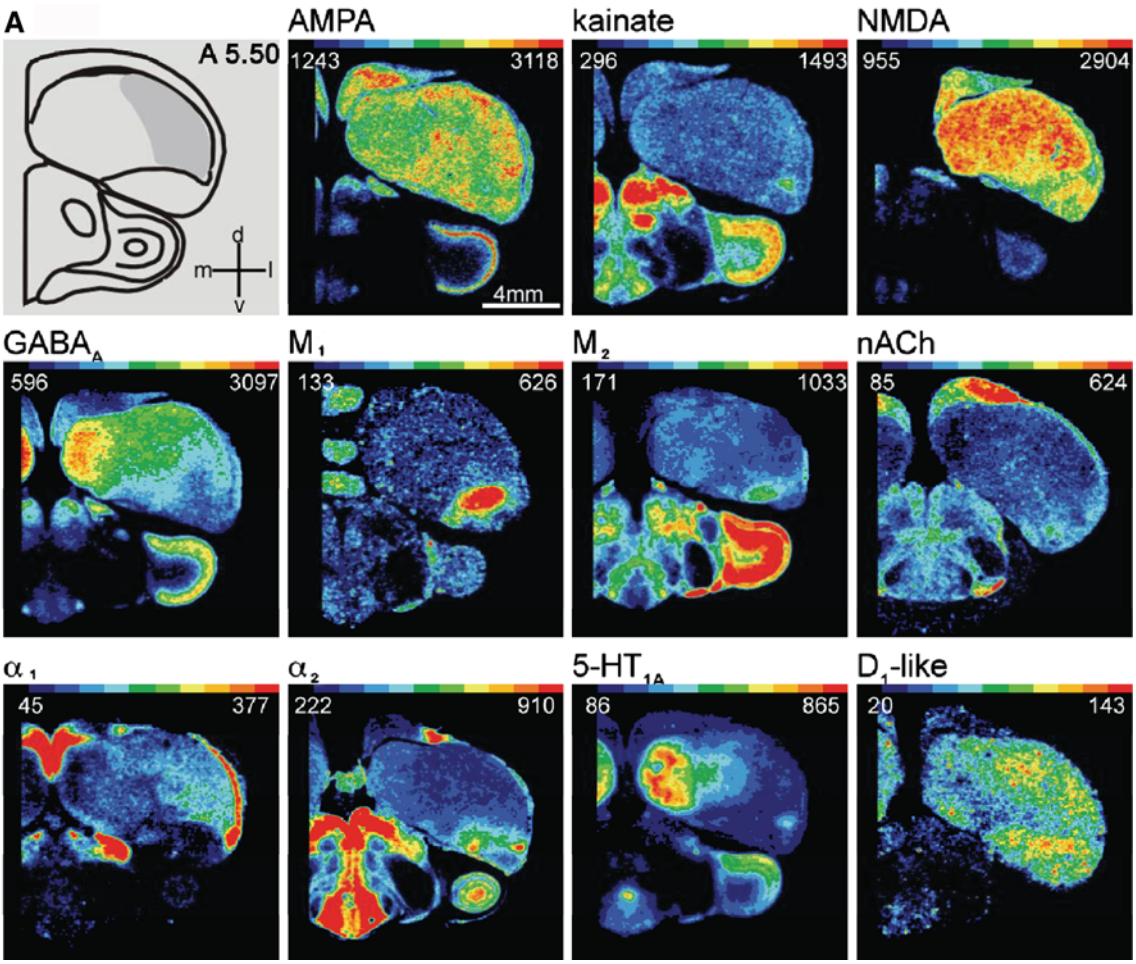

Fig. 1 Color-coded autoradiographs showing the distribution of AMPA, kainate, NMDA, $GABA_A$, M_1, M_2, nicotinic cholinergic (nACh), α_1, α_2, 5-HT_{1A} and D_1-like receptors in coronal sections through the pigeon brain at rostrocaudal levels A 5.50 (**a**) and A 6.75 (**b**). Extent of the NCL at each of these levels is highlighted in gray in the schematic drawing. *Scale bars* code for receptor densities in fmol/mg protein

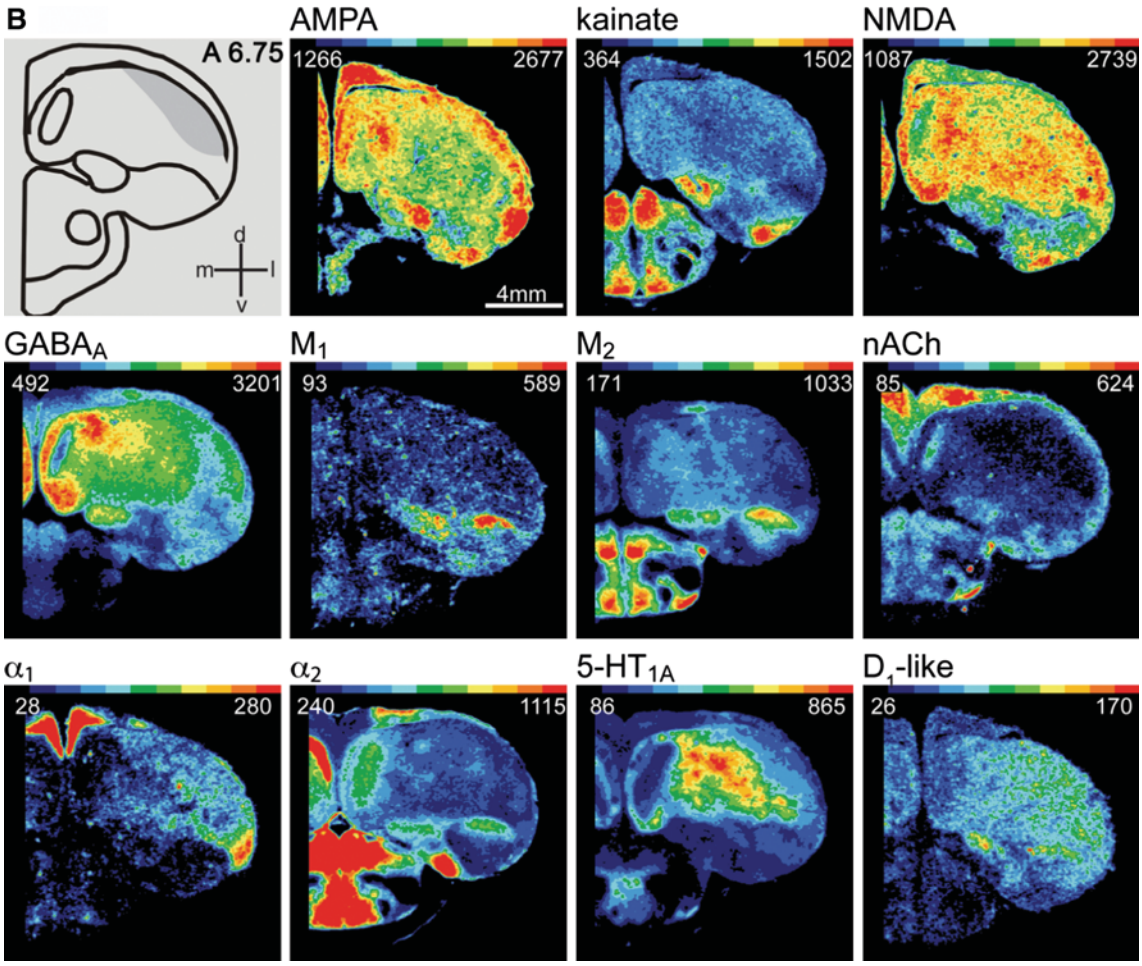

Fig. 1 continued

significantly stepwise increase of binding strength from CDL over NCL to NCM ($N = 6$, $T \leq 1$, $p < 0.05$) and a parcellation of NCLm and NCLl ($N = 6$, $T = 0$, $p < 0.05$; Fig. 3).

Binding of [^{3}H]cytisine to nicotinic receptors was very low in the whole lateral aspect of the nidopallium (144 ± 12 fmol/mg protein, Fig. 1a/b and Fig. 2a), indicating low densities of nACh receptors (Fig. 2a). The Friedman ANOVA showed a significant overall effect [Chi Square ($N = 6$, df $= 2$) $= 12$, $p < 0.005$]. Subsequent Wilcoxon tests revealed a significantly stepwise decrease of binding strength from CDL over NCL to NCC ($N = 6$, $T = 0$, $p < 0.05$). Further, binding densities between NCLm and NCLl differed significantly ($N = 6$, $T = 0$, $p < 0.05$; Fig. 3).

The noradrenergic α_1 receptor was visualized by means of [^{3}H]prazosin (127 ± 16 fmol/mg protein; Fig. 1a/b). Although in few cases the ventral aspect of the NCL, abutting the arcopallium, displayed some higher binding, this was not consistently observed. A differentiation between NCLl and NCLm was not evident. The Friedman ANOVA comparing NCL, NCC and CDL showed a significant overall effect [Chi Square ($N = 6$, df $= 2$) $= 12$, $p < 0.005$]. Subsequent Wilcoxon tests revealed a significantly stepwise decrease of binding strength from CDL over NCL to NCC (all $N = 6$, $T = 0$, $p < 0.05$; Fig. 2a).

[^{3}H]RX821002 binds to noradrenergic α_2 receptor and displayed moderate binding in NCL (308±27 fmol/mg protein). Substructures within the NCL were not visible (Fig. 1a/b). The Friedman ANOVA showed a significant overall effect [Chi Square ($N = 6$, df $= 2$) $= 9.33$, $p < 0.01$]. Subsequent Wilcoxon tests revealed that binding in NCC was significantly higher than both in NCL and CDL (all $N = 6$, $T = 0$, $p < 0.05$; Fig. 2).

Serotonergic 5-HT$_{1A}$ receptor-binding sites were visualized with [^{3}H]8-OH-DPAT. NCL revealed lower densities (374 ± 67 fmol/mg protein) than the medially abutting nidopallial areas, again providing the possibility to clearly identify the medial wall of the NCL (Fig. 1a/b). The Friedman ANOVA showed a significant overall effect

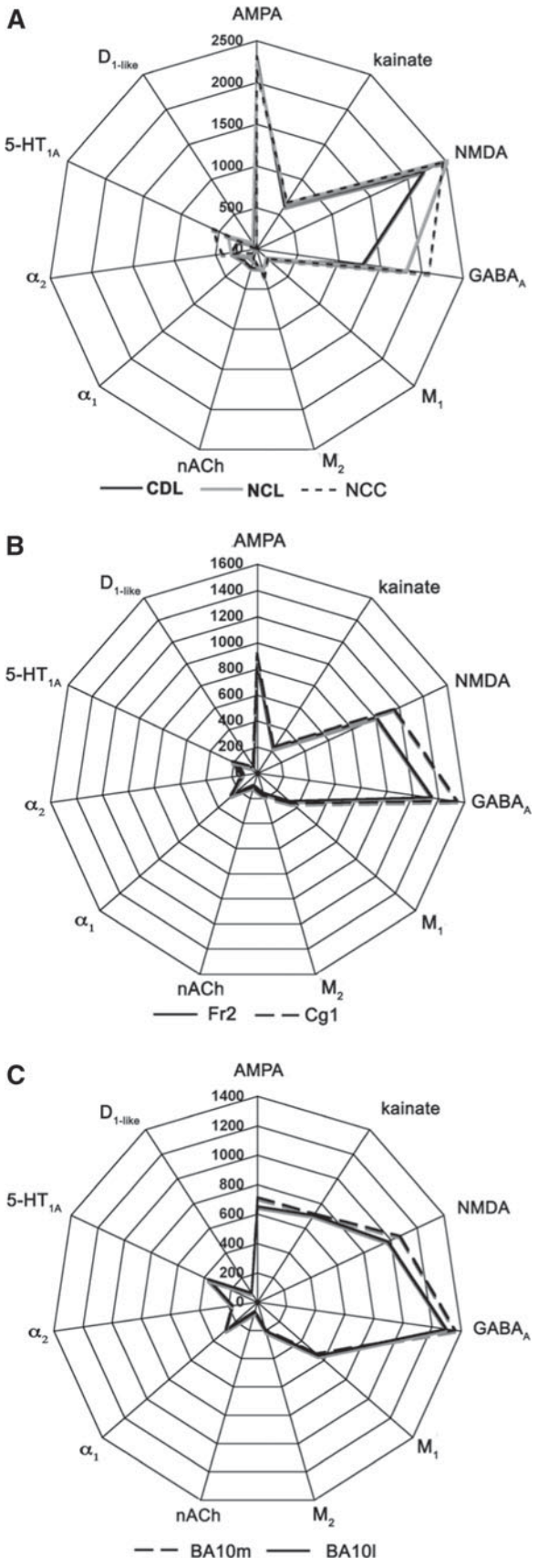

◀ **Fig. 2** Receptor fingerprints for CDL, NCL, NCC of the pigeon pallium (**a**), for Fr2 and Cg1 of the rat cortex (**b**) and for the BA10l and BA10m of the human cortex (**c**). The mean densities (fmol/mg protein) of glutamatergic (AMPA, kainate, NMDA), GABAergic ($GABA_A$), acetylcholinergic muscarinic (M_1, M_2) and nicotinic (nACh), adrenergic (α_1, α_2), serotonergic ($5\text{-}HT_{1A}$) and dopaminergic (D_1-like) receptors are displayed in polar coordinate plots. The lines connecting the mean densities define the shape of the fingerprint based on 11 different binding sites for each area. Note that the scales in **a**–**c** are different. *BA10l* Brodmann area 10 lateral, *BA10m* Brodmann area 10 medial, *CDL* area corticoidea dorsolateralis, *NCL* nidopallium caudolaterale, *NCC* nidopallium caudocentrale, *Fr2* frontal area 2, *Cg1* cingulate cortex 1

[Chi Square ($N = 6$, df $= 2$] $= 12$, $p < 0.005$). Subsequent Wilcoxon tests revealed a significantly stepwise increase of binding strength from CDL over NCL to NCC (all $N = 6$, $T = 0$, $p < 0.05$, Fig. 2a). Furthermore, $5\text{-}HT_{1A}$ receptors were more abundant in NCLm than NCLl ($N = 6$, $T = 0$, $p < 0.05$; Fig. 3).

[^{3}H]SCH23390 was used to reveal the location and density of dopaminergic D_1-like receptors. Ligand binding was mainly concentrated within the NCL without showing a difference between the lateral and the medial component (Fig. 1a/b). Although density in NCL was rather low (92 ± 12 fmol/mg protein), a Friedman ANOVA comparing NCL, NCC, and CDL showed a significant overall effect [Chi Square ($N = 6$, df $= 2$) $= 12$, $p < 0.01$]. A subsequent Wilcoxon test revealed significantly higher values for NCL and CDL over NCC ($N = 6$, $T = 0$, $p < 0.05$; Fig. 2) as well as significantly higher values for NCL than for CDL ($N = 6$, $T = 0$, $p < 0.05$; Fig. 2).

Based on the different binding site densities for kainate, NMDA, $GABA_A$, M_1, M_2, nACh, α_1, α_2, $5\text{-}HT_{1A}$ and D_1-like receptors a detailed outline of the NCL is depicted in Fig. 4.

Comparison of receptor-binding site densities in the avian NCL to mammalian prefrontal structures

In the rat (Fig. 2b) and human (Fig. 2c) prefrontal areas examined, AMPA and $GABA_A$ receptors showed the highest densities of all measured receptor types, and were followed by NMDA receptor densities (Fig. 2b/c). Lowest values were found for nACh, and D_1-like receptor densities.

Human and rat prefrontal areas differed considerably in their relative balance of ionotropic glutamatergic receptors. In human areas, BA10l and BA10m, kainate receptor densities were comparable to those of AMPA receptors, and only slightly lower than those of NMDA receptors (Fig. 2c). In rat areas, Fr2 and Cg1, similar to the situation described for the pigeon nidopallial areas, kainate receptor

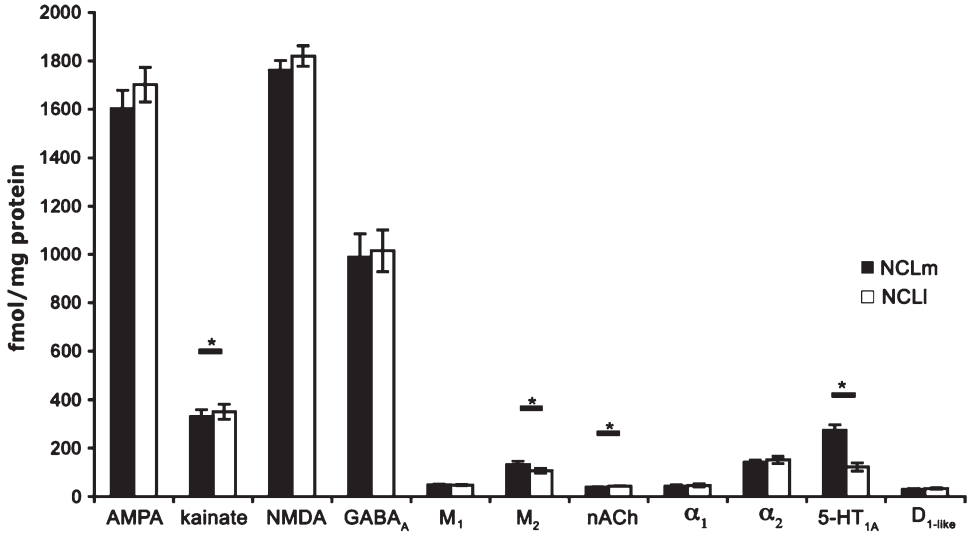

Fig. 3 Histogram of the mean receptor densities (fmol/mg protein) of the pigeon's areas NCLm and the NCLl. *Error bars* represent standard deviations. *Asterisks* indicate significant differences between receptor densities

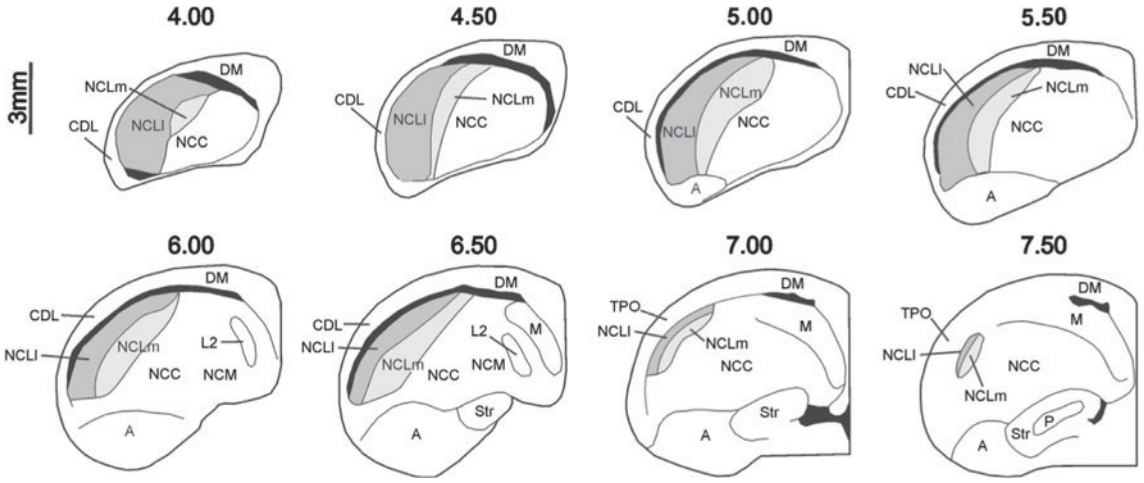

Fig. 4 Atlas of the NCL in serial frontal sections based on different receptor densities. The length of the bar represents 3 mm

densities were considerably lower than those of AMPA (fourfold lower) or NMDA (five to sixfold lower) receptor densities (Fig. 2b). Thus, the pigeon and rat, but not the human fingerprints presented a conspicuous indentation at the level of the kainate receptors.

The examined human and rat prefrontal areas presented the same balance of cholinergic receptor densities, with highest concentrations for the muscarinic M_1 cholinergic type and lowest values for the nicotinic receptor (Fig. 2b/c). This pattern differs however, from that of pigeons, since nidopallial areas contain higher M_2 than M_1 receptor densities (Fig. 2a).

In the group of monoaminergic receptors, noradrenergic α_1 receptor densities were higher than those of α_2 receptors in both human and rat prefrontal areas (Fig 2b/c). Conversely, α_1 receptor densities were lower than of α_2 receptor densities in the pigeon nidopallium (Fig. 2a). Serotoninergic 5-HT_{1A} receptor densities were higher than those of α_1 receptors in human areas BA10l and BA10m, whereas the opposite holds true for rat areas Fr2 and Cg1 (Fig. 2b/c). D_1-like binding-site densities showed neither differences between the analyzed prefrontal structures nor the pigeon's NCL (Fig. 2b/c).

Discussion

Using a quantitative analysis of 11 different receptor-binding sites, the present study aimed to (1) analyze the areal borders of the constituents of the caudolateral part of the pigeons' telencephalon, (2) to reveal possible subdivisions within the NCL, (3) to compare the receptor fingerprints of NCL and the surrounding NCC and CDL with those of frontal areas in mammals.

Areal delineation in the pigeons' caudolateral telencephalon

Moving from centromedial to lateral, the avian caudolateral telencephalon is constituted by the three areas: NCC, NCL, and CDL. The NCC receives its input predominantly from the dorsal intermediate mesopallium and projects to arcopallial subfields. The arcopallial outflow to the medial hypothalamus could imply that NCC is involved in neuroendocrine and autonomic functions and is limbic in nature (Yamamoto and Reiner 2005; Atoji and Wild 2009). The interconnectivity between NCC and NCL seems to be surprisingly weak (Atoji and Wild 2009; Kröner and Güntürkün 1999). Further, the pattern of afferents and efferents of NCC and NCL is considerably different (Leutgeb et al. 1996; Metzger et al. 1998; Kröner and Güntürkün 1999; Atoji and Wild 2009). Thus, although NCC and NCL cannot be delineated by cytoarchitectonic means and were subsumed into area Ne16 in the quantitative cytoarchitectonic study of Rehkämper and Zilles (1991), they show marked differences in hodology. The study of Atoji and Wild (2009) placed the borderline between NCC and NCL far more laterally than the immunocytochemical and connectivity analyses conducted on the NCL (Waldmann and Güntürkün 1993; Leutgeb et al. 1996; Kröner and Güntürkün 1999; Riters et al. 1999). In fact, according to Atoji and Wild (2009), NCLm would be part of NCC. Interestingly, the reconstruction of the location of retrogradely labeled neurons in Atoji and Wild (2009) reveals a border that is more close to that of the present study and similar to the original delineation by Waldmann and Güntürkün (1993) and this is reflected by the distribution patterns of α_1, 5-HT_{1A} and D_1-like receptors. However, the caudal aspect of the avian nidopallium is organized in clusters with fuzzy borders; in addition, not all receptor-binding sites defined clear boundaries between areas. Thus, the distribution patterns of the receptors confirm a smooth transition at the caudal site and both areas probably do not have a clear boundary at that point. Therefore, in the most caudal portion of the nidopallium, the delineation between NCC and NCL becomes extremely difficult and may have led to different findings in the past (Atoji and Wild 2009).

Towards the lateral border, the distinction between NCL and CDL is easy due to the ventricle that separates these two areas. The CDL is considered to be mostly limbic in nature and was hodologically compared to the mammalian cingulate cortex (Yamamoto and Reiner 2005; Atoji and Wild 2005; Csillag and Montagenese 2005). It shares similarities with the receptor architecture of the hippocampal formation (data not shown) and nidopallial structures. CDL extents rostrally up to A 6.75 where NCL and CDL are no longer separated by the lateral ventricle but directly abut each other. At this point, the autoradiographic data revealed a less fuzzy transition when compared to the caudal aspects of NCL and NCC, depicting that NCL follows the outer curvature of the telencephalon but always stays about 1 mm away from the pial surface. Similarly, the rostral border of the NCL is easier to define as it tapers up to A 7.50.

Subdivisions of the NCL

Our findings reveal a clear parcellation of the avian nidopallium that is in line with tracing studies (Rehkämper and Zilles 1991; Leutgeb et al. 1996; Kröner and Güntürkün 1999; Atoji and Wild 2009). Earlier studies have shown functional and neurochemical subdivisions of the NCL (Leutgeb et al. 1996; Braun et al. 1999; Kröner and Güntürkün 1999; Riters et al. 1999). Here, a new subdivision into a medial and a lateral part is proposed by the differences of the mean receptor densities of nACh, M_2, kainate, and 5-HT_{1A} receptors. Some earlier tracing and neurochemical studies revealed a possible dorsal and ventral component (Leutgeb et al. 1996; Braun et al. 1999; Riters et al. 1999). The neurochemical subdivision into a dorsal and a ventral component also coincides with hodological data showing that only dorsal NCL receives afferents from multimodal thalamic nuclei (Korzeniewska and Güntürkün 1990; Güntürkün and Kröner 1999) and contributes more significantly to working memory performance (Diekamp et al. 2002a, b). Dorsal, but not ventral NCL, is connected with a complex of association structures in the rostromedial nidopallium and ventral hyperpallium in different species of birds. In domestic chicken two extensively overlapping structures, the mediorostral nidopallium/hyperpallium (MNH) and the intermediate and medial mesopallium ventrale (IMM), play a pivotal role in auditory and visual filial imprinting, respectively (Horn 1981; Braun et al. 1999). These areas are activated during imprinting and lesions cause deficits in recognizing the imprinting stimulus (Horn 1981; Horn et al. 1985). In chicken, IMM is also a nodal point of initial memory formation in one-trial passive avoidance learning with gustatory cues (Rose 2000). Both MNH and IMM project to dorsomedial NCL as shown in chicken (Metzger et al. 1998) and pigeons (Kröner and Güntürkün 1999). However, we could not confirm a border between dorsal and ventral NCL based on the receptor-density profiles. On the other hand, Kröner and Güntürkün (1999) demonstrated that the component labeled NCLl in our preparations receives input from secondary areas of sensory representation and projects back to these structures. Furthermore, a large number of neurons from NCL projects to the arcopallium and these output neurons are close to the densest catecholaminergic innervations that are located in the

lateral part of the NCL (Waldmann and Güntürkün 1993; Kröner and Güntürkün 1999). In addition, a large number of medial NCL neurons project to the basal ganglia in pigeons (Veenman et al. 1995; Kröner and Güntürkün 1999). Therefore, NCLl displayed a different connectivity pattern from NCLm. Due to the curvature of the NCL, NCLl is positioned more dorsally than NCLm. Thus, a dorsoventral subdivision of the NCL could mistakenly be concluded from the lateromedial differentiation of a semilunar structure.

The neurochemistry of the caudolateral avian forebrain

In NCL, NCC, and CDL the highest receptor densities were detected for glutamatergic and $GABA_A$ receptors. This is in line with earlier studies that determined receptor levels in the nidopallium of various bird species (Dietl and Palacios 1988; Stewart et al. 1988,1999; Mitsacos et al. 1990; Aamodt et al. 1992; Veenman et al. 1994; Ben-Ari et al. 1997; Salvatierra et al. 1997). Pigeons showed higher AMPA and NMDA receptor concentrations in the nidopallium when compared to other birds, while the amount of $GABA_A$ receptor densities seemed to be similar in pigeons, chicks and zebra finches (Stewart et al. 1988; Henley and Barnard 1990; Veenman et al. 1994; Martinez de la Torre et al. 1998; Stewart et al. 1999; Pinaud and Mello 2007). The present study reports for the first time kainate receptor densities in the pigeon's pallium. If compared to AMPA and NMDA receptors, kainate binding was about four times lower in all of the above-mentioned structures. However, like for the NMDA receptors, kainate binding differed between the CDL and the nidopallial structures, showing a clear segregation. This is in line with an immunohistochemical study in quails, showing that AMPA and NMDA receptors have higher densities than kainate receptors in the nidopallium. In addition, kainate and NMDA binding is lower in the CDL while the AMPA receptor subunit GluR1 was intensely labeled in the CDL (Cornil et al. 2000). Binding of the $GABA_A$ receptor also increased from the surface to the deeper nidopallial areas, confirming earlier immunohistochemical und receptor autoradiographic studies (Rehkämper and Zilles 1991; Veenman et al. 1994). In the nidopallium, cholinergic muscarinic and nicotinic receptors showed an intermediate to low density, which is in line with results from other studies of muscarinic or nicotinic binding sites in the telencephalon of pigeons, chicks, quails, sparrows, and starlings (Dietl et al. 1988; Ball et al. 1990; Sorenson and Chiappinelli 1992). As described for the $GABA_A$ receptor, the M_2 receptor density increases from the superficial CDL over the NCL to the NCM while the nACh receptor densities decreases. The boundaries of the NCL were revealed by all cholinergic receptors.

The monoaminergic receptors were differentially distributed. Their densities ranged from very low (D_1-like receptors) to moderate (5-HT_{1A} receptors). Densities of the α_2 receptors varied across different bird species in the CDL and in the nidopallium (Balthazart and Ball 1989; Ball et al. 1995; Diez-Alarcia et al. 2006). To our knowledge to date no specific information about the densities of 5-HT_{1A} receptor densities is available on the avian pallium, although it was shown in a competition assay with [^{3}H]5-HT binding that 5-HT_{1A} receptors were abundant in the pigeon's telencephalon (Waeber et al. 1989). Comparable results were reported for the D_1-like receptor in the nidopallium of pigeons (Dietl and Palacios 1988).

Comparison to mammals and functional considerations

As first shown by lesion experiments (Mogensen and Divac 1982), the NCL is involved in executive functions. More recent studies have confirmed that the NCL shares many similarities with the mammalian prefrontal cortex (Güntürkün, 2005a, b; Kirsch et al. 2008). These findings can be seen in parallel to observations in corvids and parrots which possess cognitive abilities that are comparable to those of monkeys and apes (Bird and Emery 2010; Hunt and Gray 2003; Emery and Clayton 2004; Kenward et al. 2005; Seed et al. 2006; Prior et al. 2008; Taylor et al. 2009; Pollok et al., 2000). As observed for other mammals (Harvey and Krebs 1990) this is accompanied by an increased encephalization (Cnotka et al. 2008) and a relative growth of associative forebrain areas (Mehlhorn et al. 2010). Based on topographical and genetic arguments both the NCL and the prefrontal cortex seem to be a case of homoplasy (Puelles et al. 2000). Additionally, the morphological organization of avian and mammalian forebrains differs importantly, with the avian pallium having a nuclear organization while the mammalian dorsal pallium assumes a laminar structure. Thus, a layered cortical structure appears not to be a prerequisite for higher cognitive functions (Kirsch et al. 2008). In contrast to the NCL, less is known about the CDL and its functions. The connections of the avian CDL share similarities with those of the mammalian cingulate cortex (Vogt and Pandya 1987; Atoji and Wild 2005). Neurobehavioral studies in which the CDL was lesioned as part of larger lesions to the lateral nidopallium or the hippocampal formation indicate a role for the CDL in spatial memory (Hartmann and Güntürkün 1998; Bingman et al. 1985; Colombo et al. 2001; Gagliardo et al. 2001). Only one study showed that CDL lesions did not impair performance in simultaneous pattern or delayed alternation discrimination tasks (Gagliardo et al. 1996). Receptor autoradiography and receptor fingerprints of brain regions provide a tool to compare the chemoarchitecture between different species.

Therefore, our results will be further discussed in the light of comparative studies in birds, primates and rats.

As in the pigeon's NCL and CDL, high receptor densities for glutamatergic and GABAergic receptors were found in the prefrontal regions investigated here, as well as in other cortical regions of rats, monkeys and humans (Gebhard et al. 1995; Geyer et al. 1998; Zilles et al. 2002a, b; Palomero-Gallagher and Zilles 2004). However, there were differences in the amount of distinct glutamate receptors between species. AMPA and NMDA receptors showed high concentrations in the NCL and the CDL of pigeons and chicks (Bock et al. 1997) if compared to frontal structures of mammals. Kainate receptors seemed to be very low in rat FR2 and Cg1, while they did not differ substantially between human BA10 and the NCL, and between the CDL and the human cingulate cortex (Palomero-Gallagher et al. 2009). By contrast, the amounts of $GABA_A$ receptors were equally distributed in the prefrontal areas of all the investigated species here and also in the NCL of pigeons and chicks (Stewart et al. 1988). The same is true for the CDL and the human as well as the macaque cingulate cortex (Bozkurt et al. 2005; Palomero-Gallagher et al. 2009). Thus, there seems to be a shift towards higher densities of glutamate receptors in avian nidopallial structures. Therefore, the top right quadrant of the fingerprints for the birds' nidopallial structures differs in size when compared to the rodent frontal areas, and differ in shape for both species, if compared to human BA10.

Cholinergic M_1 receptors were highest in human if compared to macaque monkey, rhesus monkey, rat and pigeon, while M_2 and nicotinic receptors showed equal densities (Bozkurt et al. 2005; Lidow et al. 1989). However, pigeons showed an inverted pattern of M_1/M_2 binding if compared to other species. ACh is an essential regulator of cortical excitability and plays important roles for arousal, attention, and cognitive processes (Sarter and Bruno 2000; Hasselmo and Stern 2006; Briand et al. 2007; Sarter et al. 2009). These functions are mediated by muscarinic and nicotinic ACh receptors. In the cerebral cortex the M_1 receptor is preferentially expressed in pyramidal cells and enriched on the extrasynaptic membrane of their dendrites and spines (Yamasaki et al. 2010). The M_2 receptor is the primary muscarinic autoreceptor presynaptically regulating ACh release in the forebrain of rodents and primates including humans (Mrzljak et al. 1995; Zhang et al. 2002). Both receptor subtypes are metabotropic. M_1 couples to a stimulatory G-protein whereas M_2 couples to an inhibitory G-protein. Genetic variation of the CHRM2 gene encoding the M_2 receptor selectively influence muscarinic presynaptic inhibition (Comings et al. 2003). The nACh receptors are fast-acting ligand-gated ion channels producing EPSPs. A recent genetic approach showed that both, fast-acting nicotinic receptors and slow-acting muscarinic receptors influence in a synergistic system the efficiency of shifting visuospatial attention in the PFC (Greenwood et al. 2009). In pigeons, central cholinergic systems are important for temporal memory processes and spatial orientation during homing, two processes that also involve the NCL (Gagliardo and Divac 1993; Santi and Weise 1995; Kohler et al. 1996; Riters and Bingman 1999).

Like for the muscarinic cholinergic receptors, the same inverted ratio was detected in the NCL and in the CDL for the noradrenergic α_1 and α_2 receptors if compared to prefrontal or cingulate structures in mammals. In humans, macaque monkeys and rats higher amounts of α_1 than of α_2 receptors were described (Goldman-Rakic et al. 1990; Bozkurt et al. 2005; Palomero-Gallagher et al. 2009). Both receptor types are metabotropic and α_1 receptors are coupled to stimulatory G-proteins, while α_2 receptors are coupled to inhibitory G-proteins. In the PFC of monkeys, α_2 receptors are located postsynaptically at the dendritic spines of pyramidal neurons where glutamate receptors are concentrated (Aoki et al. 1998). Behavioral pharmacological studies in rodents, monkeys, and humans demonstrated that systemically or locally administered α_2 receptor agonists could improve PFC cognitive performances (Robbins and Arnsten 2009). Further, it was shown that stimulation of α_2 receptors suppresses glutamate synaptic transmission in the PFC and tunes the synaptic output to an optimal state for working memory function (Wang et al. 2007; Ji et al. 2008). In songbirds noradrenalin is involved in song learning at different developmental stages by controlling local circuits in the higher vocal center (HVC) (Fortune and Margoliash 1995) and modulation of auditory responses through attention processes (Castelino and Schmidt 2010). The HVC could be an oscine specialization of the dorsal NCL (Farries 2001). Because both the M_1/M_2 and the α_1/α_2 ratio show an inverted pattern in the NCL resulting in an increased inhibitory control on local circuits this may be a compensating mechanism for the shift to glutamatergic processing.

The densities of 5-HT_{1A} receptors were equal in the prefrontal areas of humans, monkeys and pigeons, while rats showed lower densities (Goldman-Rakic et al. 1990). The 5-HT_{1A} subtype is of particular interest, since it is one of the main mediators of 5-HT and contributes to a lot of prefrontal functions (Sakaue et al. 2000; de Almeida et al. 2008). In the human cingulate cortex the density of the 5-HT_{1A} subtype is slightly higher than in the CDL (Palomero-Gallagher et al. 2009). In birds less is known about the serotonergic contribution to executive functions, but it was shown that serotonin release was increased in the NCL during a working memory task (Karakuyu et al. 2007).

D_1-like receptors showed the lowest densities of all measured receptor types in the assumed prefrontal and cingulate regions of pigeons, rats, monkeys, cats, tree

shrews and humans (Richfield et al. 1989; Goldman-Rakic et al. 1990; Palomero-Gallagher et al. 2009). In mammals, low densities of D_1-like receptors in frontal areas are associated with volume transmission of dopamine and a diffuse action of dopamine on multiple components of cortical networks (reviewed in Gonzalez-Burgos et al. 2007). These results also reveal that the dopaminergic system seems to be highly conserved across species, although prefrontal structures evolved independently (Callier et al. 2003). Thus, the dopaminergic system and its interactions with other systems might constitute a key element for our understanding of the anatomical/chemical traits that are necessary for proper executive functions. The low density of D_1-like receptors might also explain why species share similar deficits if signaling via this receptor-type is disturbed (Zahrt et al. 1997; Williams and Castner 2006; Herold et al. 2008; McNab and Klingberg 2008; Rose et al. 2010).

In summary, it appears that the GABAergic and dopaminergic systems are highly conserved across the species studied here, which have a long history of separate evolution (Jarvis et al. 2005). This could result from a common selection pressure for a structure that serves executive functions, i.e., the control of higher order processes. This includes the integration and manipulation of information from all modalities in order to generate a proper behavior in a given situation. These functions rely on specific connections to other brain structures and the modulation of information flow through these circuits. Thus, similar evolutionary pressures on information processing in birds might result in a comparable or analogue pattern of specific receptor compositions that would resemble those in the neocortex of mammals. Future studies need to examine differences between various bird species, as well as between different mammalian species to confirm these conclusions.

Acknowledgments Supported by a grant from the BMBF through the Bernstein Focus Group "Varying Tunes" to O.G.

Conflict of interest The authors declare that they have no conflict of interest.

References

Aamodt SM, Kozlowski MR, Nordeen EJ, Nordeen KW (1992) Distribution and developmental change in [3H]MK-801 binding within zebra finch song nuclei. J Neurobiol 23:997–1005

Amunts K, Weiss PH, Mohlberg H, Pieperhoff P, Eickhoff S, Gurd JM, Marshall JC, Shah JN, Fink GR, Zilles K (2004) Analysis of the neural mechanisms underlying verbal fluency in cytoarchitectonically defined stereotaxic space—the roles of Brodmann areas 44 and 45. NeuroImage 22:42–56

Amunts K, Schleicher A, Zilles K (2007) Cytoarchitecture of the cerebral cortex—more than localization. NeuroImage 37:1061–1065

Aoki C, Venkatesan C, Go CG, Forman R, Kurose H (1998) Cellular and subcellular sites for noradrenergic action in the monkey dorsolateral prefrontal cortex as revealed by the immunocytochemical localization of noradrenergic receptors and axons. Cereb Cortex 8:269–277

Atoji Y, Wild JM (2005) Afferent and efferent connections of the dorsolateral corticoid area and a comparison with connections of the temporo-parieto-occipital area in the pigeon (*Columba livia*). J Comp Neurol 485:165–182

Atoji Y, Wild JM (2009) Afferent and efferent projections of the central caudal nidopallium in the pigeon (*Columba livia*). J Comp Neurol 517:350–370

Ball GF, Nock B, Wingfield JC, McEwen BS, Balthazart J (1990) Muscarinic cholinergic receptors in the songbird and quail brain: a quantitative autoradiographic study. J Comp Neurol 298:431–442

Ball GF, Casto JM, Balthazart J (1995) Autoradiographic localization of D1-like dopamine receptors in the forebrain of male and female Japanese quail and their relationship with immunoreactive tyrosine hydroxylase. J Chem Neuroanat 9:121–133

Balthazart J, Ball GF (1989) Effects of the noradrenergic neurotoxin DSP-4 on luteinizing hormone levels, catecholamine concentrations, alpha 2-adrenergic receptor binding, and aromatase activity in the brain of the Japanese quail. Brain Res 492:163–175

Bast T, Diekamp B, Thiel C, Schwarting RK, Güntürkün O (2002) Functional aspects of dopamine metabolism in the putative prefrontal cortex analogue and striatum of pigeons (*Columba livia*). J Comp Neurol 446:58–67

Ben-Ari Y, Khazipov R, Leinekugel X, Caillard O, Gaiarsa JL (1997) GABAA, NMDA and AMPA receptors: a developmentally regulated 'menage a trois'. Trends Neurosci 20:523–529

Bingman VP, Ioalè P, Casini G, Bagnoli P (1985) Dorsomedial forebrain ablations and home loft association behavior in homing pigeons. Brain Behav Evol 26:1–9

Bird CD, Emery NJ (2010) Rooks perceive support relations similar to six-month-old babies. Proc Biol Sci 277:147–151

Bock J, Schnabel R, Braun K (1997) Role of the dorso-caudal neostriatum in filial imprinting of the domestic chick: a pharmacological and autoradiographical approach focused on the involvement of NMDA-receptors. Eur J Neurosci 9:1262–1272

Bozkurt A, Zilles K, Schleicher A, Kamper L, Arigita ES, Uylings HB, Kötter R (2005) Distributions of transmitter receptors in the macaque cingulate cortex. Neuroimage 25:219–229

Braun K, Bock J, Metzger M, Jiang S, Schnabel R (1999) The dorsocaudal neostriatum of the domestic chick: a structure serving higher associative functions. Behav Brain Res 98:211–218

Briand LA, Gritton H, Howe WM, Young DA, Sarter M (2007) Modulators in concert for cognition: modulator interactions in the prefrontal cortex. Prog Neurobiol 83:69–91

Brodmann K (1909) Vergleichende Lokalisationslehre der Großhirnrinde in ihren Prinzipien dargestellt auf Grund des Zellenbaues, Barth, Leipzig; English translation available in Garey, L. J. Brodmann's Localization in the Cerebral Cortex (Smith Gordon, London, 1994)

Callier S, Snapyan M, Le Crom S, Prou D, Vincent JD, Vernier P (2003) Evolution and cell biology of dopamine receptors in vertebrates. Biol Cell 95:489–502

Castelino CB, Schmidt MF (2010) What birdsong can teach us about the central noradrenergic system. J Chem Neuroanat 39:96–111

Cnotka J, Güntürkün O, Rehkämper G, Gray RD, Hunt GR (2008) Extraordinary large brains in tool-using New Caledonian crows (*Corvus moneduloides*). Neurosci Lett 433:241–245

Colombo M, Broadbent NJ, Taylor CS, Frost N (2001) The role of the avian hippocampus in orientation in space and time. Brain Res 919:292–301

Comings DE, Wu S, Rostamkhani M, McGue M, Lacono WG, Cheng LS, MacMurray JP (2003) Role of the cholinergic muscarinic 2 receptor (CHRM2) gene in cognition. Mol Psychiatry 8:10–11

Cornil C, Foidart A, Minet A, Balthazart J (2000) Immunocytochemical localization of ionotropic glutamate receptors subunits in the adult quail forebrain. J Comp Neurol 428:577–608

Csillag A, Montagnese CM (2005) Thalamotelencephalic organization in birds. Brain Res Bull 66:303–310

de Almeida J, Palacios JM, Mengod G (2008) Distribution of 5-HT and DA receptors in primate prefrontal cortex: implications for pathophysiology and treatment. Prog Brain Res 172:101–115

Diekamp B, Kalt T, Güntürkün O (2002a) Working memory neurons in pigeons. J Neurosci 22:RC210

Diekamp B, Gagliardo A, Güntürkün O (2002b) Nonspatial and subdivision-specific working memory deficits after selective lesions of the avian prefrontal cortex. J Neurosci 22:9573–9580

Dietl MM, Palacios JM (1988) Neurotransmitter receptors in the avian brain. I. Dopamine receptors. Brain Res 439:354–359

Dietl MM, Cortes R, Palacios JM (1988) Neurotransmitter receptors in the avian brain. II. Muscarinic cholinergic receptors. Brain Res 439:360–365

Diez-Alarcia R, Pilar-Cuellar F, Paniagua MA, Meana JJ, Fernandez-Lopez A (2006) Pharmacological characterization and autoradiographic distribution of alpha2-adrenoceptor antagonist [3H]RX 821002 binding sites in the chicken brain. Neuroscience 141:357–369

Divac I, Mogensen J, Bjorklund A (1985) The prefrontal 'cortex' in the pigeon. Biochemical evidence. Brain Res 332:365–368

Durstewitz D, Kröner S, Hemmings HC Jr, Güntürkün O (1998) The dopaminergic innervation of the pigeon telencephalon: distribution of DARPP-32 and co-occurrence with glutamate decarboxylase and tyrosine hydroxylase. Neuroscience 83:763–779

Eickhoff S, Amunts K, Mohlberg H, Zilles K (2006) The human parietal operculum. II. Stereotaxic maps and correlation with functional imaging results. Cereb Cortex 16:268–279

Emery NJ, Clayton NS (2004) The mentality of crows: convergent evolution of intelligence in corvids and apes. Science 306:1903–1907

Farries MA (2001) The oscine song system considered in the context of the avian brain: lessons learned from comparative neurobiology. Brain Behav Evol 58:80–100

Fortune ES, Margoliash D (1995) Parallel pathways and convergence onto HVc and adjacent neostriatum of adult zebra finches (*Taeniopygia guttata*). J Comp Neurol 360:413–441

Gagliardo A, Divac I (1993) Effects of ablation of the presumed equivalent of the mammalian prefrontal cortex on pigeon homing. Behav Neurosci 107:280–288

Gagliardo A, Bonadonna F, Divac I (1996) Behavioural effects of ablations of the presumed 'prefrontal cortex' or the corticoid in pigeons. Behav Brain Res 78:155–162

Gagliardo A, Ioalè P, Odetti F, Bingman VP, Siegel JJ, Vallortigara G (2001) Hippocampus and homing in pigeons: left and right hemispheric differences in navigational map learning. Eur J Neurosci 13:1617–1624

Gebhard R, Zilles K, Schleicher A, Everitt BJ, Robbins TW, Divac I (1995) Parcellation of the frontal cortex of the New World monkey *Callithrix jacchus* by eight neurotransmitter-binding sites. Anat Embryol (Berl) 191:509–517

Geyer S, Matelli M, Luppino G, Schleicher A, Jansen Y, Palomero-Gallagher N, Zilles K (1998) Receptor autoradiographic mapping of the mesial motor and premotor cortex of the macaque monkey. J Comp Neurol 397:231–250

Goldman-Rakic PS (1999) The "psychic" neuron of the cerebral cortex. Ann N Y Acad Sci 868:13–26

Goldman-Rakic PS, Lidow MS, Gallager DW (1990) Overlap of dopaminergic, adrenergic, and serotoninergic receptors and complementarity of their subtypes in primate prefrontal cortex. J Neurosci 10:2125–2138

Gonzalez-Burgos G, Kröner S, Seamans JK (2007) Cellular mechanisms of working memory and its modulation by dopamine in the prefrontal cortex of primates and rats. In: Tseng KY, Atzori M (eds) Monoaminergic Modulation of Cortical Excitability. Springer, Berlin, pp 125–152

Greenwood PM, Lin MK, Sundararajan R, Fryxell KJ, Parasuraman R (2009) Synergistic effects of genetic variation in nicotinic and muscarinic receptors on visual attention but not working memory. Proc Natl Acad Sci USA 106:3633–3638

Güntürkün O (1997) Cognitive impairments after lesions of the neostriatum caudolaterale and its thalamic afferent: functional similarities to the mammalian prefrontal system? J Brain Res 38:133–143

Güntürkün O (2005a) Avian and mammalian "prefrontal cortices": limited degrees of freedom in the evolution of the neural mechanisms of goal-state maintenance. Brain Res Bull 66:311–316

Güntürkün O (2005b) The avian 'prefrontal cortex' and cognition. Curr Opin Neurobiol 15:686–693

Güntürkün O, Kröner S (1999) A polysensory pathway to the forebrain of the pigeon: the ascending projections of the nucleus dorsolateralis posterior thalami (DLP). Eur J Morphol 37:185–189

Hartmann B, Güntürkün O (1998) Selective deficits in reversal learning after neostriatum caudolaterale lesions in pigeons: possible behavioral equivalencies to the mammalian prefrontal system. Behav Brain Res 96:125–133

Harvey PH, Krebs JR (1990) Comparing brains. Science 249:140–146

Hasselmo ME, Stern CE (2006) Mechanisms underlying working memory for novel information. Trends Cogn Sci 10:487–493

Henley JM, Barnard EA (1990) Autoradiographic distribution of binding sites for the non-NMDA receptor antagonist CNQX in chick brain. Neurosci Lett 116:17–22

Herold C, Diekamp B, Güntürkün O (2008) Stimulation of dopamine D1 receptors in the avian fronto-striatal system adjusts daily cognitive fluctuations. Behav Brain Res 194:223–229

Horn G (1981) Neural mechanisms of learning: an analysis of imprinting in the domestic chick. Proc R Soc Lond B Biol Sci 213:101–137

Horn G, Bradley P, McCabe BJ (1985) Changes in the structure of synapses associated with learning. J Neurosci 5:3161–3168

Hunt GR, Gray RD (2003) Diversification and cumulative evolution in New Caledonian crow tool manufacture. Proc Biol Sci 270:867–874

Jarvis ED, Güntürkün O, Bruce L, Csillag A, Karten H, Kuenzel W, Medina L, Paxinos G, Perkel DJ, Shimizu T, Striedter G, Wild JM, Ball GF, Dugas-Ford J, Durand SE, Hough GE, Husband S, Kubikova L, Lee DW, Mello CV, Powers A, Siang C, Smulders TV, Wada K, White SA, Yamamoto K, Yu J, Reiner A, Butler AB (2005) Avian brains and a new understanding of vertebrate brain evolution. Nat Rev Neurosci 6:151–159

Ji XH, Cao XH, Zhang CL, Feng ZJ, Zhang XH, Ma L, Li BM (2008) Pre- and postsynaptic beta-adrenergic activation enhances excitatory synaptic transmission in layer V/VI pyramidal neurons of the medial prefrontal cortex of rats. Cereb Cortex 18:1506–1520

Kalenscher T, Diekamp B, Güntürkün O (2003) Neural architecture of choice behaviour in a concurrent interval schedule. Eur J Neurosci 18:2627–2637

Kalenscher T, Güntürkün O, Calabrese P, Gehlen W, Kalt T, Diekamp B (2005) Neural correlates of a default response in a delayed go/no-go task. J Exp Anal Behav 84:521–535

Karakuyu D, Herold C, Güntürkün O, Diekamp B (2007) Differential increase of extracellular dopamine and serotonin in the 'prefrontal cortex' and striatum of pigeons during working memory. Eur J Neurosci 26:2293–2302

Karten HJ (1969) The ascending auditory pathway in the pigeon (*Columba livia*). II. Telencephalic projections of the nucleus ovoidalis thalami. Brain Res 11:134–53

Karten H, Hodos W (1967) A stereotaxic atlas of the brain of the pigeon (*Columba livia*). The Johns Hopkins University Press, Baltimore

Kenward B, Weir AA, Rutz C, Kacelnik A (2005) Behavioural ecology: tool manufacture by naive juvenile crows. Nature 433:121

Kirsch JA, Güntürkün O, Rose J (2008) Insight without cortex: lessons from the avian brain. Conscious Cogn 17:475–483

Kohler EC, Riters LV, Chaves L, Bingman VP (1996) The muscarinic acetylcholine antagonist scopolamine impairs short-distance homing pigeon navigation. Physiol Behav 60:1057–1061

Korzeniewska E, Güntürkün O (1990) Sensory properties and afferents of the N. dorsolateralis posterior thalami of the pigeon. J Comp Neurol 292:457–479

Kröner S, Güntürkün O (1999) Afferent and efferent connections of the caudolateral neostriatum in the pigeon (*Columba livia*): a retro- and anterograde pathway tracing study. J Comp Neurol 407:228–260

Leutgeb S, Husband S, Riters LV, Shimizu T, Bingman VP (1996) Telencephalic afferents to the caudolateral neostriatum of the pigeon. Brain Res 730:173–181

Levy R, Goldman-Rakic PS (1999) Association of storage and processing functions in the dorsolateral prefrontal cortex of the nonhuman primate. J Neurosci 19:5149–5158

Lidow MS, Gallager DW, Rakic P, Goldman-Rakic PS (1989) Regional differences in the distribution of muscarinic cholinergic receptors in the macaque cerebral cortex. J Comp Neurol 289:247–259

Lissek S, Güntürkün O (2005) Out of context: NMDA receptor antagonism in the avian 'prefrontal cortex' impairs context processing in a conditional discrimination task. Behav Neurosci 119:797–805

Martinez de la Torre M, Mitsacos A, Kouvelas ED, Zavitsanou K, Balthazart J (1998) Pharmacological characterization, anatomical distribution and sex differences of the non-NMDA excitatory amino acid receptors in the quail brain as identified by CNQX binding. J Chem Neuroanat 15:187–200

McNab F, Klingberg T (2008) Prefrontal cortex and basal ganglia control access to working memory. Nat Neurosci 11:103–107

Medina L, Reiner A (2000) Do birds possess homologues of mammalian primary visual, somatosensory and motor cortices? Trends Neurosci 23:1–12

Mehlhorn J, Hunt GR, Gray RD, Rehkämper G, Güntürkün O (2010) Tool-making new caledonian crows have large associative brain areas. Brain Behav Evol 75:63–70

Merker B (1983) Silver staining of cell bodies by means of physical development. J Neurosci Methods 9:235–241

Metzger M, Jiang S, Braun K (1998) Organization of the dorsocaudal neostriatal complex: a retrograde and anterograde tracing study in the domestic chick with special emphasis on pathways relevant to imprinting. J Comp Neurol 395:380–404

Metzger M, Jiang S, Braun K (2002) A quantitative immuno-electron microscopic study of dopamine terminals in forebrain regions of the domestic chick involved in filial imprinting. Neuroscience 111:611–623

Mitsacos A, Dermon CR, Stassi K, Kouvelas ED (1990) Localization of L-glutamate binding sites in chick brain by quantitative autoradiography. Brain Res 513:348–352

Mogensen J, Divac I (1982) The prefrontal 'cortex' in the pigeon. Behavioral evidence. Brain Behav Evol 21:60–66

Mrzljak L, Pappy M, Leranth C, Goldman-Rakic PS (1995) Cholinergic synaptic circuitry in the macaque prefrontal cortex. J Comp Neurol 357:603–617

Naito E, Scheperjans F, Eickhoff SB, Amunts K, Roland P, Zilles K, Ehrsson HH (2008) Cytoarchitectonic areas in human superior parietal lobule are functionally implicated by an illusion of bimanual interaction with an external object. J Neurophysiol 99:695–703

Palomero-Gallagher N, Zilles K (2004) Isocortex. In: Paxinos G (ed) The rat nervous system, 3rd edn edn. Acadamic Press, San Diego, pp 729–757

Palomero-Gallagher N, Mohlberg H, Zilles K, Vogt B (2008) Cytology and receptor architecture of human anterior cingulate cortex. J Comp Neurol 508:906–926

Palomero-Gallagher N, Vogt B, Mayberg HS, Schleicher A, Zilles K (2009) Receptor architecture of human cingulate cortex: insights into the four-region neurobiological model. Hum Brain Mapp 30:2336–2355

Pinaud R, Mello CV (2007) GABA immunoreactivity in auditory and song control brain areas of zebra finches. J Chem Neuroanat 34:1–21

Pollok B, Prior H, Güntürkün O (2000) Development of object permancence in the food storing magpie (Pica pica). J Comp Psychol 114:148–157

Prior H, Schwarz A, Güntürkün O (2008) Mirror-induced behavior in the magpie (*Pica pica*): evidence of self-recognition. PLoS Biol 6:e202

Puelles L, Kuwana E, Puelles E, Bulfone A, Shimamura K, Keleher J, Smiga S, Rubenstein JL (2000) Pallial and subpallial derivatives in the embryonic chick and mouse telencephalon, traced by the expression of the genes Dlx-2, Emx-1, Nkx-2.1, Pax-6, and Tbr-1. J Comp Neurol 424:409–438

Rehkämper G, Zilles K (1991) Parallel evolution in mammalian and avian brains: comparative cytoarchitectonic and cytochemical analysis. Cell Tissue Res 263:3–28

Reiner A, Perkel DJ, Bruce LL, Butler AB, Csillag A, Kuenzel W, Medina L, Paxinos G, Shimizu T, Striedter G, Wild M, Ball GF, Durand S, Güntürkün O, Lee DW, Mello CV, Powers A, White SA, Hough G, Kubikova L, Smulders TV, Wada K, Dugas-Ford J, Husband S, Yamamoto K, Yu J, Siang C, Jarvis ED (2004) Revised nomenclature for avian telencephalon and some related brainstem nuclei. J Comp Neurol 473:377–414

Richfield EK, Young AB, Penney JB (1989) Comparative distributions of dopamine D-1 and D-2 receptors in the cerebral cortex of rats, cats, and monkeys. J Comp Neurol 286:409–426

Riters LV, Bingman VP (1999) The effects of lesions to the caudolateral neostriatum on sun compass based spatial learning in homing pigeons. Behav Brain Res 98:1–15

Riters LV, Erichsen JT, Krebs JR, Bingman VP (1999) Neurochemical evidence for at least two regional subdivisions within the homing pigeon (*Columba livia*) caudolateral neostriatum. J Comp Neurol 412:469–487

Robbins TW, Arnsten AF (2009) The neuropsychopharmacology of fronto-executive function: monoaminergic modulation. Annu Rev Neurosci 32:267–287

Rose SP (2000) God's organism? The chick as a model system for memory studies. Learn Mem 7:1–17

Rose J, Colombo M (2005) Neural correlates of executive control in the avian brain. PLoS Biol 3:e190

Rose J, Schiffer AM, Dittrich L, Güntürkün O (2010) The role of dopamine in maintenance and distractability of attention in the "prefrontal cortex" of pigeons. Neuroscience 167:232–237

Sakaue M, Somboonthum P, Nishihara B, Koyama Y, Hashimoto H, Baba A, Matsuda T (2000) Postsynaptic 5-hydroxytryptamine (1A) receptor activation increases in vivo dopamine release in rat prefrontal cortex. Br J Pharmacol 129:1028–1034

Salvatierra NA, Torre RB, Arce A (1997) Learning and novelty induced increase of central benzodiazepine receptors from chick forebrain, in a food discrimination task. Brain Res 757:79–84

Santi A, Weise L (1995) The effects of scopolamine on memory for time in rats and pigeons. Pharmacol Biochem Behav 51:271–277

Sarter M, Bruno JP (2000) Cortical cholinergic inputs mediating arousal, attentional processing and dreaming: differential afferent regulation of the basal forebrain by telencephalic and brainstem afferents. Neuroscience 95:933–952

Sarter M, Parikh V, Howe WM (2009) nAChR agonist-induced cognition enhancement: integration of cognitive and neuronal mechanisms. Biochem Pharmacol 78:658–667

Schleicher A, Palomero-Gallagher N, Morosan P, Eickhoff SB, Kowalski T, de Vos K, Amunts K, Zilles K (2005) Quantitative architectural analysis: a new approach to cortical mapping. Anat Embryol (Berl) 210:373–386

Schnabel R, Metzger M, Jiang S, Hemmings HC Jr, Greengard P, Braun K (1997) Localization of dopamine D1 receptors and dopaminoceptive neurons in the chick forebrain. J Comp Neurol 388:146–168

Seed AM, Tebbich S, Emery NJ, Clayton NS (2006) Investigating physical cognition in rooks, *Corvus frugilegus*. Curr Biol 16:697–701

Sorenson EM, Chiappinelli VA (1992) Localization of 3H-nicotine, 125I-kappa-bungarotoxin, and 125I-alpha-bungarotoxin binding to nicotinic sites in the chicken forebrain and midbrain. J Comp Neurol 323:1–12

Stewart MG, Bourne RC, Chmielowska J, Kalman M, Csillag A, Stanford D (1988) Quantitative autoradiographic analysis of the distribution of [3H]muscimol binding to GABA receptors in chick brain. Brain Res 456:387–391

Stewart MG, Cristol D, Philips R, Steele RJ, Stamatakis A, Harrison E, Clayton N (1999) A quantitative autoradiographic comparison of binding to glutamate receptor sub-types in hippocampus and forebrain regions of a food-storing and a non-food-storing bird. Behav Brain Res 98:89–94

Taylor AH, Hunt GR, Medina FS, Gray RD (2009) Do New Caledonian crows solve physical problems through causal reasoning? Proc Biol Sci 276:247–254

Uylings HBM, Sanz-Arigita E, de Vos K, Smeets WJAJ, Pool CW, Amunts K, Rajkowska G, Zilles K (2000) The importance of a human 3D database and atlas for studies of prefrontal and thalamic functions. Progr Brain Res 126:357–368

Uylings HB, Groenewegen HJ, Kolb B (2003) Do rats have a prefrontal cortex? Behav Brain Res 146:3–17

Van De Werd HJ, Rajkowska G, Evers P, Uylings HB (2010) Cytoarchitectonic and chemoarchitectonic characterization of the prefrontal cortical areas in the mouse. Brain Struct Funct 214:339–353

Van Eden CG, Lamme VA, Uylings HB (1992) Heterotopic cortical afferents to the medial prefrontal cortex in the rat. A combined retrograde and anterograde tracer study. Eur J Neurosci 4:77–97

Veenman CL, Albin RL, Richfield EK, Reiner A (1994) Distributions of GABAA, GABAB, and benzodiazepine receptors in the forebrain and midbrain of pigeons. J Comp Neurol 344:161–189

Veenman CL, Wild JM, Reiner A (1995) Organization of the avian "corticostriatal" projection system: a retrograde and anterograde pathway tracing study in pigeons. J Comp Neurol 354:87–126

Vogt BA, Pandya DN (1987) Cingulate cortex of the rhesus monkey: II. Cortical afferents. J Comp Neurol 262:271–289

Waeber C, Dietl MM, Hoyer D, Palacios JM (1989) 5.HT1 receptors in the vertebrate brain. Regional distribution examined by autoradiography. Naunyn Schmiedebergs Arch Pharmacol 340:486–494

Waldmann C, Güntürkün O (1993) The dopaminergic innervation of the pigeon caudolateral forebrain: immunocytochemical evidence for a 'prefrontal cortex' in birds? Brain Res 600:225–234

Wang M, Ramos BP, Paspalas CD, Shu Y, Simen A, Duque A, Vijayraghavan S, Brennan A, Dudley A, Nou E, Mazer JA, McCormick DA, Arnsten AF (2007) Alpha2A-adrenoceptors strengthen working memory networks by inhibiting cAMP-HCN channel signaling in prefrontal cortex. Cell 129:397–410

Williams GV, Castner SA (2006) Under the curve: critical issues for elucidating D1 receptor function in working memory. Neuroscience 139:263–276

Wynne B, Güntürkün O (1995) Dopaminergic innervation of the telencephalon of the pigeon (*Columba livia*): a study with antibodies against tyrosine hydroxylase and dopamine. J Comp Neurol 357:446–464

Yamamoto K, Reiner A (2005) Distribution of the limbic-system associated membran protein (LAMP) in pigeon forebrain and midbrain. J Comp Neurol 486:221–242

Yamasaki M, Matsui M, Watanabe M (2010) Preferential localization of muscarinic M1 receptor on dendritic shaft and spine of cortical pyramidal cells and its anatomical evidence for volume transmission. J Neurosci 30:4408–4418

Zahrt J, Taylor JR, Mathew RG, Arnsten AF (1997) Supranormal stimulation of D1 dopamine receptors in the rodent prefrontal cortex impairs spatial working memory performance. J Neurosci 17:8528–8535

Zhang W, Yamada M, Gomeza J, Basile AS, Wess J (2002) Multiple muscarinic acetylcholine receptor subtypes modulate striatal dopamine release, as studied with M1–M5 muscarinic receptor knock-out mice. J Neurosci 22:6347–6352

Zilles K (1985) The cortex of the rat, a stereotaxic atlas. Springer Verlag, Berlin

Zilles K, Amunts K (2010) Centenary of Brodmann's map—conception and fate. Nat Rev Neurosci 11:139–145

Zilles K, Schleicher A, Palomero-Gallagher N, Amunts K (2002a) Quantitative analysis of cyto- and receptor architecture of the human brain. In: Mazziotta JC, Toga A (eds) Brain mapping: the methods. Elsevier, Amsterdam, pp 573–602

Zilles K, Palomero-Gallagher N, Grefkes C, Scheperjans F, Boy C, Amunts K, Schleicher A (2002b) Architectonics of the human cerebral cortex and transmitter receptor fingerprints: reconciling functional neuroanatomy and neurochemistry. Eur Neuropsychopharmacol 12:587–599

OPEN ACCESS Freely available online

PLoS one

Plasticity in D1-Like Receptor Expression Is Associated with Different Components of Cognitive Processes

Christina Herold[1,3]*, Illah Joshi[2], Omar Chehadi[1], Michael Hollmann[2], Onur Güntürkün[1]

1 Institute for Cognitive Neuroscience, Department of Biopsychology, Faculty of Psychology, Ruhr University Bochum, Bochum, Germany, **2** Department of Biochemistry I—Receptor Biochemistry, Faculty of Chemistry and Biochemistry, Ruhr University Bochum, Bochum, Germany, **3** C. & O. Vogt Institute for Brain Research, Heinrich-Heine-University, Düsseldorf, Germany

Abstract

Dopamine D1-like receptors consist of D1 (D1A) and D5 (D1B) receptors and play a key role in working memory. However, their possibly differential contribution to working memory is unclear. We combined a working memory training protocol with a stepwise increase of cognitive subcomponents and real-time RT-PCR analysis of dopamine receptor expression in pigeons to identify molecular changes that accompany training of isolated cognitive subfunctions. In birds, the D1-like receptor family is extended and consists of the D1A, D1B, and D1D receptors. Our data show that D1B receptor plasticity follows a training that includes active mental maintenance of information, whereas D1A and D1D receptor plasticity in addition accompanies learning of stimulus-response associations. Plasticity of D1-like receptors plays no role for processes like response selection and stimulus discrimination. None of the tasks altered D2 receptor expression. Our study shows that different cognitive components of working memory training have distinguishable effects on D1-like receptor expression.

Citation: Herold C, Joshi I, Chehadi O, Hollmann M, Güntürkün O (2012) Plasticity in D1-Like Receptor Expression Is Associated with Different Components of Cognitive Processes. PLoS ONE 7(5): e36484. doi:10.1371/journal.pone.0036484

Editor: Verner Peter Bingman, Bowling Green State Universtiy, United States of America

Received December 1, 2011; **Accepted** April 9, 2012; **Published** May 4, 2012

Copyright: © 2012 Herold et al. This is an open-access article distributed under the terms of the Creative Commons Attribution License, which permits unrestricted use, distribution, and reproduction in any medium, provided the original author and source are credited.

Funding: This work was supported by a fellowship of the Wilhelm and Günter Esser Stiftung to C.H. and a DFG grant to O.G. via the SFB874. I.J. was supported by a fellowship of the Deutsche Forschungsgemeinschaft Graduate School 736. The funders had no role in study design, data collection and analysis, decision to publish, or preparation of the manuscript.

Competing Interests: The authors have declared that no competing interests exist.

* E-mail: Christina.Herold@uni-duesseldorf.de

Introduction

The prefrontal cortex (PFC) provides the capacity to interpret and predict incoming information based on past events and to select alternative responses. This capability requires working memory (WM) – a cognitive process in which information is held online and manipulated [1]. One key modulator of WM in the PFC is the neurotransmitter Dopamine (DA) [2]. The tuning of PFC neurons during WM processes and WM performance depend on DA D1-like receptor stimulation [1,3,4].

In vertebrates, DA mediates its physiological functions through two pharmacologically and physiologically distinct subfamilies of G protein-coupled receptors, D1-like (D1 and D5) and D2-like (D2, D3, and D4) receptors. The D1-like receptor family is extended in birds, comprising the D1A/D1, D1B/D5, and the D1D receptors, the latter of is physiologically compared to the D1 receptor [5,6]. DA receptors are differentially expressed in the brain [7]. Both D1 and D5 receptors are coexpressed in prefrontal pyramidal neurons and interneurons, showing a complex pattern of localization at the synapse. [8–11]. This difference in subcellular localization suggests that although D1 and D5 receptors exhibit similar pharmacology, they are not functionally redundant. Probably, they are able to complement each other at the behavioral level since D1 receptor knockout mice with intact D5 receptors display normal WM performance, despite showing some learning impairment [12].

Recently, it was shown that cortical D1-like receptor binding changed in association with cognitive training in humans [13]. Further, DA receptors can stimulate their own expression [7]. These results open up the possibility that different cognitive processes induce the expression of different dopamine receptors in various forebrain structures, thereby importantly altering the neurochemical architecture of the cortex. However, several problems have to be solved before such a scenario can be considered likely. First, functions like "working memory" or "cognitive training" involve several subprocesses that reach from the acquisition and retrieval of simple stimulus-response associations to higher cognitive functions. Without separating these components, it remains unclear which function is related to changes in receptor binding. Second, drugs or ligands that specifically affect or bind to D1A, D1B, or D1D are not available, making a classic behavioral or physiological pharmacological approach difficult. Third, different brain structures may show divergent alterations of training-induced changes in receptor binding.

We therefore conducted a behavioral working memory paradigm that works like Russian Matryoshka dolls: The four tasks were designed with increasing cognitive demands such that task 2 had one cognitive component more than task 1, task 3 had more components than task 2 and so on (Figure 1 and 2). By subtraction of cognitive faculties between tasks, expression changes of D1A, D1B, and D1D in striatum and avian nidopallium caudolaterale, an avian functional analogue to the prefrontal cortex, could therefore be mapped to specific subcomponents of cognitive training.

Results

Analysis of DA Receptors in the Pigeon's Brain

Prior to testing, we successfully confirmed the presence of the D1A, D1B, D1D, and D2 receptor in pigeons. We isolated parts of the coding DNA sequence for the different receptor genes in the

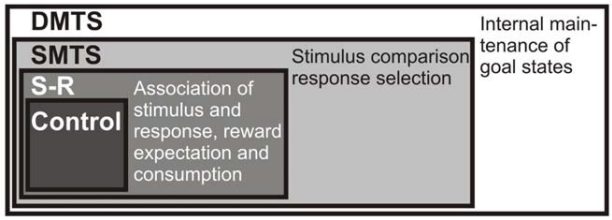

Figure 1. Schematic depiction of the logical structure of the behavioral approach. Expression levels of dopamine receptors are tested in different animal groups under control conditions (no operant behavioral task involved), and during execution of an S-R, an SMTS, or a DMTS task. Much like Russian "Matryoshka" dolls, each of the tasks involves the cognitive components of the previous one, but adds new components that are depicted on the right side of each box.
doi:10.1371/journal.pone.0036484.g001

pigeon's brain after mRNA isolation by using PCR with oligonucleotides that were designed based on the highly homologues sequences for each receptor gene in humans, mice, and chicken. We verified the PCR products by sequence analysis and compared the obtained sequences with sequences in the GenBank® library by using the software tool BLAST®. The derived parts of the coding regions for the different dopamine receptors in the pigeon were deposited in GenBank (EU190460, EU190461, EU190462, EU190463). To analyze the expression of the dopamine receptors after different behavioral training procedures, we redesigned the oligonucleotides based on the pigeon's sequence to create a subunit-specific set of primers (Table 1). When comparing the obtained cDNA sequences to dopamine receptor sequence in other species, we found that D1A and D1B display substantial similarities to mammalian D1 and D5 receptors, respectively. By contrast, D1D, which is also found in chicken and zebra finch [5,6], does not have a counterpart in the mammalian brain (Table 2). Recently, the chicken D1D receptor was renamed D1C (gi:118092829 replaced 50749575); however, it is not clear whether this change was based on established similarity to the D1C gene found in other vertebrates. Therefore, we will continue to use the old term D1D. The avian D2 receptor appears to be similar to the mammalian D2 receptor (Table 2).

Changes in Dopamine Receptor Gene Expression after Prolonged Cognitive Training

The pigeons used for the real-time RT-PCR analysis were age-matched and housed under standard conditions. Pigeons in the control group were inexperienced to any operant or cognitive task, while the pigeons in the experimental groups had learned the described S-R, SMTS, or the DMTS task (Figure 2). Animals in the S-R group were trained in 39±13 sessions, in the SMTS group 40±6, and in the DMTS group 52±26 sessions (all data mean ± SD; $F_{2.27} = 1,84$, $p = 0.18$ n.s.). This corresponds to a period of 9±3 (mean ± SD) weeks of training in a specific task. The animals' forebrains were subsequently extracted and divided into two areas of interest. The first and critical one was the nidopallium caudolaterale (NCL) in the posterior telencephalon (caudal to stereotaxic coordinates A 6.25). As outlined in the discussion, the NCL is a functional analogue to the PFC. The second area of interest consisted of the anterior forebrain frontal to A 8.00. This anterior chunk included a major part of the striatum, although visual and somatosensory areas were also present. Since levels of DA innervation and DA receptor densities are very low in this part of the anterior pallium, the data from the anterior chunk mostly represent striatal DA receptors [14].

RNA was extracted from both areas and a two-step real-time RT-PCR was performed. Data for DA receptor expression levels were normalized to the expression level of the housekeeping gene histone H3.3B from each particular sample of analyzed brain areas and groups.

DA receptor expression levels in the control, the S-R, the SMTS, and the DMTS groups for the NCL and the anterior forebrain (aFB) were analyzed with repeated measurement ANOVAs (4×4×2). Significant main effects for the expression levels of DA receptors were detected between groups ($F_{3.36} = 12.14$, $p<0.001$), brain regions ($F_{1.36} = 28.04$, $p<0.001$), and DA receptors ($F_{3.108} = 55.40$, $p<0.001$). Further interactions were observed between DA receptors and groups ($F_{9,108} = 5.09$, $p = 0.001$) as well as brain regions and DA receptors ($F_{3,108} = 16.08$, $p<0.001$), and a triple interaction was confirmed between brain regions, DA receptor, and groups ($F_{9,108} = 2.28$, $p = 0.02$).

Post-hoc analysis revealed that D1A receptor expression decreased in the NCL and the aFB of the S-R and of the SMTS group if compared to the control condition (all $p \leq 0.002$, *Fisher-LSD;* Figure 3A and B). Additionally, D1A receptors were expressed at lower levels in the NCL and the aFB of the S-R and the SMTS groups than in the DMTS group (all: $p \leq 0.002$, *Fisher-LSD;* Figure 3A and B). Neither in the NCL nor in the aFB did we find differences between the DMTS and the control group. That means D1A receptors were down-regulated after training in the S-R task and in the SMTS task, and up-regulated to control levels after training in the DMTS task. This is illustrated in Figure 4, where the additive logic of our behavioral program was used to calculate differences in receptor expression by subtracting expression levels of different behavioral paradigms. Generally, D1A receptors were expressed equally in both brain regions.

In contrast to the D1A receptor, D1B receptor expression in NCL and aFB was higher after prolonged training in the DMTS task when compared to the expression levels of the control, the S-R, and the SMTS groups (all $p<0.05$, *Fisher-LSD*; Figure 3A and B). No differences in D1B receptor expression levels were seen between the control, the S-R, and the SMTS groups in both brain regions. Thus, only the DMTS training increased D1B receptor levels, while in the other groups levels persisted at control values (Figure 4). Apart from that, under control conditions we found higher expression levels for the D1B receptor in the aFB than in the NCL ($p<0.001$, *Fisher LSD*).

In the NCL and the aFB, D1D receptor expression levels showed the same pattern as for D1A (Figure 4). Lower mRNA levels in the NCL and the aFB were detected between the control and both, the S-R and the SMTS groups (all $p<0.01$, *Fisher-LSD*; Figure 3A and B). The same results were observed if the D1D mRNA levels in the NCL and the aFB were compared to the levels of the DMTS group (all $p<0.001$, *Fisher-LSD*; Figure 3A and B). Further, D1D receptor levels in the aFB were higher in the DMTS if compared to the S-R and the SMTS groups (all $p<0.001$, *Fisher LSD*; Figure 2B). Thus, D1D receptor expression in the aFB initially decreased after training in the S-R and the SMTS tasks, and then rose again to eventually increase above control levels (Figure 4). D1D receptors were equally expressed in both brain regions.

Expression levels of the D2 receptors were stable under all conditions. None of the training procedures altered D2 receptor expression levels in the two investigated brain regions (Figure 3A and B). Further, no significant difference was detected between the expression levels of D2 receptors in the two regions.

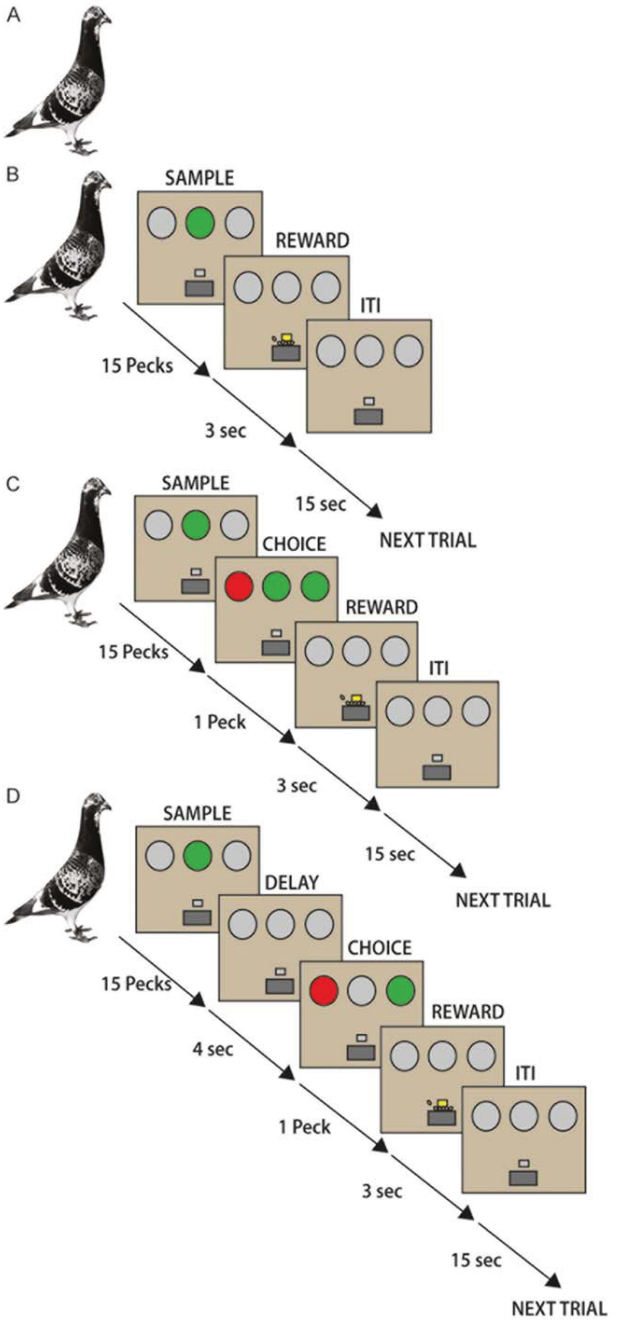

Figure 2. Schematic illustration of the different paradigms for the animal groups in cognitive training. (A) Control group without training in an operant task. (B) S-R task. During training with colored operant keys, each trial started with the presentation of either a green or a red stimulus on one of the three keys. After 15 correct pecks the REWARD phase started with 3 s food access. This was followed by an intertrial interval (ITI) before the next trial started. (C) SMTS task. Training in the simultaneous matching-to-sample task always started with the presentation of either a green or red stimulus as the SAMPLE on the central key. 15 pecks onto this directly started the CHOICE period, where the pigeons had to peck the lateral key that matched the color of the sample. During this phase all keys were simultaneously illuminated. No maintaining of information was required. A single correct peck started the REWARD phase with 3 s food access. This was followed by an ITI before the next trial started. (D) DMTS task. During training of the delayed matching-to-sample task each trial started with the presentation of either a green or red stimulus as the SAMPLE on the central key. 15 pecks onto this started a 4 s DELAY period during which the animals had to memorize the sample color. Then, the lateral keys lit and started the CHOICE period, where the pigeons had to peck the lateral key that matched the color of the sample. A single correct peck started the REWARD phase with 3 s food access. This was followed by an ITI before the next trial started.
doi:10.1371/journal.pone.0036484.g002

Discussion

This study reports that training of cognitive subcomponents of a working memory task results in a specific pattern of dopamine (DA) receptor expression changes in the pigeons' "prefrontal cortex" and anterior forebrain. Our results imply that behavioral procedures that were used in most prior studies involved components that had differentially regulated the expression of D1-like receptors; a fact that was not taken into account before. Additionally, we show that D1A, D1D, and D1B differ considerably in the way their expression patterns change after cognitive training.

The regions of interest are the nidopallium caudolaterale (NCL) and the striatum. The NCL is the functional analogue of the mammalian prefrontal cortex (PFC). Numerous studies have shown that both structures share very similar anatomical [14,15], neurochemical [16,17], electrophysiological [18,19], and functional [20,21] characteristics. This is especially true for the dopaminergic modulation of 'prefrontal' functions in birds and mammals [14,16,22–24]. Thus, despite the non-homologues character of NCL and PFC, DA systems are converging on these two structures for playing very similar roles. The functional similarities of NCL and PFC possibly result from the fact that the dopaminergic systems that derive from the dopaminergic cell groups in the midbrain are homologues in birds and mammals [5,25–27]. One reason for this might be that the development of these dopaminergic systems is older than the divergence of lines of mammals and birds, although some differences in the divers DA systems between species still exist [25,26,28]. The anterior forebrain (aFB) sample of the pigeon encompasses several structures of which the striatum is only one. However, only the striatum has very high levels of DA receptors while the mesopallial and hyperpallial visual and somatosensory areas that are also included show moderate densities [14]. Recently, in situ hybridization studies in the zebra finch and in the chicken brain have shown that the expression of D1-like receptors differs in regions that are included in the aFB sample. For example, D1D receptor transcripts are more prominent in the mesopallial and hyperpallial areas than in the striatal parts, while D1A and D1B receptors showed much more higher densities in the striatum [6,29]. Further D1B receptors were abundant in the chicken mesopallium [6,29]. To date, no in situ hybridization data for the expression pattern of DA receptors is available for the pigeon, and even the zebra finch and the chicken showed differences in the expression pattern of DA receptors [6]. Thus, we cannot exclude that non-striatal areas also contributed to our results, and therefore the results for the aFB have to be interpreted with caution. On the other hand, the avian basal ganglia are densely innervated by midbrain dopaminergic fibers [14,30,31]. Parallel to the situation in mammals, the striatum in pigeons showed higher DA levels compared to the PFC/NCL and the same differences between striatum and PFC/NCL in release and reuptake mechanisms of DA and its metabolites measured by vivo microdialysis studies [16,32]. Furthermore, the avian basal ganglia are homologous to their mammalian counterparts [27] and process the same functions as in other vertebrates [33]. Since levels of DA innervation and DA

Table 1. Primers used for real-time RT-PCR.

Gene	Forward primer 5′–3′	Reverse primer 5′–3′	GenBank accession # for amplicon	Size (bp)
D1A	TTTCCGCAAGGCGTTTTCAAC	TGATCTTTTCCAAAGAAACATCAG	EU190460	304
D1B	CTTCTCCAACCTCCTGGGATG	AGTTATTTTGCCTAGTGAAATCTC	EU190462	276
D1D	TACTGGGCCATCGCCAGCC	TAGGTGATGATCATGATGGGC	EU190461	266
D2	ATGGCTGTGTCCAGGGAAAAA	CCCTGCGCTTCGAGCTGTAGC	EU190463	286
H3.3B	GTGCAGCCATCGGTGCGCT	TGCGAGCCAACTGGATATCT	EU196043	128

The primers were used for quantitative RT-PCR. Each primer pair binds specifically the indicated gene without cross-reactions. The obtained fragments were verified by sequence analysis.

doi:10.1371/journal.pone.0036484.t001

receptor densities in the pigeon seemed to be much lower in the meso- and hyperpallial parts of the aFB sample, we assume that the data from the anterior chunk not entirely but mostly represent striatal DA receptors [14].

Studies in humans show that WM training results in an increase in prefrontal, parietal, and striatal activity [34]. WM training improves intelligence [35], and boosts performance in related but untrained tasks by altering striatal activity [36]. Moreover, it was demonstrated that WM training results in decreased D1-like receptor binding of the ligand [^{11}C]SCH23390 in the human prefrontal and parietal cortex, concomitant with an increase in WM capacity [13]. The effect could best be explained by a non-linear, inverted U-function that is typical for the dopaminergic effect on D1-like receptors [3]. Similarly, an excessive expression of prefrontal D1-like receptors was associated with impaired WM performance in schizophrenic patients [37]. However, participants of all of these studies were tested in multiple tasks and in procedures that involve diverse cognitive skills. Furthermore, SCH23390 binds to D1A and D1B [38]. Thus, several independent and partly inversely organized effects could have contributed to these results.

Both, D1A and D1D expression in NCL and striatum was decreased when animals performed an S-R or an SMTS task. Because expression levels after S-R and SMTS training did not differ between each other, SMTS-related cognitive operations like stimulus comparison or response selection had no impact on DA receptor expression levels. A hallmark of reward-related stimulus-response learning is the feedback by DA encoding a reward prediction error signal [39]. After learning, DA neurons of the midbrain show reward-predictive activity in response to stimuli that are associated with variables like reward magnitude and reward probability [40]. Cues associated with food consumption elicit PFC DA efflux as well as retrieval of trial-specific information during an SMTS task [41–43]. This is also true for pigeons. An elevation of extracellular DA in the NCL was found after SMTS training [16]. D1-like receptors in the NCL are critically involved in learning new S-R contingencies [21] and stimulus selection [24]. Therefore, S-R and SMTS training presumably had produced an increase of DA release and a concomitant binding to D1A and D1D receptors. Long-term DA influx into the n. accumbens resulted in a down-regulation of D1 receptor expression [44]. Further, physical activity not only increases striatal DA [45] but can suppress striatal D1 receptor mRNA transcripts [46]. Therefore, we assume that the training-elicited down-regulation of D1A and D1D receptors in NCL and striatum result from extended periods of training in which external stimuli had to be associated with own actions, and high performance rates resulted in regular bouts of reward.

No alterations in D2 receptor expression were observed, unlike what was seen after motor learning in the striatum of rats [47]. However, Soiza-Reilly et al. (2004) obtained their results during the ontogenetic development of rats. Thus, the observed changes could be influenced by maturational factors of the dopaminergic system. Recently, it was shown that updating training in humans results in higher DA levels in the striatum that is associated with D2 receptor activity without changing D2 receptor densities [48].

Expression levels of D1A, D1B, and D1D were significantly increased after DMTS training when compared with SMTS (Fig. 4). The difference between DMTS and SMTS is the delay component, which characterizes a DMTS-task. Thus, all D1-like receptors are up-regulated when information has to be maintained in WM, and the animal is being faced with delay periods in which the relevant stimuli are physically absent. During delay periods, a memory trace of the relevant information has to be held active. Some PFC and NCL neurons display sustained activity during delay that could hold a memory trace for a subsequent response or

Table 2. Comparison of pigeon DA receptor probe sequences to gene sequences in chicken (c) and human (h).

	D1A/D1 gene	D1B/D5 gene	D1D gene	D2 gene
D1A probe	284/305 (93%) (c) 220/304 (72%) (h)			
D1B probe		250/275 (90%) (c) 195/293 (66%) (h)		
D1D probe		97/266 (36%) (c) 71/266 (27%) (h)	219/266 (82%) (c) n.a. (h)	
D2 probe				264/286 (92%) (c) 235/286 (82%) (h)

Data is presented as x/y (%), with x the number of identical bases and y the total length of the fragment followed by the percentage value of sequence identity. Similarities to pigeon sequences differ between chicken and human and are generally larger for chicken sequences. For the D1D probe only low correspondences were detected to the D1B/D5 gene, while high correlations were found with the chicken D1D gene. Empty boxes indicate absence of any significant identities.

doi:10.1371/journal.pone.0036484.t002

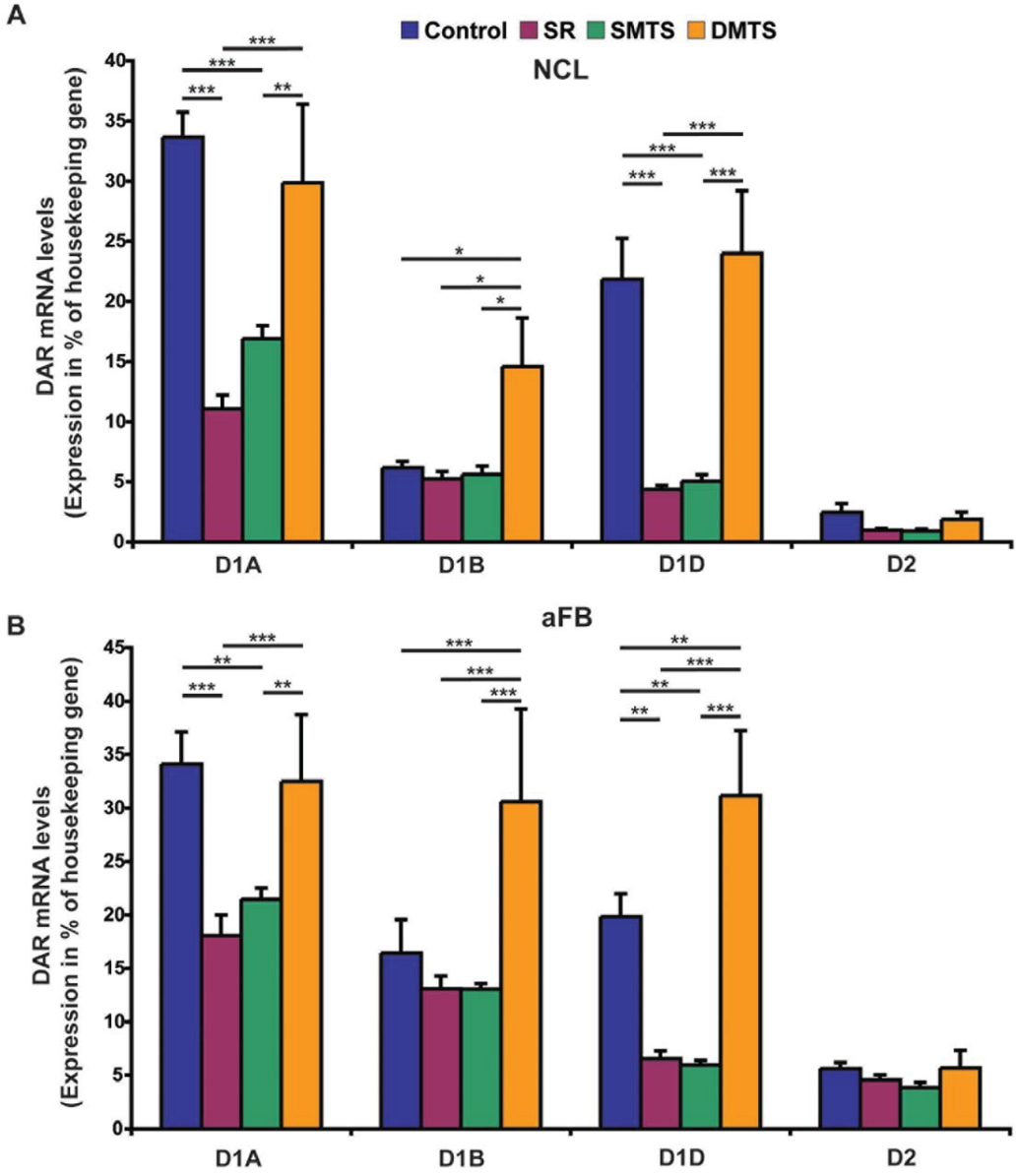

Figure 3. Quantification of dopamine receptor (DAR) mRNA levels in the NCL (A) and the anterior forebrain (aFB; B) of the control and the trained groups. Expression of different DA receptors at the mRNA level is shown relative to the expression of the housekeeping gene histone H3.3B (mean ± SEM; n = 10 each group). Significant differences between groups are marked with asterisks (*p<0.05; **p<0.01; ***p<0.001).
doi:10.1371/journal.pone.0036484.g003

an expected outcome [18,49]. If this activity within the NCL breaks down, the animal is likely to err [18,50]. Delay time-specific activations of PFC neurons are modulated by the dopaminergic system via D1-like receptors [1,3,51]. Blockade of dopaminergic D1-like receptors in the NCL or the PFC disrupts WM performance [1,52,53]. Possibly, DA via D1-like receptors stabilizes active prefrontal neural representations against interfering input by altering ionic and synaptic conductance that enhances spike frequencies of preactivated assemblies [4,54]. Similar results were reported from the songbird basal ganglia [55]. In addition, in monkeys [2] and pigeons [16] increased DA levels in the PFC and the NCL has been observed in DMTS tasks. Our data indicate that expression levels of all three subclasses of D1-like receptors are up-regulated when being confronted over lengthy periods of time with the task to hold a memory trace active during delay periods. However, because D1A and D1D receptor transcripts are down-regulated prior training of the DMTS- task, it may be necessary to have an optimal range or basis level of D1A and D1D receptors to show an excellent performance in the DMTS task that might be not advantageous for the S-R or the SMTS task. Such a dynamic range in modulation of DA receptor transcripts seemed to be also true in the juvenile zebra finch for different processes during song learning [6]. It is important to note that also- the time to obtain a reward was prolonged in the DMTS task, since the reward always followed the response. Thus, the delay to reward delivery was not equalized between tasks. In principle it is possible that this constitutes a further explanation for the different regulation of DA receptor expression profiles in the DMTS task.

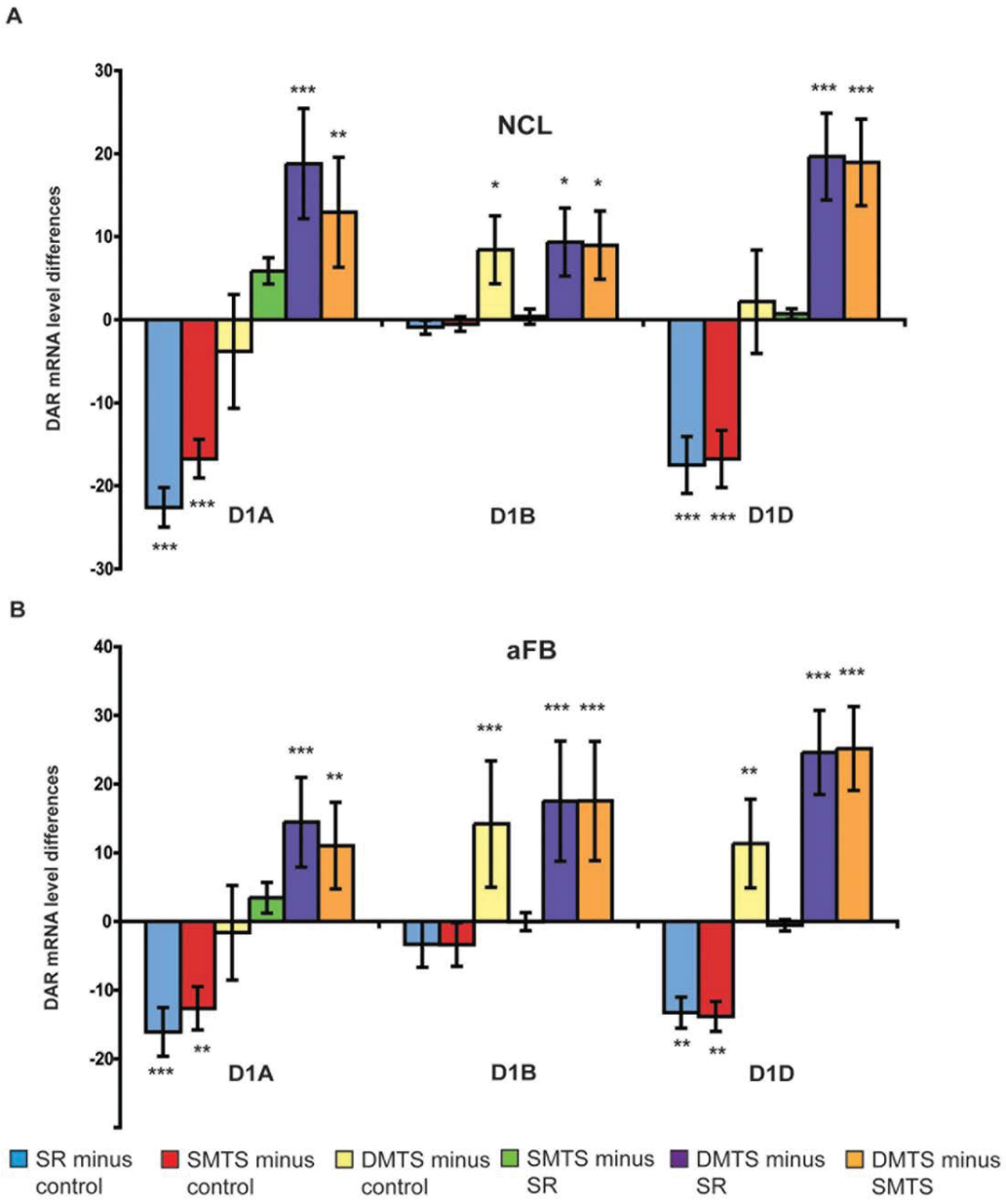

Figure 4. Differences of D1-like mRNA levels in the NCL (A) and the anterior forebrain (aFB; B) between the trained groups. In the NCL and in the aFB, D1A receptor expression levels decreased in the S-R and in the SMTS groups, and increased to control levels after training in the DMTS group. D1B receptor expression increased in both areas in the DMTS group. D1D receptor expression levels decreased in the S-R and the SMTS groups in both areas, and increased to control levels in the NCL while increasing above control levels in the aFB. Thus, a rigid training program that involved a reward-dependent learning of an association between external stimuli and own responses resulted in a down-regulation of the expression of D1A and D1D. D1B expression is only affects after DMTS training. A sole comparison of control and DMTS tasks would have resulted in the wrong conclusion that a DMTS procedure increases D1B expression levels but has no effect on D1A or D1D. All data is presented as mean ± SEM; n = 10 each group. All statistical analyses were only performed on the original data (Figure 3). Significant differences between groups are marked with asterisks (*$p<0.05$; **$p<0.01$; ***$p<0.001$).
doi:10.1371/journal.pone.0036484.g004

Our inverse experimental approach shows that D1 and D5 receptor expression is variably tuned by different cognitive demands. In mammals D1-like receptors not only have differential intracellular trafficking properties [9,56] but also different densities in spines, dendrites, somata, and axons [8,10,11]. Both, in mammals and birds, D1 receptors are often localized in synaptic triads of pyramidal neurons, where glutamatergic and dopaminergic terminals shape the biophysical properties of individual spines [8,57,58]. In mammals, D1 but not D5 receptors form heteromeric assemblies with NMDA receptor subunits by selectively coupling to NR1-1a and NR2A subunits [59]. Indeed, during maintenance periods of DMTS-tasks, forebrain neurons in mammals [60–64] and birds [18] show sustained activity that are modulated by D1 receptors by increasing the NMDA receptor-

induced EPSCs [4,52]. Our findings of task-dependent altered D1-like expression could imply that these molecular dynamics affect the synaptic surrounding of spines.

By contrast, D5 receptors are predominantly localized within dendritic shafts, where inhibitory GABAergic neurons form postsynaptic contacts [8,10]. D5 receptors couple through binding to the $GABA_A$ receptor γ2 subunit [65,66]. This D5-$GABA_A$ receptor cross-talk allows induction of reciprocal inhibitory interactions. As we found training-induced increased levels of D5 receptor mRNA in the avian forebrain, this opens the possibility of an increased D5 receptor cross-talk with $GABA_A$ receptors. Indeed, an increased overall activity of the PFC after cognitive training was reported [34]. Our results support the idea that, at least in birds, D1 and D5 receptors serve distinct cognitive functions and presumably mediate different effects at the cellular level.

Materials and Methods

Animals

40 experimentally naive, adult, unsexed pigeons (*Columba livia*) of local stock, where they live in a natural environment, were used in the experiments. For each group ten pigeons were used. All pigeons were age-matched between one and five years. Animals in the control group (Figure 2A) were experimentally inexperienced, while the rest of the pigeons participated in the cognitive training. Dependent on the task they were trained they were divided into the S-R group, the simultaneous matching-to-sample (SMTS) group, and the delayed matching-to-sample (DMTS) group. All pigeons were housed in individual cages in a temperature-controlled room on a 12-hr light-dark cycle. One week before the experiment started, pigeons from all groups were food-deprived to 80% of their normal free feeding weights. They always had *ad libitum* access to water and grit. Thereafter, pigeons of local stock for the control group were directly used for brain tissue preparation. Pigeons participating in the cognitive training were trained and tested four to five days a week in an operant chamber.

Ethics Statement

The animal procedures were conducted in accordance with the NIH *Guide for the Care and Use of Laboratory Animals* and under adherence to the German laws to protect animals, and hence, the European Communities Council Directive of 18 June 2007. The experimental protocol was approved by national authorities and the ethics committee of the *Landesamt für Natur, Umwelt und Verbraucherschutz* (LANUV) of North Rhine-Westphalia, Germany.

Apparatus and Stimuli

Two operant chambers (34×33×36 cm) were used in the cognitive training. Each chamber was controlled via a digital input-output board (CIO-PDISO8; Computer Boards, Inc.) and illuminated by a 24 W, centrally fixed light bulb. Three opaque operant keys (2 cm in diameter) with a distance of 10 cm between them were located at the back panel of each box, 22 cm above the floor. The pecking keys were homogeneously transilluminated either by white, red, or green light, without matching the brightness of the colors. White lights were used in the operant conditioning and pretraining sessions, while red and green lights were used during the pick training, the SMTS, and the DMTS tasks. The feeder, combined with a light-emitting diode, was fixed in the center of the back panel, 5 cm above the floor.

Behavioral Procedures

The logical structure of the behavioral approach is depicted in Figure 1 and Figure 2.

Pretraining. During the first sessions pigeons were trained to peck reliably on the center key, whenever it was illuminated with white light. After a single peck, the light was turned off, and the pigeons were reinforced with 3 s access to food, followed by an inter-trial interval of 5 s. In the next steps each trial began with the illumination of the center key. One peck on the lateral keys during this phase terminated the trial that was then followed by an inter-trial interval of 15 s and a retry of the trial. Pecking on the central key led to the extinction of the central light and, immediately thereafter, to the illumination of one of the lateral choice keys. After pecking the illuminated lateral key, pigeons were reinforced, whereas pecking the dark choice key caused punishment by a 10 s time-out period during which all lights were turned off. One session included 80 trials with a 15 s inter-trial interval between each trial. Throughout the next training sessions, the number of pecks required on the center key to extinguish the center light and to turn on the lateral lights was constantly increased from 1, 3, 6 to 15 pecks. The criterion for the pretraining was 100% correct responses in one session.

The S-R task. After pretraining, pigeons were trained for a simple stimulus-response (S-R) task. For this, they learned to peck reliably on one of the keys, whenever it was illuminated with colored light. No discrimination of colors was involved. After 15 pecks, the light was turned off, and the pigeons were reinforced with 3 s access to food, followed by an inter-trial interval of 5 s. Illumination of the either one of the lateral keys or the central key was randomized to exclude a spatial bias for one of the keys. Pecking one of the dark keys caused punishment by a 10 s time-out period during which all lights were turned off. One session included 80 trials with a 15 s inter-trial interval between each trial. Before decapitating the animals for quantification of the different dopamine receptor subtype mRNA levels in the nidopallium caudolaterale (NCL) and the anterior part of the forebrain (aFB), all pigeons had to reach an overall criterion of 80% correct responses on three subsequent days. Taken together, the S-R task demanded of the animals to track the location of the colored key and to repeatedly peck it to then obtain reward (Figure 2B).

SMTS task. After pretraining, the operant keys were illuminated with colored light. The illumination of the central stimulus with either red or green light started the trial. The center light stayed on until the pigeon had pecked the key 15 times. Immediately thereafter, the two lateral choice keys were illuminated simultaneously, one in red and the other in green light, while the central key stayed on. Pigeons were reinforced after pecking the lateral illuminated choice key that matched the color of the simultaneously illuminated central key with 3 access to food, and were punished after pecking the non-matching key by a 10 s time-out. No maintaining of stimulus information was required to perform the task because during the choice phase all keys were illuminated. Training went on until the pigeons reached a performance level of 80% correct responses on three subsequent days. The order in which colors were presented was randomized, so that pigeons could not learn a fixed sequence of presentation of the stimuli. Taken together, the SMTS task demanded of the animals to do the very same as in the S-R task until the 15^{th} peck on the central key. However, immediately thereafter they had to match the color of the central key to one of the choice keys and then to select a response to this identified key (Figure 2C). Thus, relative to the S-R animals, the SMTS group had to additionally perform a color matching and response selection task component.

DMTS task. To introduce WM with a short-term memory component, we used a DMTS task. Each trial began with the illumination of the central key, the sample stimulus, either in red or green. During this time, pecking on the lateral dark keys terminated the trial and an inter-trial interval was initiated followed by a repetition of the trial. Otherwise the sample stimulus remained active until the pigeon had pecked the sample stimulus 15 times. After that the delay period started during which the sample stimulus was no longer visible. At the end of the delay the two lateral choice keys were illuminated simultaneously, one in red and the other in green light. Matching the sample stimulus by choosing the choice key with the same color as the sample stimulus before (correct response) was rewarded immediately with free access to food for 3 s. Choosing the complementary color which was not shown at the previous sample stimulus (incorrect answer), was punished with a 10 s time-out period in darkness. The next trial started after a 15 s inter-trial interval. Each session consisted of 80 trials. The order in which colors were presented was randomized, so that pigeons could not learn a fixed sequence of presentation of the stimuli (Figure 2D).

Pigeons of the DMTS group were first trained on a 0 s delay task until they reached a performance level of 80% correct matches in at least three subsequent sessions. Afterwards the delay level was augmented from 0 to 1 s until they reached criterion after which the delay was increased again to 2 s, and later up to a maximum of 4 s. Pigeons had to reach an overall criterion of 80% correct responses on the maximum 4 s delay in at least three subsequent sessions before they were decapitated for the quantification of the different DA receptor subtype mRNAs. Thus, relative to the SMTS animals, the DMTS group had to additionally maintain color information in working memory during the delay period.

RNA Preparation and Quantitative Real-time RT-PCR

For brain tissue preparation pigeons were deeply anesthetized with Equithesin (0.5 ml/100 g body weight, i.m.) and decapitated. Brains were quickly removed and stored on ice. The NCL and the anterior parts of the forebrain including the striatum were dissected out for the left and right hemispheres separately, frozen in liquid nitrogen and stored at −80°C for later use. First, the pigeon brain was adjusted under a binocular microscope with a µm scale. Second, the anterior chunk of the forebrain (aFB) frontal to A 8.00 was cut off straightly from each brain half. Herein, the cerebellar-forebrain junction was used as a reference point and additionally the length of the forebrain itself. According to the atlas of Karten and Hodos [67] these sample included a major part of the basal ganglia as well as visual and somatosensory areas like the entopallium and the frontal parts of the meso-, hyper- and nidopallial regions. Third, the NCL sample according to Waldmann and Güntürkün [68] was prepared (For a detailed atlas of the NCL see [17]). Because a large part of the half-moon-shaped NCL starts caudal from the stereotactic coordinate A 6.25, we cut off a further slice with a thickness of 2 mm to achieve A 6.00. After that we removed the ventrally positioned arcopallial parts. We used the tractus dorso-arcopallialis to orientate because this tract is highly visible in the native preparation. In the next step we cut off the medial parts of the nidopallium, namely the nidopallium caudolaterale central and the nidopallium caudo mediale as well as the hippocampal and the overlaying CDL regions that are naturally separated from the NCL by the ventricle. Therefore, this sample consists mostly of NCL material. Total RNA was extracted to process for real-time RT-PCR by using the NucleoSpin®RNA II Kit (Macherey-Nagel, Düren, Germany). RNA quality was checked for each probe. cDNA was obtained with the Superscript^{TM}II RT First Strand Synthesis System for RT-PCR (Invitrogen, Karlsruhe, Germany). For each probe 300 ng of total RNA was used for the RT reaction. Each probe was replicated twice.

Real-time PCR was performed on a LightCycler® (Roche, Mannheim, Germany) to determine the mRNA expression in the NCL or the anterior parts of the forebrain. For the preparation of the PCR standard reaction the protocol from LightCycler® FastStart DNA Master^{PLUS} SYBR Green I (Roche, Mannheim, Germany) at a total volume of 20 µl was used. For each sample 1 µl cDNA diluted with 4 µl PCR-grade water was used as template for the reaction, with 10 µM forward and backward primers. Both, targets and reference amplifications were performed in triplicate in separate capillaries. The primers for the different DA receptors and the housekeeping gene histone H3.3B used in the real-time PCR are listed in Table 1. Thermal cycling conditions included 10 min at 95°C preincubation, followed by 40 amplification cycles comprising 95°C for 10 s, 60°C for 10 s, and 72°C for 20 s, and one cycle for melting curve analysis comprising 95°C for 0 s, 65°C for 15 s, and 95°C with a slope of 0.1°C/s, followed by cool-down to at least 40°C. Under these conditions the efficiency for all primers was in the range of 2 and thus at maximum. Further, expression of the reference gene was controlled in all groups. None of the groups showed regulation in H3.3B expression.

Real-time PCR products were verified by melting curve analysis, 2% agarose gel electrophoresis (ethidium bromide staining), and sequence analysis on an ABI PRISM Genetic Analyzer 3100C (Applied Biosystems, Darmstadt, Germany). Sequence identities of PCR products to homologues in chicken and human are listed in Table 2.

Data Analysis

Behavioral data was analyzed with a one-way ANOVA with group as "between subject" factor and training days as "within subject" factor. For analysis of real-time RT-PCR data the levels of target gene expression were normalized to the levels of the housekeeping gene histone H3.3B. Ratios between different groups were calculated with the 2-ΔΔCT method. For statistical analysis of real-time RT-PCR data, all values for the different DA receptor types given as percent expression relative to the housekeeping gene were analyzed between groups with repeated measurement ANOVAs (4×4×2). Therein, group was defined as "between subject" factor, and receptors (D1A, D1B, D1D, D2) and brain regions (NCL and anterior forebrain) were defined as "within subject" factors. If main or interaction effects were confirmed this was followed by post-hoc analysis with *Fisher LSD* tests using Statistica 9 (StatSoft, Tulsa, USA). For all analyses the p-level was set at 0.05.

Author Contributions

Conceived and designed the experiments: CH OG. Performed the experiments: CH OC. Analyzed the data: CH. Contributed reagents/materials/analysis tools: CH IJ OC MH OG. Wrote the paper: CH IJ MH OG. Technical assistance: IJ.

References

1. Castner SA, Williams GV (2007) Tuning the engine of cognition: a focus on NMDA/D1 receptor interactions in prefrontal cortex. Brain Cogn 63: 94–122.

2. Watanabe M, Kodama T, Hikosaka K (1997) Increase of extracellular dopamine in primate prefrontal cortex during a working memory task. J Neurophysiol 78: 2795–2798.
3. Vijayraghavan S, Wang M, Birnbaum SG, Williams GV, Arnsten AFT (2007) Inverted-U dopamine D1 receptor actions on prefrontal neurons engaged in working memory. Nature Neurosci 10: 376–384.
4. Seamans JK, Yang CR (2004) The principal features and mechanisms of dopamine modulation in the prefrontal cortex. Prog Neurobiol 74: 1–58.
5. Callier S, Snapyan M, Le Crom S, Prou D, Vincent J-D, et al. (2003) Evolution and cell biology of dopamine receptors in vertebrates. Biol Cell 95: 489–502.
6. Kubikova L, Wada K, Jarvis ED (2009) Dopamine receptors in a songbird brain. J Comp Neurol 518: 741–769.
7. Missale C, Nash SR, Robinson SW, Jaber M, Caron MG (1998) Dopamine receptors: from structure to function. Physiol Rev 78: 189–225.
8. Bergson C, Mrzljak L, Smiley JF, Pappy M, Levenson R, et al. (1995) Regional, cellular, and subcellular variations in the distribution of D1 and D5 dopamine receptors in primate brain. J Neurosci 15: 7821–7836.
9. Yao W-D, Spealman RD, Zhang J (2008) Dopaminergic signaling in dendritic spines. Biochem Pharmacol 75: 2055–2069.
10. Bordelon-Glausier JR, Khan ZU, Muly EC (2008) Quantification of D1 and D5 dopamine receptor localization in layers I, III, and V of Macaca mulatta prefrontal cortical area 9: coexpression in dendritic spines and axon terminals. J Comp Neurol 508: 893–905.
11. Glausier JR, Khan ZU, Muly EC (2009) Dopamine D1 and D5 receptors are localized to discrete populations of interneurons in primate prefrontal cortex. Cereb Cortex 19: 1820–1834.
12. El-Ghundi M, Fletcher PJ, Drago J, Sibley DR, O'Dowd BF, et al. (1999) Spatial learning deficit in dopamine D(1) receptor knockout mice. Eur J Pharmacol 383: 95–106.
13. McNab F, Varrone A, Farde L, Jucaite A, Bystritsky P, et al. (2009) Changes in cortical dopamine D1 receptor binding associated with cognitive training. Science 323: 800–802.
14. Durstewitz D, Kröner S, Güntürkün O (1999) The dopaminergic innervation of the avian telencephalon. Prog Neurobiol 59: 161–195.
15. Kröner S, Güntürkün O (1999) Afferent and efferent connections of the caudolateral neostriatum in the pigeon (Columba livia): a retro- and anterograde pathway tracing study. J Comp Neurol 407: 228–260.
16. Karakuyu D, Herold C, Güntürkün O, Diekamp B (2007) Differential increase of extracellular dopamine and serotonin in the 'prefrontal cortex' and striatum of pigeons during working memory. European J Neurosci 26: 2293–2302.
17. Herold C, Palomero-Gallagher N, Hellmann B, Kröner S, Theiss C, et al. (2011) The receptor architecture of the pigeons' nidopallium caudolaterale: an avian analogue to the mammalian prefrontal cortex. Brain Struct Funct 216: 239–254.
18. Diekamp B, Kalt T, Güntürkün O (2002) Working memory neurons in pigeons. J Neurosci 22: RC210.
19. Kröner S, Gottmann K, Hatt H, Güntürkün O (2002) Electrophysiological and morphological properties of cell types in the chick neostriatum caudolaterale. Neuroscience 110: 459–473.
20. Diekamp B, Gagliardo A, Güntürkün O (2002) Nonspatial and subdivision-specific working memory deficits after selective lesions of the avian prefrontal cortex. J Neurosci 22: 9573–9580.
21. Güntürkün O (2005) The avian 'prefrontal cortex' and cognition. Curr Opin Neurobiol 15: 686–693.
22. Herold C, Diekamp B, Güntürkün O (2008) Stimulation of dopamine D1 receptors in the avian fronto-striatal system adjusts daily cognitive fluctuations. Behav Brain Res.
23. Herold C (2010) NMDA and D2-like receptors modulate cognitive flexibility in a color discrimination reversal task in pigeons. Behav Neurosci 124: 381–390.
24. Rose J, Schiffer AM, Dittrich L, Güntürkün O (2010) The role of dopamine in maintenance and distractability of attention in the "prefrontal cortex" of pigeons. Neuroscience 167: 232–237.
25. Smeets WJ, Gonzalez A (2000) Catecholamine systems in the brain of vertebrates: new perspectives through a comparative approach. Brain Res Brain Res Rev 33: 308–379.
26. Yamamoto K, Vernier P (2011) The evolution of dopamine systems in chordates. Front Neuroanat 5: 21.
27. Reiner A, Perkel DJ, Bruce LL, Butler AB, Csillag A, et al. (2004) Revised nomenclature for avian telencephalon and some related brainstem nuclei. J Comp Neurol 473: 377–414.
28. Jarvis ED, Güntürkün O, Bruce L, Csillag A, Karten H, et al. (2005) Avian brains and a new understanding of vertebrate brain evolution. Nat Rev Neurosci 6: 151–159.
29. Sun Z, Reiner A (2000) Localization of dopamine D1A and D1B receptor mRNAs in the forebrain and midbrain of the domestic chick. J Chem Neuroanat 19: 211–224.
30. Durstewitz D, Kröner S, Hemmings HC Jr., Güntürkün O (1998) The dopaminergic innervation of the pigeon telencephalon: distribution of DARPP-32 and co-occurrence with glutamate decarboxylase and tyrosine hydroxylase. Neuroscience 83: 763–779.
31. Reiner A (2002) Functional circuitry of the avian basal ganglia: implications for basal ganglia organization in stem amniotes. Brain Res Bull 57: 513–528.
32. Bast T, Diekamp B, Thiel C, Schwarting RKW, Güntürkün O (2002) Functional aspects of dopamine metabolism in the putative prefrontal cortex analogue and striatum of pigeons (Columba livia). J Comp Neurol 446: 58–67.
33. Reiner A (2005) A new avian brain nomenclature: why, how and what. Brain Res Bull 66: 317–331.
34. Klingberg T (2010) Training and plasticity of working memory. Trends Cogn Sci 14: 317–324.
35. Jaeggi SM, Buschkuehl M, Jonides J, Perrig WJ (2008) Improving fluid intelligence with training on working memory. Proc Natl Acad Sci U S A 105: 6829–6833.
36. Dahlin E, Neely AS, Larsson A, Backman L, Nyberg L (2008) Transfer of learning after updating training mediated by the striatum. Science 320: 1510–1512.
37. Abi-Dargham A, Mawlawi O, Lombardo I, Gil R, Martinez D, et al. (2002) Prefrontal dopamine D1 receptors and working memory in schizophrenia. J Neurosci 22: 3708–3719.
38. Seeman P, Van Tol HH (1994) Dopamine receptor pharmacology. Trends Pharmacol Sci 15: 264–270.
39. Schultz W (2002) Getting formal with dopamine and reward. Neuron 36: 241–263.
40. Nomoto K, Schultz W, Watanabe T, Sakagami M (2010) Temporally extended dopamine responses to perceptually demanding reward-predictive stimuli. J Neurosci 30: 10692–10702.
41. Bassareo V, Di Chiara G (1997) Differential influence of associative and nonassociative learning mechanisms on the responsiveness of prefrontal and accumbal dopamine transmission to food stimuli in rats fed ad libitum. J Neurosci 17: 851–861.
42. Ahn S, Phillips AG (2002) Modulation by central and basolateral amygdalar nuclei of dopaminergic correlates of feeding to satiety in the rat nucleus accumbens and medial prefrontal cortex. J Neurosci 22: 10958–10965.
43. Phillips AG, Ahn S, Floresco SB (2004) Magnitude of dopamine release in medial prefrontal cortex predicts accuracy of memory on a delayed response task. J Neurosci 24: 547–553.
44. Alsio J, Olszewski PK, Norback AH, Gunnarsson ZE, Levine AS, et al. (2010) Dopamine D1 receptor gene expression decreases in the nucleus accumbens upon long-term exposure to palatable food and differs depending on diet-induced obesity phenotype in rats. Neuroscience 171: 779–787.
45. Petzinger GM, Walsh JP, Akopian G, Hogg E, Abernathy A, et al. (2007) Effects of treadmill exercise on dopaminergic transmission in the 1-methyl-4-phenyl-1,2,3,6-tetrahydropyridine-lesioned mouse model of basal ganglia injury. J Neurosci 27: 5291–5300.
46. Fisher BE, Petzinger GM, Nixon K, Hogg E, Bremmer S, et al. (2004) Exercise-induced behavioral recovery and neuroplasticity in the 1-methyl-4-phenyl-1,2,3,6-tetrahydropyridine-lesioned mouse basal ganglia. J Neurosci Res 77: 378–390.
47. Soiza-Reilly M, Fossati M, Ibarra GR, Azcurra JM (2004) Different dopamine D1 and D2 receptors expression after motor activity in the striatal critical period. Brain Res 1004: 217–221.
48. Bäckman L, Nyberg L, Soveri A, Johansson J, Andersson M, et al. (2011) Effects of working-memory training on striatal dopamine release. Science 333: 718.
49. Machens CK, Romo R, Brody CD (2005) Flexible control of mutual inhibition: a neural model of two-interval discrimination. Science 307: 1121–1124.
50. Rose J, Colombo M (2005) Neural correlates of executive control in the avian brain. PLoS Biol 3: e190.
51. Sawaguchi T, Goldman-Rakic PS (1991) D1 dopamine receptors in prefrontal cortex: involvement in working memory. Science 251: 947–950.
52. Durstewitz D, Seamans JK (2006) Beyond bistability: biophysics and temporal dynamics of working memory. Neuroscience 139: 119–133.
53. Güntürkün O, Durstewitz D (2001) Multimodal areas of the avian forebrain: blueprints for cognition. In: Brain evolution cognition. (Roth G, Wulliman MF, eds): 431–450. New York: Wiley.
54. Durstewitz D, Seamans JK, Sejnowski TJ (2000) Neurocomputational models of working memory. Nat Neurosci 3 Suppl. pp 1184–1191.
55. Ding L, Perkel DJ (2002) Dopamine modulates excitability of spiny neurons in the avian basal ganglia. J Neurosci 22: 5210–5218.
56. He Y, Yu LP, Jin GZ (2009) Differential distributions and trafficking properties of dopamine D1 and D5 receptors in nerve cells. Neurosci Bull 25: 43–53.
57. Goldman-Rakic PS, Leranth C, Williams SM, Mons N, Geffard M (1989) Dopamine synaptic complex with pyramidal neurons in primate cerebral cortex. Proc Natl Acad Sci U S A 86: 9015–9019.
58. Schnabel R, Metzger M, Jiang S, Hemmings HC Jr., Greengard P, et al. (1997) Localization of dopamine D1 receptors and dopaminoceptive neurons in the chick forebrain. J Comp Neurol 388: 146–168.
59. Lee FJS, Xue S, Pei L, Vukusic B, Chery N, et al. (2002) Dual regulation of NMDA receptor functions by direct protein-protein interactions with the dopamine D1 receptor. Cell 111: 219–230.
60. Quintana J, Yajeya J, Fuster JM (1988) Prefrontal representation of stimulus attributes during delay tasks. I. Unit activity in cross-temporal integration of sensory and sensory-motor information. Brain Res 474: 211–221.
61. Funahashi S, Bruce CJ, Goldman-Rakic PS (1989) Mnemonic coding of visual space in the monkey's dorsolateral prefrontal cortex. J Neurophysiol 61: 331–349.
62. Funahashi S, Kubota K (1994) Working memory and prefrontal cortex. Neurosci Res 21: 1–11.
63. Rainer G, Asaad WF, Miller EK (1998) Memory fields of neurons in the primate prefrontal cortex. Proc Natl Acad Sci U S A 95: 15008–15013.

64. Takeda K, Funahashi S (2002) Prefrontal task-related activity representing visual cue location or saccade direction in spatial working memory tasks. J Neurophysiol 87: 567–588.
65. Liu F, Wan Q, Pristupa ZB, Yu XM, Wang YT, et al. (2000) Direct protein-protein coupling enables cross-talk between dopamine D5 and gamma-aminobutyric acid A receptors. Nature 403: 274–280.
66. Wang M, Lee FJ, Liu F (2008) Dopamine receptor interacting proteins (DRIPs) of dopamine D1-like receptors in the central nervous system. Mol Cells 25: 149–157.
67. Karten H, Hodos W (1967) A stereotaxic atlas of the brain of the pigeon: Columba livia. Johns Hopkins Press.
68. Waldmann C, Güntürkün O (1993) The dopaminergic innervation of the pigeon caudolateral forebrain: immunocytochemical evidence for a 'prefrontal cortex' in birds? Brain Res 600: 225–234.

Neuroscience 200 (2012) 1–12

SEROTONIN 5-HT$_{1A}$ RECEPTOR BINDING SITES IN THE BRAIN OF THE PIGEON (*COLUMBA LIVIA*)

C. HEROLD,[a]* N. PALOMERO-GALLAGHER,[b] O. GÜNTÜRKÜN[c] AND K. ZILLES[a,b]

[a]*C. & O. Vogt-Institute for Brain Research, Heinrich-Heine-University, 40225 Düsseldorf, Germany*

[b]*Institute of Neuroscience and Medicine (INM-2), Research Center Jülich, 52425 Jülich, Germany*

[c]*Institute for Cognitive Neuroscience, Faculty of Psychology, Ruhr-University, Bochum, 44780 Bochum, Germany*

Abstract—Present knowledge about the serotonergic system in birdbrains is very limited, although the pigeon was used as an animal model in various studies focused on the behavioral effects of serotonergic transmission. In the mammalian brain the 5-HT$_{1A}$ receptor is the most widespread serotonin receptor type, and is involved in various functions. Less is known about the distribution of 5-HT$_{1A}$ receptors in the avian species. Therefore, we analyzed serotonin 5-HT$_{1A}$ receptor binding sites in the pigeon brain using quantitative *in vitro* receptor autoradiography with the selective radioligand [^{3}H]-8-hydroxy-2-(di-n-propylamino)tetralin ([^{3}H]-8-OH-DPAT). The receptor is differentially distributed throughout the pigeon brain. High levels of 5-HT$_{1A}$ receptors are found in the nucleus pretectalis (PT). Moderate densities were detected in the tectum, as well as in the telencephalic nidopallium and hyperpallium. Very low levels were found in the hippocampal formation, the amygdaloid complex, the basal ganglia, and several thalamic nuclei. Furthermore, local variations in 5-HT$_{1A}$ receptor densities support the concept of further subdivisions of the entopallium. The regional distribution patterns of 5-HT$_{1A}$ receptors mostly display a similar distribution as found in homologue brain structures of mammals. **© 2011 IBRO. Published by Elsevier Ltd. All rights reserved.**

Key words: 5-HT$_{1A}$ receptor, [^{3}H]-8-OH-DPAT, avian, nucleus pretectalis, entopallium, MVL.

Serotonin (5-HT) is a modulatory neurotransmitter that is involved in a variety of physiological and behavioral functions. In mammals, dysfunction of the serotonergic system has been linked to various diseases such as depression, schizophrenia, Alzheimer's disease, and eating disorders (Müller et al., 2007; Michelsen et al., 2008; Remington, 2008; Terry et al., 2008; Akimova et al., 2009; Polter and Li, 2010). In addition, growing evidence found in many species indicates that 5-HT modulates learning and memory (Jacobs and Azmitia, 1992; Winsauer et al., 1996; Meneses, 1999; Clarke et al., 2004; Meneses and Perez-Garcia, 2007; Müller et al., 2007; Bert et al., 2008; Gasbarri et al., 2008; González-Burgos and Feria-Velasco, 2008; Sitaraman et al., 2008; Sambeth et al., 2009; Bari et al., 2010).

Serotonin binds to multiple receptors (Hoyer et al., 2002; Green, 2006), which are widely distributed throughout the brain (Chalmers and Watson, 1991; Baumgarten and Grozdanovic, 1995; Barnes and Sharp, 1999; Riad et al., 2000). One of the most prominent is the 5-HT$_{1A}$ receptor, which was first cloned and described by Fargin et al. (1988). The 5-HT$_{1A}$ receptor belongs to the G protein coupled receptor superfamily and binds to a Gi/o protein (Innis and Aghajanian, 1987; Polter and Li, 2010). It displays a high affinity for 5-HT and occurs both pre- and postsynaptically (Hall et al., 1985; van Wijngaarden et al., 1990; Riad et al., 2000). As somatodendritic autoreceptors, 5-HT$_{1A}$ receptors modulate the activity of 5-HT neurons, whereas they modify neuronal activity in terminal areas as postsynaptic receptors (Müller et al., 2007).

The distribution of 5-HT$_{1A}$ receptors in the brain has been investigated by several methods in rodents, nonhuman primates, and humans. Thereby, a high correlation between receptor binding with [3H]-8-hydroxy-2-(di-n-propylamino)tetralin ([^{3}H]-8-OH-DPAT) and 5-HT$_{1A}$ mRNA densities has been shown (Chalmers and Watson, 1991; Pompeiano et al., 1992). High 5-HT$_{1A}$ receptor densities were detected in the dorsal and median raphe nuclei and in areas of the limbic system such as the hippocampus, the lateral septum, the amygdala, as well as the entorhinal and cingulate cortices (Glaser et al., 1985; Zilles et al., 1985, 2000; Palacios et al., 1990; Yilmazer-Hanke et al., 2003). Moderate binding was detected in the olfactory bulb, the thalamus, hypothalamus, and several brain stem nuclei as well as neocortical areas. Low levels, or no binding, were reported in the basal ganglia and cerebellum (Gozlan et al., 1983; Marcinkiewicz et al., 1984; Zilles et al., 1985, 2000; Hall et al., 1997; Vergé et al., 1986; Albert et al., 1990; Palacios et al., 1990; Pompeiano et al., 1992; Khawaja, 1995; Kia et al., 1996a,b; Farde et al., 1997; Raurich et al., 1999; Hume et al., 2001; Maeda et al., 2001; Geyer et al., 2005; Palchaudhuri and Flügge, 2005; Eickhoff et al., 2007; Topic et al., 2007). 5-HT$_{1A}$ receptors play a role in executive functions, anxiety related behavior, learning and reinforcement, feeding behavior, and locomotor activity (Zilles et al., 2000; Yilmazer-Hanke et al., 2003; Müller

*Corresponding author. Tel: +49-211-81-12666; fax: +49-211-81-12366.
E-mail address: Christina.Herold@uni-duesseldorf.de.

Abbreviations: AI, arcopallium intermedium; APH, area parahippocampalis; Ee, entopallium externum; Eie, entopallium internum pars externale; Eii, entopallium internum pars internale; Gld, lateral geniculate nucleus; HA, hyperpallium apicale; HD, hyperpallium densocellulare; HI, hyperpallium intercalatum; IP, nucleus interpeduncularis; MVL, mesopallium ventrolaterale; NCL, nidopallium caudolaterale; NIL, nidopallium intermedium laterale; PT, nucleus pretectalis; Rt, nucleus rotundus; TnA, nucleus taenia amygdalae; TPO, temporo-parieto-occipitalis; [3H]-8-OH-DPAT, [3H]-8-hydroxy-2-(di-n-propylamino)tetralin.

0306-4522/12 $36.00 © 2011 IBRO. Published by Elsevier Ltd. All rights reserved.
doi:10.1016/j.neuroscience.2011.10.050

et al., 2007; Sumiyoshi et al., 2007; Topic et al., 2007; Borg, 2008; Perez-Garcia and Meneses, 2009).

In pigeons, immunohistochemical studies revealed serotonin fibers and terminals to be broadly distributed throughout the brain. They were particularly prominent in several structures of the telencephalon (arcopallium pars dorsalis, nucleus taeniae, area parahippocampalis, septum), diencephalon (nuclei preopticus medianus, magnocellularis, nucleus geniculatus lateralis pars ventralis, nucleus triangularis, nucleus pretectalis), mesencephalon-rhombencephalon (superficial layers of the optic tectum, nucleus of the basal optic root, nucleus isthmo-opticus), and in most of the cranial nerve nuclei (Krebs et al., 1991; Challet et al., 1996). To date, detailed information about the distribution of 5-HT receptors in the avian brain is very sparse. One study described binding sites for [^{3}H]-8-OH-DPAT in the basal ganglia (Dietl and Palacios, 1988), and a second study used [^{3}H]-5-HT binding in the telencephalon of pigeons, which is non-selective for the different receptor types (Waeber et al., 1989). In addition, the role of 5-HT$_{1A}$ receptor signaling in behavioral outcome and cognitive functions is less investigated in the avian brain compared with mammals. Only a few studies suggest a role for this receptor type in ingestive behavior, circadian rhythm, sleep (Tejada et al., 2011; Fuchs et al., 2006; Garau et al., 2006; Da Silva et al., 2007; Campanella et al., 2009; Dos Santos et al., 2009), and impulsive reactions (Wolff and Leander, 2000). It was demonstrated that 5-HT modulates executive function during working memory in pigeons (Karakuyu et al., 2007) and possibly plays a role in visual attention switching (Miceli et al., 1999, 2002) and ingestive behavior (Güntürkün et al., 1989). Hence, comprehensive information about the regional distribution of 5-HT$_{1A}$ receptor densities is needed to constitute a relevant fundament for behavioral and pharmacological studies in birds. Furthermore, since the avian and mammalian pallia are partly homologous but differ in their morphological organization (Jarvis et al., 2005), 5-HT$_{1A}$ receptor densities could be relevant to compare homologue and analogue structures in birds and mammals. Therefore, we analyzed the distributions of the 5-HT$_{1A}$ receptor with the selective radioligand [^{3}H]-8-OH-DPAT in the pigeon's CNS.

EXPERIMENTAL PROCEDURES

We examined a total of six pigeons (*Columba livia*) of unknown sex. Animals were decapitated and the brains removed from the skull, frozen immediately in isopentane at −40 °C and stored at −70 °C. Serial coronal 10 μm sections were cut with a cryostat microtome (2800 Frigocut E, Reichert-Jung, Vienna, Austria). Sections were thaw-mounted on gelatinized slides and freeze-dried before use for receptor autoradiography or histological staining for the visualization of cell bodies (Merker, 1983).

RECEPTOR AUTORADIOGRAPHY

Binding sites for serotonergic 5-HT$_{1A}$ receptors were labeled with [^{3}H]8-OH-DPAT (Arvidsson et al., 1981; Hjorth and Carlsson, 1982) according to a previously published standardized protocol (Zilles et al., 2002a,b), which consists of three steps: (1) A preincubation step of 30 min at room temperature in buffer (170 mM Tris–HCl buffer with 4 mM $CaCl_2$ and 0.01% ascorbic acid, pH 7.6) removed endogenous ligand from the tissue. (2) During the main incubation step, binding sites were labeled with 1 nM [^{3}H]8-OH-DPAT in buffer for 60 min at room temperature either in the presence of 1 μm 5-hydroxy tryptamine as a displacer (non-specific binding), or without the displacer (total binding). Specific binding is the difference between total and non-specific binding. Since non-specific binding sites amounted to less than 10% of total binding sites, total binding was considered equivalent to specific binding. (3) A final rinsing step of 5 min at 4 °C in buffer eliminated unbound radioactive ligand from the sections.

Sections were air-dried overnight and subsequently coexposed for 8 weeks against a tritium-sensitive film (Hyperfilm, Amersham, Braunschweig, Germany) with plastic [^{3}H]-standards (Microscales, Amersham) of known concentrations of radioactivity. Adjacent sections were stained with a Nissl staining for cytoarchitectonic analysis.

IMAGE ANALYSIS

Autoradiographs were digitized (Schleicher et al., 2005; Zilles et al., 2002a) by means of a KS-400 image analyzing system (Kontron, Germany) connected to a CCD camera (Sony, Tokyo) equipped with an S-Orthoplanar 60-mm macro lens (Zeiss, Germany). The images were stored with a resolution of 512×512 pixels and 8-bit gray value. Images of coexposed microscales were used to compute a calibration curve by nonlinear, least squares fitting, which defined the relationship between gray values in the autoradiographs and concentrations of radioactivity. This enabled the pixel-wise conversion of the gray values of an autoradiograph into the corresponding concentrations of radioactivity. These concentrations of binding sites occupied by the ligand under incubation conditions are transformed into receptor binding site densities at saturation conditions by means of the equation: $(K_D+L)/A_S \times L$, where K_D is the equilibrium dissociation constant of ligand-binding kinetics, L is the incubation concentration of ligand, and A_S the specific activity of the ligand.

ANATOMICAL IDENTIFICATION

The borders of the structures as defined by the atlas of Karten and Hodos (1967) were microscopically identified in the sections processed for the visualization of cell bodies and traced on prints of the digitized autoradiographs. The mean gray values in anatomically identified brain regions (one to five sections per animal and region) are transformed into binding site concentrations (fmol/mg protein). The 5-HT$_{1A}$ receptor densities measured in numerous anatomical structures are summarized in Table 1.

STATISTICAL ANALYSIS

To investigate the binding site density differences between the subdivisions in the entopallium a Friedman ANOVA was conducted. For post hoc analysis, pair-wise comparisons were run with Wilcoxon rank test. All analysis was

Table 1. [^{3}H]8-OH-DPAT binding in the pigeon brain

Brain area	Binding density			
	fmol/mg protein	±SD	Relative density compared with MBV (%)	
Hyperpallium accesorium (HA)	494	115	41	++
Hyperpallium densocellulare (HD)	378	71	31	++
Hyperpallium intercalatum (HI)	688	146	57	+++
Mesopallium (M)	300	49	25	++
Mesopallium dorsale (MD)	313	59	26	++
Mesopallium ventrale (MV)	286	58	24	+
Nucleus MVL	425	50	35	++
Nidopallium (N)	587	90	49	++
Nidopallium caudolaterale (NCL)	374	67	31	++
Nidopallium intermedium laterale (NIL)	629	86	52	+++
Entopallial belt (Ep)	338	70	28	++
Entopallium externum (Ee)	208	54	17	+
Entopallium internum pars externale (Eie)	99	33	8	+
Entopallium internum pars internale (Eii)	n.d.	n.d.	n.d.	n.d.
Nucleus commissuralis septi (CoS)	269	116	22	+
Nucleus sepatalis lateralis (SL)	378	54	31	++
Nucleus septalis medialis (SM)	408	96	34	++
Nucleus diagonalis Brocae (NDB)	342	63	28	++
Nucleus basorostralis pallii (Bas)	121	15	10	+
Arcopallium anterius (AA)	175	13	14	+
Arcopallium intermedium (AI)	229	28	19	+
Arcopallium dorsale (AD)	194	21	16	+
Arcopallium mediale (AM)	n.d.	n.d.	n.d.	n.d.
Nucleus posterioris amygdalopallii (PoA)	175	20	14	+
Hippocampus (Hp)	136	12	11	+
Area parahippocampalis (APH)	156	25	13	+
Area corticoidea dorsolateralis (CDL)	236	101	20	+
Area temporo-parieto-occipitalis (TPO)	252.	115.	21	+
Field L2 (L2)	296	75	24	+
Medial striatum (MSt)	136	14	11	+
Lateral striatum (LSt)	116	13	10	+
Globus pallidus (GP)	94	14	8	+
Nucleus intrapeduncularis (INP)	120	12	10	+
Olfactory tubercle (Otu)	194	74	16	+
Bed nucleus of the stria terminalis, (BST)	164	24	14	+
Nucleus taeniae amygdalae (TnA)	133	15	11	+
Ventral pallidum (VP)	134	6	11	+
Nucleus dorsolateralis anterior thalami, pars lateralis dorsolateralis (DLLdl)	164	100	14	+
Nucleus dorsolateralis anterior thalami, pars lateralis dorsomedialis (DLLdm)	127	37	10	+
Nucleus dorsolateralis anterior thalami, pars lateralis ventrolateralis (DLLvl)	160	95	13	+
Nucleus dorsolateralis anterior thalami, pars lateralis ventromedialis (DLLvm)	126	71	10	+
Nucleus rotundus (Rt)	59	27	5	+
Nucleus subrotundus (SRt)	n.d.	n.d.	n.d.	n.d.
Nucleus ovoidalis (Ov)	76	3	6	+
Nucleus superficialis parvocellularis (SPC)	120	16	10	+
Nucleus triangularis (T)	71	11	6	+
Nucleus pretectalis (PT)	1210	160	100	MBV++++
Nucleus spiriformis medialis (SpM)	n.d.	n.d.	n.d.	n.d.
Nucleus spiriformis lateralis (SpL)	n.d.	n.d.	n.d.	n.d.
Nucleus principalis precommisuralis (PPC)	259	50	21	+
Nucleus geniculatus lateralis. Pars ventralis (Glv)	370	72	31	++
Nucleus subpretectalis/nucleus interstitio-pretecto-subpretectalis (Sp/IPS)	40	3	3	+
Tectum opticum lamina 1	132	22	11	+
Tectum opticum laminae 2–4	597	104	49	++
Tectum opticum lamina 5	620	116	51	+++
Tectum opticum laminae 6–7	545	87	45	++
Tectum opticum laminae 8–13	200	28	17	+

Table 1. Continued

Brain area	Binding density			
	fmol/mg protein	±SD	Relative density compared with MBV (%)	
Tectum opticum lamina 14	66	10	5	+
Nucleus interpeduncularis (IP)	550	138	45	++
Nucleus intercollicularis (ICo)	408	116	34	++
Molecular layer	23	6	2	+
Purkinje+granular cell layer	33	12	3	+

[3H]8-OH-DPAT binding values are shown in fmol/mg protein. Data is presented as mean±SD. The percentage binding values for each structure and the qualitative classification are compared with the structure with the maximal binding (MBV). ++++, very high; +++, high; ++, moderate; +, low; n.d., non detectable.

performed using Statistica 9.0 (StatSoft, Europe GmbH, Hamburg, Germany).

RESULTS

Quantitative receptor autoradiography

Telencephalon. Autoradiographic analysis revealed a widespread, but heterogeneous distribution of 5-HT_{1A} receptors in the pigeon's telencephalon (Table 1). In the following, we will provide a detailed account of our findings.

Pallial structures. High 5-HT_{1A} receptor densities were seen in the hyperpallium intercalatum (HI), one of the pseudolayers of the avian Wulst. In contrast, the most dorsal layer of the Wulst, the hyperpallium apicale (HA) and the hyperpallium densocellulare (HD) showed moderate densities (Fig. 1A–D; Table 1). The second area with a high 5-HT_{1A} receptor concentration was the nidopallium. Therein, the nidopallium intermedium laterale (NIL) showed the highest binding values. The area temporo-parieto-ocipitalis (TPO) could be easily discriminated from the nidopallium because TPO showed only low densities. In contrast to the nidopallium, the overall labeling in the entopallium was relatively low with the notable exception of its belt subregion, which showed comparable densities to those of the nidopallium caudolaterale (NCL) (Fig. 1B–H; Table 1). Different subdivisions of the entopallium were visible (Fig. 2). A comparison of binding site densities between the entopallial belt (Ep), the entopallium externum (Ee), and the entopallium internum pars externale (Eie) using a Friedman ANOVA showed a significant overall effect [chi square (n=6, df=2)=12, $P<0.01$). Binding site densities decreased from Ep to Ee to Eie (all $P<0.05$; Wilcoxon). 5-HT_{1A} receptors were not detectable in the entopallium internum pars internale (Eii). Within the mesopallium, the mesopallium ventrolaterale (MVL) showed a high binding site density (Fig. 1A–C; Table 1). All septal nuclei showed moderate binding site densities (Fig. 1D–F; Table 1). Only low 5-HT_{1A} receptor concentrations were detected in the arcopallium, with lowest values in the nucleus taenia amygdalae (TnA) (Fig. 1G–L; Table 1). Additionally, low densities of 5-HT_{1A} receptors were found in the dorsolateral corticoid area (CDL), area parahippocampalis (APH) and hippocampus (Hp) (Fig. 1D–L; Table 1).

Subpallial structures. The basal ganglia showed relatively low 5-HT_{1A} receptor concentrations when compared with those of the Wulst or the nidopallium. Densities were similar in all subpallial areas, with highest values in the olfactory tubercle (Otu) and the bed nucleus of the stria terminalis (BST), and with lowest concentrations in the globus pallidus (GP) (Fig. 1A–H; Table 1).

Diencephalon. In the thalamic nuclei overall densities were low. Highest 5-HT_{1A} receptor densities were found in the nucleus geniculatus lateralis, pars ventralis (Glv), and lowest in the nucleus subrotundus (SRt). All parts of the nucleus dorsolateralis anterior thalami, pars lateralis (DLL) were labeled, with higher densities in the lateral regions than in the medial ones. Low receptor densities were also detected in the nucleus rotundus (Rt) and in the nucleus ovoidalis (Ov) (Fig. 1H–L, Table 1).

The highest 5-HT_{1A} receptor densities in the pigeon's brain were detected in the nucleus pretectalis (PT). They were two-fold higher than those in the visual Wulst or the nidopallium, and almost 12-fold higher when compared with other diencephalic nuclei.

The nucleus principalis precommisuralis (PPC) contained moderate densities, whereas binding densities in the nucleus subpretectalis/nucleus interstitio-pretecto-subpretectalis (Sp/IPS) were close to zero (Fig. 1H–L; Table 1).

Mesencephalon-rhombencephalon. The nucleus interpeduncularis (IP) showed quite high 5-HT_{1A} receptor densities. The nucleus intercollicularis (ICo) was moderately labeled. In the optic tectum a stepwise increase of 5-HT_{1A} receptor densities was found from layer 1 to layer 5, with a peak in layer 5 and a stepwise decrease until layer 14, which presented the lowest densities in this structure. For comparison, 5-HT_{1A} receptor densities in layer 5 of the optic tectum were comparable with those measured in the Wulst or the nidopallium (Fig. 1I–L, Table 1).

Cerebellum. 5-HT_{1A} receptors occurred at very low densities in the cerebellar cortex with higher concentration in the Purkinje cell layer and in the granule cell layer than in the molecular layer (Table 1).

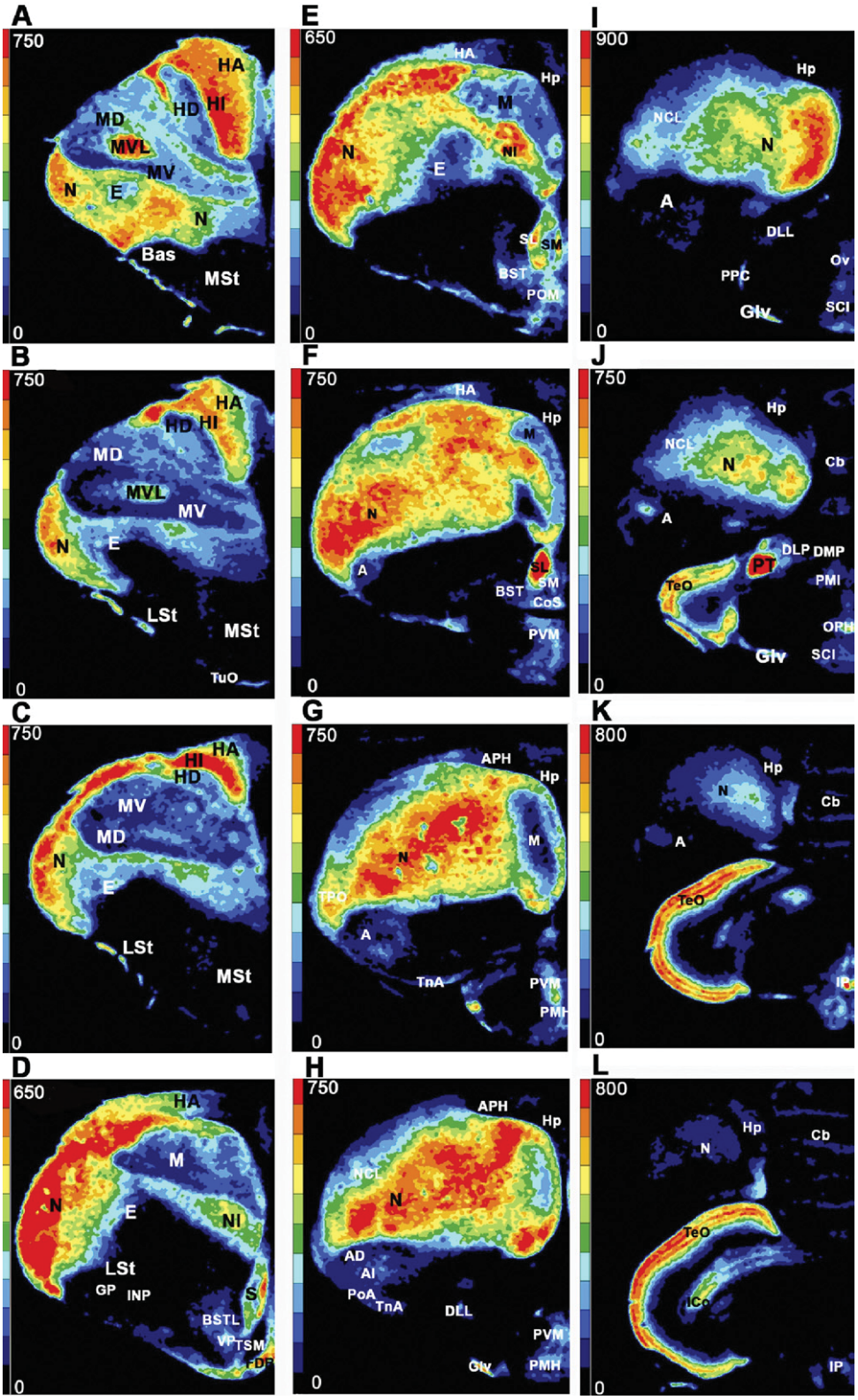

Fig. 1. Color-coded autoradiographs of [^{3}H]8-OH-DPAT binding in the pigeon's CNS. For each sectioning level in a series of coronal sections the color-coded autoradiograph is shown (A–L). Images were arranged in rostro-caudal sequence (left, middle, and right column). Color coding indicates density of 5-HT$_{1A}$ receptor binding sites in fmol/mg protein. Note that color-coding of each image is optimized to the overall density. The maximum binding level is not included in the color graphs but is shown in the table (Table 1). Abbreviations used are defined in the autoradiography binding data table (Table 1). For interpretation of the references to color in this figure legend, the reader is referred to the Web version of this article.

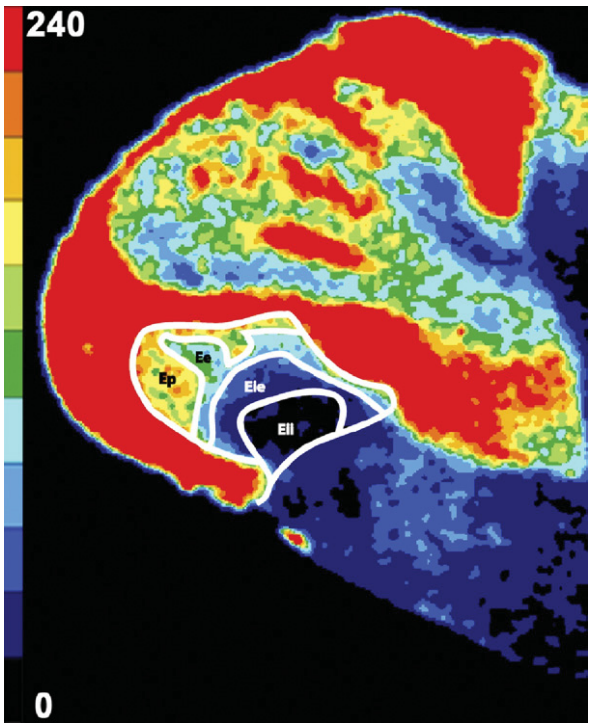

Fig. 2. Color-coded autoradiograph showing the heterogenous 5-HT_{1A} receptor distribution in the pigeon's entopallium. Contrast enhancement is optimized to the density of 5-HT_{1A} receptors in the entopallium. The 5-HT_{1A} receptors showed a lamina-type allocation in the entopallium. Densities increased from the ventromedial area to the belt region. Ep, Entopallial belt; Ee, Entopallium externum; Eie, Entopallium internum pars externale; Eii, Entopallium internum pars internale. For interpretation of the references to color in this figure legend, the reader is referred to the Web version of this article.

DISCUSSION

5-HT_{1A} receptors were widely and heterogeneously distributed throughout the pigeon's brain. The highest density was found in the PT. This is in line with the dense innervation of the avian PT by serotonergic fibers (Cozzi et al., 1991; Challet et al., 1996; Metzger et al., 2002). Since PT is the source of visual and nonvisual input to the superficial layers of the optic tectum, it may modulate the inhibitory control of retinotectal transmission (Gamlin and Cohen, 1988; Gamlin et al., 1996) through 5-HT_{1A} receptors. Lesions of PT as well as of the nucleus spiriformis lateralis (SpL) result in impairment of behavior involving tracking and pecking moving targets (Bugbee, 1979). Further, PT has reciprocal connections with the subpretectal nucleus SP and therefore, PT may control attention shift from one eye to the other (Theiss et al., 2003). The PT receives further input from the basal ganglia that underlines its function in visuomotor processing (Reiner et al., 1982). Like in birds, a prominent innervation of the area pretectalis with serotonergic fibers was reported for rats, turtles, and fish (Ueda et al., 1983; Lüth and Seidel, 1987; Cuadrado et al., 1993).

In the optic tectum 5-HT_{1A} receptors showed a laminar specific distribution. The major retino-recipient layer 5 displays the highest density of 5-HT_{1A} receptors in the optic tectum, and is also densely innervated by serotonergic fibers (Metzger et al., 2006). Layer 5b of the optic tectum, which is a major retino-recipient layer, receives further input from PT (Gamlin et al., 1996). Since the optic tectum and PT showed a high density of 5-HT_{1A} receptors, the receptors may play a substantial role of 5-HT_{1A} receptors in controlling the output of these regions.

A nucleus in the brain stem, the IP, also showed a quite high density of 5-HT_{1A} receptors. This finding matches with the presence of a high density of 5-HT fibers and terminals in IP (Challet et al., 1996), and is in line with other autoradiography studies in human and rats that also showed high binding sites for 5-HT receptors in IP (Palacios et al., 1983; Kaulen et al., 1986). In birds IP has been implicated in appetitive and consummatory male sexual behavior (Dermon et al., 1999). Further, a lesion study in rats showed that IP is enclosed in a network of controlling avoidance behavior (Hammer and Klingberg, 1990). Rats with IP lesions were hypoactive and showed diminished exploratory behavior. Because behavioral drug tests in mammals have shown that 5-HT_{1A} receptors are also involved in appetitive and avoidance behavior, the same may be true for the avian species. Indeed, it was detected in ringdoves that systemic injections of 8-OH-DPAT increased locomotor activity (Tejada et al., 2011).

In the thalamic nuclei 5-HT_{1A} receptors are found to occur at moderate densities. The relatively highest density was detected in the ventral part of the lateral geniculate nucleus (Glv), which receives a strong serotonergic innervation, though to a lesser extent than PT (Cozzi et al., 1991; Challet et al., 1996). Furthermore, the Glv receives direct input from the retina and afferents from the visual Wulst, has reciprocal connections with the optic tectum, and projects to the pretectal nuclei (Guiloff et al., 1987; Güntürkün and Karten, 1991). Lesions of the Glv had shown that this area is involved in visuomotor function (Guiloff et al., 1987). The dorsal part of the lateral geniculate nucleus (Gld), contains relatively low 5-HT_{1A} receptor densities. The Gld is also a retinorecipient optic center in the thalamus, projects to the Wulst, and is part of one of the two ascending visual pathways in birds, the thalamofugal pathway (Karten et al., 1973). In addition, the Rt, which is the thalamic in- and output structure of the second visual pathway, the tectofugal pathway (Rogers and Deng, 1999; Hellmann and Güntürkün, 2001; Schmidt and Bischof, 2001; Folta et al., 2004), also contained very low 5-HT_{1A} receptor densities.

The overall 5-HT_{1A} receptor density in the pigeon Wulst was high. This implicates that 5-HT_{1A} receptors are critically involved in the function of the avian Wulst, which is in part comparable with the function of primary visual, somatosensory and motor cortices in mammals (Keary et al., 2010; Ng et al., 2010; Reiner et al., 2005; Iwaniuk and Wylie, 2006). The avian Wulst is also a part of the thalamofugal pathway in birds (Hodos et al., 1973; Karten et al., 1973; Shimizu and Bowers, 1999). It was suggested that the processing of visual information in the thalamofugal tract is associated with the performance of more complex visual tasks that include a more detailed analysis of infor-

mation, like during migration behavior (Budzynski et al., 2002). The thalamofugal pathway corresponds to the mammalian geniculostriate pathway (Shimizu and Karten, 1990). The Gld, the thalamic relay station of the thalamofugal projection receives input from the central area of the pigeon's retina, and thus, from the lateral visual field (Remy and Güntürkün, 1991). Consequently, lesions of the thalamofugal system affect discrimination tasks in the lateral but not in the frontal field of view (Güntürkün and Hahmann, 1999; Budzynski and Bingman, 2004). The highest 5-HT_{1A} receptor density was detected in the HI, which is one of the pseudolayers of the avian Wulst. Pseudolayers are nuclear structures that do not display the laminar organization of the mammalian cerebral cortex where columns have an orthogonal position to laminae (Medina and Reiner, 2000; Butler et al., 2005). HI receives visual input from the Gld and is also part of the thalamofugal system (Güntürkün and Hahmann, 1999). In addition, HI is the output layer that gives rise to projections to the dorsocaudal telencephalon like the area parahippocampalis and the area corticoidea dorsolateralis (Shimizu et al., 1995). In most avian species the Wulst contains three further pseudolayers (Medina and Reiner, 2000). The intermediate layer is a thin band of granule cells, the interstitial part of the hyperpallium apicale (IHA), which is a major recipient for sensory thalamic input (Watanabe et al., 1983; Wild, 1987; Shimizu et al., 1995). The HD receives only visual thalamic input and mainly projects to subpallial and pallial parts. The most superficial layer, the HA, is the main output layer and projects to the striatum, the thalamus and the brainstem, as well as to other pallial structures (Reiner and Karten, 1982; Veenman et al., 1995; Shimizu et al., 1995; Medina and Reiner, 2000). In addition, HA receives afferents from all other layers of the Wulst (Shimizu et al., 1995). 5-HT_{1A} receptor had lower densities in HA and HD than in HI. HI/HD showed comparable concentrations of 5-HT_{1A} receptors to those measured in layers II-III of human V1 (Eickhoff et al., 2007). Taken together, 5-HT_{1A} receptors can play a crucial role in controlling Gld output to the Wulst and hence to higher associative structures.

The nidopallium was also enriched in 5-HT_{1A} receptors, with higher amounts in the NIL than in its medial parts. In addition, the associative (Güntürkün, 2005) forebrain structure NCL was also densely labeled, and could be subdivided into a medial and a lateral part (Herold et al., 2011). The dense receptor labeling is in contrast to the few serotonergic terminals within NCL (Challet et al., 1996). However, our findings are in accordance with the results of Karakuyu et al. (2007), who examined serotonin efflux during a working memory paradigm in pigeons. They observed serotonin release in the NCL, but not in the striatum during working memory tasks. Since the serotonin release was independent of a short term memory component, the authors concluded that serotonin within NCL could control executive functions like attention switching without being involved in the process of memorization of stimulus information. Because of the relatively high 5-HT_{1A} receptor densities measured in the NCL, future studies should confirm a specific role of this receptors type for executive functions. For example, in rats, 5-HT_{1A} receptor modulations in the mPFC have been shown to be very important for optimal attention functioning (Carli et al., 2006). 5-HT_{1A} receptor densities in the nidopallium are comparable with those found in frontal areas of humans and monkeys (Herold et al., 2011; Goldman-Rakic et al., 1990) but are different from the findings in rats (Herold et al., 2011; Pazos and Palacios, 1985).

In birds the former archistriatum has been subdivided into a somatosensory arcopallium and a complex of structures that are comparable with the mammalian amygdaloid complex (Reiner et al., 2004; Saint-Dizier et al., 2009). In birds, the amygdaloid complex includes the nucleus posterior amygdalopallialis (PoA), the TnA, and the area subpallialis amygdalae (SpA), and has been linked to visceral and limbic functions because of its connections with the hypothalamus and caudal brain stem nuclei. A dense 5-HT innervation was found for limbic structures like the TnA, the parahippocampal area (APH), hippocampus (HP), and area septalis in pigeons, chicken, and quails (Yamada et al., 1985; Cozzi et al., 1991; Challet et al., 1996). Recently it was shown that injections of the 5-$HT_{1/2/7}$ receptor antagonist Metergoline and the 5-$HT_{1B/1D}$ agonist GR46611 into TnA induced hypophagic responses, whereas the same treatment in the arcopallium intermedium (AI) resulted in a selective increase in water intake (Campanella et al., 2009). These effects seemed to be regionally specific because Metergoline and GR46611 injections into the arcopallium mediale (AM) failed to affect those behaviors. In line with this, we found only low 5-HT_{1A} densities in TnA and AI, supporting the view that transmission through 5-HT_{1A} receptors in those regions plays no, or only a minor role in ingestive behavior (Campanella et al., 2009). However, our findings are in contrast to those of the mammalian amygdaloid nuclei, which contain high or intermediate 5-HT_{1A} receptor concentrations (Hall et al., 1997; Yilmazer-Hanke et al., 2003; Palchaudhuri and Flügge, 2005; Perez-Garcia and Meneses, 2008). Further, a strong serotonergic innervation of the hippocampus and the parahippocampal area has been reported, however the 5-HT_{1A} receptor density observed in the present study is low. This is not a contradictory finding, since 5-HT binds to a variety of further 5-HT receptors. Moreover, the boundaries of the avian hippocampal formation are still not completely determined. Krebs et al. (1991) detected dense 5-HT termination fields in the dorsomedial hippocampus. In our data, we could identify this field in the hippocampus by the highest concentration of 5-HT_{1A} receptors at the dorsomedial hippocampus, and a further field at the caudal and ventromedial site of the hippocampus. Future studies are clearly needed to clarify the exact boundaries of different areas in the hippocampal formation of the avian species. The low overall density of 5-HT_{1A} receptors in the avian hippocampus is in contrast to that in rats and other mammals (Topic et al., 2007; Pazos and Palacios, 1985; Zilles et al., 1985, 2000; Wree et al., 1987; Zilles, 1989; Kraemer et al., 1995; Aznavour et al., 2009).

Thus, low 5-HT_{1A} receptor densities in the pigeon's hippocampal formation may demonstrate an avian-specific situation and implicate that this receptor type might have a different role in the avian hippocampal formation than in mammals. In contrast, all septal nuclei showed dense labeling that is in line with a strong serotonergic innervation in pigeons (Challet et al., 1996) and published 5-HT_{1A} receptor densities for cats, rats, non-human primates, and humans (Aznavour et al., 2009; Aznavour and Zimmer, 2007; Khawaja, 1995; Pazos and Palacios, 1985).

Within the telencephalon, the entopallium is the end station of the tectofugal pathway (Hodos and Karten, 1970; Manns et al., 2007; Valencia-Alfonso et al., 2009). Because of the projections and connectivity of the entopallium, this structure was compared with the human extrastriate cortex (Veenman et al., 1995). Only a few serotonergic terminals were found in the entopallium of pigeons (Challet et al., 1996). In line with this, labeling of 5-HT_{1A} receptors in the entopallium was low, except for the entopallial belt (perientopallium; Ep), which showed comparable densities to those of the NCL. The Ep serves as an intermediary between the core components of the entopallium and the subsequent projections to the nidopallium and the arcopallium, although the Ep is also reached by a minute thalamic projection (Krützfeldt and Wild, 2004, 2005). Some authors compare the neurons of the Ep to layers II and III neurons of the mammalian neocortex (Shimizu and Karten, 1990; Shimizu et al., 1995; Veenman et al., 1995). Herein, our results support this suggestion, because layers II and III of the human extrastriate cortex also contain the highest numbers of 5-HT_{1A} receptors when compared with the other neocortical layers (Zilles et al., 2004; Eickhoff et al., 2007). The input region of the entopallium is the entopallial core, which can be further subdivided into an entopallium externum (Ee) and internum (Ei) (Hellmann et al., 1995; Krützfeldt and Wild, 2005). Our results in principle support such a subdivision. We found a heterogeneous 5-HT_{1A} receptor distribution within the entopallial core, with higher densities in the Ee than in the Eie, and no labeling in the Eii. This could imply that these subdivisions have functional implications, which have to be analyzed in further studies determining the role of the entopallium within the tectofugal pathway. To date, it is not clear whether neurons of the core components are comparable with layer IV neurons in the neocortex of mammals, or whether they are a mixture composed of layer IV and V neurons (Krützfeldt and Wild, 2005). Our results show a low concentration for 5-HT_{1A} receptors in Eie and Eii. This was also found in layers IV and V of the human extrastriate cortex (Eickhoff et al., 2007). In line with the finding of a laminar and columnar organization in the avian auditory cortex (Wang et al., 2010), our results support the idea that the entopallium may have a similar laminar-type organization (Wild and Krützfeldt, 2010).

In pigeons, the medial entopallium has strong reciprocal connections to an area of the ventrolateral mesopallium dorsal to the entopallium (Krützfeldt and Wild, 2005). This area is distinct in Nissl-stained sections and was described in the former hyperstriatum ventrale as hyperstriatum ventrale ventrolaterale (HVvl) (Husband and Shimizu, 1999). This area may be compared with the nucleus MVL in the zebra finch (Krützfeldt and Wild, 2004), and could be also observed in sparrows, canaries, and chicken (Huber and Crosby, 1929; Stokes et al., 1974; Alpár and Tömböl, 2000). In our study, this area showed a dense labeling for 5-HT_{1A} receptors that differed clearly from the rest of the mesopallium confirming a nuclear structure. Therefore, our findings support the idea of Krützfeldt and Wild (2005) that this area is comparable with the nucleus MVL in the zebra finch.

In the basal ganglia low 5-HT_{1A} receptor densities were detected. These findings are in line with one of the few studies that determined the distributions of serotonin 5-HT_{1A} receptors in the avian brain (Dietl and Palacios, 1988). Low densities were also found in the basal ganglia of mammals (Dietl and Palacios, 1988; Palomero-Gallagher et al., 2009). Thus, this result underlines the conservation of receptor distribution patterns in the basal ganglia of different species over a long span of separate evolution.

CONCLUSION

In conclusion, 5-HT_{1A} receptors were prominent in regions that process visual information and higher cognitive functions. In contrast to mammals, low binding sites were detected in limbic structures such as the hippocampus or the amygdala. Future functional studies should address these differences and similarities between the serotonergic systems in avian and mammalian brains. We detected comparable densities of 5-HT_{1A} receptors in pallial structures that have been compared with different layers of specific structures in the mammalian neocortex. Herein, our results support the idea of a nucleus to lamina homology between avian and mammalian brain structures. However, it seems to be necessary to delineate some structures more precisely because as in case of the entopallium it is indicated that the entopallium itself has a laminar-type organization.

Acknowledgments—Supported by a grant from the BMBF through the Bernstein Focus Group "Varying Tunes" to OG.

REFERENCES

Akimova E, Lanzenberger R, Kasper S (2009) The serotonin-1A receptor in anxiety disorders. Biol Psychiatry 66:627–635.

Albert PR, Zhou QY, Van Tol HH, Bunzow JR, Civelli O (1990) Cloning, functional expression, and mRNA tissue distribution of the rat 5-hydroxytryptamine1A receptor gene. J Biol Chem 265:5825–5832.

Alpár A, Tömböl T (2000) Efferent connections of the ectostriatal core. An anterograde tracer study. Ann Anat 182:101–110.

Arvidsson LE, Hacksell U, Nilsson JL, Hjorth S, Carlsson A, Lindberg P, Sanchez D, Wikstrom H (1981) 8-Hydroxy-2-(di-n-propylamino-)tetralin, a new centrally acting 5-hydroxytryptamine receptor agonist. J Med Chem 24:921–923.

Aznavour N, Benkelfat C, Gravel P, Aliaga A, Rosa-Neto P, Bedell B, Zimmer L, Descarries L (2009) MicroPET imaging of 5-HT 1A receptors in rat brain: a test-retest [18F]MPPF study. Eur J Nucl Med Mol Imaging 36:53–62.

Aznavour N, Zimmer L (2007) [18F]MPPF as a tool for the *in vivo* imaging of 5-HT1A receptors in animal and human brain. Neuropharmacology 52:695–707.

Bari A, Theobald DE, Caprioli D, Mar AC, Aidoo-Micah A, Dalley JW, Robbins TW (2010) Serotonin modulates sensitivity to reward and negative feedback in a probabilistic reversal learning task in rats. Neuropsychopharmacology 35:1290–1301.

Barnes NM, Sharp T (1999) A review of central 5-HT receptors and their function. Neuropharmacology 38:1083–1152.

Baumgarten HG, Grozdanovic Z (1995) Psychopharmacology of central serotonergic systems. Pharmacopsychiatry 28 (Suppl 2):73–79.

Bert B, Fink H, Rothe J, Walstab J, Bönisch H (2008) Learning and memory in 5-HT(1A)-receptor mutant mice. Behav Brain Res 195:78–85.

Borg J (2008) Molecular imaging of the 5-HT(1A) receptor in relation to human cognition. Behav Brain Res 195:103–111.

Budzynski CA, Bingman VP (2004) Participation of the thalamofugal visual pathway in a coarse pattern discrimination task in an open arena. Behav Brain Res 153:543–556.

Budzynski CA, Gagliardo A, Ioalé P, Bingman VP (2002) Participation of the homing pigeon thalamofugal visual pathway in sun-compass associative learning. Eur J Neurosci 15:197–210.

Bugbee N (1979) The effect of bilateral lesions in the nucleus spiriformis lateralis on visually guided behavior in the pigeon. Ph.D. Thesis, University of Maryland, College Park, MD.

Butler AB, Manger PR, Lindahl BI, Arhem P (2005) Evolution of the neural basis of consciousness: a bird-mammal comparison. Bioessays 2005(27):923–936.

Campanella LC, da Silva AA, Gellert DS, Parreira C, Ramos MC, Paschoalini MA, Marino-Neto J (2009) Tonic serotonergic control of ingestive behaviours in the pigeon (*Columba livia*): the role of the arcopallium. Behav Brain Res 205:396–405.

Carli M, Baviera M, Invernizzi RW, Balducci C (2006) Dissociable contribution of 5-HT1A and 5-HT2A receptors in the medial prefrontal cortex to different aspects of executive control such as impulsivity and compulsive perseveration in rats. Neuropsychopharmacology 31:757–767.

Challet E, Miceli D, Pierre J, Repérant J, Masicotte G, Herbin M, Vesselkin NP (1996) Distribution of serotonin-immunoreactivity in the brain of the pigeon (*Columba livia*). Anat Embryol (Berl) 193:209–227.

Chalmers DT, Watson SJ (1991) Comparative anatomical distribution of 5-HT1A receptor mRNA and 5-HT1A binding in rat brain—a combined *in situ* hybridisation/*in vitro* receptor autoradiographic study. Brain Res 561:51–60.

Clarke HF, Dalley JW, Crofts HS, Robbins TW, Roberts AC (2004) Cognitive inflexibility after prefrontal serotonin depletion. Science 304:878–880.

Cozzi B, Viglietti-Panzica C, Aste N, Panzica GC (1991) The serotoninergic system in the brain of the Japanese quail. An immunohistochemical study. Cell Tissue Res 263:271–284.

Cuadrado MI, Coveñas R, Tramu G (1993) Neuropeptides and monoamines in the carp (*Cyprinus carpio*) pretectum: an immunocytochemical study. Tissue Cell 25:549–561.

Da Silva RA, Da Silva AS, Poffo MJ, Ribas DC, Faria MS, Marino-Neto J, Paschoalini MA (2007) Feeding behavior after metergoline or GR-46611 injections into the paraventricular nucleus of the hypothalamus in the pigeon. Behav Brain Res 179:248–257.

Dermon CR, Stamatakis A, Tlemçani O, Balthazart J (1999) Performance of appetitive or consummatory components of male sexual behavior is mediated by different brain areas: a 2-deoxyglucose autoradiographic study. Neuroscience 94:1261–1277.

Dietl M, Palacios JM (1988) Receptor autoradiography as a tool for the study of the phylogeny of the basal ganglia. J Recept Res 8:521–532.

Dos Santos MM, Hoeller AA, dos Santos TS, Felisbino MB, Herdt MA, da Silva ES, Paschoalini MA, Marino-Neto J (2009) Behavioural and electroencephalographic effects of systemic injections of 8-OH-DPAT in the pigeon (*Columba livia*). Behav Brain Res 201:244–256.

Eickhoff SB, Rottschy C, Zilles K (2007) Laminar distribution and co-distribution of neurotransmitter receptors in early human visual cortex. Brain Struct Funct 212:255–267.

Farde L, Ginovart N, Ito H, Lundkvist C, Pike VW, McCarron JA, Halldin C (1997) PET-characterization of [carbonyl-11C]WAY-100635 binding to 5-HT1A receptors in the primate brain. Psychopharmacology (Berl) 133:196–202.

Fargin A, Raymond JR, Lohse MJ, Kobilka BK, Caron MG, Lefkowitz RJ (1988) The genomic clone G-21 which resembles a beta-adrenergic receptor sequence encodes the 5-HT1A receptor. Nature 335:358–360.

Folta K, Diekamp B, Güntürkün O (2004) Asymmetrical modes of visual bottom-up and top-down integration in the thalamic nucleus rotundus of pigeons. J Neurosci 24:9475–9485.

Fuchs T, Siegel JJ, Burgdorf J, Bingman VP (2006) A selective serotonin reuptake inhibitor reduces REM sleep in the homing pigeon. Physiol Behav 87:575–581.

Gamlin PD, Cohen DH (1988) Projections of the retinorecipient pretectal nuclei in the pigeon (*Columba livia*). J Comp Neurol 269:18–46.

Gamlin PD, Reiner A, Keyser KT, Brecha N, Karten HJ (1996) Projection of the nucleus pretectalis to a retinorecipient tectal layer in the pigeon (*Columba livia*). J Comp Neurol 368:424–438.

Garau C, Aparicio S, Rial RV, Nicolau MC, Esteban S (2006) Age-related changes in circadian rhythm of serotonin synthesis in ring doves: effects of increased tryptophan ingestion. Exp Gerontol 41:40–48.

Gasbarri A, Cifariello A, Pompili A, Meneses A (2008) Effect of 5-HT(7) antagonist SB-269970 in the modulation of working and reference memory in the rat. Behav Brain Res 195:164–170.

Geyer S, Luppino G, Ekamp H, Zilles K (2005) The macaque inferior parietal lobule: cytoarchitecture and distribution pattern of serotonin 5-HT1A binding sites. Anat Embryol (Berl) 210:353–362.

Glaser T, Rath M, Traber J, Zilles K, Schleicher A (1985) Autoradiographic identification and topographical analysis of high affinity serotonin receptor subtypes as a target for the novel putative anxiolytic TVX Q 7821. Brain Res 358:129–136.

Goldman-Rakic PS, Lidow MS, Gallager DW (1990) Overlap of dopaminergic, adrenergic, and serotoninergic receptors and complementarity of their subtypes in primate prefrontal cortex. J Neurosci 10:2125–2138.

González-Burgos I, Feria-Velasco A (2008) Serotonin/dopamine interaction in memory formation. Prog Brain Res 172:603–623.

Gozlan H, El Mestikawy S, Pichat L, Glowinski J, Hamon M (1983) Identification of presynaptic serotonin autoreceptors using a new ligand: 3H-PAT. Nature 305:140–142.

Green AR (2006) Neuropharmacology of 5-hydroxytryptamine. Br J Pharmacol 147 (Suppl 1):S145–S152.

Guiloff GD, Maturana HR, Varela FJ (1987) Cytoarchitecture of the avian ventral lateral geniculate nucleus. J Comp Neurol 264:509–526.

Güntürkün O (2005) The avian "prefrontal cortex" and cognition. Curr Opin Neurobiol 15:686–693.

Güntürkün O, Grothues A, Hautkappe A, Visé F, Wawrzyniak N, Zwilling U (1989) Serotonergic modulation of ingestive behavior in pigeons. Pharmacol Biochem Behav 32:415–420.

Güntürkün O, Hahmann U (1999) Functional subdivisions of the ascending visual pathways in the pigeon. Behav Brain Res 98:193–201.

Güntürkün O, Karten HJ (1991) An immunocytochemical analysis of the lateral geniculate complex in the pigeon (*Columba livia*). J Comp Neurol 314:721–749.

Hall H, Lundkvist C, Halldin C, Farde L, Pike VW, McCarron JA, Fletcher A, Cliffe IA, Barf T, Wikström H, Sedvall G (1997) Autoradiographic localization of 5-HT1A receptors in the post-mortem

human brain using [3H]WAY-100635 and [11C]WAY-100635. Brain Res 745:96–108.

Hall MD, El Mestikawy S, Emerit MB, Pichat L, Hamon M, Gozlan H (1985) [3H]8-hydroxy-2-(di-n-propylamino)tetralin binding to pre- and postsynaptic 5-hydroxytryptamine sites in various regions of the rat brain. J Neurochem 44:1685–1696.

Hammer KH, Klingberg F (1990) Active avoidance is permanently abolished after lesions of the nucleus interpeduncularis in rat. Biomed Biochim Acta 49:489–497.

Hellmann B, Güntürkün O (2001) Structural organization of parallel information processing within the tectofugal visual system of the pigeon. J Comp Neurol 429:94–112.

Hellmann B, Waldmann C, Güntürkün O (1995) Cytochrome oxidase activity reveals parcellations of the pigeon's ectostriatum. Neuroreport 6:881–885.

Herold C, Palomero-Gallagher N, Hellmann B, Kröner S, Theiss C, Güntürkün O, Zilles K (2011) The receptor architecture of the pigeons' nidopallium caudolaterale: an avian analogue to the mammalian prefrontal cortex. Brain Struct Funct 216:239–254.

Hjorth S, Carlsson A (1982) Buspirone: effects on central monoaminergic transmission—possible relevance to animal experimental and clinical findings. Eur J Pharmacol 83:299–303.

Hodos W, Karten HJ (1970) Visual intensity and pattern discrimination deficits after lesions of ectostriatum in pigeons. J Comp Neurol 140:53–68.

Hodos W, Karten HJ, Bonbright JC Jr (1973) Visual intensity and pattern discrimination after lesions of the thalamofugal visual pathway in pigeons. J Comp Neurol 148:447–467.

Hoyer D, Hannon JP, Martin GR (2002) Molecular, pharmacological and functional diversity of 5-HT receptors. Pharmacol Biochem Behav 71:533–554.

Huber GC, Crosby EC (1929) The nuclei and fiber paths of the avian diencephalon, with consideration of telencephalic and certain mesencephalic centers and connections. J Comp Neurol 48:1–225.

Hume S, Hirani E, Opacka-Juffry J, Myers R, Townsend C, Pike V, Grasby P (2001) Effect of 5-HT on binding of [(11)C] WAY 100635 to 5-HT(IA) receptors in rat brain, assessed using *in vivo* microdialysis nd PET after fenfluramine. Synapse 41:150–159.

Husband SA, Shimizu T (1999) Efferent projections of the ectostriatum in the pigeon (*Columba livia*). J Comp Neurol 406:329–345.

Innis RB, Aghajanian GK (1987) Pertussis toxin blocks 5-HT1A and GABAB receptor-mediated inhibition of serotonergic neurons. Eur J Pharmacol 143:195–204.

Iwaniuk AN, Wylie DR (2006) The evolution of stereopsis and the Wulst in caprimulgiform birds: a comparative analysis. J Comp Physiol A Neuroethol Sens Neural Behav Physiol 192:1313–1326.

Jacobs BL, Azmitia EC (1992) Structure and function of the brain serotonin system. Physiol Rev 72:165–229.

Jarvis ED, Güntürkün O, Bruce L, Csillag A, Karten H, Kuenzel W, Medina L, Paxinos G, Perkel DJ, Shimizu T, Striedter G, Wild JM, Ball GF, Dugas-Ford J, Durand SE, Hough GE, Husband S, Kubikova L, Lee DW, Mello CV, Powers A, Siang C, Smulders TV, Wada K, White SA, Yamamoto K, Yu J, Reiner A, Butler AB (2005) Avian brains and a new understanding of vertebrate brain evolution. Nat Rev Neurosci 6:151–159.

Karakuyu D, Herold C, Güntürkün O, Diekamp B (2007) Differential increase of extracellular dopamine and serotonin in the "prefrontal cortex" and striatum of pigeons during working memory. Eur J Neurosci 26:2293–2302.

Karten H, Hodos W (1967) A stereotaxic atlas of the brain of the pigeon (*Columba livia*). Baltimore, MD: The Johns Hopkins University Press.

Karten HJ, Hodos W, Nauta WJ, Revzin AM (1973) Neural connections of the "visual wulst" of the avian telencephalon. Experimental studies in the piegon (*Columba livia*) and owl (*Speotyto cunicularia*). J Comp Neurol 150:253–278.

Kaulen P, Brüning G, Rommelspacher H, Baumgarten HG (1986) Characterization and quantitative autoradiography of [3H]tryptamine binding sites in rat brain. Brain Res 366:72–88.

Keary N, Voss J, Lehmann K, Bischof HJ, Löwel S (2010) Optical imaging of retinotopic maps in a small songbird, the zebra finch. PLoS One 5(8):e11912.

Khawaja X (1995) Quantitative autoradiographic characterisation of the binding of [3H]WAY-100635, a selective 5-HT1A receptor antagonist. Brain Res 673:217–225.

Kia HK, Brisorgueil MJ, Hamon M, Calas A, Verge D (1996a) Ultrastructural localization of 5-hydroxytryptamine1A receptors in the rat brain. J Neurosci Res 46:697–708.

Kia HK, Miquel MC, Brisorgueil MJ, Daval G, Riad M, El Mestikawy S, Hamon M, Verge D (1996b) Immunocytochemical localization of serotonin1A receptors in the rat central nervous system. J Comp Neurol 365:289–305.

Kraemer M, Zilles K, Schleicher A, Gebhard R, Robbins TW, Everitt BJ, Divac I (1995) Quantitative receptor autoradiography of eight different transmitter-binding sites in the hippocampus of the common marmoset, *Callithrix jacchus*. Anat Embryol 191:213–225.

Krebs JR, Erichsen JT, Bingman VP (1991) The distribution of neurotransmitters and neurotransmitter-related enzymes in the dorsomedial telencephalon of the pigeon (*Columba livia*). J Comp Neurol 314:467–477.

Krützfeldt NO, Wild JM (2004) Definition and connections of the entopallium in the zebra finch (*Taeniopygia guttata*). J Comp Neurol 468:452–465.

Krützfeldt NO, Wild JM (2005) Definition and novel connections of the entopallium in the pigeon (*Columba livia*). J Comp Neurol 490:40–56.

Lüth HJ, Seidel I (1987) Immunohistochemical characterization of serotoninergic afferent pathways in the visual system of the rat. J Hirnforsch 28:591–600.

Maeda J, Suhara T, Ogawa M, Okauchi T, Kawabe K, Zhang MR, Semba J, Suzuki K (2001) *In vivo* binding properties of [carbonyl-11C]WAY-100635: effect of endogenous serotonin. Synapse 40:122–129.

Manns M, Freund N, Patzke N, Güntürkün O (2007) Organization of telencephalotectal projections in pigeons: impact for lateralized top-down control. Neuroscience 144:645–653.

Marcinkiewicz M, Vergé D, Gozlan H, Pichat L, Hamon M (1984) Autoradiographic evidence for the heterogeneity of 5-HT1 sites in the rat brain. Brain Res 291:159–163.

Medina L, Reiner A (2000) Do birds possess homologues of mammalian primary visual, somatosensory and motor cortices? Trends Neurosci 23:1–12.

Meneses A (1999) 5-HT system and cognition. Neurosci Biobehav Rev 23:1111–1125.

Meneses A, Perez-Garcia G (2007) 5-HT(1A) receptors and memory. Neurosci Biobehav Rev 31:705–727.

Merker B (1983) Silver staining of cell bodies by means of physical development. J Neurosci Methods 9:235–241.

Metzger M, Britto LR, Toledo CA (2006) Monoaminergic markers in the optic tectum of the domestic chick. Neuroscience 141:1747–1760.

Metzger M, Toledo C, Braun K (2002) Serotonergic innervation of the telencephalon in the domestic chick. Brain Res Bull 57:547–551.

Miceli D, Repérant J, Bertrand C, Rio JP (1999) Functional anatomy of the avian centrifugal visual system. Behav Brain Res 98:203–210.

Miceli D, Repérant J, Rio JP, Hains P, Medina M (2002) Serotonin immunoreactivity in the retinal projecting isthmo-optic nucleus and evidence of brainstem raphe connections in the pigeon. Brain Res 958:122–129.

Michelsen KA, Prickaerts J, Steinbusch HW (2008) The dorsal raphe nucleus and serotonin: implications for neuroplasticity linked to major depression and Alzheimer's disease. Prog Brain Res 172:233–264.

Müller CP, Carey RJ, Huston JP, De Souza Silva MA (2007) Serotonin and psychostimulant addiction: focus on 5-HT1A-receptors. Prog Neurobiol 81:133–178.

Ng BS, Grabska-Barwińska A, Güntürkün O, Jancke D (2010) Dominant vertical orientation processing without clustered maps: early visual brain dynamics imaged with voltage-sensitive dye in the pigeon visual Wulst. J Neurosci 30:6713–6725.

Palacios JM, Probst A, Cortes R (1983) The distribution of serotonin receptors in the human brain: high density of [3H]LSD binding sites in the raphe nuclei of the brainstem. Brain Res 274:150–155.

Palacios JM, Waeber C, Hoyer D, Mengod G (1990) Distribution of serotonin receptors. Ann N Y Acad Sci 600:36–52.

Palchaudhuri M, Flügge G (2005) 5-HT1A receptor expression in pyramidal neurons of cortical and limbic brain regions. Cell Tissue Res 321:159–172.

Palomero-Gallagher N, Bidmon HJ, Cremer M, Schleicher A, Kircheis G, Reifenberger G, Kostopoulos G, Häussinger D, Zilles K (2009) Neurotransmitter receptor imbalances in motor cortex and basal ganglia in hepatic encephalopathy. Cell Physiol Biochem 24:291–306.

Pazos A, Palacios JM (1985) Quantitative autoradiographic mapping of serotonin receptors in the rat brain. I. Serotonin-1 receptors. Brain Res 346:205–230.

Perez-Garcia G, Meneses A (2008) Memory formation, amnesia, improved memory and reversed amnesia: 5-HT role. Behav Brain Res 195:17–29.

Perez-Garcia G, Meneses A (2009) Memory time-course: mRNA 5-HT1A and 5-HT7 receptors. Behav Brain Res 202:102–113.

Polter AM, Li X (2010) 5-HT1A receptor-regulated signal transduction pathways in brain. Cell Signal 22:1406–1412.

Pompeiano M, Palacios JM, Mengod G (1992) Distribution and cellular localization of mRNA coding for 5-HT1A receptor in the rat brain: correlation with receptor binding. J Neurosci 12:440–453.

Raurich A, Mengod G, Artigas F, Cortés R (1999) Displacement of the binding of 5-HT(1A) receptor ligands to pre- and postsynaptic receptors by (−)pindolol. A comparative study in rodent, primate and human brain. Synapse 34:68–76.

Reiner A, Brecha NC, Karten HJ (1982) Basal ganglia pathways to the tectum: the afferent and efferent connections of the lateral spiriform nucleus of pigeon. J Comp Neurol 208:16–36.

Reiner A, Karten HJ (1982) Laminar distribution of the cells of origin of the descending tectofugal pathways in the pigeon (*Columba livia*). J Comp Neurol 204:165–187.

Reiner A, Perkel DJ, Bruce LL, Butler AB, Csillag A, Kuenzel W, Medina L, Paxinos G, Shimizu T, Striedter G, Wild M, Ball GF, Durand S, Güntürkün O, Lee DW, Mello CV, Powers A, White SA, Hough G, Kubikova L, Smulders TV, Wada K, Dugas-Ford J, Husband S, Yamamoto K, Yu J, Siang C, Jarvis ED (2004) Revised nomenclature for avian telencephalon and some related brainstem nuclei. J Comp Neurol 473:377–414.

Reiner A, Yamamoto K, Karten HJ (2005) Organization and evolution of the avian forebrain. Anat Rec A Discov Mol Cell Evol Biol 287:1080–1102.

Remington G (2008) Alterations of dopamine and serotonin transmission in schizophrenia. Prog Brain Res 172:117–140.

Remy M, Güntürkün O (1991) Retinal afferents to the tectum opticum and the nucleus opticus principalis thalami in the pigeon. J Comp Neurol 305:57–70.

Riad M, Garcia S, Watkins KC, Jodoin N, Doucet E, Langlois X, el Mestikawy S, Hamon M, Descarries L (2000) Somatodendritic localization of 5-HT1A and preterminal axonal localization of 5-HT1B serotonin receptors in adult rat brain. J Comp Neurol 417:181–194.

Rogers LJ, Deng C (1999) Light experience and lateralization of the two visual pathways in the chick. Behav Brain Res 98:277–287.

Saint-Dizier H, Constantin P, Davies DC, Leterrier C, Lévy F, Richard S (2009) Subdivisions of the arcopallium/posterior pallial amygdala complex are differentially involved in the control of fear behaviour in the Japanese quail. Brain Res Bull 79:288–295.

Sambeth A, Riedel WJ, Tillie DE, Blokland A, Postma A, Schmitt JA (2009) Memory impairments in humans after acute tryptophan depletion using a novel gelatin-based protein drink. J Psychopharmacol 23:56–64.

Schleicher A, Palomero-Gallagher N, Morosan P, Eickhoff SB, Kowalski T, de Vos K, Amunts K, Zilles K (2005) Quantitative architectural analysis: a new approach to cortical mapping. Anat Embryol (Berl) 210:373–386.

Schmidt A, Bischof HJ (2001) Integration of information from both eyes by single neurons of nucleus rotundus, ectostriatum and lateral neostriatum in the zebra finch (*Taeniopygia guttata* castanotis Gould). Brain Res 923:20–31.

Shimizu T, Bowers AN (1999) Visual circuits of the avian telencephalon: evolutionary implications. Behav Brain Res 98:183–191.

Shimizu T, Cox K, Karten HJ (1995) Intratelencephalic projections of the visual wulst in pigeons (*Columba livia*). J Comp Neurol 359:551–572.

Shimizu T, Karten HJ (1990) Immunohistochemical analysis of the visual wulst of the pigeon (*Columba livia*). J Comp Neurol 300:346–369.

Sitaraman D, Zars M, Laferriere H, Chen YC, Sable-Smith A, Kitamoto T, Rottinghaus GE, Zars T (2008) Serotonin is necessary for place memory in Drosophila. Proc Natl Acad Sci U S A 105:5579–5584.

Stokes TM, Leonard CM, Nottebohm F (1974) The telencephalon, diencephalon, and mesencephalon of the canary, *Serinus canaria*, in stereotaxic coordinates. J Comp Neurol 156:337–374.

Sumiyoshi T, Park S, Jayathilake K, Roy A, Ertugrul A, Meltzer HY (2007) Effect of buspirone, a serotonin1A partial agonist, on cognitive function in schizophrenia: a randomized, double-blind, placebo-controlled study. Schizophr Res 95:158–168.

Tejada S, Rial RV, Gamundí A, Esteban S (2011) Effects of serotonergic drugs on locomotor activity and vigilance states in ring doves. Behav Brain Res 216:238–246.

Terry AV Jr, Buccafusco JJ, Wilson C (2008) Cognitive dysfunction in neuropsychiatric disorders: selected serotonin receptor subtypes as therapeutic targets. Behav Brain Res 195:30–38.

Theiss MP, Hellmann B, Güntürkün O (2003) The architecture of an inhibitory sidepath within the avian tectofugal system. Neuroreport 14:879–882.

Topic B, Willuhn I, Palomero-Gallagher N, Zilles K, Huston JP, Hasenöhrl RU (2007) Impaired maze performance in aged rats is accompanied by increased density of NMDA, 5-HT1A, and alpha-adrenoceptor binding in hippocampus. Hippocampus 17:68–77.

Ueda S, Takeuchi Y, Sano Y (1983) Immunohistochemical demonstration of serotonin neurons in the central nervous system of the turtle (*Clemmys japonica*). Anat Embryol (Berl) 168:1–19.

Valencia-Alfonso CE, Verhaal J, Güntürkün O (2009) Ascending and descending mechanisms of visual lateralization in pigeons. Philos Trans R Soc Lond B Biol Sci 364:955–963.

van Wijngaarden I, Tulp MT, Soudijn W (1990) The concept of selectivity in 5-HT receptor research. Eur J Pharmacol 188:301–312.

Veenman CL, Wild JM, Reiner A (1995) Organization of the avian "corticostriatal" projection system: a retrograde and anterograde pathway tracing study in pigeons. J Comp Neurol 354:87–126.

Vergé D, Daval G, Marcinkiewicz M, Patey A, el Mestikawy S, Gozlan H, Hamon M (1986) Quantitative autoradiography of multiple 5-HT1 receptor subtypes in the brain of control or 5,7-dihydroxytryptamine-treated rats. J Neurosci 6:3474–3482.

Waeber C, Dietl MM, Hoyer D, Palacios JM (1989) 5.HT1 receptors in the vertebrate brain. Regional distribution examined by autoradiography. Naunyn Schmiedebergs Arch Pharmacol 340:486–494.

Wang Y, Brzozowska-Prechtl A, Karten HJ (2010) Laminar and columnar auditory cortex in avian brain. Proc Natl Acad Sci U S A 107:12676–12681.

Watanabe M, Ito H, Masai H (1983) Cytoarchitecture and visual receptive neurons in the Wulst of the Japanese quail (*Coturnix coturnix japonica*). J Comp Neurol 213:188–198.

Wild JM (1987) The avian somatosensory system: connections of regions of body representation in the forebrain of the pigeon. Brain Res 412:205–223.

Wild JM, Krützfeldt NO, Karten HJ (2010) Neocortical-like organization of avian auditory "cortex." Commentary on Wang Y, Brzozowska-Prechtl A, Karten HJ (2010): laminar and columnar auditory cortex in avian brain. Proc Natl Acad Sci USA 107:12676–12681. Brain Behav Evol 76:89–92.

Winsauer PJ, Bixler MA, Mele PC (1996) Comparison of the effects of typical and atypical anxiolytics on learning in monkeys and rats. J Pharmacol Exp Ther 276:1111–1127.

Wolff MC, Leander JD (2000) A comparison of the behavioural effects of 5-HT2A and 5-HT2C receptor agonists in the pigeon. Behav Pharmacol 11:355–364.

Wree A, Zilles K, Schleicher A, Horváth E, Traber J (1987) Effect of the 5-HT1A receptor agonist ipsapirone on the local cerebral glucose utilization of the rat hippocampus. Brain Res 436:283–290.

Yamada J, Kitamura N, Yamashita T (1985) The relative frequency and topographical distribution of somatostatin-, GRP-, APP$^-$, glucagon-, 5-HT-, and neurotensin-immunoreactive cells in the proventriculus of seven species of birds. Arch Histol Jpn 48:305–314.

Yilmazer-Hanke DM, Roskoden T, Zilles K, Schwegler H (2003) Anxiety-related behavior and densities of glutamate, GABAA, acetylcholine and serotonin receptors in the amygdala of seven inbred mouse strains. Behav Brain Res 145:145–159.

Zilles K (1989) Codistribution of transmitter receptors in the human and rat hippocampus. In: Hippocampus: new vistas (Chan-Palay V, Köhler C, eds), pp 171–187. New York, NY: AR Liss.

Zilles K, Palomero-Gallagher N, Grefkes C, Scheperjans F, Boy C, Amunts K, Schleicher A (2002b) Architectonics of the human cerebral cortex and transmitter receptor fingerprints: reconciling functional neuroanatomy and neurochemistry. Eur Neuropsychopharmacol 12:587–599.

Zilles K, Palomero-Gallagher N, Schleicher A (2004) Transmitter receptors and functional anatomy of the cerebral cortex. J Anat 205:417–432.

Zilles K, Schleicher A, Glaser T, Traber J, Rath M (1985) The ontogenetic development of serotonin (5-HT1) receptors in various cortical regions of the rat brain. Anat Embryol 172:255–264.

Zilles K, Schleicher A, Palomero-Gallagher N, Amunts K (2002a) Quantitative analysis of cyto- and receptor architecture of the human brain. Brain mapping: the methods, 2nd ed., Vol. 21, pp 573–602. San Diego, CA: Academic Press.

Zilles K, Wu J, Crusio WE, Schwegler H (2000) Water maze and radial maze learning and the density of binding sites of glutamate, GABA, and serotonin receptors in the hippocampus of inbred mouse strains. Hippocampus 10:213–225.

(Accepted 26 October 2011)
(Available online 03 November 2011)

RESEARCH ARTICLE

Cingulate Area 32 Homologies in Mouse, Rat, Macaque and Human: Cytoarchitecture and Receptor Architecture

Brent A. Vogt,[1,2,3]* Patrick R. Hof,[4] Karl Zilles,[3,5,6] Leslie J. Vogt,[1,2] Christina Herold,[7] and Nicola Palomero-Gallagher[2,3,5]

[1]Department of Anatomy and Neurobiology, Boston University School of Medicine, Boston, Massachusetts 02118
[2]Cingulum Neurosciences Institute, Manlius, New York 13104
[3]Institute of Neuroscience and Medicine (INM-1), Research Centre Jülich, 52425 Jülich, Germany
[4]Fishberg Department of Neuroscience and Friedman Brain Institute, Ichan School of Medicine at Mount Sinai, New York, New York 10029
[5]JARA-BRAIN, Jülich-Aachen Research Alliance, 52425 Jülich, Germany
[6]Department of Psychiatry, Psychotherapy and Psychosomatics, RWTH Aachen University, 52074 Aachen, Germany
[7]C. & O. Vogt Institute of Brain Research, Heinrich-Heine-University Düsseldorf, 40225 Düsseldorf, Germany

ABSTRACT

Homologizing between human and nonhuman area 32 has been impaired since Brodmann said he could not homologize with certainty human area 32 to a specific cortical domain in other species. Human area 32 has four divisions, however, and two can be structurally homologized to nonhuman species with cytoarchitecture and receptor architecture: pregenual (p32) and subgenual (s32) in human and macaque monkey and areas d32 and v32 in rat and mouse. Cytoarchitecture showed that areas d32/p32 have a dysgranular layer IV in all species and that areas v32/s32 have large and dense neurons in layer V, whereas a layer IV is not present in area v32. Areas v32/s32 have the largest neurons in layer Va. Features unique to humans include large layer IIIc pyramids in both divisions, sparse layer Vb in area p32, and elongated neurons in layer VI, with area s32 having the largest layer Va neurons. Receptor fingerprints of both subdivisions of area 32 differed between species in size and shape, although AMPA/$GABA_A$ and NMDA/$GABA_A$ ratios were comparable among humans, monkeys, and rats and were significantly lower than in mice. Layers I–III of primate and rodent area 32 subdivisions share more similarities in their receptor densities than layers IV–VI. Monkey and human subdivisions of area 32 are more similar to each other than to rat and mouse subdivisions. In combination with intracingulate connections, the location, cytoarchitecture, and ligand binding studies demonstrate critical homologies among the four species. J. Comp. Neurol. 521:4189–4204, 2013.

© 2013 Wiley Periodicals, Inc.

INDEXING TERMS: cortex; limbic system; neurotransmitter receptors; anterior cingulate cortex; rodent; primate

Human area 32 forms the external cingulate gyrus and is bounded by the cingulate sulcus and usually the paracingulate sulcus. Although Brodmann (1909) viewed this as a homogeneous area, von Economo and Koskinas (1925) proposed that it had four subdivisions in relation to adjacent prefrontal fields referring to them (from ventral to dorsal) as FHL, FEL, FDL, and FCL. These designations correlate with our findings of four area 32 divisions; subgenual s32 is comparable to FHL, pregenual p32 to FEL and part of FDL, dorsal d32 to dorsal FDL, and midcingulate 32′ includes FCL but extends farther caudally (Vogt et al., 1995; Palomero-Gallagher et al., 2008; Vogt, 2009). The Vogts (1919) identified nine subdivisions of area 32, with three in the position of area s32, two divisions of area p32, one for area d32, and three divisions of area 32′. The s32 and p32 divisions of human anterior cingulate cortex (ACC)

© 2013 Wiley Periodicals, Inc.

Grant sponsor: James S. McDonald Foundation; Grant number: 22002078-PRH; Grant sponsor: Initiative and Networking Fund of the Helmholtz Association within the Helmholtz Alliance on Systems Biology (to K.Z.).

*CORRESPONDENCE TO: Brent A. Vogt, Department of Anatomy and Neurobiology, Boston University School of Medicine, 75 E. Concord Street, Boston, MA 02118. E-mail: bavogt@bu.edu

Received March 19, 2013; Revised May 1, 2013;
Accepted June 18, 2013.
DOI 10.1002/cne.23409
Published online July 10, 2013 in Wiley Online Library (wileyonlinelibrary.com)

are the focus of this study, because it appears that they have counterparts in murid rodent brains (Vogt and Paxinos, 2012).

Areas s32 and p32 mediate different functions and are vulnerable to different diseases. Area s32 is involved in negative (sad) emotions (Phan et al., 2002; Vogt et al., 2003). In a functional imaging study, value-dependent changes for monetary reward or physical pain activate area s32 (but not area p32) when the task requires integration of different advantages (positive values) and disadvantages (negative values) into a subjective decision (Park et al., 2011). Activation of area s32 also is proportional to the degree of confidence with which retrieval occurs (Takashima et al., 2006). In contrast, area p32 has a role in positive emotions (happiness; Phan et al., 2002; Vogt et al., 2003) and is activated during tasks requiring explicit awareness of one's emotional state (Lane et al., 1997; Piefke et al., 2003) or decisions on the affective value of sensory experiences (Grabenhorst et al., 2008; Park et al., 2011). Area p32 also has a role in memory consolidation; it links neocortical areas that store remote memory and suppress irrelevant representations (Nieuwenhuis and Takashima, 2011).

In terms of disease vulnerabilities, the following differences have been noted in the rostral divisions of area 32. Areas s32 and p32 are activated during provocation of contamination obsessions in obsessive-compulsive disorder (Saxena et al., 2009). Impairment of area p32 function occurs in schizophrenia (Preda et al., 2009), posttraumatic stress disorder (Shin et al., 2009), and apathy in probable Alzheimer's disease (Salmon and Laureys, 2009). In view of the disease vulnerabilities of areas p32 and s32, it is imperative that homologues be established between experimental animals and humans as a prelude to precise modeling of disease mechanisms.

Determining homologues between humans and nonhuman species has been impacted for more than a century by Brodmann's (1909) view that area 32 in monkeys and nonprimates could not be homologized with certainty to that in human. He emphasized this view by designating area 32 in nonhuman species "prelimbic cortex" to differentiate it from human area 32. There is overwhelming evidence that human area 32 is not homogeneous, so the issue of homologies must be revisited. Also, if area 32 in monkey and nonprimate species is "prelimbic," then, by definition, it is not part of the "limbic" cortex. Brodmann's (1909) view cannot be sustained in the context of the connections and functions of area 32; it is involved in autonomic functions (for review see Vogt and Derbyshire, 2009), projects to brainstem autonomic nuclei (Gabbott et al., 2005), and responds during and stores emotional memories (Lane et al., 1997; Phan et al., 2002; Piefke et al., 2003; Grabenhorst et al., 2008; Park et al., 2011). Thus, area 32 fits current definitions of a limbic cortex, and Brodmann's cautious statement concerning homologies between area 32 in monkey and human must be critically tested. Indeed, human areas 32′ and d32 are not present in nonhuman primates or rodents, and it is these human areas that do not have homologues in nonhuman species. The question remains of homologies of the two parts of human area 32 (p32 and s32) among the mammalian species that are frequently employed in experimental research.

A recent study of cyto- and receptor architecture of areas s32 and p32 in macaque monkey and human brains demonstrated substantial similarities, leading to the conclusion that they are homologues (Palomero-Gallagher et al., 2013). Furthermore, cytoarchitecture in mice and rats shows that area 32 comprises two parts, areas v32 and d32 (Vogt and Paxinos, 2012). This latter study, however, used Nissl-stained sections that make subtle distinctions difficult such as the dysgranular nature of layer IV, and it did not employ receptor binding analyses, which provide important quantitative information to assess area 32 subdivisions as well as establishing homologies among species. Thus, the present study seeks to extend previous rodent work (Vogt and Paxinos, 2012) with neuron-specific nuclear binding protein (NeuN) immunohistochemistry and laminar receptor binding patterns for each area in mouse, rat, macaque monkey, and human brains to evaluate homologies in the two parts of area 32 in primates (p32 and s32) and rodents (d32 and v32).

MATERIALS AND METHODS

Postmortem tissues

A human brain was obtained from the Department of Pathology at Wake Forest University School of Medicine with a postmortem interval of 3 hours and 20 minutes and a weight of 1,360 g. This is case GPC, who was an 80-year-old, right-handed, white male who died from pneumonia and a retroperitoneal hemorrhage. There was no evidence of neurological or psychiatric disorders, and the brain had an unremarkable postmortem histology. Six further human cases (ages 76 $\pm$ 3 years; four male, two female; postmortem interval 13 $\pm$ 2 hours) were obtained for receptor autoradiography through the body donor program of the Department of Anatomy, University of Düsseldorf. An adult macaque monkey was obtained at the Wake Forest University School of Medicine for immunohistochemistry, and three adult macaques were obtained from Covance

Laboratories (Münster, Germany) for receptor autoradiography. Five adult male Wistar rats (292 ± 8.6 g) and eight adult Balb mice (28.4 ± 0.79 g; five males, three females) were processed at SUNY Upstate Medical University for immunohistochemistry. Finally, eight LEW/Ztm rats were obtained from the Central Animal Facility of the Hannover Medical School and eight C57BL/6J male mice from Cerj Laboratory (Le Genest, France) and were processed for receptor autoradiography. All experimental protocols were approved by the Committee for the Humane Use of Animals at Wake Forest University School of Medicine (Winston-Salem, NC), SUNY Upstate Medical University (Syracuse, NY), and the European local committees and complied with the European Communities Council Directive.

Immunohistochemistry

The human brain was postfixed in 4% paraformaldehyde for 3 days, cryoprotected with sucrose, and sectioned on a cryostat at 50 μm thickness. The monkey was anesthetized with a lethal dose of sodium pentobarbital and intracardially perfused with 400 ml cold saline, followed by 1 liter of 4% paraformaldehyde. After 3 days of postfixation, the brain was cryoprotected in sucrose, frozen in a cryostat, and sectioned at 40 μm thickness. Mice and rats were lethally anesthetized with sodium pentobarbital and intracardially perfused with 100 ml cold saline, followed by 100–300 ml of cold 4% paraformaldehyde. After 3 days postfixation, the brains were cryoprotected in sucrose, frozen in a cryostat, and sectioned at 30 μm thickness.

The NeuN antibody (Chemicon, Temecula, CA; I.D. MAB377) is mouse monoclonal antibody AB91665 at http://antibodyregistry.org/AB 2298770. Anti-NeuN reliably detects postmitotic neurons, and Kim et al. (2009) identified it as the Fox-3 gene product with mass spectrometry of anti-NeuN immunoreactive protein, recombinant Fox-3 recognition by anti-NeuN, short hairpin RNAs targeting Fox-3 mRNA that down-regulate NeuN expression, Fox-3 expression restricted to neural tissues, anti-Fox-3 immunostaining, and complete anti-NeuN immunostaining overlapping in neuronal nuclei. The sections were pretreated with 75% methanol/25% peroxidase, followed by 3 minutes with formic acid, and then washed with distilled water and two washes in phosphate-buffered saline (PBS; pH 7.4). Sections were incubated in primary antibody in PBS (Chemicon; 1:1,000, mouse antibody) containing 0.3% Triton X-100 and 0.5 mg/ml bovine serum albumin (BSA) overnight at 4°C. After incubation in the primary antibody, the sections were rinsed in PBS and incubated in biotinylated secondary antibody at 1:200 in PBS/Triton-X/BSA for 1 hour. After rinses in PBS, sections were incubated in ABC solution (1:4; Vector Laboratories, Burlingame, CA) in PBS/Triton-X/BSA for 1 hour followed by PBS rinses and incubation in 0.05% 3.3′-diaminobenzidine and 0.01% H_2O_2 in a 1:10 dilution of PBS for 5 minutes. After final rinses in PBS, sections were mounted and counterstained with thionin.

For this comparison, we selected one case from each species, and the cytoarchitectural centroids of areas d32 and v32 in rodents and areas p32 and s32 in primates were selected for photography. The centroid was identified as the approximate center in all planes for an area and does not consider cytoarchitectural gradients that occur where two or more areas merge. These digital photographs were then entered into Photoshop CS2 and coregistered along the dorsal border of layer Va. Occasional artifacts were removed, and the contrast was enhanced in all images to reduce nonspecific neuropil staining in relation to that of individual neurons. The flat maps shown in Figure 1 were derived from previous publications for the human (Vogt, 2009), macaque monkey (Vogt et al., 2005), and rat and mouse (Vogt and Paxinos, 2012).

Receptor autoradiography

Human brains were bisected at autopsy, and each hemisphere was cut into slabs (2–3 cm thick) and frozen in isopentane at −40°C. Monkeys were killed by means of a lethal intravenous injection of sodium pentobarbital, brains immediately removed from the skull, and hemispheres frozen in isopentane at −40°C. Rats and mice were decapitated, and brains were removed from the skull and frozen in isopentane at −40°C. Unfixed frozen tissue was stored at −80°C until sectioning. Serial coronal cryosections (20 μm for human tissue, 10 μm for the other species) comprising the whole cross-section of a hemisphere were prepared using a large-scale cryostat microtome (human) or a cryostat (other species). Adjacent glass-mounted sections were processed for quantitative in vitro receptor autoradiography according to previously described protocols to label receptors for glutamate (AMPA, kainate, NMDA) and GABA ($GABA_A$, $GABA_B$, $GABA_A$-associated benzodiazepine (BZ) binding sites; Table 1; Palomero-Gallagher et al., 2008; Zilles et al., 2002), or stained with a modified silver method that produces Nissl-like images (Merker, 1983; Palomero-Gallagher et al., 2008). Binding assays consisted of a preincubation to remove endogenous ligand from the tissue, a main incubation with a tritiated ligand (total binding) or the tritiated ligand and an appropriate nonlabeled displacer (nonspecific binding), and a washing step to eliminate unbound radioactive ligand.

Radioactively labeled sections were coexposed with standards of known radioactivity concentrations against

TABLE 1.
Summary of Incubation Conditions for In Vitro Receptor Autoradiography

Receptor	[3H] ligand	Displacer	Incubation buffer	Preincubation	Main incubation	Rinsing
AMPA	AMPA (10 nM)	Quisqualate (10 μM)	50 mM Tris-acetate (pH 7.2) + 100 mM KSCN (M)[1]	3 × 10 Min at 4°C	45 Min at 4°C	4 × 4 Sec at 4°C; 2 × 2 sec fixation[2] at 4°C
Kainate	Kainate (8 nM)	Kainate (100 μM)	50 mM Tris-citrate (pH 7.1) + 10 mM Ca-acetate (M)	3 × 10 Min at 4°C	45 Min at 4°C	4 × 4 Sec at 4°C; 2 × 2 sec fixation[2] at 4°C
MDA	MK-80 (5 nM)	(+)MK-80 (100 μM)	50 mM Tris-HCl (pH7.2) + 30 μM glycine (M) + 50 μM spermidine (M)	15 Min at 22°C	60 Min at 22°C	2 × 5 Min at 4°C
$GABA_A$	Muscimol (3 nM/6 nM)[3]	GABA (10 μM)	50 mM Tris-citrate (pH 7.0)	3 × 5 Min at 4°C	40 Min at 4°C	3 × 3 Sec at 4°C
$GABA_B$	CGP 5462 (1.5 nM)	CGP 5584 (100 μM)	50 mM Tris-HCl (pH 7.2) + 2.5 mM $CaCl_2$	3 × 5 Min at 4°C	60 Min at 4°C	3 × 2 Sec at 4°C
BZ	Flumazenil (0.8 nM)	Clonazepam (2 μM)	170 mM Tris-HCl (pH 7.4)	15 Min at 4°C	60 Min at 4°C	2 × 1 Min at 4°C

[1](M): Substances added to buffer only during the main incubation.
[2]Fixation in a 100 ml/2.5 ml acetone/glutaraldehyde solution.
[3]Human and monkey sections were incubated with 3 nM of [3H]muscimol, rodents with 6 nM; BZ, $GABA_A$ associated benzodiazepine binding sites.

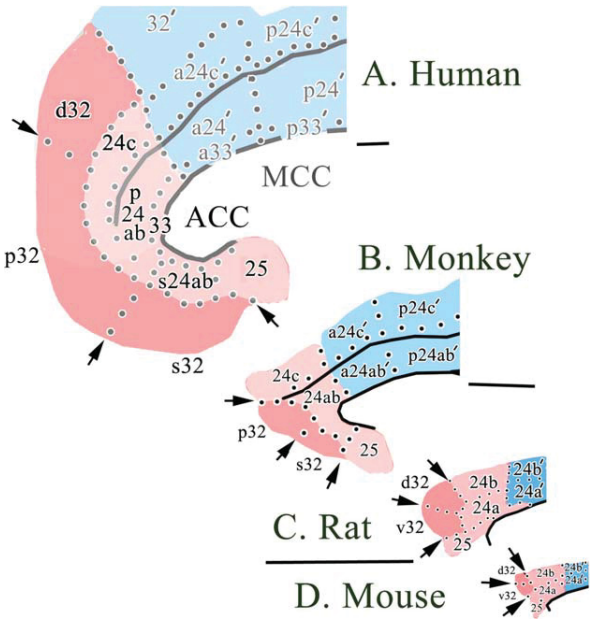

Figure 1. **A–D:** Flat maps of the medial surfaces with anterior cingulate cortex (ACC) and midcingulate cortex (MCC) color-coded for four species. The primate brains have a black line at the apex of the cingulate gyrus and one along the callosal sulcus. Arrows emphasize the areas considered in this analysis, including areas p32 and s32 for primates and areas d32 and v32 for rodents. Scale bars = 1 cm.

tritium-sensitive films for 4–18 weeks. The ensuing autoradiographs were processed densitometrically (Zilles et al., 2002). Cortical areas were anatomically identified on adjacent Nissl-stained sections, and the mean of the gray values contained in a specific area over a series of four or five sections per receptor and animal was thus transformed into a receptor concentration per unit protein (fmol/mg protein; Zilles et al. 2002). Receptor densities were extracted from linearly equidistant intensity profiles oriented vertically to the cortical surface. The area below a profile quantifies the mean areal density. Densities from layers I–III, IV and V–VI were extracted from profiles by computing the surface of discrete segments defined by the borders between layers.

Multivariate ANOVAs were applied to reveal putative, general differences in receptor densities between human and macaque monkey areas s32 and p32 as well as between rat and mouse areas d32 and v32. MANOVAs were followed by post hoc tests (paired *t*-tests) to determine which of the examined receptor types contributed to the significant difference. Multivariate ANOVAs were also applied to reveal putative, general interspecies differences in the AMPA/$GABA_A$ and NMDA/$GABA_A$ ratios for both area 32 divisions. Post

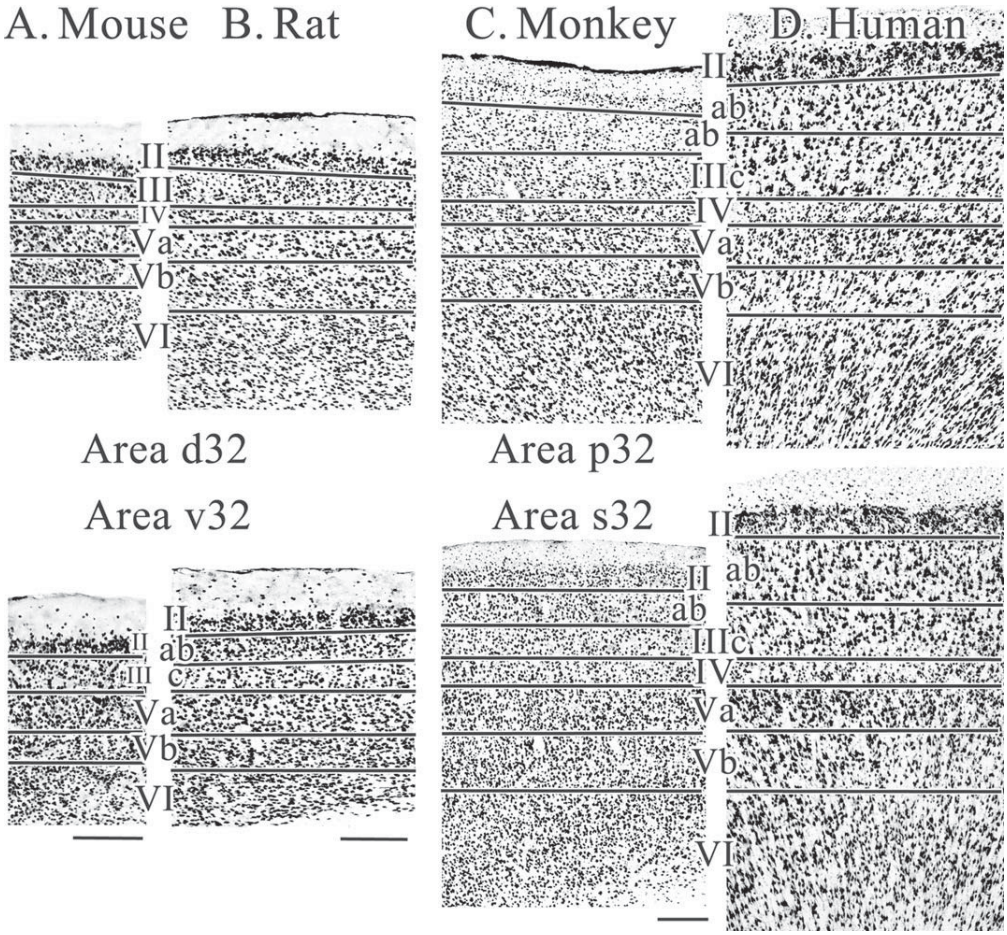

Figure 2. **A–D:** Low-magnification photographs through two area 32 divisions of four species and aligned to the top of layer Va. The key similarity in areas d32/p32 is the presence of a dysgranular layer IV. Rodent area v32 does not have a layer IV, whereas area s32 in primates does. A common feature for areas v32/s32 is the very dense layer V, with particularly large neurons. Scale bars = 250 μm.

hoc tests (*t*-tests) were then carried out to determine which species differed significantly. Significance levels for all tests were set at $P < 0.01$. Additionally, canonical (discriminant) analyses were performed with the mean areal densities or the densities extracted from layers I–III, IV, or V–VI to visualize the degree of (dis)-similarity among the four species. A hierarchical cluster analysis was conducted as previously described (Palomero-Gallagher et al., 2009) to detect putative groupings of species according to the degree of similarity of receptor architecture. Each species was represented by a matrix with four rows (two areas, each with densities extracted from superficial and deep layers) and six columns (receptors). Hierarchical clustering requires that each species be represented by a one-dimensional feature vector, so it was necessary to reduce the data. Thus, for each species, densities of a given receptor type in the set of four rows of that species were treated as a feature vector, and the Euclidean distances between all possible combinations of receptors were calculated, resulting in a new feature vector with 15 elements.

RESULTS

Cytoarchitecture

Flat maps of the divisions of ACC in Figure 1 are a schematic distillation of detailed analyses of the topography, sulcal patterns, and cytoarchitecture for the human (Vogt et al., 1995; Palomero-Gallagher et al., 2008; Vogt, 2009), macaque monkey (Vogt et al., 2005), mouse and rat (Vogt and Paxinos, 2012). Figures 2 and 3 present centroids from NeuN-immunostained sections through each part of area 32 of the four species, with the magnifications balanced slightly to enhance observation of comparative laminar similarities and differences. Figure 3 is at a higher magnification than Figure 2, showing the midcortical layers such that the structure

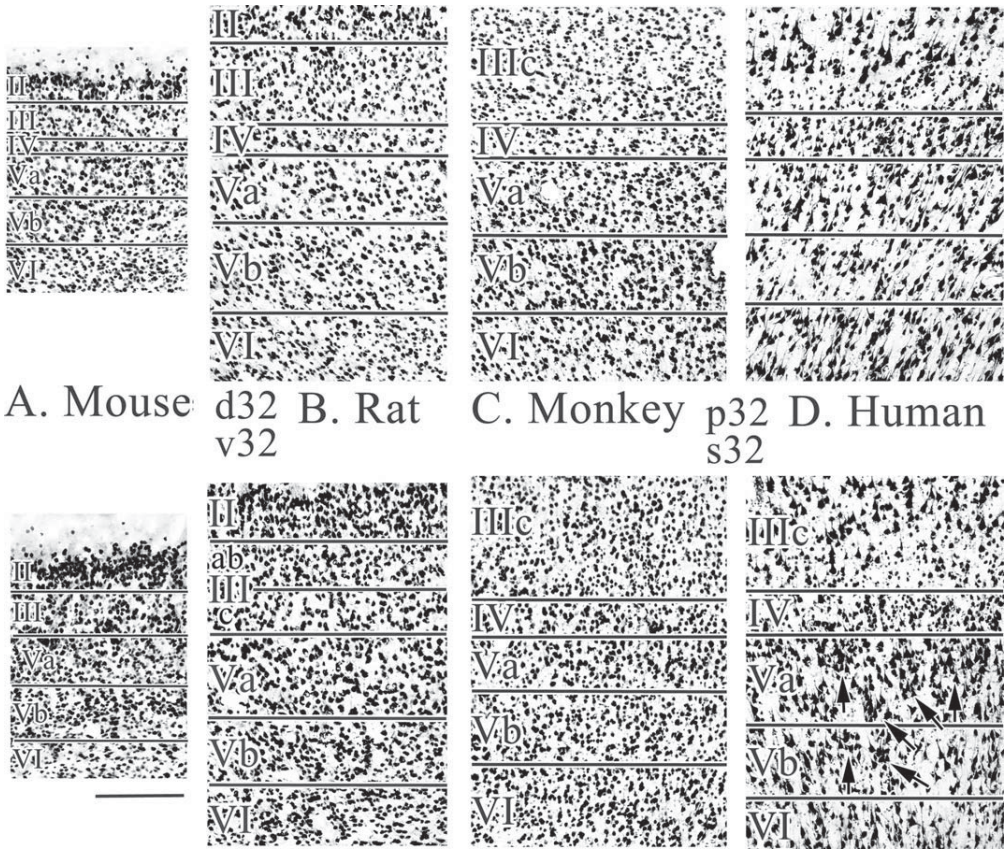

Figure 3. **A–D:** Photographs of each area 32 division through the midcortical layers at the same magnification. The sections are aligned to the top of layer Va. The arrows on human area s32 refer to clusters of neurons in layer V. Scale bar = 250 μm.

and density of neurons are more clearly appreciated. It has long been recognized that area 32 in primates has a dysgranular layer IV, and these figures also show that layer IV is present in mouse and rat area d32 but not in area v32 of either rodent. The progressive thickening of layer IV and size of neurons therein is apparent if one places mouse area d32 at one end of the spectrum and human area p32 at the other (without implying a scala naturae progression among these species). Layer III of area d32 in both rodents was not differentiated, although the rat has two divisions of layer III in area v32. Both subdivisions of area 32 in both primates had a two-part layer III. As previously noted for human (Vogt, 2009), layer IIIc neurons in area p32 are larger than those in layer IIIab, and this relationship is reversed in area s32 of both primates and the rat area v32, in which a division of layer III is notable.

Neuron densities in layers Va and Vb are particularly high in mouse area d32 and monkey area p32 and of equal densities, whereas in rat area d32 they have a higher density in layer Vb, and human area p32 densities are sparse in layer Vb. In the ventral rodent areas, layers Va and Vb both have relatively large neurons and are similarly packed, although the mouse has slightly smaller neurons in the deep part of layer Va, and packing in the rat is slightly less dense. In other words, layer V subdivisions in rodents are possible but subtle. For both primates, the relative sizes shift, with larger ones in layer Va, where neurons are also denser. Additionally, neurons in layer Va in humans form clusters (four are marked with arrows in layer Va and two in layer Vb). Similar relationships hold for layer Vb in rodents and primate areas v32 and s32, respectively, although neuron clustering appears only in the human brain. Finally, layer VI of humans is unique in both divisions of area 32, in that the neurons are generally elongated and aggregate into clusters in a cytoarchitectural feature not present in the other species (Fig. 2).

In summary, all species have a dysgranular layer IV in area d32 or p32, and areas v32 and s32 have large and dense neurons in layers Va and Vb. Features unique to rodents or primates include the following: rodent area d32 has no layer III divisions, whereas in primates there are layers IIIab and IIIc; areas v32 and

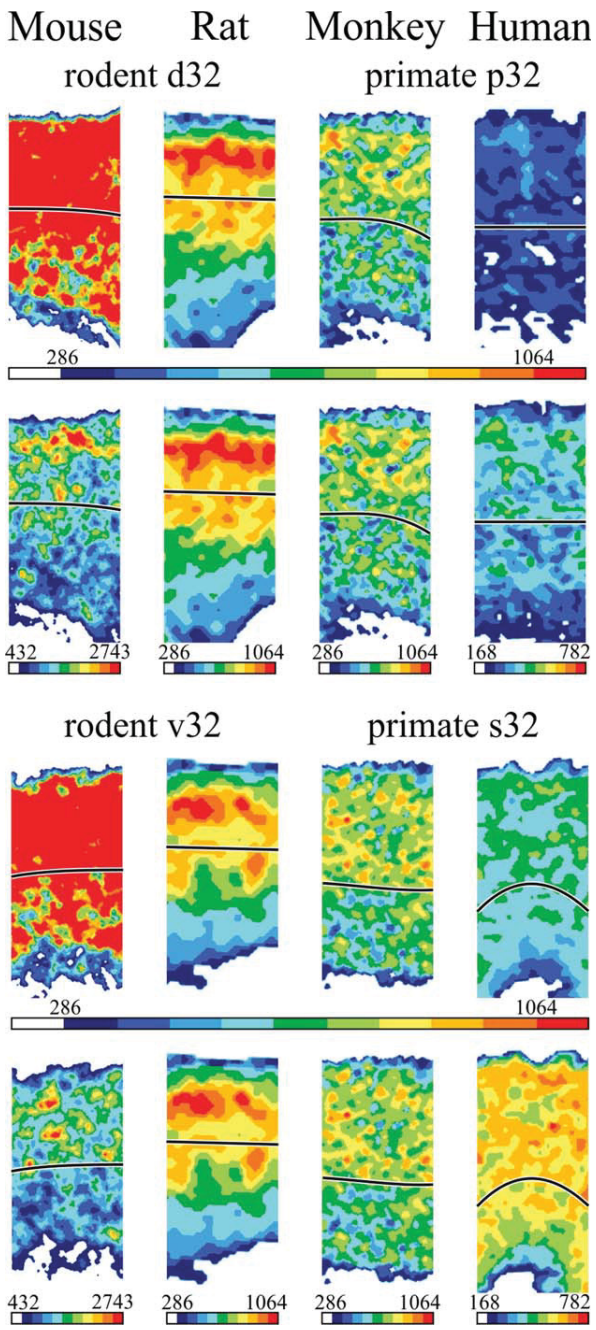

Figure 4. Color-coded autoradiographs of AMPA receptor density throughout the layers of primate areas p32 and s32 and rodent areas d32 and v32. Autoradiographs in the top row were contrast enhanced such that the scaling of absolute densities is the same for areas d32 and p32 of all species. Color-coded autoradiographs in the row below were differentially scaled to optimize the differences in receptor densities between superficial and deep layers. The different scaling is indicated by the bars, which code for densities in fmol/mg protein. Autoradiographs in the third and fourth rows show the AMPA receptor distribution in areas v32 and s32 in the same way as described above. Magnification was chosen to allow alignment of the pial surface and the layer VI/white matter border in all species, and the top of layer Va is delineated on each autoradiograph.

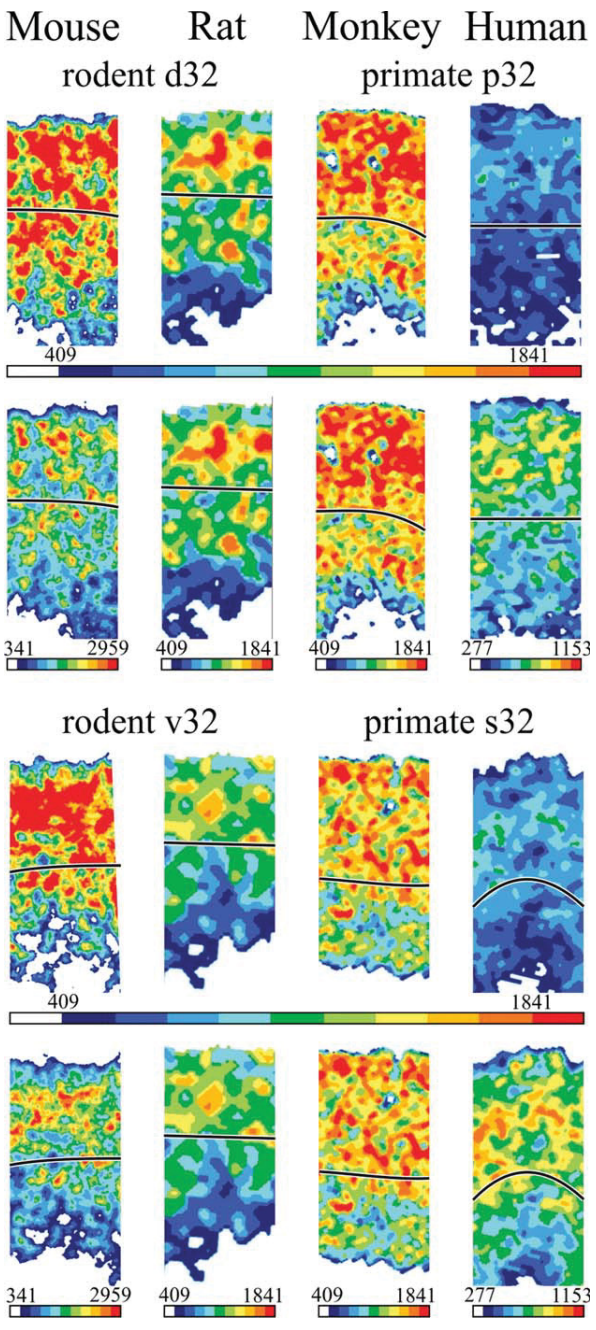

Figure 5. Color-coded autoradiographs of NMDA receptor density distribution throughout the cortical layers of primate p32 and s32 and rodent d32 and v32. For further information see Figure 4.

s32 have the relatively largest neurons in layer Va; rodent area d32 has a dysgranular layer IV, whereas area v32 in rodents does not; and area v32/s32 neuron sizes and densities are quite similar for layers Va and Vb. Features unique to human include large layer IIIc pyramids, sparse layer Vb, and elongated neurons in layer VI, and area s32 has the largest layer Va neurons that form clusters.

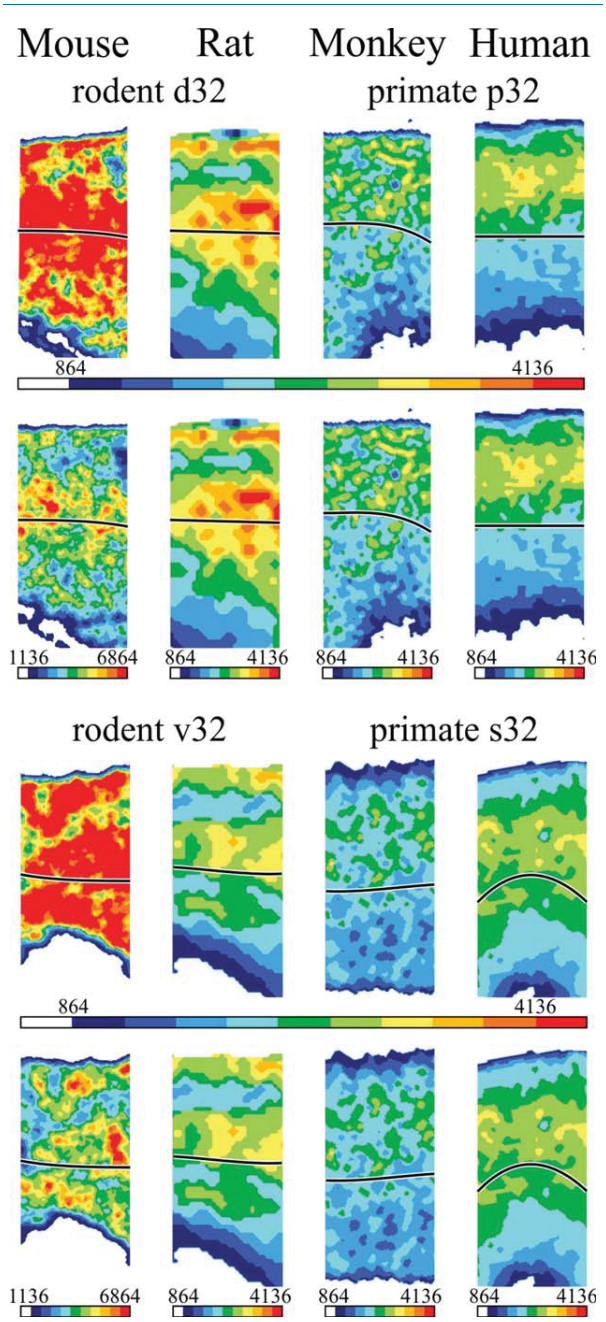

Figure 6. Color-coded autoradiographs of benzodiazepine binding site distribution throughout the cortical layers of primate p32 and s32 and rodent d32 and v32. For further information see Figure 4.

Receptor autoradiography

Six different receptor binding sites (AMPA, NMDA, kainate, $GABA_A$, $GABA_A$-associated BZ binding sites, and $GABA_B$) were studied in both subdivisions of rodent and primate area 32. As an example, the laminar distributions of AMPA, NMDA, and BZ binding sites are shown in Figures 4–6. The AMPA receptor density averaged over all cortical layers and separately for superficial and deep layers decreases with brain size (Fig. 4). In contrast to the interspecies variation in AMPA receptor densities, the NMDA receptors do not scale with brain size (Fig. 5). The NMDA receptor densities of mouse areas d32 and v32 are comparable to those of monkey areas p32 and s32, whereas rat cingulate areas have lower densities than the mouse and the human lower than the monkey (Fig. 5). The BZ binding sites of the $GABA_A$ receptor decrease in both areas d32 and v32 of rodents and p32 of monkey with brain size but increase in the superficial layers of human p32 and s32 (Fig. 6). In all species, these three receptors seem to be more densely expressed in the superficial compared with deep layers, with the notable exception of mouse area v32, where BZ binding site densities are nearly the same in superficial and deep layers.

The absolute receptor densities (fmol/mg protein) averaged over all cortical layers are depicted as receptor fingerprints in Figure 7. Here, rodent area d32 is contrasted with v32 and primate area p32 with s32. Mouse areas d32 and v32 do not differ in any of the examined receptor types (Fig. 7A). Rat areas d32 and v32 differed significantly only in their mean BZ binding site densities, which were higher in the former area (Fig. 7B). Monkey area p32 contained significantly higher NMDA but lower BZ binding site densities than did area s32 (Fig. 7C). Human areas p32 and s32 differed significantly in their AMPA, kainate, $GABA_A$, and BZ binding site densities, which were always higher in area s32 than in area p32 (Fig. 7D).

Figure 8 shows the fingerprints (fmol/mg protein) for superficial and deep layers in rodent area d32 and primate p32. Receptor densities in primate area p32 and rodent d32 tend to be more densely packed in superficial than in deep layers, with the exception of kainate receptors, which are present in higher densities in the deep layers of monkey and mouse brains (Fig. 8). However, only in mouse area d32 do kainate receptors reach significantly higher densities in the deep layers (Fig. 6A). Further significant differences between superficial and deep layers of rodent area d32 and primate p32 are demonstrated in Figure 8.

Figure 9 shows the superficial to deep layer gradients in rodent area v32 and primate s32. Again, in most cases, superficial layers show higher receptor densities than do deep layers, but only in the mouse NMDA and $GABA_A$ do receptor densities reach significant levels. Kainate receptors are more densely expressed in the deep layers and reach significance in rat area v32 and primate s32.

The search for homologies led us to evaluate the hypothesis that it is the relative proportions between excitatory and inhibitory receptors that are critical. The AMPA/$GABA_A$ and NMDA/$GABA_A$ ratios in mouse areas

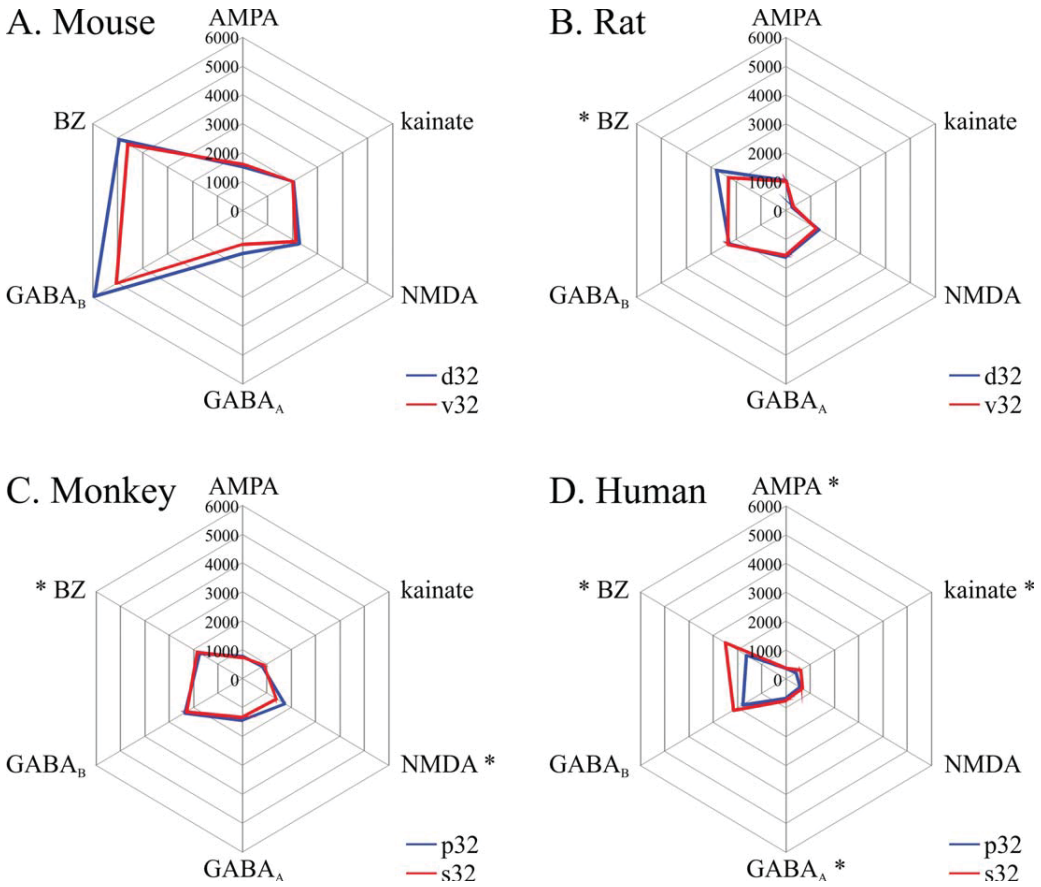

Figure 7. **A–D:** Receptor fingerprints of each area 32 subdivision. The axis codes for receptor densities in fmol/mg protein, and the same scale has been used for all plots to facilitate interspecies comparisons. Asterisks indicate significant differences ($P < 0.01$) in receptor densities between areas d32 and v32 or between areas p32 and s32; BZ, $GABA_A$-associated benzodiazepine binding sites.

d32 and v32 were significantly higher than those of their counterparts in the other three species (Fig. 10). Additionally, the NMDA/$GABA_A$ ratio in monkey area s32 was significantly higher than that of human area s32 or rat v32 (Fig. 10B).

Discriminant analyses were carried out to assess the degree of (dis)similarity of the receptor fingerprints of each area 32 division for all layers together (Fig. 11A) and separately for layers I–III (Fig. 11B), layer IV (Fig. 11C), and layers V–VI (Fig. 11D). If receptor densities are averaged over all cortical layers (Fig. 11A), it is apparent that monkey and human multireceptor fingerprints are more similar to each other than either rat or mouse, and the latter two species diverge substantially from each other. This relationship can be described by the hierarchical cluster analysis (Fig. 12), in which monkey and human contrast to rat and mouse fingerprints. The laminar discriminant analyses for the different cortical layers show the most obvious interspecies difference in layer IV, whereas layers I–III present the least interspecies divergence.

DISCUSSION

Cortical homologies among rodent areas d32/v32 and primate areas p32/s32 have been defined systematically in four ways: 1) relative location as the most rostral part of cingulate cortex in relation to landmarks (corpus callosum and callosal sulcus), rostral to midcingulate cortex (MCC), and dorsal to area 25; 2) similarities in cytoarchitecture, with a dysgranular layer IV in rodent area d32 and primate p32 and particularly large neurons in layer V of areas v32 and s32; 3) similarities of ligand binding for all receptors analyzed, with preferential binding in superficial vs. deep layers; and 4) intracingulate connection similarities, considered below.

With the present findings, we have resolved Brodmann's comparative paradox of area 32; his area 32 is not a homogeneous area but comprises areas p32/s32 in human and monkey and areas d32/v32 in rodents. The human areas d32 and 32′ have no equivalent in or homology with nonhuman primates. Although we have known this to be generally true (Vogt et al., 2005; Vogt,

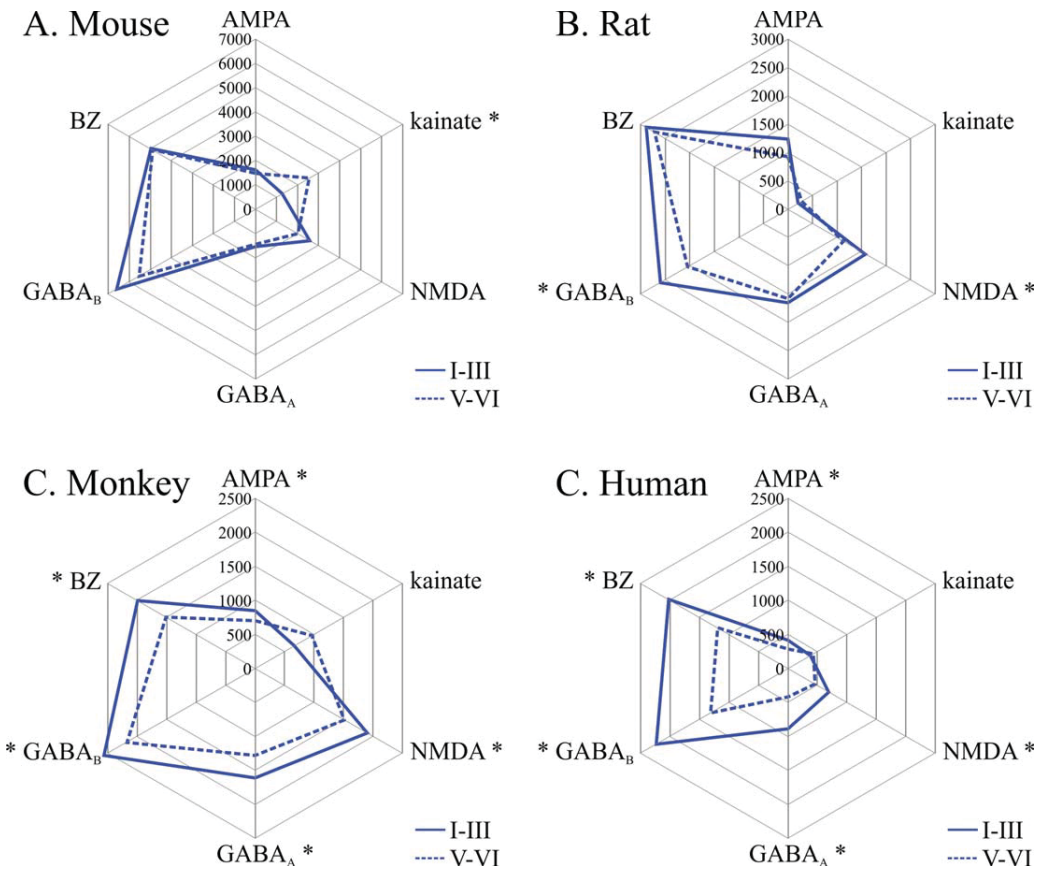

Figure 8. **A–D:** Receptor densities in the superficial (I–III) and deep (V–VI) layers of areas d32 (mouse and rat) and p32 (monkey and human). The axis codes for receptor densities in fmol/mg protein. Note that the scale has been set in such a way that differences in receptor densities of superficial and deep layers are displayed optimally within a given species. Asterisks indicate significant differences ($P < 0.01$) in receptor densities between superficial (I–III) and deep (V–VI) layers; BZ, $GABA_A$-associated benzodiazepine binding sites.

2009), it is now possible to state such a conclusion with more certainty in light of the exact comparisons of the other two components in mouse, rat, and macaque.

The cytoarchitecture of areas p32/d32 reflects differentiated neocortical structures, with the dysgranular layer IV progressively increasing in thickness from mouse to rat to monkey and human. Figure 3 emphasizes that neuron densities throughout midcortical layers are higher in mouse and monkey than in rat and human, and this is particularly notable in both divisions of layer V. However, human area p32 stands out in many ways from the other species; layers IIIc and V have large and dispersed pyramids generally associated with elaboration of the basal dendritic trees, and layer IV has many small neurons but also occasional clumps of larger neurons, as is characteristic of dysgranular cortex. These differences emphasize that, although each of the examined species have homologues in areas d32/p32, there are many differences as well, particularly in the human brain. The ventral and subgenual areas have significantly less laminar differentiation than the dorsal/pregenual areas and the most prominent and common feature among species is the very large and dense neurons in both parts of layer V (Fig. 3). Not all features are common; the rodents do not have a layer IV, which is present in primates, and, once again, the human has unique features, including very large pyramids in layers IIIc and V, the latter of which shows substantial clustering, and relatively more neuropil.

Densities of GABA receptors were higher than those of glutamate receptors in all species and areas, as has been reported for numerous other human and rat cortical areas (Zilles et al., 2002; Palomero-Gallagher and Zilles, 2004; Palomero-Gallagher et al., 2009; Amunts et al., 2010). Thus, the mammalian cortex appears to be subject to a strong inhibitory modulation by GABAergic neurons, and this may represent an evolutionarily conservative feature across rodents and primates. There is a trend toward higher AMPA receptor densities

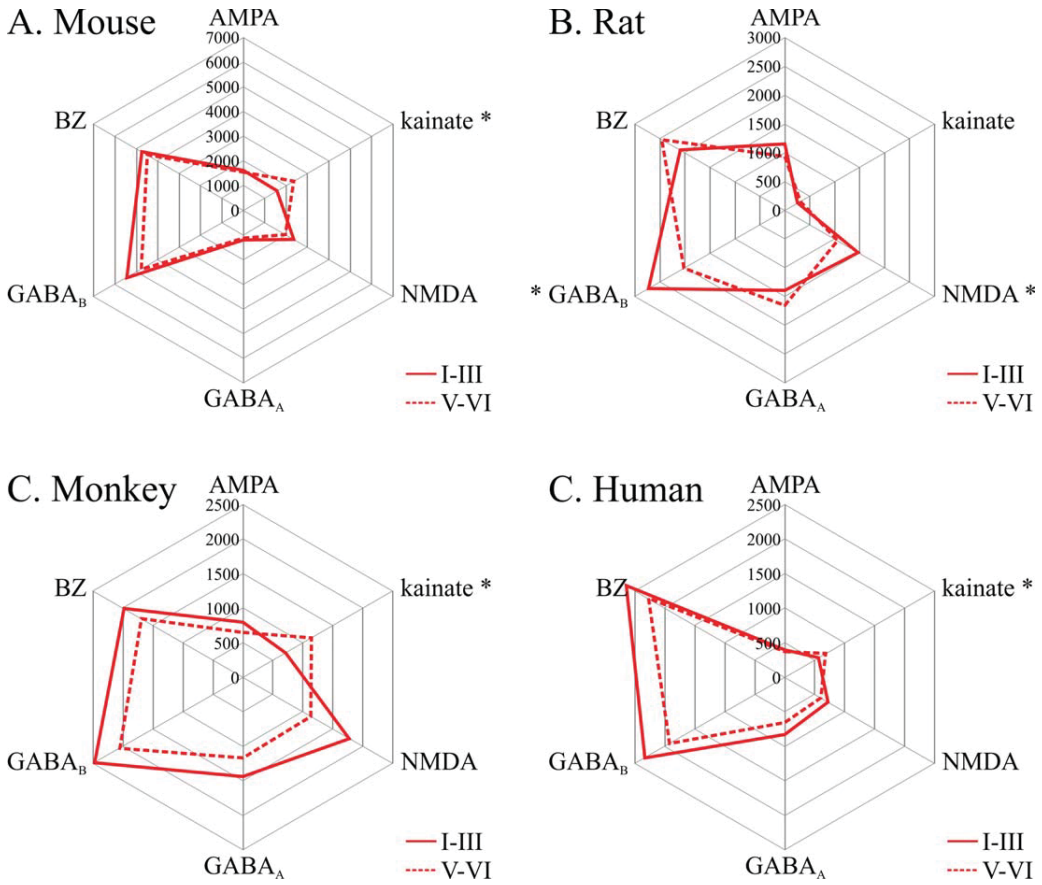

Figure 9. **A–D:** Receptor densities in the superficial (I–III) and deep (V–VI) layers of areas v32 (mouse and rat) and s32 (monkey and human). The axis codes for receptor densities in fmol/mg protein. Same scale as in Figure 5. Asterisks indicate significant differences ($P < 0.01$) in receptor densities between superficial (I–III) and deep (V–VI) layers; BZ: $GABA_A$-associated benzodiazepine binding sites.

in small brains compared with larger brains. This cannot be explained as an overproportional increase in connectivity, which would lead to more afferent and efferent fibers in all cortical layers of larger brained species, because the NMDA receptors of monkeys are more densely packed than in humans and rats, and the BZ binding sites are more densely packed in humans than in monkeys. Therefore, the differential expression of receptors between species probably reflects species-specific local differentiations in the various cortical areas and layers.

Receptor fingerprints of both subdivisions of area 32 differed between species in size and shape, supporting the notion of a species-specific pattern of multiple receptor expression, which may indicate different balances between the major excitatory and inhibitory receptors in the cingulate cortex. Indeed, AMPA/$GABA_A$ and NMDA/$GABA_A$ ratios were similar in human, monkey, and rat and differed considerably from those found in the mouse. The discriminant analyses further emphasize not only the exceptional position of receptor expression pattern in the mouse brain but also the fact that monkey and human divisions of area 32 are more similar to each other than to those of rats. Interestingly, much of the divergence among monkey, human, and rat brains disappears when binding is plotted separately for layers I–III, IV or V–VI, and this is particularly true when the discriminant analysis was carried out using only the superfical layer densities. Thus, homologies in receptor architecture are stronger in superficial than in deep layers. The examined receptors provide a substrate for homologizing human and monkey divisions of area 32 but also emphasize the differences between rodents and primates.

Most differences in receptors were found when comparing human area p32 with its counterpart in monkey, rat, and mouse brains. Human area s32 shares more similarities with monkey areas s32 and p32 than with human area p32 (Palomero-Gallagher et al., 2013). This may indicate a divergent differentiation of areas s32 and p32 between human and monkey brains at the receptor level. The cytoarchitecture of these areas in

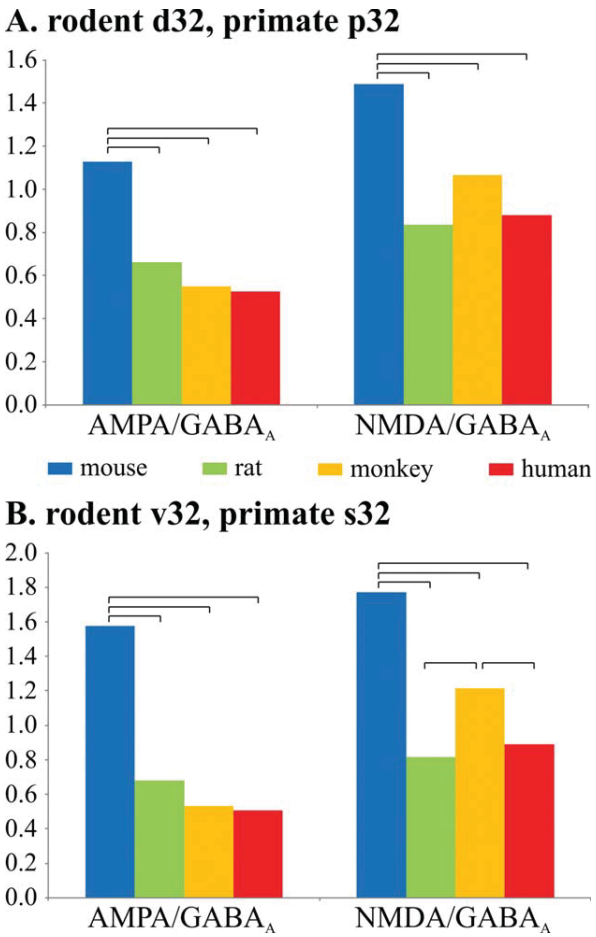

Figure 10. **A,B:** Ratios between AMPA and $GABA_A$ or NMDA and $GABA_A$ receptor densities in both area 32 divisions of human, monkey, rat, and mouse brains. Brackets indicate significant differences ($P < 0.01$).

humans and monkeys suggests the homologies indicated by the same areal designations, but further studies are necessary to understand the difference in receptor expression between human areas s32 and p32 in comparison with the monkey.

The overall pattern of cingulate cortex expansion in the four species studied here is shown in Figure 13A as a prelude to considering connections. This is a schematic drawing of each cingulate cortex based on the relative surface areas shown in Figure 1. The mouse is the smallest black oval, and surrounding ovals represent the rat, macaque, and human cingulate cortices. Each species has two parts of ACC area 32, and the arrows extend from the mouse to human brains showing this. Because the mouse and rat have but one division of MCC, this arrow stops at the monkey oval, where it splits into anterior and posterior divisions of MCC. The mouse has a retrosplenial cortex, as do all other species, so the arrow originating from the mouse retrosplenial cortex extends through all species. Finally, only the human cingulate cortex has areas d32 and 32′ (Vogt, 2009), and these are unique to humans at the apex of the cingulate expansion. The search for connection homologies must be made in the context of the extensive expansion of cingulate cortex among these species. For example, to the extent that rodents do not have areas such as dorsal and ventral posterior cingulate cortex, connections in primates cannot be assessed for these areas in rodents. The primate brain has many areas not present in rodents, including anterior cingulate area 24c, midcingulate area 24c′, a two-part MCC, and posterior cingulate areas 23 and 31.

There is one key connection similarity among these species, their intracingulate connections. Intracingulate projections of monkey area p32 terminate mainly in areas 25 and 24a–c (Pandya et al., 1981; Fig. 13B). In the rat, the connections project mainly to areas 24a,b and less to MCC areas 24a′b′ (Jones et al., 2005). The monkey retrosplenial area 30 projects to anterior cingulate area 24a but not area 32 (Morris et al., 1999), and this lack of an interaction between areas 32 and 29 is also true for the rat (van Groen and Wyss, 2003; Jones et al., 2005). In contrast, areas s32/s24a project throughout ACC and to area 23b (Vogt and Pandya, 1987; Fig. 13B). The rat and mouse do not have an area 23, so the latter connection does not exist in either species. In terms of MCC, aMCC projections in monkey terminate throughout ACC (areas p32, s32, 24, and 25; Pandya et al., 1981; Arikuni et al., 1994), whereas the one division of rat MCC projects to area 24 but not to area 32 (Jones et al., 2005). Thus, given the constraints of cytoarchitectural organization, there is a core similarity in local ACC connections of area 32 in rodents and primates.

The corticospinal system in rat is unique compared with that of the primates, in that the former originates from areas d32 and 24b and is a limbic corticospinal system. Nudo and Masterton (1990) reported a patch of retrogradely labeled neurons following cervical spinal horseradish peroxidase injections in area M2 and area 24b that is not observed in either of these areas in primates. The reason for designating this as a "limbic" system is that it directly mediates autonomic functions; i.e., a key feature of limbic areas and neurons. Area 32 projects prominently to the central autonomic area of the thoracic spinal cord, where axon terminals form asymmetric (excitatory) synapses (Bacon and Smith, 1993). This projection may also be involved in ultrasonic vocalization (Neafsey et al., 1993). Another feature that differentiates limbic corticospinal neurons is their robust innervation by the basolateral nucleus of

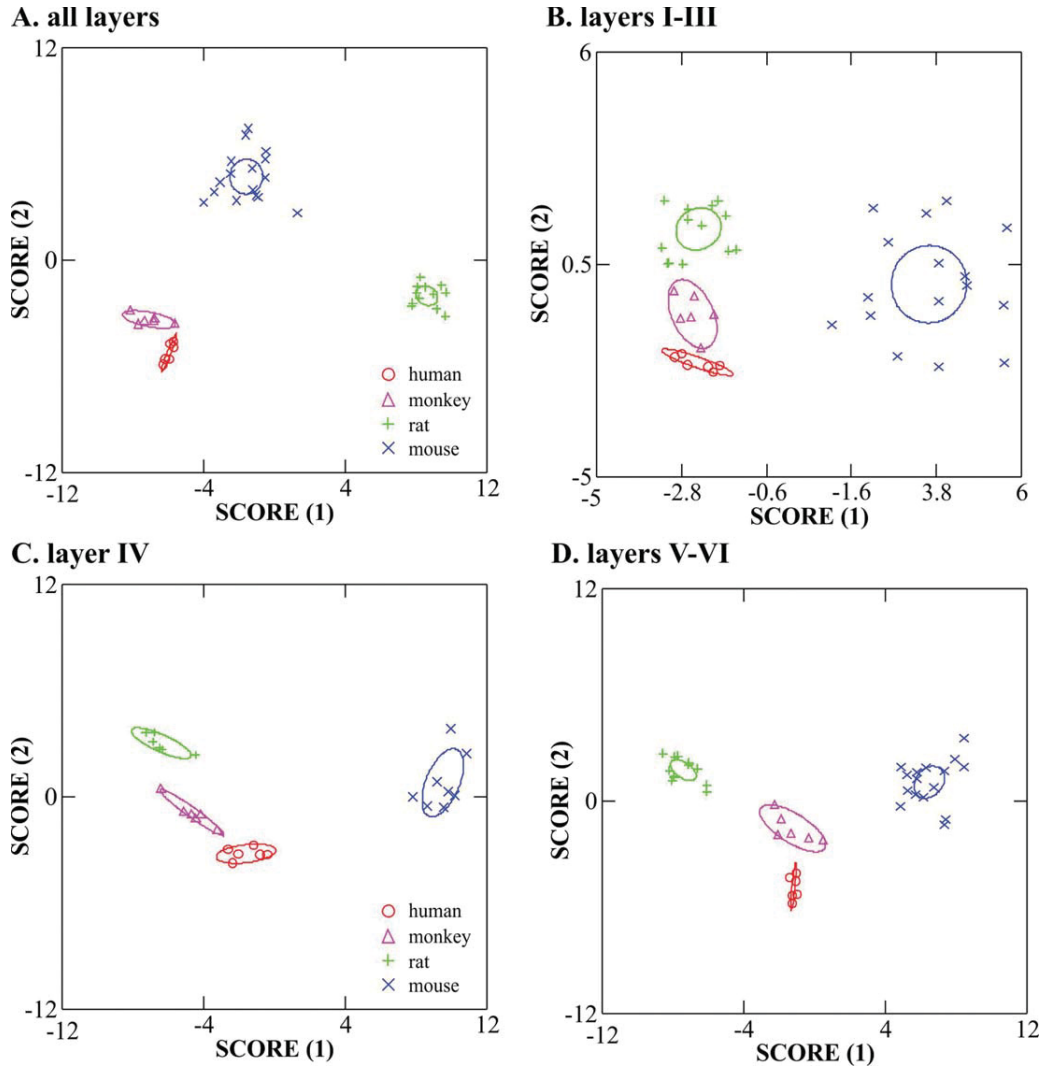

Figure 11. Plots of discriminant analyses to visualize a putative clustering of the four species based on receptor fingerprints of entire area 32 (**A**), the superficial layers (**B**), layer IV (**C**), or the deep layers (**D**). The centroids of each group are indicated by the corresponding 95% confidence intervals. Scores are the data values in a new coordinate system, with axes calculated from the original values (in this case, receptor densities) to show the differences (Euclidean distances) between the fingerprints of the four species to the greatest extent. The same scale was set for all plots. Differences are much less prominent where the superfical layers are concerned, and there is substantial overall differentiation of mouse and rat and close proximity of scores for monkey and human.

the amygdala (Vertes, 2004; Gabbott et al., 2012). Thus, the cingulospinal system in rodents mediates autonomic function and may have a small role in skeletomotor control.

The monkey area 24c on the ventral bank of the cingulate sulcus is a unique area, and it is not shared by rodents. Nevertheless, it may have a function in primates similar to that of the area d32/24b system in rodents. It is guided by auditory and visual inputs (Van Hoesen et al., 1993), it receives substantial amygdalar input (Vogt and Pandya, 1987), and it projects to the motor nucleus of the fifth nerve (Morecraft et al., 1996). It has been shown that this part of the ACC is involved in emotional vocal expressions (Müller-Preuss and Jürgens, 1976; Müller-Preuss et al., 1980). Thus, this system could have homologies to the rodent cingulospinal system in its role in emotional vocal expression. Finally, cingulate-mediated, autonomic regulation in primates is segregated from skeletomotor systems. The subgenual anterior cingulate areas s24 and s32, but not the cingulate premotor areas in the cingulate sulcus, project to autonomic brainstem structures, including the central nucleus of the amygdala, lateral hypothalamus, periaqueductal gray, and parabrachial

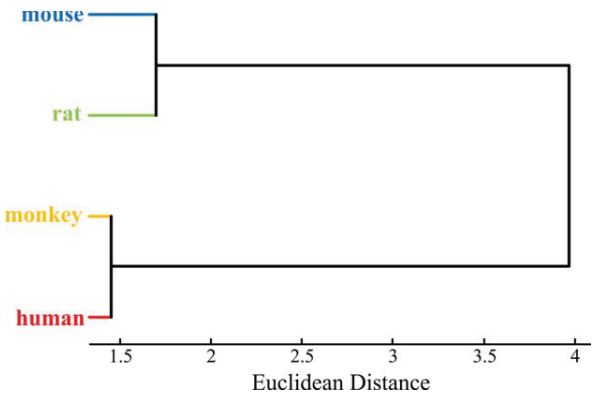

Figure 12. Hierarchical clustering of the cingulate regions of the four species examined, based on the receptor densities measured in superficial and deep layers of their area 32 divisions. Elements included in the hierarchical cluster analysis are grouped into clusters in such a way that species located in the same cluster are similar with respect to their receptor architecture and different from species in other clusters. Ward linkage algorithm; cophrenetic correlation 0.7721.

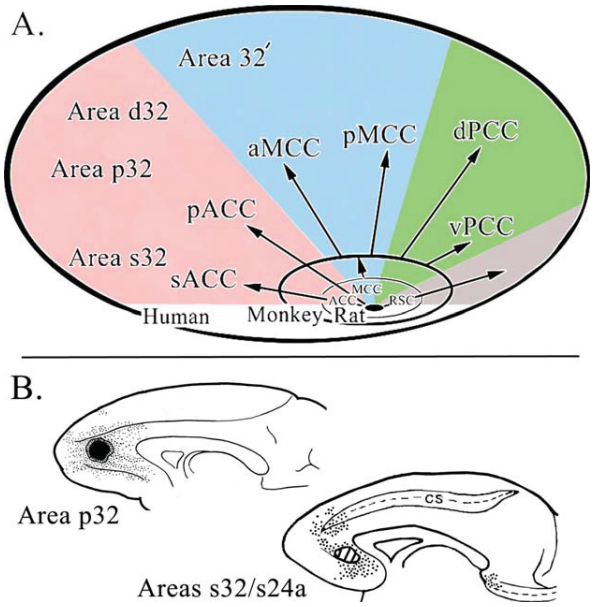

Figure 13. **A:** Differential expansion of cingulate cortex in mouse, rat, macaque, and human. The scaling for each species was derived from the proportions determined from the flat maps for the area 32 subdivisions in Figure 1. The arrows reflect the composition of each region/subregion in cingulate cortex. The ACC divisions (v32, d32, s32, and d32) appear to be homologous, and arrows are drawn through all. In contrast, the MCC has but one component in rodents, and the arrow stops at the monkey oval, where it divides into two parts and continues to the human brain for the anterior MCC (aMCC) and posterior MCC (pMCC) divisions. The human areas d32 and 32′ have no counterparts in rodents or macaque monkey and are set off as separate entities. dPCC, dorsal posterior cingulate cortex; RSC, retrosplenial cortex; vPCC, ventral posterior cingulate cortex. **B:** Intracingulate connections are shown for macaque monkey areas p32 and s32/s24a as reported by Pandya, Van Hoesen, and Mesulam (1981) and Vogt and Pandya (1987), respectively.

nucleus (Ysaui et al., 1985; Chiba et al., 2001). Thus, autonomic and skeletomotor systems are segregated in primates but not in rodents.

Homologies of cortical areas can be assessed with common ontogeny, location, structure, connections, and functions. Functional and ontogenetic homologies cannot be analyzed prior to demonstrating the location, structure, and connections of an area, and that is what has been achieved in the present studies of area 32. Areas d32 and v32 in rodents appear to be homologous to areas p32 and s32, respectively, in primates. Preuss (1995) notes that there is considerable evidence that rats possess homologues of several macaque frontal lobe areas, including the primary motor area, two divisions of premotor cortex, four divisions of cingulate cortex, and caudal orbital cortex. He also observed that rat medial frontal cortex resembles the medial frontal cortex of macaques and humans much more than the dorsolateral prefrontal cortex. This is significant in light of the evidence that the anterior cingulate cortex is involved in human diseases.

In conclusion, we have identified a number of strategies for establishing homologies among rodents and primates for two divisions of area 32. This includes the location, cytoarchitecture, laminar pattern in receptor binding, and intracingulate connections. Eventually, a multivariate model will be required to integrate the many complex factors that determine species homologues for these and other limbic cortical areas. When such models have been developed, it will be possible to search for cingulate cortex in aquatic mammals and other species that are not a routine part of experimental research but have much to offer in terms of anatomical and functional diversity.

CONFLICT OF INTEREST

The authors have no conflicts of interest to report.

ROLE OF AUTHORS

All authors had full access to all data and take responsibility for the integrity of the data and accuracy of the data analysis. Study concept and design: BAV, NP-G. Acquisition, analysis, and interpretation of the data: BAV, LJV, CH, KZ, NP-G. Drafting and critical revision of the manuscript: BAV, PRH, LJV, KZ, NP-G. Statistical analyses and illustrations: BAV, NP-G.

LITERATURE CITED

Amunts K, Lenzen M, Friederici AD, Schleicher A, Morosan P, Palomero-Gallagher N, Zilles K. 2010. Broca's region: novel organizational principles and multiple receptor mapping. PLos Biol 8.

Arikuni T, Sako H, Murata A. 1994. Ipsilateral connections of the anterior cingulate cortex with the frontal and medial temporal cortices in the macaque monkey. Neurosci Res 21:19–39.

Bacon SJ, Smith AD. 1993. A monosynaptic pathway from an identified vasomotor centre in the medial prefrontal cortex to an autonomic area in the thoracic spinal cord. Neuroscience 54:719–728.

Brodmann K. 1909. Vergleichende Lokalisationslehre der Grosshirnrinde in ihren Prinzipien dargestellt auf Grund des Zellenbaues. Leipzig: Barth.

Chiba T, Kayahara T, Nakano K. 2001. Efferent projections of infralimbic and prelimbic areas of the medial prefrontal cortex in the Japanese monkey, *Macaca fuscata*. Brain Res 888:83–101.

Gabbott PLA, Warner TA, Jays PRL, Salway P, Busby SJ. 2005. Prefrontal cortex in the rat: projections to subcortical autonomic, motor, and limbic centers. J Comp Neurol 492:145–177.

Gabbott PLA, Warner TA, Brown JB, Salway P, Gabbott T, Busby S. 2012. Amygdala afferents monosynaptically innervate corticospinal neurons in rat medial prefrontal cortex. J Comp Neurol 520:2440–2458.

Grabenhorst F, Rolls ET, Parris BA. 2008. From affective value to decision-making in the prefrontal cortex. Eur J Neurosci 28:1930–1939.

Jones BF, Groenewegen HJ, Witter MP. 2005. Intrinsic connections of the cingulate cortex in the rat suggest the existence of multiple functionally segregated networks. Neuroscience 133:193–207.

Kim KK, Adelstein RS, Kawamoto S. 2009. Identification of neuronal nuclei (NeuN) as Fox-3, a new member of the fox-1 gene family of splicing factors. J Biol Chem 284: 31052–1061.

Lane RD, Fink GR, Chau PM, Dolan RJ. 1997. Neural activation during selective attention to subjective emotional responses. Neuroreport 8:3969–3972.

Merker B. 1983. Silver staining of cell bodies by means of physical development. J Neurosci Methods 9:235–241.

Morecraft RJ, Schroeder CM, Keifer J. 1996. Organization of face representation in the cingulate cortex of the rhesus monkey. Neuroreport 7:1343–1348.

Morris R, Petrides M, Pandya DN. 1999. Architecture and connections of retrosplenial aerea 30 in the rhesus monkey (*Macaca mulatta*). Eur J Neurosci 11:2506–2518.

Müller-Preuss P, Jürgens U. 1976. Projections from the "cingular" vocalization area in the squirrel monkey. Brain Res 103:29–43.

Müller-Preuss P, Newman JD, Jürgens U. 1980. Anatomical and physiological evidence for a relationship between the "cingular" vocalization area and the auditory cortex in the squirrel monkey. Brain Res 202:307–315.

Neafsey EJ, Terreberry RR, Hurley KM, Ruitt KG, Frysztak, RJ. 1993. Anterior cingulate cortex in rodents: connections, visceral control functions, and implications for emotion. In: Vogt BA, Gabriel M, editors. Neurobiology of cingulate cortex and limbic thalamus. Boston: Birkhäuser. p 206–223.

Nieuwenhuis IL, Takashima A. 2011. The role of the ventromedial prefrontal cortex in memory consolidation. Behav Brain Res 218:325–334.

Nudo RJ, Masterton RB. 1990. Descending pathways to the spinal cord, III. Sites of origin of the corticospinal tract. J Comp Neurol 296:559–583.

Palomero-Gallagher N, Zilles K. 2004. The rat isocortex. In: Paxinos G, editor. The rat nervous system. San Diego: Academic Press. p 729–757.

Palomero-Gallagher N, Mohlberg H, Zilles K, Vogt BA. 2008. Cytology and receptor architecture of human anterior cingulate cortex. J Comp Neurol 508:906–926.

Palomero-Gallagher N, Vogt BA, Schleicher A, Mayberg HS, Zilles K. 2009. Receptor architecture of human cingulate cortex: evaluation of the four-region neurobiological model. Hum Brain Mapp 30:2336–2355.

Palomero-Gallagher N, Schleicher A, Zilles K, Vogt BA. 2013. Anterior cingulate area 32 in monkey and human: cytoarchitecture and multireceptor binding. J Comp Neurol 521:3272–3286.

Pandya DN, Van Hoesen GW, Mesulam M-M. 1981. Efferent connections of the cingulate gyrus in the rhesus monkey. Exp Brain Res 42:319–330.

Park SQ, Kahnt T, Rieskamp J, Heekeren HR. 2011. Neurobiology of value integration: when value impacts valuation. J Neurosci 31:9307–9314.

Phan KL, Wager T, Taylor SF, Liberzon I. 2002. Functional neuroanatomy of emotion: a meta-analysis of emotion activation studies in PET and fMRI. Neuroimage 16:331–348.

Piefke M, Weiss PH, Zilles K, Markowitsch HJ, Fink GR. 2003. Differential remoteness and emotional tone modulate the neural correlates of autobiographical memory. Brain 126: 650–668.

Preda A, Rilling LM, Chin RB, Tamminga CA. 2009. The cingulate gyrus in schizophrenia: Imaging and altered structure and function. In: Vogt BA, editor. Cingulate neurobiology and disease. Oxford: Oxford University Press. p 655–678.

Preuss TM. 1995. Do rats have prefrontal cortex? The Rose-Woolsey-Akert program reconsidered. J Cogn Neurosci 7: 1–24.

Salmon E, Laureys S. 2009. Brain imaging in prodromal and probable Alzheimer's disease. A focus on the cingulate gyrus. In: Vogt BA, editor. Cingulate neurobiology and disease. Oxford: Oxford University Press. p 749–762.

Saxena S, O'Neill J, Rauch SL. 2009. The role of cingulate cortex dysfunction in obsessive-compulsive disorder. In: Vogt BA, editor. Cingulate neurobiology and disease. Oxford: Oxford University Press. p 587–617.

Shin LM, Whalen PJ, Pitman RK, Rauch SL. 2009. The role of the anterior cingulate cortex in posttraumatic stress and panic disorders. In: Vogt BA, editor. Cingulate neurobiology and disease. Oxford: Oxford University Press. p 453–465.

Takashima A, Petersson KM, Rutters F, Tendolkar I, Jensen O, Zwarts MJ, McNaughton BL, Fernandez G. 2006. Declarative memory consolidation in humans: a prospective functional magnetic resonance imaging study. Proc Natl Acad Sci U S A 103:756–761.

van Groen T, Wyss JM. 2003. Connections of the retrosplenial granular b cortex in the rat. J Comp Neurol 463:249–263.

Van Hoesen GW, Morecraft RJ, Vogt BA. 1993. Connections of the monkey cingulate cortex. In: Vogt BA, Gabriel M, editors. Neurobiology of cingulate cortex and limbic thalamus. Boston: Birkhäuser. p 249–284.

Vertes RP. 2004. Differential projections of the infralimbic and prelimbic cortex in the rat. Synapse 51:32–58.

Vogt BA. 2009. Architecture, neurocytology and comparative organization of monkey and human cingulate cortices. In: Vogt BA, editor. Cingulate neurobiology and disease. Oxford: Oxford University Press. p 67–93.

Vogt BA, Derbyshire SWJ. 2009. Visceral circuits, autonomic function and human imaging. In: Vogt BA, editor.

Cingulate neurobiology and disease. Oxford: Oxford University Press. p 219–235.
Vogt BA, Palomero-Gallagher N. 2012. Cingulate cortex. In: Mai JK, Paxinos G, editors. The human nervous system, 3rd ed. Amsterdam: Academic Press. p 943–987.
Vogt BA, Pandya DN. 1987. Cingulate cortex of rhesus monkey. II. Cortical afferents. J Comp Neurol 262:271–289.
Vogt BA, Paxinos G. 2012. Cytoarchitecture of mouse and rat cingulate cortex with human homologies. Brain Struct Funct, doi 10.1007/s00429-012-0493-3.
Vogt BA, Nimchinsky EA, Vogt LJ, Hof PR. 1995. Human cingulate cortex: surface features, flat maps, and cytoarchitecture. J Comp Neurol 359:490–506.
Vogt BA, Berger GR, Derbyshire SWG. 2003. Structural and functional dichotomy of human midcingulate cortex. Eur J Neurosci 18:3134–3144.
Vogt BA, Vogt L, Farber NB, Bush G. 2005. Architecture and neurocytology of the monkey cingulate gyrus. J Comp Neurol 485:218–239.
Vogt C, Vogt O. 1919. Allegemeine Ergebnisse unserer Hirnforschung. J Psychol Neurol 25:279–462.
von Economo C, Koskinas GN. 1925. Die Cytoarchitektonik der Hirnrinde des erwachsenen Menschen. Berlin: Springer.
Yasui Y, Itoh K, Takada M, Mitani A, Kaneko T, Mizuno N. 1985. Direct cortical projections to the paraqbrachial nucleus in the cat. J Comp Neurol 234:77–86.
Zilles K, Schleicher A, Palomero-Gallagher N, Amunts K. 2002. Quantitative analysis of cyto- and receptorarchitecture of the human brain. In: Toga AW, Mazziotta JC, editors. Brain mapping. The methods. Amsterdam: Elsevier. p 573–602.

RESEARCH ARTICLE

Distribution of Neurotransmitter Receptors and Zinc in the Pigeon (*Columba livia*) Hippocampal Formation: A Basis for Further Comparison With the Mammalian Hippocampus

Christina Herold,[1]* Verner P. Bingman,[2] Felix Ströckens,[3] Sara Letzner,[3] Magdalena Sauvage,[4] Nicola Palomero-Gallagher,[5] Karl Zilles,[5,6] and Onur Güntürkün[3]

[1]C. & O. Vogt Institute of Brain Research, University of Düsseldorf, 40225 Düsseldorf, Germany
[2]Department of Psychology and J.P. Scott Center for Neuroscience, Bowling Green State University, Bowling Green, Ohio 43403
[3]Department of Biopsychology, Institute of Cognitive Neuroscience, Faculty of Psychology, Ruhr-University Bochum, 44780 Bochum, Germany
[4]Research Department of Neuroscience, Mercator Research Group "Structure of Memory," Faculty of Medicine, Ruhr-University Bochum, 44780 Bochum, Germany
[5]Institute of Neuroscience and Medicine INM-1, Research Center Jülich, 52425 Jülich, Germany
[6]Department of Psychiatry, Psychotherapy and Psychosomatics, RWTH Aachen University, and JARA–Translational Brain Medicine, 52074 Aachen, Germany

ABSTRACT

The avian hippocampal formation (HF) and mammalian hippocampus share a similar functional role in spatial cognition, but the underlying neuronal mechanisms allowing the functional similarity are incompletely understood. To understand better the organization of the avian HF and its transmitter receptors, we analyzed binding site densities for glutamatergic AMPA, NMDA, and kainate receptors; $GABA_A$ receptors; muscarinic M_1, M_2 and nicotinic (nACh) acetylcholine receptors; noradrenergic α_1 and α_2 receptors; serotonergic 5-HT_{1A} receptors; dopaminergic $D_{1/5}$ receptors by using quantitative in vitro receptor autoradiography. Additionally, we performed a modified Timm staining procedure to label zinc. The regionally different receptor densities mapped well onto seven HF subdivisions previously described. Several differences in receptor expression highlighted distinct HF subdivisions. Notable examples include 1) high $GABA_A$ and α_1 receptor expression, which rendered distinctive ventral subdivisions; 2) high α_2 receptor expression, which rendered distinctive a dorsomedial subdivision; 3) distinct kainate, α_2, and muscarinic receptor densities that rendered distinctive the two dorsolateral subdivisions; and 4) a dorsomedial region characterized by high kainate receptor density. We further observed similarities in receptor binding densities between subdivisions of the avian and mammalian HF. Despite the similarities, we propose that 300 hundred million years of independent evolution has led to a mosaic of similarities and differences in the organization of the avian HF and mammalian hippocampus and that thinking about the avian HF in terms of the strict organization of the mammalian hippocampus is likely insufficient to understand the HF of birds. J. Comp. Neurol. 522:2553–2575, 2014.

© 2014 Wiley Periodicals, Inc.

INDEXING TERMS: hippocampus; entorhinal cortex; receptor; avian; autoradiography; zinc

In both mammals and birds, the hippocampal formation (HF) plays a similar role in spatial cognition (Colombo and Broadbent, 2000; Bingman et al., 2005) and shows comparable neuroanatomical, neurochemical, and electrophysiological characteristics (Bingman et al., 2005). The overall homology between the mammalian and avian HF is well established (Reiner et al.,

© 2014 Wiley Periodicals, Inc.

Grant sponsor: Alexander von Humboldt-Stiftung (to V.P.B.); Grant sponsor: HGF Program "Function and Dysfunction of the Nervous System" (to K.Z.); Grant sponsor: Deutsche Forschungsgemeinschaft; Grant number: SFB874 (to O.G.).

*CORRESPONDENCE TO: Christina Herold, C. & O. Vogt Institute of Brain Research, University of Düsseldorf, 40225 Düsseldorf, Germany.
E-mail: christina.herold@uni-duesseldorf.de

Received August 16, 2013; Revised January 17, 2014;
Accepted January 21, 2014.
DOI 10.1002/cne.23549
Published online January 29, 2014 in Wiley Online Library (wileyonlinelibrary.com)

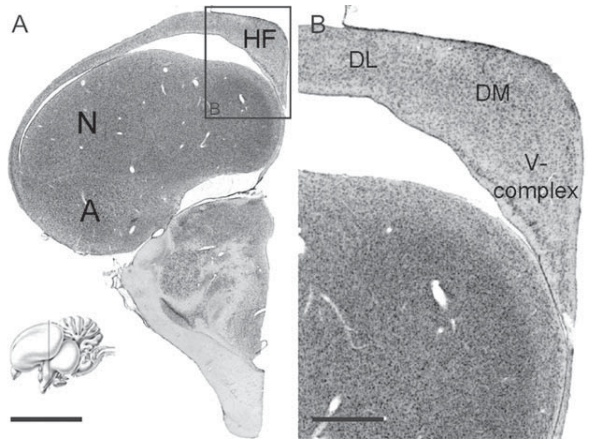

Figure 1. Nissl-stained transverse section of the forebrain of the pigeon. **A:** Full transverse section at atlas level A 6.75 (Karten and Hodos, 1967). The boxed area indicates the region of interest, the hippocampal formation. At bottom, a lateral view of the pigeons brain was prepared that indicates the location of the plane of the illustrated section (not scaled). **B:** Enlarged image of the hippocampal formation labeled in A. A, arcopallium; DM, dorsomedial region of HF; DL, dorsolateral region of HF; HF, hippocampal formation; N, nidopallium; V-complex, region that comprises the ventral subdivisions of the HF. Scale bars = 2.5 mm in A; 500 μm in B.

2004; Jarvis et al., 2013), but what continues to concern researchers is uncertainty with respect to what, if any, areas of the avian HF correspond to the well-defined dentate gyrus (DG) and Ammon's horn (CA3 and CA1 in particular) of the mammalian hippocampus. The avian HF (Fig. 1) can be coarsely divided into ventromedial (V-complex), dorsomedial (DM), and dorsolateral (DL) subdivisions. Further subdivisions (ventromedial Tr, Vl, and Vm; dorsomedial DMd and DMv; and dorsolateral DLd and DLv; Fig. 2) have been described (Erichsen et al., 1991; Kahn et al., 2003; Atoji and Wild, 2004). Erichsen et al. (1991) proposed that the medial (Vm) and lateral (Vl) dense cell layers of the V-complex correspond to areas of Ammon's horn, the area between the two cell layers (Tr) to the hilar region, and the dorsomedial HF (DMd and DMv) to the dentate gyrus (DG). However, they acknowledged uncertainty with respect to a dentate gyrus-like structure in the avian HF. The tracing study of Kahn et al. (2003) and Székély and Krebs (1996) in zebra finch (*Taeniopygia guttata*) essentially led to the same conclusions with respect to the interclass comparisons of Erichsen et al. (1991). By contrast, Atoji and Wild (2004) proposed, based on connectivity data and kainic acid lesions, that the cell layers of the V-complex actually correspond to the DG, whereas an Ammon's horn-like subdivision is found in DM. Timm staining for zinc is a powerful marker for mossy fibers in mammals and has also been used to search for a DG mossy fiber-like system in bird species other than pigeons (Faber et al., 1989; Aboitiz, 1993; Montagnese et al., 1993, 1996; Tömböl et al., 2000b), but those Timm staining studies failed to reveal distinct, rat-like fiber labeling in the HF of birds. However, zinc labeling has been used to classify different types of glutamatergic synapses that can be found numerously in the CA fields (Sindreu et al., 2003).

To understand better the organization of the avian HF and its transmitter receptors and to shed light on the extent to which there are anatomically defined structures in the avian HF that are comparable to the DG and CA regions in the mammalian hippocampus, we mapped the distribution of 11 different neurotransmitter receptors in the pigeon HF. Our goal was to describe the regional receptor expression in the pigeon hippocampal formation as well as to characterize the receptor organization of HF in distinct subdivisions. We then compared the receptor binding data with published data for the hippocampus in different mammalian species (Kraemer et al., 1995; Palomero-Gallagher et al., 2003; Topic et al., 2007; Cremer et al., 2011). To complement the receptor data, we further carried out a zinc-staining procedure in the pigeon.

MATERIALS AND METHODS

Receptor autoradiography

We examined a total of six adult pigeons (*Columba livia*) of unknown sex. Animals were obtained from local breeders and were housed in individual cages (30 × 30 × 45 cm) in a temperature (21°C ± 1°C)- and humidity-controlled room with a 12-hour light/dark circle. The subjects had access to grit, food, and water ad libitum. All experimental procedures were approved by national authorities (LANUV NRW, Germany) and were carried out in accordance with the National Institutes of Health *Guide for care and use of laboratory animals*. Animals were decapitated and the brains removed from the skull, frozen immediately in isopentane at −40°C, and stored at −70°C. Serial coronal 10-μm sections were cut with a cryostat microtome (2800 Frigocut E; Reichert-Jung). Sections were thaw mounted on gelatinized slides, freeze dried, and stained with a modified cell body staining for cytoarchitectonic analysis or processed for receptor autoradiography (Merker, 1983; Palomero-Gallagher et al., 2008).

Details of the autoradiographic labeling procedure have been published elsewhere (Zilles et al., 2002a,b; Schleicher et al., 2005). Binding protocols are summarized in Table 1. Three steps were performed in the following sequence: 1) A preincubation step removed endogenous ligand from the tissue. 2) During the main incubation step, binding sites

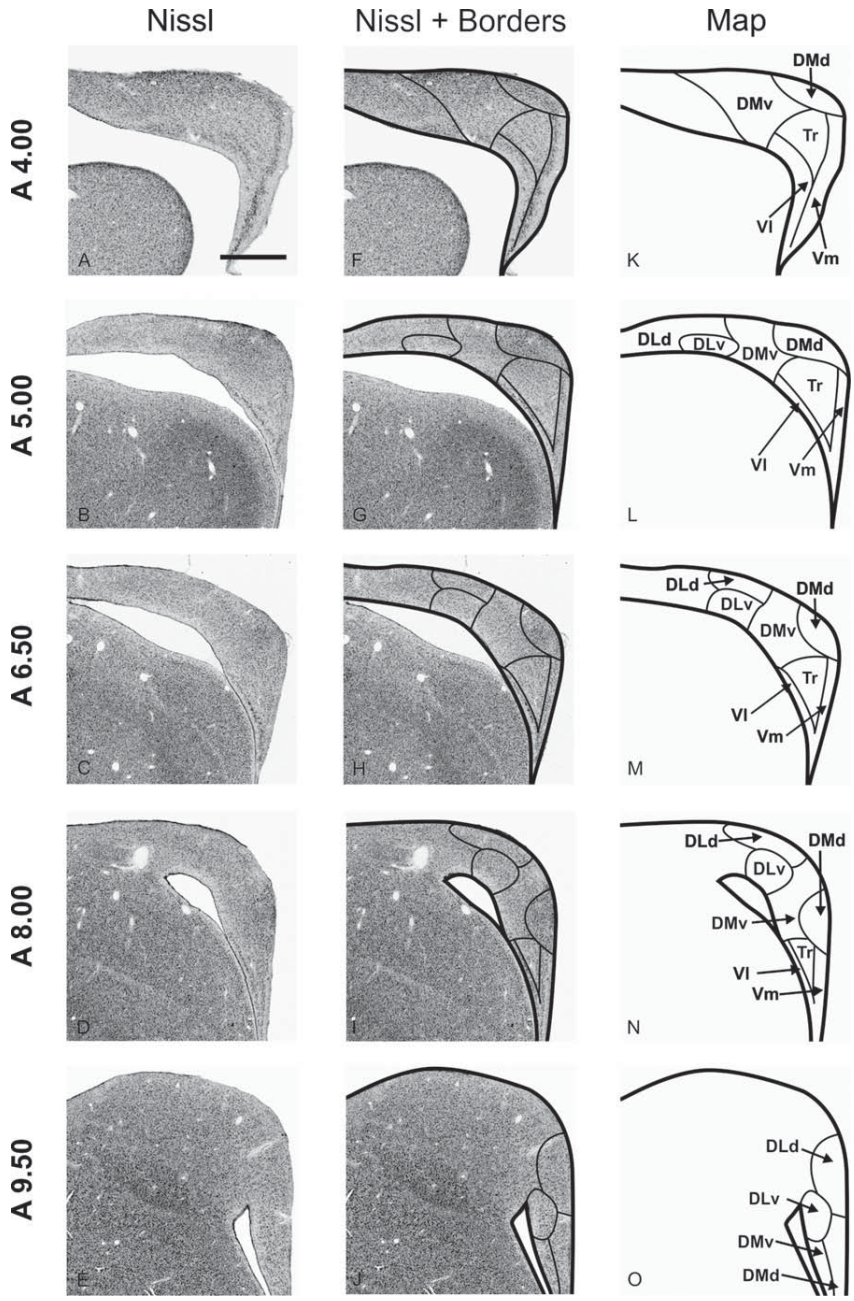

Figure 2. Nissl-stained and schematic representation of the pigeon hippocampal formation subdivision boundaries from rostrocaudal atlas levels A 4.00 to A 9.50 (Karten and Hodos, 1967). **A–E:** Nissl-stained coronal sections of the hippocampal formation. **F–J:** Nissl-stained coronal section with the boundaries following Atoji and Wild (2004, 2006). **K–O:** Schematic representation of the subdivision scheme used to map the receptor densities and zinc labeling. The hippocampal formation in the pigeon comprises seven regions: the V-complex, consisting of the ventrolateral (Vl) and ventromedial (Vm) cell bands and the cellular inner triangular region (Tr), the dorsomedial region DM and its ventral (DMv) and dorsal (DMd) subdivisions, and the dorsolateral region DL and its ventral (DLv) and dorsal (DLd) subdivisions. Scale bar = 500 μm.

were labeled with tritiated ligand (total binding). Coincubation of the tritiated ligand and a 1,000–10,000-fold excess of an appropriate nonlabeled ligand (displacer) determined nonspecific and thus nondisplaceable binding. Specific binding is the difference between total and nonspecific binding. 3) A final rinsing step eliminated unbound radioactive ligand from the sections.

The following binding sites were labeled according to the above-cited protocols: 1) α-amino-3-hydroxy-5-methyl-4-isoxalone propionic acid (AMPA) receptor with

TABLE 1.

Incubation Conditions Used for Receptor Autoradiography

Receptor	^{3}H ligand (incubation concentration)	Displacer (incubation concentration)	Incubation buffer	Preincubation step	Main incubation step	Rinsing step
AMPA	[^{3}H]AMPA (10 nM)	Quisqualate (10 μM)	50 mM Tris-acetate (pH 7.2)	3 × 10 min at 4°C in incubation buffer	45 min at 4°C in incubation buffer + 100 mM KSCN	4 × 4 sec at 4°C in incubation buffer + 2 × 2 sec at 4°C in acetone/glutaraldehyde
Kainate	[^{3}H]kainate (8 nM)	Kainate (100 μM)	50 mM Tris-citrate (pH 7.1)	3 × 10 min at 4°C in incubation buffer	45 min at 4°C in incubation buffer + 10 mM Ca-acetate	4 × 4 sec at 4°C in incubation buffer + 2 × 2 sec at 4°C in acetone/glutaraldehyde
NMDA	[^{3}H]MK-801 (5 nM)	MK-801 (100 μM)	50 mM Tris-HCl (pH 7.2)	15 min at 25°C in incubation buffer	60 min at 25°C in incubation buffer + 30 μM glycine + 50 μM spermidine	2 × 5 min at 4°C in incubation buffer
Muscarinergic cholinergic M_1	[^{3}H]pirenzepine (1 nM)	Pirenzepine (10 μM)	Modified Krebs-Ringer buffer (pH 7.4)	20 min at 25°C in incubation buffer	60 min at 25°C in incubation buffer	2 × 5 min at 4°C in incubation buffer
Muscarinergic cholinergic M_2	[^{3}H]oxotremorine-M (0.8 nM)	Carbachol (1 μM)	20 mM Hepes-Tris (pH 7.5) + 10 mM $MgCl_2$	20 min at 25°C in incubation buffer	60 min at 25°C in incubation buffer	2 × 2 min at 4°C in incubation buffer
Nicotinic cholinergic	[^{3}H]cytisine (1 nM)	Nicotine (10 μM)	50 mM Tris-HCl (pH7.4) + 120 mM NaCl + 5 mM KCl + 1 mM $MgCl_2$ + 2.5 mM $CaCl_2$	15 min at 22°C in incubation buffer	90 min at 4°C in incubation buffer	2 × 2 min at 4°C in incubation buffer
α1 Adrenoreceptor	[^{3}H]prazosin (0.2 nM)	Phentolamine (10 μM)	50 mM Tris-HCl (pH 7.4)	30 min at 37°C in incubation buffer	45 min at 30°C in incubation buffer	2 × 5 min at 4°C in incubation buffer
α2 Adrenoreceptor	[^{3}H]UK-14304 (1.4 nM) [^{3}H]RX-821002 (6 nM)	Noradrenaline (100 μM) (-) adrenaline (10 μM)	50 mM Tris-HCl (pH 7.7) + 100 μM $MnCl_2$ 50 mM Tris-HCl (pH 7.4) + 100 mM $MnCl_2$ + 0.1% Ascorbic acid + 0.3 μM 8-OH-DPAT	15 min at 22°C in incubation buffer 30 min at 22°C in incubation buffer	90 min at 22°C in incubation buffer 30 min at 22°C in incubation buffer	5 min at 4°C in incubation buffer 2 × 20 sec at 4°C in incubation buffer
$GABA_A$	[^{3}H]muscimol (6 nM)	GABA (10 μM)	50 mM Tris-citrate (pH 7.0)	3 × 5 min at 4°C in incubation buffer	40 min at 4°C in incubation buffer	3 × 3 sec at 4°C in incubation buffer
Serotoninergic 5-HT_{1A}	[^{3}H] 8-OH-DPAT (1 nM)	Serotonin (10 μM)	170 mM Tris-HCl (pH 7.6) + 4 mM $CaCl_2$ + 0.01% Ascorbic acid	30 min at 22°C in incubation buffer	60 min at 22°C in incubation buffer	1 × 5 min at 4°C in incubation buffer
Dopaminergic $D_{1/5}$	[^{3}H]SCH-23390 (0.5 nM)	SKF 83566 (1 μM)	50 mM Tris-HCl (pH 7.4) + 120 mM NaCl + 5 mM KCl + 2 mM $CaCl_2$ + 1 mM $MgCl_2$ + 1 μM Mianserin	20 min at 22°C in incubation buffer	90 min at 22°C in incubation buffer	2 × 10 min at 4°C in incubation buffer

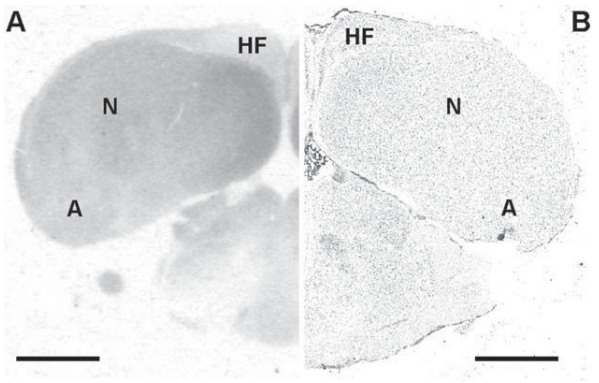

Figure 3. Original autoradiograph and its Nissl-stained counterpart of a coronal forebrain section of the pigeon. **A:** Autoradiograph at atlas level A 5.00 (Karten and Hodos, 1967). Here, binding sites of [^{3}H]muscimol to $GABA_A$ receptors are shown. Darker gray levels indicate higher densities of $GABA_A$ receptors. **B:** Nissl-stained coronal section corresponding to the autoradiograph to trace the borders of the different subdivisions on prints of the digitized autoradiographs. A, arcopallium; HF, hippocampal formation; N, nidopallium. Scale bar = 2 mm.

[^{3}H]AMPA, 2) kainate receptor with [^{3}H]kainate, 3) N-methyl-D-aspartate (NMDA) receptor with [^{3}H]MK-801, 4) γ-aminobutyric acid A ($GABA_A$) receptor with [^{3}H]muscimol, 5) muscarinic cholinergic M_1 receptor with [^{3}H]pirenzepine, 6) muscarinic cholinergic M_2 receptor with [^{3}H]oxotremorine-M, 7) nicotinic cholinergic (nACh) receptor with [^{3}H]cytosine, 8) noradrenergic α_1 adrenoreceptor with [^{3}H]prazosin, 9) noradrenergic α_2 adrenoreceptor with [^{3}H]RX-821002, 10) serotonergic 5-HT_{1A} receptor with [^{3}H]8-OH-DPAT, and 11) dopaminergic $D_{1/5}$ receptors with [^{3}H]SCH 23390. Sections were air dried overnight and subsequently coexposed for 4–5 weeks against a tritium-sensitive film (Hyperfilm; Amersham, Braunschweig, Germany) with plastic ^{3}H standards (Microscales; Amersham) of known concentrations of radioactivity.

Anatomical identification

The borders of the HF subdivisions (Fig. 2) were identified based on previous cytoarchitectural, neurochemical, and tract-tracing studies (Erichsen et al., 1991; Atoji et al., 2002; Kahn et al., 2003; Atoji and Wild, 2004, 2005, 2006; Rosinha et al., 2009). Borders of the different subdivisions were traced on prints of the digitized autoradiographs by projecting the cell body stained sections onto the digitized images of the autoradiographs (Fig. 3).

Image analysis

The resulting autoradiographs were subsequently processed via densitometry with a video-based image analyzing technique (Schleicher et al., 2005). Autoradiographs were digitized by means of a KS-400 image analyzing system (Kontron Germany) connected to a CCD camera (Sony) equipped with an S-Orthoplanar 60-mm macro lens (Zeiss). The images were stored as binary files with a resolution of 512 × 512 pixels and eight-bit

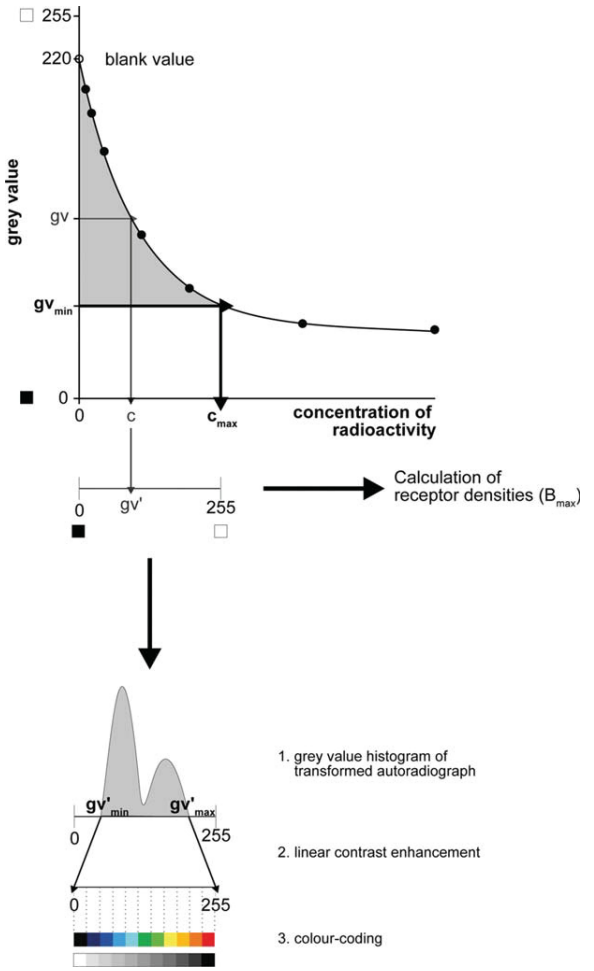

Figure 4. Example of a calibration curve based on isotope standards from which the concentration of bound ligands was calculated. The gray value images of the coexposed microscales were used to compute a calibration curve by nonlinear, least-squares fitting, which defined the relationship between gray values in the autoradiographs and concentrations of radioactivity. This allowed pixel-wise conversion of the gray values of an autoradiograph into the corresponding concentrations of radioactivity. A gray-value histogram of the transformed autoradiograph was built, followed by a linear contrast enhancement procedure. After that, the autoradiograph was color coded as indicated in the graph. The concentrations of binding sites occupied by the ligand under incubation conditions are transformed into fmol/mg protein at saturation conditions by means of the equation $(K_D + L)/A_S \times L$, where K_D is the equilibrium dissociation constant of ligand-binding kinetics, L is the incubation concentration of ligand, and A_S is the specific activity of the ligand.

gray value. The gray-value images of the coexposed microscales were used to compute a calibration curve by nonlinear, least-squares fitting, which defined the relationship between gray values in the autoradiographs and concentrations of radioactivity that were then indicated in the color-coded autoradiographs (see Fig. 4). This allowed the pixel-wise conversion of the gray values of an autoradiograph into the corresponding concentration of radioactivity. The concentrations of binding sites occupied by a ligand under incubation conditions are transformed into fmol/mg protein at saturation conditions by means of the equation $(K_D + L)/A_S \times L$, where K_D is the equilibrium dissociation constant of ligand-binding kinetics, L is the incubation concentration of ligand, and A_S is the specific activity of the ligand.

For the analysis of each ligand for each subdivision for a given pigeon, we attempted to sample HF, in the left hemisphere, at six evenly distributed anterior–posterior levels between A 9.5 and A 4.0 according to the atlas of Karten and Hodos (1967). However, for some ligands in some individuals, the tissue was not of sufficient quality to carry out an analysis at all six levels, and receptor concentrations were derived from the tissue available and based on fewer than six sections. Also, not all subdivisions extend across the entire anterior–posterior range sampled. For example, the V-complex is not discernible at more anterior levels, and DLd and DMd are not discernible at more posterior levels (Fig. 2); as a result, fewer than six sections were used for these subdivisions. The mean of the gray values contained in a specific HF subdivision over the sampled AP levels from one animal was then transformed into a receptor concentration (fmol/mg protein). The mean of each ligand in each subdivision averaged across the six animals was then reported as the receptor concentration. All receptor-binding densities are presented as mean ± SEM. Quantitative, multireceptor data are presented in regional fingerprints that were prepared as polar plots that separately show the density of a single receptor type for all subdivisions (Fig. 5).

Statistical analysis

For comparisons (see below), it was useful to determine whether any difference in receptor densities among the HF subdivisions, either visually or quantitatively revealed, was statistically verifiable. To do this, we first applied a Friedman ANOVA across all subdivisions for each ligand. If significant, pair-wise comparisons were run with the Wilcoxon-rank test. For all statistical analyses, Statistica 10 (StatSoft, Tulsa, OK) was used. The significance level was set at 0.05.

Zinc labeling

For the zinc-labeling procedure, an additional five adult pigeons of unknown sex obtained from local breeders were used. Pigeons were housed in individual cages (30 × 30 × 45 cm) in a temperature (21°C ± 1°C)- and humidity-controlled room with a 12-hour light–dark circle. The subjects had access to grit, food, and water ad libitum. All experimental procedures were approved by national authorities (LANUV NRW, Germany) and were carried out in accordance with the National Institutes of Health *Guide for care and use of laboratory animals*. All subjects were transcardially perfused for 5 min with a 0.1% Na_2S in phosphate-buffered solution (105 mM $NaH_2PO^4 \cdot 2H_2O$ in distilled H_2O, pH set to 6.35 with NaOH) using an average pressure of 15 ml/min (modified from Danscher and Zimmer, 1978). The brain was removed and incubated for 3 hours in a 5% phosphate-buffered Acrolein solution for immersion fixation, followed by rinsing for twice for 30 min and twice for 5 min in PB. After incubation for 24 hours in 30% sucrose in PB for cryoprotection, brains were cut into 25-μm thin frontal sections using a microtome (Leica Microsystems, Wetzlar, Germany). Every tenth section was mounted on slides. Slides were rinsed for 5 min in distilled water and briefly dried at 30°C.

For the zinc staining, four solutions were prepared. 1) Gum arabic, 450 g, was dissolved in 900 ml distilled H_2O and stirred for 5 days. After a few hours of precipitation, the supernatant was collected and the precipitate discarded. The Gum arabic solution can be stored at −20° until further use. 2) Citric acid monohydrate ($C_6H_8O_7 \cdot H_2O$), 5 g, was dissolved in 12.5 ml distilled H_2O. After complete dissolving of citric acid monohydrate, 4.85 g trisodium citrate dihydrate ($Na_3C_6H_5O_7 \cdot 2H_2O$) was added to the solution. The solution was then filled to 20 ml with distilled H_2O. 3) Hydroquinone, 1.7 g, was dissolved in 30 ml distilled H_2O. 4) Silver nitrate, 0.21 g, was dissolved in 30 ml distilled H_2O. Because the solution is light sensitive, it has to be protected from light all the time.

One hundred twenty-five milliliters of the gum arabic solution was mixed with solutions 2–4 and stirred for 5 min. The emergent developer solution was poured into an opaque plastic box, and sections were incubated in the developer solution for 3–4 hours. When staining had reached a sufficient intensity, as determined visually, the sections were removed from the developer solution and washed under running tap water for 15 minutes. After incubation in H_2O overnight, slices were dehydrated and embedded/coverslipped in DPX (Sigma-Aldrich). It was crucial to use high-grade H_2O to

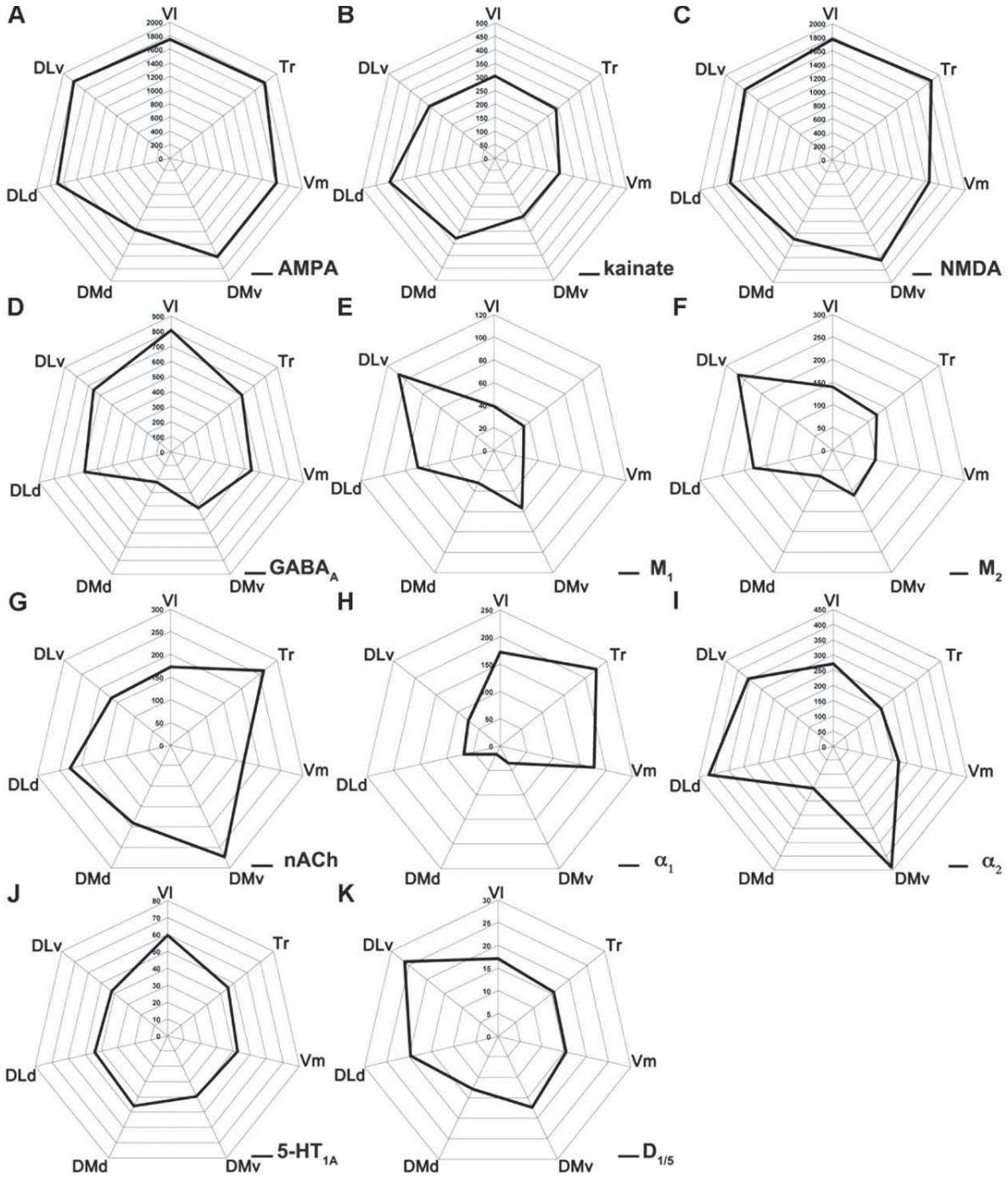

Figure 5. Receptor fingerprints of the pigeon hippocampal formation (HF) subdivisions. The coordinate polar plots (*A–K*) show the individual receptor densities in fmol/mg protein for all subdivisions. The black lines connecting the mean densities of the receptors in each subdivision define the shape of the fingerprint so the reader can quickly notice substantial differences in the distribution of receptors in all subdivisions of the HF. As demonstrated in the fingerprint, glutamatergic AMPA and NMDA receptors are very similarly distributed in the pigeon HF, with high densities in all areas and a decline in DMd, whereas the high kainate receptors densities in DMd and DLd cause a peak in these subdivisions. $GABA_A$ receptor densities peaked in the Vl region and showed a decline in DMd. Muscarinic M_1 and M_2 receptors showed the same fingerprint shape. Densities differed substantially between DLv and the other subdivisions, which resulted in a substantial peak in the west–north direction of their polar plots. By contrast, nicotinic receptors were densely distributed in DMv, Tr, and DLd. Noradrenergic α_1 and α_2 substantially differed in their distributions. Very intense labeling for α_1 was found in the V-complex, so the northeast direction dominates the shape of its fingerprint. By contrast, α_2 receptor levels were high in DMv and the DL regions. 5-HT_{1A} receptor distributions, although with much lower densities, were similar to the $GABA_A$ receptor distributions but showed no break in DMd. Finally, $D_{1/5}$ receptor distribution was similar to the M_2 distribution. Note that the scales in A–K are different. DMd, dorsal part of the dorsomedial region of HF; DMv, ventral part of the dorsomedial region of HF; DLd, dorsal part of dorsolateral region of HF; DLv, ventral part of dorsolateral region of HF; Tr, triangular region of the ventromedial region of HF; Vm, ventromedial part of the V-complex; Vl, ventrolateral part of the V-complex.

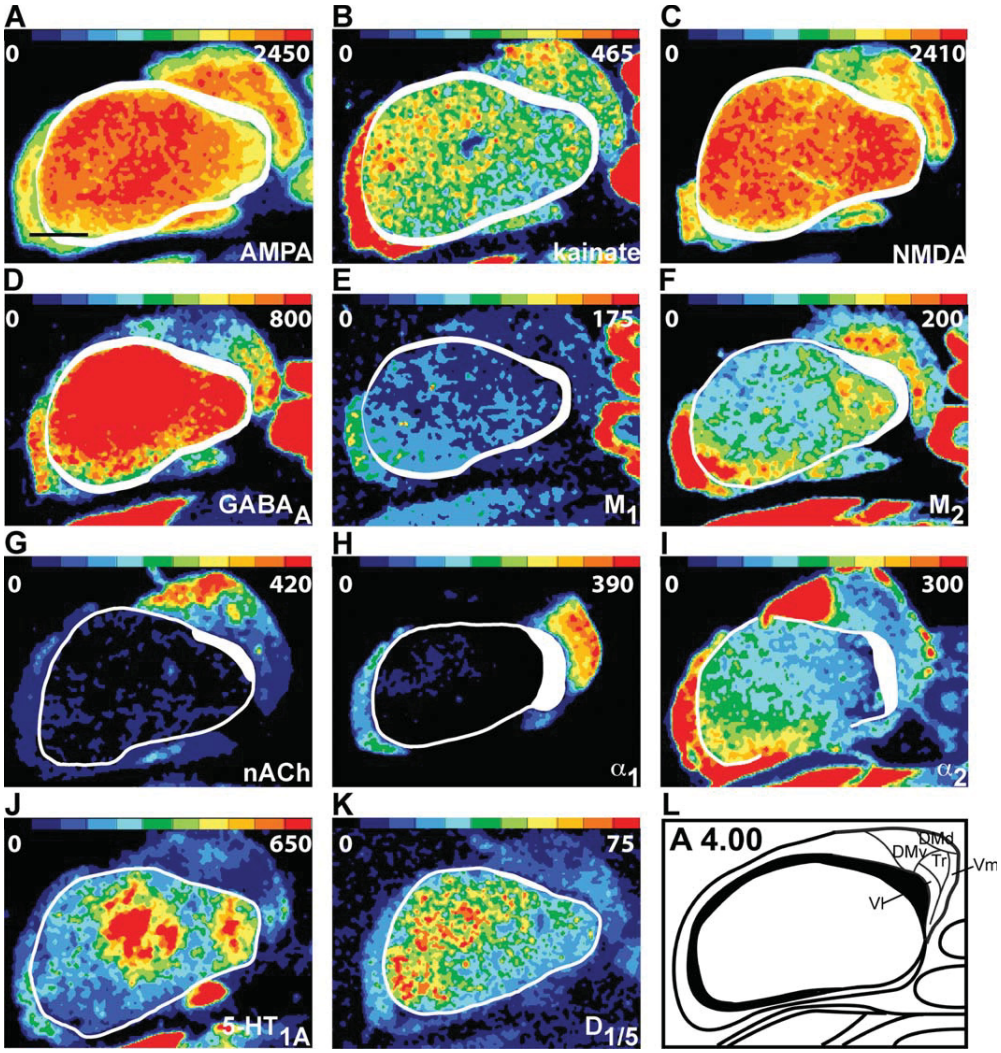

Figure 6. Color-coded autoradiographs showing the distribution and density of AMPA, kainate, NMDA, $GABA_A$, M_1, M_2, nicotinic cholinergic (nACh), α_1, α_2 $5\text{-}HT_{1A}$, and $D_{1/5}$ receptors in coronal sections through the pigeon HF around rostrocaudal level A 4.00 (**A–L**). Densities can be read using the scale for each receptor on the top of each autoradiograph. Note that the end of the red scale indicates the best fit for the investigated HF substructures but not the maximal densities. White outlines show the location of the ventricle. Scale bar = 1.3 mm.

prevent any metal or chloride ions from contaminating working solutions or labware until completing incubation in developer solution, because such ions can interfere with autometallographic zinc labeling.

Sections were analyzed with a Zeiss Axio Imager M1 Microscope (Carl Zeiss) with ×2.5 objective. HF images at A 9.50, A 8.00, A 6.50, and A 5.00 (according to the atlas of Karten and Hodos, 1967) were taken with an AxioCam MRM (Carl Zeiss) and the software AxioVison 4.8 (Carl Zeiss) with an exposure time of 8.4 msec.

To demonstrate that the observed labeling was specific to zinc, we carried out two control procedures. One control pigeon was perfused without using Na_2S. For a second control pigeon, the developer solution was prepared without silver nitrate. Further steps were performed as described above.

RESULTS

Figure 2 displays representative Nissl-stained sections and schematic images of the HF subdivisions used to map the receptor radiographs and zinc labeling. Beginning ventromedially and moving dorsolaterally, we subdivided HF into a ventromedial region (V-complex) with a medial cell layer (Vm), triangular region (Tr), lateral cell layer (Vl), dorso-dorsomedial region (DMd), ventro-dorsomedial region (DMv), dorso-dorsolateral region (DLd) and ventro-dorsolateral region (DLv).

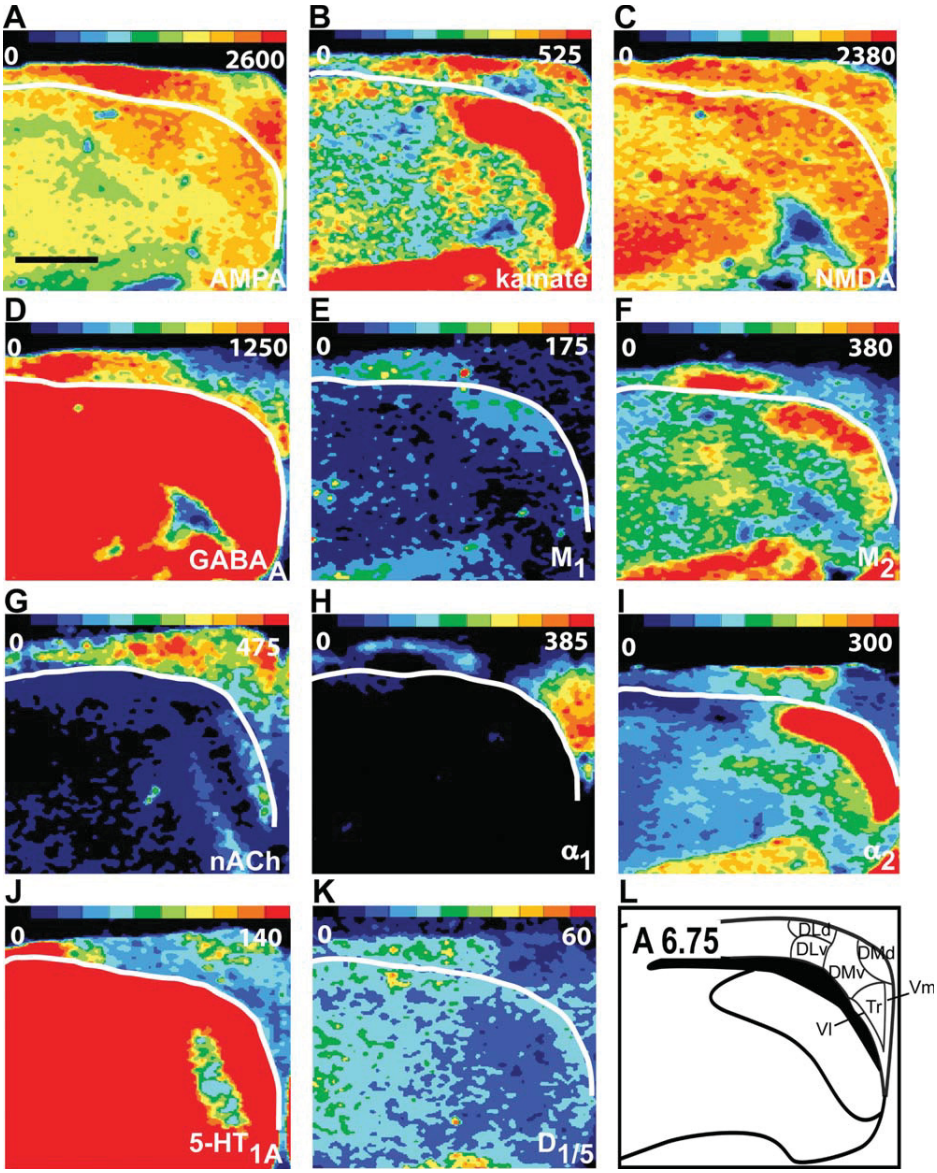

Figure 7. Color-coded autoradiographs showing the distribution and density of AMPA, kainate, NMDA, $GABA_A$, M_1, M_2, nicotinic cholinergic (nACh), α_1, α_2 5-HT_{1A}, and $D_{1/5}$ receptors in coronal sections through the pigeon HF around rostrocaudal level A 6.50 (**A–L**). Densities can be read using the scale for each receptor on the top of each autoradiograph. Note that the end of the red scale indicates the best fit for the investigated HF substructures but not the maximal densities. The white outlines show the location of the ventricle. Scale bar = 1.1 mm.

Receptor-binding site densities in the HF

Binding site densities of all receptors are presented in a two-dimensional polar coordinate plot to construct a multireceptor fingerprint for each analyzed receptor for all HF subdivisions (see Fig. 5). Glutamatergic AMPA and NMDA receptors and GABAergic $GABA_A$ receptors displayed the highest densities. By contrast, muscarinergic cholinergic M_1, serotonergic 5-HT_{1A}, and dopaminergic $D_{1/5}$ receptors displayed low densities throughout HF (see Fig. 5). As illustrated in the color-coded autoradiographs, in general, most of the HF subdivisions were labeled by glutamate and $GABA_A$ receptors, and it is noteworthy that noradrenergic α_1 and α_2 receptors nicely resolved some subdivisions (Figs. 6, 7). All receptor binding site densities are given in fmol/mg protein.

AMPA

Comparisons between all studied subdivisions using a Friedman ANOVA showed significant regional differences

of the AMPA receptor densities (χ^2 [N = 6, df = 6] = 25.64, $P < 0.001$). AMPA receptor concentrations varied from 1,164 ± 77 fmol/mg in DMd to 1,802 ± 58 fmol/mg in Dlv (Figs. 5–7). A high receptor density was also found in Tr (1,777 ± 80 fmol/mg). In general, densities of the dorsolateral subdivisions were higher than those of the dorsomedial subdivisions, with DMd showing the lowest binding site densities among the dorsal regions. Densities in DLd were higher than densities in DMd (N = 6, T = 1, $P < 0.05$), and DLv was different from DMv and DMd (both N = 6, T = 0, $P < 0.05$). AMPA receptor labeling clearly separated DMd and DMv from the V-complex, which showed higher binding site densities. DMv and DMd showed lower densities of AMPA receptors than Tr and Vl (all N = 6, T = 0, $P < 0.05$), and only DMd was additionally different from Vm (N = 6, T = 0, $P < 0.05$). DMd was also different from DMv. DMv displayed a binding site density of 1,611 ± 67 fmol/mg, which was about 50% higher compared with DMd (N = 6, T = 0, $P < 0.05$). Within the V-complex, the higher receptor density in Tr can be distinguished from Vm (N = 6, T = 0, $P < 0.05$).

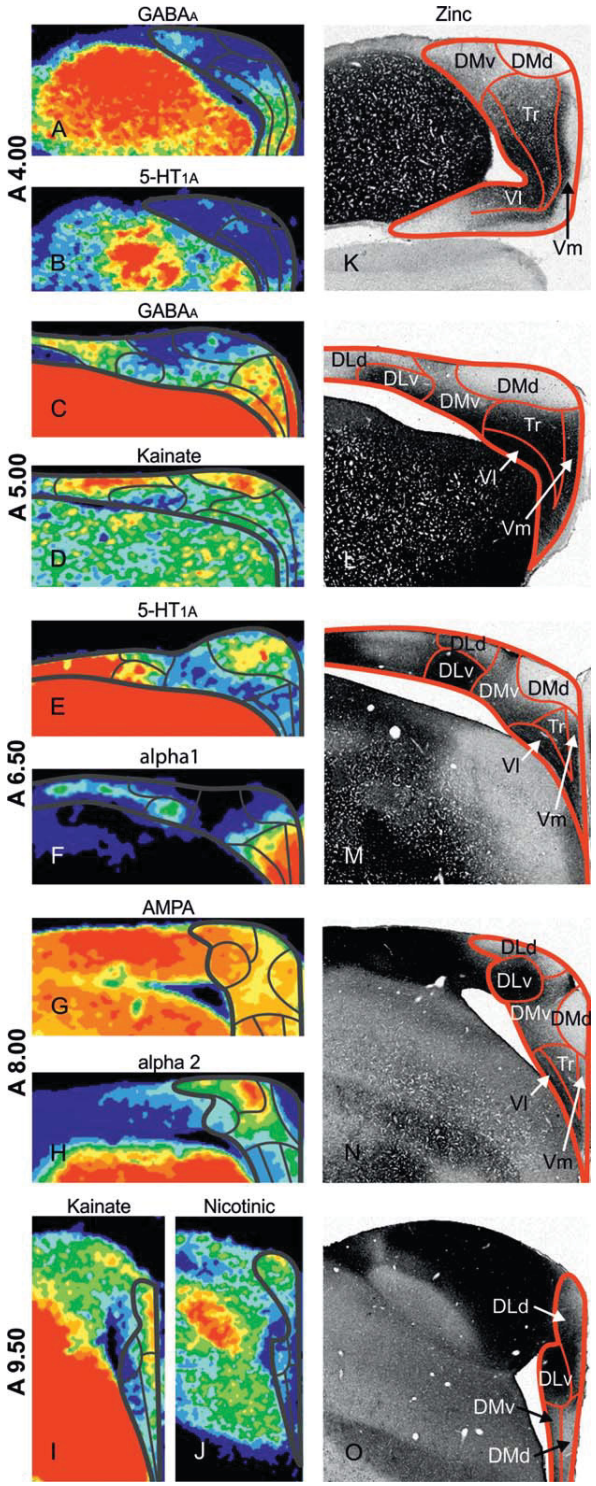

Kainate

The densities of kainate receptors varied between the HF subdivisions (χ^2 [N = 6, df = 6] = 29.50, $P < 0.001$). Highest densities for kainate receptors were detected in DLd (398 ± 15 fmol/mg) and lowest in DMv (238 ± 23 fmol/mg; Figs. 5–7). In the dorsolateral region, DLd and DLv showed different binding site densities (N = 6, T = 0, $P < 0.05$). More than any other ligand, labeling of kainate in DMd, with a concentration of 328 ± 23 fmol/mg, clearly separated it from surrounding subdivisions as DMd displayed lower densities than DLd and higher densities than DMv (both N = 6, T = 0, $P < 0.05$; Fig. 8). In the V-complex, a stepwise decrease in kainate binding site concentration could be observed from Vl (303 ± 29 fmol/mg) to Tr (289 ± 27 fmol/mg) to Vm (245 ± 23 fmol/mg; Vl and Tr: N = 6, T = 1, $P < 0.05$; Tr and Vm: N = 6, T = 0, $P < 0.05$; Vl and Vm: N = 6, T = 0, $P < 0.05$; Fig. 5).

NMDA

Similarly to AMPA receptors, NMDA receptors were highly expressed in HF. The Friedman ANOVA revealed a significant overall effect (χ^2 [N = 6, df = 6] = 26.57, $P < 0.001$). The highest amounts of NMDA labeling were detected in Tr (1,855 ± 83 fmol/mg) and the

Figure 8. Color-coded autoradiographs and zinc labeling in the pigeon hippocampal formation (HF). **A–J:** Color-coded autoradiographs of selected receptors at selected rostrocaudal levels from A 4.00 to A 9.50 highlighting subdivision differences designated by different receptor densities. Red areas indicated high receptor densities; blue areas showed low receptor densities. **K–O:** Subdivision differences in zinc labeling observed in the pigeon HF from rostrocaudal levels A 4.00 to A 9.50. Black areas were high in zinc, and light gray areas were low in zinc.

lowest in DMd (1,297 ± 76 fmol/mg; Figs. 5–7). Binding site densities for NMDA receptors were homogeneously distributed throughout DLd (1,543 ± 141 fmol/mg) and DLv (1,646 ± 85 fmol/mg; N = 6, T = 5, n.s.). Dorsomedially, DMv showed considerably higher concentrations of NMDA receptor labeling (1639 ± 98 fmol/mg) than DMd (N = 6, T = 0, $P < 0.05$). Furthermore, DMv was clearly distinct with respect to the V-complex (DMv and Tr: N = 6, T = 0, $P < 0.05$; DMv and Vl and DMv and Vm: both N = 6, T = 1, $P < 0.05$). In the V-complex, Tr showed a higher density of NMDA receptors compared with Vm (N = 6, T = 0, $P < 0.05$) but not Vl (N = 6, T = 2, n.s.). However, Vl showed a higher density (1,768 ± 82 fmol/mg) than Vm (1,456 ± 93 fmol/mg; N = 6, T = 0, $P < 0.05$). Notably, NMDA displayed a relatively more homogeneous binding site pattern in rostral HF compared with the more regionally distinctive pattern in caudal HF (Figs. 6, 7).

GABA$_A$

$GABA_A$ receptor densities varied from 807 ± 72 fmol/mg protein in Vl to 221 ± 33 fmol/mg in DMd (χ^2 [N = 6, df = 6] = 28.79, $P < 0.001$; Figs. 5–8). The dorsolateral regions DLd (588 ± 54 fmol/mg) and DLv (658 ± 40 fmol/mg) showed an approximately threefold higher receptor concentration compared with DMd (221 ± 33 fmol/mg). DMd showed lower $GABA_A$ receptor density than DLv, DLd, and DMv (all N = 6, T = 0, $P < 0.05$), and DMv (415 ± 55 fmol/mg) showed lower densities than DLd (N = 6, T = 1, $P < 0.05$) and DLv (N = 6, T = 0, $P < 0.05$). Furthermore, DMv and DMd differed from all V-complex subdivisions (all N = 6, T = 0, $P < 0.05$, except for DMv and Vm: N = 6, T = 1, $P < 0.05$). Indeed, the low $GABA_A$ receptor densities in DMd and DMv clearly separate the entire DM from the neighboring ventromedial and dorsolateral regions (Figs. 6–8). In the V-complex, $GABA_A$ receptor densities decreased from Vl (807 ± 72 fmol/mg) to Tr (601 ± 57 fmol/mg) to Vm (546 ± 43 fmol/mg; Figs. 5–8). However, significant differences could be detected only between Vl and Tr (N = 6, T = 0, $P < 0.05$) and Vl and Vm (N = 6, T = 0, $P < 0.05$).

M$_1$

Muscarinergic cholinergic M_1 receptors were barely detectable throughout HF (Figs. 5–7). Modestly high receptor densities could be seen in DLd (69 ± 7 fmol/mg) and DLv (107 ± 5 fmol/mg). In the rest of HF, M_1 receptor density ranged between 27 ± 3 fmol/mg in Vm and 57 ± 7 fmol/mg in DMv. Statistical analysis revealed a significant regional overall effect (χ^2 [N = 6, df = 6] = 34.64, $P < 0.001$). Subsequent post hoc analyses showed that all subdivisions displayed different densities of M_1 receptors compared with each other (all N = 6, T = 0, $P < 0.05$), except for the comparisons between DLd and DMv (N = 6, T = 4, n.s.) and DMd and Tr (N = 6, T = 5, n.s.; Figs. 5–7).

M$_2$

M_2 receptor binding resulted in a clear parcellation of HF into its subdivisions (Figs. 5–7). Lowest densities were detected in DMd (64 ± 13 fmol/mg), with highest densities (267 ± 24 fmol/mg) in DLv. The Friedman ANOVA resulted in a significant overall effect (χ^2 [N = 6, df = 6] = 29.43, $P < 0.001$). DLv showed higher amounts of M_2 receptors than DLd (179 ± 13 fmol/mg; N = 6, T = 1, $P < 0.05$) and DMv (111 ± 22 fmol/mg; N = 6, T = 0, $P < 0.05$). The densities of M_2 receptor in DMd were lower than in all other regions (all N = 6, T = 0; $P < 0.05$). Receptor density decreased from Vl (140 ± 20 fmol/mg) to Tr (125 ± 23 fmol/mg; N = 6, T = 0, $P < 0.05$) to Vm (97 ± 14 fmol/mg protein; compared with Tr N = 6, T = 1, $P < 0.05$). DMv densities were not different from any subdivision of the V-complex (Vl N = 6, T = 3, n.s.; TR and Vm N = 6, T = 6, n.s.; Figs. 5–7).

nACh

Binding sites for nACh receptors showed an inverse pattern of densities in DLd and DLv compared with both muscarinergic cholinergic receptor types (Figs. 5–8). A significant overall effect was detected with the Friedman ANOVA (χ^2 [N = 6, df = 6] = 27.57, $P < 0.001$). The concentration of nACh receptors was higher in DLd (228 ± 22 fmol/mg) compared with DLv (167 ± 16 fmol/mg; N = 6, T = 0, $P < 0.05$). Highest binding site density was detected in DMv (273 ± 31 fmol/mg). DMd (190 ± 18 fmol/mg) displayed a lower binding density for nACh receptors than DMv and DLd (both N = 6, T = 0, $P < 0.05$). Density for nACh receptors in DMv was also higher compared with DLd, DLv, Vl (172 ± 15 fmol/mg) and Vm (166 ± 18 fmol/mg; all N = 6, T = 0, $P < 0.05$) but not Tr (262 ± 32 fmol/mg; Figs. 5–8).

α_1

The Friedman ANOVA revealed a significant regional effect of noradrenergic α_1 receptors in the pigeon HF (χ^2 [N = 6, df = 6] = 31,57, $P < 0.001$). Noradrenergic α_1 receptors were detected at only 16 ± 1 fmol/mg in DMd, but substantially higher amounts of 226 ± 11 fmol/mg were found in Tr (Figs. 5–8). DLd (67 ± 5 fmol/mg) and DLv (74 ± 4 fmol/mg) displayed intermediate densities of α_1 adrenoreceptors. Vl (172 ± 14 fmol/mg) and Vm (177 ± 27 fmol/mg) showed similar α_1 receptor densities. The α_1 receptor binding with [^{3}H]prazosin generally rendered the entire V-complex

distinctive (Figs. 6–8). DMv displayed at least a fourfold lower density (36 ± 4 fmol/mg) than any ventromedial region and was distinct from all other regions (all N = 6, T = 0, $P < 0.05$). The lowest density of noradrenergic α_1 receptors in the HF was detected in DMd (all N = 6, T = 0, $P < 0.05$).

α_2

Whereas α_1 adrenoreceptors were highly expressed in the V-complex, α_2 adrenoreceptors showed high densities in the dorsolateral and dorsomedial regions. Densities of α_2 adrenoreceptors in the HF varied from 441 ± 48 fmol/mg in DMv to 153 ± 19 fmol/mg in DMd (Figs. 5–8). The Friedman ANOVA detected a significant regional overall effect (χ^2 [N = 6, df = 6] = 30.07, $P < 0.001$). Densities of α_2 adrenoreceptors in DMd were threefold lower than in DMv (N = 6, T = 0, $P < 0.05$; Figs. 5–7). Densities in DMv were also higher in comparison with the regions of the V-complex (Vl & Tr N = 6, T = 0, $P < 0.05$; Vm N = 6, T = 1, $P < 0.05$). In the V-complex, Vl (271 ± 28 fmol/mg) showed higher densities than Tr (201 ± 21 fmol/mg; N = 6, T = 0, $P < 0.05$) but not Vm (220 ± 19 fmol/mg; N = 6, T = 4, $P = 0.17$). The noradrenergic α_2 adrenoreceptors were also abundant but unequally distributed in DLd (418 ± 31 fmol/mg) and DLv (354 ± 18 fmol/mg; N = 6, T = 0, $P < 0.05$).

5-HT_{1A}

The expression of serotonergic 5-HT_{1A} receptors was generally low throughout the pigeon HF (Figs. 5–8), and no significant regional overall differences were detected (χ^2 [N = 6, df = 6] = 10.00, $P = 0.15$). However, a notably stronger signal could be found in DMd in some sections, especially at the border between DMd and DMv (see, e.g., Fig. 8). However, this stronger signal seemed to be highly variable across pigeons; no significant difference was detected between DMd (46 ± 3 fmol/mg) and neighboring DMv (40 ± 3 fmol/mg), DLd (44 ± 5 fmol/mg), or DLv (42 ± 3 fmol/mg). Densities in the V-complex varied and showed the highest value in Vl (60 ± 10 fmol/mg).

$D_{1/5}$

Dopaminergic $D_{1/5}$ receptors showed the lowest densities of all measured receptor types (Figs. 5–7). However, the Friedman ANOVA detected a significant regional overall effect (χ^2 [N = 6, df = 6] = 22.86, $P < 0.001$). The maximal density was 26 ± 3 fmol/mg in DLv (all comparisons N = 6, T = 0, $P < 0.05$; except for the comparison between DLv & DLd N = 6, T = 1, $P < 0.05$). Although $D_{1/5}$ receptors provided little obvious separation among the HF subdivisions, the boundary between DMd and DMv was rendered distinctive by an almost complete lack of $D_{1/5}$ receptors in DMd (Figs. 5–7). DMd showed the lowest receptor density compared with all other DM and DL structures (13 ± 1 fmol/mg; all N = 6, T = 0, $P < 0.05$).

Zinc staining

Although we did not see distinct layers of mossy fibers as found in rat hippocampus (but see Discussion), there is heterogeneity in the density of labeling that maps remarkably well onto our subdivision boundaries (Fig. 8). Moving from ventromedially to dorsolaterally, high zinc density indicated by the dense black labeling is clearly seen throughout Vl, Vm, and Tr. This dense labeling is diminished in DMv, and labeling is virtually nonexistent in DMd. In dorsolateral DLv, dense labeling is seen again, but moderate labeling, similarly to DMv, is seen in DLv. The zinc data clearly indicate a well-defined boundary between the rich labeling in the V-complex and the absence of labeling in DMd. Also noteworthy is that zinc does not seem to distinguish between DMv and DLv.

DISCUSSION

Summary of main findings

By using receptor autoradiography for 11 different neurotransmitter receptors and zinc staining, we show that the hippocampal formation of the pigeon can be subdivided into seven subdivisions, which match well with other subdivisional schemes based on neurotransmitter distribution (Erichsen et al., 1991) and connectivity (Kahn et al., 2003; Atoji and Wild, 2004). Additionally, our data offer a further basis for comparing subdivisions of the mammalian and avian hippocampal formation. Our approach has the advantage that we can compare the receptor architecture of an evolutionarily ancient brain structure, which retains a similar role in spatial cognition in species that have had independent evolutionary histories for about 300 million years. Similarities between birds and mammals may offer insight into how selective pressure may conserve basic receptor traits regardless of structural differences. In addition, it remains uncertain whether clear similarities exist among the subdivisions of avian and mammalian HF. Therefore, an important goal of our study was to compare the receptor architecture of the pigeon and mammalian HF to assess better which, if any, avian subdivisions may correspond best to the mammalian hippocampal DG, CA fields, subiculum, and EC.

Subdivisional organization of the avian hippocampal formation: previous studies

Different criteria have been used to define subdivisions of the HF in diverse bird species (Casini et al.,

1986; Erichsen et al., 1991; Krebs et al., 1991; Montagnese et al., 1996; Székély, 1999; Atoji et al., 2002; Kahn et al., 2003; Atoji and Wild, 2006; Nair-Roberts et al., 2006; Suarez et al., 2006; Mayer et al., 2009; Sherry, 2011). During the first part of the twentieth century, judging from comparative studies between reptiles and different types of mammals (e.g., rodents, insectivores, and chiroptera; Rose, 1912) and birds (e.g., chicken and pigeons; Rose, 1914), Rose divided the caudal part of the avian dorsomedial forebrain into a ventrally located Ammon's formation and a dorsally located entorhinal area, which, in his opinion, were comparable to the similarly named regions in mammals (Rose, 1914, 1926). In 1930, Craigie studied the kiwi's (*Apteryx australis*) brain and named the dense cellular layer between Rose's Ammon's formation and entorhinal area the *fascia dentate*, which was not included in Rose's earlier analysis. A few years later, Craigie (1935) studied the emu's (*Dromiceius novaehollandiae*) brain. He introduced the terms *hippocampal area* and *parahippocampal area* (APH) based on cell types and their arrangement. However, a clear border between the ventral and dorsal parts of HF as well as between the APH and the hyperpallium apicale (HA) were not defined. Furthermore, the HF in most other bird species is considerably smaller than that in the emu, so the emu classification is difficult to apply to other bird species.

Using Nissl staining and the previous data, Karten and Hodos (1967) divided the pigeon hippocampal formation into two regions, a hippocampus proper and the APH. Analysis of neurotransmitters and related enzymes with immunohistochemical methods offered the first higher resolution HF subdivision scheme and revealed seven candidate subdivisions (Erichsen et al., 1991; Krebs et al., 1991). A later electrophysiological study was able to resolve five of these subdivisions (Siegel et al., 2000). Probably the most influential subdivisional scheme of the avian HF comes from the work of Atoji and Wild (2004, 2006). Using tract tracing and Nissl staining, they divided the pigeon hippocampal formation into a dorsomedial region (DM), a dorsolateral region (DL), a medial V-complex region (V), which included a triangular region (Tr) with adjacent ventromedial (Vml) and ventrolateral (Vll) cell layers. Also located dorsomedially were three smaller areas, a magnocellular (Ma), a parvocellular (Pa), and a cell-poor (Po) region (Atoji and Wild, 2004, 2006). Additionally, Atoji and Wild (2004, 2006) showed that DM could be further subdivided into a lateral portion (DMl) and a medial portion (DMm). DL could also be further subdivided into a dorsal portion (DLd) and a ventral portion (DLv). It is the subdivisional scheme of Atoji and Wild (2004) that we used to create our provisional subdivisional map, and indeed it is remarkable how well many of the receptors studied here, as well as the zinc labeling, respected the borders of these subdivisions.

Boundaries and subdivisions of the pigeon HF based on receptor autoradiography

Consistent with earlier studies using immunohistochemical (Krebs et al., 1991; Erichsen et al., 1991) and tract tracing (Atoji and Wild, 2004, 2006; Kahn et al., 2003) analyses, the receptor data indicated relatively sharp boundaries between the most lateral portions of HF, namely, DLd and DLv, and laterally adjacent areas (for some examples see Figs. 6–8). The border between HA and dorsolateral HF was especially visible with AMPA, $GABA_A$, M_2, α_1, α_2, and 5-HT_{1A} receptor labeling. Densities of AMPA, $GABA_A$, M_2, and 5-HT_{1A} receptors were higher in HA than in neighboring DLd and DLv, whereas densities of α_1 and α_2 receptors were lower (quantitative HA data not presented).

More posteriorly, dorsolateral HF has been typically distinguished from the neighboring dorsolateral corticoid area (CDL) based on its shape; CDL is characterized as a uniformly thin wall, whereas DL decreases in thickness as it approaches CDL laterally (Montagnese et al., 1993; Atoji and Wild, 2004, 2006). Our ligand maps, by contrast, reveal a much clearer boundary. The border between HF and CDL is particularly distinct with $GABA_A$, M_2, α_1, α_2, and 5-HT_{1A} receptor labeling (Figs. 6, 7). Densities of $GABA_A$, α_1, and 5-HT_{1A} receptors are higher in the CDL than in dorsolateral HF, whereas M_2 and α_2 receptor densities are lower (quantitative data for CDL not presented; Herold et al., 2011, 2012). Also notable is that in more caudal HF CDL borders DMd and DMv as DLd and DLv disappear (for examples see Fig. 8).

Receptor imaging also allowed identification of a boundary between the HF dorsolateral subdivisions, DLd and DLv, and the adjacent dorsomedial structures, DMd and DMv. Densities of AMPA, kainate, $GABA_A$, M_1, M_2, and α_1 receptors were higher in DLd and DLv, whereas nACh receptors were lower in DLd and DLv compared with, in particular, DMv (Figs. 5–7). In general, the multireceptor mapping supports the identification of seven subdivisions as proposed by Erichsen et al. (1991) and Atoji and Wild (2004, 2006).

Glutamate receptors

Glutamate AMPA and NMDA receptor densities were high in all regions of the pigeon HF. AMPA binding did not vary between DLd and DLv, but clearly separated DL from DMv. Furthermore, DMd displayed a relatively low concentration compared with the other regions and could be clearly separated from DMv. In general, DM

showed lower densities than the surrounding DL and V-complex ventromedial regions. In the V-complex, AMPA binding was lower in Vm compared with Tr. Our results showed higher AMPA densities in the pigeon HF compared with those reported for [^{3}H]AMPA binding in marsh tits (*Parus palustris*) and blue tits (*Parus caeruleus*; Stewart et al., 1999). Furthermore, there seemed to be no differences in AMPA receptor densities between DL (their APH) and DM/V-complex (their Hp) in tits.

An immunhistochemical analysis of glutamatergic AMPA receptor subunits revealed that GluR1, GluR2/3, and GluR4 are expressed in the pigeon HF (Rosinha et al., 2009). Especially GluR1 and GluR2/3 were expressed pre dominantly in so-called IR and T neurons, whereas GluR4 was expressed predominantly in so-called R neurons. IR neurons are multipolar projection neurons, T neurons are triangular pyramidal neurons, and R neurons are ovoid or stellate cells that may be glial cells or local interneurons (Tömböl et al., 2000a; Atoji et al., 2002). Rosinha et al. (2009) observed intense labeling for GluR1 and GluR2/3 in the V-complex, in which we detected high AMPA receptor densities as well.

Generally fewer kainate receptors were expressed compared with NMDA or AMPA, but kainate receptors showed a differential regional distribution pattern. Kainate receptor density reached a maximum in DLd and DMd, and the lowest densities were measured in DMv. Again, DMv was distinct from the surrounding DL, ventromedial regions, and DMd. In the V-complex, a stepwise decrease in receptor density could be detected from Vl to Tr to Vm. We are aware of no other studies that have looked at kainate receptor binding in birds.

NMDA receptor binding discriminated mainly among DMd, DMv, and the V-complex. Highest NMDA receptor densities were found in Vl and Tr, and the lowest densities were detected in DMd. Similarly to AMPA receptors, NMDA receptor binding in the V-complex separated Tr from Vm but not Vl. Furthermore, the pattern of NMDA receptors seemed to become increasingly distinctive in the subdivisions of the more caudal part of HF. Compared with our present results, densitometric measurements of NMDA receptor binding with [^{3}H]MK801 in blue and marsh tits showed the same overall densities in the HF of blue tits and slightly lower densities for marsh tits (Stewart et al., 1999). However, in both marsh and blue tits, there seemed to be only small overall differences in NMDA receptor densities between DL (their APH) and DM/V-complex (their Hp).

$GABA_A$ receptor

Examination of $GABA_A$ receptor densities showed again a clear boundary between HF dorsolateral and dorsomedial regions. Densities decreased overall from DL to DMv to DMd. In addition, DMv was different from the V-complex, which showed higher $GABA_A$ receptor densities. Within the V-complex, a decrease from Vl to Tr to Vm was observed. Earlier binding studies in pigeons did not show differences in $GABA_A$ receptor labeling in the Hp/APH region (Veenman et al., 1994). However, our pattern of $GABA_A$ receptor density is in general agreement with results from other bird species looking at GABAergic neurochemistry. In members of the Corvidae and Paridae, calbindin distribution divides HF into five main regions, and the medial and the lateral branches of what would be the V-complex are different (Montagnese et al., 1993). Glutamate decarboxylase (GAD; an enzyme in GABAergic interneurons) was found homogeneously distributed in the neuropil of the pigeon DM and DL, and in small to medium-sized immunoreactive cells throughout the entire HF (Krebs et al., 1991). The pattern of GAD was approximately coextensive with the calbindin staining of Montagnese et al. (1993). As with the intensely GAD- and calbindin-labeled areas, we found high densities of $GABA_A$ receptors throughout the entire pigeon DL and Vl. By contrast, $GABA_A$ receptors were relatively weakly expressed in DM, particularly in DMd.

Cholinergic receptors

The different cholinergic receptors were each distinctly distributed throughout the HF. M_1 densities were highest, followed by M_2 and nACh. M_1 receptors showed the highest concentration in DLv and lower densities in DLd, DMv, and Tr. A low M_1 receptor density rendered DMd distinct from the other regions. In the V-complex, densities decreased from Vl to Tr to Vm, again showing a difference in receptor profile between the medial and the lateral dense cell layers. A similar receptor distribution pattern was also found for M_2 receptors. By contrast, nACh receptor binding showed higher densities in DLd compared with DLv. Both DLv and DLd were different from DMv, whereas DMv again was not distinguishable from Tr. However, higher densities in Tr separated this region from Vl and Vm.

Analysis of muscarinic (M-type) receptors with [^{3}H]N-methyl scopolamine showed no differences in densities between DM/V-complex (their Hp) and DL (their APH) in quail (*Coturnix coturnix japonica*) but higher amounts of M-type receptors in DL compared with DM/V-complex in starlings (*Sturnus vulgaris*; Ball et al., 1990). The densities of M-type receptors in the quail and starling HF were higher across all major subdivisions compared with our findings in pigeon. Although the difference could be explained by species variation, probably more important is the use of subtype-specific ligands for the

group of M-type receptors in our study. Our binding protocols label M_1 and M_2 subtypes separately, which can explain the higher densities for all M-type receptors found by Ball et al. (1990). Our findings are also in line with an earlier autoradiographic study, which showed only low to moderate densities of M-type receptors, 25–250 fmol/mg protein, in DL and DM/V-complex of the pigeon (Dietl et al., 1988). As with starlings (Ball et al., 1990), pigeons showed higher densities of M-type receptors in DL than in all other HF subregions. Weak labeling of muscarinic cholinergic receptors was found in DMd, but nACh receptors occurred at a relatively high density in DMd (see Fig. 5).

Monoaminergic receptors

Monoaminergic receptors showed highly variable densities in the pigeon HF. Highest densities were observed for noradrenergic α receptors and lowest for $D_{1/5}$ receptors α_1 Receptors were expressed in the V-complex region, with highest densities both in Tr and in Vm. This finding is in contrast to the lower density in Vl. The α_1 receptor density of the V-complex was clearly different from that of DMv. DMv can be separated from DMd, DLd, and DLv by differences in α_1 receptor density. However, DLd and DLv could not be discriminated by their α_1 receptor binding. α_2 Receptor binding was higher in DMv and the DL regions. By contrast, α_2 receptors were more dense in DLd compared with DLv but did not differ from DMv. Again, DMd was rendered distinct by its lower α_2 receptor density compared with DMv, DLd, and DLv. In the V-complex, a relatively homogeneous distribution of α_2 receptors was detected. Vl showed higher densities compared with Tr but not Vm. Our results seem to be in line with the distribution of α_2 receptors in the European starling (Heimovics et al., 2011). Although not quantified in their publication, the autoradiographs of the starling HF look similar to the autoradiographs that we obtained for pigeons.

Serotonergic 5-HT_{1A} receptors did not differ among any of the subdivisions. This has already been reported for DL and the DM/V-complex (APH and Hp, respectively, in Herold et al., 2012). The quantitative result is somewhat surprising, because a higher density in DMd was detected by visual inspection in a number of brain sections (see Figs. 6, 7). Similarly to the neurotransmitter 5-HT labeling in DMd and DMv (DMs and parts of DMi in Krebs et al., 1991), 5-HT_{1A} receptor labeling in our study seemed to slowly decrease from rostral to caudal HF, perhaps obscuring subdivision differences in 5-HT_{1A} receptor density.

Dopaminergic $D_{1/5}$ receptors were differentially distributed between DLv and all other subregions. They reach their highest densities in DLv compared with the other subregions. Additionally, lower $D_{1/5}$ densities were observed in DMd compared with the surrounding regions. As in our results, tyrosine hydroxylase (TH) was detected mainly in the dorsal parts of the pigeon HF (Krebs et al., 1991). In general, the low densities of $D_{1/5}$ receptors observed in the pigeon HF are in line with former studies in pigeons, quails, and chicken (*Gallus gallus*; Dietl and Palacios, 1988; Ball et al., 1995; Schnabel and Braun, 1996; Kleitz et al., 2009).

Comparison with the mammalian hippocampal formation

The avian HF and mammalian hippocampus develop from the same portion of the telencephalon (Kallen, 1962; Rodriguez et al., 2002), share the same cell types (Molla et al., 1986; Tömböl et al., 2000a), and have similar neurochemical profiles (Erichsen et al., 1991; Krebs et al., 1991). A special characteristic of both the avian HF and the mammalian hippocampus is adult neurogenesis (Altman, 1962; Barnea and Nottebohm, 1994; Eriksson et al., 1998; Hoshooley et al., 2005; Ming and Song, 2005; Pytte et al., 2007). The similarities may explain the presumably conserved role of both the avian HF and the mammalian hippocampus in cognition (Sherry et al., 1992; Colombo and Broadbent, 2000). However, the connections to other brain areas, e.g., septum, hypothalamus, brainstem nuclei, and telencephalic sensory processing areas, are not fully identical (Casini et al., 1986; Atoji and Wild, 2006). Furthermore, the cytoarchitectural differences between the avian and the mammalian HF have made it difficult to identify similarities in subdivisional organization (but see Erichsen et al., 1991; Kahn et al., 2003; Atoji and Wild, 2006; Papp et al., 2007).

The mammalian hippocampus is divided into distinct subregions based on anatomical criteria, DG with the hilus region, Ammon's horn (comprising the fields CA1–CA4), and the subiculum (Amaral and Witter, 1989; Insausti, 1993; Amunts et al., 2005; Witter, 2007). Because of the distinct cytoarchitecture of DG and Ammon's horn regions, they can be distinguished from the laterally positioned subiculum and EC. Typically, the CA regions are densely packed with pyramidal neurons, whereas the DG is densely packed with granular cells. In contrast, the avian HF is a more nuclear-like structure, densely packed with heterogeneous populations of neurons with a slow transition into the parahippocampal area (DL). In the mammalian hippocampus, the EC is part of the parahippocampal area (gyrus parahippocampalis) and differs considerably from the hippocampal

regions (Amaral and Witter, 1989; Insausti, 1993; Amunts et al., 2005; Witter, 2007).

Different regions of the avian HF, based on tracing studies, have been proposed to be homologues of the mammalian DG. Székély and Krebs (1996) and Kahn et al. (2003) proposed that DM is a homologue of DG and that the V-complex is a homologue of unspecified CA fields. Atoji and Wild (2004, 2006), by contrast, claimed that DM shows properties of both CA and subiculum, whereas the V-shaped structure (our V-complex), because of its intrinsic connections, seems to be more similar to DG. However, seemingly all researchers agree that DL is comparable to EC (Székély, 1999; Siegel et al., 2002; Atoji and Wild, 2004; Puelles et al., 2007; Rattenborg and Martinez-Gonzalez, 2011).

In general, the receptor autoradiographic analysis of 10 different receptor types in the hippocampus of 11 different mammalian species showed that α_1, M_1, 5-HT_2, $GABA_A$, AMPA, kainate, and NMDA receptor densities were minimally variable across species, whereas α_2, 5-HT_{1A}, and M_2 were highly variably expressed (Palomero-Gallagher, 1999). In many of the species studied and compared with all other hippocampal structures, CA3 showed the lowest receptor densities (Kraemer et al., 1995; Palomero-Gallagher, 1999; Zilles et al., 2000; Cremer et al., 2009). To compare and identify better the subdivision similarities (and differences) between pigeon HF and mammalian hippocampus, we created a summary of the already published receptor data in the mammalian HF (Table 2). This table provides the relative receptor densities for each mammalian hippocampal substructure normalized to the mean value of the investigated receptor type in the total hippocampus. For better comparisons, we also added the relative densities for each substructure of the pigeon HF. As in the pigeon, glutamate receptors showed high densities in the mammalian hippocampus, with higher densities for AMPA and NMDA compared with kainate receptors (Palomero-Gallagher, 1999; Zilles et al., 2000; Topic et al., 2007). In rats (*Rattus norvegicus*) and mice (*Mus musculus*), CA1 showed the highest densities for AMPA and NMDA receptors, followed by DG. In contrast, CA3 and DG were high in kainate receptors (Table 2). Overall, the following conclusions can be drawn: in comparing the relative densities of glutamatergic receptors in the different subdivisions of the rodent hippocampus and pigeon HF, the most striking similarities exist between high kainate receptor densities in Vl, Tr, DMd, and DG/CA3, as well as DLd vs. EC, and low kainate receptor concentrations in Vm/DMv and CA1/CA2. NMDA and AMPA receptor densities were mostly comparable between Vl/Tr/DMv and DG/CA1 (Table 2). Binding of $GABA_A$ receptors with [^{3}H]muscimol showed high receptor densities in the pigeon HF and mammalian hippocampus (Kraemer et al., 1995; Topic et al., 2007; Cremer et al., 2009, 2010). $GABA_A$ receptor densities decreased from Ent to DG to CA1 to CA2 to CA3 in mouse, rat, and marmoset (*Callithrix jacchus*) brains. Again, Vl/Tr/Vm and the DL regions resembled DG/CA1 and EC, respectively. DMv was similar to CA2, and DMd, with its very low $GABA_A$ densities, was comparable to CA3. M receptors were more highly expressed in the marmoset and the rodent hippocampus compared with the pigeon HF, but nACh showed higher densities in pigeons compared with rodents (Pauly et al., 1989; Kraemer et al., 1995; Topic et al., 2007; Wolff et al., 2008; Cremer et al., 2009). In pigeons, cholinergic binding sites nicely discriminated among the different subdivisions; however, no pattern was observed to indicate any correspondence among mammalian and avian hippocampal substructures based on density variation in cholinergic receptors (Table 2). This lack of correspondence may reflect interspecies variability with respect to cholinergic receptor types that may obscure detection of general differences in the hippocampal–cholinergic systems in mammals and birds. The analysis of the monoaminergic receptors revealed that α_2 receptor binding suggests a similarity for CA1/DG and Vl/DMv, whereas lower densities in CA2/CA3 appear to resemble more Tr/Vm/DMd (Table 2; Zilles et al., 1993). 5-HT_{1A} receptors showed comparable relative densities only between DG and Vl and between CA1 and Vm for the rat, but not for mice or other mammals (Table 2; Palomero-Gallagher, 1999). $D_{1/5}$ receptors also suggest a DG more similar to Vl and DMv. The high densities of $D_{1/5}$ receptors in the DL regions are also detected in EC.

Overall, we propose close similarity between DG/CA1 and the Vl/Tr/DMv regions, whereass DMd/Vm might be more comparable to the CA2/CA3 regions. DMd shared several receptor characteristics with CA3, and generally DMv was more similar to CA1 and Vm resembled CA2. The DL regions seemed to be comparable to EC (Fig. 9). This latter finding is in line with the generally accepted similarity between DL and EC (for review see Atoji and Wild, 2006).

Zinc staining

High levels of zinc in the mossy fiber system of rats have led avian researchers to seek a DG equivalent in birds, relying on Timm staining. In previous studies (Faber et al., 1989; Montagnese et al., 1993; Tömböl et al., 2000b) of chick and zebra finch brains, an obvious parallel to DG could not be revealed. An examination of our zinc staining (Fig. 8) also failed to reveal the distinctive labeling suggestive of the layered

TABLE 2.

Comparison of Neurotransmitter Receptor Densities in the Pigeon and Mammalian Hippocampal Formation (HF)[1]

	Relative binding densities in the pigeon HF (%)							Relative binding densities in the mammalian HF (%)					
Receptor	Vl	Tr	Vm	DMv	DMd	DLd	DLv	CA1	CA2	CA3	DG	EC	Species
AMPA	107	109	99	99	71	104	111	109 (1), 114 (2), 117 (5), 102 (6), 110 (4), 115 (7)	90 (1), 87 (2), 94 (5)	86 (1), 78 (2), 94 (5), 95 (4), 90 (7)	97 (1), 104 (2), 95 (5), 98 (6), 96 (4), 94 (7)	68 (6)	Rat, Mouse
Kainate	101	96	81	79	109	132	102	52 (1), 67 (2,6), 59 (5), 71 (4), 63 (7)	74 (1), 58 (2), 69 (5)	140 (1), 127 (2), 174 (5), 116 (4), 113 (7)	124 (1), 113 (2), 132 (6), 97 (5), 113 (4), 125 (7)	134 (6)	Rat, Mouse
NMDA	110	116	91	102	81	96	103	120 (1), 124 (2), 130 (5), 105 (6), 126 (4), 135 (7), 110 (3)	84 (1), 83 (2), 99 (5), 88 (3)	74 (1), 71 (2), 83 (5), 81 (4), 69 (7), 82 (3)	90 (1), 101 (2), 89 (5), 95 (6), 93 (4), 97 (7), 94 (3)	77 (6)	Rat, Mouse, Marmoset
$GABA_A$	147	110	100	76	40	107	120	80 (2), 87 (6), 122 (4), 106 (7), 111 (3)	70 (2), 72 (3)	47 (2), 62 (4), 58 (7), 60 (3)	119 (2), 111 (6), 114 (4), 137 (7), 112 (3)	118 (6)	Rat, Mouse, Marmoset
M_1	74	65	52	109	61	132	206	118 (2), 128 (12), 119 (7), 113 (8), 101 (3)	74 (2), 67 (12), 104 (3)	65 (2), 94 (12), 71 (7), 70 (8), 97 (3)	109 (2), 139 (12), 110 (7), 117 (8), 99 (3)	111(12)	Rat, Mouse, Marmoset
M_2	99	89	69	79	46	127	190	115 (2), 141 (12), 91 (7), 124 (8), 103 (3)	101 (2), 86 (12), 110 (3)	105 (2), 104 (12), 142 (7), 79 (8), 111 (3)	86 (2), 89 (12), 74 (7), 97 (8), 88 (3)	146 (12)	Rat, Mouse, Marmoset
nACh	83	126	80	131	91	109	80	56 (12), 103 (7),	56 (12)	56 (12), 45 (7)	260 (12), 152 (7)	185 (12)	Rat, Mouse
α_1	156	206	161	33	15	61	67	95 (2), 108 (7), 88 (3)	102 (2), 101 (3)	101 (2), 104 (7), 95 (3)	103 (2), 88 (7), 110 (3)	104 (13)	Rat, Mouse, Marmoset
α_2	92	68	75	150	52	142	120	103 (2)	90 (2)	86 (2)	105 (2)	132 (13)	Rat
$5\text{-}HT_{1A}$	130	100	93	87	101	97	93	93 (2), 79 (9), 205 (7)	44 (2)	73 (2), 29 (7)	130 (2), 119 (9), 66 (7)	27 (13)	Rat, Mouse
$D_{1/5}$	96	89	87	98	72	110	148	39 (2), 76 (10)	58 (2)	54 (2)	177 (2), 147 (10)	170 (11)	Rat

[1]Values for each structure correspond to the receptor density in percentage relative to the mean density of the receptor type in the hippocampus (mammals) or the HF (pigeons). The conclusion of this summary is illustrated in Figure 9. (1) Palomero-Gallagher et al., 2003; (2) Topic et al., 2007; (3) Kraemer et al., 1995; (4) Zilles et al., 2000; (5) Martens et al., 1998; (6) Cremer et al., 2009; (7) Cremer et al., 2011; (8) Wolff et al., 2008; (9) Zavitsanou et al., 2010; (10) Savosta et al., 1986; (11) Cremer et al., 2010; (12) Sihver et al., 1997; (13) our unpublished data.

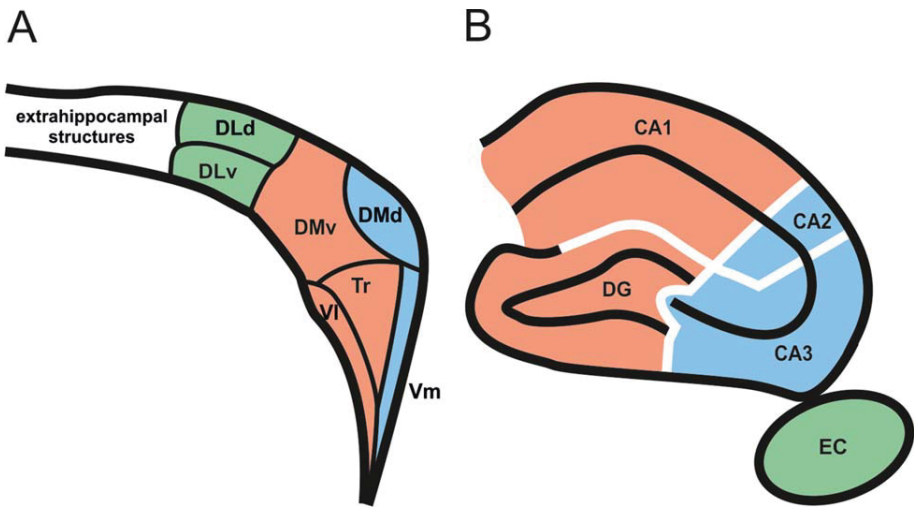

Figure 9. Similarities between receptor distribution in the subdivisions of the pigeon HF (**A**) and receptor distribution in the subdivisions of a typical (idealistic) mammalian hippocampus (**B**). The same colors indicate substantial overlap in relative receptor densities based on semiquantitative comparisons between the pigeon HF and the rat hippocampus (Table 2). Here DMv, Vl, and Tr share similarities with DG and CA1 (indicated in orange), and DMd and Vm share similarities with CA2 and CA3 (indicated in blue), whereas DLd/DLv share similarities with entorhinal cortex (EC; indicated in green). CA1, cornu ammonis field 1; CA2, cornu ammonis field 2; CA3, cornu ammonis field 3; DG, dentate gyrus; DMd, dorsal part of the dorsomedial region of HF; DMv, ventral part of the dorsomedial region of HF; DLd, dorsal part of dorsolateral region of HF; DLv, ventral part of dorsolateral region of HF; EC, entorhinal cortex; Tr, triangular region of the ventromedial region of HF; Vm, ventromedial part of the V-complex; Vl, ventrolateral part of the V-complex.

organization of mossy fibers in rats (Danscher et al., 1973; Danscher and Zimmer, 1978; Zimmer and Haug, 1978). At first glance, our findings also call into question whether mossy fibers, and by inference a strict equivalent to the DG, is present in birds, despite the indicators of our autoradiographic analysis. However, a further examination of Figure 8 shows that the V-complex of the avian HF is densely labeled with zinc, whereas in the DMv area staining is low, and the DMd is almost devoid of zinc staining. In the DL region, high levels of zinc could be observed in the DLv region but not in the DLd. No distinctive laminar-like labeling similar to the rat hippocampus could be observed. In fact, the diffuse but dense labeling in our V-complex resembles the diffuse and dense labeling in the CA regions of the primate hippocampus (Amaral et al., 2007). Therefore, if one considers the density of zinc labeling rather than looking for distinct mossy fibers, our V-complex resembles more the CA regions of mammals and particularly primates. On the other hand, not only the mossy fibers in the mammalian hippocampus are labeled with zinc. Zinc labeling occurred also in the granular cell layer and the molecular layer of DG (Zimmer and Haug, 1978; De Biasi and Bendotti, 1998). Given this fact, our zinc results do not exclude a correspondence between Vl/Tr and DG or Vm/DMv/DMd and the CA regions as suggested by the receptor data. Dense zinc labeling in the DLv and low labeling in DLd is in line with the nonhomogeneous labeling of EC and subiculum in the rat HF (Zimmer and Haug, 1978; Riba-Bosch and Perez-Clausell, 2004).

The colocalization of NMDA receptors and zinc characterizes much of Ammon's horn of the mammalian hippocampus, where glutamate and zinc (Zn^{2+}) are coreleased (Sindreu et al., 2003; Qian and Noebels, 2005). Thus, the extent to which NMDA receptors and zinc colocalize in the avian HF is of additional comparative interest. However, one limitation of our staining technique is that it labeled only vesicular zinc, leaving extracellular zinc undetected. Despite this limitation, examination of the NMDA fingerprint in Figure 5 and the zinc labeling in Figure 8 reveals some notable similarities. Based on the fingerprints, the highest density of NMDA receptors were found in Vl and Tr of the V-complex, where there was also dense labeling for zinc. Vm, by contrast, had lower NMDA receptor densities and less dense zinc labeling. Similarities continue in the two DM subdivisions, where higher NMDA and zinc labeling densities were found in DMv compared with DMd. Overall, there is an apparent correlation between the density of NMDA receptors and the zinc labeling density in the avian HF, a pattern also found in the mammalian hippocampus. From the perspective of possible subdivision parallels, the dense coupling of NMDA

receptors and zinc in Vl and Tr argues for similarity with the CA fields of Ammon's horn.

CONCLUSIONS

Although the mammalian hippocampus and avian HF derive from the same portion of the developing pallium (Reiner et al., 2004; Jarvis et al., 2013), their relationship to the rest of the forebrain is somewhat different. Whereas the mammalian hippocampus interacts, indirectly, with virtually the entire neocortex (Bird and Burgess, 2008), the avian HF has more limited connectivity (Csillag et al., 1994; Leutgeb et al., 1996; Kröner and Güntürkün, 1999; Atoji et al., 2002; Atoji and Wild, 2005). For example, unlike the case for the mammalian hippocampus, only a small projection from the medial septum to HF has been detected (Casini et al., 1986; Atoji and Wild, 2004; Montagnese et al., 2004). Given the incomplete correspondence in the subdivisional organization of the mammalian and avian HF, it is tempting to speculate that the differences in connectivity can in part explain how the two systems evolved different internal characteristics (Aboitiz, 1993; Manns and Eichenbaum, 2005; Papp et al., 2007; Rattenborg and Martinez-Gonzalez, 2011). However, in both mammals and birds, the hippocampal formation shares a number of morphological, physiological, and neurochemical similarities (Krebs et al., 1989; Bingman and Mench, 1990; Erichsen et al., 1991; Montagnese et al., 1993; Colombo et al., 1997; Margrie et al., 1998; Gagliardo et al., 1999; Tömböl et al., 2000a; Atoji et al., 2002; Budzynski et al., 2002; Bingman et al., 2003, 2005; Kahn et al., 2003; Atoji and Wild, 2004, 2005, 2006; Hough and Bingman, 2004; Bischof et al., 2006; Nair-Roberts et al., 2006; Hoshooley and Sherry, 2007; Sherry, 2011; Gupta et al., 2012) and plays a similar role in cognition, especially in spatial cognition (Bingman et al., 1998; Colombo and Broadbent, 2000; Suzuki and Clayton, 2000; Tommasi et al., 2003; Watanabe and Bischof, 2004; Ruploh et al., 2011; Mayer et al., 2012). By comparing the receptor architectonic profile of the pigeon HF with the mammalian hippocampus, we detected a number of shared traits (Fig. 9). However, as indicated by a study in the zebra finch that investigated the expression of immediate early genes during spatial learning, a study that detected individual patch locations that were not in line with previously described hippocampal subdivisions (Mayer et al., 2012), it may be possible that information processing in the HF of birds is, at least in part, different from that in the mammalian hippocampus (but see Kahn et al., 2003). Székély (1999) also came to the same conclusion, that the avian HF probably has a somewhat different wiring organization compared with the mammalian hippocampus. Therefore, in assuming a kind of nonlaminar, network organization for the avian HF (for review see Atoji and Wild, 2006), it may be that there was less selective pressure to organize the avian HF into anatomically discrete subdivisions such as those found in the mammalian hippocampus. Another point is that, although the avian HF and mammalian hippocampus develop from the same type of cells during development, so far expression profiles of selective markers have not clarified whether these cells are more amygdala- or more cortex-like, or both (Reiner et al., 2004; Dugas-Ford et al., 2012; Chen et al., 2013; Jarvis et al., 2013). To understand the development of hippocampal subfields, it is also very important to understand how cells originate, how cells migrate, and during which time window cells express specific genes that organize their future targets during development (Christie et al., 2013; Montiel and Molnar, 2013). As one last consideration, from analysis of gene expression profiles between different species, some researchers have proposed that the DG is one of the most recently evolved structures of the mammalian brain (see Kempermann, 2012). Thus, it may be that birds did not evolve a DG, but this would not exclude the independent evolution of a functional equivalent, as has been shown for the nidopallium caudolaterale of birds and the prefrontal cortex of mammals (Güntürkün, 2012).

Overall, our study reveals an avian HF characterized by distinct subdivisions based on differences in receptor-type distribution and zinc density. Similarities to the mammalian HF could be observed between Vl/Tr/DMv and DG/CA1, between Vm/DMd and CA2/CA3, and between DL and Ent (Table 2, Fig. 9). However, we suggest that 300 hundred million years of independent evolution has led to a mosaic of similarities and differences in the subdivisional organization of the avian HF and mammalian hippocampus and that thinking about the avian HF in terms of the strict subdivisional organization of the mammalian hippocampus is likely insufficient to understand the avian HF.

CONFLICT OF INTEREST STATEMENT

The authors declare that there are no conflicts of interest.

ROLE OF AUTHORS

All authors had full access to all the data in the study and take responsibility for the integrity of the data and the accuracy of the data analysis. Study concept and design: CH, VPB, KZ, OG. Acquisition of data: CH, NP-G, SL, FS. Analysis and interpretation of data:

CH, VPB, MS, OG. Drafting of the manuscript: CH, VPB, OG. Critical revision of the manuscript for important intellectual content: CH, VPB, MS, KZ, OG. Statistical analysis: CH. Obtained funding: VPB, Z, OG. Administrative, technical, and material support: CH, NP-G, SL, FS. Study supervision: CH, NP-G, KZ, OG.

LITERATURE CITED

Aboitiz F. 1993. Further comments on the evolutionary origin of the mammalian brain. Med Hypoth 41:409–418.

Altman J. 1962. Are new neurons formed in the brains of adult mammals? Science 135:1127–1128.

Amaral DG, Witter MP. 1989. The three-dimensional organization of the hippocampal formation: a review of anatomical data. Neuroscience 31:571–591.

Amaral DG, Scharfman HE, Lavenex P. 2007. The dentate gyrus: fundamental neuroanatomical organization (dentate gyrus for dummies). Prog Brain Res 163:3–22.

Amunts K, Kedo O, Kindler M, Pieperhoff P, Mohlberg H, Shah NJ, Habel U, Schneider F, Zilles K. 2005. Cytoarchitectonic mapping of the human amygdala, hippocampal region and entorhinal cortex: intersubject variability and probability maps. Anat Embryol 210:343–352.

Atoji Y, Wild JM. 2004. Fiber connections of the hippocampal formation and septum and subdivisions of the hippocampal formation in the pigeon as revealed by tract tracing and kainic acid lesions. J Comp Neurol 475:426–461.

Atoji Y, Wild JM. 2005. Afferent and efferent connections of the dorsolateral corticoid area and a comparison with connections of the temporo-parieto-occipital area in the pigeon (*Columba livia*). J Comp Neurol 485:165–182.

Atoji Y, Wild JM. 2006. Anatomy of the avian hippocampal formation. Rev Neurosci 17:3–15.

Atoji Y, Wild JM, Yamamoto Y, Suzuki Y. 2002. Intratelencephalic connections of the hippocampus in pigeons (*Columba livia*). J Comp Neurol 447:177–199.

Ball GF, Nock B, Wingfield JC, McEwen BS, Balthazart J. 1990. Muscarinic cholinergic receptors in the songbird and quail brain: a quantitative autoradiographic study. J Comp Neurol 298:431–442.

Ball GF, Casto JM, Balthazart J. 1995. Autoradiographic localization of D1-like dopamine receptors in the forebrain of male and female Japanese quail and their relationship with immunoreactive tyrosine hydroxylase. J Chem Neuroanat 9:121–133.

Barnea A, Nottebohm F. 1994. Seasonal recruitment of hippocampal neurons in adult free-ranging black-capped chickadees. Proc Natl Acad Sci U S A 91:11217–11221.

Bingman VP, Mench JA. 1990. Homing behavior of hippocampus and parahippocampus lesioned pigeons following short-distance releases. Behav Brain Res 40:227–238.

Bingman VP, Strasser R, Baker C, Riters LV. 1998. Paired-associate learning is unaffected by combined hippocampal and parahippocampal lesions in homing pigeons. Behav Neurosci 112:533–540.

Bingman VP, Hough GE 2nd, Kahn MC, Siegel JJ. 2003. The homing pigeon hippocampus and space: in search of adaptive specialization. Brain Behav Evol 62:117–127.

Bingman VP, Gagliardo A, Hough GE 2nd, Ioale P, Kahn MC, Siegel JJ. 2005. The avian hippocampus, homing in pigeons and the memory representation of large-scale space. Integr Comp Biol 45:555–564.

Bird CM, Burgess N. 2008. The hippocampus and memory: insights from spatial processing. Nat Rev Neurosci 9:182–194.

Bischof HJ, Lieshoff C, Watanabe S. 2006. Spatial memory and hippocampal function in a non-foodstoring songbird, the zebra finch (*Taeniopygia guttata*). Rev Neurosci 17: 43–52.

Budzynski CA, Gagliardo A, Ioale P, Bingman VP. 2002. Participation of the homing pigeon thalamofugal visual pathway in sun-compass associative learning. Eur J Neurosci 15:197–210.

Casini G, Bingman VP, Bagnoli P. 1986. Connections of the pigeon dorsomedial forebrain studied with WGA-HRP and ^{3}H-proline. J Comp Neurol 245:454–470.

Chen CC, Winkler CM, Pfenning AR, Jarvis ED. 2013. Molecular profiling of the developing avian telencephalon: regional timing and brain subdivision continuities. J Comp Neurol 521:3666–3701.

Christie KJ, Emery B, Denham M, Bujalka H, Cate HS, Turnley AM. 2013. Transcriptional regulation and specification of neural stem cells. Adv Exp Med Biol 786:129–155.

Colombo M, Broadbent N. 2000. Is the avian hippocampus a functional homologue of the mammalian hippocampus? Neurosci Biobehav Rev 24:465–484.

Colombo M, Cawley S, Broadbent N. 1997. The effects of hippocampal and area parahippocampalis lesions in pigeons: II. Concurrent discrimination and spatial memory. Q J Exp Psychol B 50:172–189.

Craigie EH. 1930. Studies on the brain of the kiwi (*Apteryx australis*). J Comp Neurol 49:223–357.

Craigie EH. 1935. The cerebral hemispheres of the kiwi and of the emu (*Apteryx* and *Dromiceius*). J Anat 69:380–393.

Cremer CM, Palomero-Gallagher N, Bidmon HJ, Schleicher A, Speckmann EJ, Zilles K. 2009. Pentylenetetrazole-induced seizures affect binding site densities for GABA, glutamate and adenosine receptors in the rat brain. Neuroscience 163:490–499.

Cremer CM, Bidmon HJ, Gorg B, Palomero-Gallagher N, Escobar JL, Speckmann EJ, Zilles K. 2010. Inhibition of glutamate/glutamine cycle in vivo results in decreased benzodiazepine binding and differentially regulated GABAergic subunit expression in the rat brain. Epilepsia 51:1446–1455.

Cremer CM, Lubke JH, Palomero-Gallagher N, Zilles K. 2011. Laminar distribution of neurotransmitter receptors in different reeler mouse brain regions. Brain Struct Funct 216:201–218.

Csillag A, Székély AD, Davies DC. 1994. Termination pattern of medial hyperstriatum ventrale efferents in the archistriatum of the domestic chick. J Comp Neurol 348:394–402.

Danscher G, Zimmer J. 1978. An improved Timm sulphide silver method for light and electron microscopic localization of heavy metals in biological tissues. Histochemistry 55:27–40.

Danscher G, Haug FM, Fredens K. 1973. Effect of diethyldithiocarbamate (DEDTC) on sulphide silver stained boutons. Reversible blocking of Timm's sulphide silver stain for "heavy" metals in DEDTC treated rats (light microscopy). Exp Brain Res 16:521–532.

De Biasi S, Bendotti C. 1998. A simplified procedure for the physical development of the sulphide silver method to reveal synaptic zinc in combination with immunocytochemistry at light and electron microscopy. J Neurosci Methods 79:87–96.

Dietl MM, Palacios JM. 1988. Neurotransmitter receptors in the avian brain. I. Dopamine receptors. Brain Res 439: 354–359.

Dietl MM, Cortes R, Palacios JM. 1988. Neurotransmitter receptors in the avian brain. II. Muscarinic cholinergic receptors. Brain Res 439:360–365.

Dugas-Ford J, Rowell JJ, Ragsdale CW. 2012. Cell-type homologies and the origins of the neocortex. Proc Natl Acad Sci U S A 109:16974–16979.

Erichsen JT, Bingman VP, Krebs JR. 1991. The distribution of neuropeptides in the dorsomedial telencephalon of the pigeon (*Columba livia*): a basis for regional subdivisions. J Comp Neurol 314:478–492.

Eriksson PS, Perfilieva E, Bjork-Eriksson T, Alborn AM, Nordborg C, Peterson DA, Gage FH. 1998. Neurogenesis in the adult human hippocampus. Nat Med 4:1313–1317.

Faber H, Braun K, Zuschratter W, Scheich H. 1989. System-specific distribution of zinc in the chick brain. A light- and electron-microscopic study using the Timm method. Cell Tissue Res 258:247–257.

Gagliardo A, Ioale P, Bingman VP. 1999. Homing in pigeons: the role of the hippocampal formation in the representation of landmarks used for navigation. J Neurosci 19: 311–315.

Güntürkün O. 2012. The convergent evolution of neural substrates for cognition. Psychol Res 76:212–219.

Gupta S, Maurya R, Saxena M, Sen J. 2012. Defining structural homology between the mammalian and avian hippocampus through conserved gene expression patterns observed in the chick embryo. Dev Biol 366:125–141.

Heimovics SA, Cornil CA, Ellis JM, Ball GF, Riters LV. 2011. Seasonal and individual variation in singing behavior correlates with alpha2-noradrenergic receptor density in brain regions implicated in song, sexual, and social behavior. Neuroscience 182:133–143.

Herold C, Palomero-Gallagher N, Hellmann B, Kröner S, Theiss C, Güntürkün O, Zilles K. 2011. The receptor architecture of the pigeons' nidopallium caudolaterale: an avian analogue to the mammalian prefrontal cortex. Brain Struct Funct 216:239–254.

Herold C, Palomero-Gallagher N, Güntürkün O, Zilles K. 2012. Serotonin 5-HT_{1A} receptor binding sites in the brain of the pigeon (*Columba livia*). Neuroscience 200:1–12.

Hoshooley JS, Sherry DF. 2007. Greater hippocampal neuronal recruitment in food-storing than in non-food-storing birds. Dev Neurobiol 67:406–414.

Hoshooley JS, Phillmore LS, Macdougall-Shackleton SA. 2005. An examination of avian hippocampal neurogenesis in relationship to photoperiod. Neuroreport 16:987–991.

Hough GE, Bingman VP. 2004. Spatial response properties of homing pigeon hippocampal neurons: correlations with goal locations, movement between goals, and environmental context in a radial-arm arena. J Comp Physiol A Neuroethol Sens Neural Behav Physiol 190:1047–1062.

Insausti R. 1993. Comparative anatomy of the entorhinal cortex and hippocampus in mammals. Hippocampus 3(Spec No.):19–26.

Jarvis ED, Yu J, Rivas MV, Horita H, Feenders G, Whitney O, Jarvis SC, Jarvis ER, Kubikova L, Puck AE, Siang-Bakshi C, Martin S, McElroy M, Hara E, Howard J, Pfenning A, Mouritsen H, Chen CC, Wada K. 2013. Global view of the functional molecular organization of the avian cerebrum: mirror images and functional columns. J Comp Neurol 521:Spc1.

Kahn MC, Hough GE 2nd, Ten Eyck GR, Bingman VP. 2003. Internal connectivity of the homing pigeon (*Columba livia*) hippocampal formation: an anterograde and retrograde tracer study. J Comp Neurol 459:127–141.

Kallen B. 1962. II. Embryogenesis of brain nuclei in the chick telencephalon. Ergeb Anat Entwicklungsgesch 36:62–82.

Karten H, Hodos W. 1967. A stereotaxic atlas of the brain of the pigeon (*Columba livia*). Baltimore: The Johns Hopkins University Press.

Kempermann G. 2012. New neurons for "survival of the fittest." Nat Rev Neurosci 13:727–736.

Kleitz HK, Cornil CA, Balthazart J, Ball GF. 2009. Species differences in the relative densities of D1- and D2-like dopamine receptor subtypes in the Japanese quail and rats: an in vitro quantitative receptor autoradiography study. Brain Behav Evol 73:81–90.

Kraemer M, Zilles K, Schleicher A, Gebhard R, Robbins TW, Everitt BJ, Divac I. 1995. Quantitative receptor autoradiography of eight different transmitter-binding sites in the hippocampus of the common marmoset, *Callithrix jacchus*. Anat Embryol 191:213–225.

Krebs JR, Sherry DF, Healy SD, Perry VH, Vaccarino AL. 1989. Hippocampal specialization of food-storing birds. Proc Natl Acad Sci U S A 86:1388–1392.

Krebs JR, Erichsen JT, Bingman VP. 1991. The distribution of neurotransmitters and neurotransmitter-related enzymes in the dorsomedial telencephalon of the pigeon (*Columba livia*). J Comp Neurol 314:467–477.

Kröner S, Güntürkün O. 1999. Afferent and efferent connections of the caudolateral neostriatum in the pigeon (*Columba livia*): a retro- and anterograde pathway tracing study. J Comp Neurol 407:228–260.

Leutgeb S, Husband S, Riters LV, Shimizu T, Bingman VP. 1996. Telencephalic afferents to the caudolateral neostriatum of the pigeon. Brain Res 730:173–181.

Manns JR, Eichenbaum H. 2005. Time and treason to the trisynaptic teachings: theoretical comment on Kesner et al. (2005). Behav Neurosci 119:1140–1143.

Margrie TW, Rostas JA, Sah P. 1998. Long-term potentiation of synaptic transmission in the avian hippocampus. J Neurosci 18:1207–1216.

Mayer U, Watanabe S, Bischof HJ. 2009. Hippocampal activation of immediate early genes Zenk and c-Fos in zebra finches (*Taeniopygia guttata*) during learning and recall of a spatial memory task. Neurobiol Learn Mem 93:322–329.

Mayer U, Watanabe S, Bischof HJ. 2012. Spatial memory and the avian hippocampus: research in zebra finches. J Physiol Paris doi: 10.1016/j.jphysparis.2012.05.002.

Merker B. 1983. Silver staining of cell bodies by means of physical development. J Neurosci Methods 9:235–241.

Ming GL, Song H. 2005. Adult neurogenesis in the mammalian central nervous system. Annu Rev Neurosci 28:223–250.

Molla R, Rodriguez J, Calvet S, Garcia-Verdugo JM. 1986. Neuronal types of the cerebral cortex of the adult chicken (*Gallus gallus*). A Golgi study. J Hirnforsch 27:381–390.

Montagnese CM, Geneser FA, Krebs JR. 1993. Histochemical distribution of zinc in the brain of the zebra finch (*Taeniopygia guttata*). Anat Embryol 188:173–187.

Montagnese CM, Krebs JR, Meyer G. 1996. The dorsomedial and dorsolateral forebrain of the zebra finch, *Taeniopygia guttata*: a Golgi study. Cell Tissue Res 283:263–282.

Montagnese CM, Székély AD, Adam A, Csillag A. 2004. Efferent connections of septal nuclei of the domestic chick (*Gallus domesticus*): an anterograde pathway tracing study with a bearing on functional circuits. J Comp Neurol 469:437–456.

Montiel JF, Molnar Z. 2013. The impact of gene expression analysis on evolving views of avian brain organization. J Comp Neurol 521:3604–3613.

Nair-Roberts RG, Erichsen JT, Reboreda JC, Kacelnik A. 2006. Distribution of substance P reveals a novel subdivision in the hippocampus of parasitic South American cowbirds. J Comp Neurol 496:610–626.

Palomero-Gallagher N. 1999. Transmitterrezeptoren im Hippocampus verschiedener Säugetiere: Vergleichend-anatomische Untersuchungen und Analyse geschlechts-

und zyklusabhängiger Verteilungsmuster. Dissertation, Heinrich-Heine-Universität Düsseldorf.

Palomero-Gallagher N, Bidmon HJ, Zilles K. 2003. AMPA, kainate, and NMDA receptor densities in the hippocampus of untreated male rats and females in estrus and diestrus. J Comp Neurol 459:468–474.

Palomero-Gallagher N, Schleicher A, Lindemann S, Lessenich A, Zilles K, Loscher W. 2008. Receptor fingerprinting the circling ci2 rat mutant: insights into brain asymmetry and motor control. Exp Neurol 210:624–637.

Papp G, Witter MP, Treves A. 2007. The CA3 network as a memory store for spatial representations. Learn Mem 14:732–744.

Pauly JR, Stitzel JA, Marks MJ, Collins AC. 1989. An autoradiographic analysis of cholinergic receptors in mouse brain. Brain Res Bull 22:453–459.

Puelles L, Martinez-de-la-Torre M, Paxinos G, Watson C, Martinez S. 2007. The chick brain in stereotaxic coordinates: an atlas featuring neuromeric subdivisions and mammalian homologies. San Diego: Acadamic Press.

Pytte CL, Gerson M, Miller J, Kirn JR. 2007. Increasing stereotypy in adult zebra finch song correlates with a declining rate of adult neurogenesis. Dev Neurobiol 67:1699–1720.

Qian J, Noebels JL. 2005. Visualization of transmitter release with zinc fluorescence detection at the mouse hippocampal mossy fibre synapse. J Physiol 566:747–758.

Rattenborg NC, Martinez-Gonzalez D. 2011. A bird-brain view of episodic memory. Behav Brain Res 222:236–245.

Reiner A, Perkel DJ, Bruce LL, Butler AB, Csillag A, Kuenzel W, Medina L, Paxinos G, Shimizu T, Striedter G, Wild M, Ball GF, Durand S, Gunturkun O, Lee DW, Mello CV, Powers A, White SA, Hough G, Kubikova L, Smulders TV, Wada K, Dugas-Ford J, Husband S, Yamamoto K, Yu J, Siang C, Jarvis ED, Avian Brain Nomenclature F. 2004. Revised nomenclature for avian telencephalon and some related brainstem nuclei. J Comp Neurol 473:377–414.

Riba-Bosch A, Perez-Clausell J. 2004. Response to kainic acid injections: changes in staining for zinc, FOS, cell death and glial response in the rat forebrain. Neuroscience 125:803–818.

Rodriguez F, Lopez JC, Vargas JP, Broglio C, Gomez Y, Salas C. 2002. Spatial memory and hippocampal pallium through vertebrate evolution: insights from reptiles and teleost fish. Brain Res Bull 57:499–503.

Rose M. 1912. Histologische Lokalisation der Großhirnrinde bei kleinen Säugetieren. J Psychol Neurol 19.

Rose M. 1914. Über die cytoarchitektonische Gleiderung des Vorderhinrs der Vögel. J Psychol Neurol 21:278–352.

Rose M. 1926. Der Allocortex bei Tier und Mensch 1. Teil. Jour Psychol Neurol 34:1–111.

Rosinha MU, Ferrari EA, Toledo CA. 2009. Immunohistochemical distribution of AMPA-type label in the pigeon (*C. livia*) hippocampus. Neuroscience 159:438–450.

Ruploh T, Kazek A, Bischof HJ. 2011. Spatial orientation in Japanese quails (*Coturnix coturnix japonica*). PLoS One 6: e28202.

Schleicher A, Palomero-Gallagher N, Morosan P, Eickhoff SB, Kowalski T, de Vos K, Amunts K, Zilles K. 2005. Quantitative architectural analysis: a new approach to cortical mapping. Anat Embryol 210:373–386.

Schnabel R, Braun K. 1996. Development of dopamine receptors in the forebrain of the domestic chick in relation to auditory imprinting. An autoradiographic study. Brain Res 720:120–130.

Sherry DF. 2011. The hippocampus of food-storing birds. Brain Behav Evol 78:133–135.

Sherry DF, Jacobs LF, Gaulin SJ. 1992. Spatial memory and adaptive specialization of the hippocampus. Trends Neurosci 15:298–303.

Siegel JJ, Nitz D, Bingman VP. 2000. Hippocampal theta rhythm in awake, freely moving homing pigeons. Hippocampus 10:627–631.

Siegel JJ, Nitz D, Bingman VP. 2002. Electrophysiological profile of avian hippocampal unit activity: a basis for regional subdivisions. J Comp Neurol 445:256–268.

Sihver W, Günther P, Schiebs R, Bigl V. 1997. Repeated administration of tacrine to normal rats: effects on cholinergic, glutamamtergic and gabaergic receptor subtypes in rat using receptor autoradiography. Neurochem Int 31: 693–703.

Sindreu CB, Varoqui H, Erickson JD, Perez-Clausell J. 2003. Boutons containing vesicular zinc define a subpopulation of synapses with low AMPAR content in rat hippocampus. Cereb Cortex 13:823–829.

Stewart MG, Cristol D, Philips R, Steele RJ, Stamatakis A, Harrison E, Clayton N. 1999. A quantitative autoradiographic comparison of binding to glutamate receptor sub-types in hippocampus and forebrain regions of a food-storing and a non-food-storing bird. Behav Brain Res 98:89–94.

Suarez J, Davila JC, Real MA, Guirado S, Medina L. 2006. Calcium-binding proteins, neuronal nitric oxide synthase, and GABA help to distinguish different pallial areas in the developing and adult chicken. I. Hippocampal formation and hyperpallium. J Comp Neurol 497:751–771.

Suzuki WA, Clayton NS. 2000. The hippocampus and memory: a comparative and ethological perspective. Curr Opin Neurobiol 10:768–773.

Székély AD. 1999. The avian hippocampal formation: subdivisions and connectivity. Behav Brain Res 98:219–225.

Székély AD, Krebs JR. 1996. Efferent connectivity of the hippocampal formation of the zebra finch (*Taenopygia guttata*): an anterograde pathway tracing study using *Phaseolus vulgaris* leucoagglutinin. J Comp Neurol 368: 198–214.

Tömböl T, Davies DC, Nemeth A, Alpar A, Sebesteny T. 2000a. A golgi and a combined Golgi/GABA immunogold study of local circuit neurons in the homing pigeon hippocampus. Anat Embryol 201:181–196.

Tömböl T, Davies DC, Nemeth A, Sebesteny T, Alpar A. 2000b. A comparative Golgi study of chicken (*Gallus domesticus*) and homing pigeon (*Columba livia*) hippocampus. Anat Embryol 201:85–101.

Tommasi L, Gagliardo A, Andrew RJ, Vallortigara G. 2003. Separate processing mechanisms for encoding of geometric and landmark information in the avian hippocampus. Eur J Neurosci 17:1695–1702.

Topic B, Willuhn I, Palomero-Gallagher N, Zilles K, Huston JP, Hasenohrl RU. 2007. Impaired maze performance in aged rats is accompanied by increased density of NMDA, 5-HT_{1A}, and alpha-adrenoceptor binding in hippocampus. Hippocampus 17:68–77.

Veenman CL, Albin RL, Richfield EK, Reiner A. 1994. Distributions of $GABA_A$, GABAB, and benzodiazepine receptors in the forebrain and midbrain of pigeons. J Comp Neurol 344:161–189.

Watanabe S, Bischof HJ. 2004. Effects of hippocampal lesions on acquisition and retention of spatial learning in zebra finches. Behav Brain Res 155:147–152.

Witter MP. 2007. Intrinsic and extrinsic wiring of CA3: indications for connectional heterogeneity. Learn Mem 14: 705–713.

Wolff SC, Hruska Z, Nguyen L, Dohanich GP. 2008. Asymmetrical distributions of muscarinic receptor binding in the

hippocampus of female rats. Eur J Pharmacol 588:248–250.

Zilles K, Qu M, Schleicher A. 1993. Regional distribution and heterogeneity of alpha-adrenoceptors in the rat and human central nervous system. J Hirnforsch 34:123–132.

Zilles K, Wu J, Crusio WE, Schwegler H. 2000. Water maze and radial maze learning and the density of binding sites of glutamate, GABA, and serotonin receptors in the hippocampus of inbred mouse strains. Hippocampus 10: 213–225.

Zilles K, Palomero-Gallagher N, Grefkes C, Scheperjans F, Boy C, Amunts K, Schleicher A. 2002a. Architectonics of the human cerebral cortex and transmitter receptor fingerprints: reconciling functional neuroanatomy and neurochemistry. Eur Neuropsychopharmacol 12:587–599.

Zilles K, Schleicher A, Palomero-Gallagher N, Amunts K. 2002b. Quantitative analysis of cyto- and receptor architecture of the human brain. In: Mazziotta JC, Toga A, editors. Brain mapping: the methods. Amsterdam: Elsevier. p 573–602.

Zimmer J, Haug FM. 1978. Laminar differentiation of the hippocampus, fascia dentata and subiculum in developing rats, observed with the Timm sulphide silver method. J Comp Neurol 179:581–617.

Behavioural Brain Research 295 (2015) 45–63

Contents lists available at ScienceDirect

Behavioural Brain Research

journal homepage: www.elsevier.com/locate/bbr

Research report

Distribution of serotonin 5-HT_{1A}-binding sites in the brainstem and the hypothalamus, and their roles in 5-HT-induced sleep and ingestive behaviors in rock pigeons (*Columba livia*)

Tiago Souza dos Santos[a,1], Jéssica Krüger[a,1], Fernando Falkenburger Melleu[a,1], Christina Herold[d,3], Karl Zilles[f,g,h,4], Anicleto Poli[c,2], Onur Güntürkün[e,5], José Marino-Neto[a,b,*]

[a] *Department of Physiological Sciences, CCB, Federal University of Santa Catarina, 88040-900 Florianópolis, SC, Brazil*
[b] *Institute of Biomedical Engineering, EEL-CTC, Federal University of Santa Catarina, 88040-900 Florianópolis, SC, Brazil*
[c] *Department of Pharmacology, CCB, Federal University of Santa Catarina, 88040-900 Florianópolis, SC, Brazil*
[d] *C & O. Vogt Institute for Brain Research, Heinrich Heine University, 40225 Düsseldorf, Germany*
[e] *Institute for Cognitive Neuroscience, Faculty of Psychology, Ruhr University Bochum, 44780 Bochum, Germany*
[f] *Institute of Neuroscience and Medicine INM-1, Research Center Jülich, 52425 Jülich, Germany*
[g] *Department of Psychiatry, Psychotherapy and Psychosomatics, RWTH Aachen University, 52074 Aachen, Germany*
[h] *JARA – Translational Brain Medicine, 52074 Aachen, Germany*

HIGHLIGHTS

- 5-HT_{1AR} was found in brainstem 5-HT areas and in the hypothalamus of pigeons.
- ICV 5-HT or DPAT evokes drinking, sleep, and c-Fos expression in these areas.
- 5-HT_{1AR} heteroreceptor antagonist blocks 5-HT- and DPAT-evoked drinking and sleep.
- 5-HT-specific neurotoxin 5,7-DHT does not alter 5-HT activity but does increase sleep.
- 5-HT_{1ARs} play crucial but complex roles in ingestive and postprandial behavior.

ARTICLE INFO

Article history:
Received 1 October 2014
Received in revised form 20 February 2015
Accepted 26 March 2015
Available online 3 April 2015

ABSTRACT

Serotonin 1A receptors (5-HT_{1ARs}), which are widely distributed in the mammalian brain, participate in cognitive and emotional functions. In birds, 5-HT_{1ARs} are expressed in prosencephalic areas involved in visual and cognitive functions. Diverse evidence supports 5-HT_{1AR}-mediated 5-HT-induced ingestive and sleep behaviors in birds. Here, we describe the distribution of 5-HT_{1ARs} in the hypothalamus and brainstem of birds, analyze their potential roles in sleep and ingestive behaviors, and attempt to determine

Abbreviations: A6, caudal part of locus coeruleus; A8, rostral part of locus coeruleus; AL, ansa lenticularis; AM, nucleus anterior medialis hypothalami; Anl, nucleus annularis; BC, brachium conjunctivum; BNSTl, bed nucleus of stria terminalis, pars lateral; CA, anterior commissure; CO, chiasma opticum; CP, posterior commissure; CS, nucleus centralis superior; DMN, nucleus dorsomedialis hypothalami; DSD, dorsal supraoptic decussation; DSV, ventral supraoptic decussation; FDB, fasciculus diagonalis brocae; FLM, fasciculus longitudinalis medialis; GCt, griseum centralis; IF, infundibular tract; IN, nucleus infundibuli; LC, nucleus linearis caudalis; LHy, lateral hypothalamic area; ML, nucleus mamillar lateralis; MM, nucleus mamillaris medialis; n.IV, nucleus trochlearis; n.V, nucleus principalis nervi trigemini; OM, occipitomesencephalic tract; PD, nucleus preopticus dorsalis; PLH, nucleus lateralis hypothalami posterioris; PMH, nucleus medialis hypothalami posterioris; PMM, nucleus pre-mamillaris; POA, nucleus preopticus anterior; POM, nucleus preopticus medialis; PPM, nucleus preopticus magnocellularis; PVNm, nucleus paraventricularis, pars magnocellularis; PVNp, nucleus paraventricularis, pars parvocellularis; PVO, paraventricular organ; QF, quinto frontalis tract; R, nucleus raphe pontis; RPO, nucleus reticularis pontis oralis; Rt, nucleus rotundus; ScD, nucleus subcoeruleus dorsalis; SCE, stratum cellulare externum; SCI, stratum cellulare internum; ScV, nucleus subcoeruleus ventralis; SFO, subfornical organ; SL, septal lateral nucleus; SOE, nucleus supraopticus externus; TSM, tractus septomesencephalicus; VMN, nucleus ventromedialis hypothalami; ZpFLM, zone peri-fasciculus longitudinalis medialis.

* Corresponding author at: Department of Physiological Sciences CCB, Federal University of Santa Catarina, 88040-900 Florianópolis, SC, Brazil. Tel.: +55 48 3721 8760; fax: +55 48 3331 8686.
E-mail addresses: santos.ts@hotmail.com (T.S. dos Santos), jessica.kkruger@hotmail.com (J. Krüger), fmelleu@gmail.com (F.F. Melleu), christina.herold@uni-duesseldorf.de (C. Herold), k.zilles@fz-juelich.de (K. Zilles), poli@ccb.ufsc.br (A. Poli), onur.guentuerkuen@ruhr-uni-bochum.de (O. Güntürkün), marino@ieb.ufsc.br, marino@ccb.ufsc.br (J. Marino-Neto).
[1] Tel.: +55 21 48 37218760.
[2] Tel.: +55 21 48 37214861.
[3] Tel.: +49 211 81 12666; fax: +49 211 81 12366.
[4] Tel.: +49 2461 613015.
[5] Address: Biopsychology, Institute of Cognitive Neuroscience, Faculty of Psychology, Ruhr-University Bochum, 44780 Bochum, Germany. Tel.: +49 234 3226213; fax: +49 234 3214377.

http://dx.doi.org/10.1016/j.bbr.2015.03.059
0166-4328/© 2015 Elsevier B.V. All rights reserved.

Keywords:
Serotonin
Sleep
Drinking
Feeding
5-HT-1A receptor
Cerebrospinal fluid

the involvement of auto-/hetero-5-HT_{1ARs} in these behaviors. In 6 pigeons, the anatomical distribution of [^{3}H]8-OH-DPAT binding in the rostral brainstem and hypothalamus was examined. Ingestive/sleep behaviors were recorded (1 h) in 16 pigeons pretreated with MM77 (a heterosynaptic 5-HT_{1AR} antagonist; 23 or 69 nmol) for 20 min, followed by intracerebroventricular ICV injection of 5-HT (N:8; 150 nmol), 8-OH-DPAT (DPAT, a 5-$HT_{1A,7R}$ agonist, 30 nmol N:8) or vehicle. 5-HT- and DPAT-induced sleep and ingestive behaviors, brainstem 5-HT neuronal density and brain 5-HT content were examined in 12 pigeons, pretreated by ICV with the 5-HT neurotoxin 5,7-dihydroxytryptamine (5,7-DHT) or vehicle (N:6/group). The distribution of brainstem and diencephalic c-Fos immunoreactivity after ICV injection of 5-HT, DPAT or vehicle (N:5/group) into birds provided with or denied access to water is also described. 5-HT_{1ARs} are concentrated in the brainstem 5-HTergic areas and throughout the periventricular hypothalamus, preoptic nuclei and circumventricular organs. 5-HT and DPAT produced a complex c-Fos expression pattern in the 5-HT_{1AR}-enriched preoptic hypothalamus and the circumventricular organs, which are related to drinking and sleep regulation, but modestly affected c-Fos expression in 5-HTergic neurons. The 5-HT-induced ingestivebehaviors and the 5-HT- and DPAT-induced sleep behaviors were reduced by MM77 pretreatment. 5,7-DHT increased sleep per se, decreased tryptophan hydroxylase expression in the raphe nuclei and decreased prosencephalic 5-HT release but failed to affect 5-HT- or DPAT-induced drinking or sleep behavior. 5-HT- and DPAT-induced ingestive and sleep behaviors in pigeons appear to be mediated by heterosynaptic and/or non-somatodendritic presynaptic 5-HT_{1ARs} localized to periventricular diencephalic circuits.

© 2015 Elsevier B.V. All rights reserved.

1. Introduction

Postprandial states in both mammals [1–3] and birds [4–6] are characterized by an increased incidence of grooming, drinking and resting. These behaviors, which occur in a relatively fixed temporal setting, constitute the so-called behavioral satiety sequence (BSS) in both classes of vertebrates. Additionally, BSS expression appears to be selectively affected by changes in serotonin (5-HT) neurotransmission in both vertebrate classes. Increased activity of 5-HT circuits exerts suppressive effects on food and water intake in mammals (e.g., [7]) and in pigeons [8–10]. Intracerebroventricular (ICV) injection of 5-HT in pigeons [9,11–13] evoked a sequence of hypophagia, drinking and sleep that parallels the BSS in pigeons [6]. On the other hand, increased feeding was observed in free-feeding pigeons after intra-hypothalamic and intra-amygdalar injection of a 5-$HT_{1/2}$ receptor antagonist or intra-raphe injection of 8-OH-DPAT (DPAT; a 5-$HT_{1A/7}$ receptor agonist) [14], indicating that5-HT afferents exert tonic inhibitory control on feeding-related prosencephalic circuits in free-feeding pigeons, similar to the findings in mammals.

Furthermore, increased activity of 5-HTergic circuits also exerts an inhibitory effect on sleep in both vertebrate classes [15,16,12,13]. Brainstem 5-HTergic neurons in mammals are active during waking but display reduced firing rates, and may not fire at all, during sleep states [17,15,18]. Activating 5-HT receptors via ICV injection of 5-HT evokes hypophagia and behavioral/electrographic sleep-like states in carnivores and rodents (e.g., [19]). Furthermore, in mammals, intra-raphe injection of DPAT increases sleep signs [20,21], indicating an important role of the presynaptic 5-HT_{1A} receptor subtype (5-HT_{1AR}) in decreasing the activity of 5-HT-related mechanisms that promote wakefulness in mammals [15,18]. ICV injection of DPAT into free-feeding pigeons at the identical ventricular regions to which 5-HT evokes the hypophagia/drinking/sleep sequence and increases feeding and drinking behaviors; these effects are followed by increased behavioral and electrographic signs of sleep [12,13]. Thus, it is possible that the activity of central 5-HT circuits may coordinate satiety processes, influencing the expression and sequential appearance of the major components of the mammalian and avian BSS.

The similarities between the effects of ICV-injected 5-HT and DPAT on behaviors in pigeons indicate a crucial role of 5-HT_{1ARs} in satiety-related circuits. Similar to mammals, systemic DPAT injection reduces serotonergic neurotransmission in pigeons [22–24,24], possibly by acting on inhibitory 5-HT_{1A} autoreceptor-mediated mechanisms, similar to those found in mammals. Accordingly, pretreatment with a 5-HT_{1AR} antagonist, such as WAY100635 decreases drinking and sleep behaviors induced by ICV 5-HT injection and antagonizes DPAT-induced feeding and drinking behaviors [13]. Furthermore, the density of c-Fos protein expression in midline and dorsal brainstem 5-HTergic cell populations double-labeled for tryptophan hydroxylase (TPH) was reduced in 5-HT (ICV)-injected pigeons compared to vehicle-injected animals. Moreover, the activity of these double-labeled neurons negatively correlated to sleep [12]. These data suggest that the drinking- and sleep-inducing effects of ICV 5-HT injection into pigeons result from the 5-HT-induced inhibition of 5-HTergic neurons (via activation of 5-HT_{1ARs}) [12,13]. Taken together, these results indicate a mechanistic hypothesis in which a feeding-evoked increase in ventricular 5-HT results in 5-HT-mediated hypophagia. This mechanism, subsequently, results in a 5-HT_{1AR}-mediated reduction in the activity of drinking- and sleep-inhibitory 5-HTergic neurons, thus favoring the post-prandial satiety-related appearance of these behaviors. In addition to the possible relevance of such mechanisms to coordinating BSS behavior in pigeons, these data also suggest that the roles and mechanisms of 5-HT represent shared, evolutionarily conserved functional attributes of the serotonergic circuits in the amniote brain.

However, before proceeding to a closer examination of the circumventricular, BSS-related functions of intraventricular 5-HTergic neurons, the hypothesis described above must be further tested on anatomical and pharmacological bases. In mammals, 5-HT_{1ARs} are localized to both synaptic terminals: as an autoreceptor that regulates serotonergic neuronal activity and as a heteroreceptor that modulates 5-HT-mediated effects via several serotonergic targets [25]. In mammalian brains, a high density of 5-HT_{1ARs} was detected in 5-HTergic areas of the brainstem [26] and the forebrain, such as the cingulate and entorhinal cortices, the hippocampus, the amygdala, the septum, the thalamus and the hypothalamus [27–32]. An autoradiographic study using pigeons indicated moderate to high expression of binding sites to [^{3}H]8-OH-DPAT in forebrain regions including the nidopallium, the hyperpallium, the hippocampus, the basal ganglia, and the amygdala [33]. However, the distribution of these receptors in the brainstem and in periventricular areas, such as the hypothalamus, of birds remains unknown.

Furthermore, the 5-HT_{1AR} antagonist used to examine these activities, WAY100635, acts at both pre- and postsynaptic 5-HT_{1ARs} [34,35], obscuring the localization of these receptors. A suitable

approach to assess these functions of 5-HT is pretreatment with a postsynaptic selective 5-HT_{1AR} antagonist and/or injection of the 5-HTergic neuronal neurotoxin 5,7-dihydroxytryptamine (5,7-DHT). This toxin is known to reduce the brain levels of 5-HT in both rats [36] and pigeons [37]. Moreover, 5,7-DHT decreases the density of binding sites to [^{3}H]8-OH-DPATin the brainstem of rats [38,39]. Additionally, behavioral studies have shown that this toxin is effective in discriminating between the functions of pre- and postsynaptic 5-HT_{1ARs} in rats [40,41] and pigeons [42]. In the present report, we first describe the distribution of [^{3}H]8-OH-DPAT-binding sites in the brainstem and the hypothalamus of pigeons, as well as that of neurons activated (c-Fos-immunoreactive) by ICV injection of DPAT in the brainstem and in periventricular diencephalic areas. Furthermore, the effects of pretreatment with 5,7-DHT or a 5-HT_{1AR} antagonist (MM77) that primarily acts at postsynaptic 5-HT_{1ARs} [43] on 5-HT- and DPAT-evoked behaviors were examined.

2. Materials and methods

All experimental procedures described here were conducted in adherence to the recommendations of the "Principles of Animal Care" (NIH, 1985) and were approved by the local Committees for Ethics in Animal Research (protocols: Federal University of Santa Catarina, 23080.0383262/2008-65; Ruhr Universität, 8.87-50.10.37). Adult domestic pigeons (*Columba livia* of both sexes, 400–500 g body weight) were supplied by the central vivarium facilities of each university and were maintained in individual cages at a temperature of 22–24 °C in a 12:12 light-dark cycle (lights on at 07:00 a.m.; fluorescent daylight lamps generating 80–90 lx light intensity) with free access to food and water until the experiments.

2.1. Lateral ventricle cannula implant and 5,7-DHT injection procedures

The pigeons received an injection of desipramine hydrochloride (25 mg/kg/1 ml in 0.9% NaCl, i.p.; Sigma–Aldrich Co., St. Louis, MO, USA) to preserve the noradrenergic circuits from the deleterious effects of the neurotoxin 5,7-DHT (5,7-dihydroxytryptamine creatinine sulfate salt, Sigma–Aldrich Co., St. Louis, MO, USA); 30 min later, they were anesthetized (ketamine: 0.15 ml/100 g, xylazine: 0.05 ml/100 g, i.m.) and placed in the stereotaxic apparatus (David Kopf Instruments, Tujunga, CA, USA). All wound margins and the external acoustic meati (into which the stereotaxic inner bar was inserted) were infiltrated with lidocaine solution (5%). The animals received bilateral ICV injections (at AP = +6 mm; L = 1.5 mm; H = −5 mm; the stereotaxic coordinates were derived from the stereotaxic atlas of the pigeon brain [44]) of 5,7-DHT (Lesion group, 200 μg/ventricle) or vehicle (Veh group) using a guide cannula (21 G). 5,7-DHT was dissolved in 10 μl of 0.1% ascorbic acid/0.9% NaCl solution 10 min prior to the injections. In the 5-HT- and DPAT-treated animals (see Section 2.10.3 for details), the guide cannula was inserted into the right lateral ventricle, fixed to the skull using dental cement and 2 jeweler's screws, and maintained patent using a removable inner stylet. The injections were performed using an inner cannula (30 G) extending 1 mm from the tip of the guide cannula; and the inner cannula was connected to a Hamilton microsyringe using polyethylene tubing (injection rate; 0.5 μl/min). After these surgeries, the animals were treated (daily for the next 5 days) with the antibiotic Baytril® (5% enrofloxacin, Bayer; 0.1 ml/kg, i.m.) and the analgesic Ketofen® (Ketoprofen1%; Merial; 0.2 ml/kg, i.m.). The wound was treated daily with Furacin® cream (Nitrofural; Mantecorp). A post-operation recovery period of at least 10 days was observed before the experiments.

2.2. Drugs and ICV injections

5-HT (5-hydroxytryptamine hydrochloride; Sigma–Aldrich, St. Louis, MO, USA; dose 150 nmol) and DPAT [8-hydroxy-2 (di-*n*-propylamino) tetralin; Sigma–Aldrich, St. Louis, MO, USA; dose 30 nmol], a 5-$HT_{1A/7}$ receptor agonist, were dissolved in 5% ascorbic acid in 0.9% NaCl solution (used as the vehicle), and MM77 [1-(2-methoxyphenyl)-4-(4-succinimid-obutyl) piperazinedihydrochloride; Tocris Bioscience, Bristol, UK; dose 23 or 69 nmol], a postsynaptic 5-HT_{1A} receptor antagonist, was dissolved in 0.3% DMSO (in 0.02 M phosphate buffer solution; PBS); this solution was used as the vehicle for the MM77 pre-treatment experiments. 5-HT and DPAT were used in a dose range previously shown to induce ingestive and sleep-waking responses in free-feeding pigeons [9,12,13], and the MM77 doses were based on the effective systemic dose (divided by 1000) used to block DPAT-induced anxiolytic effects in rats [45]. The ICV injections were performed using a Hamilton microsyringe as described above. The volume injected (2 μl) was administered over a period of 2 min, and for the subsequent 2 min, the inner cannula was maintained in the cannula guide to avoid potential reflux of the solution.

2.3. Immunohistochemistry

Unless otherwise stated, all washing and incubation steps during the following procedures were performed under gentle shaking at room temperature (RT). The washing steps consisted of three washes (5 min each) with 0.1 M PBS containing 0.25% Triton X-100 (PBST). To detect c-Fos protein expression, free-floating sections were washed, blocked for 40 min in 2% bovine serum albumin (BSA) in PBST and incubated in the anti-c-Fos primary antibody (1:2000; rabbit anti-c-Fos; K-25 – Sc-253 – Santa Cruz Biotechnology, Dallas, TX, USA) in PBST solution containing 1% BSA in a humidified chamber for 18 h at 4–8 °C. Next, the sections were washed, the endogenous peroxidase activity was blocked by incubation in 0.3% H_2O_2 in 100% methanol for 40 min, and the sections were incubated (in PBST at RT) in a goat anti-rabbit biotinylated secondary antibody (1:1000; Vector Laboratories, Burlingame, CA, USA). After 2 h of incubation, the sections were incubated in the avidin–biotin complex (1.5 h; 1:1000 in PBST, Vector Laboratories). After washing, c-Fos labeling was visualized using 0.05% 3,3-diaminobenzidine (DAB; Sigma–Aldrich, St. Louis, MO, USA), 0.05% nickel ammonium sulfate and 0.015% H_2O_2 in 0.1 M PBS for 4–5 min, staining the immunopositive nuclei as dark gray/black. To detect c-Fos expression in serotonergic neurons, brainstem sections were stained with an antibody against the enzyme tryptophan hydroxylase (TPH) as described in [12]. Free-floating sections were washed, blocked for 40 min with 2% normal rabbit serum (NRS) in PBST and incubated in the anti-TPH primary antibody (1:1000; sheep anti-TPH: AB 1541, Millipore Corporation, Billerica, MA, USA) in PBST containing 1% NRS in a humidified chamber for 18 h at 4–8 °C. Next, the sections were washed and incubated (2 h in PBST at RT) in a rabbit anti-sheep biotinylated secondary antibody (1:1000; Vector Laboratories), followed by incubation in the avidin-biotin complex (1.5 h; 1:250 in PBST). TPH labeling was visualized using 0.05% DAB and 0.0075% H_2O_2 in 0.1 M PBS for 9 min, resulting in reddish-brown staining. The reaction was stopped by washing for 5 min in cold (4 °C) distilled water, and the sections were mounted on chrome-alum-gelatin-coated glass slides, air-dried for 48 h, and dehydrated in a graded alcohol series and xylene, followed by coverslipping using DPX (Fluka BioChemika, Sigma–Aldrich, St. Louis, MO, USA).

2.4. Cell counting

The sections were analyzed under an optical microscope (Olympus, BH-2), and images were captured using an attached camera

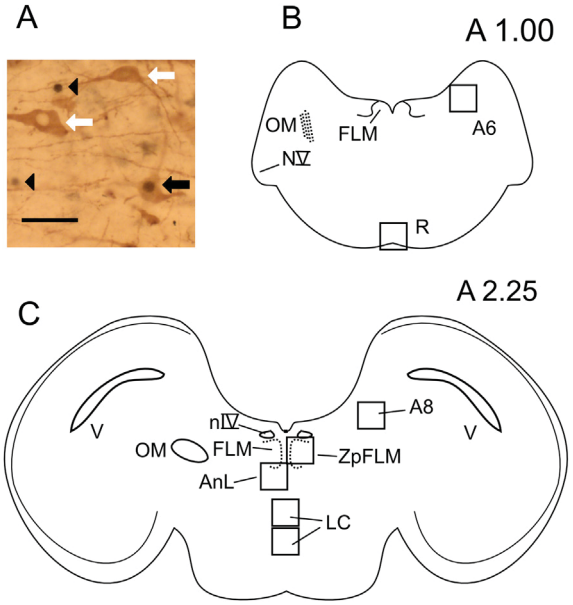

Fig. 1. (A) Photomicrograph illustrating c-Fos expression (black arrowhead) in a representative counted field indicating TPH-immunoreactive (TPH+, white arrow) and c-Fos− and TPH-immunoreactive cells (c-Fos+/TPH+, black arrow). Scale bar = 100 μm. (B) and (C) Schematic drawings of frontal sections of the pigeon brainstem showing the location of the quantified fields in the analyzed areas. The approximate rostrocaudal levels based on the Karten and Hodos' [44] atlas of the pigeon brain are indicated in the upper right corner of each drawing. For abbreviations, see the list.

(PixeLink, Ontario, Canada). The TPH- and c-Fos immunoreactive cells were analyzed according to our previous studies on the brainstem distribution of serotonergic neurons in pigeons [46,12], and the atlas of the pigeon brain of Karten and Hodos [44] was used to standardize the rostrocaudal levels (Figs. 1 and 2). To ensure that sections at the same rostrocaudal level were selected across the groups, the sections were selected based on their relative position to landmarks specific for each nucleus (see Figs. 1 and 2). Three representative sections of each nucleus from each animal in the experimental groups were selected for counting. For bilateral structures, such as n.A6 in the brainstem, or for hypothalamic nuclei, the counts in each hemisphere were averaged. The landmarks used for brainstem structures were detailed in a former report [12]. In short, c-Fos-labeled (c-Fos+), TPH-labeled (TPH+) or double-labeled (c-Fos+/TPH+) cells were quantified in six brainstem nuclei (Fig. 1), by a single blind-to-condition person (TSS) on 1–2 entire field photomicrographs with ImageJ software (www.rsbweb.nih.gov/ij/) of sections containing the nucleus raphe pontis (R; 1 quantification field (QF; 0.47 mm × 0.36 mm) in sections corresponding to the A 1.00 stereotaxic level of the pigeon brain atlas [44]), A6 (or caudal LoC; 1 QF were positioned between the ventrolateral border of the fasciculus longitudinalis medialis (flm), the BC and the floor of IV ventricle at the A 1.00 stereotaxic level), nucleus linearis caudalis (LC; 2 QF located over the 2 midline cell rows of the LC, at A 2.25 stereotaxic level), A8 (rostral part of the LoC; 1 QF were aligned vertically to the TIO and horizontally aligned to the flm at the A 2.25 stereotaxic level), nucleus annularis (Anl, 1 QF positioned immediately ventral to the flm along its mediolateral extent and dorsally to the DBC fibers, at the A 2.25 stereotaxic level) and the zone perifasciculus longitudinalis medialis (Zp-flm; 1 QF placed laterally to the IV ventricle, and medially to the flm and ventral to the nIV (Fig. 1) dorsomedial to the flm and lateral to the 4th IV ventricle, and 2 fields were placed laterally to the flm) (Fig. 3).

The identification and nomenclature of hypothalamic areas and other prosencephalic structures were based on the reviews by Kuenzel and Van Tienhoven [47] and Reiner and cols [48]. Counting of c-Fos labeling in these regions and landmarks used to locate the diencephalic QFs are described as following. The paraventricular organ (PVO; 1 QF positioned at a particular spot in periventricular region of the recessus infundibuli characterized by the presence of juxtaposed cells aligned in a bended way into the ventricular wall) and nucleus infundibuli (IN; 1 QF centrally positioned in the infundibulus region) were evaluated at the A 4.75 stereotaxic level [44], with the IF as landmark (Fig. 2). The nucleus paraventricularis (PVN; 2 QFs vertically aligned at paraventricular region of the dorsal hypothalamus); the nucleus dorsomedialis hypothalami (DMN; 1 QF, dorsally); the nucleus ventromedialis hypothalami (VMN; 1 QF, medioventrally) and the lateral hypothalamic area (LHy; 1 QF, laterally located) were analyzed at the A 6.75 stereotaxic level [44], where the DSD and DSV are very visible in the ventral part of hypothalamus (Fig. 2). The bed nucleus of stria terminalis, pars lateral (BSTNl; 1 QF, ventrolateraly located to the lateral ventricle); the septal lateral nucleus (SL; 1 QF, ventromedialy located to lateral ventricle) and the subfornical organ (SFO; 1 QF, located at the "roof" of the III ventricle, posterior to the CA) were evaluated in the A 7.25 stereotaxic level [44], where OM's ascending fibers are visible. To evaluation of the nucleus preopticus medialis (POM), 2 QFs were vertically arranged on this nucleus ventrally to the CA (at A 7.75 stereotaxic level [44]), and to the nucleus preopticus anterior (POA), 1 QF was positioned on its entire area, with the TSM dorsolaterally located as reference (stereotaxic level A 9.25 [44]) (Fig. 2).

2.5. Behavioral analysis

During the first hour after the second injection (see the experimental protocols below), video recordings (Orbit QuickCam, V-UCC22, Logitech, Newark, CA, USA) of the home cage were captured. The latency to the first event, the total duration and frequency of drinking, feeding, preening, locomotor, exploratory, alert immobility and sleep-like behavior (SLB) were scored using the behavioral analysis software EthoWatcher® ([49]; freely available at www.ethowatcher.ufsc.br). The behavioral events have been described previously (e.g., [12,13]) and are shown in a movie clip that is available online [50]. Food pellets were delivered via plastic cups, and water was provided in plastic bottles. The experiments were performed between 10:00 and 16:00 h during the illuminated period of the light/dark cycle, when the ingestive behavior of pigeons is stable and low [12]. Food and water were weighed 1 h after the final injection.

2.6. Receptor autoradiography

The 5-HT-binding sites of the 5-HT_{1AR} were labeled with [^{3}H] 8-OH-DPAT [51,52] according to a previously published standardized protocol [53,54,33], which consisted of three steps. (1) The samples were preincubated for 30 min (at RT) in buffer (170 mM Tris–HCl buffer containing 4 mM $CaCl_2$ and 0.01% ascorbic acid, pH 7.6) to remove endogenous ligands from the tissue; (2) The 5-HT binding sites were labeled via incubation in 1 nM [^{3}H]8-OH-DPAT in buffer for 60 min at room temperature in the presence or absence of 1 μM 5-hydroxytryptamine as a displacer (non-specific binding or total binding, respectively). Specific binding was calculated as the difference between total and non-specific binding. Because non-specific binding accounted for less than 10% of total binding, total binding was considered to be equivalent to specific binding. (3) The samples were rinsed for 5 min at 4 °C in buffer to eliminate the unbound radioactive ligand from the sections. The sections were air-dried overnight and subsequently co-exposed for 8 weeks to a tritium-sensitive film (Hyperfilm, Amersham, Braunschweig, Germany) and plastic [^{3}H]-standards (Microscales, Amersham) of

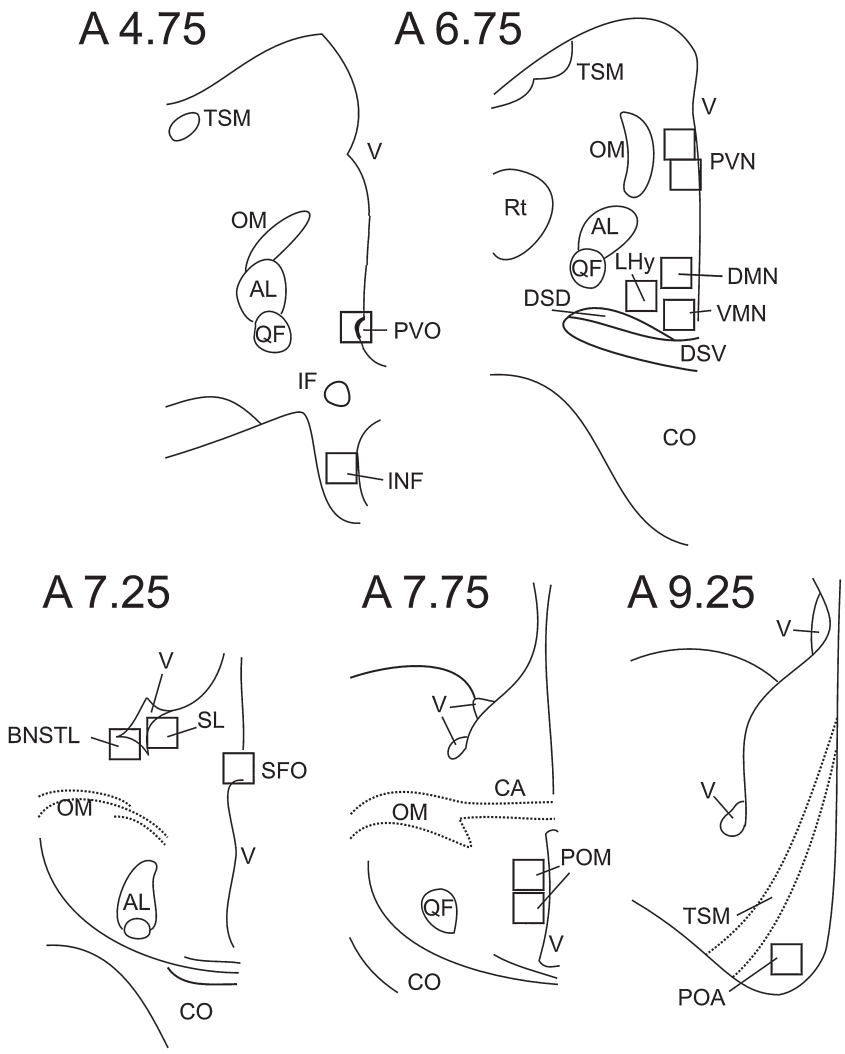

Fig. 2. Schematic drawings of frontal sections of the pigeon brain showing the hypothalamic and subpallial structures (SL and BNSTl) and the location of the quantified fields in the analyzed areas. The approximate rostrocaudal levels based on Karten and Hodos' [44] atlas of the pigeon brain are indicated in the upper right corner of each drawing. For abbreviations, see the list.

known levels of radioactivity. Adjacent sections were Nissl stained for cytoarchitectonic analysis.

2.7. Image analysis and anatomical identification

Autoradiographs were digitized [55,53] using a KS-400 image analysis system (Kontron, Germany) connected to a CCD camera (Sony, Tokyo) equipped with an S-Orthoplanar60-mm macro lens (Zeiss, Germany). The images were collected at a resolution of 512×512 pixels and 8-bit gray value. Images of the co-exposed microscales were used to compute a calibration curve via nonlinear, least-squares fitting, which defined the relationship between the gray values in the autoradiographs and the levels of radioactivity. This calculation enabled the pixel-wise conversion of the gray values of an autoradiograph to the corresponding levels of radioactivity. These concentrations of the binding sites occupied by the incubated ligand were transformed into receptor binding site densities under saturation conditions according to the function $(K_d + L)/A_s \times L$, where K_d is the equilibrium dissociation constant of ligand-binding, L is the concentration of the incubated ligand, and A_s is the specific activity of the ligand. The borders of the structures as defined by the atlas of Karten and Hodos [44] were microscopically identified in the sections processed for the visualization of cell bodies and were traced on prints of the digitized autoradiographs. For the identification of anteroposterior levels of the different structures, we used the same landmarks as those used to cell counting (Section 2.5; Figs. 1 and 2). The DMN and PVN nucleus, through autoradiographs process, were separated into PMH and PLH (the DMN) and into pars magnocellularis (PVNm) and pars parvocellularis (PVNp) (the PVN). The mean of the gray values of the anatomically identified brain regions (from one to five sections per animal and region) were transformed into the binding site concentration (fmol/mg protein).

2.8. High pressure liquid chromatography (HPLC)

2.8.1. Drugs and reagents

Standards of 5-HT, 5-hydroxyindoleacetic acid (5-HIAA), noradrenaline (NA), their metabolites 5-hydroxyindoleacetic acid (5-HIAA) and homovalenic acid (HVA), and all salts for mobile-phase extraction were acquired from Sigma–Aldrich (St. Louis, MO, USA). HPLC grade solvents (J.T. Baker, Mexico) and Milli-Q water (Millipore, São Paulo, Brazil) were used without further purification.

2.8.2. HPLC apparatus

HPLC was performed using a Waters e2695 Alliance Separation Module composed of a quaternary pump, a degasser, a column

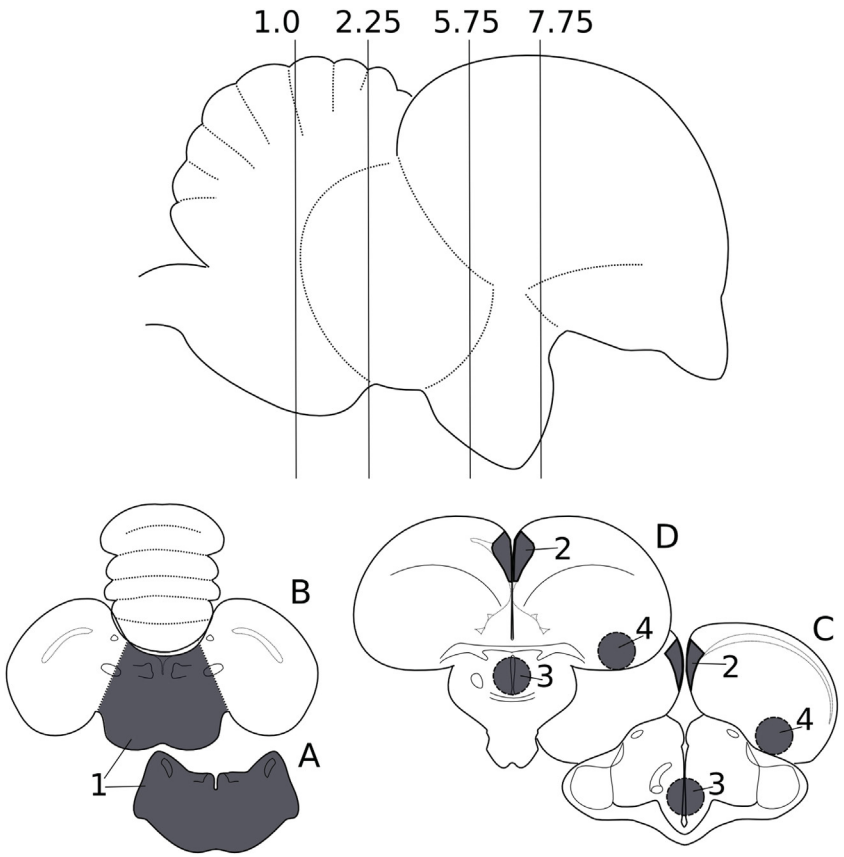

Fig. 3. Upper panel: sagittal view of the pigeon brain showing the anterior-posterior levels at which different sections were evaluated. Lower panels: schematic drawings of the frontal sections of the pigeon brain showing the dissected structures (dark area) at which the levels of 5-HT were measured. The numbers indicate the following structures: 1 – brainstem; 2 – hippocampus; 3 – hypothalamus; and 4 – arcopallium. The letters A–D correspond to the specific antero-posterior levels indicated in upper panel: (A) A1.0; (B) A2.25; (C) A5.75; and (D) A7.75. These coordinates are derived from the atlas of the pigeon brain of Karten and Hodos [44].

heater and a refrigerated autosampler (maintained at 4 °C) coupled to a Waters 2465 amperometric electrochemical detector. The chromatograms were acquired and processed using Empower® 2 software (Waters, Milford, MA, USA).

2.8.3. Chromatographic conditions

The chromatographic analysis was adapted from Linder and cols. [56]. The mobile phase mixture was prepared as 90 mM sodium dihydrogen phosphate, 50 mM citric acid, 50 μM disodium EDTA, 1.7 mM sodium 1-heptanesulfonate:acetonitrileat 90:10, which was adjusted to pH 3.0 using concentrated NaOH, filtered using a 0.45 μm cellulose acetate membrane (Merck Millipore, Billerica, MA, USA), and degassed under vacuum in an ultrasonic bath prior to use. The mobile phase was pumped in an isocratic mode at a flow rate of 0.30 ml/min through a reverse-phase (C18) semi-μHPLC column (150 mm length × 2 mm inner diameter, 4 μm diameter particle size; Synergi Hydro RP, Phenomenex, Torrance, CA, USA), protected with a C18 guard-column (20 mm length × 2 mm inner diameter; Alltech, Deerfield, IL USA), both maintained at 35 °C. The electrochemical reactions occurred in an electrochemical flow cell equipped with a glassy carbon working electrode (GC-WE) operated in direct current (DC) mode set at an oxidation potential of +400 mV vs. an "In Situ Ag/AgCl" (ISAAC) reference electrode and a stainless steel wire auxiliary electrode (Waters, part # 205004215). The peaks of the analytes were identified via comparison of the retention times to the respective standards. The peak areas were integrated to quantify the samples via linear regression of the standard calibration curve. The values obtained were expressed as ng/mg wet tissue.

2.8.4. Sample preparation for HPLC analysis

The sample preparation protocol was adapted from Alesci and Bagnoli [37]. To section the brain of different pigeons at similar predetermined levels (Fig. 1), we developed an acrylic matrix adapted for the pigeon brain (similar to a rodent brain slicer, commercially available) based on the atlas of the pigeon brain by Karten and Hodos [44]. Briefly, the brain tissues (brainstem, hypothalamus, hippocampus, and arcopallium; Fig. 1) were removed from the skull on ice and stored in Eppendorf tubes containing 0.3 ml of refrigerated buffer (0.1 M perchloric acid + 0.02% sodium meta-bisulfide) and immediately stored at −80 °C until analysis. The tissue samples were crushed manually and sonicated in an ultrasonic cooling bath for 10 min. Then, the Eppendorf tubes were promptly centrifuged (14,000 rpm) at 4 °C for 20 min, and 20 μl of the supernatant was injected into the HPLC column.

2.9. Statistical analysis

The behavioral, food and water intake data were analyzed via 2-way ANOVA (factors: pretreatment × treatment, experiment 2.9.2; lesion × treatment, experiment 2.9.3) followed by Scheffé post hoc analysis for any significant results. The cell labeling density (number of cells per mm^2) was analyzed separately for each brain area in each experimental group (experiments 2.9.4 and 2.9.5). First, the counting data were analyzed using Shapiro–Wilk's test to verify the normality of the particular data sample. Then, the data were analyzed via a parametric (one way ANOVA) or non-parametric (Kruskal–Wallis test) analysis, followed by respective post hoc analysis (parametric: Sheffé post hoc analysis; non-parametric: Mann–Whitney *U* test) when appropriate. For experiment 2.9.3, the

alterations in the 5-HT levels (expressed as the % of the 5-HT levels in the control animals) were analyzed using the non-parametric Kruskal–Wallis test followed by the Mann–Whitney *U* post hoc test to evaluate the inter-group differences. To demonstrate the [^{3}H]-8-OH-DPAT-binding sites in the brainstem and the hypothalamus, we performed descriptive analysis of the data expressed as the means and standard deviation (SD). All analyses were performed using Statistica 8.0 software (Stasoft, Tulsa, OK, USA). For all tests, p values of <0.05 were considered to be statistically significant.

2.10. Experimental procedures

2.10.1. Distribution of 5-HT$_{1AR}$ binding sites in the brainstem and the hypothalamus of the pigeon brain

The animals (N = 6 pigeons, of both sexes) were deeply anesthetized with equithesin (i.m.; 0.5 ml/kg bw), decapitated and their brains were removed from the skull, frozen immediately in isopentane at −40 °C and stored at 70 °C. Serial coronal 10 μm sections were generated using a cryostat microtome (2800 Frigocut E, Reichert-Jung, Vienna, Austria). The sections were thaw-mounted on gelatinized slides and freeze-dried before use for receptor autoradiography or histological staining to visualize cell bodies [57].

2.10.2. Effects of pretreatment with MM77 on the ingestive and behavioral responses evoked by ICV injection of 5-HT or DPAT

Sixteen experimentally naïve pigeons were cannulated ICV (see procedures in the Section 2.1) and were separated into two groups: (1) 5-HT group: 8 animals treated with vehicle and 5-HT (150 nmol) (7 days interval between the treatments) and (2) DPAT group: 8 animals treated with vehicle and DPAT (30 nmol) (7 days interval between injections). In both groups, the injections (5-HT; DPAT or vehicle) were preceded (20 min) with an injection of MM77 or vehicle. For the 5-HT-injected animals, we tested two different doses of MM77: 23 and 69 nmol; for the DPAT animals, we tested only the most effective MM77 dose, 69 nmol (based on a previous finding of the most evident 5-HT-mediated effect, a dipsogenic response). Each pigeon received all treatments corresponding to its specific experimental group, which was assigned according to a Latin-squared design. In the end, each group was formed by the following treatments: 5-HT group: veh × veh; veh × 5-HT; MM77 (23) × veh; MM77 (69) × veh; MM77 (23) × 5-HT; MM77 (69) × 5-HT; DPAT group: veh × DPAT; MM77 (69) × DPAT. As to 5-HT and DPAT we used the same vehicle (ascorbic acid), we did not repeated the treatments veh × veh and MM77 × veh in the DPAT group.

2.10.3. Effects of the neurotoxin 5,7-DHT on the ingestive and behavioral responses evoked by 5-HT and DPAT and on the density of brainstem serotonergic neurons

Twenty-four animals were cannulated ICV billateraly (see procedures in the Section 2.1) and divided into 2 groups: (1) 12 animals (6 injected with 5,7-DHT and 6 sham-injected), sacrificed 12 days after the lesion (group DHT12) and (2) 12 animals (6 injected with 5,7-DHT and 6 sham-injected), sacrificed 28 days after the lesion (group DHT28). The animals from group DHT12 were used to verify the effects of 5,7-DHT on the 5-HT levels at the 12th day after 5,7-DHT treatment. The animals from group DHT28 were subjected to pharmacological experiments (from day 12–27) to evaluate the effects of 5,7-DHT on the ingestive and behavioral responses produced by 5-HT and DPAT (according to protocols similar to those described above). Each animal in the group DHT28 were evaluated using all drugs (7-day interval between treatments). On 12th or 28th day, the animals were sacrificed via anesthetic overdose (50 mg/kg ketamine hydrochloride and 10 mg/kg xylazine, IM) and decapitated. Then, the brains were quickly removed from the skull and immediately stored at −80 °C until analysis. To examine the effects of 5,7-DHT on the density of brainstem serotonergic neurons, we used another 12 naïve pigeons (6 treated with 5,7-DHT and 6 sham-injected). These animals were anesthetized (50 mg/kg ketamine hydrochloride and 10 mg/kg xylazine, IM) and perfused (see details in Section 2.10.4) 12 days after the injection, and their brains were prepared for immunohistochemistry to verify the effects of 5,7-DHT on the number of TPH-immunoreactive cells.

2.10.4. Effects of DPAT ICV injection on c-Fos expression in TPH-immunoreactive and -non-immunoreactive neurons in serotonergic brainstem areas

In a previous study [12], we described the effects of ICV injection of 5-HT into free-feeding pigeons on c-Fos activation in serotonergic (TPH+) and non-serotonergic (c-Fos+/TPH−) cells in the brainstem. DPAT and 5-HT exert similar effects on drinking and sleep [13]. Here, we examined the effects of ICV injection of DPAT on the pattern of c-Fos expression in TPH-immunoreactive and non-immunoreactive cells. Moreover, as we noted previously [12], water intake after these injections produced a different pattern of c-Fos expression. Therefore, we used the same experimental design to test the effects of 5-HT [12]. Fifteen pigeons (both sex, 480–540 g) were cannulated ICV (see procedures in the Section 2.1), assigned to one of three groups (N:5/group) and injected ICV as follows: (1) vehicle (5% ascorbic acid in 0.9% NaCl solution; vehicle group), (2) DPAT (30 nmol) with free access to water after the injection (DPAT + W group) or (3) DPAT (30 nmol) with no access to water (DPAT group). The vehicle-treated animals were provided with free access to water. The behaviors of the animals were recorded for the first 90 min after injection, and water/food intake was quantified at the end of this period. Then, the animals were deeply anesthetized (50 mg/kg ketamine hydrochloride and 10 mg/kg xylazine, IM) and were transcardially perfused with heparin (IVC bolus of 1500 IU) and a sucrose solution (9.25% in 0.02 M phosphate buffer (PB), pH 7.2, at 37 °C) followed by 4% paraformaldehyde in PB. The brains were removed, blocked, post-fixed for 4 h in the same fixative, sectioned at 40 μm using a vibratome (Vibratome 1500 Plus, Vibratome Company, St. Louis, MO, USA) and stored in a cryoprotectant solution at −20 °C until use.

2.10.5. Effects of DPAT and 5-HT ICV injection on c-Fos activation in the hypothalamus and in the prosencephalic periventricular areas

A group of 10 ICV-cannulated, experimentally naive pigeons, which were maintained as described above, were separated into two groups and treated as follows: (1) 5-HT (150 nmol) ICV injection with free access to water (5-HT + W group) and (2) 5-HT ICV injection with no access to water (5-HT group). The experimental procedures, including perfusion and brain preparation, were the same as those described in Section 2.10.4. The data from these groups were compared to the vehicle group described in Section 2.10.4. In Figs. 9 and 10 and in Table 3, the DPAT (N:5) and 5-HT groups (N:5) were only compared to the control group (N:5).

3. Results

3.1. Distribution of 5-HT$_{1AR}$ binding sites in the brainstem and the hypothalamus of the pigeon brain

In both the brainstem and the hypothalamus, [^{3}H]8-OH-DPAT binding sites were most apparent in structures located at the midline or in periventricular (third ventricle) and periaqueductal regions (Table 1; Fig. 4). [^{3}H]8-OH-DPAT binding was intense in the dorsal region of the pons, concentrated in the peri-fasciculus longitudinalis medialis zone (ZpFLM; Fig. 4A; Table 1), in area A6 (the caudal portion of the locus coeruleus; Fig. 4A, Table 1), and in the caudal portion of the griseum centralis (GCt; Fig. 4A; Table 1).

Table 1
[^{3}H]8-OH-DPAT binding values (fmol/mg protein) in brainstem and hypothalamus of the pigeon (N = 6 animals). Data is presented as mean ± SD. The percentage binding values for each structure and the qualitative classification are compared to structure with the maximal binding value (MBV). Brainstem and hypothalamic nuclei are presented in a caudorostral arrangement. ++++, very high; +++, high; ++, moderate; + low.

Brain area	Binding density			
	fmol/mg protein	±SD	Relative density compared with MBV (%)	
Brainstem				
R (nucleus raphe pontis)	180	133	34	++
LoC caudalis (A6)	351	238	68	+++
LoC rostralis (A8)	41	19	8	+
SCd (N. Subcoeruleus dorsalis)	46	19	9	+
SCv (N. Subcoeruleus ventralis)	33	15	6	+
LC (N. Linearis caudalis)	345	161	66	+++
CS (N. Centralis Superior)	138	144	26	++
ZpFLM (Zone Peri Fasciculus Longitudinalis Medialis)	510	289	98	++++
Anl (N. Annularis)	517	222	100	MBV ++++
GCt caudalis (Substantia Gricea Centralis, pars caudalis)	315	166	61	+++
GCt rostralis (Substantia Gricea Centralis, pars rostralis)	38	13	7	+
PME (Posterior median eminence)	144	71	27	++
RPO (N. Reticularis Pontis Oralis)	24	15	5	+
Hypothalamus				
IN (N. Infundibuli Hypothalami)	57	44	11	+
PVO (Organum Pavaventriculare)	444	179	86	+++
MM (N. Mamillaris Medialis)	250	137	48	++
ML (N. Mamillaris Lateralis)	36	13	7	+
PMM (N. Premamillaris)	179	64	34	++
VMN (N. Ventromedialis Hypothalami)	102	24	20	+
LHy (N. Lateralis Hypothalami)	98	29	19	+
SCI (Stratum Cellulare Internum)	31	26	6	+
SCE (Stratum Cellulare Externum)	25	3	5	+
PVNm (N. Paraventricularis, pars magnocellularis)	171	35	33	++
PVNp (N. Paraventricularis, pars parvocellularis)	82	51	16	+
PLH (N. Lateralis Hypothalami Posterioris)	112	72	22	++
PMH (N. Medialis Hypothalami Posterioris)	229	164	44	++
AM (N. Anterior Medialis Hypothalami)	48	61	9	+
POM (N. Preopticus Medialis)	103	35	20	+
POA (N. Preopticus Anterior)	357	115	69	+++
PPM (N. Magnocellularis Preopticus)	143	77	27	++
FDB (Fasciculus Diagonalis Brocae)	273	133	53	+++
SOe (N. Supraopticus externus)	258	85	50	++
PD (N. Preopticus Dorsalis)	274	90	53	+++

Discrete labeling was detected in the rostral portion of the GCt (Fig. 4B; Table 1). Moderate labeling was detected in the midline ventral raphe nucleus (Fig. 4A; Table 1). In the mesencephalon, the highest densities of [^{3}H]8-OH-DPAT labeling were detected in the medial portion of the nucleus annularis (Anl) and in the rostral portion of ZpFLM (Fig. 4B; Table 1). The Anl displayed the maximal binding value (MBV; 517 fmol/mg protein = 100%), to which all other structures were compared. In the pontomesencephalic midline, the linearis caudalis (LC) and centralis superior (CS) nuclei displayed high and moderate levels of [^{3}H]8-OH-DPAT binding, respectively (Fig. 4B; Table 1). Modest labeling was observed in the lateral monoamine-containing nuclei sub coeruleus dorsalis (SCd) and in the sub coeruleus ventralis (SCv) (Table 1), in area A8 (the rostral portion of the locus coeruleus; Fig. 4B; Table 1), and in the reticularis pontis oralis nucleus (RPO) (Table 1).

Binding to [^{3}H]8-OH-DPAT in the hypothalamus and the preoptic region was highly localized to medial structures. In the posterior hypothalamus, the highest concentration of all hypothalamic nuclei investigated was detected in the paraventricular organ (PVO; 86% of the staining in the MBV, the Anl; Fig. 4D; Table 1), a bilateral circumventricular organ that is located at the posteroventral wall of the third ventricle. The posterior median eminence (PME; another circumventricular organ), displayed moderate expression of [^{3}H]8-OH-DPAT-binding sites (Fig. 4C; Table 1). We also found moderate labeling abutting the mamillaris medialis nucleus (MM; Fig. 4D; Table 1) and in the pre-mamillaris nucleus (PMM; Table 1). Discrete labeling was detected in the nuclei infundibuli (IN; Fig. 4D; Table 1) and in the mamillar lateralis (ML) (Table 1). In the medial hypothalamus, we detected moderate [^{3}H]8-OH-DPAT binding in the paraventricular nucleus (magnocellular portion, PVNm; 171 ± 35 fmol/mg protein; parvocellular portion, PVNp; 82 ± 51 fmol/mg protein; Fig. 4E; Table 1), in the nucleus preopticus medialis (POM) (Table 1), in the nucleus medialis hypothalami posterioris (PMH) and in the nucleus lateralis hypothalami posterioris (PLH, Fig. 4E; Table 1). Low levels of [^{3}H]8-OH-DPAT binding were detected in the nucleus lateralis hypothalami (LHy) (Fig. 4E; Table 1), in the stratum cellular internum (SCI), in the stratum cellulare externum (SCE) (Table 1) and in the anterior medialis hypothalami (AM) (Fig. 4E; Table 1). In the anterior hypothalamic and preoptic areas, medial (preopticus anterior, POA; magnocellularis preopticus, PPM; and preopticus dorsalis, PD) and lateral structures (supraopticus externus, SOe; fasciculus diagonalis Brocae, FDB) displayed moderate (PPM and SOe) to high (POA, PD and FDB; Fig. 4E; Table 1) levels of [^{3}H]8-OH-DPAT binding.

3.2. Effects of pretreatment with MM77 on the ingestive and behavioral responses induced by ICV injection of 5-HT or DPAT

Two-way ANOVA revealed that 5-HT injection produced significant changes in drinking behavior and SLB. 5-HT injection increased water intake ($F_{1,42}$ = 149, p = 0.001; interaction: $F_{1,42}$ = 9.2, p = 0.0004) (Fig. 5) and drinking frequency ($F_{1,42}$ = 149, p < 0.0001) and duration ($F_{1,42}$ = 32, p < 0.0001) and also decreased the latency to the first episode of drinking ($F_{1,42}$ = 7.5, p = 0.008; Table 1, Supplementary material). 5-HT also increased the SLB duration ($F_{1,42}$ = 12,

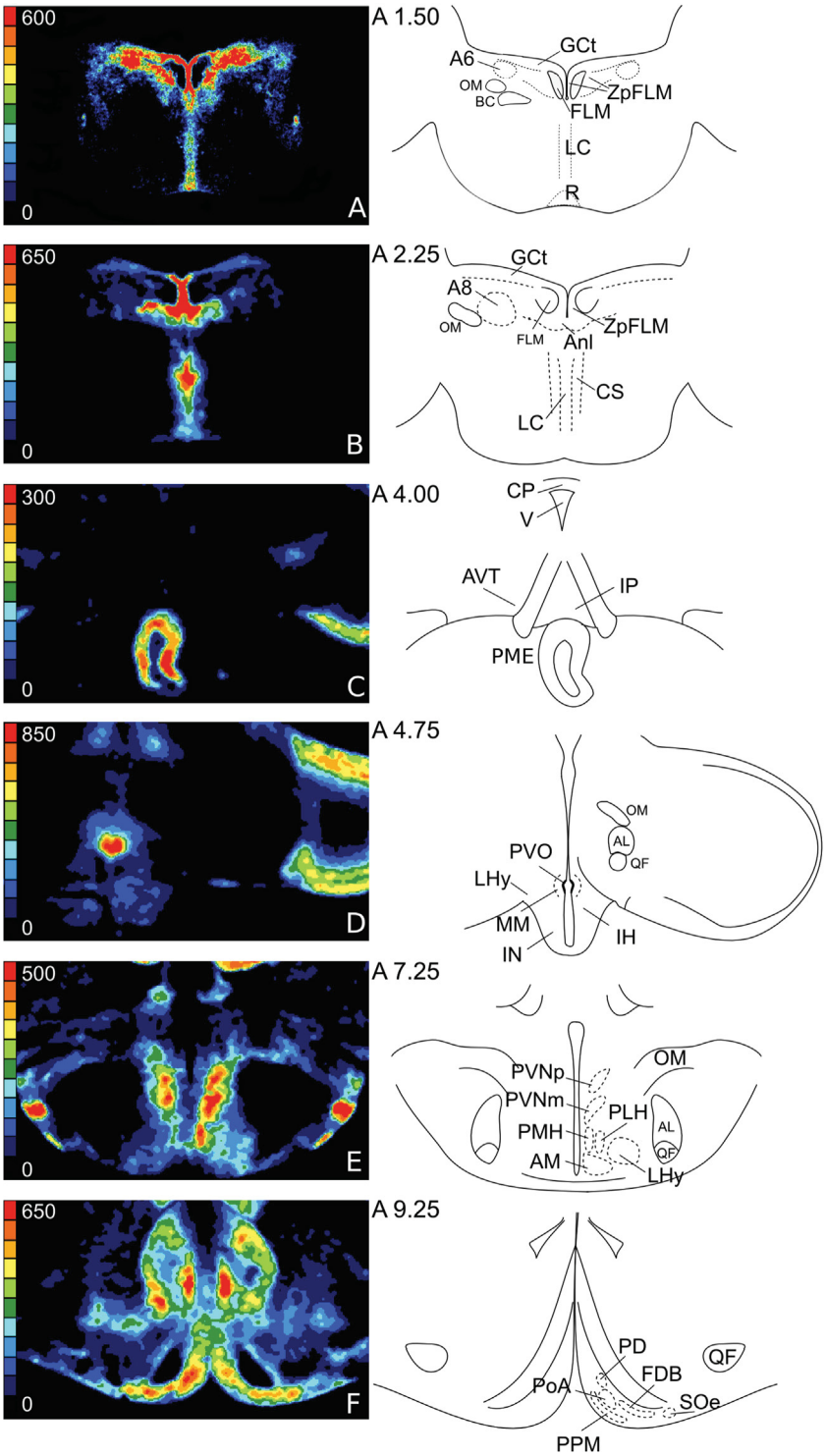

Fig. 4. Color-coded autoradiographs of [^{3}H]8-OH-DPAT binding in the pigeon brainstem (left column, A and B, letters in the lower right corner) and hypothalamus (C–F), arranged in caudo-rostral order. (N = 6 animals). The color-coding indicates the density of [^{3}H]8-OH-DPAT-binding sites in terms of fmol/mg protein. Note that the color-coding of each image is optimized to the overall DPAT-binding site density. The maximum DPAT binding level was detected in the AnI (Panel B). In the right column, schematic drawings of frontal sections of the pigeon brain show the structures examined. Alphanumeric characters placed at the upper left corner indicate the approximate stereotaxic levels according to the Karten and Hodos atlas [44]. For abbreviations, see the list and Table 1.

$p = 0.0004$; interaction: $F_{2,42} = 3.6$, $p = 0.0004$) (Fig. 5) and frequency (5-HT: $F_{1,42} = 6.2$, $p = 0.01$; interaction: $F_{2,42} = 3.2$, $p = 0.05$) and decreased the latency to the first SLB episode ($F_{1,42} = 6.1$, $p = 0.02$; interaction: $F_{2,42} = 3.2$, $p = 0.05$; Table 1, Supplementary material). However, 5-HT injection did not alter food intake or feeding behavior (Fig. 5). Pretreatment with MM77 reduced the effects of 5-HT on water intake (Fig. 5) and drinking duration (Table 1, Supplementary material). The MM77 23 nmol dose decreased the effect of 5-HT on drinking latency, and the 69 nmol dose blocked the effect of 5-HT on drinking frequency (Table 1, supplementary material). MM77 failed to alter food or water intake or feeding or drinking behavior (Fig. 5). Both MM77 doses completely blocked

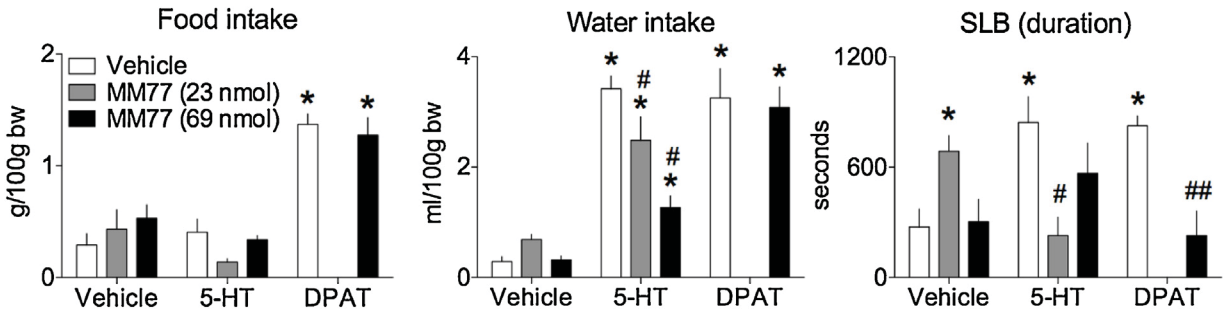

Fig. 5. The effects of ICV injection of 5-HT (0 or 150 nmol, $N = 8$) or DPAT (0 or 30 nmol, $N = 8$) on food and water intake and on sleep-like behavior (SLB duration after pretreatment with MM77 (0, 23 or 69 nmol)). The data are expressed as the means ± standard error of the mean (S.E.M.). $^{*}p < 0.05$ compared to animals treated with vehicle followed by vehicle injection; $^{\#}p < 0.05$ compared to animals treated with vehicle followed by 5-HT injection; and $^{\#\#}p < 0.05$ compared to animals treated with vehicle followed by DPAT injection.

the 5-HT-induced increase in the duration and latency of SLB (Fig. 5).

Supplementary Table S1 related to this article can be found, in the online version, at http://dx.doi.org/10.1016/j.bbr.2015.03.059.

Similarly, DPAT affected drinking behavior and SLB. Moreover, this treatment produced significant effects on feeding. DPAT injection increased water intake ($F_{1,20} = 40$, $p < 0.0001$) (Fig. 5) and drinking duration ($F_{1,20} = 34$, $p < 0.0001$) and frequency ($F_{1,20} = 7$, $p = 0.01$), and decreased the latency to the first drinking episode ($F_{1,20} = 14$, $p < 0.0001$) (Table 2, Supplementary material). DPAT injection increased food intake ($F_{1,20} = 43$, $p < 0.0001$) (Fig. 5) and feeding frequency ($F_{1,20} = 6.7$, $p = 0.01$) and duration ($F_{1,20} = 63$, $p < 0.0001$) and decreased the latency to the first episode of feeding ($F_{1,20} = 20$, $p = 0.0002$) (Table 2, Supplementary material). DPAT also increased the SLB duration ($F_{1,20} = 8.6$, $p = 0.008$; interaction: $F_{1,20} = 8.5$, $p = 0.008$) (Fig. 5) and decreased the latency to the first SLB episode ($F_{1,20} = 5.6$, $p < 0.0001$) (Table 2, Supplementary material). MM77 did not affect feeding or drinking behavior induced by DPAT. However, MM77 effectively blocked the effects of DPAT on SLB duration ($F_{1,20} = 8.5$, $p = 0.008$) (Fig. 5) and latency ($F_{1,20} = 6.6$, $p = 0.008$) (Table 2, supplementary material). The only per se effect of MM77 injection was a significant increase in SLB duration at the 23 nmol dose (Fig. 5).

Supplementary Table S2 related to this article can be found, in the online version, at http://dx.doi.org/10.1016/j.bbr.2015.03.059.

3.3. Effects of the neurotoxin 5,7-DHT on the ingestive and behavioral responses induced by ICV injection of 5-HT or DPAT

5,7-DHT injection reduced the 5-HT levels in the brainstem ($H_{4,29} = 17.2$, $p = 0.0017$), the hypothalamus ($H_{4,29} = 14.6$, $p = 0.005$) and the hippocampus ($H_{4,29} = 11.8$, $p = 0.01$) compared to the controls. However, 5,7-DHT did not alter the 5-HT levels in the arcopallium (Table 2). The analyses revealed no significant alteration in the 5-HT,NA or HVA levels in sham-injected compared to control pigeons. In the brainstem, a 56 ± 10% reduction in group DHT12 ($p = 0.02$) and a 65 ± 7% reduction in group DHT28 ($p = 0.013$) were detected (Table 2) compared to the corresponding vehicle-treated groups. In the hypothalamus, this reduction was of 80 ± 33% ($p = 0.003$) in group DHT12 and 70 ± 22% in group DHT28 ($p = 0.012$; Table 2). In the hippocampus, we detected 66 ± 35% and 40 ± 20% reductions in the DHT12 and DHT28 groups, respectively (Table 2). 5,7-DHT injection also decreased the level of the 5-HT metabolite 5-HIAA in the hypothalamus ($H_{4,29} = 10$, $p = 0.01$) and in the hippocampus ($H_{4,29} = 7.4$, $p = 0.001$) in both the DHT12 and DHT28 groups. We did not detect any significant change in the 5-HIAA levels in the brainstem or the arcopallium in any group injected with 5,7-DHT (data not shown). Moreover, 5,7-DHT did not affect the NA or HVA levels in any examined structure (data not shown). Furthermore, injection of 5,7-DHT decreased the number of TPH+ neurons in the brainstem. This effect of 5,7-DHT was detected in all serotonergic areas, and the most affected nuclei are depicted in Fig. 6. Two-way ANOVA revealed that 5-HT and DPAT increased water intake ($F_{2,24} = 88$, $p < 0.0001$) and SLB ($F_{2,24} = 20$, $p < 0.0001$). Moreover, DPAT increased food intake ($F_{2,24} = 53$, $p < 0.0001$) (Fig. 7). Injection of 5,7-DHT did not affect the ingestive or hypnogenic effect of 5-HT or DPAT. Additionally, 5,7-DHT increased SLB induced by 5HT but did not affect SLB or feeding stimulated by DPAT (Fig. 7).

3.4. Effects of DPAT ICV injection on c-Fos activation in TPH-immunoreactive and -non-immunoreactive neurons in serotonergic brainstem areas

Injection of DPAT increased the number of c-Fos-immunoreactive (c-Fos+) cells in Anl ($H_{2,15} = 10$, $p = 0.006$) and ZpFLM ($H_{2,15} = 13$, $p = 0.001$) (Fig. 8). Moreover, DPAT increased the number of double-labeled (c-Fos+/TPH+) cells in the LC ($H_{2,15} = 9.8$, $p = 0.007$), Anl ($H_{2,15} = 7.3$, $p = 0.02$) and ZpFLM ($H_{2,15} = 9.2$, $p = 0.01$). When animals were allowed to drink (DPAT + W), c-Fos activity increased in the nucleus raphe pontis ($F_{2,12} = 11$, $p = 0.001$) and the LC (Fig. 8). In Anl and ZpFLM, allowance of water intake decreased the effect of DPAT injection on the number of c-Fos+ cells ($p < 0.002$ for DPAT vs. DPAT + W, Mann–Whitney post hoc test for both nuclei) (Fig. 8). The density of double-labeled cells was increased in the LC, Anl and ZpFLM in both DPAT-treated groups. ANOVA did not indicate any significant effect of DPAT injection on TPH labeling among the different groups (Fig. 8). No change in the number of

Table 2
Effects of the neurotoxin 5,7-DHT on the 5-HT levels in different areas of the pigeon brain ($n = 6$/experimental group). The values are presented as the % of the values in the control animals. The (−) symbol in front of a number indicates a reduction. The data are expressed as the medians ± interquartile range.

Groups	Brainstem	Hypothalamus	Hippocampo	Arcopalium
Sham 12	−3.9 ± 14.2	−2.1 ± 53.1	−1.4 ± 38.8	−2.5 ± 24.5
Sham 28	−1.8 ± 13.3	−2.6 ± 86.8	18.3 ± 39.4	−0.5 ± 58.6
DHT 12	−56.6 ± 10.5*	−80.08 ± 33.2*	−66.4 ± 35.6*	−0.18 ± 45.4
DHT 28	−64.8 ± 7.2*	−70.1 ± 22.4*	−40.4 ± 20.6*	36.7 ± 25.2

* $p < 0.05$ compared to the control untreated animals (set as 100%, data not shown).

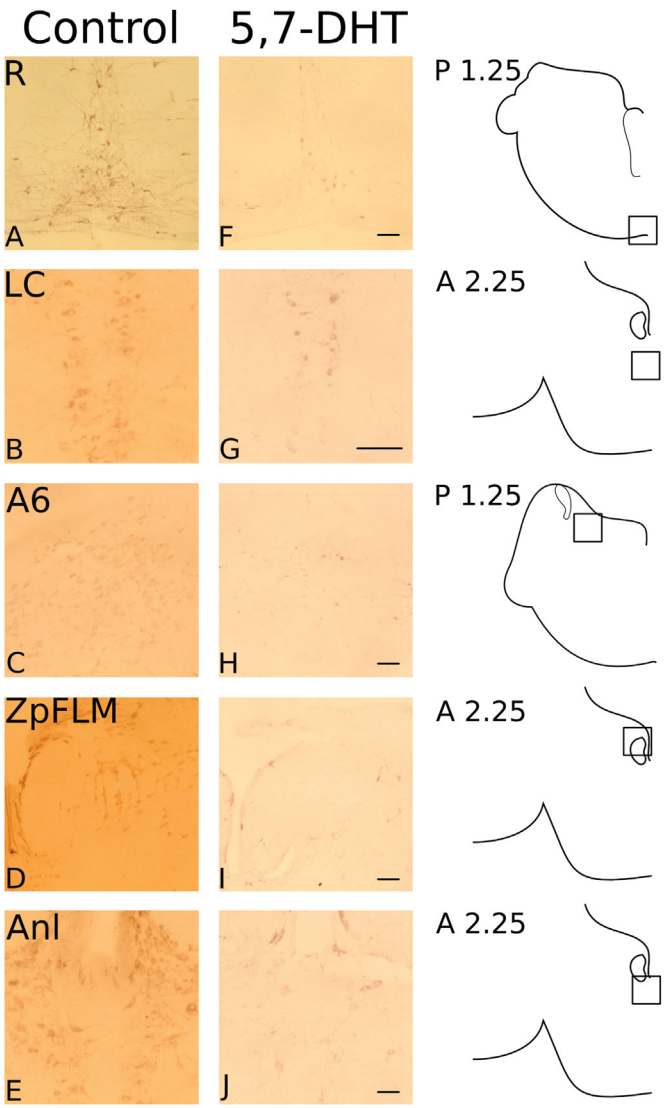

Fig. 6. Effects of 5,7-DHT injections on the density of TPH-immunoreactive cells in brainstem nuclei containing 5-HT neurons ($N = 6$). Left two columns: photomicrographs of control untreated animals (panels A–E) and animals injected ICV with 5,7-DHT (panels F–J). Right column: schematic drawings of frontal sections of the pigeon brain showing the anatomical location of the analyzed structures. The alphanumeric characters placed at the upper left corner indicate the approximate stereotaxic levels according to the Karten and Hodos atlas [44]. Scale bar = 100.

c-Fos+ or double-labeled cells in area A6 or A8 was detected (data not shown).

3.5. Effects of DPAT and 5-HT ICV injection on c-Fos activation in the hypothalamus and in prosencephalic periventricular areas

DPAT injection increased c-Fos labeling in the subfornical organ (SFO: $H_{2,15} = 9.4$, $p = 0.009$), the preopticus medialis (POM: $F_{2,12} = 12.5$, $p = 0.002$), the preopticus anterior (POA: $F_{2,12} = 27$, $p < 0.0003$) (Table 3), the dorso medialis hypothalami (DMN: $F_{2,12} = 26$, $p < 0.001$), the ventro medialis hypothalami (VMN: $F_{2,12} = 34$, $p = 0.001$) and in the LHy ($F_{2,12} = 21$, $p = 0.001$) (Fig. 9). DPAT also increased the number of c-Fos+ cells in bed nucleus of the stria terminalis pars lateralis (BNSTl: $H_{2,15} = 12$, $p = 0.002$) and in septal lateral areas (SL: $H_{2,15} = 93$, $p < 0.0001$) (Table 3). In the animals allowed to drink after DPAT injection, we detected an increase in the number of c-Fos+ cells in the SFO ($H_{2,15} = 9.4$, $p = 0.009$), the PVN ($H_{2,15} = 7.9$, $p = 0.001$) and the POA (Table 3; Figs. 9 and 10). In the SL and the POM, the effects of DPAT on c-Fos expression were increased after water intake (post hoc analysis, $p < 0.001$ for DPAT vs. DPAT + W for both nuclei) (Table 3). Conversely, a decrease in DPAT-induced c-Fos+ cells was detected in the BNSTl after water intake (Mann–Whitney U test, $p = 0.009$) (Table 3). In the PVO ($F_{2,12} = 48.1$ $p < 0.0001$) and the PVN, we detected an increase in c-Fos+ cells only in the animals that were allowed to drink after injection (Fig. 9; Table 3).

5-HT increased the number of c-Fos+ cells in almost all hypothalamic nuclei examined (PVO: $F_{2,12} = 9.4$, $p = 0.02$; SFO: $H_{2,15} = 14$, $p = 0.002$; PVN: $H_{2,15} = 21$, $p = 0.001$; POM: $F_{2,12} = 37$, $p = 0.001$; and POA: $F_{2,12} = 18$, $p = 0.002$) (Table 3). Moreover, 5-HT increased the number of c-Fos+ cells in the SL ($H_{2,15} = 12{,}5$, $p = 0{,}002$) and the BSTNl ($H_{2,15} = 37.3$, $p < 0.0001$). Water intake decreased the effect of 5-HT on c-Fos activity in the SL, the BSTNl and the POM and blocked the 5-HT-mediated increase in the number of c-Fos+ cells in the PVO and the SFO (Fig. 9; Table 3). However, 5-HT injection decreased the number of c-Fos+ cells in the DMN ($F_{2,12} = 14$, $p < 0{,}03$) and the LHy ($F_{2,12} = 16$, $p < 0{,}05$) (Fig. 9).

4. Discussion

The present data indicate that 5-HT$_{1ARs}$ are densely concentrated in the brainstem and in the periventricular preoptic-hypothalamic areas of the pigeon brain, extending previous findings that these receptors are widely distributed in the pallial and pretectal/tectal regions in this species [33]. The radioligand [^{3}H]-8-OH-DPAT appeared to bind most strongly to post- and pre-synaptic 5-HT$_{1ARs}$; DPAT is a highly specific 5-HT$_{1AR}$agonist [58,59,60] that has been used as a radioligand to determine the distribution of 5-HT$_{1ARs}$ in various vertebrate species [61,27,54,62–65]. However, DPAT also displays moderate affinity for the 5-HT$_{7R}$ subtype (in guinea-pig: [66,67]), rat and human

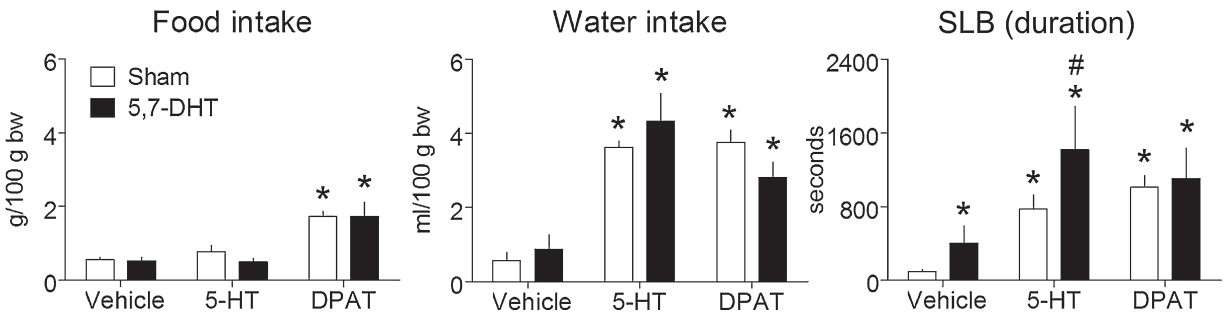

Fig. 7. Effects of ICV injection of 5-HT (150 nmol) or DPAT (30 nmol) on food and water intake and SLB after pre-treatment with 5,7-DHT or vehicle (Sham; $N = 6$/experimental group). The data are expressed as the means ± S.E.M. $^*p < 0.05$ compared to sham animals treated with vehicle; $^\#p < 0.05$ compared to sham animals treated with 5-HT.

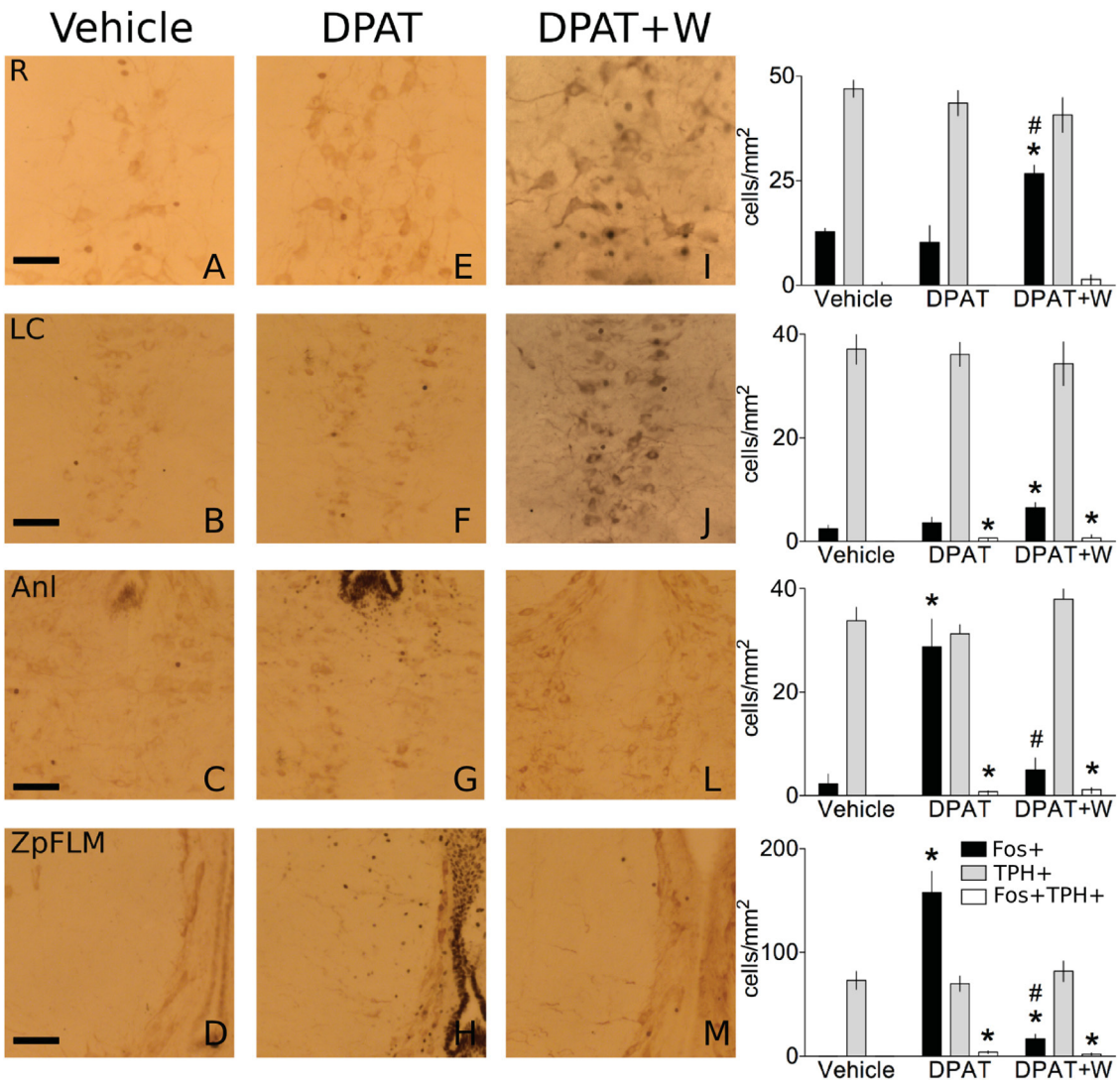

Fig. 8. Representative photomicrographs showing the effects of ICV injection of DPAT (30 nmol) on the number of c-Fos+, TPH+ and double-labeled cells in brainstem nuclei (N = 8/experimental group). DPAT-injected animals were provided with no (DPAT; panels E–H) or with free access to water (DPAT + W; panels I–M) after injection. $^{*}p < 0.05$ compared to the vehicle group (panels A–D). Scale bar = 100 μm. $^{\#}p < 0.05$ compared to DPAT. The c-Fos countsin the R nucleus and the LC are expressed as the means ± S.E.M. The c-Fos counts in Anl and ZpFLM and all TPH+ and double-labeled cells are expressed as the medians ± interquartile range. For abbreviations, see the list.

brain tissue [68]. To avoid the binding of [^{3}H]-8-OH-DPAT to 5-HT$_{7Rs}$, we used a concentration that does not bind to 5-HT$_{7Rs}$ in 5-HT$_{1AR}$ knockout mice. Bonaventure and colleagues [69] demonstrated that 1 or 2 nmol [^{3}H]-8-OH-DPAT does not bind or displays a very low binding density in the septal area of knockout mice compared to the moderate to high binding densities in the area of wild-type animals [69]. Consistently, lower K_D values (1.3 nM, 95% confidence interval 0.35–2.25 nM) were obtained in the septum of wild-type animals than in that of knockout animals (5-HT$_{1AR}$ knockout animals: 20 nM, 95% confidence interval 14–27 nM). At 10 nM [^{3}H]8-OH-DPAT, high densities were detected in both wild-type and 5-HT$_{1AR}$ knockout mice [69], suggesting that at higher doses than the one used in this study, DPAT binds to receptors other than 5-HT$_{1ARs}$.

Table 3
Effects of ICV injection of vehicle, DPAT (30 nmol) or 5-HT (150 nmol) on c-Fos protein expression in hypothalamic nuclei (PVO, SFO, PVN, POM and POA) and in the SL and the BNSTl (N = 8/experimental group). The symbol +W indicates the animals treated with DPAT or 5-HT that were provided with free access to water after injection. Vehicle-treated animals also received free access to water for all experiments. For the structure names, see Table 1. The data for the SFO, the PVN, the BNSTl and the SL are expressed as the medians ± interquartile range. For abbreviations, see the list.

Groups/nuclei	PVO	SFO	PVN	BSTNl	SL	POM	POA
Vehicle	7 ± 1.4	17.6 ± 4.5	56.4 ± 5.9	21.8 ± 4.2	9 ± 1.2	9.6 ± 1.3	4.8 ± 1.4
DPAT	14.4 ± 2	123 ± 16*	71.6 ± 8.6	421 ± 36*	346 ± 25*	30.4 ± 3.6*	40.4 ± 3*
DPAT + W	57.6 ± 8*,#	128 ± 10*	120 ± 3*,#	79.2 ± 6.2*,#	786 ± 65*,#	117 ± 9*#	27.6 ± 5*
5-HT	26 ± 5.5*	60.2 ± 7.3*	137 ± 3*	118 ± 11*	835 ± 100*	108 ± 11*	24.6 ± 3.3*
5-HT + W	4.4 ± 1.4#	24.2 ± 5.7#	153 ± 5*	86.2 ± 6.6*,#	285 ± 37*,#	56 ± 8*#	34 ± 4.8*

* $p < 0.05$ compared to the vehicle group.
# $p < 0.05$ for DPAT vs. DPAT + W or 5-HT vs. 5-HT + W.
The c-Fos counts in the PVO, the POM and the POA are expressed as the means ± S.E.M.

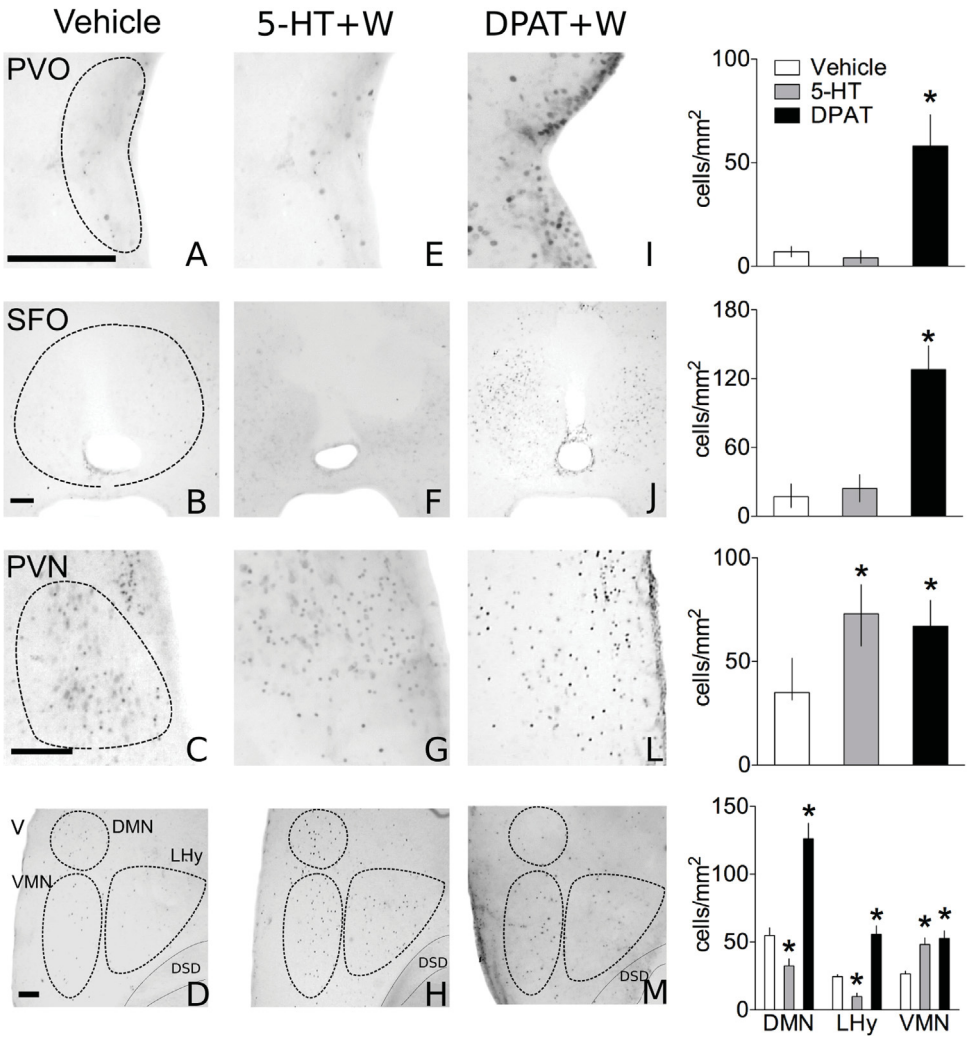

Fig. 9. Representative photomicrographs showing the effects of ICV injection of 5-HT (150 nmol) or DPAT (30 nmol) on the number of c-Fos+ cells in hypothalamic nuclei: vehicle group (panels A–D); 5-HT + W group (panels E–H);and DPAT + W group (panels I–M; $N = 6$/experimental group). All animals were provided with free access to water after injection. $^{*}p < 0{,}05$ compared to the vehicle group. Scale bar = 100 μm. The c-Fos counts for the PVO, the VMN, the DMN and the LHy are expressed as the means ± S.E.M. The data for the SFO and the PVN are expressed as the medians ± interquartile range. For abbreviations, see the list.

In those pontomesencephalic areas that were examined, [^{3}H]-8-OH-DPAT binding was localized to nuclei previously reported to contain high concentrations of 5-HT-immunoreactive cell bodies in pigeons, chickens and quails (e.g., [70–73,14]) and TPH (the rate-limiting enzyme in the biosynthesis of 5-HT)-immunoreactive cell bodies in pigeons [46,12]. These nuclei (R, Anl, ZpFLM, LC, A6 and A8) constitute the rostral or superior raphe nuclei in birds; areas A6 and A8 in pigeons also contain dense populations of dopaminergic (A8) or noradrenergic (A6) neurons [74,75] that appear to partially overlap with the serotonergic perikarya. Dense populations of 5-HT_{1ARs} are found in the raphe nuclei are comparable to those in mammals (rodents: [28,38]); humans: [76]. In the mammalian midbrain raphe nuclei, 5-HT_{1ARs} control 5-HTergic neuron firing and 5-HT release [77–79], acting as somatodendritic autoreceptors to inhibit 5-HTergic neuron firing and release upon stimulation with endogenous 5-HT or 5-HT_{1AR} agonists. These 5-HT_{1ARs} are not tonically activated by endogenous 5-HT under resting, physiological conditions, but 5-HT_{1ARs} can inhibit the 5-HTergic neuron firing rate and 5-HT efflux in response to endogenous 5-HT surges evoked by changes in the behavioral state of the animal [80–82].

In pigeons, systemic injection of DPAT decreases the levels of 5-HIAA (a 5-HT metabolite) but does not change the levels of other monoaminergic metabolites in the cerebrospinal fluid (CSF) [22,23,83], suggesting that in this species, this 5-HT_{1AR} agonist decreases the activity of 5-HTergic neurons. The 5-HIAA levels in the mammalian ventricular CSF have been shown to reliably indicate serotonergic activity in the brain (e.g., [84]). Along these lines, it is interesting that ICV 5-HT injection into pigeons *reduced* c-Fos expression in TPH+ neurons in the LC and areas A6 and A8 but not in the pontine raphe nucleus [12]. These results suggest that, although the precise cellular localization of these binding sites cannot be determined based on the autoradiography method used here, the observed labeling may be at least partially associated with somatodendritic inhibitory 5-HT_{1ARs} on serotonergic neurons in the raphe nuclei.

However, it appears that inhibition of 5-HTergic neurons due to activation of somatodendritic 5-HT_{1ARs} is not sufficient to account for the acute neural and behavioral effects of ICV 5-HT or DPAT injection. Injection of DPAT produced a modest increase in the number of c-Fos+ (in Anl and ZpFLM) and c-Fos+/TPH+ cells (in the LC, Anl and ZpFLM, present data) predominantly in the *animals that were allowed to drink*. Alternatively, ICV 5-HT injection consistently *reduced* the number of c-Fos+/TPH+ neurons when the animals *were not allowed* to drink [12]. These data suggest that 5-HTergic neuronal activity in the raphe nuclei tends to increase slightly or return to basal levels when the animal satisfies its 5-HT- or DPAT-evoked

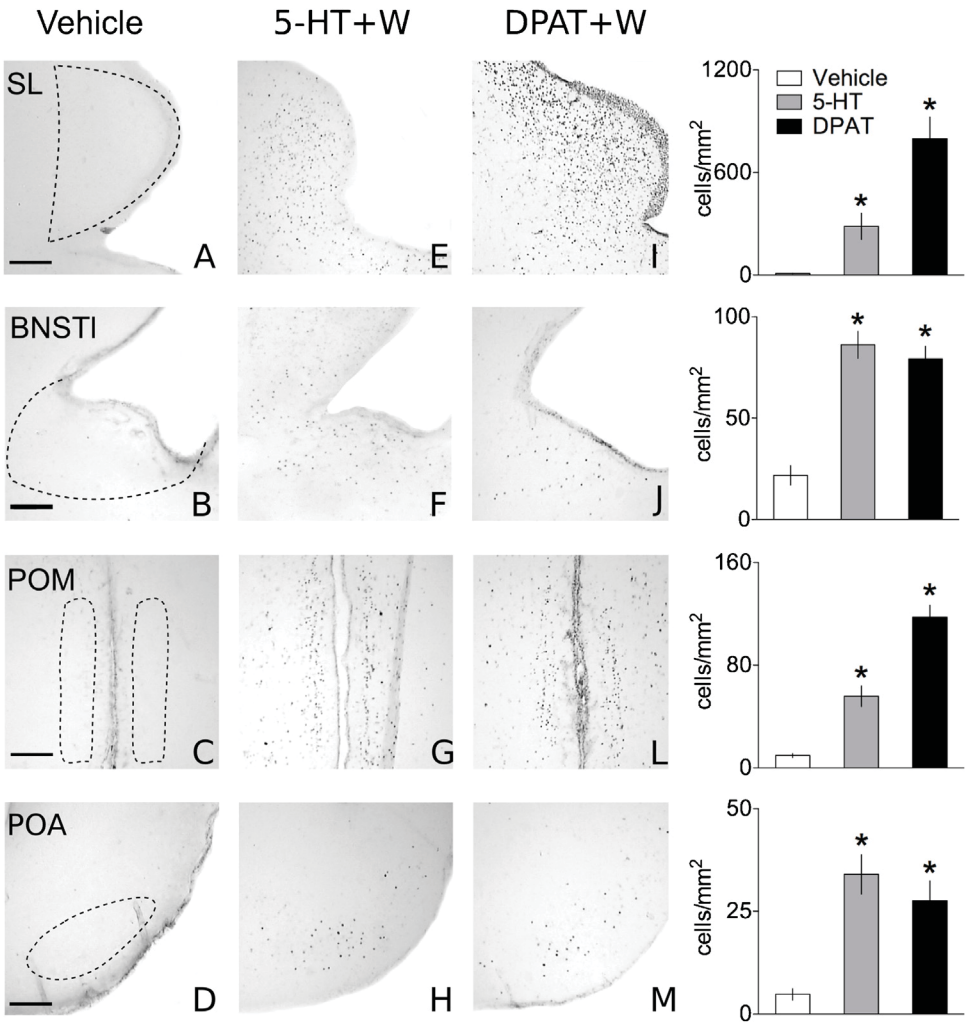

Fig. 10. Representative photomicrographs showing the effects of ICV injection of 5-HT (150 nmol) or DPAT (30 nmol) on the number of c-Fos+ cells in the hypothalamic nuclei: vehicle group (panels A–D); 5-HT + W group (panels E–H); and DPAT + W group (panels I–M; $N = 6$/experimental group). All animals were provided with free access to water after injection. Scale bar = 100 μm. $^{*}p < 0.05$ compared to the vehicle-treated group. The c-Fos counts in the POM and the POA are expressed as the means ± S.E.M. The data for the BNSTl and the SL are expressed as the medians ± interquartile range. For abbreviations, see the list.

search for water and that the reduced activity of 5-HTergic neurons in the raphe nuclei may be associated with a thirst-like state or may be associated to the act of drinking per se.

Furthermore, bilateral ICV injection of 5,7-DHT (200 μg/ventricle) decreased the 5-HT levels in the upper brainstem, the hypothalamus and the hippocampus and reduced the number of TPH+ neurons in the raphe nuclei. Our findings differed quantitatively from those of a previous study that administered the same toxin to pigeons [37]. They performed a single intraaqueductal injection of 5,7-DHT (600 μg), and 9 and 60 days after injection, they detected a decrease in the 5-HT levels in a pallial visual area (the Wulst) and in the optic tectum but not in the brainstem. The causes of these conflicting results remain unclear, but they may be related to the differences in the injection volume/site or the different size and rostrocaudal span of the brainstem samples examined; they used 5.5 mm long samples from the caudal medulla oblongata (P3.00) to the rostral pontine levels (A2.50), whereas we sampled only the rostral pons (between A1.00 and A2.25 levels). In rodents, intense reductions in TPH activity and the 5-HT levels in the hippocampus and cerebral cortex and decreases in [^{3}H]-8-OH-DPAT binding exclusively in the midbrain raphe nuclei were detected after intracerebral injection of 5,7-DHT (e.g., [38]). Intracisternal [85] or intra-raphe nuclear (median or dorsal; [40]) injection of 5,7-DHT impaired feeding induced by systemic injection of DPAT, suggesting that DPAT-induced feeding is dependent on activation of somatodendritic, inhibitory 5-HT$_{1A}$Rs in rats.

Conversely, and despite the apparently intense and selective 5,7-DHT-induced reduction in 5-HT activity in our pigeons, the ingestive and hypnogenic effects of 5-HT and DPAT ICV injection were not changed in the 5,7-DHT-treated animals. These results may indicate that drinking and sleep induced by DPAT and 5-HT, as well as hyperphagia induced by DPAT, are not dependent on a reduction in the activity of the central 5-HTergic circuitry mediated by activation of inhibitory somatodendritic 5-HT$_{1A}$Rs in pigeons. In fact, 5,7-DHT-induced lesion increased sleep duration in both the vehicle- and 5-HT-treated animals, suggesting that a chronic reduction in brain 5-HT activity induces plastic changes in sleep-related circuits, leading to sleepiness and an increased susceptibility to the sleep-evoking effects of 5-HT. We have shown that ICV injection of DPAT or 5-HT increases the duration of electrographically characterized desynchronized sleep (or rapid-eye-movement, REM) and slow wave sleep (SWS) based on hippocampal EEG recordings [13].

In mammals, sleep states have been associated with decreased activity or inactivity of serotonergic neurons (compared to wakefulness). Dorsal raphe neurons fire intensely during wakefulness

but exhibit decreased firing during SWS and cease firing during REM sleep [17,18]. Perfusion of the dorsal raphe nucleus with DPAT decreased 5-HT release and increased REM sleep in cats [21] and rats [86], indicating that a somatodendritic 5-HT_{1AR}-mediated decrease in the activity of serotonergic neurons is associated with this sleep state. Interestingly, similar to the findings in pigeons [13], sleep and electroencephalographic activity typical of SWS was detected after ICV injection of low doses of 5-HT into mammals [19,87]. The role of 5-HT_{1ARs} has been studied via systemic and intra-raphe injection of the 5-$HT_{1A/7R}$ agonist DPAT. In free-feeding rats, DPAT increases food intake when administered systemically [88,89] or into the dorsal or median raphe nuclei [34,90], and these effects are most likely dependent on the activation of somatodendritic, inhibitory 5-HT_{1ARs} in rats [85,40]. Thus, it appears that DPAT-induced hyperphagia, as well as DPAT- and 5-HT-induced sleep, depend on distinct 5-HT_{1AR}-mediated mechanisms in mammals and pigeons.

We have previously shown that ICV pretreatment with low doses of the 5-HT_{1AR} antagonist WAY100635 attenuates the dipsogenic and hypnogenic effects of low doses of 5-HT (50 nmol), and reduced the DPAT-evoked increases in feeding, drinking and sleep in pigeons [13], confirming that these effects may be dependent on the activation of 5-HT_{1ARs}. WAY100635 displays high affinity for 5-HT_{1ARs} (K_i = 4.5 nM) and antagonist-like activity on both presynaptic and postsynaptic 5-HT_{1ARs} [91,92,35]. Here, we further explored the effects of 5-HT_{1AR} antagonists by injecting MM77 (an agent that acts primarily on postsynaptic 5-HT_{1ARs}) before ICV injection of 5-HT or DPAT. MM77 is characterized as a postsynaptic 5-HT_{1AR} antagonist [43], and its antagonistic effect on postsynaptic 5-HT_{1ARs} has been described [93,45]. In one study [94], the anti-conflict effects of WAY100636 and MM77 were compared in rats whose 5-HTergic neurons were destroyed by prior administration of p-chloroamphetamine (which reduced the hippocampal concentration of 5-HT by ca. 85%). In these animals, the anti-conflict effect of WAY100635, but not MM77, was abolished, indicating that the anxiolytic-like activity of MM77 does not appear to depend on the integrity of presynaptic 5-HT_{1ARs}. The present data indicate that pretreatment with MM77 reduces 5-HT-induced drinking and both 5-HT- and DPAT-induced sleep. If MM77 indeed acts preferably at postsynaptic 5-HT_{1ARs} in pigeons, these results reinforce the concept that the somatodendritic 5-HT_{1AR}-mediated decrease in the activity of serotonergic neurons is of little relevance to these 5-HT-evoked behavioral effects. Surprisingly, MM77 failed to affect DPAT-induced feeding or drinking, indicating that WAY100635 (which attenuated these DPAT-induced responses) and MM77 may display distinct pharmacological profiles with respect to their interactions with DPAT-sensitive receptors.

Beyond the likely expression of somatodendritic 5-HT_{1ARs} on serotonergic neurons in the raphe nuclei, our autoradiographic data indicate that 5-HT_{1ARs} (pre- and/or post-synaptic) are especially concentrated in periventricular hypothalamic and preoptic areas and in the circumventricular organs. These dense [^{3}H]-8-OH-DPAT binding patterns agree with the evidence for dense serotonergic innervation of these medial/paraventricular hypothalamic regions in pigeons [72] and for 5-HT+ and TPH+ cell clusters in the cerebrospinal fluid (CSF)-contacting neurons of circumventricular areas (in the hypothalamic recessus infundibularis, in the PVO and in sub- and supra-ependymal patches in aqueductal levels and throughout the lateral and third ventricles; [95,73,46]) of the pigeon. Furthermore, the medial preoptic nucleus, the anterior-medial hypothalamic area, including the paraventricular and the posteromedial hypothalamic nucleus, have been shown to be extensively inter-connected [96–98] in pigeons. Efferent from these regions innervate the septal lateral, posterior hypothalamic and medial mammillary areas, the median eminence and neurohypophysis, as well as the brainstem, whereas afferent input to these regions originates from CSF-contacting cells (including 5-HT+ neurons), circumventricular organs (SFO, OVLT, area postrema), and limbic and autonomic areas of the brainstem and the prosencephalon in birds. Thus, these periventricular preoptico-hypothalamic receptors are positioned to mediate the important serotonergic functions in reproductive and chronobiologically dependent states (e.g., [99]), in sleep [100,101], in the control of thermal and fuel-related metabolism [100,102,103], and in the performance of ingestive behaviors [103,10,104,12,13], as suggested by local, ICV and systemic injection of 5-HT or drugs that interact with 5-HT_{1ARs} in pigeons and chickens.

The [^{3}H]8-OH-DPAT labeling patterns described here and by Herold and colleagues [33] are in line with the intense c-Fos labeling induced by 5-HT or DPAT ICV injection in these preoptic-hypothalamic periventricular regions and in the SL and the BNSTl. 5-HT injection increased the number of c-Fos+ cells in the parenchyma (PVN, BNSTl, SL, POM and POA) the circumventricular organs (PVO, SFO), which were, exception for the PVN, *attenuated or abolished by drinking*. These data suggest that the 5-HT-induced increase in c-Fos expression in these nuclei may be associated with thirst-related phenomena, whereas that in the PVN may be related to other 5-HT-induced functions. Interestingly, injection of metergoline (an antagonist of 5-$HT_{1/2Rs}$) or GR-46611 (a 5-$HT_{1B/1DR}$ agonist) into the PVN, the posterior medial hypothalamus and the caudal preoptic region evoked feeding without changing water intake in free-feeding pigeons [10], indicating that 5-HT-induced c-Fos activity in the PVN may be related to a 5-HT_{1BR}-mediated effect of 5-HT on feeding behavior. The number of c-Fos+ cells was increased in the PVN, the medial preoptic area, the SFO and the SL of chickens, quails, zebra finches and starlings that had been injected intraperitoneally with hypertonic saline 3 h earlier [105], which increased drinking behavior and the plasma vasotocin and angiotensin II levels in birds [106]. Hypertonic saline-induced c-Fos labeling was shown to co-localize with vasotocin-immunoreactive neurons in the PVN (in magnocellular cells known to project to the neurohypophysis), in the posterior hypothalamus and in the ventral floor of the rostral preoptic area. These data may underscore the relevance of serotonergic mechanisms to hypothalamic that regulate the hydrosaline balance in birds.

Interestingly, DPAT injection altered c-Fos expression in the same regions that were reactive to 5-HT injection, although in a different (even divergent) pattern: the number of c-Fos+ neurons was *increased* in the PVO, PVN, SL and POM among animals allowed to drink. These data suggest that these effects of DPAT on c-Fos expression in these nuclei may be associated with the drinking behavior itself, to the satiation of DPAT-induced thirst, or to other DPAT-induced effects (including hyperphagia and sleep). In addition, the complex pattern of c-Fos activity produced by DPAT injection in hypothalamic areas, in contrast to the limited level of c-Fos activation in serotonergic brainstem areas, contributes to the concept that heterosynaptic or non-somatodendritic presynaptic 5-HT_{1ARs} are crucial for the dipsogenic and hypnogenic effects of 5-HT. Moreover, the differences in c-Fos activity between the 5-HT- and DPAT-injected animals indicate that 5-HT receptors other than 5-HT_{1ARs} also participate in the functions mediated by hypothalamic serotonergic circuits.

The distribution of hypothalamic [^{3}H]-8-OH-DPAT-binding sites in the pigeon is comparable to that in the rodent brain [28,69], including intense expression in the choroid plexus and moderate expression in the paraventricular, dorsomedial, ventromedial, posterior, anterior, mammillary and arcuate nuclei, as well as the preoptic area. The ventromedial, lateral, anterior, and dorsomedial hypothalamus and the paraventricular, magnocellular preoptic and supraoptic nuclei contain cells and cellular processes displaying 5-HT_{1AR}-like immunoreactivity [107,31,32]. Many of these cells also display immunoreactivity to sleep- and feeding-related

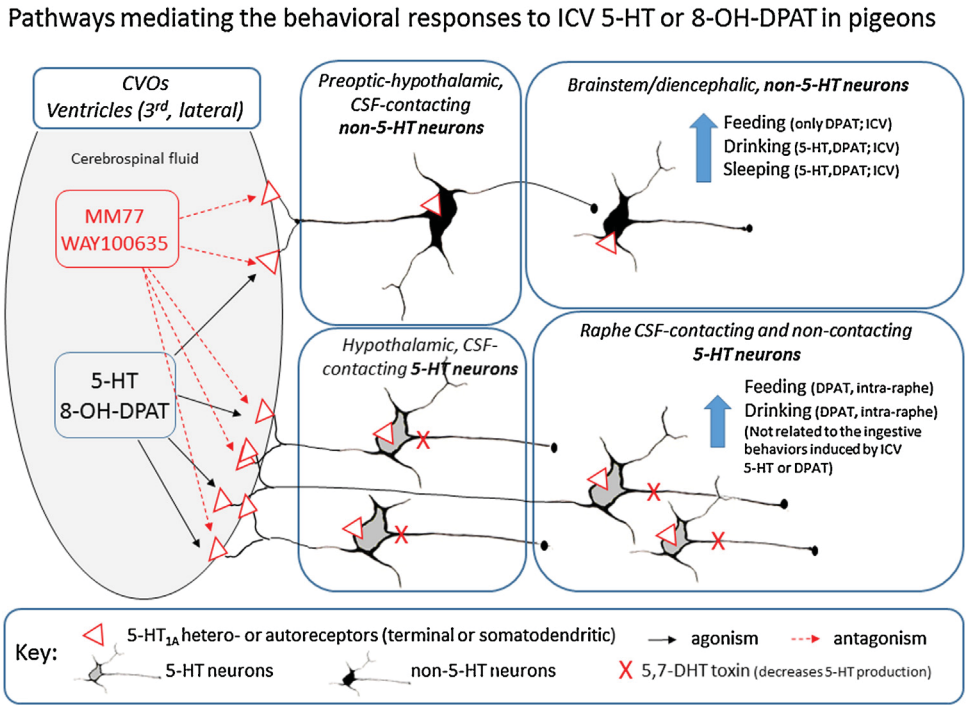

Fig. 11. Schematic diagram summarizing the rationale of the experiments and the main findings of the present report, and showing the putative brain circuits involved in organizing behavioral responses to ICV injections of 5-HT and 8-OH-DPAT in pigeons. As indicated by [^{3}H]8-OH-DPAT labeling, 5-HT1A hetero- or autoreceptors (terminal or somatodendritic) are localized in brainstem raphe, rich in 5-HT-producing neurons, as well as in circumventricular organs (CVOs) and periventricular preoptico-hypothalamic regions. Some of these regions are endowed with cerebrospinal fluid (CSF)-contacting serotonergic and non-serotonergic neurons. ICV injections of 5-HT [13] or 8-OH-DPAT (5-HT1AR agonist; present results) changes c-Fos expression in these regions, and evokes prompt and intense drinking, sleeping and feeding (for 8-OH-DPAT only) responses in free-feeding pigeons. These behavioral responses are blocked by WAY-100635 (5-HT 1AR antagonist of hetero and autoreceptors [13]) and by MM77 (5-HT 1AR antagonist at heteroreceptors; present results). ICV injection of the toxin 5,7-DHT, which decreased the 5-HT levels in the upper brainstem and the hypothalamus and reduced the number of 5-HT-producing neurons in the raphe nuclei, left unchanged the behavioral responses to ICV 5-HT or 8-OH-DPAT. These evidence suggest that the behavioral responses to ICV 5-HT and DPAT are mediated by 5-HT1AR heteroreceptors located at CVOs or diencephalic, CFS-contacting, non-serotonergic neurons and circuits, while 5-HT neurons and circuits located in the hypothalamus or in the raphe nuclei are not involved in these responses. The latter may be also involved in circuits controlling ingestive behaviors, since intra-raphe 8-OH-DPAT injections evoke feeding and drinking in this species [14].

peptides (neuropeptide Y, agouti-related peptide, cocaine- and amphetamine-regulated transcript, melanin-concentrating hormone and orexin; [31]). These results suggest that serotonin acts via postsynaptic 5-HT$_{1ARs}$ to influence the release of feeding-regulated peptides. In line with this hypothesis, it was found that local injections of DPAT into the lateral, arcuate [108,109] and PVN [110] evoked hypophagia in rats. At least in the lateral hypothalamus and the arcuate nucleus, this effect of DPAT was blocked by pretreatment with WAY100635 [108,109].

The massive accumulation of [^{3}H]-8-OH-DPAT labeling and 5-HT-induced c-Fos reactivity in the periventricular hypothalamic and septal areas containing CSF-contacting neurons may indicate an important role of the ventricular wall and intraventricular 5-HT levels in regulating sleep, feeding and drinking in pigeons. 5-HT-immunoreactive processes containing dense core vesicles invade and heavily populate the ventricular ependymal lining in all vertebrate species examined to date [111,112,95,113,114], and 5-HT+ cells in the PVO and the posterior hypothalamic recess extend processes that protrude into the ventricular lumen and that proceed ependymofugally in all studied non-mammalian species [95,114], including the pigeon [73,46]. Some of these CSF-contacting PVO cells also display TPH immunoreactivity and, thus, may produce 5-HT [46]. Therefore, these subependymal CSF-contacting elements are positioned to synthesize/release 5-HT into the CSF. Some of these cells are also influenced by the intra-CSF 5-HT levels via 5-HT$_{1AR}$ activation [115,114]. The circumventricular organs were repeatedly shown to be associated with both blood- and CSF-borne substances to regulate a variety of functions, including feeding, drinking and circadian sleep regulation (e.g., [116–119]). However, since 5,7-DHT treatment decreased brainstem and hypothalamic 5-HT, but failed to affect the 5-HT$_{1AR}$-mediated, 5-HT behavioral responses to intraventricular 5-HT and DPAT, the fluid-contacting serotonergic neurons (located either in the raphe nuclei or in the periventricular diencephalon) may not be directly responsible for the 5-HT-evoked responses. Thus, it is conceivable that non-serotonergic neurons endowed with 5-HT$_{1A}$ receptors, located in circumventricular organs or parenchymal hypothalamus, with CSF-contacting processes, may constitute the circuit through which ventricular 5-HT influences ingestive and sleep behaviors in pigeons (Fig. 11). The mechanisms controlling the 5-HT content of the CSF, which are located upstream to these non-serotonergic circuits, are unknown and warrant further investigation. Furthermore, these data suggest that the changes in the c-Fos+/TPH+ neurons observed after intraventricular 5-HT and DPAT injections may not be associated to the behavioral effects of these treatments examined in the present report.

Central 5-HT circuits display neurochemical and neuroanatomical characteristics that appear to be highly conserved in vertebrates [120–122]. The present data indicate that the distribution of 5-HT$_{1ARs}$ in the brainstem raphe nuclei and in the periventricular diencephalic structures is comparable to that found in mammals and suggest that 5-HT circuits and 5-HT$_{1ARs}$ play important functional roles in the performance of ingestive and sleep behaviors in an avian species, in parallel with the findings in mammals. However, despite these similarities, the mechanisms by which these circuits generate these similar behavioral effects may depend on distinct or opposing neurobiological mechanisms between rodents (somatodendritic autoreceptor-related) and pigeons

(heterosynaptic- or non-somatodendritic autoreceptor-related). It is conceivable that species- (or taxa-) specific attributes of central 5-HTergic mechanisms co-exist with phylogenetically ancient traits. Further comparative studies of the functional roles of 5-HTergic circuits may discriminate the primitive or shared functional characteristics (that may be of general relevance for vertebrates or result from convergent evolutionary mechanisms) from those which are unique to a given taxon.

Conflict of interest statement

All authors state that they have no actual or potential conflict of interest, including any financial, personal or other relationship with other individuals or organizations that could inappropriately influence the work submitted here.

Role of the funding source

The funding agencies, including CNPq, Capes, FAPESC and DFG, had no influence or role in the study design, in the collection/analysis/interpretation of the data, in the writing of the report, or in the decision to submit the paper for publication.

Authors contribution

Tiago Souza dos Santos: behavioral experiments and design, collection and analysis of behavioral data; writing the manuscript; Jéssica Krueger: behavioral experiments; collection of the neurochemical and behavioral data; Fernando Falkenburger Melleu: collection and analysis of behavioral data; Anicleto Poli: collection and chromatographic analysis of neurochemical data; Christina Herold: autoradiography procedures and image processing; Karl Zilles: experimental design, approval of the final version of the article; Onur Güntürkün: experimental design, approval of the final version of the article; José Marino Neto: experimental design, selection of the theme, data analysis, writing the paper, approval of the final version of the article.

Acknowledgments

This study was supported by CNPq and FAPESC research grants to J. Marino-Neto (proc. 471888/03-6 and 300308/2007-8) and by DFG via grants FOR1581 and SFB874 to O. Güntürkün. F. Melleu and T.S. dos Santos received Graduate (PhD) fellowships from Capes. T.S. dos Santos also received a PhD sandwich fellowship from the CNPq "Science without Borders" Program. J. Kruger received a PIBIC-CNPq undergraduate research fellowship. We wish to thank the helpful comments and suggestions made by Dr. Cilene Lino-de-Oliveira (CCB-CFS-UFSC) to the final version of the manuscript. We wish to thank also the excellent and devoted technical assistance and animal care provided by Mr. Eduardo H. Gonçalves, Mr. Carlos H. Espíndola, Mrs. Joanésia M.J. Rothstein, Mr. Emerson V. Fornalski, Mrs. Sandra R B de Oliveira and Mr. Sandro M. de Jesus throughout the experiments.

References

[1] Blundell J. Serotonin manipulations and the structure of feeding-behaviour. Appetite 1986;7(Suppl.):39–56.
[2] Halford J, Wanninayake S, Blundell J. Behavioral satiety sequence (BSS) for the diagnosis of drug action on food intake. Pharmacol Biochem Behav 1998;61(2):159–68.
[3] Rodgers R, Holch P, Tallet A. Behavioural satiety sequence (BSS): separating wheat from chaff in the behavioural pharmacology of appetite. Pharmacol Biochem Behav 2010;97(1):3–14.
[4] Canello M, Ravazio MR, Paschoalini MA, Marino-Neto J. Food deprivation- vs. intraventricular adrenaline-induced feeding and postprandial behaviors in the pigeon (*Columba livia*). Physiol Behav 1993;54(6):1075–9.
[5] Dario AJ, Lopes PR, Freitas CG, Paschoalini MA, Marino-Neto J. Electrographic patterns of postprandial sleep after food deprivation or intraventricular adrenaline injections in pigeons. Brain Res Bull 1996;39(4):249–54.
[6] Spudeit WA, Sulzbach NS, BITTENCOURT MDEA, DUARTE AM, LIANG H, Lino-de-Oliveira C, et al. The behavioral satiety sequence in pigeons (*Columba livia*). Description and development of a method for quantitative analysis. Physiol Behav 2013;122(62–71):2013.
[7] De Vry J, Schereiber R. Effects of selected serotonin 5-HT1 and 5-HT2 receptor agonists on feeding behavior: possible mechanisms of action. Neurosci Biobehav 2000;24(3):341–53.
[8] Güntürkün O, Grothues A, Hautkappe A, Visé F, Wawrzyniak N, Zwilling U. Serotonergic modulation of ingestive behavior in pigeons. Pharmacol Biochem Behav 1989;32(2):415–20.
[9] Steffens SM, Casas DC, Milanez BC, Freitas CG, Paschoalini MA, Marino-Neto J. Hypophagic and dipsogenic effects of central 5-HT injections in pigeons. Brain Res Bull 1997;44(6):681–8.
[10] Da Silva RA, Da Silva AS, Poffo MJ, Ribas DC, Faria MS, Marino-Neto J, et al. Feeding behavior after metergoline or GR-46611 injections into the paraventricular nucleus of the hypothalamus in the pigeon. Behav Brain Res 2007;179(2):248–57.
[11] Brun S, da Luz V, Fernandez M, Paschoalini MA, Marino-Neto J. Atypical angiotensin receptors may mediate water intake induced by central injections of angiotensin II and of serotonin in pigeons. Regul Pept 2001;98(3):127–35.
[12] Dos Santos TS, Meneghelli C, Hoeller AA, Paschoalini MA, Arckens L, Lino-de-Oliveira C, et al. Behavioral profile and Fos activation of serotonergic and non-serotonergic raphe neurons after central injections of serotonin in the pigeon (*Columba livia*). Behav Brain Res 2011;220(1):173–84.
[13] Hoeller AA, Dos Santos TS, Bruxel RR, Dallazen AR, Silva HTA, André ES, et al. Serotonergic control of ingestive and post-ingestive behaviors in pigeons (*Columba livia*): the role of 5-HT1A receptor-mediated central mechanisms. Behav Brain Res 2013;236(1):118–30.
[14] Häckl LPN, Richter GO, Faria MS, Paschoalini MA, Marino-Neto J. Behavioral effects of 8-OH-DPAT injections into pontine and mesencephalic areas containing 5-HT-immunoreactive perikarya in the pigeon. Brain Res 2005;1035(2):154–67.
[15] Portas C, Bjorvatn B, Ursin R. Serotonin and the sleep/wake cycle: special emphasis on microdialysis studies. Prog Neurobiol 2000;60(1):13–35.
[16] Tejada S, Rial RV, Gamundí A, Esteban S. Effects of serotonergic drugs on locomotor activity and vigilance states in ring doves. Behav Brain Res 2011;216(1):238–46.
[17] Jacobs B, Fornal C. Activity of brain serotonergic neurons in the behaving animal. Pharmacol Rev 1991;43(4):563–78.
[18] Monti J. The role of dorsal raphe nucleus serotonergic and non-serotonergic neurons, and of their receptors, in regulating waking and rapid eye movement (REM) sleep. Sleep Med Rev 2010;14(5):319–27.
[19] Koella W, Czicman J. Mechanism of the EEG-synchronizing action of serotonin. Am J Physiol 1966;211(4):926–34.
[20] Bjorvatn B, Fagerland S, Eid T. Sleep/waking effects of a selective 5-HT1A receptor agonist given systemically as well as perfused in the dorsal raphe nucleus in rats. Brain Res 1997;770(1–2):81–8.
[21] Portas CM, Thakkar M, Rainnie D, Mccarley RW. Microdialysis perfusion of 8-hydroxy-2-(di-*n*-propylamino) tetralin (8-OH-DPAT) in the dorsal raphe nucleus decreases serotonin release and increases rapid eye movement sleep in the freely moving cat. J Neurosci 1996;16(8):2820–8.
[22] Gleeson S, Weissman BA, Seggel MR, Barrett JE. Neurochemical effects of 5-HT1 receptor ligands in pigeons. Eur J Pharmacol 1992;229(2–3):109–15.
[23] Mansbach RS, Harrod C, Hoffmann SM, Nader MA, Lei Z, Witkin JM, et al. Behavioral studies with anxiolytic drugs. V. Behavioral and in vivo neurochemical analyses in pigeons of drugs that increase punished responding. J Pharmacol Exp Ther 1988;246(1):114–20.
[24] Bonvento G, Scatton B, Claustre Y, Rouquier L. Effect of local injection of 8-OH-DPAT into the dorsal or median raphe nuclei on extracellular levels of serotonin in serotonergic projection areas in the rat brain. Neurosci Lett 1992;137(1):101–4.
[25] Müller CP, Carey RJ, Huston JP, De Souza Silva MA. Serotonin and psychostimulant addiction: focus on 5-HT1A-receptors. Prog Neurobiol 2007;81(3):133–78.
[26] Sotelo C, Cholley B, El Mestikawy S, Gozlan H, Hamon M. Direct immunohistochemical evidence of the existence of 5-HT1A autoreceptors on serotoninergic neurons in the midbrain raphe nuclei. Eur J Neurosci 1990;2(12):1144–54.
[27] Zilles K, Schleicher A, Glaser T, Traber J, Rath M. The ontogenetic development of serotonin (5-HT1) receptors in various cortical regions of the rat brain. Anat Embryol 1985;172(3):255–64.
[28] Pazos A, Palacios J. Quantitative autoradiographic mapping of serotonin receptors in the rat brain. I. Serotonin-1 receptors. Brain Res 1985;346(2):205–30.
[29] Palchaudhuri M, Flügge G. 5-HT1A receptor expression in pyramidal neurons of cortical and limbic brain regions. Cell Tissue Res 2005;321(2):159–72.
[30] Miquel MC, Doucet IE, Boni AC, El Mestikawy LS, Matthiessen L, Daval G, et al. Central serotonin 1A receptors respective distributions of encoding mRNA, receptor protein and binding sites by in situ hybridization histochemistry, radioimmunohistochemistry and autoradiographic mapping in the rat brain. Neurochem Int 1991;19(4):453–65.
[31] Collin M, Backberg M, Onnestam K, Meister B. 5-HT1A receptor immunoreactivity in hypothalamic neurons involved in body weight control. NeuroReport 2002;13(7):945–51.

[32] Marvin E, Scrogin K, Dudás B. Morphology and distribution of neurons expressing serotonin 5-HT1A receptors in the rat hypothalamus and the surrounding diencephalic and telencephalic areas. J Chem Neuroanat 2010;39(4):235–41.
[33] Herold C, Palomero-Gallagher, A N, Güntürkün O, Zilles K. Serotonin 5-HT1A receptor binding sites in the brain of the pigeon (*Columba livia*). Neuroscience 2012;200:1–12.
[34] Fletcher A, Cliffe I, Dourish C. Silent 5-HT1A receptor antagonists: utility as research tools and therapeutic agents. Trends Pharmacol Sci 1993;14(12):41–8.
[35] Forster EA, Cliffe IA, Bill DJ, Dover GM, Jones D, Reilly Y, et al. A pharmacological profile of the selective silent 5-HT1A receptor antagonist, WAY-100635. Eur J Pharmacol 1995;281(1):81–8.
[36] Monti JM, Jantos H, Silveira R, Reyes-Parada M, Scorza C, Prunell G. Depletion of brain serotonin by 5,7-DHT: effects on the 8-OH-DPAT-induced changes of sleep and waking in the rat. Psychopharmacology (Berl) 1994;115(1–2):273–7.
[37] Alesci R, Bagnoli P. Endogenous levels of serotonin and 5-hydroxyindoleacetic acid in specific areas of the pigeon CNS: effects of serotonin neurotoxins. Brain Res 1988;450(1–2):259–71.
[38] Vergé D, Daval G, Marcinkiewicz M, Patey A, El Mestikawy S, Gozlan H, et al. Quantitative autoradiography of multiple 5-HT1 receptor subtypes in the brain of control or 5,7-dihydroxytryptamine-treated rats. J Neurosci 1986;6(12):3474–82.
[39] Pranzatelli M, Durkin M, Barkai A. Quantitative autoradiography of 5-hydroxytryptaminela binding sites in rats with chronic neonatal 5,7-dihydroxytryptamine lesions. Dev Brain Res 1994;80(1–2):1–6.
[40] Currie P, Coscina D, Fletcher P. Reversal of fenfluramine and fluoxetine anorexia by 8-OH-DPAT is attenuated following raphe injection of 5,7-dihydroxytryptamine. Brain Res 1998;800(1):62–8.
[41] Choi M, Jonak E, Fernstrom J. Serotonin reuptake inhibitors do not prevent 5,7-dihydroxytryptamine-induced depletion of serotonin in rat brain. Brain Res 2004;1007(1–2):19–28.
[42] Ison M, Fachinelli C, Rodriguez Echandia E. Effect of the i.c.v. injection of 5,7-di-hydroxytryptamine on the aggressive behavior of dominant and submissive pigeons (*Columba livia*). Pharmacol Biochem Behav 1996;53(4):951–5.
[43] Mokrosz MJ, Chojnacka-Wójcik E, Tatarczyńska E, Klodzińska A, Filip M, Boksa J, et al. 1-(2-Methoxyphenyl)-4-[(4-succinimido) butyl] piperazine (MM-77): a new, potent, postsynaptic antagonist of 5-HT1A receptors. Med Chem Res 1994;4:161–9.
[44] Karten H, Hodos W. A stereotaxic atlas of the brain of the pigeon (*Columba livia*). Baltimore: Johns Hopkins Press; 1967.
[45] Alfredo B, Picazo O. Effect of the postsynaptic 5-HT1A receptor antagonist MM-77 on stressed mice treated with 5-HT1A receptor agents. Eur J Pharmacol 2005;508(1–3):155–8.
[46] Meneghelli C, Rocha NH, Mengatto V, Hoeller AA, Santos TS, Lino-De-Oliveira C, et al. Distribution of tryptophan hydroxylase-immunoreactive neurons in the brainstem and diencephalon of the pigeon (*Columba livia*). J Chem Neuroanat 2009;38(1):34–46.
[47] Kuenzel W, Van Tienhoven A. Nomenclature and location of avian hypothalamic nuclei and associated circumventricular organs. J Comp Neurol 1982;206(3):293–313.
[48] Reiner A, Perkel DJ, Bruce LL, Butler AB, Csillag A, Kuenzel W, et al. Revised nomenclature for avian telencephalon and some related brainstem nuclei. J Comp Neurol 2004;473(3):377–414.
[49] Crispim Junior C, Pederiva CN, Bose RC, Garcia VA, Lino-De-Oliveira C, Marino-Neto J. ETHOWATCHER: validation of a tool for behavioral and video-tracking analysis in laboratory animals. Comput Biol Med 2012;42(2):257–64.
[50] Da Silva E, Dos Santos TV, Hoeller AA, Dos Santos TS, Pereira GV, Meneghelli C, et al. Behavioral and metabolic effects of central injections of orexins/hypocretins in pigeons (*Columba livia*). Regul Pept 2008;147(1–3):9–18.
[51] Arvidsson LE, Hacksell U, Nilsson JL, Hjorth S, Carlsson A, Lindberg P, et al. 8-Hydroxy-2-(di-*n*-propylamino-)tetralin, a new centrally acting 5-hydroxytryptamine receptor agonist. J Med Chem 1981;24(8):921–3.
[52] Hjorth S, Carlsson A, Buspirone:. Effects on central monoaminergic transmission – possible relevance to animal experimental and clinical findings. Eur J Pharmacol 1982;83(3–4):299–303.
[53] Zilles K, Schleicher A, Palomero-Gallagher N, Amunts K. Quantitative analysis of cyto- and receptor architecture of the human brain. In: Toga A, Mazziotta J, editors. Brain mapping: the methods, 21, 2nd. ed. San Diego: Academic Press; 2002. p. 573–602.
[54] Zilles K, Palomero-Gallagher N, Grefkes C, Scheperjans F, Boy C, Amunts K, et al. Architectonics of the human cerebral cortex and transmitter receptor fingerprints: reconciling functional neuroanatomy and neurochemistry. Eur Neuropsychopharmacol 2002;12(6):587–99.
[55] Schleicher A, Palomero-Gallagher N, Morosan P, Eickhoff SB, Kowalski T, De Vos K, et al. Quantitative architectural analysis: a new approach to cortical mapping. Anat Embriol (Berl) 2005;210(5–6):373–86.
[56] Linder AE, Diaz J, NI W, Szasz T, Burnett R, Watts SW. Vascular reactivity, 5-HT uptake, and blood pressure in the serotonin transporter knockout rat. Am J Physiol Heart Circ Physiol 2008;294(4):H1745–52.
[57] Merker B. Silver staining of cell bodies by means of physical development. J Neurosci Methods 1983;9(3):235–41.
[58] Gozlan H, Elmestikawy S, Pichat L, Glowinski J, Hamon M. Identification of presynaptic serotonin autoreceptors using a new ligand: 3H-PAT. Nature 1983;305(5930):140–2.
[59] Boess F, Martin I. Molecular biology of 5-HT receptors. Neuropharmacol 1994;33(3–4):275–317.
[60] Hoyer D, Clarke DE, Fozard JR, Hartig PR, Martin GR, Mylecharane EJ, et al. International Union of Pharmacology classification of receptors for 5-hydroxytryptamine (serotonin). Pharmacol Rev 1994;46(2):157–63.
[61] Zilles K. Evolution of the human brain and comparative cyto- and receptor architecture. In: Dehaene S, Duhamel S, Hauser JR, Rizzolatti M, editors. From monkey brain to human brain. 2005. p. 41–56.
[62] Zilles K, Bacha-Trams M, Palomero-Gallagher N, Amunts K, Friederici AD. Comon molecular basis of the sentence comprehension network revealed by neurotransmitter receptor fingerprints. Cortex 2015;63:79–89.
[63] Dupuis D, Palmier C, Colpáert FC, Pauwels PJ. Autoradiography of serotonin 5-HT1A receptor-activated G proteins in guinea pig brain sections by agonist-stimulated [35S] GTPγS binding. J Neurochem 1998;70:1258–68.
[64] Simpson MD, Lubman DI, Slater P, Deakin JF. Autoradiography with [3H] 8-OH-DPAT reveals increases in 5-HT (1A) receptors in ventral prefrontal cortex in schizophrenia. Biol Psychiatry 1996;39(11):919–28.
[65] Assié M-B, Koek W. [3H]-8-OH-DPAT binding in the rat brain raphe area: involvement of 5-HT1A and non-5-HT1A receptors. Br J Pharmacol 2000;130(6):1348–52.
[66] To ZP, Bonhaus DW, Eglen RM, Jakeman LB. Characterization and distribution of putative 5-ht7 receptors in guinea-pig brain. Br J Pharmacol 1995;115(1):107–16.
[67] Thomas DR, Middlemiss DN, Taylor SG, Nelson P, Brown AM. 5-CT stimulation of adenylylcyclase activity in guinea-pig hippocampus: evidence for involvement of 5-HT7 and 5-HT1A receptors. Br J Pharmacol 1999;128(1):158–64.
[68] Martín-Cora F, Pazos A. Autoradiographic distribution of 5-HT7 receptors in the human brain using [3H] mesulergine: comparison to other mammalian species. Br J Pharmacol 2004;141(1):92–4.
[69] Bonaventure P, Nepomuceno D, Kwok A, Chai W, Langlois X, Hen R, et al. Reconsideration of 5-hydroxytryptamine (5-HT) 7 receptor distribution using [3H]5-carboxamidotryptamine and [3H]8-hydroxy-2-(di-npropylamino)tetraline: analysis in brain of 5-HT1A knockout and 5-HT1A/1B double-knockout mice. JPET 2002;302:240–8.
[70] Yamada H, Sano Y. Immunohistochemical studies on the serotonin neuron system in the brain of the chicken (*Gallus domesticus*). II. The distribution of the nerve fibers. Biog Amines 1985;2:21–36.
[71] Cozzi B, Viglietti-Panzica C, Aste N, Panzica GC. The serotoninergic system in the brain of the Japanese quail. An immunohistochemical study. Cell Tissue Res 1991;263(2):271–84.
[72] Challet E, Miceli D, Pierre J, Reperant J, Masicotte G, Herbin M, et al. Distribution of serotonin-immunoreactivity in the brain of the pigeon (*Columba livia*). Anat Embryol (Berl) 1996;193(3):209–27.
[73] Hirunagi K, Hasegawa M, Vígh B, Vígh-Teichmann I. Immunocytochemical demonstration of serotonin-immunoreactive cerebrospinal fluid-contacting neurons in the paraventricular organ of pigeons and domestic chickens. Prog Brain Res 1992;91:327–30.
[74] Reiner A, Karle EJ, Anderson KD, Medina L. Catecholaminergic perikarya and fibers in the avian nervous system. In: Smeets W, Reiner A, editors. Phylogeny and development of catecholamine systems in the CNS of vertebrates. Cambridg: Cambridge University Press; 1994. p. 135–81.
[75] Mello C, Pinaud R, Ribeiro S. Noradrenergic system of the zebra finch brain: immunocytochemical study of dopamine-*b*-hydroxylase. J Comp Neurol 1998;400(2):207–28.
[76] Palacios J, Probst A, Cortes R. The distribution of serotonin receptors in the human brain: high density of [3H] LSD binding sites in the raphe nuclei of the brainstem. Brain Res 1983;274(1):150–5.
[77] Sprouse J, Aghajanian G. (−)-Propranolol blocks the inhibition of serotonergic dorsal raphe cell firing by 5-HT1A selective agonists. Eur J Pharmacol 1986;128(3):295–8.
[78] Adell A, Carceller A, Artigas F. In vivo brain dialysis study of the somatodendritic release of serotonin in the raphe nuclei of the rat: effects of 8-hydroxy-2-(di-*n*-propylamino) tetralin. J Neurochem 1993;60(5):1673–81.
[79] Kreiss D, Lucki I. Differential regulation of serotonin (5-HT) release in the striatum and hippocampus by 5-HT1A autoreceptors of the dorsal and median raphe nuclei. J Pharmacol Exp Ther 1994;269(3):1268–79.
[80] Adell A, Celada P, Abellan MT, Artigas F. Origin and functional role of the extracellular serotonin in the midbrain raphe nuclei. Brain Res Rev 2002;39(2–3):154–80.
[81] Johnson A, Gartside S, Ingram C. 5-HT1A receptor-mediated autoinhibition does not function at physiological firing rates: evidence from in vitro electrophysiological studies in the rat dorsal raphe nucleus. Neuropharmacology 2002;43(6):959–65.
[82] Bortolozzi A, Amargos-Bosch M, Miklos T, Artigas F, Adell A. In vivo efflux of serotonin in the dorsal raphe nucleus of 5-HT1A receptor knockout mice. J Neurochem 2004;88(6):1373–9.
[83] Nader M, Barret J. Neurochemical changes in pigeon cerebrospinal fluid during chronic administration of buspirone or 8-hydroxy-2-(di-*n*-propylamino)tetralin (8-OH-DPAT). Pharmacol Biochem Behav 1989;32(1):227–32.
[84] Mignot E, Serrano A, Laude D, Elghozi J-L, Dedek J, Scatton B. Measurement of 5-HIAA levels in ventricular CSF (by LCEC) and in striatum (by in vivo

voltammetry) during pharmacological modifications of serotonin metabolism in the rat. J Neural Transm 1985;62(1–2):117–24.
[85] Coscina D, De Rooy E. Effects of intracisternal vs. intrahypothalamic 5,7-DHT on feeding elicited by hypothalamic infusion of NE. Brain Res 1992;579(2):310–20.
[86] Bjorvatn B, Fagerland S, Eid T, Ursin R. Sleep/waking effects of a selective 5-HT1A receptor agonist given systemically as well as perfused in the dorsal raphe nucleus in rats. Brain Res 1997;770:81–8.
[87] Findlay P, Thompson G. The effect of intraventricular injections of noradrenaline, 5-hydroxytryptamine, acetylcholine and tranylcypromine on the ox (*Bos taurus*) at different environmental temperatures. J Physiol 1968;194(3):809–16.
[88] Dourish C, Hutson P, Curzon G. Characteristics of feeding induced by the serotonin agonist 8-hydroxy-2-(di-*n*-propylamino) tetralin (8-OH-DPAT). Brain Res Bull 1985;15(4):377–84.
[89] Bendotti C, Samanin R. 8-Hydroxy-2-(di-*n*-propylamino) tetralin (8-OH-DPAT) elicits eating in free-feeding rats by acting on central serotonin neurons. Eur J Pharmacol 1986;121(1):147–50.
[90] Currie P, Fletcher P, Coscina D. Administration of 8-OH-DPAT into the midbrain raphe nuclei: effects on medial hypothalamic NE-induced feeding. Am J Physiol 1994;266(5 (Pt 2)):R1645–51.
[91] Fletcher A, Bill DJ, Cliffe IA, Forster EA, Jones D, Reilly Y. A pharmacological profile of WAY-100635, a potent and selective 5-HT1A receptor antagonist. Br J Pharmacol 1994;112:91P.
[92] Fletcher A, Forster EA, Bill DJ, Brown G, Cliffe IA, Hartley JE, et al. Electrophysiological, biochemical, neurohormonal and behavioural studies with WAY-100635, a potent, selective and silent 5-HT1A receptor antagonist. Behav Brain Res 1996;73(1–2):337–53.
[93] Wesolowska A, Borycz J, Paluchowska MH, Chojnacka-Wójcik E. Pharmacological analysis of the hypothermic effects of nan-190 and its analogs, postsynaptic 5-HT1A receptor antagonists, in mice. Pol J Pharmacol 2002;54(4):391–9.
[94] Wesolowska A, Paluchowska M, Chojnacka-Wójcik E. Involvement of presynaptic 5-HT1A and benzodiazepine receptors in the anticonflict activity of 5-HT1A receptor antagonists. Eur J Pharmacol 2003;471(1):27–34.
[95] Sano Y, Ueda S, Yamada H, Takeuchi Y, Goto M, Kawata M. Immunohistochemical demonstration of serotonin-containing CSF-contacting neurons in the submammalian paraventricular organ. Histochemistry 1983;77(4):423–30.
[96] Berk M, Butler A. Efferent projections of the medial preoptic nucleus and medial hypothalamus in the pigeon. J Comp Neurol 1981;203(3):379–99.
[97] Korf H, Simon-Oppermann C, Simon E. Afferent connections of physiologically identified neuronal complexes in the paraventricular nucleus of conscious Pekin ducks involved in regulation of salt- and water-balance. Cell Tissue Res 1982;226(2):275–80.
[98] Korf H. Neuronal organization of the avian paraventricular nucleus: intrinsic, afferent, and efferent connections. J Exp Zool 1984;232(3):387–95.
[99] Haida Y, Ubuka T, Ukena K, Tsutsui K, Oishi T, Tamotsu S. Photoperiodic response of serotonin- and galanin-immunoreactive neurons of the paraventricular organ and infundibular nucleus in Japanese quail, *Cortunix cortunix japonica*. Zool Sci 2004;21(5):575–82.
[100] Marley E, Whelan J. Some central effects of 5-hydroxytryptamine in young chickens at and below thermoneutrality. Br J Pharmacol 1975;53(1):37–41.
[101] Fuchs T, Siegel JJ, Burgdorf J, Bingman VP, et al. A selective serotonin reuptake inhibitor reduces REM sleep in the homing pigeon. Physiol Behav 2006;87(3):575–81.
[102] Pyörnillä A, Hissa R. Opposing temperature responses to intrahypothalamic injections of 5-hydroxytryptamine in the pigeon exposed to cold. Experentia 1979;35(1):59–60.
[103] Da Silva RA, De Oliveira ST, Hackl LP, Spilere CI, Faria MS, Marino-Neto J, et al. Ingestive behaviors and metabolic fuels after central injections of 5-HT1A and 5-HT1D/1B receptors agonists in the pigeon. Brain Res 2004;1026(2):275–83.
[104] Campanella LC, Da Silva AA, Gellert DS, Parreira C, Ramos MC, Paschoalini MA, et al. Tonic serotonergic control of ingestive behaviours in the pigeon (*Columba livia*): the role of the arcopallium. Behav Brain Res 2009;205(2):396–405.
[105] D'hondt E, Vermeiren J, Peeters K, Balthazart J, Tlemcani O.,, Ball GF, et al. Validation of a new antiserum directed towards the synthetic c-terminus of the FOS protein in avian species: immunological, physiological and behavioral evidence. J Neurosci Methods 1999;91(1–2):31–45.
[106] Simon E, Gerstberger R, Gray D. Central nervous angiotensin II responsiveness in birds. Prog Neurobiol 1992;39(2):179–87.
[107] Kia HK, Miquel M-C, Brisorgueil M-J, Daval G, Riad M, El Mestikawy S, et al. Immunocytochemical localization of serotonin1A receptors in the rat central nervous system. J Comp Neurol 1996;365(2):289–95.
[108] Steffens SM, Da Cunha IC, Beckman D, Lopes AP, Faria MS, Marino-Neto J, et al. The effects of metergoline and 8-OH-DPAT injections into arcuate nucleus and lateral hypothalamic area on feeding in female rats during the estrous cycle. Physiol Behav 2008;95(3):484–91.
[109] Steffens S, Beckman D, Faria MS, Marino-Neto J, Paschoalini MA. WAY100635 blocks the hypophagia induced by 8-OH-DPAT in the hypothalamic nuclei. Physiol Behav 2010;99(5):632–7.
[110] López-Alonso V, E, Mancilla-Díaz JM, Rito-Domingo M, González-Hernández B, Escartín-Pérez RE. The effects of 5-HT1A and 5-HT2C receptor agonists on behavioral satiety sequence in rats. Neurosci Lett 2007;416(3):285–8.
[111] Aghajanian G, Gallager D. Raphe origin of serotonergic nerves terminating in the cerebral ventricles. Brain Res 1975;88(2):221–31.
[112] Chan-Palay V. Serotonin axons in the supra- and subependymal plexuses and in the leptomeninges; their roles in local alterations of cerebrospinal fluid and vasomotor activity. Brain Res 1976;102(1):103–30.
[113] Simpson KL, Fisher TM, Waterhouse BD, Lin RCS. Projection patterns from the raphe nuclear complex to the ependymal wall of the ventricular system in the rat. J Comp Neurol 1998;399(1):61–72.
[114] Vígh B, et al. The system of cerebrospinal fluid-contacting neurons. Its supposed role in the nonsynaptic signal transmission of the brain. Histol Histopathol 2004;19(2):607–28.
[115] Vigh-Teichmann I, Vígh B. The system of cerebrospinal fluid-contacting neurons. Its supposed role in the nonsynaptic signal transmission of the brain. Arch Histol Cytol 1989;52(Suppl.):195–7.
[116] Danguir L, et al. LCEC monitoring of 5-hydroxyindolic compounds in the cerebrospinal fluid of the rat related to sleep and feeding. Brain Res Bull 1982;8(3):293–7.
[117] Hurtson P, et al. Monitoring 5HT metabolism in the brain of the freely moving rat. Ann N Y Acad Sci 1986;473:321–36.
[118] Johnson A, Gross P. Sensory circumventricular organs and brain homeostatic pathways. FASEB J 1993;7(8):678–86.
[119] Castillo-Ruiz A, et al. Day-night differences in neural activation in histaminergic and serotonergic areas with putative projections to the cerebrospinal fluid in a diurnal brain. Neuroscience 2013;250:352–63.
[120] Parent A. Comparative anatomy of the serotoninergic systems. J Physiol 1981;77(2–3):147–56.
[121] Azmitia E. Serotonin and brain: evolution, neuroplasticity, and homeostasis. Int Rev Neurobiol 2007;(77):31–56.
[122] Norton W, Folchert A, Bally-Cuif L. Comparative analysis of serotonin receptor (HTR1A/HTR1B families) and transporter (slc6a4a/b) gene expression in the zebrafish brain. J Comp Neurol 2008;511(4):521–42.

Received: 10 October 2016 | Revised: 9 October 2017 | Accepted: 10 October 2017

DOI: 10.1002/cne.24344

RESEARCH ARTICLE

WILEY The Journal of Comparative Neurology

Transmitter receptors reveal segregation of the arcopallium/amygdala complex in pigeons (*Columba livia*)

Christina Herold[1] | Christina Paulitschek[1] | Nicola Palomero-Gallagher[2] | Onur Güntürkün[3] | Karl Zilles[2,4]

[1]C. and O. Vogt Institute of Brain Research, Medical Faculty, Heinrich-Heine University of Düsseldorf, Düsseldorf, Germany

[2]Institute of Neuroscience and Medicine INM-1, Research Center Jülich, Jülich, Germany

[3]Department of Biopsychology, Institute of Cognitive Neuroscience, Faculty of Psychology, Ruhr-University Bochum, Bochum, Germany

[4]Department of Psychiatry, Psychotherapy and Psychosomatics, RWTH Aachen University, and JARA – Translational Brain Medicine, Aachen, Germany

Correspondence
Christina Herold, C. & O. Vogt-Institute of Brain Research, University of Düsseldorf, Düsseldorf 40225, Germany.
Email: christina.herold@uni-duesseldorf.de

Funding information
Grant sponsor: Deutsche Forschungsgemeinschaft, Grant No.: SFB 1280 (O.G.).

Abstract

At the beginning of the 20th century it was suggested that a complex group of nuclei in the avian posterior ventral telencephalon is comparable to the mammalian amygdala. Subsequent findings, however, revealed that most of these structures share premotor characteristics, while some indeed constitute the avian amygdala. These developments resulted in 2004 in a change of nomenclature of these nuclei, which from then on were named arcopallial or amygdala nuclei and referred to as the arcopallium/amygdala complex. The structural basis for the similarities between avian and mammalian arcopallial and amygdala subregions is poorly understood. Therefore, we analyzed binding site densities for glutamatergic AMPA, NMDA and kainate, GABAergic $GABA_A$, muscarinic M_1, M_2 and nicotinic acetylcholine (nACh; $\alpha_4\beta_2$ subtype), noradrenergic α_1 and α_2, serotonergic 5-HT_{1A} and dopaminergic $D_{1/5}$ receptors using quantitative in vitro receptor autoradiography combined with a detailed analysis of the cyto- and myelo-architecture. Our approach supports a segregation of the pigeon's arcopallium/amygdala complex into the following subregions: the arcopallium anterius (AA), the arcopallium ventrale (AV), the arcopallium dorsale (AD), the arcopallium intermedium (AI), the arcopallium mediale (AM), the arcopallium posterius (AP), the nucleus posterioris amygdalopallii pars basalis (PoAb) and pars compacta (PoAc), the nucleus taeniae amgygdalae (TnA) and the area subpallialis amygdalae (SpA). Some of these subregions showed further subnuclei and each region of the arcopallium/amygdala complex are characterized by a distinct multi-receptor density expression. Here we provide a new detailed map of the pigeon's arcopallium/amygdala complex and compare the receptor architecture of the subregions to their possible mammalian counterparts.

KEYWORDS

amygdala, arcopallium, avian, autoradiography, receptor, RRID:SCR_013566, RRID:SCR_001905, RRID:SCR_015627

Abbreviations: A, Arcopallium; AA, Arcopallium anterius; ACh, Acetylcholine; AD, Arcopallium dorsale; ADl, Arcopallium dorsale pars lateralis; ADm, Arcopallium dorsale pars medialis; ADp, Arcopallium dorsale pars posterior; AI, Arcopallium intermedium; AId, Arcopallium intermedium pars dorsalis; AIv, Arcopallium intermedium pars ventralis; AIvm, Arcopallium intermedium pars ventromedialis; AM, Arcopallium mediale; AMm, Arcopallium mediale pars magnocellularis; AMp, Arcopallium mediale pars parvocellularis; AMPA, α-amino-3-hydroxy-5-methyl-4-isoxazolepropionic acid; AP, Arcopallium posterioris; AV, Arcopallium ventrale; AVm, Arcopallium ventrale pars medialis; BSTL, Bed nucleus of the Stria Terminalis, pars lateralis; CDL, Area corticoidea dorsolateralis; CPi, Cortex piriformis; DA, Tractus dorso-arcopallialis; FA, Tractus fronto-arcopallialis; GABA, γ-Amino-butyric acid; GP, Globus pallidus; HF, Hippocampal formation; LAD, Lamina arcopallialis dorsalis; LSt, Lateral striatum; M, Mesopallium; N, Nidopallium; NCL, Nidopallium caudolaterale; NCVl, Nidopallium caudoventrale pars lateralis; NMDA, N-Methyl-D-aspartic acid; PoA, Nucleus posterioris amygdalopallii; PoAb, Nucleus posterioris amygdalopallii pars basalis; PoAc, Nucleus posterioris amygdalopallii pars compacta; SpA, Area subpallialis amygdalae; ST, Striatum; TnA, Nucleus taeniae amygdalae; TPO, Area temporo-parieto-occipitalis; V, Ventricle.

 © 2017 Wiley Periodicals, Inc.

1 | INTRODUCTION

New concepts of vertebrate brain evolution resulted recently in a better understanding of the organization of the avian telencephalon (Jarvis et al., 2005; Reiner et al., 2004). Furthermore, in the last couple of years, novel but conflicting hypotheses on homologies of avian and mammalian pallial structures and cell types have been claimed and new genetic models were developed (Belgard et al., 2013; Butler, Reiner, & Karten, 2011; Chen, Winkler, Pfenning, & Jarvis, 2013; Dugas-Ford, Rowell, & Ragsdale, 2012; Jarvis et al., 2013; Karten, 2015; Puelles, 2011; Vicario, Abellán, Desfilis, & Medina, 2014). Beside the known homologies of brain regions that are based on the same developmental origin, some regions also share anatomical and molecular traits, which seem to be a result of convergent evolution based on functional specialization (Güntürkün & Bugnyar, 2016; Herold, Coppola, & Bingman, 2015; Herold, Joshi, Chehadi, Hollmann, & Güntürkün, 2012; Herold et al., 2011; Pfenning et al., 2014). One region that has been intensely discussed in this context is the avian arcopallium/amygdaloid complex. According to the old and outdated nomenclature (Karten & Hodos, 1967), this ventrolateral part of the posterior telencephalon was called archistriatum and was suggested to be partly comparable to the mammalian amygdala (Zeier & Karten, 1971). However, evidence from neurochemical, developmental, and behavioral data showed that most parts of the archistriatum are largely of premotor nature (Butler et al., 2011; Kuenzel, Medina, Csillag, Perkel, & Reiner, 2011; Reiner et al., 2004; Yamamoto, Sun, Wang, & Reiner, 2005). Accordingly, these premotor areas were termed arcopallium in the new nomenclature while the remaining subnuclei were assumed to constitute the amygdala (Reiner et al., 2004). In mammals, the amygdala is also a complex structure, with multiple subnuclei, and various neuronal subtypes and connections. Similarly, developmental and genetic studies have confirmed that both the avian and the mammalian amygdala complexes share several expression profiles of specific markers (Dugas-Ford et al., 2012; Jarvis et al., 2013; Kuenzel et al., 2011; Montiel & Molnar, 2013; Moreno & Gonzalez, 2007; Pfenning et al., 2014; Puelles et al., 2015; Vicario et al., 2014; Vicario, Abellán, & Medina, 2015). Not only genetic but also connectional analyses demonstrate that the premotor subregions of the arcopallium share similar connectivity patterns as the mammalian premotor areas, while the limbic nuclei showed comparable connections to parts of the mammalian amygdala (Atoji & Wild, 2012; Güntürkün & Bugnyar, 2016; Hanics, Teleki, Alpar, Szekely, & Csillag, 2016; Reiner et al., 2004; Shanahan, Bingman, Shimizu, Wild, & Güntürkün, 2013; Zeier & Karten, 1971). This is also true for functional, pharmacological and electrophysiological studies in various bird species that make it likely that the avian arcopallium/amygdaloid complex is constituted by diverse subregions that have either premotor or limbic functions and participate in visual, vocal, auditory, and emotional learning, fear and reproduction behavior as well as neuroendocrine control and homeostasis (Campanella et al., 2009; Cohen, 1975; Cross et al., 2013; da Silva et al., 2009; Dafters, 1975; Kuenzel et al., 2011; Pfenning et al., 2014; Saint-Dizier et al., 2009; Scarf, Stuart, Johnston, & Colombo, 2016; Whitney et al., 2014; Winkowski & Knudsen, 2007). However, the heterogeneity of this region constitutes a major challenge to understand the functional organization and evolutionary origin of the arcopallium/amygdala complex in birds (Medina & Abellán, 2009). In addition, a common consensus of homologies between birds and mammals is still missing.

Since the expression of multiple transmitter receptors in the brain has been proven as a powerful tool to delineate different areas, and to identify similarities among regions between various mammalian species (Palomero-Gallagher, Zilles, Schleicher, & Vogt, 2013; Vogt et al., 2013; Zilles, 2005; Zilles & Palomero-Gallagher, 2016) and also between birds and mammals (Herold et al., 2015; Herold et al., 2011; Jarvis et al., 2013; Kubikova, Wada, & Jarvis, 2010; Lovell, Clayton, Replogle, & Mello, 2008; Sun & Reiner, 2000; Wada, Sakaguchi, Jarvis, & Hagiwara, 2004), we analyzed the neurotransmitter receptor-, myelo- and cellular-architecture of the pigeon's arcopallium/amygdala complex. The resulting detailed map of this region can be used as a basis for comparisons to the mammalian amygdala complex and cortical areas in the future.

2 | MATERIAL AND METHODS

2.1 | Receptor autoradiography and histology

We examined six adult pigeon brains (*Columba livia*) of unknown sex. Animals were obtained from local breeders and were housed in individual cages (30 × 30 × 45 cm) at 21 ± 1°C temperature and in a humidity controlled room with a 12-hr light/dark circle. The birds had free access to grit, food and water ad libitum. All experimental procedures were approved by the national authority (LANUV NRW, Germany) and were carried out in accordance with the National Institute of Health Guide for Care and Use of Laboratory Animals. Animals were decapitated, brains were removed from the skull, frozen immediately in isopentane at −40°C and stored at −70°C. Serial coronal 10 μm sections were cut with a cryostat microtome (2800 Frigocut E, Reichert-Jung). Sections were thaw-mounted on gelatinized glass slides, freeze-dried and stained with a modified cell body staining or Gallyas myelin staining (Gallyas, 1971; Merker, 1983) for cyto- and myelo-architectonic analysis, or processed for receptor autoradiography.

Details of the autoradiographic labeling procedure have been published elsewhere (Herold et al., 2014; Zilles, Palomero-Gallagher, et al., 2002; Zilles, Schleicher, Palomero-Gallagher, & Amunts, 2002). Binding protocols are summarized in Table 1. Three steps were performed in the following sequence:

1. A preincubation step removed endogenous ligand from the tissue.
2. During the main incubation step binding sites were labeled with the respective tritiated ligand (total binding), or co-incubated with the tritiated ligand and a 1,000–10,000-fold excess of specific non-labeled ligand (displacer) determined non-displaceable, and thus, non-specific binding. Specific binding is the difference between total and non-specific binding. It was less than 5% in all cases.
3. A final rinsing step eliminated unbound radioactive ligand from the sections.

The following binding sites were labeled according to the above cited protocols: (a) α-amino-3-hydroxy-5-methyl-4-isoxalone propionic acid (AMPA) receptor with [^{3}H] AMPA, (b) kainate receptor with [^{3}H]kainate, (c) *N*-methyl-D-aspartate (NMDA) receptor with [^{3}H]MK-801, (d) γ-aminobutyric acid A ($GABA_A$) receptor with [^{3}H]muscimol, (e) muscarinic cholinergic M_1 receptor with [^{3}H]pirenzepine, (f) muscarinic cholinergic M_2 receptor with [^{3}H]oxotremorine-M, (g) nicotinic cholinergic (nACh; $\alpha_4\beta_2$ subtype) receptor with [^{3}H]cytisine, (h) noradrenergic α_1 adrenoreceptor with [^{3}H]prazosin, (i) noradrenergic α_2 adrenoreceptor with [^{3}H]RX-821002, (j) serotonergic 5-HT_{1A} receptor with [^{3}H]8-OH-DPAT, and (k) dopaminergic $D_{1/5}$ receptors with [^{3}H]SCH 23390. Sections were air-dried overnight and subsequently co-exposed for 4–5 weeks against a tritium-sensitive film (Hyperfilm, Amersham, Braunschweig, Germany, RRID:SCR_013566) with plastic [^{3}H]-standards (Microscales, Amersham) of known concentrations of radioactivity.

2.2 | Image analysis

The resulting autoradiographs were subsequently processed using densitometry with a video-based image analyzing technique (Zilles, Schleicher, et al., 2002). Autoradiographs were digitized by means of a KS-400 image analyzing system (Kontron, Germany) connected to a CCD camera (Sony, Japan) equipped with a S-Orthoplanar 60-mm macro lens (Zeiss, Germany). The images were stored as binary files with a resolution of 512 × 512 pixels and 8-bit gray value. The gray value images of the co-exposed microscales were used to compute a calibration curve by nonlinear, least-squares fitting, which defined the relationship between gray values in the autoradiographs and concentrations of radioactivity. This enabled the pixel-wise conversion of the gray values of an autoradiograph into the corresponding concentration of radioactivity. The concentrations of binding sites occupied by a ligand under incubation conditions are transformed into fmol/mg protein at saturation conditions by means of the equation: $(K_D + L)/A_S \times L$, where K_D is the equilibrium dissociation constant of ligand-binding kinetics, L is the incubation concentration of ligand, and A_S the specific activity of the ligand. The results of these calculations were used for binding site density measurements. The digitized autoradiographic images were color-coded only to facilitate the detection of regional differences in binding site densities by visual inspection.

2.3 | Anatomical identification

The borders of the arcopallium/amygdala complex and its subregions were identified based on our cyto-, myelo- and receptor-architectonic data, and previous cytoarchitectural, neurochemical, tract-tracing, and imaging studies (Atoji, Saito, & Wild, 2006; Atoji & Wild, 2009; H. Karten & Hodos, 1967; Kröner & Güntürkün, 1999; Reiner et al., 2004; Shanahan et al., 2013; Yamamoto & Reiner, 2005; Zeier & Karten, 1971). Borders of the different subregions were traced on prints of the digitized autoradiographs by projecting the cell body and the myelin stained sections onto the digitized images of the autoradiographs between anterior–posterior levels A 7.75 and A 4.50 according to the atlas of Karten and Hodos (1967). The mean of the concentration of each binding site (fmol/mg protein) in each subregion of the arcopallium/amygdala complex was calculated over the sampled anterior-posterior levels from each animal, averaged across the six animals, and is reported as the overall receptor concentration (mean ± standard error of mean (*SEM*)). Quantitative, multi-receptor data are presented in color-coded autoradiographs and in regional fingerprints that are prepared as polar plots or histograms that separately show the density for the receptors in each subregion.

2.4 | Statistical analysis

To determine differences in receptor densities among subregions and adjacent structures we compared the main subregions of the arcopallium/amygdala complex and included also the lateral division of the nidopallium caudoventrale (NCVl). To do so, we first applied a Friedman ANOVA across all subregions for each ligand (Table 2). If significant, pair-wise comparisons were run with the Wilcoxon-rank test (Table 3). Differences between intra-nuclear substructures were directly analyzed with Wilcoxon-rank tests. For the general statistical analyses, Statistica 10 (StatSoft, Tulsa, RRID:SCR_015627) was used. The significance level was set at 0.05. Further, a hierarchical cluster analysis was carried out to detect putative groupings of areas according to the degree of (dis) similarity of their receptor architecture (Palomero-Gallagher et al., 2009). The Euclidean distance was applied as a measure of (dis)similarity since it takes both differences, the size and the shape of receptor fingerprints into account, and the Ward linkage algorithm as the linkage method. This combination yielded the maximum cophenetic correlation coefficient as compared to any combination of alternative linkage methods and measurements of (dis)similarity. Prior to this analysis, the densities of each receptor type were transformed to *z*-scores across all areal densities of that specific receptor, thus ensuring an equal weighting of each receptor without eliminating relative differences in receptor densities among areas. The hierarchical cluster analysis was carried out with in house R-scripts (R Foundation for Statistical Computing, http://www.r-project.org, RRID:SCR_001905).

3 | RESULTS

3.1 | Qualitative analysis of the cyto- and myeloarchitecture of the arcopallium/amygdala complex

Figure 1 shows the arcopallium/amygdala complex in a Nissl (a)- and a myelin (b)-stained transverse section of a pigeon brain at the anterior–posterior coordinate A 6.50 (Karten & Hodos, 1967) and a magnification of the region of interest (1c) clipped from the Nissl image in Figure 1a. For a more detailed overview, different atlas levels are shown in representative coronal cell body- and myelin-stained sections depicting the outlines of the arcopallium/amgydala complex and surrounding structures in Figure 2 (a–l; Nissl) and Figure 3 (a–l; myelin) that were used as an orientation for the identification of subregions in the receptor autoradiographs. Thereby, the boundaries to map the different arcopallium/amygdala subdivisions followed previous cytoarchitectural, neurochemical, tract-tracing, and imaging studies (Atoji et al., 2006;

TABLE 1 Incubation conditions used for receptor autoradiography

Receptor	[^{3}H] ligand (incubation concentration)	Displacer (incubation concentration)	Incubation buffer	Preincubation step	Main incubation step	Rinsing step
glutamatergic AMPA	[^{3}H] AMPA (10 nM)	Quisqualate (10 μM)	50 mM Tris-acetate (pH 7.2)	3 × 10 min at 4°C in incubation buffer	45 min at 4°C in incubation buffer + 100 mM KSCN	4 × 4 s at 4°C in incubation buffer + 2 × 2 s at 4°C in acetone/glutaraldehyde
glutamatergic Kainate	[^{3}H] kainate (8 nM)	Kainate (100 μM)	50 mM Tris-citrate (pH 7.1)	3 × 10 min at 4°C in incubation buffer	45 min at 4°C in incubation buffer + 10 mM Ca-acetate	4 × 4 sec at 4°C in incubation buffer + 2 × 2 sec at 4°C in acetone/glutaraldehyde
glutamatergic NMDA	[^{3}H] MK-801 (5 nM)	MK-801 (100 μM)	50 mM Tris-HCl (pH 7.2)	15 min at 25°C in incubation buffer	60 min at 25°C in incubation buffer + 30 μM glycine + 50 μM spermidine	2 × 5 min at 4°C in incubation buffer
muscarinic cholinergic M_1	[^{3}H] pirenzepine (1 nM)	Pirenzepine (10 μM)	Modified Krebs-Ringer buffer (pH 7.4)	20 min at 25°C in incubation buffer	60 min at 25°C in incubation buffer	2 × 5 min at 4°C in incubation buffer
muscarinic cholinergic M_2	[^{3}H] oxotremorine-M (0.8 nM)	Carbachol (1 μM)	20 mM Hepes-Tris (pH 7.5) + 10 mM $MgCl_2$	20 min at 25°C in incubation buffer	60 min at 25°C in incubation buffer	2 × 2 min at 4°C in incubation buffer
nicotiniccholinergic $\alpha_4\beta_2$	[^{3}H] cytisine (1 nM)	Nicotine (10 μM)	50 mM Tris–HCl (pH 7.4) + 120 mM NaCl + 5 mM KCl + 1 mM MgCl2 + 2.5 mM CaCl2	15 min at 22 °C in incubation buffer	90 min at 4°C in incubation buffer	2 × 2 min at 4°C in incubation buffer
adrenergic α_1	[^{3}H] prazosin (0.2 nM)	Phentolamine (10 μM)	50 mM Tris-HCl (pH 7.4)	30 min at 37°C in incubation buffer	45 min at 30°C in incubation buffer	2 × 5 min at 4°C in incubation buffer
adrenergic α_2	[^{3}H] RX-821002 (6nM)	(-) adrenaline (10μM)	50 mM Tris-HCl (pH 7.4) + 100 mM $MnCl_2$ +0.1% Ascorbic acid +0.3 μM 8-OH-DPAT	30 min at 22°C in incubation buffer	30 min at 22°C in incubation buffer	2 × 20 s at 4°C in incubation buffer
GABAergic $GABA_A$	[^{3}H] muscimol (6 nM)	GABA (10 μM)	50 mM Tris-citrate (pH 7.0)	3 × 5 min at 4°C in incubation buffer	40 min at 4°C in incubation buffer	3 × 3 s at 4°C in incubation buffer
serotoninergic $5\text{-}HT_{1A}$	[^{3}H] 8-OH-DPAT (1 nM)	Serotonin (10 μM)	170 mM Tris-HCl (pH 7.6)+4 mM $CaCl_2$ +0.01% Ascorbic acid	30 min at 22°C in incubation buffer	60 min at 22°C in incubation buffer	1 × 5 min at 4°Cin incubation buffer
dopaminergic $D_{1/5}$	[^{3}H] SCH-23390 (0.5nM)	SKF 83566 (1μM)	50 mM Tris-HCl (pH 7.4) + 120 mM NaCl + 5 mM KCl + 2 mM $CaCl_2$ + 1 mM $MgCl_2$ + 1 μM Mianserin	20 min at 22°C in incubation buffer	90 min at 22°C in incubation buffer	2 × 10 min at 4°C in incubation buffer

TABLE 2 Neurotransmitter receptor densities (fmol/mg protein) in different subregions of the arcopallium/amygdala complex, the nidopallium caudale ventro-laterale and the posterior lateral striatum (mean ± *SEM*) and results of the Friedman ANOVA displaying regional differences for all subregions for each receptor type (all $N = 6$, $df = 10$; LSt not included)

Subregion/ Receptor	AA	AD	AM	AI	AV	AP	PoAb	PoAc	TnA	SpA	NCVl	LSt	Friedman ANOVA (χ_r^2)
AMPA	1325 ± 133	1551 ± 101	1601 ± 62	1534 ± 77	1722 ± 87	1651 ± 85	1264 ± 93	1610 ± 105	1403 ± 164	1147 ± 100	1554 ± 98	1438 ±47	28.82**
Kainate	774 ± 160	323 ± 30	275 ± 35	362 ± 35	796 ± 81	266 ± 26	316 ± 39	333 ± 18	225 ± 38	636 ± 37	256 ± 30	878 ±41	43.21***
NMDA	1238 ± 248	1330 ± 52	1338 ± 29	1234 ± 51	1690 ± 79	1478 ± 75	1359 ± 126	1685 ± 107	1133 ± 58	741 ± 54	1589 ± 78	1205 ±50	44.52***
$GABA_A$	906 ± 196	535 ± 50	414 ± 48	654 ± 60	677 ± 63	402 ± 40	361 ± 43	577 ± 76	332 ± 34	578 ± 48	605 ± 86	1539 ±76	43.82***
M_1	107 ± 20	172 ± 11	64 ± 11	115 ± 10	42 ± 3	48 ± 5	54 ± 15	61 ± 4	27 ± 7	56 ± 12	42 ± 9	78 ±11	43.21***
M_2	235 ± 42	359 ± 34	200 ± 17	324 ± 33	129 ± 17	185 ± 25	98 ± 16	142 ± 18	206 ± 25	327 ± 47	151 ± 36	390 ±39	45.67***
$\alpha_4\beta_2$	41 ± 2	41 ± 3	47 ± 1	41 ± 2	58 ± 4	62 ± 6	52 ± 3	69 ± 4	72 ± 3	57 ± 5	51 ± 5	59 ±4	40.00***
α_1	13 ± 4	17 ± 2	14 ± 2	10 ±1	11 ± 1	10 ± 4	10 ± 2	110 ± 16	7 ± 2	13 ± 2	78 ± 5	14 ±2	37.36***
α_2	231 ± 32	270 ± 20	247 ± 7	221 ± 6	121 ± 9	590 ± 130	233 ± 17	254 ± 14	831 ± 49	415 ± 27	206 ± 38	347 ±20	41.67***
5-HT_{1A}	86 ± 22	64 ± 4	54 ± 5	96 ± 8	77 ± 5	41 ± 6	40 ± 5	99 ± 13	43 ± 3	40 ± 4	65 ± 8	34 ±2	41.55***
$D_{1/5}$	41 ± 18	22 ± 1	19 ± 2	20 ± 2	16 ± 1	26 ± 4	14 ± 1	35 ± 4	14 ± 1	16 ± 1	33 ± 5	41 ±2	35.76***

*$p < .05$, **$p < .01$, ***$p < .001$. Abbreviations see list.

Atoji & Wild, 2009; H. Karten & Hodos, 1967; Kröner & Güntürkün, 1999; Reiner et al., 2004; Shanahan et al., 2013; Yamamoto & Reiner, 2005; Zeier & Karten, 1971) and our own analysis. Beginning at anterior positions and moving posteriorly, we subdivided the arcopallium into the following divisions: the arcopallium anterius (AA), the arcopallium ventrale (AV), the arcopallium dorsale (AD), the arcopallium intermedium (AI), the arcopallium mediale (AM), and the arcopallium posterius (AP). AA, the anterior tip of the arcopallium, is the beginning of a spherical structure that is encompassed dorsally by the tractus fronto-arcopallialis (FA) and is located laterally from the lateral striatum (LSt) in the ventrolateral telencephalon (Figures 2a, g and 3a, g). Through its course along the anterior–posterior axis, AA is further encompassed dorsomedially by the beginning of AD around the anterior–posterior coordinate A 7.80 (Figures 2a, 3a) and AI and is medially displaced by AI and ventrally by AV. AA showed very thin, fine fibers if compared to AD, AV, and AI (Figure 3a, b). AA-cells showed comparable cell sizes to AD. AD and AI can be easily delineated by their different cyto- and myelo-architecture (Figures 2b, c, h, i, 3a–l). AD is delineated from the nidopallium by the Lamina arcopallialis dorsalis (LAD; Figures 2b–d, 3b–e). Additionally, AD could be further subdivided into the intra-nuclear structures lateral arcopallium dorsale (ADl) and medial arcopallium dorsale (ADm) based on different myeloarchitectures (Figure 3b–l). Particularly, crossing fibers from the tractus dorsoarcopallialis (DA) demarcated ADl. The cyto- and myeloarchitecture of AI differed conspicuously from the surrounding regions. AI cells showed relatively large cell bodies compared to the other arcopallial regions (Figures 4–6). Further, many thick fibers that join the tractus occipitomesencephalicus (OM) characterized AI (Figure 3b–f, h–l). The finer and thinner fibers seen at the more posterior levels of AI belong to the tractus occipitomesencephalicus, pars hypothalami (HOM; Figure 3f, l). Additionally, a dorsal and a ventral part of AI (AId and AIv) were noticed. AId mostly corresponds to Aidv while AIv corresponds to Ai as defined in Kröner and Güntürkün (1999). Both substructures differ in their cellular- and myelo-architecture, with thinner fibers in AId compared to AIv (Figure 3b–f, h–l). As described earlier, AV showed differences in the cellular architecture and connectivity compared to the surrounding regions AI, AM, and PoAb (Zeier & Karten, 1971, Kröner & Güntürkün, 1999; Atoji et al., 2006; Shanahan et al., 2013, Letzner, Simon, & Güntürkün, 2016). Particularly, the cross sections of thick fibers that travel along the anterior posterior axis around atlas level 6.75 and pass across AV at more anterior levels characterized the shape of AV. Around atlas levels 7.50–7.25 an intra-nuclear substructure was detectable, which we named the medial part of the arcopallium ventral (AVm). AVm showed larger cell bodies compared to AV (Figure 4a–c) and thick fiber bundles that join OM (Figure 3b, c, h–i). According to Atoji and colleagues (2006, 2009), AM was subdivided into a medially located cell-dense, dark stained division with large cells (AMm) and a less cell-dense, parvocellular division (AMp) located laterally (Figures 2c–f, i–l, 5g, h, 6d). AMp was further characterized by a many thick fibers that travel through AM in the median axis (Figure 3d–f, j–l). The most caudal part of the arcopallium is a small, crescent-shaped subregion of the arcopallium that begins around atlas level 5.25 and is located between the amygdala nuclei PoAc and PoAb (Figures

TABLE 3 Significant differences between receptor densities in the main subregions of the arcopallium/amygdala complex

Subregion	AA	AD	AM	AI	AV	AP	PoAb	PoAc	TnA	SpA	NCVl
AA		M_2**	AMPA** Kainate** $GABA_A$* M_1**	M_2**	AMPA** M_1** M_2** $\alpha_4\beta_2$** α_2**	AMPA* Kainate** $GABA_A$* M_1** $\alpha_4\beta_2$*	$GABA_A$* M_2** $\alpha_4\beta_2$**	AMPA* Kainate** M_1** $\alpha_4\beta_2$** α_1**	Kainate** $GABA_A$** M_1** $\alpha_4\beta_2$** α_2** $D_{1/5}$**	NMDA** M_1** M_2** $\alpha_4\beta_2$** α_2**	AMPA* Kainate* M_1** M_2** α_1**
AD	M_2**		Kainate** $GABA_A$** M_1** M_2** $\alpha_4\beta_2$** 5-HT_{1A}**	NMDA* $GABA_A$** M_1** M_2* α_1** α_2* 5-HT_{1A}**	Kainate** NMDA** $GABA_A$** M_1** M_2** $\alpha_4\beta_2$** α_1** α_2** 5-HT_{1A}** $D_{1/5}$**	$GABA_A$** M_1** M_2* $\alpha_4\beta_2$* 5-HT_{1A}**	AMPA* $GABA_A$** M_1** M_2** α_1** 5-HT_{1A}* $D_{1/5}$**	NMDA** M_1** M_2** $\alpha_4\beta_2$** α_1** $D_{1/5}$*	Kainate** NMDA** $GABA_A$** M_1** M_2** $\alpha_4\beta_2$** α_1** α_2** 5-HT_{1A}** $D_{1/5}$**	AMPA** Kainate** NMDA** M_1** $\alpha_4\beta_2$** α_2** 5-HT_{1A}** $D_{1/5}$**	NMDA** M_1** M_2** α_1** $D_{1/5}$*
AM	AMPA** Kainate** $GABA_A$* M_1**	Kainate** $GABA_A$** M_1** M_2** $\alpha_4\beta_2$** 5-HT_{1A}**		Kainate** NMDA** $GABA_A$** M_1** M_2** $\alpha_4\beta_2$** α_1* α_2** 5-HT_{1A}**	Kainate** NMDA** $GABA_A$** M_1* M_2** $\alpha_4\beta_2$** α_1** α_2** 5-HT_{1A}**	5-HT_{1A}*	AMPA** $GABA_A$** M_2** $D_{1/5}$*	NMDA* $GABA_A$** M_1** M_2* $\alpha_4\beta_2$** α_1** 5-HT_{1A}** $D_{1/5}$**	Kainate* NMDA** $GABA_A$** M_1** $\alpha_4\beta_2$** α_1* α_2** $D_{1/5}$*	AMPA* Kainate** NMDA** M_2** $\alpha_4\beta_2$* α_2** 5-HT_{1A}*	NMDA* $GABA_A$** α_1** $D_{1/5}$**
AI	M_2**	NMDA* $GABA_A$** M_1** M_2* α_1** α_2* 5-HT_{1A}**	Kainate** NMDA** $GABA_A$** M_1** M_2** $\alpha_4\beta_2$** α_1* α_2** 5-HT_{1A}**		AMPA** Kainate** NMDA** M_1** M_2** $\alpha_4\beta_2$** α_2** 5-HT_{1A}**	Kainate** NMDA** $GABA_A$** M_1** M_2* α_2* 5-HT_{1A}**	AMPA* Kainate** $GABA_A$** M_1* M_2** $\alpha_4\beta_2$* 5-HT_{1A}** $D_{1/5}$**	NMDA** M_1** M_2** $\alpha_4\beta_2$** α_1** α_2** $D_{1/5}$**	Kainate** $GABA_A$** M_1** M_2* $\alpha_4\beta_2$** α_2** 5-HT_{1A}** $D_{1/5}$*	AMPA** Kainate** NMDA** M_1** $\alpha_4\beta_2$** α_2** 5-HT_{1A}**	Kainate* NMDA** M_1** M_2** α_1**
AV	AMPA** M_1** M_2** $\alpha_4\beta_2$** α_2**	Kainate** NMDA** $GABA_A$** M_1** M_2** $\alpha_4\beta_2$** α_1** α_2** 5-HT_{1A}** $D_{1/5}$**	Kainate** NMDA** $GABA_A$** M_1* M_2** $\alpha_4\beta_2$** α_1** α_2** 5-HT_{1A}**	AMPA** Kainate** NMDA** M_1** M_2** $\alpha_4\beta_2$** α_2** 5-HT_{1A}**		Kainate** $GABA_A$** α_2** 5-HT_{1A}** $D_{1/5}$*	AMPA** Kainate** NMDA** $GABA_A$** M_2** $\alpha_4\beta_2$* α_2** 5-HT_{1A}**	Kainate** M_1** $\alpha_4\beta_2$* α_1** α_2** $D_{1/5}$**	AMPA* Kainate** NMDA** $GABA_A$** M_1** M_2** $\alpha_4\beta_2$** α_2** 5-HT_{1A}**	AMPA** Kainate* NMDA** M_2** α_2** 5-HT_{1A}**	Kainate** α_1** α_2** $D_{1/5}$**
AP	AMPA* Kainate** $GABA_A$* M_1** $\alpha_4\beta_2$*	$GABA_A$** M_1** M_2* $\alpha_4\beta_2$* 5-HT_{1A}**	5-HT_{1A}*	Kainate** NMDA** $GABA_A$** M_1** M_2* α_2* 5-HT_{1A}**	Kainate** NMDA** $GABA_A$** α_2** 5-HT_{1A}** $D_{1/5}$*		AMPA** M_2* α_2** $D_{1/5}$*	Kainate* NMDA** $GABA_A$** M_1** α_1** 5-HT_{1A}**	AMPA** NMDA** $D_{1/5}$*	AMPA** Kainate** NMDA** $GABA_A$* $D_{1/5}$*	NMDA** $GABA_A$** α_1** 5-HT_{1A}*
PoAb	$GABA_A$* M_2** $\alpha_4\beta_2$**	AMPA* $GABA_A$** M_1** M_2** α_1** 5-HT_{1A}* $D_{1/5}$**	AMPA** $GABA_A$** M_2** $D_{1/5}$*	AMPA* Kainate** $GABA_A$** M_1* M_2** $\alpha_4\beta_2$* 5-HT_{1A}** $D_{1/5}$**	AMPA** Kainate** NMDA** $GABA_A$** M_2** $\alpha_4\beta_2$* α_2** 5-HT_{1A}**	AMPA** M_2* α_2** $D_{1/5}$*		AMPA** NMDA* $GABA_A$** M_2* $\alpha_4\beta_2$** α_1** 5-HT_{1A}** $D_{1/5}$**	Kainate** M_2** $\alpha_4\beta_2$** α_2**	Kainate** NMDA* $GABA_A$** M_2** α_2**	AMPA* $GABA_A$** M_2* α_1** 5-HT_{1A}** $D_{1/5}$**

(Continues)

TABLE 3 (Continued)

Subregion	AA	AD	AM	AI	AV	AP	PoAb	PoAc	TnA	SpA	NCVl
PoAc	AMPA* Kainate** M_1** $\alpha_4\beta_2$** α_1**	NMDA** M_1** M_2** $\alpha_4\beta_2$** α_1** $D_{1/5}$*	NMDA* $GABA_A$** M_2* $\alpha_4\beta_2$** α_1** 5-HT_{1A}** $D_{1/5}$**	M_1** M_2** $\alpha_4\beta_2$** α_1** α_2** $D_{1/5}$**	Kainate** M_1** $\alpha_4\beta_2$* α_1** α_2** $D_{1/5}$**	Kainate* NMDA** $GABA_A$** M_1** α_1** 5-HT_{1A}**	AMPA** NMDA* $GABA_A$** M_2* $\alpha_4\beta_2$** α_1** 5-HT_{1A}** $D_{1/5}$**		Kainate** NMDA** $GABA_A$** M_1** α_1** α_2** 5-HT_{1A}** $D_{1/5}$**	AMPA* Kainate** NMDA** M_2** $\alpha_4\beta_2$** α_1** α_2** 5-HT_{1A}** $D_{1/5}$**	Kainate* M_1** $\alpha_4\beta_2$* 5-HT_{1A}**
TnA	Kainate** $GABA_A$** M_1** $\alpha_4\beta_2$** α_2** $D_{1/5}$**	Kainate** NMDA** $GABA_A$** M_1** M_2** $\alpha_4\beta_2$** α_1** α_2** 5-HT_{1A}** $D_{1/5}$**	Kainate* NMDA** $GABA_A$** M_1** $\alpha_4\beta_2$** α_1* α_2** $D_{1/5}$*	Kainate** $GABA_A$** M_1** M_2* $\alpha_4\beta_2$** α_2** 5-HT_{1A}** $D_{1/5}$*	AMPA* Kainate** NMDA** $GABA_A$** M_1** M_2** $\alpha_4\beta_2$** α_2** 5-HT_{1A}**	AMPA** NMDA** $D_{1/5}$*	Kainate** M_2** $\alpha_4\beta_2$** α_2**	Kainate** NMDA** $GABA_A$** M_1** α_1** α_2** 5-HT_{1A}** $D_{1/5}$**		Kainate** NMDA** $GABA_A$** M_1** M_2* $\alpha_4\beta_2$* α_2**	NMDA** $GABA_A$** $\alpha_4\beta_2$** α_1** α_2** 5-HT_{1A}** $D_{1/5}$**
SpA	NMDA** M_1** M_2** $\alpha_4\beta_2$** α_2**	AMPA** Kainate** NMDA** M_1** $\alpha_4\beta_2$** α_2** 5-HT_{1A}** $D_{1/5}$**	AMPA* Kainate** NMDA** M_2** $\alpha_4\beta_2$* α_2** 5-HT_{1A}*	AMPA** Kainate** NMDA** M_1** $\alpha_4\beta_2$** α_2** 5-HT_{1A}**	AMPA** Kainate* NMDA** M_2** α_2** 5-HT_{1A}**	AMPA** Kainate** NMDA** $GABA_A$* $D_{1/5}$*	NMDA* $GABA_A$** M_2** α_2**	AMPA* Kainate** NMDA** M_2** $\alpha_4\beta_2$** α_1** α_2** 5-HT_{1A}** $D_{1/5}$**	Kainate** NMDA** $GABA_A$** M_1** M_2* $\alpha_4\beta_2$* α_2**		Kainate** NMDA** M_2** α_1** α_2** 5-HT_{1A}** $D_{1/5}$**
NCVl	AMPA* Kainate* M_1** M_2** α_1**	NMDA** M_1** M_2** α_1** $D_{1/5}$*	NMDA* $GABA_A$** α_1** $D_{1/5}$**	Kainate* NMDA** M_1** M_2** α_1**	Kainate** α_1** α_2** $D_{1/5}$**	NMDA** $GABA_A$** α_1** 5-HT_{1A}*	AMPA* $GABA_A$** M_2* α_1** 5-HT_{1A}** $D_{1/5}$**	Kainate* M_1** $\alpha_4\beta_2$* 5-HT_{1A}**	NMDA** $GABA_A$** $\alpha_4\beta_2$** α_1** α_2** 5-HT_{1A}** $D_{1/5}$**	Kainate** NMDA** M_2** α_1** α_2** 5-HT_{1A}** $D_{1/5}$**	

Each receptor type was tested separately with pair-wise Wilcoxon-rank test if the Friedman ANOVA showed regional differences between subregions. $^{**}T = 0$; $p < .05$, * $T = 1$; $p < .05$.

2e, f, k, l, 6). It was also described in Atoji et al. (2006) as the posterior part of AI. AP has a different connectivity from PoAc and PoAb (Atoji et al., 2006) and showed cells with larger cell bodies if compared to PoAc. Cells in PoAb also showed large cell bodies, but cells were less dense and patchier distributed compared to AP (Figure 6e, f). AP and AI differed considerably in their myelo-architecture. AP showed intra nuclear thin fiber labeling and no larger crossing fibers like AI.

The amygdala nuclei were subdivided into the area subpallialis amygdalae (SpA), which is a subpallial part of the extended amygdala in birds (Yamamoto et al., 2005), the nucleus taeniae amgygdalae (TnA; Reiner et al., 2004) and according to Atoji and colleagues (2006) in a basal and a compact division of the nucleus posterioris amygdalopallii (PoAb and PoAc). Further, we included the bed nucleus of the stria terminals pars lateralis (BSTL), that was defined based on its cytoarchitectonic characteristics that have been described in detail earlier (Atoji et al., 2006). The borders of TnA were nicely resolved with the cell staining and TnA could be distinguished from the surrounding areas by its small-sized cells (Figures 2c, 5b). The myelin staining showed thin fibers in TnA and a few thick fibers but with a smaller diameter compared to AI and AM that travel along the anterior–posterior axis of TnA at the border to AM (fascicles from OM; Figure 3d, e). Both, PoAc and PoAb differed considerably in their cyto- and myelo-architecture (Figures 2d–f, 3d–f). While PoAc showed a compact mass of small cells, PoAb is speckled with cells with larger cell bodies (Figures 6c, e). Further, PoAb is characterized by thin and short fibers that were often transversally directed, while in PoAc many longitudinal fibers were detected.

3.2 | Quantitative analysis of the receptor-binding site densities in the arcopallium/amygdala complex

Quantitative receptor data of the arcopallium/amygdala complex is presented in form of color-coded autoradiographs for each receptor at different atlas levels of a series of five cross sections with a gap of approximately 500 μm between each slice to highlight the regional differences in receptor expression that nicely resolve distinct subregions and intra-nuclear substructures (Figures 7–10). Additionally, binding site densities of all receptors ± *SEM* are presented in a 2-dimensional polar coordinate-plot to construct a multi-receptor fingerprint for each

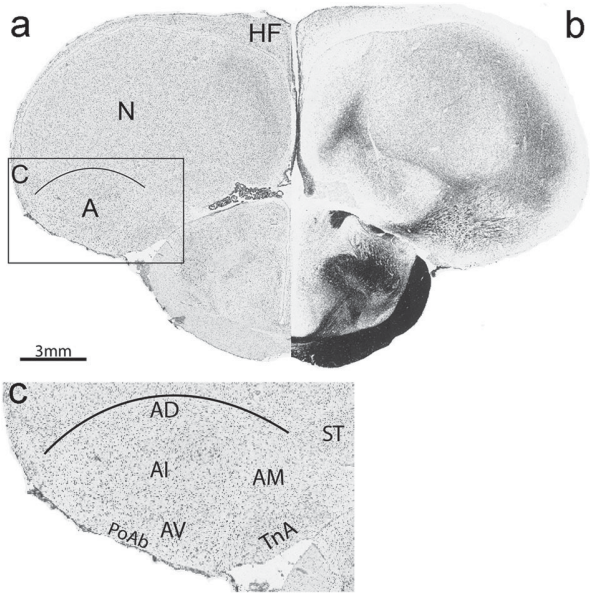

FIGURE 1 Nissl and myelin stained coronal section of the forebrain of the pigeon. (a) Nissl stained and (b) myelin stained coronal section at atlas level A 6.75 (Karten & Hodos, 1967). The boxed area indicates the region of interest: the arcopallium/amygdala complex. Scale bar 3 mm. (c) Enlarged image of the arcopallium/amygdala complex labeled in (a). A, arcopallium; AD, arcopallium dorsale; AI, arcopallium intermedium; AM, arcopallium mediale; AV, arcopallium ventrale; HF, hippocampal formation; N, nidopallium; PoAb, Nucleus posterioris amygdalopallii pars basalis; ST, striatum; TnA, Nucleus taeniae amygdalae

analyzed subregion (Figure 11a–l). We also present the receptor data for the adjacent areas of the arcopallium/amygdala complex, the posterior lateral striatum (LSt, from atlas level A 6.75–6.25; Figure 11c) and the lateral division of the nidopallium caudoventrale (NCVl); Figure 11i). Data for the intra-nuclear substructures is provided separately in histograms (Figure 12a–k). Detailed numbers of receptor densities and statistics are summarized in Tables 2 and 3. In the following subsections, we describe the highlights in receptor densities that resolved the different subregions and intra-nuclear structures one by one.

AA The anterior tip of the arcopallium is high in AMPA, kainate and $GABA_A$ receptor densities (Table 2). In contrast to the surrounding regions AD and AI, AA expressed lower M_2-receptor densities and a trend towards higher kainate receptor densities was detected. If compared to AV, higher M_1, M_2 and α_2-receptor and lower AMPA and nACh ($\alpha_4\beta_2$ subtype) receptor levels were found (Tables 2 & 3). The overall receptor expression was comparable to AD and AI (Figures 11 a, d, e; Tables 2, 3).

AD Receptor densities in AD differed from the dorsally located PoAc for NMDA, M_1, M_2, nACh ($\alpha_4\beta_2$ subtype), α_1- and $D_{1/5}$ receptors (Figures 7–10; Table 3). Additionally, AD had conspicuously high M_1 and M_2 receptor densities if compared to the other arcopallial regions (Figure 8; Table 2) and α_2-receptor expression rendered distinctively the crescent structure of AD (Figure 9). Except AMPA receptors, all measured receptors were differentially expressed in AD compared to AV (Figures 7–10; Tables 2, 3). The fingerprints of AD and AI appeared very similar (Figure 11d, e). ADl and ADm differed in kainate, NMDA, $GABA_A$, and 5-HT_{1A} receptors (Figure 12b–d, j). This delineation was primarily observed with the heterogeneously distribution of kainate receptors in ADl and ADm (Figure 7).

AI AI showed higher densities of M_2 receptors and lower densities of kainate receptors compared to the ventral region of the arcopallium (Figures 7, 8; Tables 2, 3). $GABA_A$ receptor expression was higher in AI compared to AM, AD, and AP and nicely resolved the borders to these neighboring regions (Figure 8). Further, the borders of the intermediate arcopallial region were covered with a higher 5-HT_{1A}-receptor density compared to the surrounding regions (Figure 10). The sub differentiation of AI into AId and AIv was supported by six significant differences in receptor binding sites (Figure 12c–f, i, j) and highlighted by a higher M_1-, M_2- α_2-, and 5-HT_{1A}-receptor expression in AId (Figures 8–10).

AV A high kainate receptor density delineates the ventral arcopallium from the dorsally located regions AI and AD and the medially located regions AM and TnA (Figure 7). AV additionally showed higher AMPA receptor densities if compared to AA, AI, TnA, SpA, and PoAb, and higher NMDA receptor densities if compared to AD, AI, AM, AP, PoAb, TnA, and SpA (Figure 7; Tables 2, 3). Further, a high $GABA_A$ receptor expression and relatively low M_2 receptor densities compared to the other arcopallial regions characterized AV (Figure 8; Tables 2, 3). AVm differed in kainate-, NMDA-, $GABA_A$-, M_1-, α_2-, 5-HT_{1A}-, and $D_{1/5}$- receptor densities from AV and AVm showed particularly lower $GABA_A$ receptor amounts if compared to AV (Figures 8, 12b–e, i–k).

AM Kainate and $GABA_A$ receptors showed relatively low levels in the medial arcopallium if compared to the other arcopallial regions, except AP (Figures 7, 8). AMPA receptor expression in AM was comparable to AD, AV and AP, and higher compared to AA and AI and the ventrally located TnA (Figure 7; Tables 2, 3). The receptor architecture of AM was different if compared to the other arcopallial regions AI and AV (Tables 2, 3) that is also visualized in the receptor fingerprint (Figure 11d, e, g). The substructures AMm and AMp were nicely resolved by the heterogeneously distribution of NMDA and 5-HT_{1A} receptors in AM (Figures 7, 10) and receptor densities differed in 8 out of the 11 measured types (Figure 12a–k).

AP AP differed from AI by its higher amounts of NMDA, α_2 and lower amounts of kainate, $GABA_A$, M_1, M_2, and 5-HT_{1A} receptors (Figures 7–11e, l; Tables 2, 3). Particularly, the glutamatergic receptors demarcated PoAc, AP and PoAb (Figure 7; Tables 2, 3), and α_2 receptors showed intense labeling of AP compared to PoAc (Figure 9; Tables 2, 3). AP showed only a significant difference in 5-HT_{1A} receptor expressions compared to AM, but further comparisons between both regions indicated differences by a trend for NMDA, $\alpha_4\beta_2$ and α_2 receptor densities. The overall receptor architecture of AP is highly similar to AM (Figure 11g, l).

PoA High densities of kainate, α_1, 5-HT_{1A} or $D_{1/5}$ receptors highlighted PoAc if compared to the surrounding structures AD, AP and NCVl (Figures 7, 9, 10; Tables 2, 3), whereas PoAb was separated from AV by lower AMPA, kainate, NMDA, $GABA_A$, M_2, nACh ($\alpha_4\beta_2$ subtype) and 5-HT_{1A} receptor densities (Figures 7–10; Tables 2, 3). PoAc and PoAb differed significantly from each other in AMPA, NMDA, $GABA_A$, M_2, nACh ($\alpha_4\beta_2$ subtype), α_1, 5-HT_{1A} and $D_{1/5}$ receptor densities (Figure 12a, c–d, f–h, j–k; Tables 2, 3).

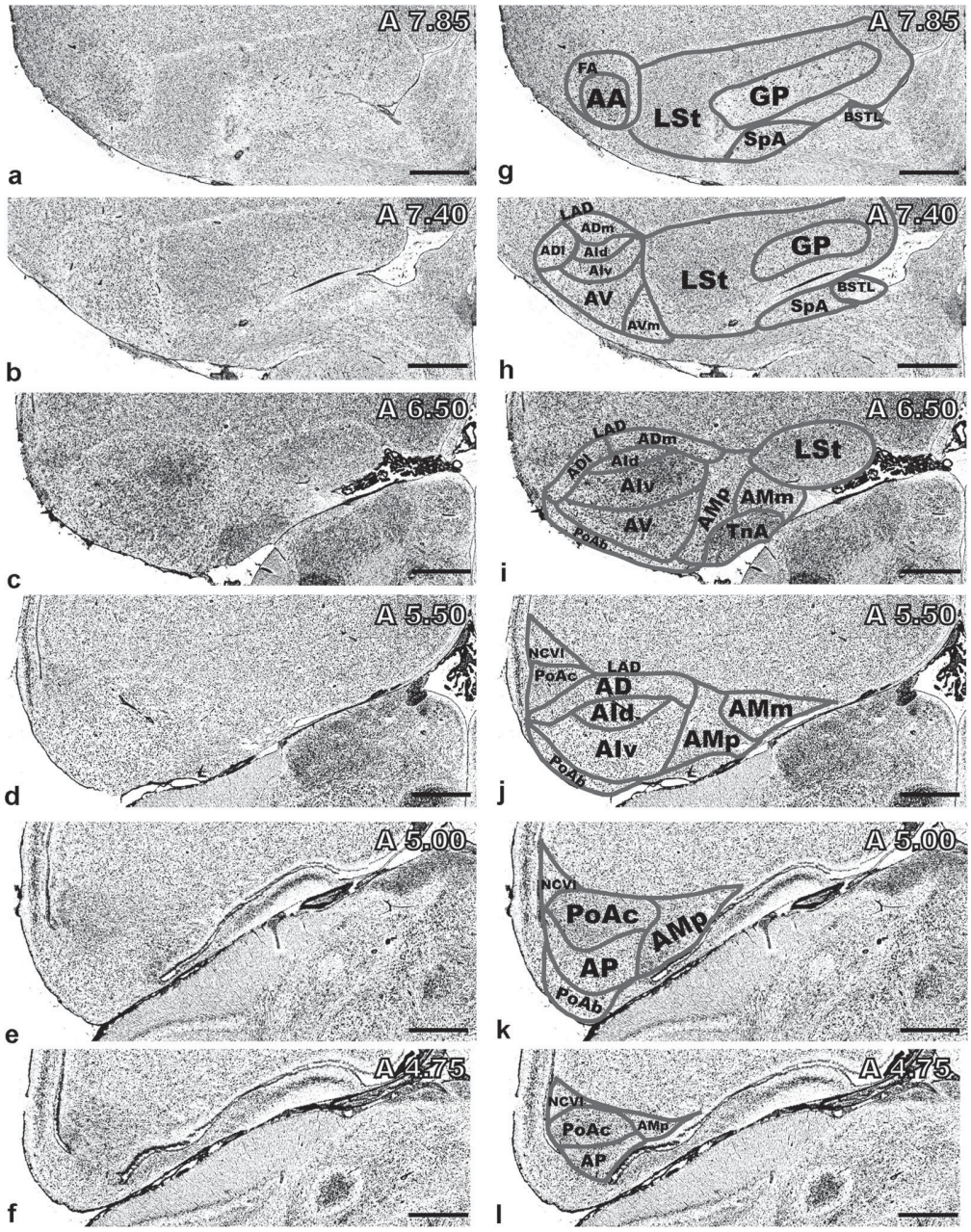

FIGURE 2 Representative Nissl stained coronal sections through the pigeon arcopallium/amygdala complex showing subregion boundaries at different rostro-caudal levels. (a–f) Nissl stained coronal sections of the arcopallium/amygdala complex. (g–l) Nissl stained coronal sections of the arcopallium/amygdala complex with the boundaries defined by (Atoji et al., 2006; Atoji & Wild, 2009; Karten & Hodos, 1967; Kröner & Güntürkün, 1999; Reiner et al., 2004; Shanahan et al., 2013; Yamamoto & Reiner, 2005; Zeier & Karten, 1971) and our own observations. These boundaries were defined solely based on cytoarchitectonical criteria and were used to identify regions of interest in receptor autoradiographs. The arcopallium/amygdala complex and the extended amygdala of pigeons comprises the following regions: AA, arcopallium anterius; AD, arcopallium dorsale; ADm, arcopallium dorsale pars medialis; ADl, arcopallium dorsale pars lateralis; AI, arcopallium intermedium; Ald, arcopallium intermedium pars dorsalis; Alv, arcopallium intermedium pars verntralis; AM, arcopallium mediale; AMp, arcopallium mediale pars parvocellularis; AMm, arcopallium mediale pars magnocellularis; AP, arcopallium posterioris; AV, arcopallium ventrale; AVm, arcopallium ventrale pars medialis; BSTL, Bed nucleus of the Stria Terminalis, pars lateralis; PoAb, nucleus posterioris amygdalopalii pars basalis; PoAc, nucleus posterioris amygdalopalii pars compacta; SpA, area subpallialis amygdalae; TnA, nucleus taeniae amygdalae. Scale bar 1200 μm in (a), 1000 μm in (b), 1160 μm in (c), 1125 μm in (d), 1150 μm in (e), 1125 μm in (f), 1200 μm in (g), 1000 μm in (h), 1160 μm in (i), 1125 μm in (j), 1150 μm in (k), 1125 μm in (l)

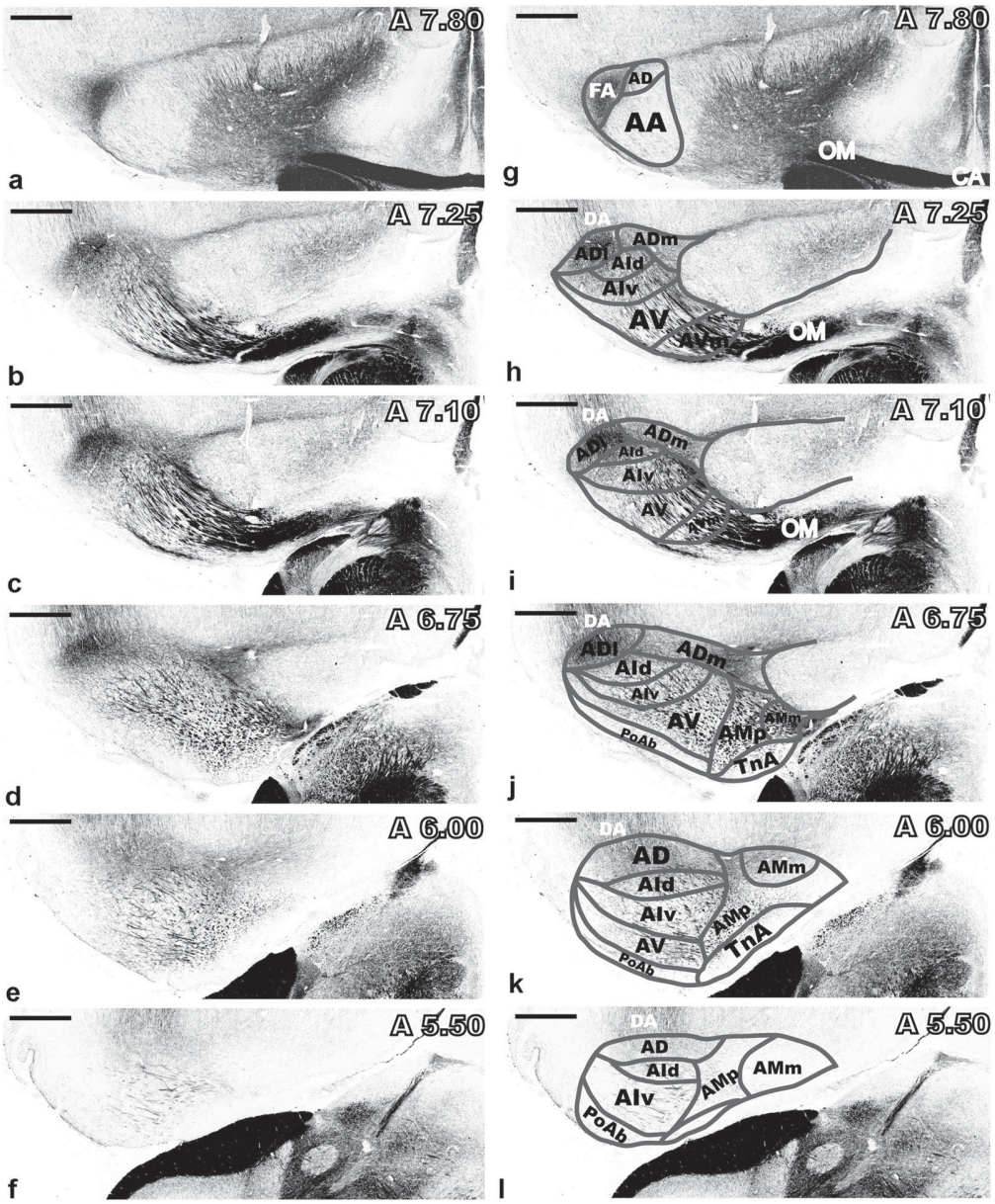

FIGURE 3 Representative myelin stained coronal sections of the pigeon arcopallium/amygdala complex showing subregion boundaries at different rostro-caudal levels. (a–f) Myelin-stained coronal sections of the arcopallium/amygdala complex. (g–l) Myelin-stained coronal sections of the arcopallium/amygdala complex with boundaries and labels. Differences in fiber architecture in the arcopallial subregions and their intra-nuclear substructures were of particular help for the delineation of structures in receptor autoradiographs and defining boundaries between ADl and ADm. For abbreviations see legend of Figure 2. Scale bar 1300 μm in (a), 1190 μm in (b), 1400 μm in (c), 1300 μm in (d), 1300 μm in (e), 1250 μm in (f), 1300 μm in (g), 1190 μm in (h), 1400 μm in (i), 1300 μm in (j), 1300 μm in (k), 1250 μm in (l)

TnA High M_2, nACh ($\alpha_4\beta_2$ subtype) and α_2 receptor densities characterized this subdivision of the arcopallium/amgygdala complex (Figures 8, 9). TnA further differed from the neighboring AM by eight receptors and showed a substantial peak in α_2 receptor density (Figures 9, 11l; Tables 2, 3). The majority of similarities in the overall receptor architecture were detected between TnA and AP (Table 3) and visualized in Figure 11h, l.

SpA This area, which is a subpallial part of the extended amygdala in birds, expressed 2.6-fold lower amounts of $GABA_A$ receptors compared to LSt that nicely resolved the border between those areas (Figure 8). SpA further showed higher densities of kainate, M_2, nACh ($\alpha_4\beta_2$ subtype) and α_2 receptors and lower AMPA, NMDA, and 5-HT_{1A} receptors if compared to the neighboring subregion AM (Tables 2, 3). If compared to the other analyzed regions, the receptor fingerprint of SpA appeared differentially (Figure 12b).

In some slices, we also managed to analyze the bed nucleus of the stria terminals pars lateralis (BSTL), which is considered to be a part of the extended amygdala of birds. However, we could not sample a sufficient receptor data set to quantify it.

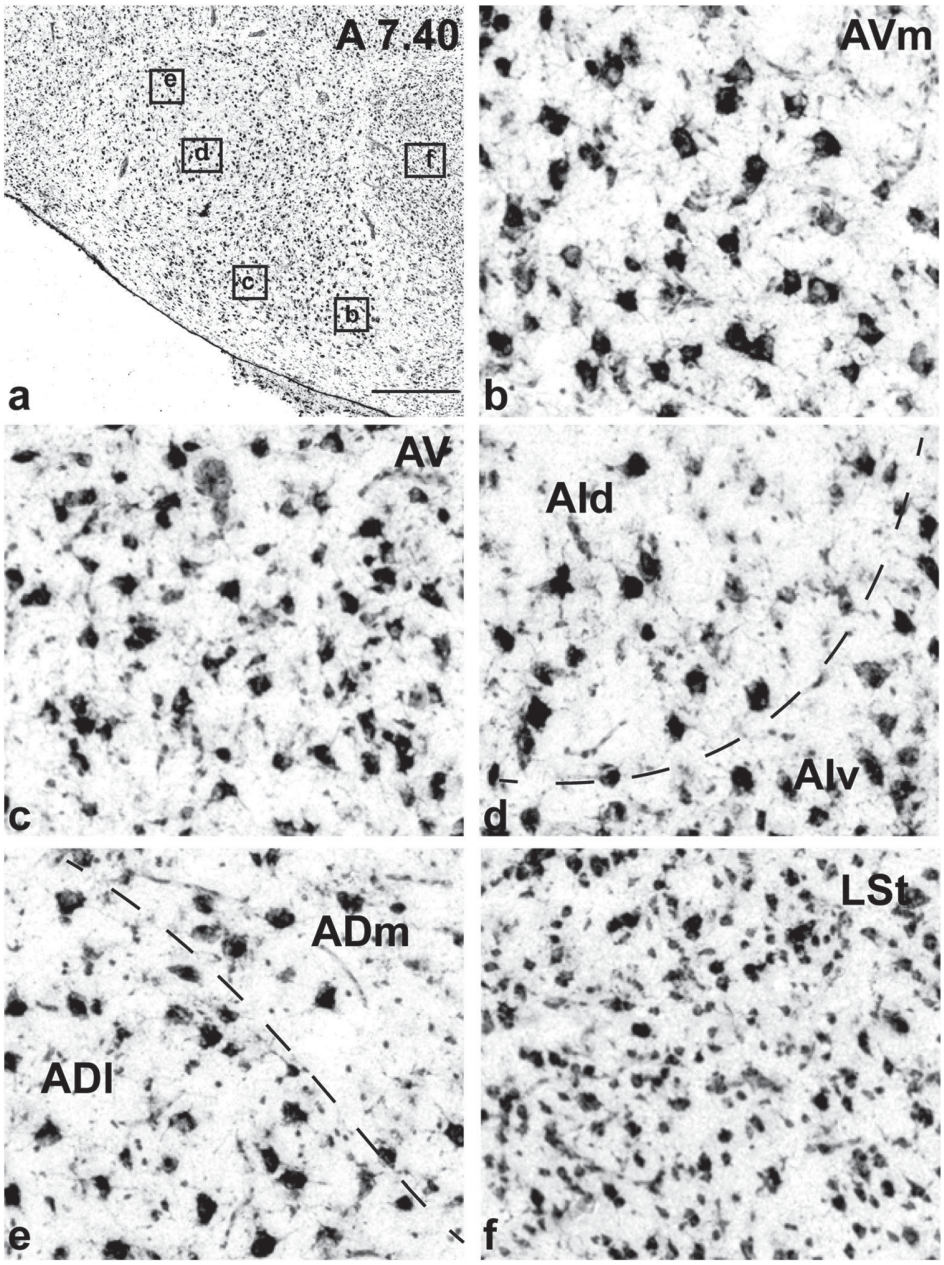

FIGURE 4 Enlarged image of the arcopallium at atlas level A 7.40 (a) and details of the cellular architecture (b–f). (b–f) Enlargement of boxes labeled in a (6× magnification) showing the cellular densities and cell sizes in the different subregions of the arcopallium. Scale bar 600 μm

The resulting new atlas from the AP coordinate A 7.75–4.50 is based, therefore, on the overlay of cellular/fiber-architectonic and receptor-density information, and is presented in Figure 13.

3.3 | Combined analysis of the overall receptor architecture in the arcopallium/amygdala complex

Overall (dis)similarities in the neurotransmitter receptor architecture between subregions of the arcopallium/amygdala complex, NCVl and posterior LSt are shown in a cladogram of a hierarchical cluster analysis (Figure 14). The hierarchical cluster analysis provided two main clusters of the analyzed subdivisions that split further up in different branches (cophenetic correlation coefficient $c = 0.60$). One main cluster groups the seven regions NCVl, PoAc, TnA, AP, AV, PoAb and AM (Cluster I), and the other cluster comprises the five regions posterior LSt, SpA, AA, AI, and AD (Cluster II, Figure 14). Further, in Cluster I, NCVl and PoAc are separated from TnA, AP, AV, PoAb, and AM, and in Cluster II, LSt and SpA are separated from AA, AI, and AD. In Cluster I, the lowest Euclidian distance was observed between PoAb and AM, while in Cluster II, the lowest Euclidian distance was observed between AI and AD.

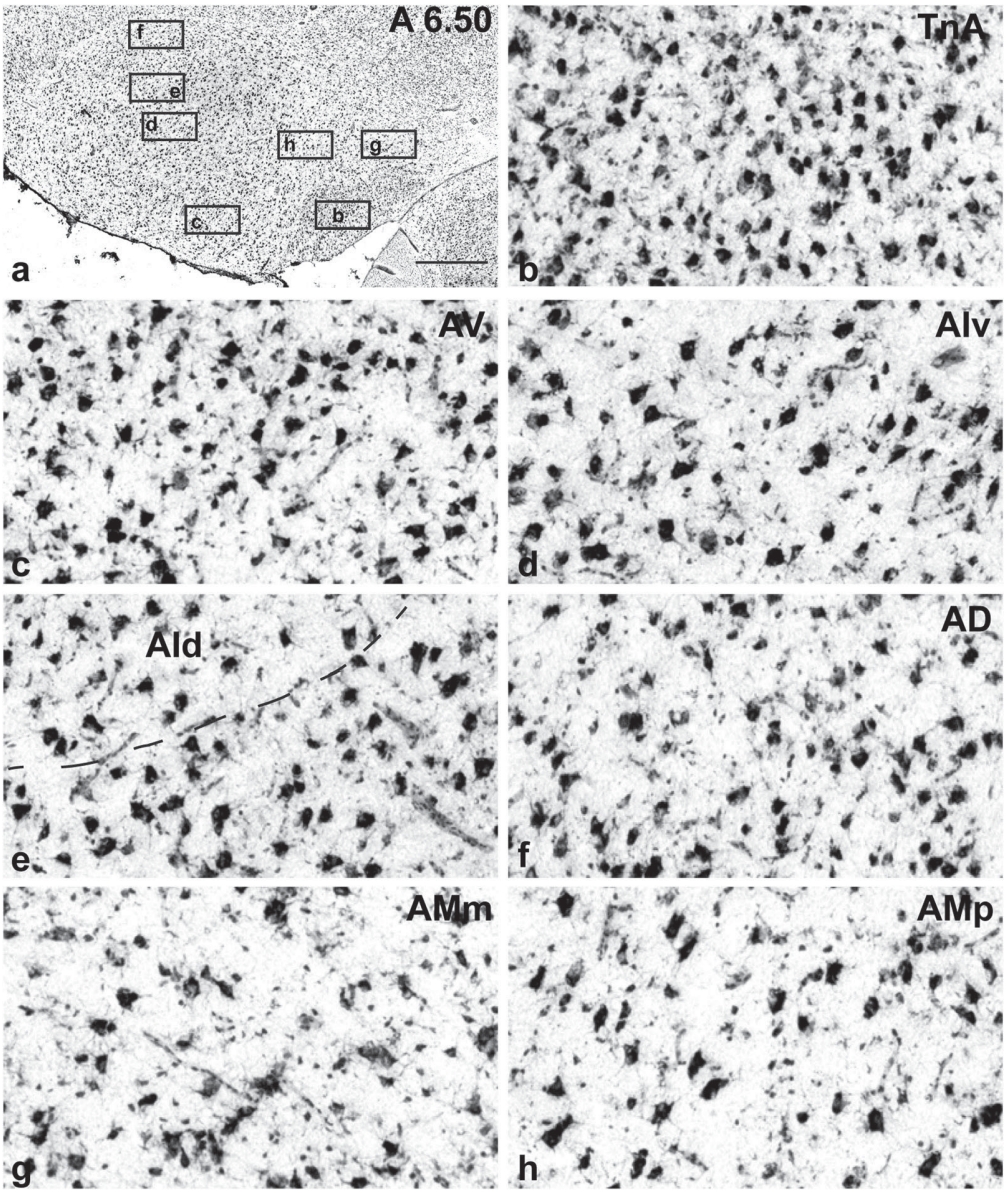

FIGURE 5 Enlarged image of the arcopallium/amygdala complex at atlas level A 6.50 (a) and details of the cellular architecture (b–h). (b–h) Enlargement of boxes labeled in a (8× magnification) showing the cellular densities and cell sizes in the different subregions of the arcopallium. Scale bar 700 μm

4 | DISCUSSION

The regionally different receptor densities mapped well onto several subregions of the arcopallium/amygdala complex in pigeons that have been in part previously described based on connectivity data and cellular analysis (Atoji et al., 2006; Karten & Hodos, 1967; Kröner & Güntürkün, 1999; Puelles, Martinez-de-la-Torre, Paxinos, Watson, & Martinez, 2007; Shanahan et al., 2013; Yamamoto et al., 2005). These subregions are: the arcopallium anterius (AA), the arcopallium ventrale (AV), the arcopallium dorsale (AD), the arcopallium intermedium (AI), the arcopallium mediale (AM), the arcopallium posterius (AP), the nucleus posterioris amygdalopallii pars basalis (PoAb) and pars compacta (PoAc), the nucleus taeniae amgygdalae (TnA) and the area subpallialis amygdalae (SpA). Based on our results, AV, AM, AD, and AI can be further subdivided into intra-nuclear substructures. Several important differences in receptor- cyto- and myelo-architecture highlighted the distinct subregions and intra-nuclear substructures that resulted into a new map of the pigeon arcopallium/amygdala complex. Together with data from previous studies, our results provide a high-resolution scheme of the pigeon's arcopallium/amygdala complex that can be used for future structural and functional studies. This will also improve the anatomic identification in different types of data sets from genetic approaches to functional studies in various avian species, may help to assess species-specific adaptations, and discover important basic neurochemical traits that may be conserved in the arcopallium/amygdala complex. Further, our data will facilitate the comparison

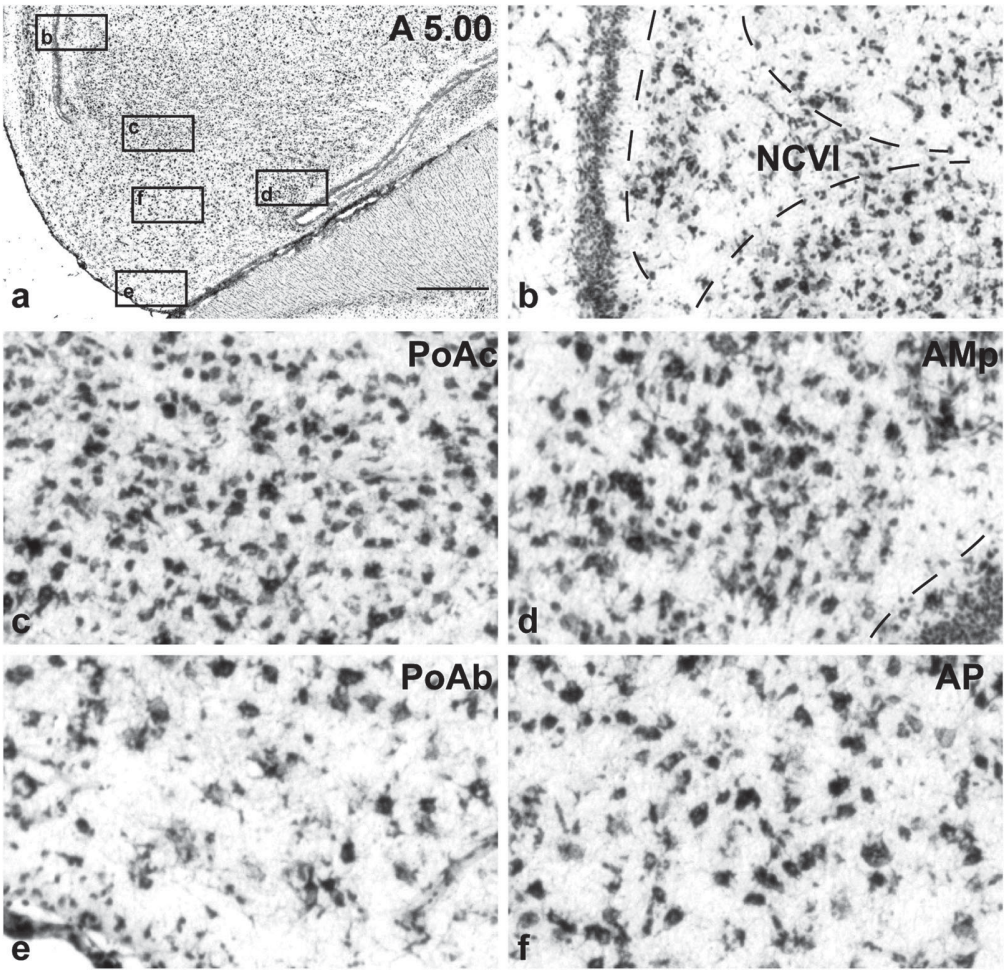

FIGURE 6 Enlarged image of the arcopallium/amygdala complex at atlas level A 5.00 (a) and details of the cellular architecture (b–f). (b–f) Enlargement of boxes labeled in a (8× magnification) showing the cellular densities and cell sizes in the different subregions of the arcopallium. Scale bar 600 μm

between the avian premotor and amygdala subregions with possibly corresponding homolog or homoplastic mammalian structures.

4.1 | The avian arcopallium/amygdala complex: previous studies and thoughts on homologies

According to the classic view of the 19th century, most of the avian telencephalon was supposed to be homologous to the mammalian basal ganglia (Edinger, 1896). This interpretation resulted in an avian brain nomenclature were Greek prefixes and the root word 'striatum' were combined to label the different substructures of the bird telencephalon (Ariens-Kappers, Huber, & Crosby, 1936; Edinger, 1903). Accordingly, the caudal ventrolateral portion of the telencephalon was termed archistriatum and suggested to be partly comparable to the mammalian amygdala. Much later and based on connectivity data, Zeier and Karten (1971) subdivided this area into four major regions: the archistriatum anterior, intermedium (with a dorsal portion), posterior (with a postero-ventral portion) and mediale. This delineation differs to some extent from the pigeon atlas of Karten and Hodos (1967). According to Zeier and Karten (1971) the posterior and medial archistriatum correspond to the amygdala since they are connected via the tractus occipitomesencephalicus, pars hypothalami (HOM) to the hypothalamus. In contrast, the archistriatum intermedium and anterior were supposed to be part of the sensorimotor system since they lack limbic projections and are connected via the tractus occipitomesencephalicus (OM) to various sensory and motor entities of thalamus and brainstem. According to Zeier and Karten (1971), only the anterior archistriatum received fibers both from the anterior commissure and from the tractus fronto-arcopallialis (FA), whereas the intermediate part received its input from the tractus arcopallialis dorsalis (DA). However, a new study revealed that the anterior commissure derives from both the anterior and the intermediate arcopallium (Letzner et al., 2016). Over the years, further subnuclei of the archistriatum were defined which will be discussed below.

At the beginning of the new millennium, neuroanatomists had reached the consensus that the view of the striatally dominated bird forebrain was outmoded and wrong. Accordingly, a revised nomenclature of the avian telencephalon was conceived (Reiner et al., 2004;

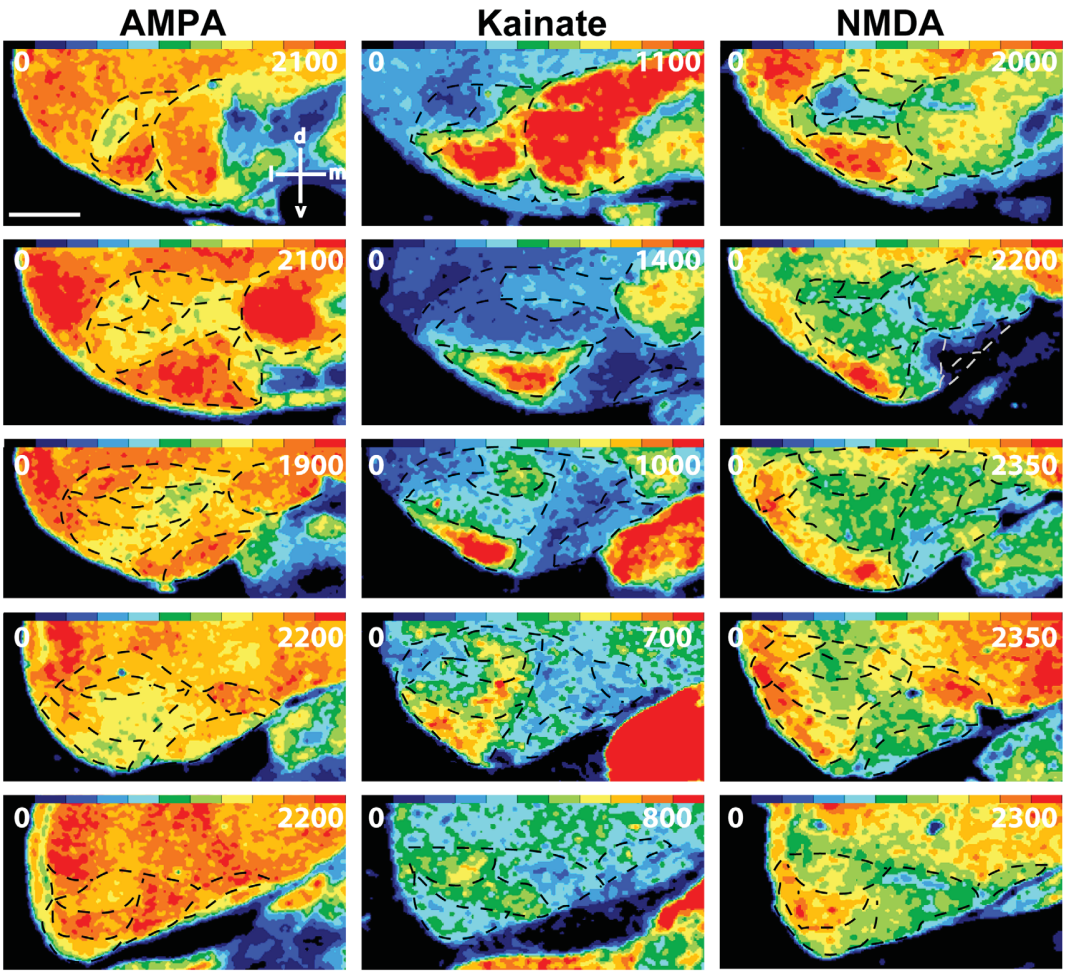

FIGURE 7 Color-coded autoradiographs showing the distribution and density of glutamate receptors at different rostro-caudal atlas levels of a series of five cross sections with a gap of approximately 500 μm between each slice of the arcopallium/amygdala complex. Left column: AMPA receptor expression in the arcopallium/amygdala complex from anterior (top) to posterior (down) levels. Middle column: Kainate receptor expression in the arcopallium/amygdala complex from anterior (top) to posterior (down) levels. Right column: NMDA receptor expression in the arcopallium/amygdala complex from anterior (top) to posterior (down) levels. Dashed lines show boundaries as depicted in Figures 2 and 3. Color scales code for the receptor densities in fmol/mg protein and are specific for each receptor type. Note that the red end of the scale bar indicates the best fit for the investigated arcopallium/amygdala substructures but not the maximum receptor density. Please use the atlas in Figure 13 to trace the labels of the different brain regions. Scale bar row 1–2: 1.8 mm, row 3–5: 3.5 mm [Color figure can be viewed at wileyonlinelibrary.com]

Jarvis et al., 2005) and along that line the archistriatum was subdivided into a premotor arcopallium complex and a limbic amygdala assembly of nuclei. Only the medial arcopallium was left undecided since it seemed to display both limbic and premotor features. Meanwhile further limbic associations of the medial arcopallium have been discovered and will be discussed further below (Atoji & Wild, 2009; Medina, Bupesh, & Abellán, 2011). In addition, some subnuclei of the arcopallial/amygdala complex can only be found in certain avian groups like those that learn their vocalizations (songbirds: robust nucleus of the arcopallium (RA); parrots: central nucleus of the anterior arcopallium (AAC); hummingbirds: vocal nucleus of the arcopallium (VA)).

To shed some light into the ongoing discussion of which subregions of the arcopallium/amygdala complex are limbic, Yamamoto and colleagues (2005a, 2005b) used different markers like the limbic associated membrane protein (LAMP) and the subpallial marker glutamate decarboxylase 65 (GAD65), to discover limbic and or subpallial components of the arcopallium/amygdala complex. This approach did not only show co-expression of these markers in TnA and SpA but also brought forward that the lateral and medial nuclei of the stria terminalis (BSTM and BSTL) of birds may be a part of the extended amygdala. Furthermore, these authors concluded that TnA should be subdivided into a lateral and medial pallial subnucleus. The weak labeling of the anterior two thirds of the arcopallium (including AA and AI) supported the suggestion of Zeier and Karten (1971) that these parts are of premotor nature. However, the dorsal arcopallium showed intense LAMP labeling which would be inconsistent with the former conclusion that this subregion is not limbic but is in line with other connectivity studies that showed inputs to AD from limbic regions like the piriform cortex, hippocampal formation, and TnA and outputs to the limbic medial and somatic lateral striatum (Atoji & Wild, 2006; Bingman, Casini, Nocjar, &

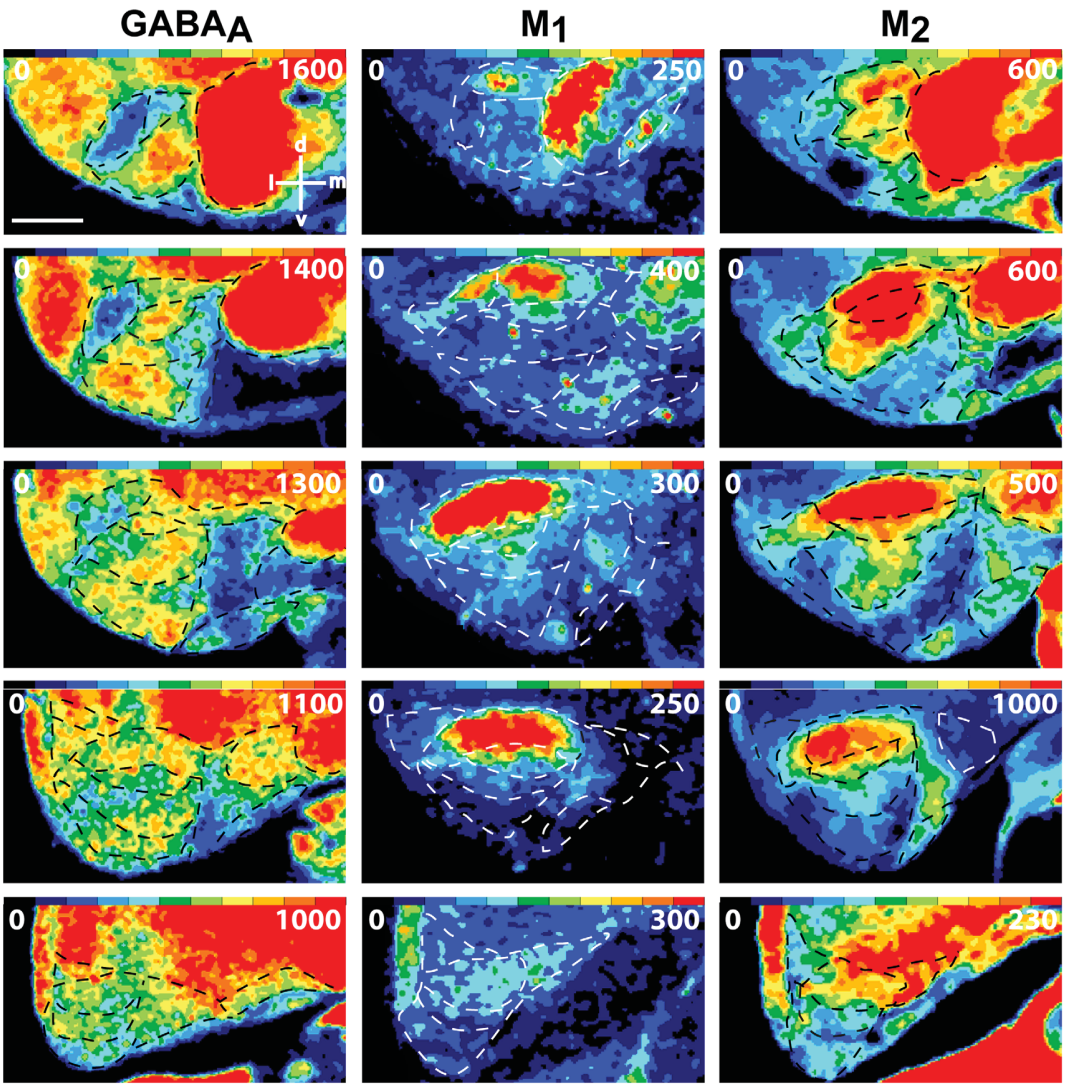

FIGURE 8 Color-coded autoradiographs showing the distribution and density of $GABA_A$ and muscarinergic cholinergic receptors at different rostro-caudal atlas levels of a series of five cross sections with a gap of approximately 500 μm between each slice of the arcopallium/amygdala complex. Left column: $GABA_A$ receptor expression in the arcopallium/amygdala complex from anterior (top) to posterior (down) levels. Middle column: M_1 receptor expression in the arcopallium/amygdala complex from anterior (top) to posterior (down) levels. Right column: M_2 receptor expression in the arcopallium/amygdala complex from anterior (top) to posterior (down) levels. Further explanations see Figure 7 [Color figure can be viewed at wileyonlinelibrary.com]

Jones, 1994; Veenman, Wild, & Reiner, 1995). Further, LAMP labeling showed that AD is distinct from AA (Yamamoto & Reiner, 2005). The posterior pallial amygdala (PoA) is also LAMP-rich, which is in line with its viscero-limbic connectivity (Zeier & Karten, 1971; Reiner et al., 2004). AM showed intense LAMP labeling as well, which would support the idea that AM is limbic (Zeier & Karten, 1971; Yamamoto & Reiner, 2005).

4.2 | The delineation of the arcopallium/amygdala complex based on receptor autoradiography, cyto- and myeloarchitecture

The cluster analysis of the overall receptor architecture of arcopallial, amygdala, striatal, and nidopallial subdivisions divided the investigated subdivisions into two main clusters with further subgroups that may be interpreted as either functionally or anatomically (dis)similar, possibly involved in different neuronal circuits. Herein, our results fit very well with the findings of a study that analyzed several pathway-tracing studies to construct a connectivity matrix ("structural connectome") for the telencephalon of the pigeon (Shanahan et al., 2013). In Cluster I, one group comprises PoAc and NCVl, both pallial subdivisions, adjacent regions and involved in viscero-limbic functions (Shanahan et al., 2013), and the second group comprises TnA, AP, AV, PoAb, and AM, which challenges the question if TnA is a subpallial part of the amygdala because all other regions of this cluster are of pallial origin. Further, the second group of Cluster I also splits up in more subgroups, one subgroup comprises TnA and AP, and the other AV, PoAb, and AM, with AV more distinct from AM/PoAb that is consistent with the finding

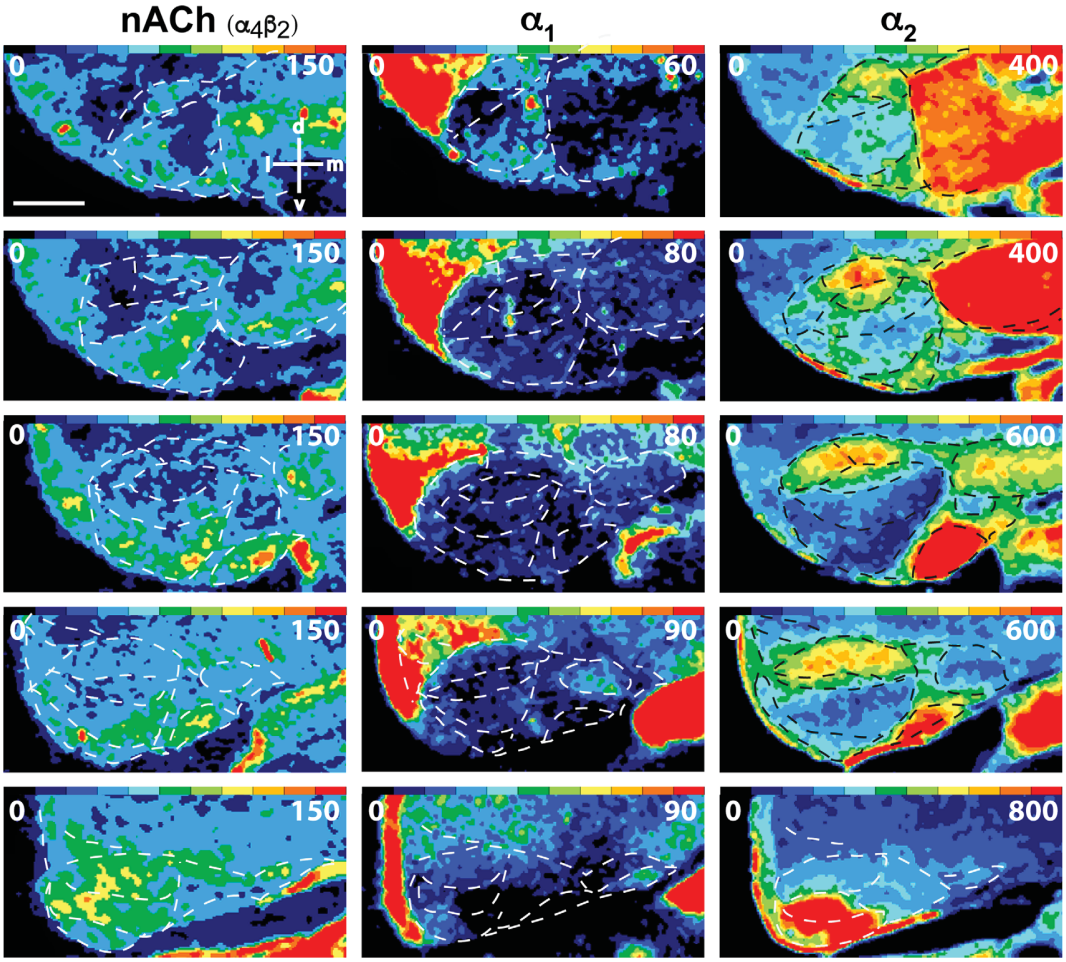

FIGURE 9 Color-coded autoradiographs showing the distribution and density of nACh receptors ($\alpha_4\beta_2$ subtype) and noradrenergic receptors at different rostro-caudal atlas levels of a series of five cross sections with a gap of approximately 500 μm between each slice of the arcopallium/amygdala complex. Left column: nACh ($\alpha_4\beta_2$ subtype) receptor expression in the arcopallium/amygdala complex from anterior (top) to posterior (down) levels. Middle column: α_1 receptor expression in the arcopallium/amygdala complex from anterior (top) to posterior (down) levels. Right column: α_2 receptor expression in the arcopallium/amygdala complex from anterior (top) to posterior (down) levels. Further explanations see Figure 7 [Color figure can be viewed at wileyonlinelibrary.com]

that functionally PoAb and AM belong to the viscero-limbic network, while AV is involved in auditory-associative processing (Shanahan et al., 2013). The second Cluster II comprises two groups, the posterior LSt and SpA, two subpallial structures that were recognized earlier as functionally closely related as caudal LSt (CLSt) and SpA (Abellán & Medina, 2009; Kuenzel et al., 2011). The second subgroup in Cluster II comprises AA, AD, AI that are more centrally located in the arcopallium and adjacent to each other. All three subdivisions are of pallial origin and have premotor-associative functions (Shanahan et al., 2013). We will now discuss these findings in more detail for each subregion below.

In the past, the arcopallium anterius (AA) was considered to be a trigeminal component because of its connectivity to the tractus fronto-arcopallialis and the anterior commissure (Schall, Güntürkün, & Delius, 1986; Wild, Arends, & Zeigler, 1984; Zeier & Karten, 1971). Therefore, together with AD and AI, AA was located in the high level associative module within the premotor submodule of the "structural connectome" in the telencephalon of the pigeon (Shanahan et al., 2013). In our receptor study, all three arcopallial subdivisions were also in the same cluster if the overall receptor densities were analyzed. Based on a study that measured the Euclidian distance of diverse mRNA expression levels within different subregions of the arcopallium in the zebra finch (*Taeniopygia guttata*), AA seems to differ from all other nuclei in this area (Jarvis et al., 2013). This does not match the current analysis based on receptor binding densities as confirmed by our cluster analysis. One explanation could be species differences in brain subdivisions or gene expression. However, it could be also possible that in vocal learning birds the arcopallium is located more medial in the forebrain and somewhat rotated medially compared to other avian species (Wang et al., 2015). Thus, it is possible that what is anterior arcopallium in the zebra finches could be more anterior-medial in pigeons, or in some other position.

Arcopallium dorsale (AD) was clearly labeled by the expression of α_2, M_1, and M_2 receptors, which is comparable to the results of former autoradiography studies in birds (Ball, Nock, Wingfield, McEwen, &

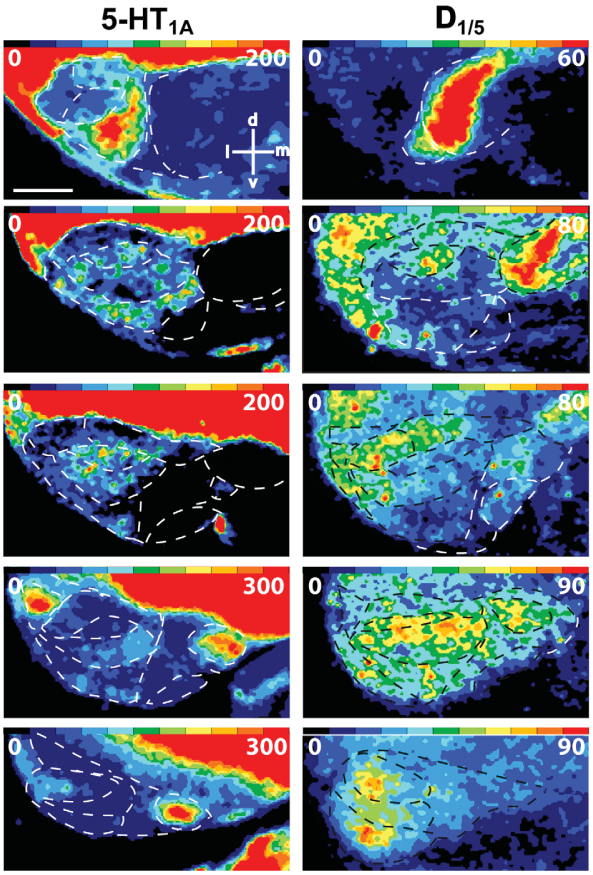

FIGURE 10 Color-coded autoradiographs showing the distribution and density of 5-HT_{1A} and $D_{1/5}$ receptors at different rostro-caudal atlas levels of a series of five cross sections with a gap of approximately 500 μm between each slice of the arcopallium/amygdala complex. Left column: 5-HT_{1A} receptor expression in the arcopallium/amygdala complex from anterior (top) to posterior (down) levels. Right column: $D_{1/5}$ receptor expression in the arcopallium/amygdala complex from anterior (top) to posterior (down) levels. Further explanations see Figure 7 [Color figure can be viewed at wileyonlinelibrary.com]

Balthazart, 1990; Herold et al., 2011; Kohler, Messer, & Bingman, 1995). AD was defined earlier by Nissl staining, tract-tracing, neurochemical and immunohistochemical studies (Atoji et al., 2006; Atoji & Wild, 2009; Herold et al. 2012; Karten & Hodos, 1967; Kröner & Güntürkün, 1999; Reiner et al., 2004; Yamamoto & Reiner, 2005). Based on our results, the receptor profile of AD showed a closer similarity to AA and AI, and is more different from AV, AM and AP. Other studies that used in situ hybridization further observed relatively high D_{1A} receptor mRNA labeling in AD in seven day old chicks (*Gallus gallus*), but low D_{1B} receptors (Sun & Reiner, 2000) and high D_{1C} mRNA levels in zebra finch (Jarvis et al., 2013). Despite the fact that the $D_{1/5}$ receptor ligand used here labels D_{1A} and D_{1B} (and possible $D_{1C/D}$) receptors together, adult expression levels of DA receptors may differ from hatchlings, which may result in lower densities in adults. This was also observed for mRNA expression profiles of different D_1 receptor types in the arcopallium of zebra finches, which tend to lower expression levels in adults compared to hatchlings (Kubikova et al., 2010). For the first time, we described a further sub-differentiation of AD, based on the observed distinct fiber architecture of ADl and ADm, particularly in the more anterior portions. Four different receptor subtypes confirmed such an intranuclear subdivision. Based on its known connectivity AD is considered to be premotor in its nature (Zeier & Karten, 1971; Shanahan et al., 2013). However, the dorsal arcopallium showed intense LAMP labeling which would go along with limbic functions (Yamamoto & Reiner, 2005). Intense LAMP labeling of AD is in line with connectivity studies that showed inputs to AD from limbic regions like the piriform cortex, hippocampal formation and TnA, and outputs to the limbic medial and somatic lateral striatum (Bingman et al., 1994; Veenman et al., 1995; Atoji & Wild, 2006). Recently reported visual stimulus selective neurons in AD, however questions both, the limbic and the premotor nature of AD (Scarf et al., 2016). However, at this time point, none of the analysis seems to be sufficient to explain the di(tri)chotomy of AD.

Arcopallium intermedium (AI) could be separated from the neighboring regions AD, AV, and AM by many differences in receptor expression, underlining the neurochemical diversity of these two arcopallial regions. Comparable to our findings, in chickens higher α_2 receptors were reported in AM compared to AI (Diez-Alarcia, Pilar-Cuellar, Paniagua, Meana, & Fernandez-Lopez, 2006). In the zebra finch brain, expression analysis of different mRNAs for kainate receptors showed higher amounts of RA, in the intermediate arcopallium if compared to the rest of the arcopallium, while AMPA receptor mRNAs showed lower amounts (Wada et al., 2004). Further, while NR2A receptor subunit is higher expressed in RA, other subunits were lower expressed, which in sum would possibly result in similar levels of NDMA receptors if measured together in all arcopallial structures. Here we found lower kainate levels of AI compared to other arcopallial structures, except AP, which is in sum in contrast to the above-mentioned study. In our study, further lower or similar amounts of AMPA receptors were detected, and lower, similar or higher densities of NMDA receptors in the different arcopallial subdivision were shown, which would be in sum possibly in line with the expression study (Wada et al., 2004). However, the caveat of ligand binding studies is that most ligands bind to multiple gene products of the same gene, so that they do not have the anatomical high resolution of mRNA binding studies that provide information of distinctively expressed single gene profiles, so in general some differences between mRNA levels and overall protein levels may exist. Further, to some extent, mRNA levels may differ in general from protein levels. Several previous studies have reported intra-nuclear subregions for AI (Atoji & Wild, 2009; Kröner & Güntürkün, 1999; Shanahan et al., 2013; Wynne & Güntürkün, 1995; Zeier & Karten, 1971). However, no consistent view could be established. In our receptor analysis, the significant differences were observed between a dorsal and a ventral component of AI in 6 out of 11 measured receptors. This was particularly visible for the muscarinergic receptors. Additionally, the cellular as well as fiber architecture of AId and AIv differed. AI is a major hub of the "structural connectome" of the telencephalon of the pigeon and as mentioned above, located in the associative module and premotor submodule (Shanahan et al., 2013). This means that AI

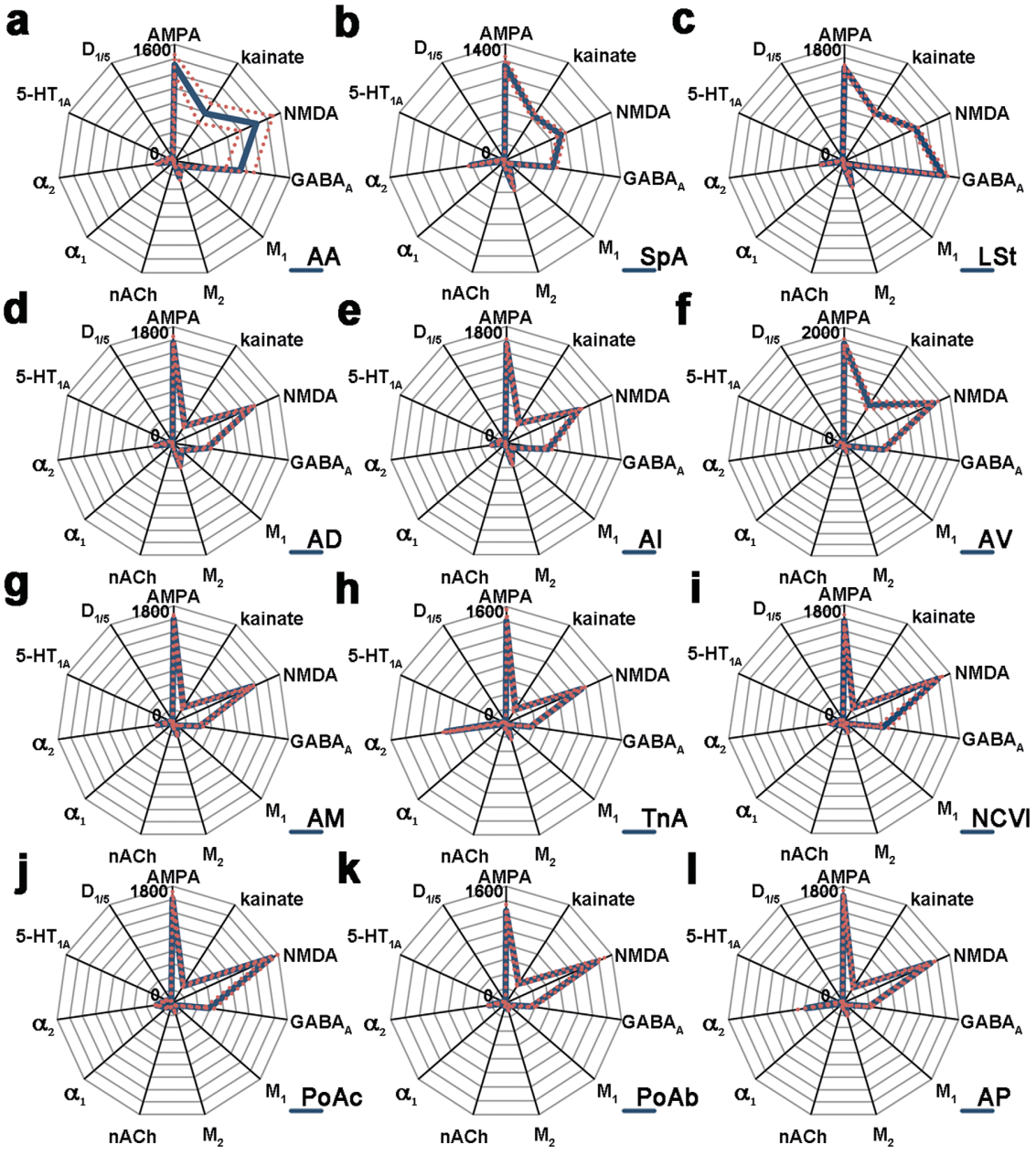

FIGURE 11 Receptor fingerprints of the subregions defined within pigeon arcopallium/amygdala complex, the lateral striatum and the nidopallium caudoventrale pars lateralis (a–l). The coordinate polar plots show the different mean receptor densities in fmol/mg protein for the arcopallial and amygdala subregions and adjacent regions. Blue lines connecting the mean densities of the 11 receptors in each subregion define the shape of the fingerprint. Light red dotted lines represent the standard errors of means of the different receptor densities in each region. Note that the scales in (a–l) are different. For abbreviations see list [Color figure can be viewed at wileyonlinelibrary.com]

innervates pallial, diencephalic and brain stem entities and at the same time receives input from associative, multimodal structures in the nidopallium and the dorsolateral region of the hippocampal formation, and from visual associative subregions of the hyperpallium and from many more (see Shanahan et al., 2013 for review).

Arcopallium ventrale (AV) showed the highest concentrations of glutamate receptors of the arcopallium/amygdala complex and high kainate receptor densities nicely resolved the borders of AV, which would be comparable to the reported high mRNA levels of kainate receptors of Ai in zebra finches (Wada et al., 2004) that was not separated into Ai and Av in the study of Wada and colleagues. However, differences between RA and the region ventral to RA in the zebra finch were mentioned in a recent study (Olson, Hodges, & Mello, 2015). In the pigeon, AV showed further substantial differences in various receptor densities, cell densities and fiber architectural details if compared to the surrounding AI, PoAb, and AM. Thus, it could be recognized as a separate

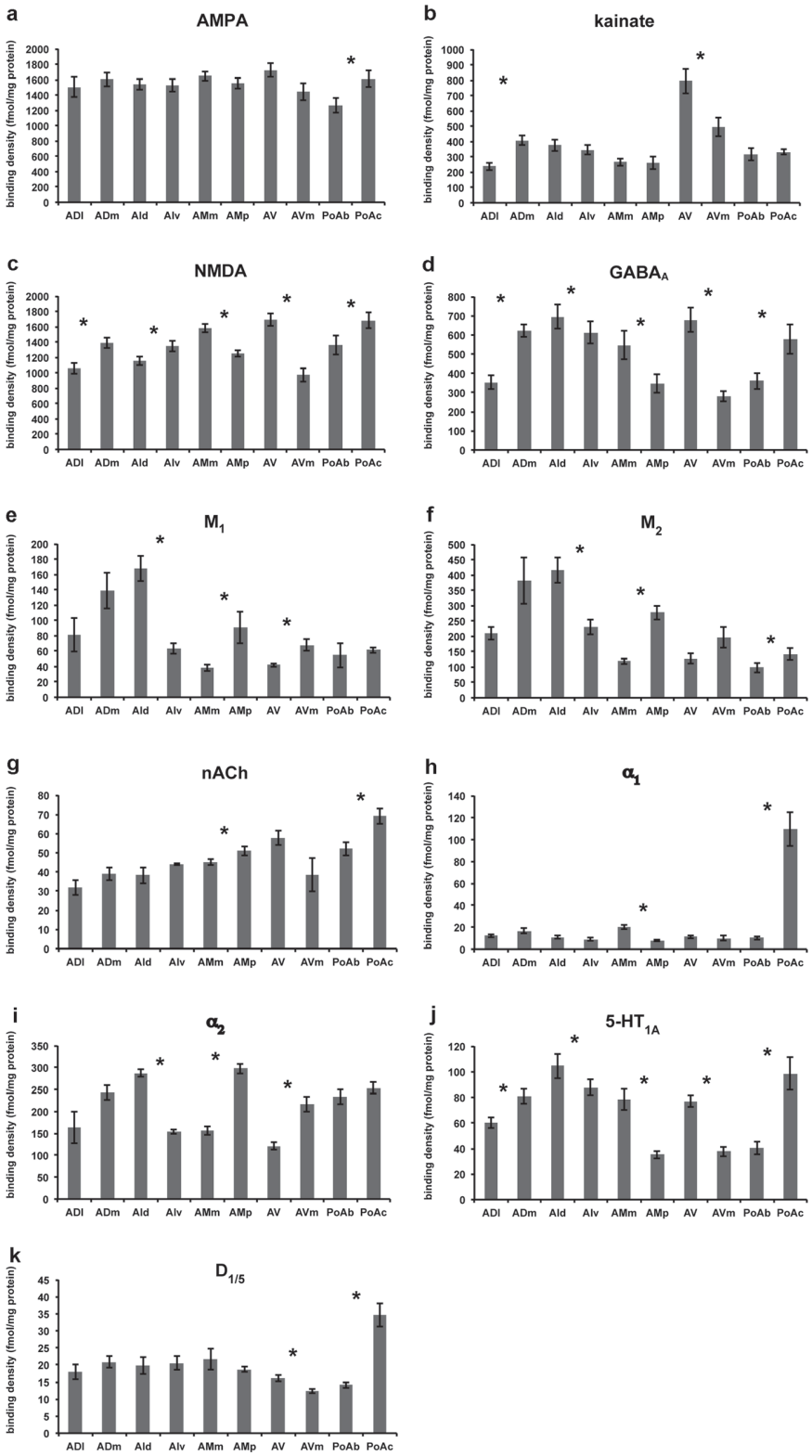

FIGURE 12 Histograms of the mean receptors densities (fmol/mg protein) of intra-nuclear substructures of the pigeon arcopallium/amygdala complex (a–k). PoA and AV showed the highest numbers of receptor density differences between the intra-nuclear substructures PoAc and PoAb or AV and AVm. NMDA, $GABA_A$, and $5\text{-}HT_{1A}$ receptors confirmed all intra-nuclear substructures. Error bars represent standard errors of the means. Asterisks represent significant differences between intra-nuclear substructures of an examined subregion ($p < .05$; *Wilcoxon-rank test*). For abbreviations see list

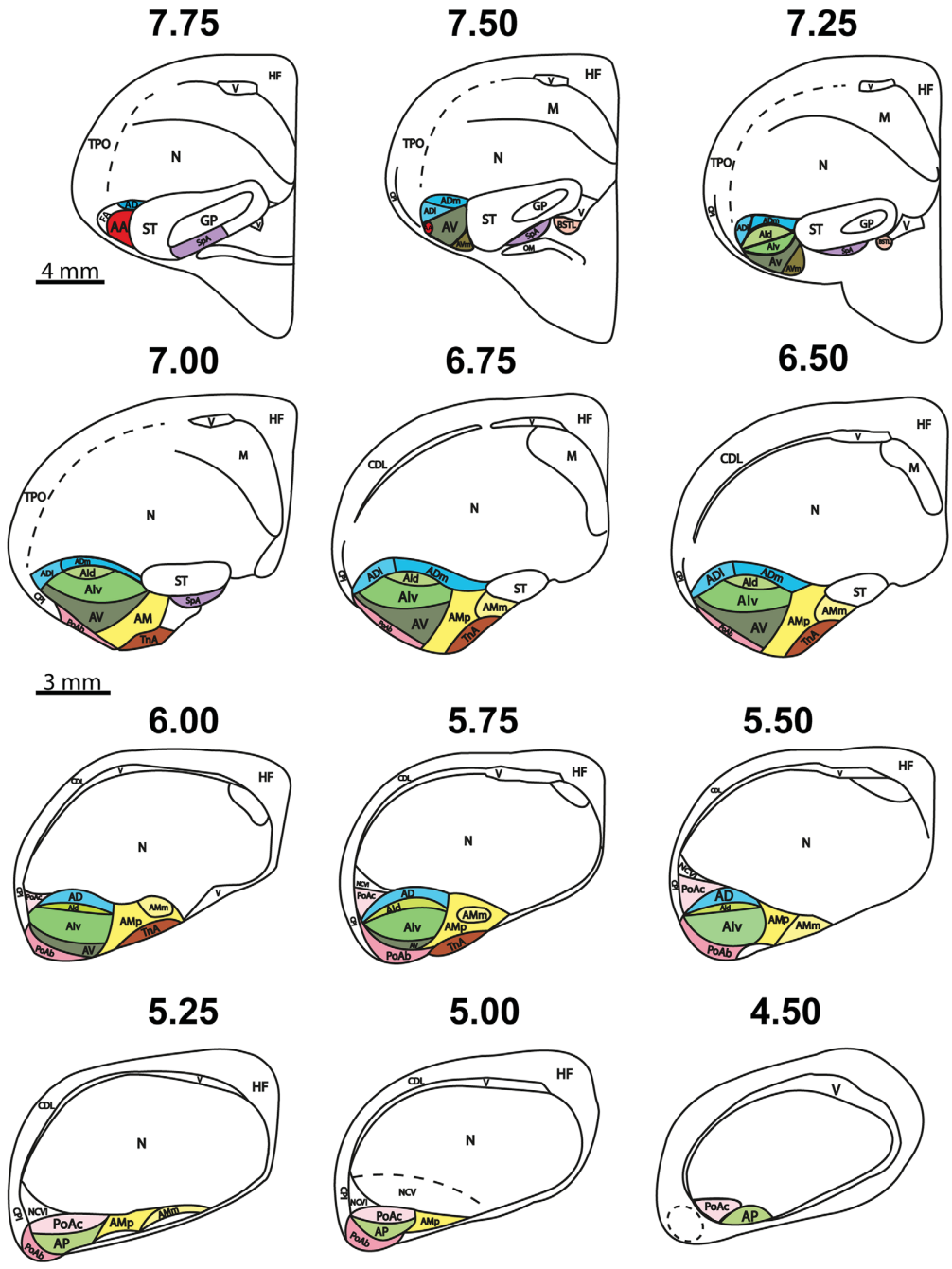

FIGURE 13 Schematic atlas of the arcopallium/amygdala complex in serial frontal sections. The atlas map is based on differences in the cyto-, myelo-, and receptor-architecture. Atlas levels correspond to the rostro-caudal atlas levels A 7.75 to A 4.50 (Karten & Hodos, 1967). For abbreviations see list [Color figure can be viewed at wileyonlinelibrary.com]

arcopallial region. Our results were supported by findings from tracing studies and further analysis of connectivity, which described AV as different from AI (Atoji & Wild, 2004; Kröner & Güntürkün, 1999; Shanahan et al., 2013; Wild, Karten, & Frost, 1993). In the more anterior portion of AV an intranuclear subregion was recognized that we named AVm. AVm showed different densities in 8 out of 11 receptors. Atoji and Wild (2009) showed that both the limbic central caudal nidopallium (NCC) and the dorsal intermediate mesopallium have tight connections with a structure named AIvm that is located in about the same location as our AVm. In a prior publication, Wild and colleagues (1993), however, had proposed AIvm to be part of an auditory premotor structure. According to Shanahan et al. (2013), AV could be an associative structure that is part of the avian prefrontal submodule, while AIvm is located in the auditory module. Like AA, AV projects via the anterior commissure to the contralateral arcopallium (Letzner et al., 2016).

Arcopallium mediale (AM) was first described in a study of Zeier and Karten (1971). Later on, tract-tracing experiments confirmed its existence and a detailed analysis of the cytoarchitecture with Nissl

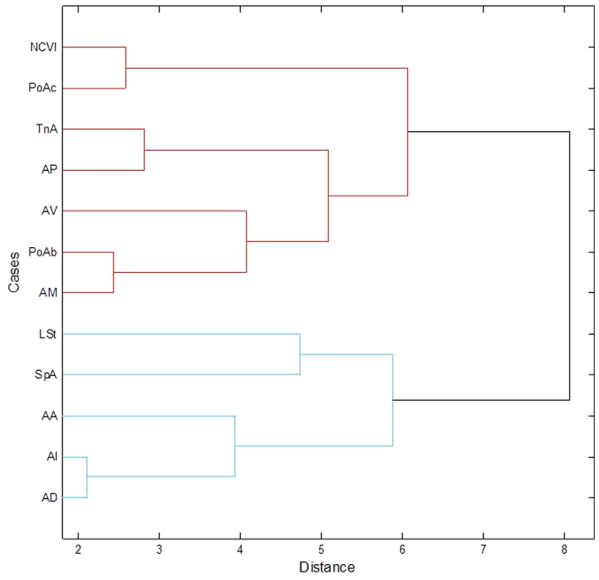

FIGURE 14 Relationships of the overall mean receptor densities between subregions of the amygdala, the arcopallium, the nidopallium caudolaterale pars lateralis and the posterior lateral striatum. X-axis: Euclidian distance. Y-axis: Subregions. The cladogram shows two different main clusters with further subgroups at different branches (cophenetic correlation coefficient $c = 0.60$) [Color figure can be viewed at wileyonlinelibrary.com]

staining offered a more precise definition of the AM in pigeons (Atoji et al., 2006). The AM is divided into a medially located cell-dense, dark stained division with large cells (AMm) and a less cell-dense, parvocellular division (AMp) located laterally (Atoji et al., 2006). In our study, the borders of AM are identical to the studies of Atoji and colleagues (2006, 2009) and fibers showed different densities and directions in both subnuclei. Tracing studies have shown that AM projects extensively to PoAc and to a lesser extent to BSTL (Atoji et al., 2006). In a follow-up study by Atoji and Wild (2009), it was shown that the central caudal nidopallium (NCC) has reciprocal connections with AMm and AMp. Both areas are associated with neuroendocrine and autonomic functions in various bird species and have connections to TnA and the postero-medial hypothalamus via HOM (Cheng, Chaiken, Zuo, & Miller, 1999; Cohen, 1975; Thompson, Goodson, Ruscio, & Adkins-Regan, 1998; Zeier & Karten, 1971). The ventrolateral part of AMp together with AIvm from Wild and colleagues (1993) were called Avpm in Zeier and Karten (1971) and based on their connectivity pattern are limbic-associated. Additionally, the overall receptor architecture of AM seemed to be more comparable to limbic regions as confirmed by the cluster analysis.

Arcopallium posterioris (AP) is the most caudal part of the arcopallium and is positioned between atlas levels A5.25 and A4.50. In line with other studies, we recognized this differentiation of PoAc, PoAb and the arcopallium intermedium in the more posterior sections based on our receptor data as well as cyto- and myelo-architecture. This area was described earlier in pigeons as the most posterior part of Al (Atoji et al., 2006) and with gene expression and cellular analysis in zebra finches (Jarvis et al., 2013). In zebra finches Ap is enriched in D_1 receptors (Jarvis et al., 2013), while here D_1 receptor expression of AP was only higher if compared to AV. As mentioned above, overall receptor densities of AP showed more similarities to TnA than to other arcopallial regions. Future studies and possibly a more detailed analysis of other gene expression profiles in the pigeon have to find out how this relationship may be interpreted and to which functional circuit AP is belonging.

Nucleus posterioris amygdalopallii (PoA) can be separated into a basal (PoAb) and a compact part (PoAc). All researchers agree that this nucleus is part of the avian amygdala (Reiner et al., 2004). A higher cell density defines PoAc, while PoAb shows a smaller number of cells with greater cell bodies (Atoji et al., 2006). This is particularly visible at the atlas level A5.00. The analysis of the receptor autoradiographs confirmed differences between PoAc and PoAb, thereby supporting a separation of these two nuclei. The highest divergences between PoAc and PoAb were detected for α_1, 5-HT_{1A}, and $D_{1/5}$ receptors. For example, PoAc showed two-times higher densities of $D_{1/5}$-receptors and 11-times higher densities of α_1 receptors. This is in line with the findings that PoAc is also characterized by high tyrosine hydroxylase (TH) immunoreactivity, while PoAb has more or less no TH positive cells (Kröner & Güntürkün, 1999). PoAb, but not PoAc participates in interhemispheric projections via the anterior commissure, a result that underlines the difference of these two subnuclei (Letzner et al., 2016). The region overlaying PoAc is named NCVl. It can be distinguished by the absence of TH immunoreactivity and darkly stained cell aggregates (Atoji et al., 2006; Kröner & Güntürkün, 1999; Wild, Arends, & Zeigler, 1985). PoAc and PoAb showed differences in receptor densities from the overlaying NCVl. NCVl together with the subnidopallium were discussed to be a part of the insular cortex (Atoji et al., 2006) or to form the endopiriform nucleus (Yamamoto & Reiner, 2005). Atoji and colleagues (2006) further analyzed and defined the borders of limbic BSTL at the ventral tip of the lateral ventricle more precisely and showed extensive connections to PoAc but not to PoAb in birds (Atoji et al., 2006). PoAb on the other hand is connected to CDL and TPO (Atoji & Wild, 2005). Both, PoAc and BSTL receive fibers from the dorsomedial subregion of the hippocampal formation (HF) but send only a small number of efferent fibers to the dorsomedial and the dorsolateral region of the HF (Atoji & Wild, 2004). In addition, AM projects extensively to PoAc and to a lesser extent to BSTL (Atoji et al., 2006). As mentioned above, PoA and NCVl belong to the viscero-limbic module in the pigeon's connectome (Shanahan et al., 2013).

Nucleus taenia amygdala (TnA) is considered to be amygdaloid and subpallial (Reiner et al., 2004). However, the subpallial nature of TnA has been questioned by some researchers of the avian brain consortium (Reiner et al., 2004), which is further underlined by our cluster analysis. Future studies have to be performed to bring more clarity at this point. No clear subdifferentiation of TnA was recognized although this was mentioned in other studies in chickens and budgerigars (*Melopsittacus undulates*; Roberts, Hall, & Brauth, 2002; Yamamoto et al., 2005). TnA is specifically visible by labeling of M_2 and α_2 receptors. A high α_2 receptor binding of TnA was also reported in Fernandez-Lopez et al. (1997) and visible in Herold et al. (2011). Generally, TnA showed a high number of differences in receptor densities if

compared to other subregions of the arcopallium/amygdala complex. This distinction had already been identified using immunostaining in various bird species (de Lanerolle, Elde, Sparber, & Frick, 1981; Deviche & Güntürkün, 1992; Martinez-Vargas, Stumpf, & Sar, 1976; Roberts et al., 2002). Based on its connections to the hippocampal formation, the olfactory bulb (Casini, Bingman, & Bagnoli, 1986; Reiner & Karten, 1985; Székély & Krebs, 1996) and its role in social behavior (Cheng et al., 1999), TnA had always been discussed as part of the avian amygdala. This is strengthened by the additional connections of TnA to the hypothalamus, the septal region, the medial striatum, the hyperpallium, and the nidopallium caudolaterale (Cheng et al., 1999; Leutgeb, Husband, Riters, Shimizu, & Bingman, 1996; Zeier & Karten, 1971). TnA was included in the septo-hippocampal network of the pigeon's telencephalic connectome (Shanahan et al., 2013).

Area subpallialis amygdala (SpA) was separated from neighboring structures AM and posterior LSt by distinct receptor densities. SpA is considered to belong to the extended amygdala and is basically defined by its different neurochemistry and connectivity as a region ventral to the globus pallidus at the level of OM (Reiner et al., 2004; Yamamoto et al., 2005). The overall receptor analysis indicated a similarity between SpA and posterior LSt that has to be further investigated in future studies, but as mentioned above was also recognized in the past (Abellán & Medina, 2009).

4.3 | General comparisons of the avian amygdala complex to the mammalian amygdala

The mammalian amygdala is molecularly and structurally heterogeneous, comprising lateral and ventral pallial parts and striatal and pallidal subpallial portions, which can be extended rostrally (Puelles et al., 2000). The pallial subregions comprise the lateral (LA), basolateral (BLA), basomedial (BM) and cortical nuclei (CoA) of the amygdala, and the subpallial subregions comprise the central (CeA) and medial nuclei of the amygdala (MeA) (Sah, Faber, Lopez De Armentia, & Power, 2003; Swanson & Petrovich, 1998). As described above, in birds, PoAc, PoAb, TnA, SpA, and BSTL are considered to form the avian amygdala.

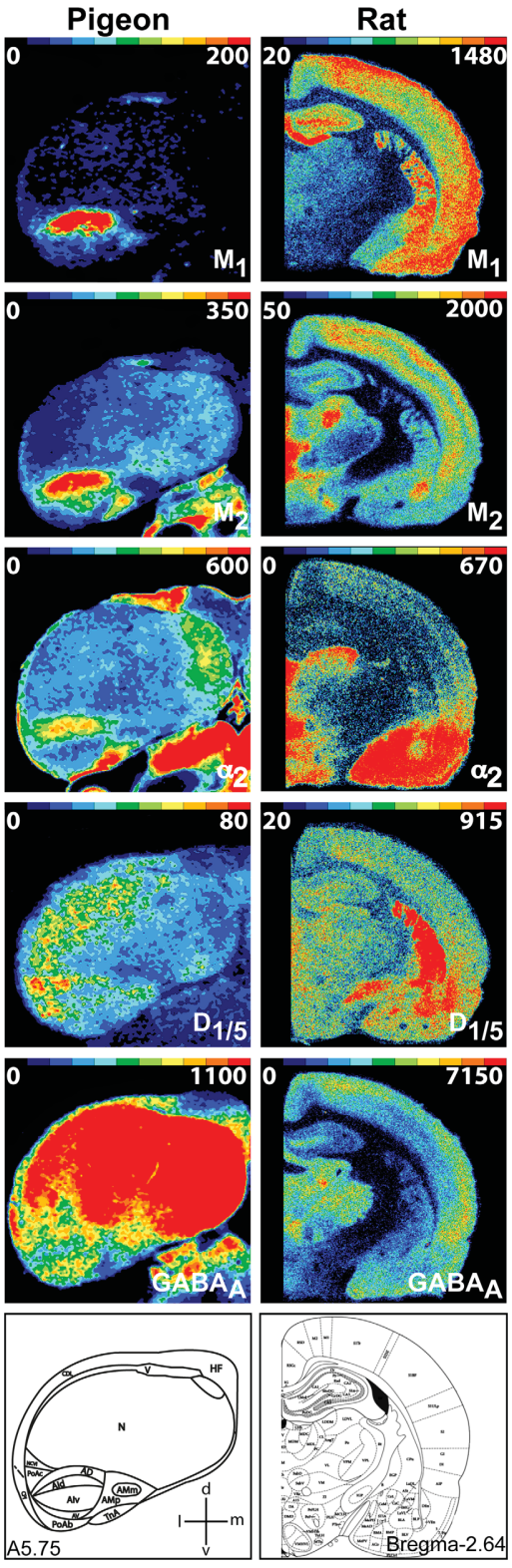

FIGURE 15.

FIGURE 15 Comparisons of different receptors between the pigeon arcopallium/amygdala complex around atlas level A 5.75 (left column) and the rat amygdala complex/cortical areas around atlas level bregma -2.16 (Paxinos and Watson, 2005; right column). Pigeon: for abbreviations see list. Rat: AIP, posterior agranular insular cortex; BLA, basolateral amygdaloid nucleus, anterior part; BLP, basolateral amygdaloid nucleus, posterior part; BLV, basolateral amygdaloid nucleus, ventral part; BMA, basomedial amygdaloid nucleus, anterior part; BMP, basomedial amygdaloid nucleus, posterior part; CPu, Caudate/Putamen; CeC, central amygdaloid nucleus, capsular part; CeM, central amygdaloid nucleus, medial division; CeL, central amygdaloid nucleus, lateral division; DI, dysgranular insular cortex; GI, granular insular cortex; LAVL, lateral amygdaloid nucleus, ventrolateral part; LAVM, lateral amygdaloid nucleus, ventromedial part; M1, primary motor cortex, M2, secondary motor cortex; MeAD, medial amygdaloid nucleus anterodorsal part; MePD, medial amygdaloid nucleus posterodorsal part; MePV, medial amygdaloid nucleus posteroventral part; S1, primary somatosensory cortex; S2, secondary somatosensory cortex; STIA, bed nucleus of the stria terminalis, intra-amygdaloid division [Color figure can be viewed at wileyonlinelibrary.com]

PoA: Genoarchitecture and fate mapping studies in diverse species revealed that PoA expressed various pallial markers and is therefore considered to be part of the pallial amygdala in birds (Puelles et al., 2000; Reiner et al., 2004; Puelles et al., 2007; Abellán & Medina, 2008; Abellán et al., 2009, 2010; Butler et al., 2011; Medina et al., 2011; Kuenzel et al., 2011). The projections of PoAc showed a comparable connectivity pattern of commissural fibers to the mammalian amygdala, which projects contralaterally to cortical, medial, and lateral nuclei of the amygdala, olfactory tubercle and pre-piriform cortex (De Olmos & Ingram, 1972; Letzner et al., 2016; Sah et al., 2003). However, PoAc shares connectional characteristics of both, the autonomic and the fronto-temporal system of mammals and thus with both the central and the basolateral/lateral nuclei of the mammalian amygdala (Veenman et al., 1995; Swanson & Petrovich, 1998; Puelles et al., 2000; Atoji et al., 2006). Here, PoAc showed the high amounts of α_1, 5-HT_{1A} and $D_{1/5}$ receptors compared to the other amygdala subregions. In rodents, α_1, α_2, and $D_{1/5}$ receptors are densely expressed in the amygdala, and in humans in LA and BLA (Cremer et al., 2010; Cremer et al., 2009; Lillethorup et al., 2015; Sanders et al., 2006). Further, α_1 receptors showed higher densities in LA compared to BLA in humans (Graebenitz et al., 2011). The most striking differences within the mouse amygdala complex were reported for M_1 receptors densities showing higher amounts in the lateral region compared to the medial and central nucleus (Yilmazer-Hanke, Roskoden, Zilles, & Schwegler, 2003). In pigeons, M_1 receptors were higher expressed in PoAb, PoAc, SpA compared to TnA. Further, PoAc and PoAb express higher numbers of NMDA receptors that are also densely expressed in the lateral and medial regions compared to the central region in mice (Yilmazer-Hanke et al., 2003). Further, TH-positive fibers and the absence of acetylcholine-esterase immune-reactivity define LA in rats (Paxinos, Kus, Ashwell, & Watson, 1999). TH-positive fibers were also reported for PoAc (Kröner & Güntürkün, 1999). Taken together, no unitary pattern could be observed, but at least PoAc showed some similarities in the receptor expression profile of the mammalian lateral regions of the amygdala.

TnA: Based on their similarities in olfactory input, hippocampal, and hypothalamic output, enrichment in androgen and estrogen receptors and involvement in sexual behavior, TnA was considered to be comparable to the MeA of mammals (Reiner et al., 2004; Yamamoto et al., 2005). It has been speculated that lateral TnA in chickens (pallial) is comparable to the anterior division of the corticoid nucleus of the amygdala (CoAa), whereas medial TnA (subpallial) is comparable to MeA (Roberts et al., 2002; Yamamoto et al., 2005; Yamamoto & Reiner, 2005). However, we did not observe this subdifferentiation of TnA in pigeons. TnA showed very high amounts of α_2-receptors that are also densely expressed in the pallial as well as subpallial nuclei of the amygdala (MeA, LA, and BLA) of mice, rats and humans if compared to cortical probes (Graebenitz et al., 2011; Lillethorup et al., 2015; Sanders et al., 2006; Scheperjans, Grefkes, Palomero-Gallagher, Schleicher, & Zilles, 2005; Scheperjans, Palomero-Gallagher, Grefkes, Schleicher, & Zilles, 2005).

Extended amygdala: In mammals, some researchers divide the subpallial amygdaloid nuclei (including the extended amygdala) into the central and medial extended amygdala complex (Kuenzel et al., 2011). The central extended amygdala complex consists of the CeA and BSTL and the medial extended amygdala complex consists of MeA and BSTM. Both, CeA and MeA are the major output nuclei of the amygdala and confluent with the BST nuclei (Swanson, 2000). Comparative studies in chick and mouse embryo with subpallial and pallial genetic markers, as well as connectivity data suggests that the BST nuclei BSTM and BSTL in birds belong to the extended amygdala nuclei (Abellán & Medina, 2008, 2009; Abellán, Menuet, Dehay, Medina, & Retaux, 2010; Bruce, Erichsen, & Reiner, 2016; Butler et al., 2011; Medina et al., 2011; Puelles et al., 2000; Puelles et al., 2007). In birds, it has been further postulated that SpA and BSTL form the central extended amygdala complex, while TnA and BSTM form another functional unit and may correspond to the medial extended amygdala complex (Puelles et al., 2000; Reiner et al., 2004; Abellán & Medina, 2009; Kuenzel et al., 2011). To test these hypotheses, researchers investigated secretagogin-binding that selectively labels the subpallial and extended amygdala in mammals (Gati, Lendvai, Hokfelt, Harkany, & Alpar, 2014; Mulder et al., 2010). In chickens, TnA, SpA and the BNST nuclei were densely populated with secretagogin-positive neurons. However, the pallial amygdala PoA as well as AV and AD also contained labeled neurons, which questions the use of this marker as subpallial-specific in birds. On the other hand, analysis of the connections of BSTL strongly supports the idea that BSTL belong to the extended amygdala in birds (Atoji et al., 2006; Veenman et al., 1995). SpA has been suggested to be comparable to the sublenticular part of the mammalian extended amygdala (Yamamoto & Reiner, 2005; Kuenzel et al., 2011). Both structures show similarities in location (ventral to GP), connections with the parabrachial area, the nucleus of the solitary tract, the dorsal motor nucleus of the vagus, the arcopallium, efferents to the BSTL (Atoji et al., 2006; Reiner et al., 2004; Wild, Arends, & Zeigler, 1990) as well as neurotransmitter traits such as enrichment in CGRP immunopositive fibers, enkephalinergic, and neurotensinergic neurons (Atoji, Shibata, Yamamoto, & Suzuki, 1996; Lanuza, Davies, Landete, Novejarque, & Martinez, 2000; Yamamoto et al., 2005). In our study, SpA showed the lowest densities of NMDA receptors. Lower NMDA receptors were also observed in the mice central amygdala if compared to the lateral and medial nuclei (Yilmazer-Hanke et al. 2003), which would fit with recent theories that SpA is part of the central extended amygdala complex (Vicario et al., 2014). On the other hand, the central nucleus in mice is also conspicuously low in $GABA_A$ receptors (Yilmazer-Hanke et al., 2003), while the lowest amounts of $GABA_A$ receptors in the pigeon amygdala subregions were detected in PoAb and TnA.

4.4 | General comparisons of the avian arcopallium complex to mammalian (pre)-motor cortical areas

The arcopallial subregions of birds are considered to be functionally comparable to (pre)motor cortical areas by some researchers (Reiner et al., 2004; Jarvis et al., 2005; Chen et al., 2013; Whitney et al., 2014; Pfenning et al., 2014; Karten, 2015; Güntürkün & Bugnyar, 2016), while others still assume that all arcopallial regions belong to the

amygdala (Puelles et al., 2000, 2007; Medina et al., 2011; Bupesh et al., 2011). In pigeons the arcopallial subregions receive input from the NCL, the functional analog of the mammalian prefrontal cortex (Güntürkün & Bugnyar, 2016; Herold, Diekamp, & Güntürkün, 2008; Herold, Joshi, et al., 2012; Leutgeb et al., 1996), as well as auditory (Wild et al., 1993), trigeminal (Wild et al., 1985), somatosensory (Kröner & Güntürkün, 1999) and visual pallial areas (Husband & Shimizu, 1999). Based on layer-specific gene expression analysis and cell type homologies Dugas-Ford and colleagues (2012) postulated that regions of the arcopallium are comparable to layer V neurons of the neocortex. One example, ER81 showed homogeneous labeling throughout the whole zebra finch arcopallium, including RA. Another marker, PCP4, showed intense labeling of subregions in chicken and zebra finch that correspond to AD and AId in our study. However, PCP4 and ER81 are also expressed in the basolateral amygdala of mammals, a pallial derivative, and not exclusively in layer V neurons (Jarvis et al., 2013; Nomura, Hattori, & Osumi, 2009). One explanation for this could be that the pallial amygdala is an extension of cortex layers V and VI, and therefore shares the expression of the same marker genes (Swanson, 2000). A more extensive gene expression pattern analysis by Pfenning and colleagues (2014) revealed for nearly thousand genes a close functional similarity of RA and the surrounding intermediate arcopallium in songbirds with the primate primary motor cortex. A cell type specific analysis from different layers in motor and sensory cortices, showed that layer V cells of macaque (*Macaca mulatta*) primary motor cortex had the strongest match with RA and surrounding arcopallium compared to all other layers and sensory cortex (Pfenning et al., 2014). Further, for 55 genes, a "convergence" of RA to the human laryngeal motor and adjacent primary somatosensory cortex was found, since these genes had similarly different expression profiles from the surrounding arcopallium. Here we think that to analyze different brain regions and cell types based on expression profiles of gene orthologs and other characteristics more precisely, a detailed brain map with higher resolution is needed for better comparisons of similarities between cortical layers/areas in mammals, cortical areas in reptiles and nuclei in birds.

Our new schematic map of the arcopallium/amygdala complex allows a more precise comparison of the receptor architecture to mammalian (pre)-motor, other cortical as well as amygdala subregions. Although absolute densities of binding sites vary between different species, relative differences between regional densities are mostly comparable (Herold et al., 2015; Zilles & Palomero-Gallagher, 2016). For example, in the (pre)-motor regions of different mammalian species, NMDA and $GABA_A$ receptors showed the highest densities, and M_1/α_1 receptors were higher expressed compared to M_2/α_2 receptors (Gebhard et al., 1995; Geyer et al., 1998; Herold et al., 2011; Palomero-Gallagher, Schleicher, Zilles, & Loscher, 2010; Palomero-Gallagher & Zilles, 2004; Zilles et al., 1995). In humans, M_2 and $GABA_A$ receptors are more densely expressed in primary visual (BA17), somatosensory (BA3) and primary auditory cortex if compared to the primary motor cortex (BA4; Zilles, Palomero-Gallagher, & Schleicher, 2004; Scheperjans, Grefkes et al., 2005; Scheperjans, Palomero-Gallagher et al., 2005). Particularly the dense M_2-receptor expression seems to be a conservative aspect of cortical organization (Zilles et al. 2004). Referring to this, it is of further interest that the pallial nuclei, LA and BLA in humans and BLA in rats have high amounts of M_2-receptors (Graebenitz et al., 2011; Mash & Potter, 1986). Additionally, in humans and rats, $D_{1/5}$ receptors are higher expressed and $GABA_A$ receptors are lower expressed in the amygdala if compared to the above-mentioned cortical areas (Scheperjans, Grefkes et al., 2005; Scheperjans, Palomero-Gallagher et al., 2005; Cremer et al., 2009, 2010; Graebenitz et al., 2011). Figure 15 provides examples of the above-mentioned receptors in the rat amygdala and cortex and the pigeon arcopallium/amygdala complex that showed differences between divers subregions in mammalian species. The receptor data of relevant brain regions in rats have been published earlier (Herold et al., 2011; Cremer et al., 2009, 2010; Palomero-Gallagher & Zilles, 2004). Comparisons of relative densities of M_1, M_2, $D_{1/5}$, α_2, and $GABA_A$ receptors between pigeons and rats support the idea that AA, AD, AI, AV, and AP share receptor expression characteristics with FR1 (M1), FR2 (M2), and the insular cortex (AIP, GI, DI). Here, high levels of $D_{1/5}$ and α_2 receptor densities of AP support the idea that AP could be comparable to AIP while dense levels of $GABA_A$, $D_{1/5}$ and M_1-receptors in AA support a comparison with FR1/FR2 and GI/DI/AIP. High $GABA_A$ receptor levels in AV point to a comparison with FR1/FR2 and AIP. In case of AI high levels of $GABA_A$, M_1, and M_2 receptors allow further comparison to FR1/FR2, S1/S2, and GI/DI/AIP. However, as visible in Figure 15 beside similar binding patterns also differences are detectable, which may be a result of parallel evolution, analogies, and species-specific adaptations.

5 | CONCLUSIONS

The pigeon arcopallium/amygdala complex is a highly heterogeneous area of the avian brain, characterized by a large number of subregions and a diversity of connectional patterns. This complexity is the reason why scientists still can't find a consensus on the number and location of subdivisions or the premotor or limbic nature of all or parts of this area. We believe that we need proper anatomical maps before embarking onto such scientific voyages. This was the motivation for our study and the reason we now present a new detailed map of this region, based on quantitative methods. In addition, our study may promote the discussions on functional similarities of premotor or limbic components, by providing details on the neurotransmitter receptor densities in pigeons in comparison with similar data in rats.

ORCID

Christina Herold http://orcid.org/0000-0002-6530-115X

REFERENCES

Abellán, A., & Medina, L. (2008). Expression of cLhx6 and cLhx7/8 suggests a pallido-peduncolo-preoptic origin for the lateral and medial parts of the avian bed nucleus of the stria terminalis. *Brain Research Bulletin*, *75* (2–4), 299–304. https://doi.org/10.1016/j.brainresbull.2007.10.034

Abellán, A., & Medina, L. (2009). Subdivisions and derivatives of the chicken subpallium based on expression of LIM and other regulatory genes and markers of neuron subpopulations during development.

The Journal of Comparative Neurology, *515*(4), 465–501. https://doi.org/10.1002/cne.22083

Abellán, A., Legaz, I., Vernier, B., Rétaux, S., & Medina, L. (2009). Olfactory and amygdalar structures of the chicken ventral pallium based on the combinatorial expression patterns of LIM and other developmental regulatory genes. *The Journal of Comparative Neurology*, *516*(3), 166–186. https://doi.org/10.1002/cne.22102

Abellán, A., Menuet, A., Dehay, C., Medina, L., & Retaux, S. (2010). Differential expression of LIM-homeodomain factors in Cajal-Retzius cells of primates, rodents, and birds. *Cerebral Cortex*, *20*(8), 1788–1798. https://doi.org/10.1093/cercor/bhp242

Ariens-Kappers, C. U., Huber, G. C., & Crosby, E. C. (1936). *The comparative anatomy of the nervous system of vertebrates, inlcuding man*. New York: MacMillan.

Atoji, Y., Saito, S., & Wild, J. M. (2006). Fiber connections of the compact division of the posterior pallial amygdala and lateral part of the bed nucleus of the stria terminalis in the pigeon (*Columba livia*). *The Journal of Comparative Neurology*, *499*(2), 161–182. https://doi.org/10.1002/cne.21042

Atoji, Y., Shibata, N., Yamamoto, Y., & Suzuki, Y. (1996). Distribution of neurotensin-containing neurons in the central nervous system of the pigeon and the chicken. *The Journal of Comparative Neurology*, *375*(2), 187–211. https://doi.org/10.1002/(SICI)1096-9861(19961111)375:2<187::AID-CNE2>3.0.CO;2-Z

Atoji, Y., & Wild, J. M. (2004). Fiber connections of the hippocampal formation and septum and subdivisions of the hippocampal formation in the pigeon as revealed by tract tracing and kainic acid lesions. *The Journal of Comparative Neurology*, *475*(3), 426–461. https://doi.org/10.1002/cne.20186

Atoji, Y., & Wild, J. M. (2005). Afferent and efferent connections of the dorsolateral corticoid area and a comparison with connections of the temporo-parieto-occipital area in the pigeon (*Columba livia*). *The Journal of Comparative Neurology*, *485*(2), 165–182. https://doi.org/10.1002/cne.20490

Atoji, Y., & Wild, J. M. (2006). Anatomy of the avian hippocampal formation. *Reviews in the Neurosciences*, *17*(1–2), 3–15.

Atoji, Y., & Wild, J. M. (2009). Afferent and efferent projections of the central caudal nidopallium in the pigeon (*Columba livia*). *The Journal of Comparative Neurology*, *517*(3), 350–370. https://doi.org/10.1002/cne.22146

Atoji, Y., & Wild, J. M. (2012). Afferent and efferent projections of the mesopallium in the pigeon (*Columba livia*). *The Journal of Comparative Neurology*, *520*(4), 717–741. https://doi.org/10.1002/cne.22763

Ball, G. F., Nock, B., Wingfield, J. C., McEwen, B. S., & Balthazart, J. (1990). Muscarinic cholinergic receptors in the songbird and quail brain: A quantitative autoradiographic study. *The Journal of Comparative Neurology*, *298*(4), 431–442. https://doi.org/10.1002/cne.902980405

Belgard, T. G., Montiel, J. F., Wang, W. Z., Garcia-Moreno, F., Margulies, E. H., Ponting, C. P., & Molnar, Z. (2013). Adult pallium transcriptomes surprise in not reflecting predicted homologies across diverse chicken and mouse pallial sectors. *Proceedings of the National Academy of Sciences of the United States of America*, *110*(32), 13150–13155. https://doi.org/10.1073/pnas.1307444110

Bingman, V. P., Casini, G., Nocjar, C., & Jones, T. J. (1994). Connections of the piriform cortex in homing pigeons (*Columba livia*) studied with fast blue and WGA-HRP. *Brain, Behavior and Evolution*, *43*(4–5), 206–218.

Bruce, L. L., Erichsen, J. T., & Reiner, A. (2016). Neurochemical compartmentalization within the pigeon basal ganglia. *Journal of Chemical Neuroanatomy*, *78*, 65–86. https://doi.org/10.1016/j.jchemneu.2016.08.005

Bupesh, M., Legaz, I., Abellán, A., Medina, L. (2011). Multiple telencephalic and extratelencephalic embryonic domains contribute neurons to the medial extended amygdala. *The Journal of Comparative Neurology*, *519*(8), 1505–1525. https://doi.org/10.1002/cne.22581

Butler, A. B., Reiner, A., & Karten, H. J. (2011). Evolution of the amniote pallium and the origins of mammalian neocortex. *Annals of the New York Academy of Sciences*, *1225*, 14–27. https://doi.org/10.1111/j.1749-6632.2011.06006.x

Campanella, L. C., da Silva, A. A., Gellert, D. S., Parreira, C., Ramos, M. C., Paschoalini, M. A., & Marino-Neto, J. (2009). Tonic serotonergic control of ingestive behaviours in the pigeon (*Columba livia*): The role of the arcopallium. *Behavioural Brain Research*, *205*(2), 396–405. https://doi.org/10.1016/j.bbr.2009.07.017

Casini, G., Bingman, V. P., & Bagnoli, P. (1986). Connections of the pigeon dorsomedial forebrain studied with WGA-HRP and 3H-proline. *The Journal of Comparative Neurology*, *245*(4), 454–470. https://doi.org/10.1002/cne.902450403

Chen, C. C., Winkler, C. M., Pfenning, A. R., & Jarvis, E. D. (2013). Molecular profiling of the developing avian telencephalon: Regional timing and brain subdivision continuities. *Journal of Comparative Neurology*, *521*(16), 3666–3701. https://doi.org/10.1002/cne.23406

Cheng, M., Chaiken, M., Zuo, M., & Miller, H. (1999). Nucleus taenia of the amygdala of birds: Anatomical and functional studies in ring doves (*Streptopelia risoria*) and European starlings (*Sturnus vulgaris*). *Brain, Behavior and Evolution*, *53*(5–6), 243–270. https://doi.org/6597

Cohen, D. H. (1975). Involvement of the avian amygdalar homologue (archistriatum posterior and mediale) in defensively conditioned heart rate change. *The Journal of Comparative Neurology*, *160*(1), 13–35. https://doi.org/10.1002/cne.901600103

Cremer, C. M., Bidmon, H. J., Gorg, B., Palomero-Gallagher, N., Escobar, J. L., Speckmann, E. J., & Zilles, K. (2010). Inhibition of glutamate/glutamine cycle in vivo results in decreased benzodiazepine binding and differentially regulated GABAergic subunit expression in the rat brain. *Epilepsia*, *51*(8), 1446–1455. https://doi.org/EPI2562 [pii]10.1111/j.1528-1167.2010.02562.x

Cremer, C. M., Palomero-Gallagher, N., Bidmon, H. J., Schleicher, A., Speckmann, E. J., & Zilles, K. (2009). Pentylenetetrazole-induced seizures affect binding site densities for GABA, glutamate and adenosine receptors in the rat brain. *Neuroscience*, *163*(1), 490–499. https://doi.org/S0306-4522(09)00454-0[pii]10.1016/j.neuroscience.2009.03.068

Cross, D. J., Marzluff, J. M., Palmquist, I., Minoshima, S., Shimizu, T., & Miyaoka, R. (2013). Distinct neural circuits underlie assessment of a diversity of natural dangers by American crows. *Proceedings of the Royal Society*, *280*(1765), 20131046. https://doi.org/10.1098/rspb.2013.1046

da Silva, A. A., Campanella, L. C., Ramos, M. C., Parreira, C., Faria, M. S., Marino-Neto, J., & Paschoalini, M. A. (2009). Arcopallium, NMDA antagonists and ingestive behaviors in pigeons. *Physiology & Behavior*, *98*(5), 594–601. https://doi.org/10.1016/j.physbeh.2009.09.009

Dafters, R. (1975). Active avoidance behavior following archistriatal lesions in pigeons. *Journal of Comparative and Physiological Psychology*, *89*(10), 1169–1179.

de Lanerolle, N. C., Elde, R. P., Sparber, S. B., & Frick, M. (1981). Distribution of methionine-enkephalin immunoreactivity in the chick brain: An immunohistochemical study. *The Journal of Comparative Neurology*, *199*(4), 513–533. https://doi.org/10.1002/cne.901990406

De Olmos, J. S., & Ingram, W. R. (1972). The projection field of the stria terminalis in the rat brain. An experimental study. *The Journal of Comparative Neurology*, *146*(3), 303–334. https://doi.org/10.1002/cne.901460303

Deviche, P., & Güntürkün, O. (1992). Peptides for calling? An immunohistochemical study of the avian n. intercollicularis. *Brain Research*, *569*(1), 93–99.

Diez-Alarcia, R., Pilar-Cuellar, F., Paniagua, M. A., Meana, J. J., & Fernandez-López, A. (2006). Pharmacological characterization and

autoradiographic distribution of alpha2-adrenoceptor antagonist [3H] RX 821002 binding sites in the chicken brain. *Neuroscience*, *141*(1), 357–369. https://doi.org/10.1016/j.neuroscience.2006.03.025

Dugas-Ford, J., Rowell, J. J., & Ragsdale, C. W. (2012). Cell-type homologies and the origins of the neocortex. *Proceedings of the National Academy of Sciences of the United States of America*, *109*(42), 16974–16979. https://doi.org/10.1073/pnas.1204773109

Edinger, L. (1896). *Vorlesungen über den Bau der nervœsen Centralorgane des Menschen und der Tiere für Ärzte und Studierende* (5., stark verm. Aufl. ed.). Leipzig: Vogel.

Edinger, L. (1903). *5 Untersuchungen über das Vorderhirn der Vögel*.

Fernandez-Lopez, A., Revilla, V., Candelas, M. A., Gonzalez-Gil, J., Diaz, A., & Pazos, A. (1997). A comparative study of alpha2- and beta-adrenoceptor distribution in pigeon and chick brain. *The European Journal of Neuroscience*, *9*(5), 871–883.

Gallyas, F. (1971). A principle for silver staining of tissue elements by physical development. *Acta Morphologica Academiae Scientiarum Hungaricae*, *19*(1), 57–71.

Gati, G., Lendvai, D., Hokfelt, T., Harkany, T., & Alpar, A. (2014). Revival of calcium-binding proteins for neuromorphology: Secretagogin typifies distinct cell populations in the avian brain. *Brain, Behavior and Evolution*, *83*(2), 82–92. https://doi.org/10.1159/000357834

Gebhard, R., Zilles, K., Schleicher, A., Everitt, B. J., Robbins, T. W., & Divac, I. (1995). Parcellation of the frontal cortex of the New World monkey Callithrix jacchus by eight neurotransmitter-binding sites. *Anatomy and Embryology*, *191*(6), 509–517.

Geyer, S., Matelli, M., Luppino, G., Schleicher, A., Jansen, Y., Palomero-Gallagher, N., & Zilles, K. (1998). Receptor autoradiographic mapping of the mesial motor and premotor cortex of the macaque monkey. *The Journal of Comparative Neurology*, *397*(2), 231–250. https://doi.org/10.1002/(SICI)1096-9861(19980727)397:2<231::AID-CNE6>3.0.CO;2-1 [pii]

Graebenitz, S., Kedo, O., Speckmann, E. J., Gorji, A., Panneck, H., Hans, V., … Pape, H. C. (2011). Interictal-like network activity and receptor expression in the epileptic human lateral amygdala. *Brain*, *134*(Pt 10), 2929–2947. https://doi.org/10.1093/brain/awr202

Güntürkün, O., & Bugnyar, T. (2016). Cognition without Cortex. *Trends in Cognitive Sciences*, *20*(4), 291–303. https://doi.org/10.1016/j.tics.2016.02.001

Hanics, J., Teleki, G., Alpar, A., Szekely, A. D., & Csillag, A. (2016). Multiple amygdaloid divisions of arcopallium send convergent projections to the nucleus accumbens and neighboring subpallial amygdala regions in the domestic chicken: A selective pathway tracing and reconstruction study. *Brain Structure & Function*, *222*, 301–315. https://doi.org/10.1007/s00429-016-1219-8

Herold, C., Bingman, V. P., Strockens, F., Letzner, S., Sauvage, M., Palomero-Gallagher, N., … Güntürkün, O. (2014). Distribution of neurotransmitter receptors and zinc in the pigeon (*Columba livia*) hippocampal formation: A basis for further comparison with the mammalian hippocampus. *Journal of Comparative Neurology*, *522*(11), 2553–2575. https://doi.org/10.1002/cne.23549

Herold, C., Coppola, V. J., & Bingman, V. P. (2015). The maturation of research into the avian hippocampal formation: Recent discoveries from one of the nature's foremost navigators. *Hippocampus*, *25*(11), 1193–1211. https://doi.org/10.1002/hipo.22463

Herold, C., Diekamp, B., & Güntürkün, O. (2008). Stimulation of dopamine D1 receptors in the avian fronto-striatal system adjusts daily cognitive fluctuations. *Behavioural Brain Research*, *194*(2), 223–229. https://doi.org/10.1016/j.bbr.2008.07.017

Herold, C., Joshi, I., Chehadi, O., Hollmann, M., & Güntürkün, O. (2012). Plasticity in D1-like receptor expression is associated with different components of cognitive processes. *PLoS One*, *7*(5), e36484. https://doi.org/10.1371/journal.pone.0036484

Herold, C., Palomero-Gallagher, N., Güntürkün, O., & Zilles, K. (2012). Serotonin 5-HT(1A) receptor binding sites in the brain of the pigeon (*Columba livia*). *Neuroscience*, *200*, 1–12. https://doi.org/S0306-4522(11)01259-0 [pii]10.1016/j.neuroscience.2011.10.050

Herold, C., Palomero-Gallagher, N., Hellmann, B., Kröner, S., Theiss, C., Güntürkün, O., & Zilles, K. (2011). The receptor architecture of the pigeons' nidopallium caudolaterale: An avian analogue to the mammalian prefrontal cortex. *Brain Structure and Function*, *216*(3), 239–254. https://doi.org/10.1007/s00429-011-0301-5

Husband, S. A., & Shimizu, T. (1999). Efferent projections of the ectostriatum in the pigeon (*Columba livia*). *The Journal of Comparative Neurology*, *406*(3), 329–345.

Jarvis, E. D., Güntürkün, O., Bruce, L., Csillag, A., Karten, H., Kuenzel, W., … Avian Brain Nomenclature, C. (2005). Avian brains and a new understanding of vertebrate brain evolution. *Nature Reviews. Neuroscience*, *6*(2), 151–159. https://doi.org/10.1038/nrn1606

Jarvis, E. D., Yu, J., Rivas, M. V., Horita, H., Feenders, G., Whitney, O., … Wada, K. (2013). Global view of the functional molecular organization of the avian cerebrum: Mirror images and functional columns. *Journal of Comparative Neurology*, *521*(16), 3614–3665. https://doi.org/10.1002/cne.23404

Karten, H., & Hodos, W. (1967). *A stereotaxic atlas of the brain of the pigeon (Columba livia)*. Baltimore: The Johns Hopkins University Press.

Karten, H. J. (2015). Vertebrate brains and evolutionary connectomics: On the origins of the mammalian 'neocortex'. *Philosophical Transactions of the Royal Society of London. Series B, Biological Sciences*, *370*(1684), https://doi.org/10.1098/rstb.2015.0060

Kohler, E. C., Messer, W. S., Jr., & Bingman, V. P. (1995). Evidence for muscarinic acetylcholine receptor subtypes in the pigeon telencephalon. *The Journal of Comparative Neurology*, *362*(2), 271–282. https://doi.org/10.1002/cne.903620209

Kröner, S., & Güntürkün, O. (1999). Afferent and efferent connections of the caudolateral neostriatum in the pigeon (*Columba livia*): A retro- and anterograde pathway tracing study. *Journal of Comparative Neurology*, *407*(2), 228–260. https://doi.org/10.1002/(SICI)1096-9861(19990503)407:2<228::AID-CNE6>3.0.CO;2-2 [pii]

Kubikova, L., Wada, K., & Jarvis, E. D. (2010). Dopamine receptors in a songbird brain. *The Journal of Comparative Neurology*, *518*(6), 741–769. https://doi.org/10.1002/cne.22255

Kuenzel, W. J., Medina, L., Csillag, A., Perkel, D. J., & Reiner, A. (2011). The avian subpallium: New insights into structural and functional subdivisions occupying the lateral subpallial wall and their embryological origins. *Brain Research*, *1424*, 67–101. https://doi.org/10.1016/j.brainres.2011.09.037

Lanuza, E., Davies, D. C., Landete, J. M., Novejarque, A., & Martinez, G., F. (2000). Distribution of CGRP-like immunoreactivity in the chick and quail brain. *The Journal of Comparative Neurology*, *421*(4), 515–532.

Letzner, S., Simon, A., & Güntürkün, O. (2016). Connectivity and neurochemistry of the commissura anterior of the pigeon (*Columba livia*). *The Journal of Comparative Neurology*, *524*(2), 343–361. https://doi.org/10.1002/cne.23858

Leutgeb, S., Husband, S., Riters, L. V., Shimizu, T., & Bingman, V. P. (1996). Telencephalic afferents to the caudolateral neostriatum of the pigeon. *Brain Research*, *730*(1–2), 173–181. https://doi.org/0006-8993(96)00444-1 [pii]

Lillethorup, T. P., Iversen, P., Fontain, J., Wegener, G., Doudet, D. J., & Landau, A. M. (2015). Electroconvulsive shocks decrease alpha2-adrenoceptor binding in the Flinders rat model of depression.

European Neuropsychopharmacology, *25*(3), 404–412. https://doi.org/10.1016/j.euroneuro.2014.12.003

Lovell, P. V., Clayton, D. F., Replogle, K. L., & Mello, C. V. (2008). Birdsong "transcriptomics": Neurochemical specializations of the oscine song system. *PLoS One*, *3*(10), e3440. https://doi.org/10.1371/journal.pone.0003440

Martinez-Vargas, M. C., Stumpf, W. E., & Sar, M. (1976). Anatomical distribution of estrogen target cells in the avian CNS: A comparison with the mammalian CNS. *The Journal of Comparative Neurology*, *167*(1), 83–103. https://doi.org/10.1002/cne.901670106

Mash, D. C., & Potter, L. T. (1986). Autoradiographic localization of M1 and M2 muscarine receptors in the rat brain. *Neuroscience*, *19*(2), 551–564.

Medina, L., & Abellán, A. (2009). Development and evolution of the pallium. *Seminars in Cell & Developmental Biology*, *20*(6), 698–711. https://doi.org/10.1016/j.semcdb.2009.04.008

Medina, L., Bupesh, M., & Abellán, A. (2011). Contribution of genoarchitecture to understanding forebrain evolution and development, with particular emphasis on the amygdala. *Brain, Behavior and Evolution*, *78*(3), 216–236. https://doi.org/10.1159/000330056

Merker, B. (1983). Silver staining of cell bodies by means of physical development. *Journal of Neuroscience Methods*, *9*(3), 235–241.

Montiel, J. F., & Molnar, Z. (2013). The impact of gene expression analysis on evolving views of avian brain organization. *The Journal of Comparative Neurology*, *521*(16), 3604–3613. https://doi.org/10.1002/cne.23403

Moreno, N., & Gonzalez, A. (2007). Evolution of the amygdaloid complex in vertebrates, with special reference to the anamnio-amniotic transition. *Journal of Anatomy*, *211*(2), 151–163. https://doi.org/10.1111/j.1469-7580.2007.00780.x

Mulder, J., Spence, L., Tortoriello, G., Dinieri, J. A., Uhlen, M., Shui, B., … Harkany, T. (2010). Secretagogin is a Ca2+-binding protein identifying prospective extended amygdala neurons in the developing mammalian telencephalon. *European Journal of Neuroscience*, *31*(12), 2166–2177. https://doi.org/10.1111/j.1460-9568.2010.07275.x

Nomura, T., Hattori, M., & Osumi, N. (2009). Reelin, radial fibers and cortical evolution: insights from comparative analysis of the mammalian and avian telencephalon. *Development, Growth & Differentiation*, *51*(3), 287–297. https://doi.org/10.1111/j.1440-169X.2008.01073.x

Olson, C. R., Hodges, L. K., & Mello, C. V. (2015). Dynamic gene expression in the song system of zebra finches during the song learning period. *Developmental Neurobiology*, *75*(12), 1315–1338. https://doi.org/10.1002/dneu.22286

Palomero-Gallagher, N., Vogt, B. A., Schleicher, A., Mayberg, H. S., Zilles, K. (2009). Receptor architecture of human cingulate cortex: evaluation of the four-region neurobiological model. *Human Brain Mapping*, *30*(8), 2336–2355. https://doi.org/10.1002/hbm.20667

Palomero-Gallagher, N., Schleicher, A., Zilles, K., & Loscher, W. (2010). The circling ci2 rat mutant revisited: Receptor architecture of the motor cortex. *Neuroscience*, *170*(2), 542–550. https://doi.org/10.1016/j.neuroscience.2010.07.043

Palomero-Gallagher, N., & Zilles, K. (2004). Isocortex. In G. Paxinos (ed), *The rat nervous system* (3rd ed., pp. 729–757). San Diego: Acadamic Press.

Palomero-Gallagher, N., Zilles, K., Schleicher, A., & Vogt, B. A. (2013). Cyto- and receptor architecture of area 32 in human and macaque brains. *The Journal of Comparative Neurology*, *521*(14), 3272–3286. https://doi.org/10.1002/cne.23346

Paxinos, G., Kus, L., Ashwell, K., & Watson, C. (1999). *Chemoarchitecture of the rat forebrain*. San Diego: Academic Press.

Paxinos, G., & Watson, C. (2005). *The Rat Brain in Stereotaxic Coordinates*. Elsevier Academic Press.

Pfenning, A. R., Hara, E., Whitney, O., Rivas, M. V., Wang, R., Roulhac, P. L., … Jarvis, E. D. (2014). Convergent transcriptional specializations in the brains of humans and song-learning birds. *Science*, *346*(6215), 1256846. https://doi.org/10.1126/science.1256846

Puelles, L. (2011). Pallio-pallial tangential migrations and growth signaling: new scenario for cortical evolution? *Brain, Behavior and Evolution*, *78*(1), 108–127. https://doi.org/10.1159/000327905

Puelles, L., Kuwana, E., Puelles, E., Bulfone, A., Shimamura, K., Keleher, J., … Rubenstein, J. L. (2000). Pallial and subpallial derivatives in the embryonic chick and mouse telencephalon, traced by the expression of the genes Dlx-2, Emx-1, Nkx-2.1, Pax-6, and Tbr-1. *The Journal of Comparative Neurology*, *424*(3), 409–438.

Puelles, L., Martinez-de-la-Torre, M., Paxinos, G., Watson, C., & Martinez, S. (2007). *The chick brain in stereotaxic coordinates: An Atlas featuring neuromeric subdivisions and mammalian homologies*. London: Academic Press.

Puelles, L., Medina, L., Borello, U., Legaz, I., Teissier, A., Pierani, A., & Rubenstein, J. L. (2015). Radial derivatives of the mouse ventral pallium traced with Dbx1-LacZ reporters. *Journal of Chemical Neuroanatomy*, *75*(Pt A), 2–19 https://doi.org/10.1016/j.jchemneu.2015.10.011

Reiner, A., & Karten, H. J. (1985). Comparison of olfactory bulb projections in pigeons and turtles. *Brain, Behavior and Evolution*, *27*(1), 11–27.

Reiner, A., Perkel, D. J., Bruce, L. L., Butler, A. B., Csillag, A., Kuenzel, W. … Avian Brain Nomenclature Forum. (2004). Revised nomenclature for avian telencephalon and some related brainstem nuclei. *The Journal of Comparative Neurology*, *473*(3), 377–414. https://doi.org/10.1002/cne.20118

Roberts, T. F., Hall, W. S., & Brauth, S. E. (2002). Organization of the avian basal forebrain: Chemical anatomy in the parrot (*Melopsittacus undulatus*). *The Journal of Comparative Neurology*, *454*(4), 383–408. https://doi.org/10.1002/cne.10456

Sah, P., Faber, E. S., Lopez De Armentia, M., & Power, J. (2003). The amygdaloid complex: Anatomy and physiology. *Physiological Reviews*, *83*(3), 803–834. https://doi.org/10.1152/physrev.00002.2003

Saint-Dizier, H., Constantin, P., Davies, D. C., Leterrier, C., Levy, F., & Richard, S. (2009). Subdivisions of the arcopallium/posterior pallial amygdala complex are differentially involved in the control of fear behaviour in the Japanese quail. *Brain Research Bulletin*, *79*(5), 288–295. https://doi.org/10.1016/j.brainresbull.2009.03.004

Sanders, J. D., Szot, P., Weinshenker, D., Happe, H. K., Bylund, D. B., & Murrin, L. C. (2006). Analysis of brain adrenergic receptors in dopamine-beta-hydroxylase knockout mice. *Brain Research*, *1109*(1), 45–53. https://doi.org/10.1016/j.brainres.2006.06.033

Scarf, D., Stuart, M., Johnston, M., & Colombo, M. (2016). Visual response properties of neurons in four areas of the avian pallium. *Journal of Comparative Physiology. A, Neuroethology, Sensory, Neural, and Behavioral Physiology*, *202*(3), 235–245. https://doi.org/10.1007/s00359-016-1071-6

Schall, U., Güntürkün, O., & Delius, J. D. (1986). Sensory projections to the nucleus basalis prosencephali of the pigeon. *Cell and Tissue Research*, *245*(3), 539–546.

Scheperjans, F., Grefkes, C., Palomero-Gallagher, N., Schleicher, A., & Zilles, K. (2005). Subdivisions of human parietal area 5 revealed by quantitative receptor autoradiography: A parietal region between motor, somatosensory, and cingulate cortical areas. *Neuroimage*, *25*(3), 975–992. https://doi.org/10.1016/j.neuroimage.2004.12.017

Scheperjans, F., Palomero-Gallagher, N., Grefkes, C., Schleicher, A., & Zilles, K. (2005). Transmitter receptors reveal segregation of cortical areas in the human superior parietal cortex: Relations to visual and somatosensory regions. *Neuroimage*, *28*(2), 362–379. https://doi.org/10.1016/j.neuroimage.2005.06.028

Shanahan, M., Bingman, V. P., Shimizu, T., Wild, M., & Güntürkün, O. (2013). Large-scale network organization in the avian forebrain: A connectivity matrix and theoretical analysis. *Frontiers in Computational Neuroscience*, *7*, 89. https://doi.org/10.3389/fncom.2013.00089

Sun, Z., & Reiner, A. (2000). Localization of dopamine D1A and D1B receptor mRNAs in the forebrain and midbrain of the domestic chick. *Journal of Chemical Neuroanatomy*, *19*(4), 211–224.

Swanson, L. W. (2000). Cerebral hemisphere regulation of motivated behavior. *Brain Research*, *886*(1–2), 113–164.

Swanson, L. W., & Petrovich, G. D. (1998). What is the amygdala? *Trends in Neurosciences*, *21*(8), 323–331.

Székély, A. D., & Krebs, J. R. (1996). Efferent connectivity of the hippocampal formation of the zebra finch (Taenopygia guttata): An anterograde pathway tracing study using Phaseolus vulgaris leucoagglutinin. *Journal of Comparative Neurology*, *368*(2), 198–214. https://doi.org/10.1002/(SICI)1096-9861(19960429)368:2<198::AID-CNE3>3.0.CO;2-Z [pii]10.1002/(SICI)1096–9861(19960429)368:2<198::AID-CNE3>3.0.CO;2-Z

Thompson, R. R., Goodson, J. L., Ruscio, M. G., & Adkins-Regan, E. (1998). Role of the archistriatal nucleus taeniae in the sexual behavior of male Japanese quail (Coturnix japonica): A comparison of function with the medial nucleus of the amygdala in mammals. *Brain, Behavior and Evolution*, *51*(4), 215–229.

Veenman, C. L., Wild, J. M., & Reiner, A. (1995). Organization of the avian "corticostriatal" projection system: A retrograde and anterograde pathway tracing study in pigeons. *The Journal of Comparative Neurology*, *354*(1), 87–126. https://doi.org/10.1002/cne.903540108

Vicario, A., Abellán, A., Desfilis, E., & Medina, L. (2014). Genetic identification of the central nucleus and other components of the central extended amygdala in chicken during development. *Frontiers in Neuroanatomy*, *8*, 90. https://doi.org/10.3389/fnana.2014.00090

Vicario, A., Abellán, A., & Medina, L. (2015). Embryonic origin of the Islet1 and Pax6 neurons of the chicken central extended amygdala using cell migration assays and relation to different neuropeptide-containing cells. *Brain, Behavior and Evolution*, *85*(3), 139–169. https://doi.org/10.1159/000381004

Vogt, B. A., Hof, P. R., Zilles, K., Vogt, L. J., Herold, C., & Palomero-Gallagher, N. (2013). Cingulate area 32 homologies in mouse, rat, macaque and human: Cytoarchitecture and receptor architecture. *The Journal of Comparative Neurology*, *521*(18), 4189–4204. https://doi.org/10.1002/cne.23409

Wada, K., Sakaguchi, H., Jarvis, E. D., & Hagiwara, M. (2004). Differential expression of glutamate receptors in avian neural pathways for learned vocalization. *The Journal of Comparative Neurology*, *476*(1), 44–64. https://doi.org/10.1002/cne.20201

Wang, R., Chen, C. C., Hara, E., Rivas, M. V., Roulhac, P. L., Howard, J. T., … Jarvis, E. D. (2015). Convergent differential regulation of SLIT-ROBO axon guidance genes in the brains of vocal learners. *The Journal of Comparative Neurology*, *523*(6), 892–906. https://doi.org/10.1002/cne.23719

Whitney, O., Pfenning, A. R., Howard, J. T., Blatti, C. A., Liu, F., Ward, J. M., … Jarvis, E. D. (2014). Core and region-enriched networks of behaviorally regulated genes and the singing genome. *Science*, *346*(6215), 1256780. https://doi.org/10.1126/science.1256780

Wild, J. M., Arends, J. J., & Zeigler, H. P. (1984). A trigeminal sensorimotor circuit for pecking, grasping and feeding in the pigeon (*Columba livia*). *Brain Research*, *300*(1), 146–151.

Wild, J. M., Arends, J. J., & Zeigler, H. P. (1985). Telencephalic connections of the trigeminal system in the pigeon (*Columba livia*): A trigeminal sensorimotor circuit. *The Journal of Comparative Neurology*, *234*(4), 441–464. https://doi.org/10.1002/cne.902340404

Wild, J. M., Arends, J. J., & Zeigler, H. P. (1990). Projections of the parabrachial nucleus in the pigeon (*Columba livia*). *The Journal of Comparative Neurology*, *293*(4), 499–523. https://doi.org/10.1002/cne.902930402

Wild, J. M., Karten, H. J., & Frost, B. J. (1993). Connections of the auditory forebrain in the pigeon (*Columba livia*). *The Journal of Comparative Neurology*, *337*(1), 32–62. https://doi.org/10.1002/cne.903370103

Winkowski, D. E., & Knudsen, E. I. (2007). Top-down control of multimodal sensitivity in the barn owl optic tectum. *The Journal of Neuroscience*, *27*(48), 13279–13291. https://doi.org/10.1523/JNEUROSCI.3937-07.2007

Wynne, B., & Güntürkün, O. (1995). Dopaminergic innervation of the telencephalon of the pigeon (*Columba livia*): A study with antibodies against tyrosine hydroxylase and dopamine. *Journal of Comparative Neurology*, *357*(3), 446–464. https://doi.org/10.1002/cne.903570309

Yamamoto, K., & Reiner, A. (2005). Distribution of the limbic system-associated membrane protein (LAMP) in pigeon forebrain and midbrain. *The Journal of Comparative Neurology*, *486*(3), 221–242. https://doi.org/10.1002/cne.20562

Yamamoto, K., Sun, Z., Wang, H. B., & Reiner, A. (2005). Subpallial amygdala and nucleus taeniae in birds resemble extended amygdala and medial amygdala in mammals in their expression of markers of regional identity. *Brain Research Bulletin*, *66*(4–6), 341–347. https://doi.org/10.1016/j.brainresbull.2005.02.016

Yilmazer-Hanke, D. M., Roskoden, T., Zilles, K., & Schwegler, H. (2003). Anxiety-related behavior and densities of glutamate, GABAA, acetylcholine and serotonin receptors in the amygdala of seven inbred mouse strains. *Behavioural Brain Research*, *145*(1–2), 145–159.

Zeier, H., & Karten, H. J. (1971). The archistriatum of the pigeon: Organization of afferent and efferent connections. *Brain Research*, *31*(2), 313–326.

Zilles, K. (2005). Evolution of the human brain and comparative cyto- and receptor architecture. In S. Dehaene, J.-R. Duhamel, M. Hauser, & G. Rizzolatti (Eds), *From monkey brain to human brain* (pp. 41–56). Cambridge: MIT Press.

Zilles, K., & Palomero-Gallagher, N. (2016). Comparative analysis of receptor subtypes that identify primary cortical sensory areas. In J. Kaas, G. Striedter, L. Krubitzer, S. Herculano-Houzel, & T. Preuss (Eds.), *Evolution of the nervous system*. Oxford: Elsevier.

Zilles, K., Palomero-Gallagher, N., Grefkes, C., Scheperjans, F., Boy, C., Amunts, K., & Schleicher, A. (2002). Architectonics of the human cerebral cortex and transmitter receptor fingerprints: Reconciling functional neuroanatomy and neurochemistry. *European Neuropsychopharmacology*, *12*(6), 587–599. https://doi.org/S0924977X02001086 [pii]

Zilles, K., Palomero-Gallagher, N., & Schleicher, A. (2004). Transmitter receptors and functional anatomy of the cerebral cortex. *Journal of Anatomy*, *205*(6), 417–432. https://doi.org/10.1111/j.0021-8782.2004.00357.x

Zilles, K., Schlaug, G., Matelli, M., Luppino, G., Schleicher, A., Qu, M., … Roland, P. E. (1995). Mapping of human and macaque sensorimotor areas by integrating architectonic, transmitter receptor, MRI and PET data. *Journal of Anatomy*, *187*(Pt 3), 515–537.

Zilles, K., Schleicher, A., Palomero-Gallagher, N., & Amunts, K. (2002). Quantitative analysis of cyto- and receptor architecture of thehuman brain. In J.C. Mazziotta & A. Toga (Eds.), *Brain mapping: The methods* (pp. 573–602). Amsterdam: Elsevier.

How to cite this article: Herold C, Paulitschek C, Palomero-Gallagher N, Güntürkün O, Zilles K. Transmitter receptors reveal segregation of the arcopallium/amygdala complex in pigeons (*Columba livia*). *J Comp Neurol*. 2018;526:439–466. https://doi.org/10.1002/cne.24344

CORTEX 118 (2019) 165–187

Available online at www.sciencedirect.com

ScienceDirect

Journal homepage: www.elsevier.com/locate/cortex

Special issue: Research report

The hippocampus of birds in a view of evolutionary connectomics

Christina Herold [a,*], Philipp Schlömer [b], Isabelle Mafoppa-Fomat [b], Julia Mehlhorn [c], Katrin Amunts [a,b] and Markus Axer [b]

[a] C. & O. Vogt-Institute of Brain Research, Medical Faculty, Heinrich Heine University of Düsseldorf, Düsseldorf, Germany

[b] Institute of Neuroscience and Medicine INM-1, Research Center Jülich, Jülich, Germany

[c] Institute of Anatomy I, Heinrich Heine University of Düsseldorf, Düsseldorf, Germany

ARTICLE INFO

Article history:
Received 12 June 2018
Reviewed 30 July 2018
Revised 26 September 2018
Accepted 26 September 2018
Published online 11 October 2018

Keywords:
Adult neurogenesis
Doublecortin
Fiber tracking
3D polarized light imaging
Avian

ABSTRACT

The avian brain displays a different brain architecture compared to mammals. This has led the first pioneers of comparative neuroanatomy to wrong conclusions about bird brain evolution by assuming that the avian telencephalon is a hypertrophied striatum. Based on growing evidence from divers analysis demonstrating that most of the avian forebrain is pallial in nature, this view has substantially changed during the past decades. Further, birds show cognitive abilities comparable to or even exceeding those of some mammals, even without a "six-layered" cortex. Beside higher associative regions, most of these cognitive functions include the processing of information in the hippocampal formation (HF) that shares a homologue structure in birds and mammals. Here we show with 3D polarized light imaging (3D-PLI) that the HF of pigeons like the mammalian HF shows regional specializations along the anterior–posterior axis in connectivity. In addition, different levels of adult neurogenesis were observed in the subdivisions of the HF per se and in the most caudal regions pointing towards a functional specialization along the anterior–posterior axis. Taken together our results point to species specific morphologies but still conserved hippocampal characteristics of connectivity, cells and adult neurogenesis if compared to the mammalian situation. Here our data provides new aspects for the ongoing discussion on hippocampal evolution and mind.

© 2019 The Authors. Published by Elsevier Ltd. This is an open access article under the CC BY license (http://creativecommons.org/licenses/by/4.0/).

1. Introduction

Understanding the routes of brain evolution in the context of cognition seems to be a challenging task for comparative neuroscientists following the fact that there are still many gaps to fill with a limited amount of species living in the 21st century. Nevertheless, in the past 50 decades researchers have presented data reporting that birds, cephalopods and even other taxa without a "six-layered" neocortex, show complex

* *Corresponding author*. C. & O. Vogt-Institute of Brain Research, Heinrich Heine University of Düsseldorf, 40225 Düsseldorf, Germany.
E-mail address: christina.herold@uni-duesseldorf.de (C. Herold).

https://doi.org/10.1016/j.cortex.2018.09.025

0010-9452/© 2019 The Authors. Published by Elsevier Ltd. This is an open access article under the CC BY license (http://creativecommons.org/licenses/by/4.0/).

and intelligent behavior, tool use, social altruism and far more other skills comparable to or even exceeding those of some mammals (Güntürkün & Bugnyar, 2016; Karten, 2015). Together all of these cognitive functions and skills involve a functional cortical–basal ganglia circuit, which seemed to be highly conserved between species, like for example, the song system of birds and speech production in humans (Chakraborty & Jarvis, 2015; Karten, 2015). These findings however, have increased comparative studies and ongoing discussions dealing with the evolution of the "six-layered" neocortex (Bolhuis & Wynne, 2009; Butler, Reiner, & Karten, 2011; Gabi et al.., 2016; Güntürkün, 2005; Güntürkün, Ströckens, Scarf, & Colombo, 2017; Herculano-Houzel, Catania, Manger, & Kaas, 2015; Hevner, 2016; Kaas & Stepniewska, 2015; Montiel, Vasistha, Garcia-Moreno, & Molnar, 2016; Olkowicz et al., 2016; Shepherd & Rowe, 2017). In contrast, debates about hippocampal evolution are relatively tame (Striedter, 2016), although hippocampal (archicortical) structures evolved sometime in-between the paleo- and the neocortex, and many cognitive functions involve hippocampal circuits that are further integrated in the cortical–basal ganglia network. In addition, recent evidence emerged that it is likely that the "six-layered" neocortex has evolved from a common ancestor with a "three-layered" cortex, a morphology that is still present in hippocampal regions of different species (Güntürkün et al., 2017; Rowe & Shepherd, 2016; Shepherd & Rowe, 2017; Striedter, 2016; Ulinski, 1983). In our view, this observation makes the hippocampus an excellent candidate to study cortical evolution because the hippocampus shares a common origin in the amniote species (Medina & Abellan, 2009; Puelles, 2001, 2011) and many features of hippocampal functions are conserved, particularly spatial memory (Bingman & Muzio, 2017; Gagliardo, Ioale, & Bingman, 1999; Herold, Coppola, & Bingman, 2015; Witter, Kleven, & Kobro Flatmoen, 2017). Even more interesting, the hippocampal formation (HF) of birds displays a special morphology along its extension through the anterior–posterior axis. Most of it exhibits no clear three-layered laminar organization like the mammalian hippocampus or its homologue in the amniote species (Herold et al., 2014; Nomura & Hirata, 2017; Striedter, 2005, 2016). This variation however, raises the question what other properties of neurons or neuronal networks are required to serve conserved functions and what differences may exist and have evolved over more than 350 Million years of separate evolution in adaption to an ecologic niche (Fig. 1).

The HF in birds can be divided into several subdivisions, the V-complex, with its ventromedial (Vm), triangular (Tr) and ventrolateral (Vl) region, the dorsomedial region with its dorso-dorsomedial (DMd) and ventro-dorsomedial (DMv) subdivision and the dorsolateral region with its dorso-dorsolateral (DLd) and ventro-dorsolateral (DLv) subdivision (Fig. 2; Herold et al., 2014). Despite the differences in the overall architecture, cell types and connections of the HF in birds show many similarities to those of mammals (Atoji, Wild, Yamamoto, & Suzuki, 2002; Casini, Bingman, & Bagnoli, 1986; Colombo & Broadbent, 2000; Hough, Pang, & Bingman, 2002; Krebs, Erichsen, & Bingman, 1991; MacPhail, 2002; Sherry, Grella, Guigueno, White, & Marrone, 2017). However, there is an ongoing discussion, which subdivisions

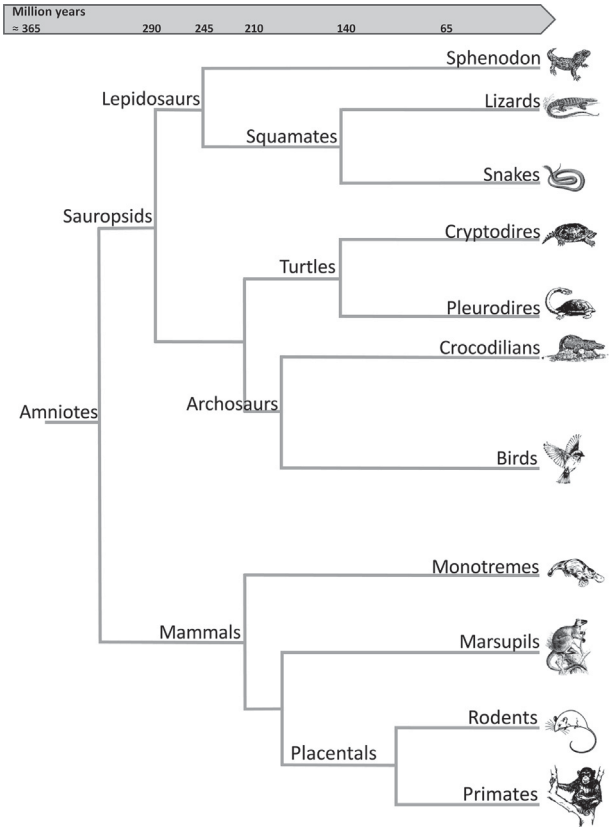

Fig. 1 – Simplified phylogenetic tree of amniotes. Analysis of single cell transcriptomics support the idea that the anlage of the hippocampal formation, i.e., dentate gyrus and cornu ammonis was already present in the ancestor of all amniotes (Tosches et al., 2018). Since then, several million years of separate evolution occurred between birds and mammals.

of the HF in birds correspond to their mammalian counterparts, i.e., the dentate gyrus (DG), the cornu ammonis (CA) fields, the subiculum and the entorhinal cortex (Abellan, Desfilis, & Medina, 2014; Atoji, Sarkar, & Wild, 2016; Herold et al., 2015; Medina, Abellán, & Desfilis, 2017). New theories of the evolution of DG as a late evolving structure and an exclusive addition to the hippocampus of mammals have further questioned whether a DG as strict as in mammals even exists in birds or not (Atoji et al., 2016; Bingman & Muzio, 2017; Bingman, Rodriguez, & Salas, 2017; Kempermann, 2012; Striedter, 2016). However, recent findings by analysis of single-cell transcriptomics of the reptilian medial most cortex, particularly the dorsomedial cortex, support the hypothesis that the hippocampal regions, including DG, CA1 and CA3 were already present in the ancestor of all amniotes (Tosches et al., 2018).

Yet, another clue comes from new insights of functionally different domains in the mammalian hippocampus. Based on genetic and connectional data the hippocampus of mammals can be compartmentalized into multiple domains along the longitudinal/dorsal-ventral axis (Dong, Swanson, Chen, Fanselow, & Toga, 2009; Ohara, Sato, Tsutsui, Witter, & Iijima, 2013; Thompson et al., 2008; Witter et al.,

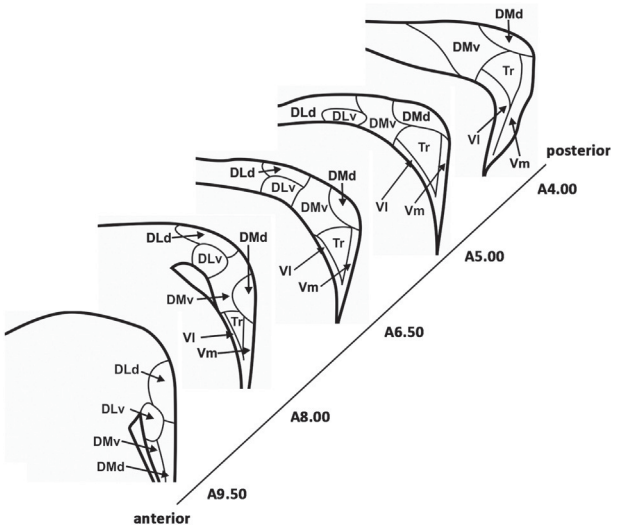

Fig. 2 – The hippocampal formation of the pigeon. Schematic outlines along the anterior–posterior axis according to Herold et al. (2014). Atlas levels referring to Karten and Hodos (1967, p. 195). The major subdivisions are the V-region comprising the lateral (Vl) and medial (Vm) layers and the triangular area in between (Tr), the dorsomedial region with its dorsal (DMd) and ventral (DMv) subdifferentiation, and the dorsolateral region (DL) including the further subdivisions dorsal (DLd) and ventral (DLv).

2017). Further, a large body of connectional and functional data, including adult neurogenesis in rodents and primates, revealed that the dorsal hippocampus (septal pole or posterior in primates) is involved in spatial memory and navigation, and showed higher levels of adult neurogenesis, while the ventral hippocampus (temporal pole or anterior in primates) mediates emotion, anxiety, stress-related behavior and cognitive flexibility, and exhibits lower levels of adult neurogenesis (Anacker & Hen, 2017; Colombo, Fernandez, Nakamura, & Gross, 1998; Fanselow & Dong, 2010; Strange, Witter, Lein, & Moser, 2014; Witter et al., 2017). This functional differentiation in case of stress-related behavior might also exist in the avian HF (Robertson et al., 2017; Smulders, 2017).

Up to now, only a few researchers have explored the rostro-caudal axis in the avian HF (Fig. 2) and less is known about the basis of functional differences along the axis. Therefore, we decided to analyze two different components of hippocampal functional circuity. First, we will present data for the homing pigeon (*Columba livia f.d.*) with a focus on rostro-caudal differences in hippocampal connectivity at the microscale level by using the newly developed method of 3D-polarized light imaging (3D-PLI). 3D-PLI has been shown to be a powerful tool to analyze fiber architecture, and the course of fibers and fiber tracts in mammals (Axer, Amunts, et al., 2011; Axer, Gräßel et al., 2011; Zeineh et al., 2017; Zilles et al., 2016). Second, we will present data of neurogenic markers for adult neurogenesis in the pigeon rostro-caudal axis of the HF.

2. Material and methods

2.1. Animals

In total, we examined eleven adult homing pigeon brains (*C. livia f.d.*) of the same age originating from our local breeding colony, which were raised in the same loft (250 cm × 190 cm × 190 cm) and lived there under identical conditions. The pigeons were allowed to fly freely and food, grit and water were provided ad libitum. All experimental procedures were approved by the national authority (LANUV NRW, Germany) and were carried out in accordance with the National Institute of Health Guide for Care and Use of Laboratory Animals.

2.2. 3D-polarized light imaging

2.2.1. Tissue-processing

Animals for the Polarized Light Imaging (n = 2) were euthanized with Pentobarbital (70 mg/kg), decapitated, brains were removed from the skull, and immediately fixed in 4% buffered formalin pH 7 and stored at 4 °C. Two weeks later brains were transferred into a solution of 10% Glycerin, 2% DMSO and 4% formalin pH 7 for five days, and subsequently transferred into a solution of 20% Glycerin, 2% DMSO and 4% formalin pH 7 for additional two weeks. Brains were frozen and stored at −80 °C. They were cut in serial coronal or sagittal 60 μm sections with a cryostat microtome (Leica Biosystems, Nussloch Germany). Slices were thaw mounted on un-gelatinized slides, freeze dried and coated in 20% Glycerin three days before the 3D-PLI measurements started. After the measurements, slices were further processed for Nissl staining with Cresyl violet.

2.2.2. Imaging

In order to make the fiber architecture of brain tissue visible, linearly polarized light has been applied to the histological sections and the light transmission has been sampled at 9 or 18 vertical polarization planes covering 180° by means of a circular analyzer (Axer, Amunts, et al., 2011; Axer, Gräßel et al., 2011). The interaction of polarized light with the birefringent components of the nerve tissue, i.e., the myelin, allows for the extraction of predominating fiber orientations in tiny volumes of 1.3 μm × 1.3 μm × 60 μm.

The polarimetric setup is based on a standard bright field microscope (with Köhler illumination) with two polarizing filters and a movable specimen stage (Märzhäuser Wetzlar, Germany) introduced into the beam path (Fig. 3). The wavelength spectrum (550 ± 5 nm) has been adapted to the polarizing filter specifications by means of a white light LED in combination with a narrowband pass filter next in line. The size of the square field of view of the monochrome CCD camera (QImaging Retiga 4000R) is 2.7 × 2.7 mm^2 providing a pixel resolution of 1.3 microns. The transmission intensity of the whole specimen is imaged with a tile overlap of 1.0 mm at 18 vertical polarization plane angles (ρ) for the frontal sections and with a tile overlap of .75 mm at 9 vertical polarization angles for the sagittal sections respectively, in order to determine accurately the predominant fiber orientation in each of 1.3 μm × 1.3 μm × 60 μm voxel (Fig. 4f).

Using the Jones calculus for flat polarization optics (Jones, 1941) three modalities can be derived from the sinusoidal dependence (Fig. 4e) of the transmission intensity I on the polarization plane angle (ρ):

$$I(\rho) = \frac{Transmittance}{2}\cdot[1 + \sin(2\rho - 2\cdot Direction)\cdot Retardation]$$

$$Retardation = \sin\left(2\pi\cdot\frac{Section\ Thickness}{Light\ WaveLength}\cdot Birefringence\cdot\cos^2(Inclination)\right)$$

Transmittance (arbitrary units) is the mean intensity of the light transmission through the tissue (Fig. 4a). *Retardation* (0–1) is the vertical projection of the cumulative tissue birefringence normalized by the transmittance at a given light wavelength (Fig. 4b). *Direction* (0°–180°) is the predominant in-plane nerve fiber orientation (Fig. 4c).

The out-of-plane elevation angle of the nerve fiber is called *Inclination* (Fig. 4d) and can be estimated from retardation and transmittance by means of four parameters determined on the basis of their gray value distributions over the whole section:

1) *retmaxwm*: maximum retardation of the white matter 2) *retmaxgm*: maximum retardation of the gray matter 3) *tmaxgm*: maximum transmittance of the gray matter 4) *tmeanwm*: mean transmittance of the white matter (Reckfort, 2015). The parameter *retmaxgm* has been introduced in addition to account for the weak influence of the gray matter retardation. These four parameters approximately determine the relation between the retardation and the inclination by means of the transmittance:

$$\frac{\sin^{-1}(Retardation)}{\cos^2(Inclination)} = \frac{\log\left(\frac{tmaxgm}{tmeanwm}\right)}{\log\left(\frac{tmaxgm}{Transmittance}\right)\cdot\sin^{-1}\left(retmaxwm + (retmaxgm - retmaxwm)\cdot\frac{Transmittance - tmeanwm}{tmaxgm - tmeanwm}\right)}$$

Due to the presence of artificial inhomogeneity in the transmittance induced by glycerol at variable time delays between tissue embedding and 3D-PLI-measurement, these parameters had to be slightly adapted subsequently to avoid the saturation of the inclination at 0° or 90° degrees in areas prone to this artifact like deep white matter or scarcely myelinated nuclei. The inclination values are compromised by this modification to the point of about +5 up to +10°.

2.2.3. Fiber orientation maps

Direction, inclination and mask provide a full set of polar coordinates for the calculation of a 3D-vector array of fiber orientations. The vector data of a single section provided by 3D-PLI are represented by color images called fiber orientation maps (FOMs). A point on the colored surface of a hemisphere represents the color of a corresponding 3D fiber orientation (Fig. 4f). Yet a quarter sphere is sufficient because flat 3D-PLI without tilting the light beam does neither differentiate forward and backward orientation nor the sign of the fiber inclination (downward or upward). The hue corresponds to the direction of the in-plane projection of the fiber orientation.

The fiber inclination on the other hand is coded by saturation and brightness (Fig. 4g). In case of the RGB-color-code (Fig. 5A) hemisphere fiber orientations are reflected by colors only. The principal directions (left–right, up–down, front–rear) are corresponding to the fundamental colors (red, green, blue). In the HSV-color-code (Fig. 5B) hemisphere fiber orientations are reflected by hue, saturation and brightness. In the HSV-black version the brightness decreases with increasing inclination staining the poles at 90° black.

The reference for a single vector representation is generally not a single fiber but all birefringent tissue compartments inside a volume element (voxel) contributing to an image pixel. There are two reasons for signal loss in the white matter: fiber crossings and steep fibers with inclinations nearby 90°. Therefore, in areas of massive fiber intermingling at scales below the section thickness of 60 microns the direct representation of the fiber orientation by color and saturation is replaced by an extinction texture. Hence fibers stay visible in the FOM, however, orientation values are getting lost (Fig. 5C).

2.3. Immunohistochemistry

Animals used for immunohistochemistry of adult neurogenesis markers (n = 9, female 5, male 4, all age-matched) were injected i.m. on three consecutive days with BrdU (50 mg/kg). Twelve weeks after the injections animals were deeply anesthetized with Pentobarbital (70 mg/kg), transcardially perfused with 4% paraformaldehyde and brains were removed. After 2 h of postfixation (4% paraformaldehyde + 30% sucrose) and 24 h of cryoprotection (30% sucrose in phosphate buffer), the brains were frozen and cut in serial coronal 40 μm sections with a microtome (Leica Biosystems, Nussloch, Germany).

Coronal sections from one series out of 10 of the whole pigeon brain were immunohistochemically processed for 1) fluorescent double-labeling detection of DCX (anti-DCX ab18723, abcam, USA, see Fig. 6A and B) and BrdU (anti-BrdU OBT0030, AbD serotec, USA), or 2) triple fluorescent labeling

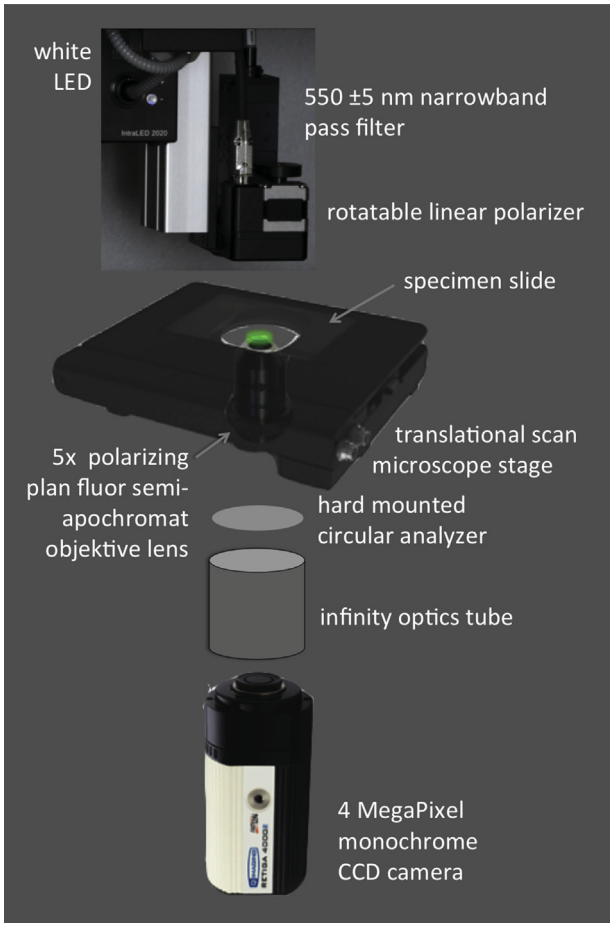

Fig. 3 – Hardware setup of the polarization microscope.

detection of BrdU (anti-BrdU OBT0030, AbD serotec, USA), NeuN (anti-NeuN MAB377, Millipore, Germany) and GFAP (ab16997, abcam, USA, see Fig. 6C and D).

1) Briefly, free-floating sections were rinsed 2 times in phosphate buffered saline (PBS). Subsequently slices were incubated in 2 N HCl at 45 °C for 30 min and .1 M borate buffer pH 8.5 for 10 min. Sections were than washed in PBS for 10 min that was followed by a blocking step with 3% goat serum (Vector, USA) in PBS + Triton-X .3% (PBS-T) for 60 min. This was followed by incubation with a primary antibody mix anti-BrdU (1:200) and anti-DCX (1:500) overnight at 4 °C. After that sections were washed 3 times in PBS that was followed by incubation with the secondary antibody mix containing goat anti-rat Alexa 488 (1:200) and goat anti-rabbit CY3 (1:500; both Jackson-Immuno Research, USA) for 2 h at darkness. At all further steps, sections were handled at a minimum of light or in complete darkness. After incubation sections were washed 3 times with PBS and 2 times with PB, mounted on gelatin-coated glass slides, air-dried for 24 h and then dipped into distilled water and directly coverslipped with Fluoromount-G (Southern Biotec, USA). The slides were than taken to a fluorescent microscope system AxioScan.Z1 (Zeiss, Germany) and the whole sections were scanned for digitalization of photomicrographs at 20× magnification. All sections were analyzed with the software Zen2 (Zeiss, Germany), by delineation of ROIs (i.e., subdivisions of the HF) and counting immunereactive cells with the counting tool so that a value for each region of the number of immunoreactive cells (either BrdU, or DCX)/area (mm^2) was determined.
2) To detect BrdU+ cells, sections were treated like in the labeling procedure of 1). After the pre-processing, sections were incubated with the primary antibody mix anti-BrdU (1:200), anti-NeuN (1:1000) and anti-GFAP (1:500)

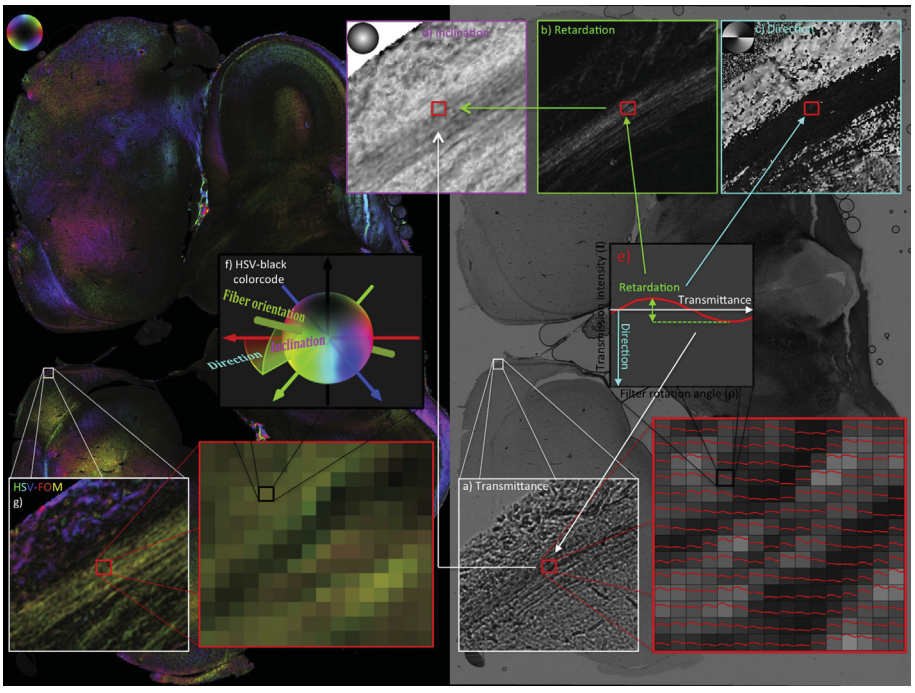

Fig. 4 – Data processing pipeline of 3D-PLI (a–f). For details see section 2.2.2 and 2.2.3 in the material and methods section.

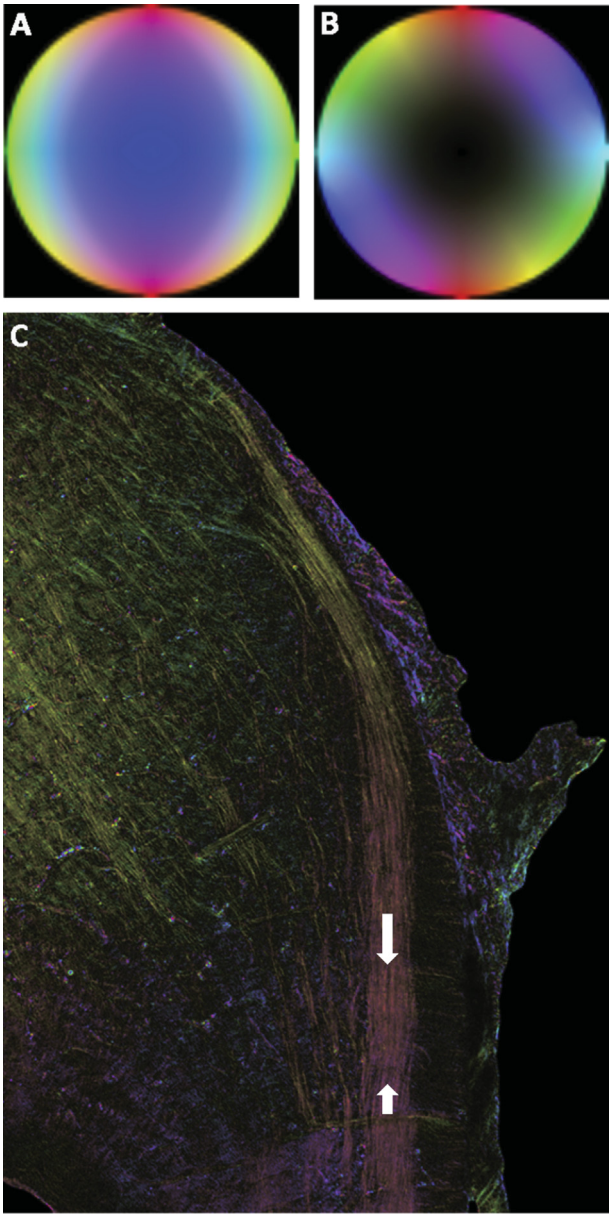

Fig. 5 – FOM color-codes and signal extinction. A: RGB color code. B: HSV-black color code. C: Signal extinction on the HSV-black map (white arrows) of radial fibers near the interhemispheric fissure crossing the septal tract in the medial part of the hippocampal formation.

overnight at 4 °C, washed (3× PBS), and then incubated with the secondary antibody mix containing donkey anti-mouse Alexa 647 (1:200; Dianova, Germany) goat anti-rabbit FITC (1:200; Cayman Chemical, USA) and goat anti-rat CY3 (1:200; Millipore, Germany) for 2 h at darkness. All further steps were identical to the labeling procedure of 1).

All antibodies were validated by Western-blotting procedures or showed specific binding in previous studies (Fig. 5E; Melleu, Santos, Lino-de-Oliveira, & Marino-Neto, 2013; Robertson et al., 2017). Tissue samples were lysed at 4 °C with 50 mM Tris–HCL buffer (pH 7.4) containing 1% IGEPAL, 150 mM NaCl, 1 mM ethylenediaminetetraacetic acid, .1% SDS, 1 mM dithiothreitol and 2% glycerin. After homogenization, the lysates were centrifuged at 20.000 *g* at 4 °C. For sodium dodecyl sulfate polyacrylamide gel electrophoresis (SDS-Page) and Western Blot analysis, the supernatant was added 1:4 to a 4× gel loading buffer containing 1.25% mercaptoethanol (pH 6.8) and heated to 95 °C for five minutes. The probes were subject to gel electrophoresis (12%) using .3 μg protein per lane. Proteins were transferred to nitrocellulose membranes using a dry transfer apparatus (Invitrogen, Carlsbad, USA). Blots were blocked for 1 h with a blocking solution containing bovine serum albumin solubilized in 20 mM Tris–HCL pH 7.6, 150 mM NaCl and .1% Tween 20, and incubated overnight with the primary antibody (see list above) at 4 °C. After several rinsing steps and incubation with horseradish peroxidase-coupled immunoglobulin G, anti-rabbit IgG or anti-mouse IgG (both Jackson-Immuno Research, USA) at room temperature for 1 h, blots were washed and developed by using enhanced chemiluminescent detection (BioRad).

2.4. *Data analysis*

At a first step, the atlas levels (Karten & Hodos, 1967, p. 195) of the brain sections from pigeons for 3D-PLI and immunohistochemistry measurements were determined.

For analysis of the 3D-PLI data, visual analyses of frontal and sagittal sections enabled us to take advantage of the extremely high in-plane resolution of 3D-PLI to optimally detect the dorsal–ventral and medial–lateral trajectories in the frontal images, and dorsal–ventral and anterior–posterior trajectories in the sagittal images. We identified the orientation of fibers by examining the color-coded fiber orientation maps, examining the color as well as the image texture (e.g., numerous lines pointing in one direction). Dark regions on transmittance images that were not cell bodies were generally considered to represent myelin. 3D-PLI is maximally sensitive for fibers oriented in-plane; on frontal section images, fibers oriented through-plane (i.e., along the anterior–posterior axis of the hippocampus formation) would appear dark on the transmittance images, but show reduced or no color orientation. Therefore, the sagittal images were used to confirm through-plane orientation of pathways. Further anterior–posterior long-range connections were first analyzed and identified in the sagittal sections, and then combined with the analysis of the frontal sections.

Combining the results of 3D-PLI with our subregion segmentation, we identified the major pathways according to known connectivity patterns from earlier avian studies (see Atoji & Wild, 2006; Shanahan, Bingman, Shimizu, Wild, & Güntürkün, 2013 for review), and compared it with the PLI data. A known limitation of 3D-PLI fiber tracking, however, is that we cannot determine, whether a fiber, or a fiber bundle, is entering or leaving the HF, so we used earlier results of tracing studies to guide the interpretation.

For immunohistochemistry, data of the hippocampal subregions defined by Herold et al. (2014) from atlas levels A 10.25 (anterior) to A 3.75 (posterior) were analyzed. The number of immunoreactive cells (BrdU+, DCX+, BrdU+/NeuN+, BrdU+/GFAP+)/area (mm^2) was averaged for the following coordinates ±500 μm: A 4.25, A 5.50, A 6.75, A 8.25 and A 9.50.

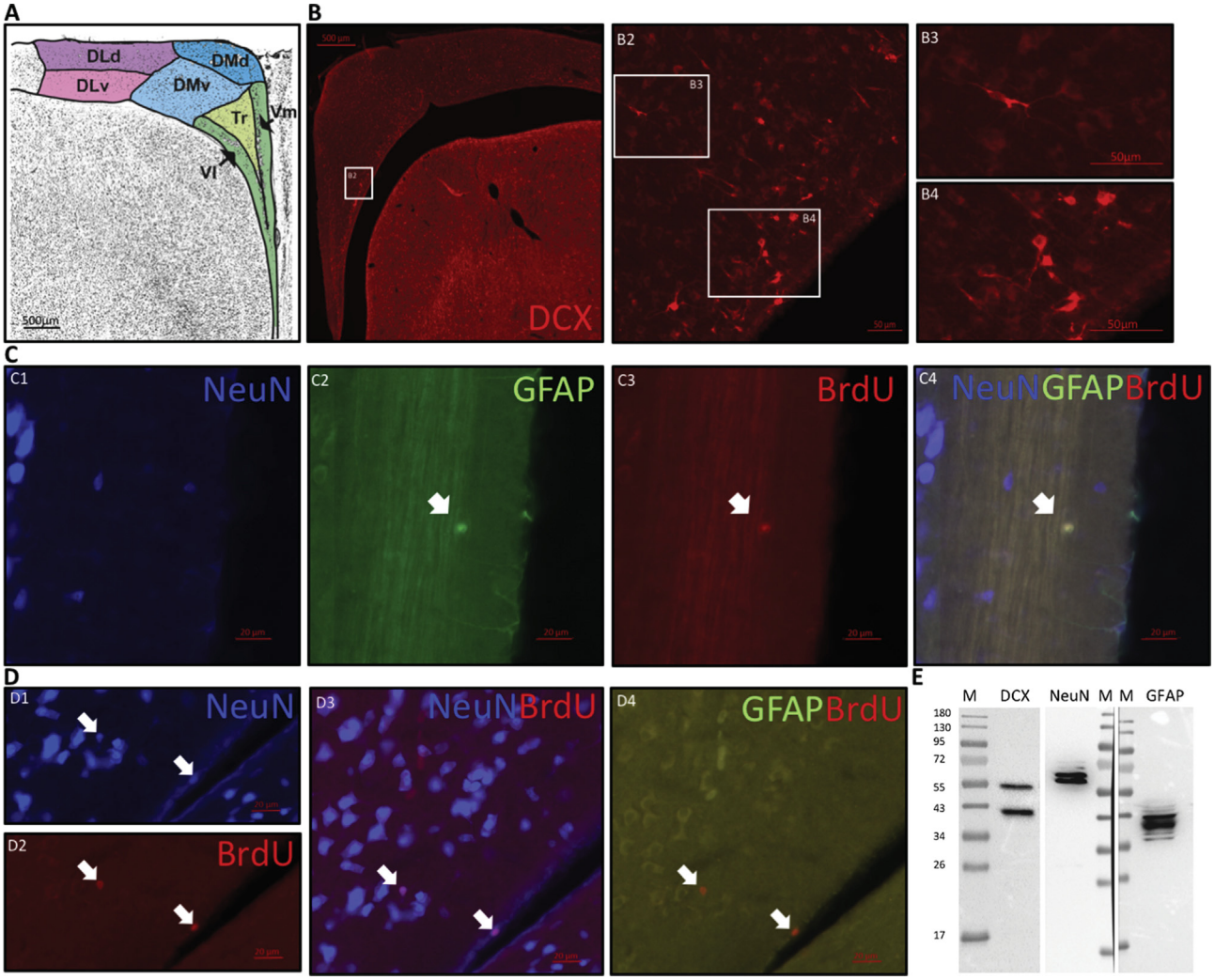

Fig. 6 – Expression of neurogenic markers in the hippocampal formation of the pigeon. A: Different subdivisions of the hippocampal formation. B: DCX expression in the hippocampal formation (B1–2) and different DCX-ir cell types characterized by shape, the ovoid cells (B3) and the triangular cells (B4) in the V-region. C: NeuN (C1), GFAP (C2), BrdU (C3) triple labeling in Vm showing double labeled BrdU/GFAP cells (C4). D: NeuN (D1), GFAP, BrdU (D2) triple labeling in Vl showing double labeled BrdU/NeuN cells (D3) excluding GFAP labeling (D4). E: Western-Blots validating the antibodies for DCX, NeuN and GFAP showing the expected bands between 55–40 kDa (DCX), 72–55 kDa (NeuN) and 43–34 kDa (GFAP). Abbreviations see text.

To determine differences in BrdU+, DCX+, BrdU+/NeuN+, BrdU+/GFAP+ cells among the HF at different anterior–posterior levels or across subdivisions, we first applied a Friedman ANOVA for each tested neurogenic marker or marker pair. If significant, pair-wise comparisons were run with the Wilcoxon-rank test. For the general statistical analyses, Statistica 13 (StatSoft, Tulsa, USA) was used. The significance level was set at .05.

3. Results

3.1. *Connectivity of the pigeon hippocampal formation along the anterior–posterior axis*

Along the anterior–posterior axis, the pigeon HF is moving from a rostro-medial to a caudo-lateral position in the dorsal forebrain (Fig. 2). We generally confirmed earlier tracing studies showing that the pigeon HF is connected to the lateral and medial septum (SL and SM), the nucleus taeniae of the amygdala (TnA), the lateral part of the bed nucleus of the stria terminalis lateralis (BSTL), the nucleus of the diagonal band (NDB), the hypothalamus, i.e., the nucleus periventricularis magnocellularis (PVM), the dorsolateral corticoid area (CDL), the hyperpallium apicale (HA) and laterale (HL), the cortex piriformis (CPi), the arcopallium ventrale (AV) and intermediale (AI) and inter-hippocampally via commissural fibers through the commissura pallii (CPa; Atoji, Saito, & Wild, 2006; Atoji & Wild, 2004; Atoji et al., 2002; Benowitz & Karten, 1976; Casini et al., 1986; Krayniak & Siegel, 1978a, 1987b; Shanahan et al., 2013; Szekely & Krebs, 1996). Because the focus of this study was to examine the differences in anterior–posterior trajectories we analyzed the above mentioned main neural pathways/long-range connections and mostly skipped the

local circuitry. To do so, we combined our observations with results of former tracing studies and included whether a connection was afferent or efferent or reciprocal (for details see Atoji and Wild, 2004; Shanahan et al., 2013 for review).

Beginning very close to the zero point of the medial level, the interhemispheric fissure (medial telencephalic wall), we observed a massive amount of fibers connecting the hippocampus with the septal region in the dorso-ventral axis that were topographically organized along the anterior–posterior axis (Fig. 7A–D). At this level, direct hypothalamic connections of the PVM and the caudal DMd region of the hippocampus were visible and hippocampal–septal projections to SL and SM were prominent (Fig. 7A–C). More dorsally fibers of the septal region joined the tractus cortico-habenularis et cortico-septalis (CHCS). Fibers that popped out from the dorso-rostral HF to the most medial portion of the tractus septopallio-mesencephalicus (TSM) were also present at this level. The commissural fibers leaving the CPa, curved to the hippocampal–septal junction, ran upwards to the medial wall before they spread into the subdivisions of the HF (caudal route). Most of them originate in the V-complex and DM of the contralateral HF. Visualization of CPa in frontal sections around A 7.50 confirmed this and showed fibers of the V-complex and DM running downwards to the contralateral side, crossing between the two hemispheres indicated by the color-switch, as soon as they reach the contralateral side along the rostral route (Fig. 7D). In the dorsal regions of the HF many thin fibers travel along the anterior–posterior axis connecting anterior and posterior regions (Fig. 7B and D).

Moving more laterally four major pathways were recognized where efferents and afferents pass through the medial wall (Fig. 8A–E). The details of the different paths are presented in Fig. 8B–E. At the lateral level around Lat .50, all subdivisions of the HF along the anterior–posterior axis could be differentiated by the fiber architecture (Fig. 8B) and an additional superficial pathway was recognized at the caudal pole of the HF along Vm and DM where fibers inclines to a 90° direction, i.e., travel in a medial–lateral direction or vice versa (Figs. 7B and 8C). Inspection of the most lateral sagittal slides showed that fibers from caudal CPi, PoA and

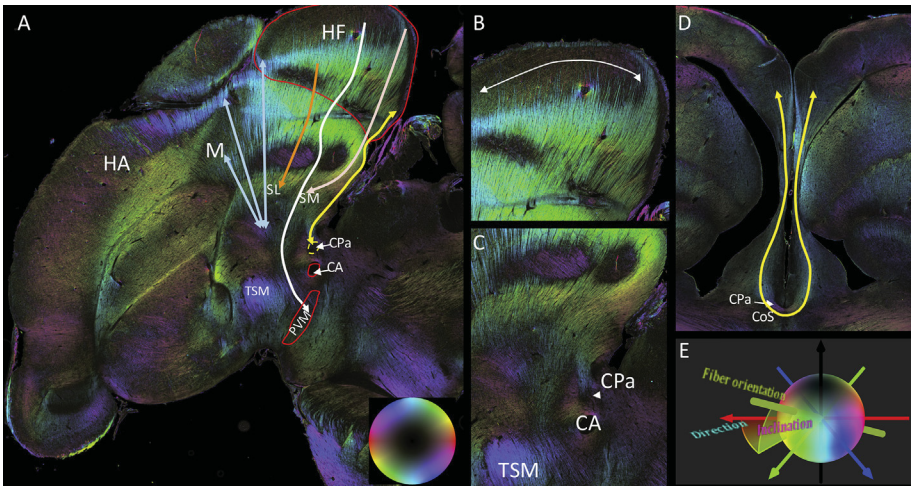

Fig. 7 – The spatial course of massive long-range connections of the hippocampal formation along the anterior–posterior axis. A: 3D-PLI image at the sagittal level around Lat .00 close to the interhemispheric fissure/medial wall. The hue of the color wheel indicates the direction of the in-plane fiber orientation (for explanation see 2.2.2), and the brightness/darkness of the color (e.g., more peripheral/central in the color wheel) indicates a primarily in-plane/through-plane orientation. Red outlines mark the hippocampal formation. White lines show direct connections of the hypothalamus, the nucleus periventricularis magnocellularis (PVM) and the caudal dorsomedial region. Hippocampal–septal connections are indicated by orange lines (lateral septum, SL) and light pink lines (medial septum, SM). The course of commissural fibers running in the commissura pallii (CPa) is marked with yellow. Fibers popping out from the most medial position of the anterior tractus septopallio-mesencephalicus (TSM) are in light blue revealing connections to rostral HF, the hyperpallium apicale (HA) and the mesopallium (M). More dorsally fibers of the septal region belong to the tractus cortico-habenularis et cortico-septalis (CHCS). B: Along the anterior–posterior axis, the V-region and the ventral dorsomedial region (DMv) show a high density of thick fibers or fiber bundles traveling in the dorso-ventral axis that are topographically organized along the anterior–posterior axis, while in the dorsal regions many thin fibers traveling along the anterior–posterior axis connecting anterior and posterior regions (white line). C: Enlargement of the connection between PVM and the dorsomedial region (DM), as well as fiber organization of the CPa and septal regions. D: Visualization of the CPa in a frontal section at A.7.50. As indicated by the color-switch (white arrow), fibers of the V-region and DM cross between the two hemispheres and run upwards to the contralateral side (yellow line). Comparisons between frontal and sagittal sections as well as inclination images show that these fibers stay in plane, i.e., running towards the same level at the anterior–posterior axis they originated. E: Additional legend showing the sinusoidal dependence of the 3D-PLI images. Hemisphere fiber orientations are reflected by hue, saturation and brightness. A change in color corresponds to a change in direction of the fiber. With increased inclination fibers appear in black.

AV as well as intra-hippocampal fibers (reciprocal) connect along this route, while at more medial sagittal levels fibers from SPC join this pathway. The four major pathways included fibers in frontal as well as sagittal sections that connect BSTL and NDB with the HF traveling together from the basal tip of the ventricle along the medial side of the ventricle close to latero-dorsal SL. Further, a few olfactory fibers also join this pathway. Fibers and fiber bundles of the hippocampal connection between SL and SM were additionally separated into two pathways at the level of the nuclei in the septal region (Fig. 8D). The fourth path comprised the crossing fibers of the HF through CPa that get intermingled with the other pathways by passing through the medial wall and then curve separately slightly rostro-ventrally to reach the commissure or vice versa (Fig. 8E).

The visualization of the fiber courses in the tractus CHCS and in the dorsal regions of the HF showed in frontal sections around atlas level A6.50 fibers traveling along the tractus CHCS started to run outwards of DM and the V-region from dorsal to ventral joining the CHCS with increased inclination in caudal direction (Fig. 9A, named post-commissural in Krayniak & Siegel, 1978b). At frontal sections around level A 7.25, at the most caudal point of the septal nuclei SL and SM, some fibers from DL and DM still travel to the medial wall along the periphery of the HF or along the ventricle in a dorso-ventral direction with increased inclination, while a few fibers already started to run further ventrally to SL (Fig. 9B). At both frontal levels, the fiber orientation maps of the DMd and DLd region mostly appeared in dark color, indicating intense fiber intermingling and/or fibers coursing in the anterior–posterior axis (Fig. 9A and B). As verified in the sagittal sections (Fig. 9C), indeed many fibers travel through/from DLd and DMd along the anterior–posterior axis. Those fibers mainly represent the connections between the CPi, the hyperpallium and the HF, as well as intrinsic connections of DM and DL. Fibers from CPi travel dorsally from anterior to posterior along the outer surface of HA reaching the HF at the border of DL (asterisk). In addition, radial fibers from HD, HL and HA cross this fiber tract (arrows), join along its path, and get indistinguishable from olfactory fibers (Fig. 9D). At lateral level Lat 1.00, the CHCS parallels the stria medullaris (SMe) as shown in a sagittal section of the right hemisphere and was clearly separated from the SMe (Fig. 9E). At this level fibers from the habenula, as well as fibers from nucleus taeniae of the amygdala (TnA) have joined the tract.

Around sagittal level Lat 1.80, the fiber courses of TnA that emerged at the ventro(basal)-medial site of the ventricle add to the medial route of afferents from TnA to HF (Fig. 10A). After reaching this point, fibers travel to the caudal end of the hippocampus and then turn into a dorso-medial direction providing the input to the caudal half of the HF. This was verified by inspection of frontal sections around atlas level A 6.25. Fibers travel from TnA medially along the bottom of the ventricle and incline to the caudal pole. Further, we observed that the fiber bundle of TnA and the fiber bundle from the habenula joined the hippocampal–septal bundle at this coordinate (Fig. 10B).

Moving more laterally to level Lat 3.50 the area corticoidea dorsolateralis (CDL) was visible (Fig. 10C and D). The analysis of the connectivity between the HF and the CDL revealed many connections between CDL and DMv, CDL and the V-

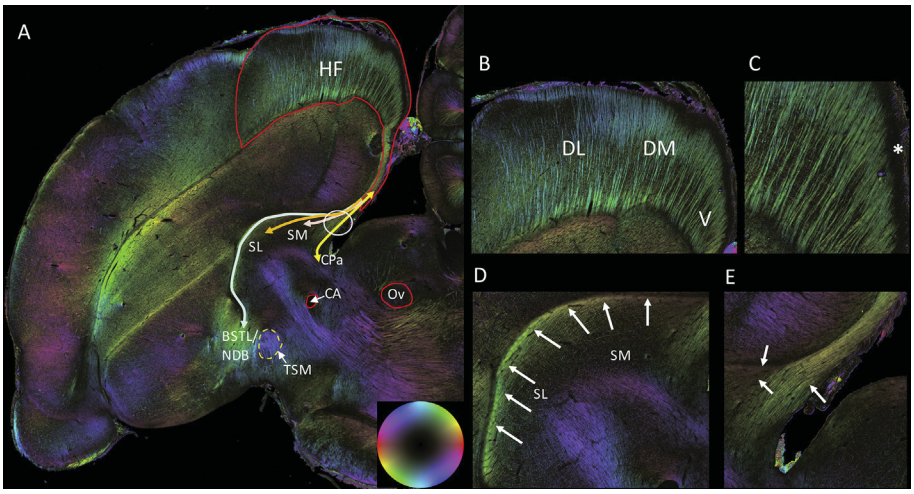

Fig. 8 – Connections of the hippocampal formation in the anterior–posterior axis at the sagittal level around Lat .50. A: Four major branches are recognized at this level were efferents and afferents pass through the medial wall (white circle). The light blue line indicates fibers between the HF and BSTL and NDB that run along this path. B: Zoom into the hippocampal formation (HF) show the organization of fibers running from the medial wall across the V-region, DM and DL. The fiber architecture revealed the subdivisions of the hippocampal formation. C: Zoom into the V-region indicates a superficial pathway at the caudal pole of the hippocampal formation along Vm (white asterisk). D: Zoom into the septal region showing the course of fibers around this region. The white arrows show the pathway of fibers from the HF to NDB and BSTL. E: Zoom into the region were fibers from the septal region and CPa get intermingled indicated by white arrows. CA, commissura anterior; Cpa, commissura pallii; BSTL, lateral part of the bed nucleus of the stria terminalis; NDB, nucleus of the diagonal band; Ov, nucleus ovoidalis; SM, medial septum; SL, lateral septum; TSM, tratcus septopallio-mesencephalicus.

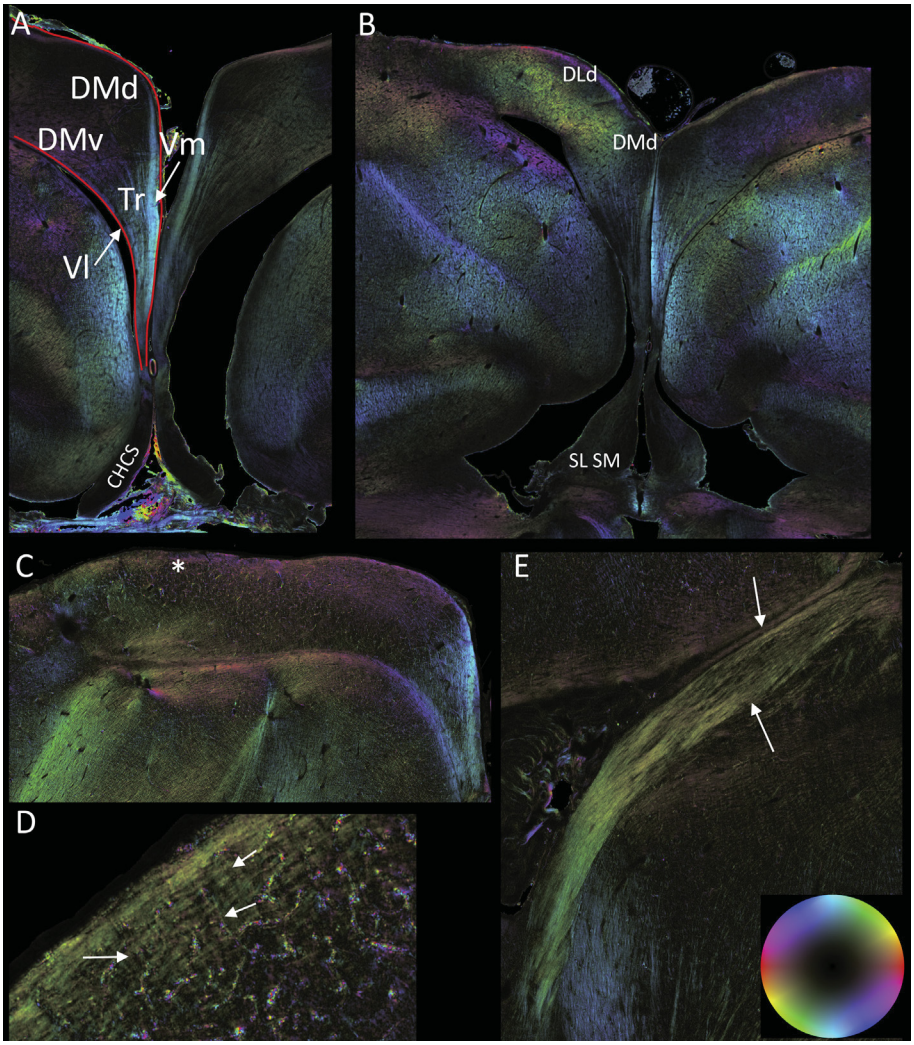

Fig. 9 – Visualization of the fiber courses in the tractus cortico-habenularis et cortico-septalis and in the dorsal regions. A: Detailed 3D-PLI image of the hippocampal formation in a frontal section at atlas level A6.50 showing the tractus cortico-Habenularis et cortico-septalis (CHCS). Fibers begin to run outwards of DM and the V-region running from dorsal to ventral joining the CHCS with increased inclination. B: Frontal section around atlas level A 7.25 at the most caudal point of the septal nuclei SL and SM. Fibers from DL and DM travel dorso-medially along the periphery of the HF or along the ventricle to a ventral direction with increased inclination. In both, (A) and (B), further inspection of the sagittal slices showed that fibers run to the septal nuclei and then travel rostral. Additionally, most of the DMd and DLd region appears dark, indicating intense fiber intermingling and/or fibers coursing in the anterior–posterior axis. As verified in (C) in an example of a sagittal section, indeed many fibers travel through/from DLd and DMd along the anterior–posterior axis. C: Fibers in DMd running in the anterior–posterior axis. Fibers from the cortex piriformis (CPi) travel dorsally from anterior to posterior along the outer surface of HA reaching the hippocampal formation at the border of DL (asterisk). In addition, radial fibers from HA/HL cross this fiber tract (arrows), join along its way particularly from more anterior portions and get indistinguishable from olfactory fibers (D). E: The CHCS parallels the stria medullaris (SMe) in a sagittal section of the right hemisphere around atlas level Lat 1.00 and is clearly separated (see white arrows; CHCS: upper arrow, SMe lower arrow).

region and to a lesser extent between CDL and DMd, and CDL and DL.

3.2. *Adult neurogenesis in the pigeon hippocampal formation along the rostro-caudal axis*

DCX+ cells were differentially expressed in the HF [$\chi^2(n = 9, df = 6) = 51.05$, $p < .001$; Fig. 11A]. The highest numbers were detected in Vl (to all subdivisions of the HF, $p < .01$, except compared to Dlv, $p < .05$) and the lowest in DMd (to all, $p < .01$). Additionally, Tr and Vm showed relatively low levels of DCX expressing cells (to all, $p < .01$, except Tr compared to Vm, $p < .05$). In DLd, DLv and DMv ovoid cells were higher expressed compared to Tr cells (to all $p < .05$), while in Vl more often Tr cells expressed DCX ($p < .01$; Fig. 11A). Along the anterior–posterior axis overall DCX+ cells showed a different distribution in the HF [$\chi^2(n = 9, df = 4) = 17.78$, $p < .01$; Fig. 11B]. The number of DCX+ cells specifically dropped at the most

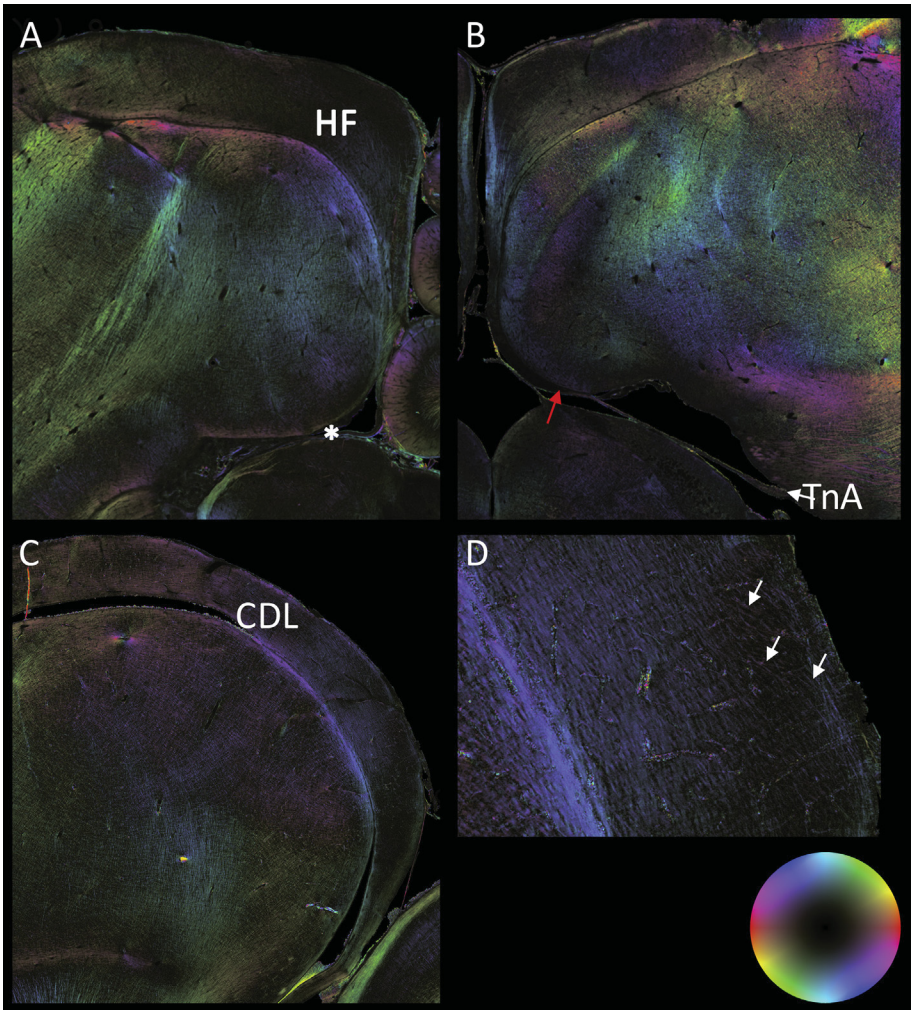

Fig. 10 – Fiber courses of the nucleus taeniae of the amygdala and the area corticoidea dorsolateralis. A: In the sagittal section, the small band of fibers (asterisk) that emerges at the ventro-medial site of the ventricle belongs to the medial route of afferents to the hippocampal formation of TnA. After reaching this point, fibers travel to the caudal end of the hippocampus and then turn into a dorso-medial direction. B: A frontal section that shows the fiber bundle of TnA that provides input to the caudal half of the hippocampus at atlas level A 6.25. As indicated, fibers travel from TnA (white arrow) medially along the bottom of the ventricle and incline (red arrow) to the caudal pole (as shown in A). C: Detail of the fiber architecture of the area corticoidea dorsolateralis (CDL) at a sagittal plane approximately at atlas level Lat 3.50 showing the connectivity of CDL and DM. D: Zoom in to visualize fibers traveling diagonally over DM at more posterior positions (white arrows).

posterior parts of the HF around atlas level A 4.25 ± .5 (to all other atlas levels, $p < .01$). This effect mainly results from a decrease of Tr DCX+ cells at the most posterior level [$\chi^2(n = 9, df = 4) = 12.18$, $p < .05$], while ovoid DCX+ cells were almost equally distributed along the anterior–posterior axis (Fig. 11B). Additionally, very few DCX+/BrdU+ positive cells in the HF were detected, indicating that even after three month of injections of BrdU immature neurons in the pigeon HF are still in a "waiting phase" on their way to mature neurons.

BrdU labeled cells were variably expressed in the subdivisions of the HF [$\chi^2(n = 9, df = 6) = 20.00$, $p < .01$; Fig. 12A], as well as double labeled BrdU+/GFAP+ cells [$\chi^2(n = 9, df = 6) = 26.81$, $p < .001$; Fig. 12A] and BrdU+/NeuN+ cells [$\chi^2(n = 9, df = 6) = 23.12$, $p < .001$; Fig. 12A]. New glial cells [BrdU+/GFAP+] were frequently higher in Vm compared to the other subdivisions (Vm: DLd, $p < .5$, DLv, DMv, Tr, $p < .01$) but not to Vl and DMd (both n.s.). Additionally, lower amounts were detected in Tr compared to DMd and DLv (both $p < .05$). The highest numbers of newborn neurons (BrdU+/NeuN+) were detected in Vl (compared to DLd, DMv, Tr, $p < .05$ and compared to DMd, Vm $p < .01$) and DLv (compared to Tr, DLd, DMd, $p < .05$ and to DMv, Vm, $p < .01$). Only low amounts were found in DMd (compared to Vl, $p < .01$ and to DLd, DLv, DMv, $p < .05$). In all hippocampal subdivisions, the number of newborn glial cells exceeded newborn neurons (all, $p < .01$; Fig. 12A). Along the rostro-caudal axis, no overall differences in BrdU+ [$\chi^2(n = 9, df = 4) = 2.22$, $p = .70$], BrdU+/GFAP+ [$\chi^2(n = 9, df = 4) = 9.16$, $p = .06$] or BrdU+/NeuN+ [$\chi^2(n = 9,$

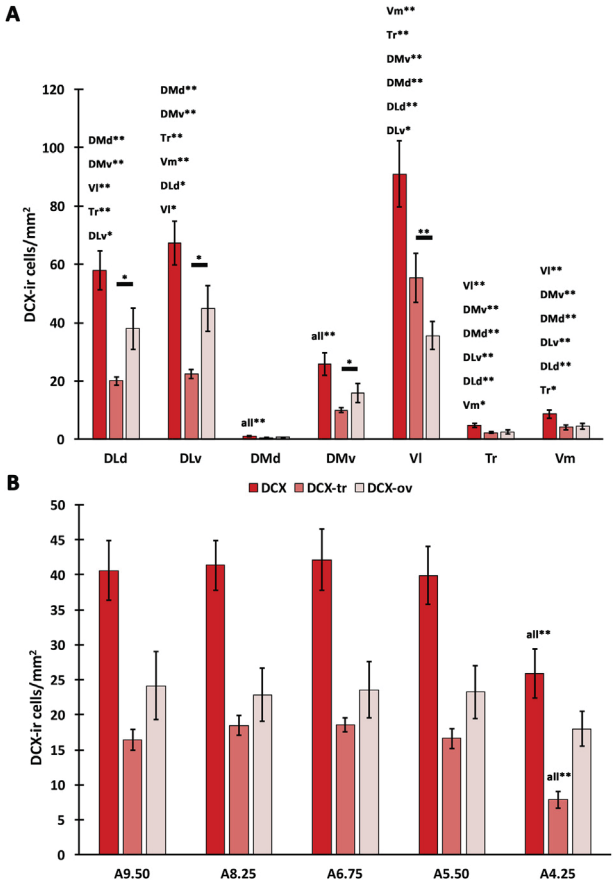

Fig. 11 – Neural plasticity in the adult hippocampal formation of the pigeon. A: Distribution of DCX-ir cells in different subregions of the hippocampal formation (n = 9). B: DCX-ir cells in the hippocampal formation along the anterior–posterior axis. Further, two different types of DCX-ir cells were recognized, triangular (tr-) and ovoid (ov-) cells (n = 9). Bars represent standard error means. Asterisks indicate significant differences (*$p < .05$; **$p < .01$).

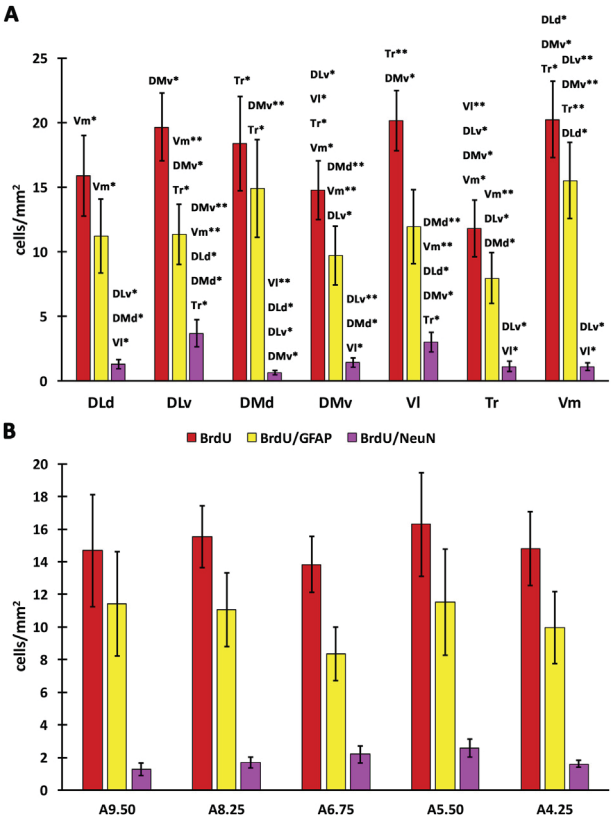

Fig. 12 – Neuro- and gliogenesis in the adult hippocampal formation of the pigeon. A: Distribution of BrdU-ir, BrdU/GFAP-ir, BrdU/NeuN-ir cells in different subregions of the hippocampal formation (n = 9). B: BrdU-ir, BrdU/GFAP-ir, BrdU/NeuN-ir in the hippocampal formation along the anterior–posterior axis (n = 9). Bars represent standard error means. Asterisks indicate significant differences (*$p < .05$; **$p < .01$).

df = 4) = 7.2, $p = .13$] cells in the HF were detected (all Fig. 12B). Selective testing of regions with high or moderate levels of plasticity, respectively Vl, Vm, DLv and DMv (Fig. 13), showed that only in Vl the BrdU+/GFAP+ cells decreased from anterior level 8.25 to posterior level 4.25 [χ^2(n = 9, df = 3) = 9.93, $p < .05$; Fig. 13A].

4. Discussion

The present study disclosed the axonal architecture of the pigeon along the anterior–posterior axis including long range connection using 3D-PLI as a high-resolution imaging approach to study the connectivity structure in the whole brain (Axer, Amunts, et al., 2011; Axer, Gräßel et al., 2011; Schubert et al., 2016; Zilles et al., 2016). It verified that subdivisions of the pigeon HF are partly topographically connected along the anterior–posterior axis with regard to the long-range connectivity and replicated earlier studies of the connectome of the HF in pigeons (Atoji & Wild, 2005; Atoji et al., 2002, 2006; Atoji and Wild, 2004, Casini et al., 1986; Krayniak & Siegel, 1978a, 1987b). To visualize the long-range connections, we used 3D-PLI in two different cutting directions, i.e., sagittal and frontal. The data presented here show for the first time the useful application of 3D-PLI in a bird brain. We furthermore demonstrate regional differences in adult neurogenesis/gliogenesis in individual subdivisions of the pigeon HF (as defined by Herold et al., 2014) by quantitative measures of different markers that have been demonstrated to reliably map neurogenesis in a wide range of species. Here, detailed analysis of five different atlas levels along the anterior–posterior axis indicated higher rates of immature neurons along the axis compared to the most caudal pole of the HF, while globally, matured newborn neurons/glia only showed a trend towards different levels. However, analysis of subdivisions with high or moderate neurogenesis levels showed that newborn glial cells decreased from anterior to posterior levels in the lateral blade of the V-region (Vl). Our

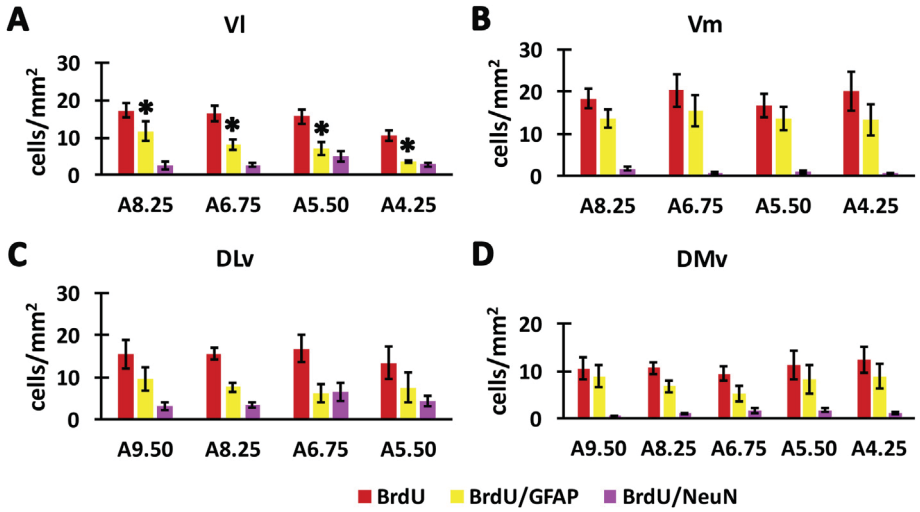

Fig. 13 – Regional distribution of BrdU labeled cells in subdivisions of the hippocampal formation with high or moderate plasticity along the anterior–posterior axis. Only BrdU/GFAP-ir cells in Vl showed decreasing quantities from anterior to posterior coordinates. Bars represent standard error means. Asterisk indicate significant differences (*$p < .05$).

data supports the idea that there is indeed a specialization to regional subdivisions of the HF along the rostro-medial to the caudo-lateral axis of the HF in birds (Smulders, 2017).

4.1. *Connectivity of the hippocampal formation along the anterior–posterior axis in the avian brain*

Numerous studies have investigated the connectome of the avian HF (see Atoji and Wild, 2006; Shanahan et al., 2013; Szekely, 1999 for review), but, none of them did explicitly studied the anterior–posterior axis, although some functional differences were reported in divers bird species. Nevertheless, a few studies mentioned or showed to some extent data of connections along the anterior–posterior axis of the HF (Atoji & Wild, 2004; Atoji et al., 2002; Krayniak & Siegel, 1978a, 1978b; Montagnese, Zachar, Bálint, & Csillag, 2008). In general, the HF projects massively to the septal nuclei and these projections are topographically organized (our data and Atoji & Wild, 2004; Atoji et al., 2002; Krayniak & Siegel, 1978a, 1978b; Montagnese et al., 2008). Caudal HF projects to the post-commissural septum and more rostral HF projects to the rostral septum and the NDB. However, the rostral reciprocal connections to NDB may be more widespread along the anterior–posterior axis according to Atoji and Wild (2002), but are in line with observations from Krayniak and Siegel (1978a). At least, more rostro-medial NDB connects along the medial wall with the HF, while connections with more caudo-lateral NDB were observed with fibers that travel from/to the tip of the ventricle on the same route that connect the HF and the BSTL. According to Atoji et al. (2006), projections from HF to BSTL originate all along the rostro-caudal axis. However, we could not confirm a lateral route from DM to BSTL via the CDL. The inter-hippocampal commissural projections are also topographically organized, i.e., rostral, middle and caudal HF projects to corresponding levels of the contralateral HF. Commissural fibers were organized in a caudal (levels posterior to A 7.5) and a rostral route (levels anterior to A 7.5). These findings are in line with observations by Atoji et al. (2002) and Krayniak and Siegel (1978a). Input from the nucleus taenia (TnA) that belongs to a group of nuclei in the arcopallium/amygdala complex (Herold, Paulitschek, Palomero-Gallagher, Güntürkün, & Zilles, 2018) is limited to the middle/caudal HF to approximately level A 6.25. Fibers between the nucleus posterioris amygdalopallii (PoA) and caudal hippocampal subdivisions course mostly transversally (dorso-laterally) along the outer surface of the telencephalon, while fibers between the ventral arcopallium (AV) or intermediate arcopallium (AI) and the HF use both, the "outer" dorsolateral and the "inner" Vm path along the ventral–medial edge of the ventricle. Hereby, more rostral levels, i.e., more laterally AV fibers travel through the dorsolateral pathway and at more caudal levels, i.e., more medially AV/AIv fibers join the Vm pathway. Whether these two pathways reflect afferent and efferent pathways, or different subtle pathways or only different rostro-caudal connectivity have to be further explored, as well as reinterpretation of data according to the different arcopallial subdivisions (Herold et al., 2018) that receive projections from the HF or vice versa. Both pathways have been described earlier, but with unclear demarcation of the arcopallium/amygdala complex nuclei (Atoji et al., 2002; Casini et al., 1986; Kröner et al., 1999). We further observed a direct connection to the nucleus PVM that was limited to a small portion in caudal DM. This connection was described earlier (Bons, Bouillé, Baylé, & Assenmacher, 1976; Bouillé & Baylé, 1973) and represents afferents from the dorsomedial HF that modulate corticosterone plasma levels. Fibers that join the TSM were limited to the anterior HF, thereby possibly connecting to brain stem sites (Reiner et al., 2004). Further connections with other extrahippocampal structures like hyperpallial subdivisions, olfactory regions or CDL did not differ in their connectivity along the anterior–posterior axis. However, from the border of HA and DL, an enlarging number of thin fibers travel along anterior–posterior axis along the dorsal regions through/over/in DL and DM to the caudal pole of the HF. Before reaching the caudal pole, some of them turn

into the V-region, and then turn ventro-laterally to Vl. To our knowledge, none of the earlier studies mentioned these numerous fibers traveling in the anterior–posterior axis before. To sum up, our results support the idea of a specialization of subdivisions of the HF along the anterior–posterior axis and may also imply functionally different contributions of dorsal and ventral DM and DL. Thereby our results may stimulate future studies to investigate these differences, for example, in relation to spatial learning and emotional behavior.

4.2. *Adult neurogenesis in the hippocampal formation in the avian brain*

In the avian HF adult neurogenesis has been demonstrated for several bird species, including pigeons, zebra finches, canaries, black-capped chickadees, chickens, sparrows, marsh tits, red warblers, corvids and parrots (Balthazart, Charlier, Barker, Yamamura, & Ball, 2008, 2010; Barkan, Roll, Yom-Tov, Wassenaar, & Barnea, 2016; Barnea, Mishal, & Nottebohm, 2006; Hall, Delaney, & Sherry, 2014; Hoshooley, Phillmore, Sherry, & Macdougall-Shackleton, 2007; Kim, Peregrine, & Arnold, 2006; Mazengenya, Bhagwandin, Manger, & Ihunwo, 2018, 2017; Melleu, Pinheiro, Lino-de-Oliveira, & Marino-Neto, 2016, 2013; Meskenaite, Krackow, & Lipp, 2016; Patel, Clayton, & Krebs, 1997; Robertson et al., 2017; Taufique, Prabhat, & Kumar, 2018; Wada, Newman, Hall, Soma, & MacDougall-Shackleton, 2014). However, only few of them have investigated adult neurogenesis in different subdivisions of the HF, and an even smaller number investigated the occurrence of adult neurogenesis regarding to anterior and posterior variations.

A number of markers that are expressed at specific stages during neuronal development or that indicate actively dividing cells have been tested in addition to the "gold standard" BrdU, a thymidine analogue that is inserted into the DNA in actively dividing cells after administration. Doublecortin (DCX), for example, is expressed in many advanced precursor or at an early post-mitotic stage of immature neurons and has been widely accepted as an indicator for adult neurogenesis and neuronal plasticity although some challenges still exist (Balthazart & Ball, 2014; Kremer et al., 2013). Other markers, like Ki67 or PCNA are strictly associated with cell proliferation (Moldovan, Pfander, & Jentsch, 2007; Scholzen & Gerdes, 2000) and Hu expression marks neuronal progenitor cells at an early stage (Barami, Iversen, Furneaux, & Goldman, 1995). NeuN and GFAP on the other hand serve as markers for mature neurons and glia cells. Although most of the antibodies used in this study were used in different species before, including different bird species, we validated the antibodies not only with negative controls but also with Western blot procedures by using fresh brain tissue, and confirmed the correct binding site through protein weights. Immature neurons were verified with DCX, and newborn neurons were proved with BrdU/NeuN double labeling, while newborn glial cells were determined with BrdU/GFAP double labeling.

In pigeons, qualitative and quantitative analysis showed lower amounts of DCX+ cells in Tr and Vm compared to Vl, while DM and DL were only sparsely labeled (Melleu et al., 2013) and lower amounts of DCX+/PCNA+ cells in Vm compared to moderate levels in Tr and Vl, and higher amounts in DL compared to DM (Mazengenya, Bhagwandin, Nkomozepi, Manger, & Ihunwo, 2017). Our quantitative approach confirmed the highest number of DCX+ cells in Vl followed by DLv and DLd, while the lowest numbers of cells/mm^2 were detected in DMd. Further, ovoid migrating immature neurons were more abundant in regions of high to moderate levels of DCX expressing cells, except in Vl, where Tr immature neurons that have already reached their destination were more frequent. We underpinned the DCX results by the finding that mature, adult-born neurons also showed the highest amounts in Vl and DLv, which was determined with BrdU+/NeuN+ labeling after three month of BrdU injections. Functionally, newborn cells in the avian HF have been related to age (Meskenaite et al., 2016), food-deprivation i.e., stress (Robertson et al., 2017; Smulders, 2017), housing, i.e., environmental enrichment (Melleu et al., 2016), food storing (Sherry & Hoshooley, 2010), seasonal changes (Sherry & MacDougall-Shackleton, 2015) and spatial memory (Hall et al., 2014). To our knowledge, none of the studies mentioned earlier in this section studied the genesis of glial cells in the HF. Here we found higher numbers of BrdU+/GFAP+ labeled cells in all estimated subdivisions compared to newborn neurons. In contrast to newborn neurons, newborn glial cells were higher in Vm and DMd compared to all other subdivisions. In general, GFAP+ cells of different size were recognized all over the pigeon HF, with some of them showing long radial branches from the outer surface of Vm and Vl into the Tr region.

Anterior–posterior differences in adult neurogenesis were reported in a study that used radioactive labeled thymidine to mark newborn cells in the HF of black-capped chickadees (Barnea & Nottebohm, 1994). In the study by Barnea and Nottebohm (1994), higher levels of adult neurogenesis in the anterior HF, compared to middle and posterior HF in wild, but not in captive hold birds was demonstrated, which was interpreted in relation to spatial memory acquisition in wild birds visiting different places to collect food. Further, newborn cell numbers were found to decline from anterior to middle to caudal levels, and in relation to the survival time of birds after the injections. In addition, higher levels in the caudal HF of birds that socially interact compared to single caged birds were described (Barnea et al., 2006). The levels of adult neurogenesis changed during season of these food-hoarding species, showing that seasonal changes of behavior affect this rostrocaudal gradient and can result in similar levels of adult neurogenesis in the HF along the anterior–posterior axis (Hoshooley et al., 2007). Under stress conditions, Robertson et al. (2017) reported increased levels of corticosterone plasma levels and reduced levels of newborn cells in the neuronal lineage (BrdU+/Hu+) in food-restricted chicken in rostral HF. However, levels of BrdU+ cells alone decreased in both, caudal and rostral HF after one week of the injection with BrdU. No general differences in BrdU+/Hu+ or BrdU+ cells between rostral and caudal HF were reported, but BrdU+ cells in the ventricular zone showed higher amounts at rostral levels (Robertson et al., 2017). In line with this we found BrdU+/GFAP+ cells gradually decrease from anterior to posterior positions in Vl, showing that a higher number of dividing cells in the more anterior subdivision most likely find their fate in providing an optimal environment for neuronal function and survival. Taken together, our results fit in with former studies, reporting lower amounts of immature neurons at the caudal

pole, and no gradient in overall BrdU+ cells, although none of the studies investigated values for individual subdivisions. In other species, like zebra finches, brown-headed cowbirds and red-winged blackbirds variable neurogenesis levels along the anterior–posterior axis dependent on different housing conditions (social interaction), food storing behavior (spatial memory) and breeding conditions were reported (Barkan et al., 2016; Barnea et al., 2006; Barnea & Nottebohm, 1994; Guigueno, MacDougall-Shackleton, & Sherry, 2016). In our view, more precise studies with respect to the different subdivisions of the HF have to be conducted to relate our findings to functional specializations along the anterior–posterior axis that depend on or impact neurogenesis. Here, our findings provide a foundation upon which future studies can be conducted. Based on previous information on connectivity, neurogenesis, volume change and neurochemical data, Smulders (2017) introduced the idea of a functional specialization of the avian HF along the anterior–posterior axis, and compared the avian anterior pole of the HF to the dorsal pole in rodents (i.e., posterior HF in humans), and the avian posterior pole to the ventral pole in rodents (i.e., anterior HF in humans). Therefore, in the following sections we will now complement this idea with our results by comparing our findings to those in mammals.

4.3. *Comparison to the mammalian hippocampal formation – connectivity*

To date, there is no general consent which subdivisions of the avian HF correspond to their mammalian counterparts, i.e., the DG, CA fields, subiculum and entorhinal cortex, although many similarities between birds and mammals exist at all levels, i.e., anatomical, neurochemical, electrophysiological and functional, many similarities between birds and mammals exist (Abellan et al., 2014; Atoji et al., 2016; Bingman et al., 2017; Herold et al., 2014, 2015; Medina et al., 2017). Some authors argued therefore that thinking about the avian HF in terms of the strict organization such as seen in the mammalian hippocampus is likely insufficient to understand the HF of birds (Bingman & Muzio, 2017; Bingman et al., 2017; Herold et al., 2014, 2015). At the time, most researchers agree that the V-region/DM corresponds to DG/CA-fields and DL corresponds to the entorhinal cortex. Given the remarkable cognitive abilities of birds and the conserved role of the hippocampus in spatial memory, this however, makes the hippocampus of birds an exciting structure to explore the relationship between structure and function against the background of divergent evolutionary paths between mammals and birds of more than 300 Million years. Beside the morphological differences of avian and mammalian hippocampal structures, both structure share many similarities in connectivity (our data; Atoji & Wild, 2006). But what about rostro-caudal differences in connectivity? Strong evidence for a functional specialization along the dorsal–ventral axis (anterior–posterior in primates) of the hippocampus in mammals originate from lesion or inactivation studies (Anacker & Hen, 2017; Colombo et al., 1998; Fanselow & Dong, 2010; O'Leary and Cryan, 2014; Strange et al., 2014; Thompson et al., 2008; Witter et al., 2017). Consequently, the dorsal (septal) hippocampus, which corresponds to the posterior hippocampus in primates is involved in spatial memory and contextual memory encoding and performs primarily cognitive functions, while the ventral (temporal) hippocampus (anterior in primates), processes emotional (stress) and social behavior. Based on the small literature of functional differences in the avian HF along the anterior–posterior axis, this would fit with the idea that the avian anterior pole of the HF corresponds to the septal pole and the posterior HF to the temporal pole of the mammalian HF (Smulders, 2017). Besides, genetic analysis of several marker genes in mice has shown that the hippocampus exhibits different regional and laminar patterns of molecular domains along the dorso-ventral axis and that it can be further compartmentalized in dorsal, intermediate and ventral regions (Fanselow & Dong, 2010; Thompson et al., 2008) that partially overlap with the classification of these domains originally illustrated by Swanson and Cowan (1977). The molecular differences in hippocampal domains are underpinned by anatomic differences in connectivity, which are more prominent between the dorsal and ventral pole, while the intermediate region exhibits a mixture of connections of both, dorsal and ventral parts that discerns on the one hand but have yet not been fully functionally elucidated.

The dorsal (septal, posterior in primates) hippocampus sends massive projections to the dorsal subiculum, while both hippocampus and dorsal subiculum further project to the retrosplenial and anterior cingulate cortices, which are involved in cognitive processing of visuospatial information and memory. The dorsal subicular complex sends further massive parallel projections through the postcommisural fornix to the mammillary nuclei and anterior thalamic regions that in turn project back to the dorsal hippocampus and retrosplenial cortex. Additionally, dorsal CA1 and CA3 project to the caudal and lesser to the dorsal part of the medial zone of the lateral septal complex, which in turn project to the medial septal complex. The lack of a subdivision that is comparable to the subiculum and a more precise classification of the lateral septum (SL) in birds, makes it hard to compare this to the avian situation, but at least we can say that more anterior SL is connected to the anterior DM and further fibers that travel through the TSM connect to anterior DM and DL. Whether these fibers connect the hippocampus to brain stem nuclei and/or diencephalic nuclei or branch to other septal nuclei was not investigated in this study, but will be of interest for future analysis. Based on prior studies, in birds, HF-septal connectivity is less reciprocal, with a significant higher number of afferents from the HF to the septum that is different compared to mammals (Atoji and Wild, 2004; Casini et al., 1986; Montagnese et al., 2004). SL in birds is further receiving a high quantity of visual inputs from diencephalic nuclei, and has prominent connections with hypothalamic nuclei, as well as dopaminergic, serotonergic, noradrenergic and cholinergic inputs (Atoji and Wild, 2004). In addition, the dorsal subiculum as well as the lateral and medial entorhinal cortex of mammals sent further projections to the rostrolateral nucleus accumbens (NAc) and rostral caudate-putamen, which are in turn connected in the so called functional "caudal behavior control column" underlying expression of exploratory behavior, including locomotion, spatial direction and orientation of movements (Swanson & Kalivas, 2000). Direct fiber connections between rostral hippocampal subfields and the NAc were not observed in this study but

between NAc and anterior SL. This finding is in contrast to the tracing study of Atoji et al. (2002) and Atoji and Wild (2004), reporting rostral projections from DL and DM to the medial striatum. However, it is possible that these small number of projections travel under the massive fiber bundles of TSM along the medial wall at the anterior position around A 10.50 (beginning of NAc) and get indistinguishable in our study. Although, no rostro-caudal differences were seen, connectivity to visual areas in the hyperpallium (HA, HL, HD) and the area CDL were confirmed, which in turn connect to the nidopallium caudolaterale (NCL), the analogue of the prefrontal cortex in the pigeon brain and other nidopallial areas (Güntürkün, 2005). This opens up the possibility for the avian HF to connect to higher order areas like the mammalian HF connects to the prefrontal and cingulate areas. Together, our data supports the idea that the anterior hippocampus in birds is stronger involved in visuo-spatial processing but the specialization is less clear compared to the mammalian situation.

The mammalian ventral CA1 on the other hand, projects to several olfactory areas, and shares, together with the ventral subiculum, a bidirectional connectivity to the amygdala nuclei, preferably those that receive massive olfactory inputs (Anderson, Morris, Amaral, Bliss, & O'Keefe, 2007; Cenquizca and Swanson, 2007; Pitkänen et al., 2000; Roberts et al., 2007; Witter & Amaral, 2004). In the pigeon, we confirmed connectivity at medial to caudal levels along the anterior–posterior axis between the HF and the nucleus taeniae of the amygdala (TnA), which is the only amygdala nucleus that receives direct olfactory input from the olfactory bulb according to Patzke, Manns, and Güntürkün (2011). Connectivity to the posterior nucleus of the amygdala (PoA) did not show any specialization along the anterior–posterior axis. In mammals, ventral CA1/subiculum and the amygdala nuclei also share a bidirectional connectivity with pre- and infralimbic and agranular insular cortices (Roberts et al., 2007; Thierry et al., 2000). It was speculated that the hyperpallium densocellulare (HD) in birds shares similarities with the insular cortex of mammals, despite a completely different connectivity (Medina & Reiner, 2000). However, we observed connections between HD and HF, but like the connectivity with the CPi no anterior–posterior specialization was revealed. In mammals, the ventral CA1 and subiculum are further connected either directly or indirectly to the central and medial amygdala, massively to rostral and ventral parts of the lateral septum and the bed nucleus of the stria terminalis to innervate the periventricular and medial zones of the hypothalamus. Thereby, the ventral hippocampus is integrated in a network controlling neuroendocrine, autonomic and somatic motor activities in motivated behaviors, which explains its involvement in fear or aversive learning tasks or stress related responses. Here, direct connections with BSTL were detected but seem to be widespread, while septal connections are topological to the medial and lateral caudal septum. In contrast to SL, the medial septum (SM) is more specifically connected to individual nuclei of the hypothalamus (Atoji and Wild, 2004). In mammals, additionally the ventral CA1 and subiculum, as well as the medial band of the lateral and medial entorhinal cortex give rise to projections to the caudomedial NAc, which plays an important role in reward processing and feeding behavior (Bagot et al., 2015; Walker, Miles, & Davis, 2009). Nothing comparable was observed in the pigeon brain. However, we detected a direct connection of caudal DM with the nucleus PVM, which is the homologue of a portion of the nucleus paraventricularis of the hypothalamus (PVN) in mammals (Berk, 1987). This connection was described earlier in pigeons as projections from the caudal dorsomedial portion of the HF to the PVM (Bons et al., 1976; Bouillé & Baylé, 1973). In mammals, the PVN receives afferents from the subiculum, primary the ventral subiculum (Silverman, Hoffmann, & Zimmermann, 1981) and CA1 (Pakhomova, 1981), which would fit with the theory that caudal HF is comparable to the temporal pole of the HF in mammals, i.e., ventral HF in rodents, and anterior HF in primates.

In rodents, commissural fibers of the hippocampus are organized topographically along the dorso-ventral axis, which is also true for the pigeon anterior–posterior axis. In monkeys, commissural fibers were detected only in the rostral part of both, the DG and the CA fields, whereas the subicular subdivisions and the entorhinal cortex show many commissural connections and most of them are topographically organized (Anderson et al., 2007), while in humans, commissural fibers seem to be absent (Wilson et al., 1991).

Further, we detected numerous thin fibers traveling along anterior–posterior axis along the dorsal regions DLd and DMd. In rodents and monkeys, longitudinally fibers were mostly found in CA3 and DG to propagate information along the septo-temporal axis. CA3 longitudinal fibers originate from the pyramidal cells of the pyramidal layer of CA3, while in DG cells of the hilar region are the source of these fibers that are called associative fibers and are very important for building associative spatial relations between cues and environment (Anderson et al., 2007). In addition, the subiculum gives rise to a longitudinal associative projection that extends from the level of origin to the subiculum at the temporal pole. Recently, in humans, a large number of longitudinally traveling fibers have been observed with 3D-PLI in the alveus of CA1 that are perforant path fibers in the stratum lacunosum-moleculare that cross the hippocampal fissure en route to the dentate molecular layer as well as between entorhinal fibers and the subiculum (Zeineh et al., 2017). However, at the moment, any comparison to the mammalian situation would be purely speculative and our findings of the local circuitry need to be further evaluated by precise tracing studies controlling for the origin of these fibers, although they do not seem to complement the unmyelinated fibers of mossy cells, which would be rarely seen in 3D-PLI due to the maximal sensitivity of PLI to the birefringent properties of myelin.

To sum up, our data and data from tracing studies clearly support a specialization along the anterior–posterior HF in birds, with anterior HF resembling the septal pole and posterior HF resembling the temporal pole of mammals. Further, the finding of a direct connection to PVM with caudal DM as well as the emergence of longitudinal fibers in DM makes it likely that DM exhibits subicular/CA1/CA3 characteristics that need to be revisited and presumably leads to an additional parceling of DM into more subdivisions instead of two (DMd, DMv).

4.4. *Comparison to the mammalian hippocampal formation – adult neurogenesis*

Although deriving from a different neurogenic niche compared to birds, the mammalian hippocampus of diverse species including humans is capable of adult neurogenesis during lifespan, i.e., generating new neurons from neural stem cells in the subgranular zone (but see Bingman et al., 2017; Gage, 2000; Kempermann, 2012; Kempermann et al., 2018; Ming and Song, 2005 for review). In mammals, the highest levels of newborn neurons marked with BrdU and additional markers were detected in DG, while we detected the highest numbers of newborn neurons in the Vl-region. However, in birds, the occurrence of immature neurons appeared not to be exclusively to the V-region but is also prominent in other subdivisions of the HF, including the proposed homologues of CA subfields, subicular and entorhinal cortex, which are relatively sparse labeled with DCX in mammals, although DCX expression is not completely absent (Kremer et al., 2013). This is a major but known species difference, reflecting generally higher levels of plasticity in the avian brain (as well as in fish, reptiles and amphibians) compared to mammals. The same is also true for DCX+ cells that have been detected outside the HF (Ernst & Frisén, 2015; Melleu et al., 2013). In rodents, it has been shown that DCX+ cells have different electrophysiological firing properties compared to mature neurons. This seems to be independent of their brain localization and presumably indicates particular plasticity that is necessary to adapt to environmental changes and to process specific information (Klempin, Kronenberg, Cheung, Kettenmann, & Kempermann, 2011; Spamanato et al., 2012). To our knowledge, no comparable studies in birds exist and thus our findings and those from others should stimulate future electrophysiological studies in birds. However, assuming that the response properties of immature neurons in the avian HF are comparable to those of mammals, birds may have additional mechanisms and faster cellular responses to adopt to environmental changes because they express higher levels of immature neurons.

Equally to the avian HF, adult neurogenesis in mammals varies according to different tasks that have been used to study the role of newborn neurons in relation to function (activity), physiological and pathological stimuli (Christian, Song, & Ming, 2014; Ming & Song, 2011; Snyder, Radik, Wojtowicz, & Cameron, 2009). In mammals, adult neurogenesis in the DG supports memory pattern separation based on space to contextualize (disambiguate) multiple memories (Clelland et al., 2009; Yassa & Stark, 2011), a function that is also supported by the avian HF (Herold et al., 2015). Further, in mammals, adult neurogenesis is involved in inflammatory pain (Zheng et al., 2017), cognitive flexibility (Anacker & Hen, 2017), stress (Tanti et al., 2013) and anxiety/depression like behaviors (O'Leary and Cryan, 2014). In line with anatomical specializations along the dorso-ventral axis, general differences and functional specializations of mammalian ventral and dorsal domains in the context of adult neurogenesis were observed. Generally, DXC+ cells were found at higher levels in the septal (dorsal) pole of the DG of marmosets and mice compared to the temporal (ventral) pole, while proliferating Ki67 + or Ki67+/PCNA+ cells did not differ (Amrein et al., 2015; Anacker & Hen, 2017). Additionally, DCX+ cells were generally higher in the suprapyramidal blade compared to the infrapyramidal blade and radial glia/progenitor cells were detected at lower levels in the infrapyramidal blade of ventral DG compared to all DG subdivisions (Jinno, 2011). Higher levels of DCX+ cells were also observed in canine dorsal hippocampus (Lowe et al., 2015). In the dorsal hippocampus of rats, DCX+, BrdU+, Ki67+ and BrdU+/DCX+ cells showed higher levels compared to ventral 9 days after BrdU injections (Ho & Wang, 2010). In line with these observations our data complement those findings and show further similarities between the avian and mammalian HF. Interestingly, we also found differences in the number of DCX+ cells and BrdU/NeuN+ newborn neurons between Vl and Vm, with higher levels of adult neurogenesis in Vl compared to Vm. In our study, pigeons generally lived in an enriched environment in their loft and were allowed to fly freely. Further, in rodents that performed complex spatial and contextual stimulation in an enriched environment neurogenesis was increased in dorsal DG (Kempermann, Kuhn, & Gage, 1997; Snyder et al., 2009; Tanti et al., 2012, 2013), while exposure to chronic stress severely reduces levels of proliferation, differentiation and survival of neurons in the ventral DG but also affects dorsal portions to some levels if simultaneously contextual memory learning is acquired (Anacker & Hen, 2017; Hawley, Morch, Christie, & Leasure, 2012; O'Leary and Cryan, 2014; Snyder et al., 2009; Tanti et al., 2013). Together, data from neurogenesis experiments further point to similarities of septal HC in mammals and anterior HF in birds, and temporal HC and posterior HF. However, one recent study in chickens showed that food deprivation, which was accompanied by increased corticosterone levels results in decreased levels of neuronal progenitors in the rostral pole, while new neurons decreased in both, caudal and rostral poles (Robertson et al., 2017). However, in rodents it was shown that sometimes chronic stress also affects neurogenesis in the septal pole, and seems to be highly dependent on the context in which animals were tested (Ho & Wang, 2010; O'Leary and Cryan, 2014; Snyder et al., 2009). Clearly more functional studies in birds, as well as in mammals are needed that explore the relationship of adult neurogenesis and functional specialization along the septo-temporal axis to a better understanding of these interactions.

4.5. *Evolutionary connectomics*

The hippocampus in all vertebrates emerges during development from the same dorsomedial region of the procencephalic alar plate (Bingman, Salas, & Rodriguez, 2009; Butler & Hodos, 2005; Hevner, 2016; Nomura & Hirata, 2017; Striedter, 2005), except ray-finned fish, where the homologue is at a dorsolateral position, which adopts because the embryonic telencephalon does not evaginate but, instead, everts (Striedter & Northcutt, 2006). In non-mammalian species, the homologue of the hippocampus is called medial or dorsomedial pallium (Hevner, 2016). During more than 300 Million years of separate evolution from a basal hippocampus of amphibians or non-sauropsids, compared to both, avian and mammalian

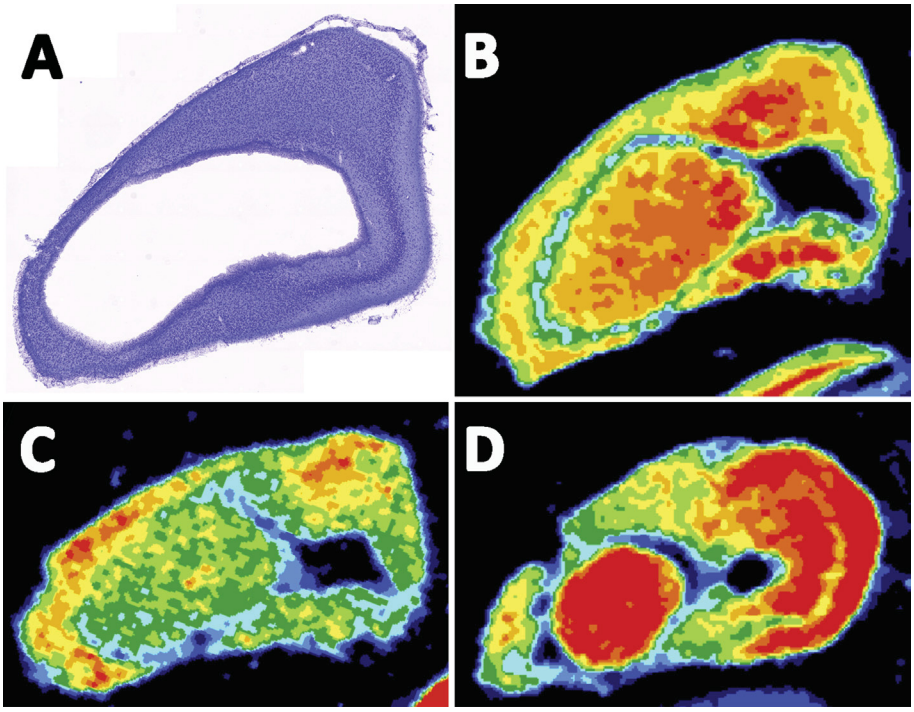

Fig. 14 – The caudal V-region of the pigeon hippocampus. A: Nissl staining showing the tri-laminated part of the V-region in a coronal section at approximately atlas level A 3.50–3.25. B–D: AMPA (B), Kainate (C) and NMDA (D) receptor expression in the caudal V-region (supplementary data figures not shown in Herold et al., 2014). Red indicates high densities while blue indicates low densities. Scales are different.

hippocampi have increased in size and complexity and evolved different cytoarchitectonical organizations (Bingman et al., 2017; Striedter, 2016). Further positional changes occurred. While in reptiles and birds, the HF is largely located periventricular in a dorsal region of the medial wall of the telencephalon, in mammals, only the primordium of the hippocampal complex (fimbria, DG, Ammon's horn, subiculum, and entorhinal cortex) is located dorso-medially but comes to lie ventrally within the development of the neocortices. In addition, the DG becomes variably convoluted among mammals (Hevner, 2016; Witter et al., 2017). However, a thin remnant of the HF surrounds the splenium of the corpus callosum that ascends dorsally over the corpus callosum to form the induseum griseum, which comprises remnants of the subiculum and other fields of the HF (Anderson et al., 2007).

In the hippocampus of reptiles, tri-lamination emerged that was accompanied by an enlargement of other pallial regions, while in birds, the HF displays a more cellular structure reflecting a presumptive reduction of lamination that was accompanied by a substantial increase in hippocampus size (Bingman et al., 2017; Hevner, 2016; Striedter, 2016). In mammals, lamination occurs inside-out in the HF, accept in DG were migration occurs outside-in. This process strongly depends on radial glia scaffold and reelin secretion of Cajal-Retzius cells (Frotscher & Seress, 2007). Cajal-Retzius cells are also prominent during development of the avian medial pallium (Nomura, Takahashi, Hara, & Osumi, 2008) but in contrast to the mammalian medial pallium do not migrate to the dorsal preplate, nor do other progenitor cells from the cortical hem or the medial pallium give rise to migrating cells to the dorsal pallium (García-Moreno et al., 2018). However, this seems to be different from lizards (Cabrera-Soccoro et al., 2007), and needs to be further explored along the axis of the cortical hem/medial pallium, but may be one reason of the different structure of mammalian, reptilian and avian hippocampal as well as neocortical regions. In case of the avian hippocampus, which derives from a more dorsomedial position and has largely expanded, this might also explain the different morphology of the most caudal–ventral parts of the V-region, where a clear tri-laminar structure is visible (Fig. 14) compared to more rostral parts of the V-region, where the cellular line splits up into two blades or becomes convoluted. Analysis of single-cell transcriptomics of the reptilian medial most pallium, particularly the dorsomedial cortex, has been shown that preliminary precursors of the hippocampal regions, including the DG, cornu ammonis 1 (CA1) and cornu ammonis (CA3) were already present in the ancestor of all amniotes (Tosches et al., 2018), which is also supported by a recently developmental analysis of chick, lizard and mouse hippocampus by Medina et al. (2017). These findings and our recent data, however, make it unlikely that the DG has recently evolved as an add-on structure of the mammalian species suggested earlier by Kempermann (2012). Instead an anlage of the DG in the least common ancestor must have been already existed that was highly morphologically transformed during million years of separate evolution with still conserved functionality.

5. Conclusion

Birds have extraordinary cognitive abilities that even exceed those of some primates, and they achieve this even without a layered structure of their pallial derivatives but with conserved functional loops between brain structures, including hippocampal connectivity and some similar properties of cells contributing to these circuits. In addition, in many cases the organization principles of hippocampal network connectivity, i.e., anterior–posterior differences seem to be conserved. On the other hand, over more than 300 Million years of separate evolution in adaption to an ecologic niche may have led to further neuronal specializations resembling an alternative route to functionally adopt, reaching the apex of avian evolution in a highly competitive world among other animals including humans. Moreover, high forms of plasticity in the avian brain, validated by DCX expression in various brain regions, may indicate the promotion of further development and evolution of brain structures, and perhaps the ability for rapid adaptation to environmental changes, which may be a selective advantage at some point.

Funding

The 3D-PLI related part of the presented study was supported by the European Union's Horizon 2020 Research and Innovation Program under Grant Agreement No. 720270 (Human Brain Project, SGA1) and No. 785907 (Human Brain Project, SGA2).

Acknowledgments

We thank Nicole Delhaes for preparing the immunohistochemistry and the Western Blots and Isabelle Masson and Dustin Hullin for help with the cell counting. We would also like to thank Christian Schramm, Patrick Nysten and Steffen Werner for preparing the pigeon brain slices for the 3D-PLI experiments and Karl Zilles for help with the data interpretation in the beginning of the 3D-PLI experiments. The authors gratefully acknowledge the computing time granted through JARA-HPC on the supercomputer JURECA at Forschungszentrum Jülich. We further thank David Gräßel who supervised the 3D-PLI work, helped with the preparation of 3D-PLI data and the methods section.

REFERENCES

Abellan, A., Desfilis, E., & Medina, L. (2014). Combinatorial expression of Lef1, Lhx2, Lhx5, Lhx9, Lmo3, Lmo4, and Prox1 helps to identify comparable subdivisions in the developing hippocampal formation of mouse and chicken. *Frontiers in Neuroanatomy, 4*, 8–59.

Amrein, I., Nosswitz, M., Slomianka, L., van Dijk, R. M., Engler, S., Klaus, F., et al. (2015). Septo-temporal distribution and lineage progression of hippocampal neurogenesis in a primate (Callithrix jacchus) in comparison to mice. *Frontiers in Neuroanatomy, 9*, 85. https://doi.org/10.3389/fnana.2015.00085.

Anacker, C., & Hen, R. (2017). Adult hippocampal neurogenesis and cognitive flexibility – linking memory and mood. *Nature Reviews. Neuroscience, 18*, 335–346.

Anderson, P., Morris, R., Amaral, D., Bliss, T., & O'Keefe, J. (2007). *The hippocampus book*. Oxford University Press.

Atoji, Y., Saito, S., & Wild, J. M. (2006). Fiber connections of the compact division of the posterior pallial amygdala and lateral part of the bed nucleus of the stria terminalis in the pigeon (Columba livia). *Journal of Comparative Neurology, 499*, 161–182.

Atoji, Y., Sarkar, S., & Wild, J. M. (2016). Proposed homology of the dorsomedial subdivision and V-shaped layer of the avian hippocampus to Ammon's horn and dentate gyrus, respectively. *Hippocampus, 26*, 1608–1617.

Atoji, Y., & Wild, J. M. (2004). Fiber connections of the hippocampal formation and septum and subdivisions of the hippocampal formation in the pigeon as revealed by tract-tracing and kainic acid lesions. *Journal of Comparative Neurology, 475*, 426–461.

Atoji, Y., & Wild, J. M. (2005). Afferent and efferent connections of the dorsolateral corticoid area and a comparison with connections of the temporo-parieto-occipital area in the pigeon (Columba livia). *Journal of Comparative Neurology, 485*, 165–182.

Atoji, Y., & Wild, J. M. (2006). Anatomy of the avian hippocampal formation. *Reviews in the Neurosciences, 17*, 3–15.

Atoji, Y., Wild, J. M., Yamamoto, Y., & Suzuki, Y. (2002). Intratelencephalic connections of the hippocampus in pigeons (Columba livia). *Journal of Comparative Neurology, 447*, 177–199.

Axer, M., Amunts, K., Gräßel, D., Palm, C., Dammers, J., Axer, H., et al. (2011). A novel approach to the human connectome: Ultra-high resolution mapping of fiber tracts in the brain. *NeuroImage, 54*, 1091–1101. https://doi.org/10.1016/j.neuroimage.2010.08.075.

Axer, M., Gräßel, D., Kleiner, M., Dammers, J., Dickscheid, T., Reckfort, J., et al. (2011). High-resolution fiber tract reconstruction in the human brain by means of three-dimensional polarized light imaging. *Frontiers in Neuroinformatics, 5*(34). https://doi.org/10.3389/fninf.2011.00034.

Bagot, R. C., Parise, E. M., Peña, C. J., Zhang, H. X., Maze, I., Chaudhury, D., et al. (2015). Ventral hippocampal afferents to the nucleus accumbens regulate susceptibility to depression. *Nature Communications, 6*, 7062. https://doi.org/10.1038/ncomms8062.

Balthazart, J., & Ball, G. (2014). Doublecortin is a highly valuable endogenous marker of adult neurogenesis in canaries. *Brain, Behavior and Evolution, 84*, 1–4.

Balthazart, J., Boseret, G., Konkle, A. T. M., Hurley, L. L., & Ball, G. F. (2008). Doublecortin as a marker of adult neuroplasticity in the canary song control nucleus HVC. *The European Journal of Neuroscience, 27*, 801–817.

Balthazart, J., Charlier, T. D., Barker, J. M., Yamamura, T., & Ball, G. F. (2010). Sex steroid-induced neuroplasticity and behavioural activation in birds. *The European Journal of Neuroscience, 32*, 2116–2132.

Barami, K., Iversen, K., Furneaux, H., & Goldman, S. A. (1995). Hu protein as an early marker of neuronal phenotypic differentiation by subependymal zone cells of the adult songbird forebrain. *Journal of Neurobiology, 28*, 82–101.

Barkan, S., Roll, U., Yom-Tov, Y., Wassenaar, L. I., & Barnea, A. (2016). Possible linkage between neuronal recruitment and flight distance in migratory birds. *Scientific Reports, 6*, 21983. https://doi.org/10.1038/srep21983.

Barnea, A., Mishal, A., & Nottebohm, F. (2006). Social and spatial changes induce multiple survival regimes for new neurons in two regions of the adult brain: An anatomical representation of time? *Behavioural Brain Research, 167*, 63–74.

Barnea, A., & Nottebohm, F. (1994). Seasonal recruitment of hippocampal neurons in adult free-ranging black-capped chickadees. *Proceedings of the National Academy of Sciences of the United States of America, 91*, 11217–11221.
Benowitz, L. I., & Karten, H. J. (1976). The tractus infundibuli and other afferents to the parahippocampal region of the pigeon. *Brain Research, 102*, 174–180.
Berk, M. L. (1987). Projections of the lateral hypothalamus and bed nucleus of the stria terminalis to the dorsal vagal complex in the pigeon. *Journal of Comparative Neurology, 260*, 140–156.
Bingman, V. P., & Muzio, R. N. (2017). Reflections on the structural-functional evolution of the hippocampus: What is the big deal about a dentate gyrus? *Brain, Behavior and Evolution, 90*, 53–61. https://doi.org/10.1159/000479095.
Bingman, V. P., Rodriguez, F., & Salas, C. (2017). The hippocampus of nonmammalian vertebrates. *Evolution of Nervous Systems, 2nd ed., 1*, 479–489. https://doi.org/10.1016/B978-0-12-804042-3.00013-0.
Bingman, V. P., Salas, C., & Rodriguez, F. (2009). Evolution of the hippocampus. In *Encyclopedia of neuroscience* (pp. 1356–1360). Berlin, Heidelberg: Springer.
Bolhuis, J. J., & Wynne, C. D. (2009). Can evolution explain how minds work? *Nature, 458*, 832–833. https://doi.org/10.1038/458832a.
Bons, N., Bouillé, C., Baylé, J. D., & Assenmacher, I. (1976). Light and electron microscopic evidence of hypothalamic afferences originating from the hippocampus in the pigeon. *Experientia, 32*(11), 1443–1445.
Bouillé, C., & Baylé, J. D. (1973). Effects of limbic stimulations or lesions on basal and stress-induced hypothalamic-pituitary-adrenocortical activity in the pigeon. *Neuroendocrinology, 13*, 264–277. https://doi.org/10.1159/000122211.
Butler, A. B., & Hodos, W. (2005). *Comparative vertebrate neuroanatomy: Evolution and adaptation*. John Wiley & Sons.
Butler, A. B., Reiner, A., & Karten, H. J. (2011). Evolution of the amniote pallium and the origins of mammalian neocortex. *Annals of the New York Academy of Sciences, 1225*, 14–27. https://doi.org/10.1111/j. 1749-6632. 2011.06006.x.
Cabrera-Socorro, A., Hernandez-Acosta, N. C., Gonzalez-Gomez, M., & Meyer, G. (2007). Comparative aspects of p73 and Reelin expression in Cajal-Retzius cells and the cortical hem in lizard, mouse and human. *Brain Research, 1132*, 59–70.
Casini, G., Bingman, V. P., & Bagnoli, P. (1986). Connections of the pigeon dorsomedial forebrain studied with WGA-HRP and 3H-proline. *Journal of Comparative Neurology, 245*, 454–470.
Cenquizca, L. A., & Swanson, L. W. (2007). Spatial organization of direct hippocampal field CA1 axonal projections to the rest of the cerebral cortex. *Brain Research Reviews, 56*, 1–26.
Chakraborty, M., & Jarvis, E. D. (2015). Brain evolution by brain pathway duplication. *Philosophical Transactions of the Royal Society of London. Series B, Biological sciences, 370*. https://doi.org/10.1098/rstb.2015.0056. pii: 20150056.
Christian, K. M., Song, H., & Ming, G. L. (2014). Functions and dysfunctions of adult hippocampal neurogenesis. *Annual Review of Neuroscience, 37*, 243–262. https://doi.org/10.1146/annurev-neuro-071013-014134.
Clelland, C. D., Choi, M., Romberg, C., Clemenson, G. D., Jr., Fragniere, A., Tyers, P., et al. (2009). A functional role for adult hippocampal neurogenesis in spatial pattern separation. *Science, 325*, 210–213. https://doi.org/10.1126/science.1173215.
Colombo, M., & Broadbent, N. (2000). Is the avian hippocampus a functional homologue of the mammalian hippocampus? *Neuroscience and Biobehavioral Reviews, 24*, 465–484.
Colombo, M., Fernandez, T., Nakamura, K., & Gross, C. G. (1998). Functional differentiation along the anterior-posterior axis of the hippocampus in monkeys. *Journal of Neurophysiology, 80*, 1002–1005.
Dong, H.-W., Swanson, L. W., Chen, L., Fanselow, M. S., & Toga, A. W. (2009). Genomic–anatomic evidence for distinct functional domains in hippocampal field CA1. *Proceedings of the National Academy of Sciences of the United States of America, 106*, 11794–11799.
Ernst, A., & Frisén, J. (2015). Adult neurogenesis in humans – common and unique traits in mammals. *PLoS Biology, 13*, e1002045. https://doi.org/10.1371/journal.pbio. 1002045.
Fanselow, M. S., & Dong, H. W. (2010). Are the dorsal and ventral hippocampus functionally distinct structures? *Neuron, 65*, 7–19.
Frotscher, M., & Seress, L. (2007). Morphological development of the hippocampus. In *The hippocampus book*. Oxford University Press.
Gabi, M., Neves, K., Masseron, C., Ribeiro, P. F., Ventura-Antunes, L., Torres, L., et al. (2016). No relative expansion of the number of prefrontal neurons in primate and human evolution. *Proceedings of the National Academy of Sciences of the United States of America, 113*, 9617–9622.
Gage, F. H. (2000). Mammalian neural stem cells. *Science, 287*, 1433–1438. https://doi.org/10.1126/science.287.5457.1433.
Gagliardo, A., Ioale, P., & Bingman, V. P. (1999). Homing in pigeons: The role of the hippocampal formation in the representation of landmarks used for navigation. *The Journal of Neuroscience: the Official Journal of the Society for Neuroscience, 19*, 311–315.
García-Moreno, F., Anderton, E., Jankowska, M., Begbie, J., Encinas, J. M., Irimia, M., et al. (2018). Absence of tangentially migrating glutamatergic neurons in the developing avian brain. *Cell Reports, 22*, 96–109. https://doi.org/10.1016/j.celrep.2017.12.032.
Guigueno, M. F., MacDougall-Shackleton, S. A., & Sherry, D. F. (2016). Sex and seasonal differences in hippocampal volume and neurogenesis in brood-parasitic brown-headed cowbirds (Molothrus ater). *Developmental Neurobiology, 76*, 1275–1290.
Güntürkün, O. (2005). The avian 'prefrontal cortex' and cognition. *Current Opinion in Neurobiology, 15*, 686–693.
Güntürkün, O., & Bugnyar, T. (2016). Cognition without cortex. *Trends in Cognitive Sciences, 20*, 291–303. https://doi.org/10.1016/j.tics.2016.02.001.
Güntürkün, O., Ströckens, F., Scarf, D., & Colombo, M. (2017). Apes, feathered apes, and pigeons: Differences and similarities. *Current Opinion in Behavioral Sciences, 16*, 35–40.
Hall, Z. J., Delaney, S., & Sherry, D. F. (2014). Inhibition of cell proliferation in black-capped chickadees suggests a role for neurogenesis in spatial learning. *Developmental Neurobiology, 74*, 1002–1010. https://doi.org/10.1002/dneu.22180.
Hawley, D. F., Morch, K., Christie, B. R., & Leasure, J. L. (2012). Differential response of hippocampal subregions to stress and learning. *PLoS One, 7*, e53126. https://doi.org/10.1371/journal.pone.0053126.
Herculano-Houzel, S., Catania, K., Manger, P. R., & Kaas, J. H. (2015). Mammalian brains are made of these: A dataset of the numbers and densities of neuronal and nonneuronal cells in the brain of glires, primates, scandentia, eulipotyphlans afrotherians and artiodactyls, and their relationship with body mass. *Brain, Behavior and Evolution, 86*, 145–163.
Herold, C., Bingman, V. P., Ströckens, F., Letzner, S., Sauvage, M., Palomero-Gallagher, N., et al. (2014). Distribution of neurotransmitter receptors and zinc in the pigeon (Columba livia) hippocampal formation: A basis for further comparison with the mammalian hippocampus. *Journal of Comparative Neurology, 522*, 2553–2575.
Herold, C., Coppola, V. J., & Bingman, V. P. (2015). The maturation of research into the avian hippocampal formation: Recent discoveries from one of the nature's foremost navigators. *Hippocampus, 25*, 1193–1211.
Herold, C., Paulitschek, C., Palomero-Gallagher, N., Güntürkün, O., & Zilles, K. (2018). Transmitter receptors reveal segregation of the arcopallium/amygdala complex in pigeons (Columba livia). *Journal of Comparative Neurology, 526*, 439–466.

Hevner, R. F. (2016). Evolution of the mammalian dentate gyrus. *Journal of Comparative Neurology, 524*, 578–594.
Hoshooley, J. S., Phillmore, L. S., Sherry, D. F., & Macdougall-Shackleton, S. A. (2007). Annual cycle of the black-capped chickadee: Seasonality of food-storing and the hippocampus. *Brain, Behavior and Evolution, 69*, 161–168.
Hough, G. E., 2nd, Pang, K. C., & Bingman, V. P. (2002). Intrahippocampal connections in the pigeon (Columba livia) as revealed by stimulation evoked field potentials. *Journal of Comparative Neurology, 452*, 297–309.
Ho, Y. C., & Wang, S. (2010). Adult neurogenesis is reduced in the dorsal hippocampus of rats displaying learned helplessness behavior. *Neuroscience, 171*, 153–161.
Jinno, S. (2011). Topographic differences in adult neurogenesis in the mouse hippocampus: A stereology-based study using endogenous markers. *Hippocampus, 21*, 467–480.
Jones, R. C. (1941). A new calculus for the treatment of optical systems. *Journal of the Optical Society of America, 31*, 488–493.
Kaas, J. H., & Stepniewska, I. (2015). Evolution of posterior parietal cortex and parietal-frontal networks for specific actions in primates. *Journal of Comparative Neurology, 524*, 595–608. https://doi.org/10.1002/cne.23838.
Karten, H. J. (2015). Vertebrate brains and evolutionary connectomics: On the origins of the mammalian 'neocortex'. *Philosophical Transactions of the Royal Society of London. Series B, Biological sciences, 370*. https://doi.org/10.1098/rstb.2015.0060. pii: 20150060.
Karten, H. J., & Hodos, W. (1967). *A stereotaxic atlas of the brain of the pigeon (Columba livia)*. Baltimore: John Hopkins University Press.
Kempermann, G. (2012). New neurons for "survival of the fittest. *Nature Reviews. Neuroscience, 13*, 727–736.
Kempermann, G., Gage, F. H., Aigner, L., Song, H., Curtis, M. A., Thuret, S., et al. (2018). Human adult neurogenesis: Evidence and remaining questions. *Cell Stem Cell*. https://doi.org/10.1016/j.stem.2018.04.004. pii: S1934-5909(18)30166-30168.
Kempermann, G., Kuhn, H. G., & Gage, F. H. (1997). More hippocampal neurons in adult mice living in an enriched environment. *Nature, 386*, 493–495.
Kim, Y. H., Peregrine, J., & Arnold, A. P. (2006). The distribution of expression of doublecortin (DCX) mRNA and protein in the zebra finch brain. *Brain Research, 1106*, 189–196.
Klempin, F., Kronenberg, G., Cheung, G., Kettenmann, H., & Kempermann, G. (2011). Properties of doublecortin-(DCX)-expressing cells in the piriform cortex compared to the neurogenic dentate gyrus of adult mice. *PLoS One, 6*, e25760. https://doi.org/10.1371/journal.pone.0025760.
Krayniak, P. F., & Siegel, A. (1978a). Efferent connections of the hippocampus and adjacent regions in the cortex. *Brain, Behavior and Evolution, 15*, 372–388.
Krayniak, P. F., & Siegel, A. (1978b). Efferent connections of the septal area in the pigeon. *Brain, Behavior and Evolution, 15*, 389–404.
Krebs, J. R., Erichsen, J. T., & Bingman, V. P. (1991). The distribution of neurotransmitters and neurotransmitter-related enzymes in the dorsomedial telencephalon of the pigeon (Columba livia). *Journal of Comparative Neurology, 314*, 467–477.
Kremer, T., Jagasia, R., Herrmann, A., Matile, H., Borroni, E., Francis, F., et al. (2013). Analysis of adult neurogenesis: Evidence for a prominent "non-neurogenic" DCX protein pool in rodent brain. *PLoS One, 8*(5). https://doi.org/10.1371/journal.pone.0059269. e59269.
Kröner, S., & Güntürkün, O. (1999). Afferent and efferent connections of the caudolaterale neostriatum in the pigeon (Columba livia): A retro-and anterograde pathway tracing study. *Journal of Comparative Neurology, 407*, 228–260.
Lowe, A., Dalton, M., Sidhu, K., Sachdev, P., Reynolds, B., & Valenzuela, M. (2015). Neurogenesis and precursor cell differences in the dorsal and ventral adult canine hippocampus. *Neuroscience Letters, 593*, 107–113. https://doi.org/10.1016/j.neulet.2015.03.017.
MacPhail, E. M. (2002). The role of the avian hippocampus in spatial memory. *Psicológica, 23*, 93–108.
Mazengenya, P., Bhagwandin, A., Manger, P. R., & Ihunwo, A. O. (2018). Putative adult neurogenesis in old world parrots: The Congo African grey parrot (Psittacus erithacus) and Timneh grey parrot (Psittacus timneh). *Frontiers in Neuroanatomy, 12*, 7. https://doi.org/10.3389/fnana.2018.00007.
Mazengenya, P., Bhagwandin, A., Nkomozepi, P., Manger, P. R., & Ihunwo, A. O. (2017). Putative adult neurogenesis in two domestic pigeon breeds (Columba livia domestica): Racing homer versus utility carneau pigeons. *Neural Regeneration Research, 12*, 1086–1096. https://doi.org/10.4103/1673-5374.211187.
Medina, L., & Abellan, A. (2009). Development and evolution of the pallium. *Seminars in Cell & Developmental Biology, 20*, 698–711.
Medina, L., Abellán, A., & Desfilis, E. (2017). Contribution of genoarchitecture to understanding hippocampal evolution and development. *Brain, Behavior and Evolution, 90*, 25–40. https://doi.org/10.1159/000477558.
Medina, L., & Reiner, A. (2000). Do birds possess homologues of mammalian primary visual, somatosensory and motor cortices? *Trends in Neurosciences, 23*, 1–12.
Melleu, F. F., Pinheiro, M. V., Lino-de-Oliveira, C., & Marino-Neto, J. (2016 May). Defensive behaviors and prosencephalic neurogenesis in pigeons (Columba livia) are affected by environmental enrichment in adulthood. *Brain Structure & Function, 221*(4), 2287–2301. https://doi.org/10.1007/s00429-015-1043-6.
Melleu, F. F., Santos, T. S., Lino-de-Oliveira, C., & Marino-Neto, J. (2013). Distribution and characterization of doublecortin-expressing cells and fibers in the brain of the adult pigeon (Columba livia). *Journal of Chemical Neuroanatomy, 47*, 57–70. https://doi.org/10.1016/j.jchemneu.2012.10.006.
Meskenaite, V., Krackow, S., & Lipp, H. P. (2016). Age-dependent neurogenesis and neuron numbers within the olfactory bulb and hippocampus of homing pigeons. *Frontiers in Behavioral Neuroscience, 10*, 126. https://doi.org/10.3389/fnbeh.2016.00126.
Ming, G. L., & Song, H. (2005). Adult neurogenesis in the mammalian central nervous system. *Annual Review of Neuroscience, 28*, 223–250.
Ming, G. L., & Song, H. (2011). Adult neurogenesis in the mammalian brain: Significant answers and significant questions. *Neuron, 70*, 687–702. https://doi.org/10.1016/j.neuron.2011.05.001.
Moldovan, G. L., Pfander, B., & Jentsch, S. (2007). PCNA, the maestro of the replication fork. *Cell, 129*, 665–679. https://doi.org/10.1016/j.cell.2007.05.003.
Montagnese, C. M., Székely, A. D., Adám, A., & Csillag, A. (2004). Efferent connections of septal nuclei of the domestic chick (Gallus domesticus): an anterograde pathway tracing study with a bearing on functional circuits. *Journal of Comparative Neurology, 469*, 437–456.
Montagnese, C. M., Zachar, G., Bálint, E., & Csillag, A. (2008). Afferent connections of septal nuclei of the domestic chick (Gallus domesticus): A retrograde pathway tracing study. *Journal of Comparative Neurology, 511*, 109–150.
Montiel, J. F., Vasistha, N. A., Garcia-Moreno, F., & Molnar, Z. (2016). From sauropsids to mammals and back: New approaches to comparative cortical development. *Journal of Comparative Neurology, 524*, 630–645.
Nomura, T., & Hirata, T. (2017). The neocortical homologues in nonmammalian amniotes: Bridging the hierarchical concepts of homology through comparative neurogenesis. *Evolution of Nervous Systems, 2nd ed., 2*, 195–204. https://doi.org/10.1016/B978-0-12-804042-3.00041-5.

Nomura, T., Takahashi, M., Hara, Y., & Osumi, N. (2008). Patterns of neurogenesis and amplitude of Reelin expression are essential for making a mammalian-type cortex. *PLoS One, 3*, e1454. https://doi.org/10.1371/journal.pone.0001454.

O'Leary, O. F., & Cryan, J. F. (2014). A ventral view on antidepressant action: Roles for adult hippocampal neurogenesis along the dorsoventral axis. *Trends in Pharmacological Sciences, 35*, 675–687. https://doi.org/10.1016/j.tips.2014.09.011.

Ohara, S., Sato, S., Tsutsui, K.-I., Witter, M. P., & Iijima, T. (2013). Organization of multisynaptic inputs to the dorsal and ventral dentate gyrus: Retrograde trans-synaptic tracing with rabies virus vector in the rat. *PLoS One, 8*, e78928. https://doi.org/10.1371/journal.pone.0078928.

Olkowicz, S., Kocourek, M., Lučan, R. K., Porteš, M., Fitch, W. T., Herculano-Houzel, S., et al. (2016). Birds have primate-like numbers of neurons in the forebrain. *Proceedings of the National Academy of Sciences of the United States of America, 113*, 7255–7260. https://doi.org/10.1073/pnas.1517131113.

Pakhomova, A. S. (1981). Diencephalic afferents of the rat hippocampus. *Journal of Neurophysiology, 13*, 267–273.

Patel, S. N., Clayton, N. S., & Krebs, J. R. (1997). Spatial learning induces neurogenesis in the avian brain. *Behavioural Brain Research, 89*, 115–128.

Patzke, N., Manns, M., & Güntürkün, O. (2011). Telencephalic organization of the olfactory system in homing pigeons (Columba livia). *Neuroscience, 194*, 53–61. https://doi.org/10.1016/j.neuroscience.2011.08.001.

Pitkänen, A., Pikkarainen, M., Nurminen, N., & Ylinen, A. (2000). Reciprocal connections between the amygdala and the hippocampal formation, perirhinal cortex, and postrhinal cortex in rat. A review. *Annals of the New York Academy of Sciences, 911*, 369–391.

Puelles, L. (2001). Thoughts on the development, structure and evolution of the mammalian and avian telencephalic pallium. *Philosophical Transactions of the Royal Society of London. Series B, Biological sciences, 356*, 1583–1598.

Puelles, L. (2011). Pallio-pallial tangential migrations and growth signaling: New scenario for cortical evolution? *Brain, Behavior and Evolution, 78*, 108–127.

Reckfort, J. (2015). *New approaches to the interpretation of 3D-polarized light imaging signals for an advanced extraction of fiber orientation* (PhD thesis). Germany: Bergische Universität Wuppertal.

Reiner, A., Perkel, D. J., Bruce, L. L., Butler, A. B., Csillag, A., Kuenzel, W., et al.Avian Brain Nomenclature F. (2004). Revised nomenclature for avian telencephalon and some related brainstem nuclei. *Journal of Comparative Neurology, 473*, 377–414.

Robertson, B.-A., Rathbone, L., Cirillo, G., D'Eath, R. B., Bateson, M., Boswell, T., et al. (2017). Food restriction reduces neurogenesis in the avian hippocampal formation. *PLoS One, 12*, e0189158. https://doi.org/10.1371/journal.pone.0189158.

Roberts, A. C., Tomic, D. L., Parkinson, C. H., Roeling, T. A., Cutter, D. J., Robbins, T. W., et al. (2007). Forebrain connectivity of the prefrontal cortex in the marmoset monkey (Callithrix jacchus): An anterograde and retrograde tract-tracing study. *Journal of Comparative Neurology, 502*, 86–112.

Rowe, T. B., & Shepherd, G. M. (2016). Role of ortho-retronasal olfaction in mammalian cortical evolution. *Journal of Comparative Neurology, 524*, 471–495. https://doi.org/10.1002/cne.23802.

Scholzen, T., & Gerdes, J. (2000). The Ki-67 protein: From the known and the unknown. *Journal of Cellular Physiology, 182*, 311–322.

Schubert, N., Axer, M., Schober, M., Huynh, A. M., Huysegoms, M., Palomero-Gallagher, N., et al. (2016). 3D reconstructed cyto-, muscarinic M2 receptor, and fiber architecture of the rat brain registered to the Waxholm Space atlas. *Frontiers in Neuroanatomy, 10*, 51. https://doi.org/10.3389/fnana.2016.00051.

Shanahan, M., Bingman, V. P., Shimizu, T., Wild, M., & Güntürkün, O. (2013). Large-scale network organization in the avian forebrain: A connectivity matrix and theoretical analysis. *Frontiers in Computational Neuroscience, 7*, 89.

Shepherd, G. M., & Rowe, T. B. (2017). Neocortical lamination: Insights from neuron types and evolutionary precursors. *Frontiers in Neuroanatomy, 11*, 100. https://doi.org/10.3389/fnana.2017.00100.

Sherry, D. F., Grella, S. L., Guigueno, M. F., White, D. J., & Marrone, D. F. (2017). Are there place cells in the avian hippocampus? *Brain, Behavior and Evolution, 90*, 73–80. https://doi.org/10.1159/000477085.

Sherry, D. F., & Hoshooley, J. S. (2010). Seasonal hippocampal plasticity in food-storing birds. *Philosophical Transactions of the Royal Society of London. Series B, Biological sciences, 365*, 933–943. https://doi.org/10.1098/rstb.2009.0220.

Sherry, D. F., & MacDougall-Shackleton, S. A. (2015). Seasonal change in the avian hippocampus. *Frontiers in Neuroendocrinology, 37*, 158–167. https://doi.org/10.1016/j.yfrne.2014.11.008.

Silverman, A. J., Hoffmann, A. J., & Zimmermann, E. A. (1981). The descending afferent connections of the paraventricular nucleus of the hypothalamus (PVN). *Brain Research Bulletin, 6*, 47–61.

Smulders, T. V. (2017). The avian hippocampal formation and the stress response. *Brain, Behavior and Evolution, 90*, 81–91. https://doi.org/10.1159/000477654.

Snyder, J. S., Radik, R., Wojtowicz, J. M., & Cameron, H. A. (2009). Anatomical gradients of adult neurogenesis and activity: Young neurons in the ventral dentate gyrus are activated by water maze training. *Hippocampus, 19*, 360–370.

Spampanato, J., Sullivan, R. K., Turpin, F. R., Bartlett, P. F., & Sah, P. (2012). Properties of doublecortin expressing neurons in the adult mouse dentate gyrus. *PLoS One, 7*, e41029. https://doi.org/10.1371/journal.pone.0041029.

Strange, B. A., Witter, M. P., Lein, E. D., & Moser, E. I. (2014). Functional organization of the hippocampal longitudinal axis. *Nature Reviews. Neuroscience, 15*, 655–669.

Striedter, G. F. (2005). *Principles of brain evolution*. Sunderland: Sinauer.

Striedter, G. F. (2016). Evolution of the hippocampus in reptiles and birds. *Journal of Comparative Neurology, 524*, 496–517.

Striedter, G. F., & Northcutt, R. G. (2006). Head size constrains forebrain development and evolution in ray-finned fishes. *Evolution & Development, 8*, 215–222.

Swanson, L. W., & Cowan, W. M. (1977). An autoradiographic study of the organization of the efferent connections of the hippocampal formation in the rat. *Journal of Comparative Neurology, 172*, 49–84.

Swanson, C. J., & Kalivas, P. W. (2000). Regulation of locomotor activity by metabotropic glutamate receptors in the nucleus accumbens and ventral tegmental area. *The Journal of Pharmacology and Experimental Therapeutics, 292*, 406–414.

Szekely, A. D. (1999). The avian hippocampal formation: Subdivisions and connectivity. *Behavioural Brain Research, 98*, 219–225.

Szekely, A. D., & Krebs, J. R. (1996). Efferent connectivity of the hippocampal formation of the zebra finch (Taeniopygia guttata): An anterograde pathway tracing study using Phaseolus vulgaris leucoagglutinin. *Journal of Comparative Neurology, 368*, 198–214.

Tanti, A., Rainer, Q., Minier, F., Surget, A., & Belzung, C. (2012). Differential environmental regulation of neurogenesis along the septo-temporal axis of the hippocampus. *Neuropharmacology, 63*, 374–384.

Tanti, A., Westphal, W. P., Girault, V., Brizard, B., Devers, S., Leguisquet, A. M., et al. (2013). Region-dependent and stage-specific effects of stress, environmental enrichment, and antidepressant treatment on hippocampal neurogenesis. *Hippocampus, 23*, 797–811.

Taufique, S. K. T., Prabhat, A., & Kumar, V. (2018). Constant light environment suppresses maturation and reduces complexity of new born neuron processes in the hippocampus and caudal nidopallium of a diurnal corvid: Implication for impairment of the learning and cognitive performance. *Neurobiology of Learning and Memory, 147*, 120–127. https://doi.org/10.1016/j.nlm.2017.12.001.

Thierry, A. M., Gioanni, Y., Degenetais, E., & Glowinski, J. (2000). Hippocampo-prefrontal cortex pathway: Anatomical and electrophysiological characteristics. *Hippocampus, 10*, 411–419.

Thompson, C. L., Pathak, S. D., Jeromin, A., Ng, L. L., MacPherson, C. R., Mortrud, M. T., et al. (2008). Genomic anatomy of the hippocampus. *Neuron, 60*, 1010–1021. https://doi.org/10.1016/j.neuron.2008.12.008.

Tosches, M. A., Yamawaki, T. M., Naumann, R. K., Jacobi, A. A., Tushev, G., & Laurent, G. (2018). Evolution of pallium, hippocampus, and cortical cell types revealed by single-cell transcriptomics in reptiles. *Science, 360*, 881–888. https://doi.org/10.1126/science.aar4237.

Ulinski, P. S. (1983). *Dorsal ventricular ridge: Treatise on forebrain organization in reptiles and birds (Neurobiology)*. John Wiley & Sons Inc.

Wada, H., Newman, A. E., Hall, Z. J., Soma, K. K., & MacDougall-Shackleton, S. A. (2014). Effects of corticosterone and DHEA on doublecortin immunoreactivity in the song control system and hippocampus of adult song sparrows. *Developmental Neurobiology, 74*, 52–62. https://doi.org/10.1002/dneu.22132.

Walker, D. L., Miles, L. A., & Davis, M. (2009). Selective participation of the bed nucleus of the stria terminalis and CRF in sustained anxiety-like versus phasic fear-like responses. *Progress in Neuro-psychopharmacology & Biological Psychiatry, 33*, 1291–1308.

Wilson, C. L., Isokawa, M., Babb, T. L., Crandall, P. H., Levesque, M. F., & Engel, J., Jr. (1991). Functional connections in the human temporal lobe. II. Evidence for a loss of functional linkage between contralateral limbic structures. *Experimental Brain Research, 85*, 174–187.

Witter, M. P., & Amaral, D. G. (2004). Hippocampal formation. In G. Paxinos (Ed.), *The rat nervous system* (pp. 635–704). Amsterdam: Elsevier.

Witter, M. P., Kleven, H., & Kobro Flatmoen, A. (2017). Comparative contemplations on the hippocampus. *Brain, Behavior and Evolution, 90*, 15–24. https://doi.org/10.1159/000475703.

Yassa, M. A., & Stark, C. E. L. (2011). Pattern separation in the hippocampus. *Trends in Neurosciences, 34*, 515–525. https://doi.org/10.1016/j.tins.2011.06.006.

Zeineh, M. M., Palomero-Gallagher, N., Axer, M., Gräßel, D., Goubran, M., Wree, A., et al. (2017). Direct visualization and mapping of the spatial course of fiber tracts at microscopic resolution in the human hippocampus. *Cerebral Cortex, 27*, 1779–1794. https://doi.org/10.1093/cercor/bhw010.

Zheng, J., Jiang, Y. Y., Xu, L. C., Ma, L. Y., Liu, F. Y., Cui, S., et al. (2017). Adult hippocampal neurogenesis along the dorsoventral axis contributes differentially to environmental enrichment combined with voluntary exercise in alleviating chronic inflammatory pain in mice. *The Journal of Neuroscience: the Official Journal of the Society for Neuroscience, 37*, 4145–4157. https://doi.org/10.1523/JNEUROSCI.3333-16.2017.

Zilles, K., Palomero-Gallagher, N., Gräßel, D., Schlömer, P., Cremer, M., Woods, R., et al. (2016). High-resolution fiber and fiber tract imaging using polarized light microscopy in the human, monkey, rat, and mouse brain. In K. S. Rockland (Ed.), *Axons and brain architecture (2016)* (pp. 369–389). London: Elsevier.